Mao-Hong Yu
Jian-Chun Li

Computational Plasticity

With Emphasis on the Application of the Unified Strength Theory

ADVANCED TOPICS
IN SCIENCE AND TECHNOLOGY IN CHINA

ADVANCED TOPICS
IN SCIENCE AND TECHNOLOGY IN CHINA

Zhejiang University is one of the leading universities in China. In Advanced Topics in Science and Technology in China, Zhejiang University Press and Springer jointly publish monographs by Chinese scholars and professors, as well as invited authors and editors from abroad who are outstanding experts and scholars in their fields. This series will be of interest to researchers, lecturers, and graduate students alike.

Advanced Topics in Science and Technology in China aims to present the latest and most cutting-edge theories, techniques, and methodologies in various research areas in China. It covers all disciplines in the fields of natural science and technology, including but not limited to, computer science, materials science, life sciences, engineering, environmental sciences, mathematics, and physics.

Mao-Hong Yu
Jian-Chun Li

Computational Plasticity

With Emphasis on the Application of the Unified Strength Theory

With 458 figures, 139 of them in color

ZHEJIANG UNIVERSITY PRESS
浙江大学出版社

Springer

Series:
1. *Unified Strength Theory and Its Applications.* Yu MH, Springer: Berlin, 2004.
2. *Generalized Plasticity.* Yu MH et al. Springer: Berlin, 2006.
3. *Structural Plasticity: Limit, Shakedown and Dynamic Plastic Analyses of Structures.* Yu MH, Ma GW and Li JC, Springer and ZJU Press, 2009.
4. *Computational Plasticity: With Emphasis on the Application of the Unified Strength Theory and Associated Flow Rule.* Yu MH and Li JC, Springer and ZJU Press, 2012.

Mao-Hong Yu
Jian-Chun Li

Computational Plasticity

With Emphasis on the Application of the Unified Strength Theory

With 458 figures, 139 of them in color

Authors
Prof. Mao-Hong Yu
Department of Civil Engineering
Xi'an Jiaotong University, Xi'an, China
E-mail: mhyu@mail.xjtu.edu.cn

Researcher Jian-Chun Li
Swiss Federal Institute of Technology
Switzerland
E-mail: jianchun.li@epfl.ch

Printed on acid-free paper

Preface

Computational plasticity is a new and important branch of computational mechanics. *Computational Plasticity*: *With Emphasis on the Application of the Unified Strength Theory and Associated Flow Rule* is the third title in the series on plasticity published by Springer and by Springer or by the collabration of Springer and ZJU Press. The other two files are: *Generalized Plasticity* (Springer, Berlin, 2006) and *Structural Plasticity: Limit, Shakedown and Dynamic Plastic Analyses of Structures* (Springer and ZJU Press, Hangzhou, 2009). The founding work in this series on plasticity is *Unified Strength Theory and its Applications* that was published by Springer in Berlin in 2004, in which the unified strength theory (UST) and its 30 years developments history are described in detail.

Generalized Plasticity, the first monograph in this series on plasticity, is a combination of traditional plasticity for metallic materials (non-SD materials) and plasticity for geomaterials (SD materials, i.e. strength difference in tension and in compression, sometimes referred to as tension-compression asymmetry). It was published by Springer in 2006, in which the unified slip line theory for plane strain problems and unified characteristics theory for plane stress and spatial axisymmetric problems, as well as the unified fracture criterion for mixed mode cracks and plastic zones at the tip of a crack using the unified strength theory are described. *Generalized Plasticity* can be used for both non-SD materials and SD materials. The time effect, however, is not taken into account in *Generalized Plasticity*. The time independent UST can be extended to time dependent UST.

The second title in this series on plasticity is *Structural Plasticity: Limit, Shakedown and Dynamic Plastic Analyses of Structures*, which was published by ZJU Press and Springer in 2009. *Structural Plasticity* deals with limit analysis, shakedown analysis and dynamic plastic analyses of structures using the analytical method. The straight line segments on the series yield surfaces of the unified strength theory make these surfaces convenient for analytical treatment of plasticity problems. A series of results of the unified solutions for elastic and plastic limit analysis, shakedown analysis and dynamic plastic analysis for structures are given by using the unified strength theory. These unified solutions can provide a very useful tool for the design of engineering structures. Most solutions in textbooks regarding the plastic analysis of structures are special cases of the unified solution, using the unified strength theory.

The third title in this series on plasticity is *Computational Plasticity*: *With Emphasis on the Application of the Unified Strength Theory and Associated Flow Rule*, in which numerical methods are applied. The unified strength theory and associated flow rule are implemented in several computational plasticity codes and applied to many engineering problems.

A series of results can be obtained in *Generalized Plasticity* (slip line theory), *Structural Plasticity* (analytical analysis of structures) and *Computational Plasticity* (numerical analysis of structures). The unified solution gives a series of new results, which can be adapted for more materials and structures. It is possible for us to adopt different values of the unified strength theory parameter *b* to meet different materials and structures. The application of the unified solution is advantageous in material and energy saving and also advantageous in environmental protection.

This monograph describes the unified strength theory and associated flow rule, the implementation of these basic theories, and shows how a series of results can be obtained by their use. A lot of numerical solutions for beams, plates, underground caves, excavations, strip foundations, circular foundations, slopes, underground structures of hydraulic power stations, pumped-storage power stations, underground mining, high-velocity penetration of concrete structures, ancient structures, rocket parts, as well as relevant computational results, are given. These theories and methods can be used for other computer codes. This will increase the function of codes. An example of numerical calculation for a slope by using the unified strength theory with the parameters $b=0$, $b=1/4$, $b=0.5$, $b=3/4$ and $b=1$ is shown in the figure below. Configurations of the plastic strain of the slope with different yield criteria are shown. The results using the Mohr-Coulomb theory and the Drucker-Prager criterion are also given for comparison.
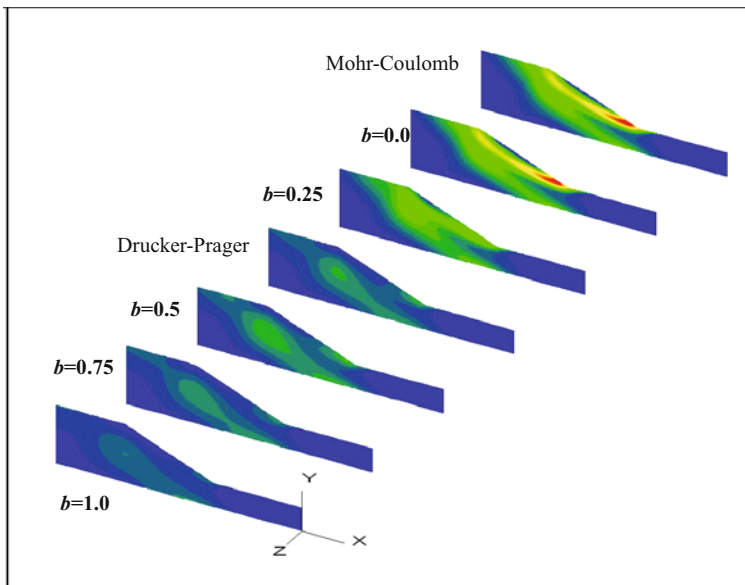
The results obtained by using various yield criteria are very different. The shape and size of the plastic zone and bearing capacity of the structure are influenced strongly by the choice of the yield criterion. The unified strength theory and its implementation in the computer code provide us with a very effective approach for studying the effect of yield criterion in various engineering problems. A series of results was obtained, which can be used for most materials from metallic materials to geomaterials. The unified model, unified constitutive relation, unified process of the corner singularity, and the program paragraph of unified implementation can be used for other FE codes, including commercial computer codes. This will also increase the power of FEM and computational plasticity codes and the fields of application for various codes.

Many new and interesting results can be obtained through the unified strength theory, such as the yield criterion effect on the bearing capacity of various structures, the effect of material strength parameters (friction angle) on plastic zones distribution (Chapter 9), the effect of tension and compression of SD materials, the relation between different yield criteria. This will bring the potential strength of the material into full play and show how we can benefit from material and energy saving, etc.

The contents of this book can be divided into four parts:

Part one: Basic theories of stress, strain, yield criterion and associated flow rule are described in Chapters 1 to 4.

Part two: Implementation of the unified strength theory and associated flow rule, the process of the singularity of the corner and several basic applications, UEPP-Unified Elasto-Plastic Program, are described in Chapters 5 to 9.

Part three: Chapters 10 to 18 are the implementation of the unified strength theory and associated flow rule in several commercial finite element codes and finite difference programs, including ABAQUS, ASYSN, AutDYN-2D, AutDYN-3D, AutDYN Hydrocode, DIANA, FLAC-2D, FLACK-3D, Non-Linear etc. The computational methods include the finite element method, finite difference method and smoothed particle hydrodynamics (SPH) method. More results can be obtained through combinations of the unified strength theory and associated flow rule and commercial finite element codes

Part four: Chapter 19 is called Mesomechanics and Multiscale Modelling for the Yield Surface. Miscellaneous issues, including ancient structures, propellant grains of solid rockets, solid rocket motors, parts of a rocket and large generators are presented in Chapter 20.

A series of research works of underground excavation were carried out for the Laxiwa Hydraulic Power Station by Northwest China Hydroelectric Power Investigation and Design Institute. 3D numerical modeling of the underground excavation of Tai'an Pumped Storage Hydraulic Power Station was done by Professors Sun, Shang, Zhang et al. of Zhejiang University, Hangzhou, China and the East China Investigation and Design Institute, State Power Corporation of China. Dynamic response and blast-resistance analysis of a tunnel subjected to blast loading was done by Professors at Zhejiang University, Hangzhou，China, in respect of a railroad tunnel (Liu and Wang, 2004). The twin-shear unified strength

theory is also used for dynamic problems. The above projects are described in brief in Chapter 10.

'Implementation of the Unified Strength Theory into ABAQUS and its application in Tunnel Engineering' was written by Professors Jun-Qi Wang and Lu (Chapter 11). 2D and 3D simulation of normal penetration and oblique penetration are presented by Prof. Xiao-Qing Zhou (Chapters 12 and 13); A 2D axi-symmetric numerical simulation for the projectile-target model is carried out using the SPH procedure and the unified strength theory by Hong-Fu Qiang and Sau-Cheong Fan at Nanyang Technological University, Singapore (Chapter 12). Underground mining excavation using the unified strength theory (Chapter 14) is a contribution by Professors Li Wang and Qing Gao, Key Laboratory of the Ministry of Education for Highly Effective Mining and Safety in Metal Mines, Beijing, China and the Beijing Science and Technical University, Beijing, China.

The unified strength theory (UST) with tension cutoff is also adopted as the failure criterion for the analysis of punching shear failure of beams and slab-column connections by Xue-Song Zhang, Hong Guan and Yew-Chaye Loo at Griffith University, Australia (Chapter 15). The multi-parameter unified strength theory with b=0.6 is used for elasto-plastic analysis of reinforced concrete slabs and high-strength concrete slabs by Fang Wang, Susanto Teng and Sau-Cheong Fan in Singapore. The unified strength theory with b=0.6 is also employed to analyze the response of an RC box sectional beam under eccentric loading conditions by Prof. Xiao-Qing Zhou. These results are introduced briefly in Chapter 15. Stability analysis of underground caverns (Huanren pumped-storage powerhouse) based on the unified strength theory and non-associated flow rule is presented by Professor Lan Qiao and Yuan Li, Beijing Science and Technical University, Beijing, China (Chapter 16).

The stability of a 170-meter high steep side slope sluice of the Three Gorges water conservation and energy project was carried out by the Yangtze River Academy of Science, in which the single-shear theory, the twin-shear theory and the Drucker-Prager criterion were used (Chapter 17). The 3D simulation of a landslip using the FLAC-3D and the unified strength theory is given by Dr. Zong-Yuan Ma and Prof. Hong-Jian Liao in Chapter 18.

Chapters 19 and 20 are Mesomechanics and Multiscale Modelling for Yield Surface and Miscellaneous Issues. Finally, several comments, reviews and research on the UST, which are presented in published papers and books, are briefly introduced in Section 20.10.

I am deeply indebted to many authors and colleagues, and especially indebted

are cited in this monograph.

We would like also to express our sincere thanks to the International Engineering Department, Springer, Germany, and the International Rights Department, Zhejiang University Press, for their excellent editorial work on our manuscript.

<div align="right">

Mao-Hong Yu
Xi'an, China
January, 2012

</div>

Contents

Notations

Stresses, Strains and Invariants

σ	normal stress
σ_{ij}	stress tensor
σ_m	hydrostatic stress or mean stress
$\sigma_1, \sigma_2, \sigma_3$	major principal stress, intermediate principal stress and minor principal stress
$\sigma_{13}, \sigma_{12}, \sigma_{23}$	normal stresses acting on the orthogonal octahedron element
σ_r	radial stress in polar coordinates
σ_θ	circumferential stress in polar coordinates
σ_z	axial stress in polar coordinates
$\tau_{13}, \tau_{12}, \tau_{23}$	maximum principal shear stress, intermediate shear stress or minimum shear stress
μ_σ	Lode stress parameter
$\mu_\tau, \mu_\tau{}'$	twin-shear parameter for stress state

$$\mu_\tau = \tau_{12} / \tau_{23}, \quad \mu_\tau{}' = \tau_{23} / \tau_{13}$$

θ	stress angle corresponding to the twin-shear parameter
τ_8 or τ_{oct}	octahedral shear stress
σ_8 or σ_{oct}	octahedral normal stress
$\varepsilon_x, \varepsilon_y, \varepsilon_z$	strains in three dimension
$\varepsilon_r, \varepsilon_\theta$	radial and circumferential strain
ε_z	longitudinal strain
I_1, I_2, I_3	invariants of the stress tensor σ_{ij}
S_1, S_2, S_3	deviatoric stresses

| J_1, J_2, J_3 | invariants of the deviatoric stress tensor |

Material Parameters

σ_y	yield stress
σ_t	uniaxial tensile strength
σ_c	uniaxial compressive strength
α	ratio of tensile strength to compressive strength
m	compressive-tensile strength ratio of materials
τ_0 or τ_y	pure shear strength or shear yield strength of materials
b	failure criterion parameter in the unified strength theory
β	coefficient in the unified strength theory that represents the effect of the normal stress on failure
C_0	cohesive strength
φ	friction angle
C_{uni}	unified cohesive strength
φ_{uni}	unified friction angle
E	Young's modulus
ν	Poisson's ratio
G	modulus of rigidity

Miscellaneous

M_r	radial bending moment per unit length
M_θ	circumferential bending moment per unit length
$\dot{W}$	rate of deflection
ρ	density of the material
u	displacement
ω_e	limit rotating speed of disc
$[\sigma]$	allowable tensile stress, $[\sigma] = \sigma_t / n$
p	internal pressure subjected on the cylinder
p_e	elastic limit pressure
p_p	plastic limit pressure
$p_{\max}$	shakedown pressure of the cylinder

r	radial variable
r_i , r_e	the internal and external radii of the cylinder
r_p	plastic zone radius of the cylinder subjected to internal pressure p

1

Introduction

1.1 Elasto-Plastic Finite Elements

The finite element method (FEM) has now become recognized as a general method with wide applications in engineering and applied mechanics. FEM was originally developed in the field of structural analysis. All the problems were linear in the sense that they involve the solution of sets of linear algebraic equations. It is the linear elastic FEM.

The elasto-plastic FEM, non-linear material problems or computational plasticity, has also been widely accepted, and many excellent books on computational plasticity have been written. Overviews and analysis can be found in Zienkiewicz (1971; 1989), Cook et al. (1989), Reddy (1993), Bathe (1996), Han and Reddy (1999), Belytschko et al. (2000), Smith and Griffiths (2004), Reddy (2009), Anandarajah (2010), etc. The theories and implementation of the plasticity FEM are described by Oden (1972), Hinton and Owen (1979), Owen and Hinton (1980), Miyoshi (1985), Kobayashi et al. (1989), Strin (1993), Pan (1995), Crisfield (1997), Bonet and Wood (1997), Simo and Hughes (1998), Belytschko et al. (2000), Smith and Griffiths (2004), Kojic and Bathe (2005) and Neto et al. (2009). *Plasticity and Geotechnics* was written by HS Yu (2006). *Lecture Notes on Computational Geomechanics: Inelastic Finite Elements for Pressure Sensitive Materials* was presented by Jeremić, et al. (2010). A detailed introduction to the plasticity FEM program (2D) can be found in Owen and Hinton (1980) and the proceedings of Owen et al. (1989), and in (Neto et al., 2009), in which a computer program of approximately 11,000 lines of FORTRAN codes is given. The 2D non-linear thermo-elastoplastic consolidation program PLASCON was given by Lewis and Schrefler (1987). The Mohr-Coulomb Theory and the Critical State Models (Roscoe et al., 1963, 1968; Schofield and Wroth, 1968) were used. The theory and implementation of nonlinear analysis in soil mechanics was described by Chen and

Mizuno (1990). The Drucker-Prager criterion and cap models were implemented for studying soil mechanics problems.

Advances in computational nonlinear mechanics before 1999 were described and edited by Wunderlich et al. (1981), Doltsinis (1989), Smith (1990) and Inoue et al. (1990), Desai and Gioda (1990), Ehlers (1999). Computational plasticity applied to metal forming can be found in Kobayashi et al. (1989), Khoei (2005), Dixit and Dixit (2008). Concrete plasticity and finite element analysis for limit-state design of concrete structures can be found in Chen (1982), Nielsen (1991), Kotsovos and Pavlovic (1995). A textbook on the combination of plasticity and geomechanics was written by Davis and Selvadural (2002). Materials including metals, soils and others are idealized as a continuum. Most engineering theories of metals and soil behavior of practical interest have depended on the continuum assumption, as indicated by Davis and Selvadural (2002). Ten serial International Conferences on Computational Plasticity (COMPLAS) have been successfully held in Barcelona, Spain since 1987. *Computational Plasticity* was published (Oñate and Owen, 2007), which contains 14 invited contributions written by distinguished authors who participated in the VIII International Conference on Computational Plasticity.

Nonlinearities can be introduced by either geometric or material property effects. Geometric nonlinearities often arise in problems involving solid media in which the strains are sufficiently large to significantly affect the shape of the solution domain. Material nonlinearities include elasto-plastic deformation characterized by an irreversible straining which can only be sustained once a certain level of stress, known as the yield limit, yield function, strength theory or material model, has been reached. Material nonlinearities also include nonlinearly elastic solids, whose properties are functions of the local state of deformation. Elasto-plastic nonlinearities are studied and applied widely in mechanics and engineering. The nonlinear elasto-plastic material model is of great importance for computational plasticity.

Elasto-plastic programs have been used for many years in the world. Material models are usually implemented in terms of the Tresca criterion and Huber-von Mises yield criterion for metallic materials and the Mohr-Coulomb criterion or the Drucker-Prager criterion for geomaterials. These material models (the single model) are suited to one kind of material. A new material model, the unified strength theory (UST), is implemented in computer codes and used for computational plasticity in this book.

The material parameters of the unified strength theory (UST) are the same as the material parameters of the Mohr-Coulomb theory and the Drucker-Prager criterion. Most parts of the computer codes are also the same as the other elasto-plastic computer codes, only the yield criteria and its associated flow rule are different. the result obtained by using the Mohr-Coulomb theory is a special case of the result using UST. The two results are identical. More results, however, can be obtained by using UST.

Unified strength theory has been applied in many research and engineering fields. UST and its implementation can be reliably employed therefore in engineering and R & D applications. UST can be adapted for more materials and

structures. It has provided more choices for researchers and engineers.

1.2 Bounds and Region of the Convex Yield Surface

As a matter of primary importance, the bounds and the region of the failure criteria have to be determined before research is started on the effect of failure criteria. There are hundreds of yield and failure criteria that can be seen (Yu, 2002, 2004). Various yield criteria and failure criteria have been proposed in the past; however, all of them must be situated between the bounds if the convexity-is considered. The lower bound is the single-shear strength theory (the Mohr-Coulomb strength theory) and the single-shear yield criterion (the Tresca yield criterion or the maximum shear stress criterion), as shown in Figs. 1.1 and 1.2. The upper bound is the twin-shear strength theory (Yu et al., 1985) for SD materials (strength difference of material in tension and in compression), as shown in Fig. 1.1, and the twin-shear yield criterion (Yu, 1961a; 1961b; 1983) or the maximum deviatoric stress criterion (Haythornthwaite, 1961) for non-SD materials, respectively (Fig. 1.2). Other yield criteria are situated between these two bounds.
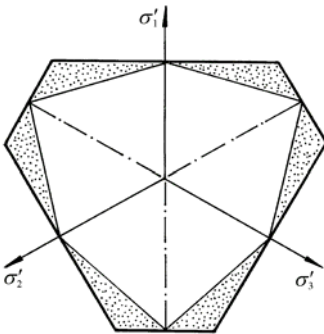
Fig. 1.1 Bounds and region of yield loci for SD materials
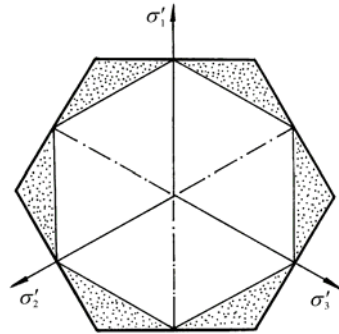
Fig. 1.2 Bounds and region of yield loci for non-SD materials

Most of the experimental results are situated between these two bounds. Figure 1.3(a) shows the experimental result for sand, given by Nakai and Matsuoka (1980). It is in good agreement with the Matsuoka-Nakai criterion, as shown in Fig. 1.3(b). It is interesting that the piece-wise linear criterion is also in very good agreement with this experimental result, as shown in Fig. 1.3(c). The piece-wise linear loci in Fig. 1.3(c) is the unified strength theory with $b=3/4$.
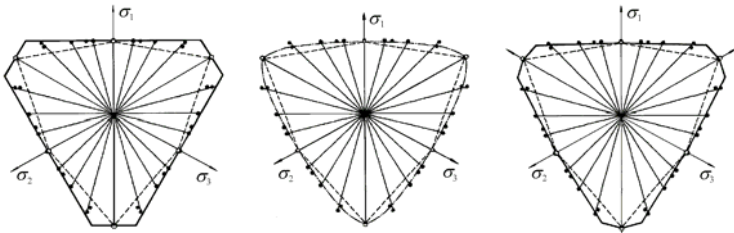
(a) Two bounds   (b) Matsuoka-Nakai criterion   (c) Unified strength theory with b=3/4

Fig. 1.3 Comparisons of test results with curve criterion and piece-wise linear criterion

1.3   Unified Strength Theory and its Implementation in Computer Codes

A unified strength theory stating that the yield loci covered the entire region from the lower bound to upper bound was proposed by Yu (1991). The details of the unified strength theory can be seen in (Yu, 1992; 2004). It is the natural development of the twin-shear idea and twin-shear yield criterion for non-SD materials (Yu, 1961) and the twin-shear strength theory for SD materials (Yu, 1985). The serial limit surfaces and three special cases in stress space of the unified strength theory are shown in Fig. 1.4.
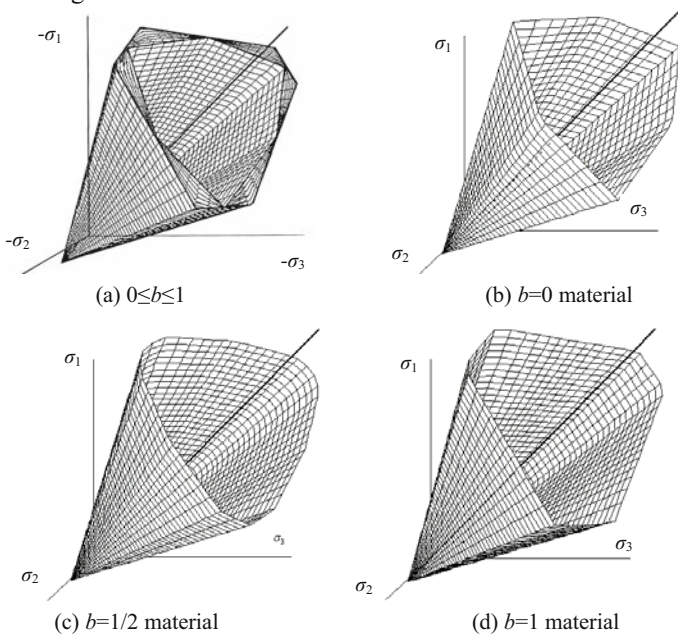
(a) $0 \leq b \leq 1$ (b) b=0 material

(c) b=1/2 material   (d) b=1 material

Fig. 1.4 Serial limit surfaces of the unified strength theory in stress space

The serial limit loci in the deviatoric plane of the unified strength theory are shown in Fig. 1.5. The yield criteria of the unified strength theory can be extended to the non-convex criteria, as shown in Fig. 1.5(a). Some well-known yield criteria and a lot of new criteria can be deduced from the unified strength theory, as shown in Fig. 1.5. The serial limit loci in the deviatoric plane of the unified strength theory can regenerate to serial yield loci for non-SD materials, as shown in Fig. 1.5(b). Limit loci for SD materials and yield loci for non-SD materials of the unified strength theory in plane stress state are shown in Fig. 1.6.

(a) Limit loci for SD materials   (b) Yield loci for non-SD materials
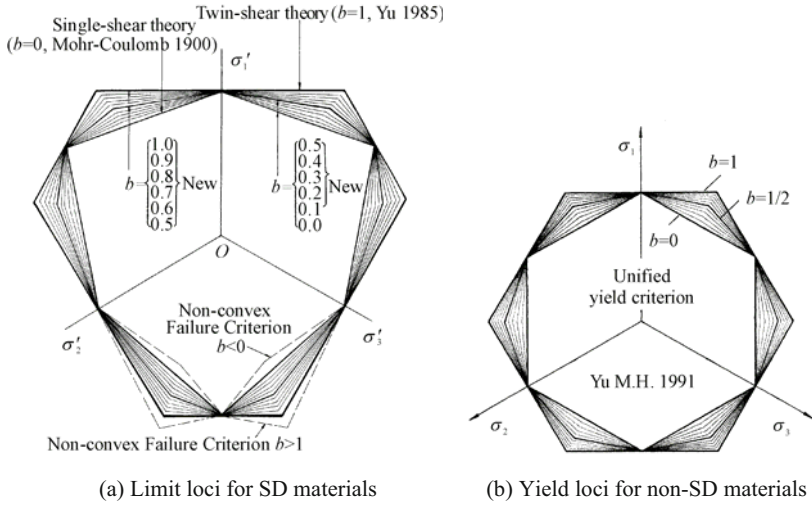
Fig. 1.5 Serial limit loci of the unified strength theory in deviatoric plane

(a) SD materials   (b) Non-SD materials
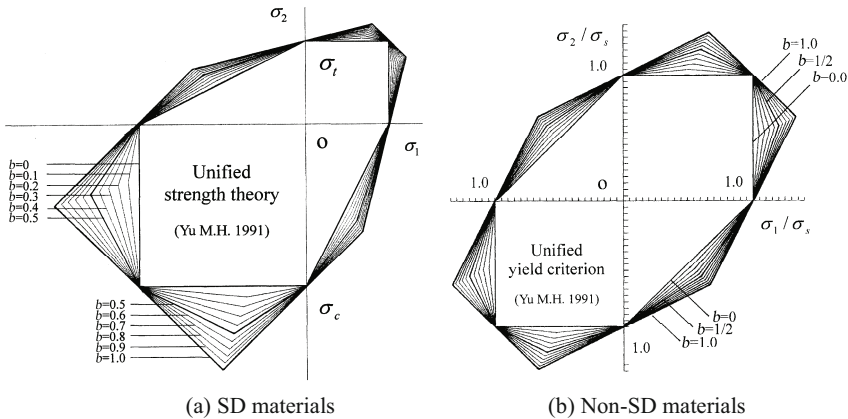
Fig. 1.6 Serial limit loci of the unified strength theory in plane stress state

A review of "Unified Strength Theory and its Applications. Springer, Berlin, 2004" was written by Teodorescu (2006) in *Zentralblatt MATH*. "Here, starting from the idea

of twin-shear and twin-shear yield criterion, the author sets up a twin-shear strength theory and then a unified strength theory, the limit loci of which cover all regions of the convex limit loci and can be extended to the region of non-convex limit loci." As pointed out by Teodorescu (2006), the serial yield criteria of the unified strength theory are piece-wise linear criteria that consist of two expressions, as follows

$$F = \sigma_1 - \frac{\alpha}{1+b}(b\sigma_2 + \sigma_3) = \sigma_t, \qquad \text{when} \qquad \sigma_2 \leq \frac{\sigma_1 + \alpha\sigma_3}{1+\alpha} \qquad (1.1a)$$

$$F' = \frac{1}{1+b}(\sigma_1 + b\sigma_2) - \alpha\sigma_3 = \sigma_t, \qquad \text{when} \qquad \sigma_2 \geq \frac{\sigma_1 + \alpha\sigma_3}{1+\alpha} \qquad (1.1b)$$

where σ_1, σ_2, σ_3 are three principal stresses; σ_t is tensile yield point of material; α is the ratio of tensile yield point to compressive yield point of material $\alpha=\sigma_t/\sigma_c$. The relations of the serial loci are shown in Fig. 1.7.
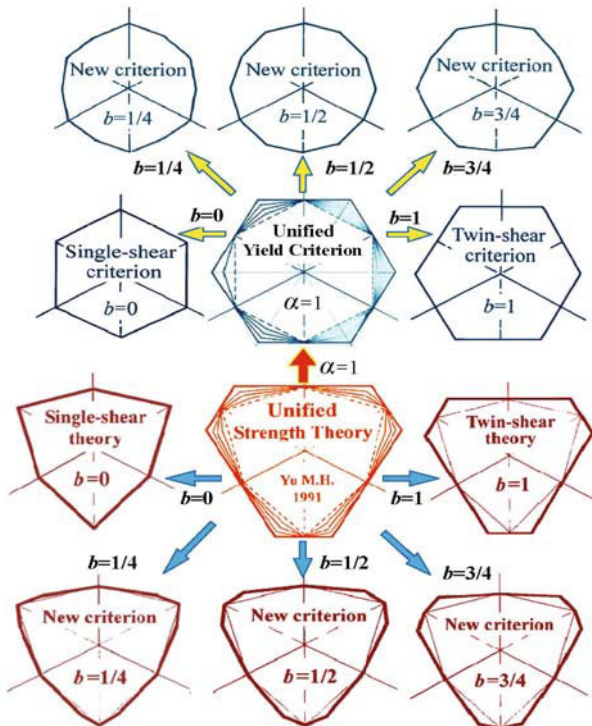
Fig. 1.7 Special cases of the unified strength theory

UST (Unified Strength Theory) has been implemented in some elasto-plastic programs including some commercial FEM codes and applied to engineering problems (Yu, 1992; Yu and Li, 1991; Yu et al., 1992; Yu and Zeng, 1994; Yu et al.,

1993; 1998; Yu et al,. 1997; 1999; Fan and Qiang, 2001; Zhang and Loo, 2001; Sun et al., 2004; Li and Ishii, 1998; Zhang et al., 2008; Wang et al., 2008; Li , 2008). The singularities at the corners of single-shear theory, twin-shear theory and the unified strength theory have been overcome by using a unified numerical procedure. A unified elasto-plastic program (UEPP) has been established, which was applied to some engineering problems (Yu and Zeng, 1994; Yu et al., 1997; 1999; Yu, 1998). UST has also been implemented in ABQUSE by Wang JQ in 2008.

The twin-shear strength theory, unified strength theory and its unified elasto-plastic constitutive model are implemented in FLAC-3D by Zhang (2008), Li (2008), Qiao and Li (2010), and Ma (2010). Before unified strength theory, the twin-shear yield criterion (for non-SD materials) and the twin-shear strength theory (for SD materials) were implemented in some FEM codes by An et al. (1991), Yu and Li (1991), Quint (1993; 1994), Shen (1993).

Therefore, unified strength theory that can be used in finite difference computation, has also developed FLAC-3D mechanical analysis serviceability. The confirmation of unified strength theory has been tested, finally demonstrating that this model is very good at taking into account the effect of intermediate principal stress. Based on unified strength theory and its constitutive relationship, as well as finite difference computation developed in FLAC-3D, the stability and protection of the underground caves at the Huanren power plant were calculated. The excavation, the spread of the plastic region around the cave area and the distribution and change in displacement were obtained by Li and Qiao. The effects of the irregular surface, the in-situ stress field's distribution and different constitutive relations concerning stability have been studied.

1.4   The Effect of Yield Criteria on the Numerical Analysis Results

The Tresca yield criterion and the Huber-von Mises criterion were described in most textbooks about metal plasticity and computational plasticity. A great deal of research has been dedicated to showing the effects of failure criteria on the numerical results of load-carrying capacities of structures. A famous example was given by Humpheson and Naylor (1975), and was further studied by Zienkiewicz and Pande (1977). Shapes of loading surfaces of concrete models and their influence on the peak load and failure mode in structural analyses were given by Pivonka et al. (2003). Figure 1.8 shows some differences between the results obtained for plane strain flexible footing on a weightless material (Humpheson and Naylor, 1975). The forms of different limit surfaces on the deviatoric plane are shown in Fig. 1.9.

The influence of different forms of yield surfaces on load-bearing capacity is obvious. The Mohr-Coulomb strength theory, the Williams-Warnke criterion, the Gudehus-Argyris criterion and various circular cone approximations, i.e. extension cone, compromise cone, compression cone and the Drucker-Prager criterion (in-

scribed cone of the Mohr-Coulomb semi-infinite hexagonal cone with unequal sides) have been used. They show a great difference between results obtained using various failure criteria. Obviously, the question arises as to which one of these results should be preferred, because there is only one reasonable result for a given material and structure.
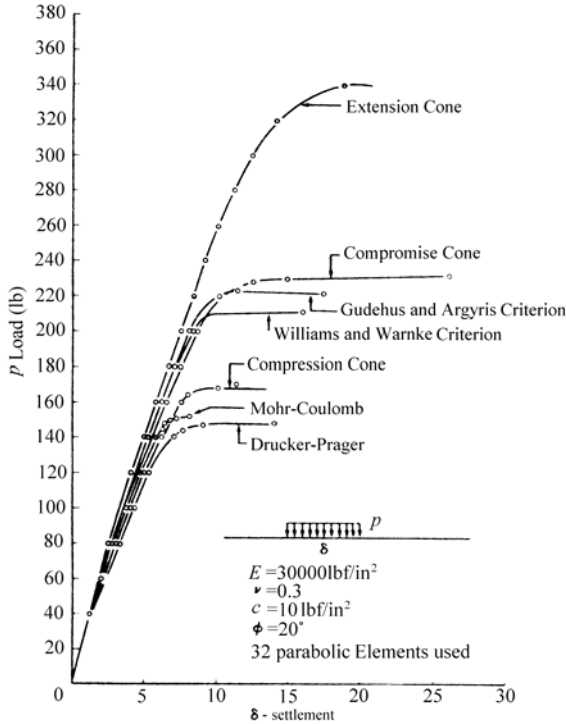
Fig. 1.8 Load-displacement curve

In this example, most of the limit surfaces of different failure criteria are cones in the stress space. The limit loci in the meridian plane are linear. This means that the strength of materials is linearly dependent on the hydrostatic stress, as has been demonstrated in a number of tests. The differences between the limit loci of various failure criteria in the deviatoric plane are shown in Fig. 1.10. Some smooth limit loci of various approximations to the Mohr-Coulomb failure criteria can be presented.

In Fig. 1.10, the limit locus 1 is the Mohr-Coulomb strength theory (1900), locus 2 is the twin-shear strength theory (Yu et al., 1985), locus 3 is the William-Warnke criterion (1975), locus 4 is the twin-shear smooth model (Yu and Liu, 1990a; 1990b) and locus 5 is the Gudehus-Argyris criterion (1973; 1974). Other smooth models can be found in the literature. Most limit loci match the two basic experimental points a and b. The circular loci cannot be matched with these two basic experimental points, as shown in Fig. 1.9.
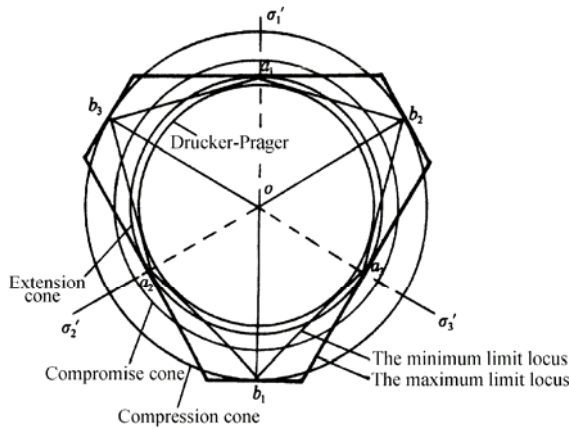
Fig. 1.9 Different limit loci on deviatoric plane

In general, the five typical limit loci of the unified strength theory with $b=0$, $b=0.25$, $b=0.5$, $b=0.75$ and $b=1$, which cover all the region of the convex area of the limit loci, can be adapted for different materials. The five typical limit loci of the unified strength theory are shown in Fig. 1.10 (b). Sometimes, the three loci (lower bound, median loci and upper bound shown in Fig. 1.10 (b) are used for analysis of structures.

(a)   (b)
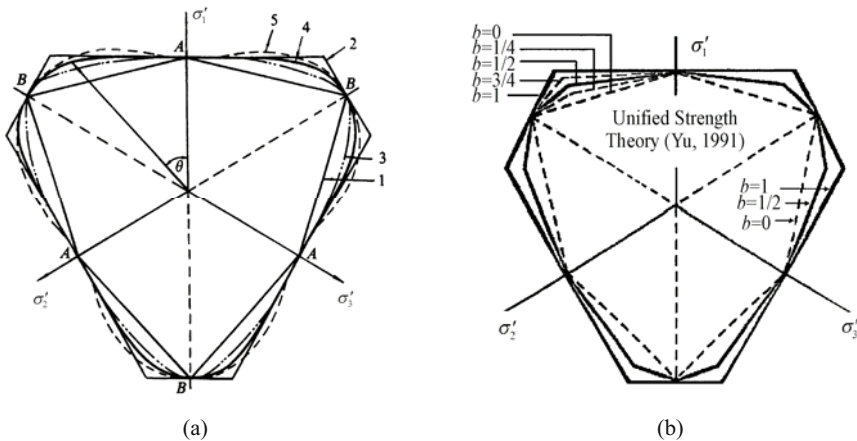
Fig. 1.10 The linear criteria and curve criteria

Nayak, Zienkiewicz (1972), Zienkiewicz and Pande (1977) have pointed out that the choice of the best limit surface is still in the hands of the analyst who has modeled the strength behavior in the best possible manner. They also indicated that the Drucker-Prager criterion and the limit loci of extensive circular cones give a very poor approximation to the real failure conditions.

The effect of the yield criterion was studied by Humpheson and Naylor (1975), Zienkiewicz and Pande (1977), Li et al. (1994; 1998), Moin and Pankaj (1998), Wang and Fan (1998), American Institute of Aeronautics and Astronautics (1999),

Yu (2004), Scheunemann (2004) and others. The choice of yield criteria has a marked effect on the analytical results of load-bearing capacities of structures, on the prediction of the forming limit diagram (FLD), on deformation, discontinuous bifurcation and localization behavior, and dynamic behavior of structures. This conclusion was also given by Chen and Baladi (1985), Wagoner and Knibloe (1989), Frieman and Pan (2000), Cao et al. (2000), Kuroda and Tvergaard (2000), Wang and Lee (2006), Huang and Cui (2006), Haderbache and Laouami (2010). Effects of the yield criterion on local deformations in numerical simulation were studied by Hopperstad (1998). The effect of failure criterion on slope stability analysis was studied by Haderbache and Laouami. The results show that the effect of failure criterion on slope stability analysis and the Mohr-Coulomb theory do not consider the intermediate principal stress, overshadowing the real behavior of soil. It is also shown that the results are correct because the intermediate principal stress exists really in the soil and may have a direct effect on the stability of a sliding slope under external actions. Wang and Lee (2006) pointed out that many factors can influence the final simulation result, the most important of which is a suitable yield criterion.

The results obtained by using the unified slip-line field theory for plane strain problems, the unified characteristics line theory for plane stress problems and spatial axisymmetric problems (Yu et al., 2006), as well as every example of unified solutions for limit, shakedown and dynamic plastic analyses of structures (Yu et al., 2009) show the serial difference. Results indicate that predictions of the limit capacity of a structure are sensitive to the selection of yield criteria. The application and choice of strength theory has a significant influence on the results.

A large number of materials models have been proposed throughout the years. So far, no general model can simulate the strength behavior of materials under complex stress. Therefore, several models are normally implemented in commercial programs to allow for simulations of different material types under various conditions. It is obviously of great importance to choose a constitutive model suitable for the material and the problem under consideration, as well as to assign proper values to the parameters included in this model. Of course, there is still a need for new models. A general but simple model that is thereby suitable for more materials may be developed.

The unified strength theory with $b=0$, $b=0.25$, $b=0.5$, $b=0.75$ and $b=1$, or the unified strength theory with $b=0$, $b=0.5$, and $b=1$ will be applied for plastic analyses of different structures in our monograph. The unified strength theory with $b=0.6$ for concrete material is used for static and dynamic analyses by Zhou at Nanyang Technological University, Singapore, and by Zhang et al. at Griffith University, Australia, which will be described in Chapters 13-15 and Chapter 22.

A slope problem is shown in Fig. 1.11. The single-shear theory of Mohr-Coulomb or the three-shear theory of Drucker-Prager do not completely match experimental data for geomaterials. It has been shown that the yield criteria of geomaterials depend not only on the maximum shear stress, but also on the intermediate principal shear stress and also on the intermediate principal stress σ_2 and the third invariant of the deviatoric stress tensor J_3. The reason that

Mohr-Coulomb theory and the Drucker-Prager criterion are not in good agreement with the experimental data is that the effect of σ_2 and the effect of J_3 are neglected. The unified strength theory with $b=0$, $b=0.25$, $b=0.5$, $b=0.75$ and $b=1$ is used. The plastic displacements of the slope with different yield criteria under the same conditions are shown in Fig. 1.12. The 3D simulation of a landslip using unified strength theory will be described in Chapter 20.
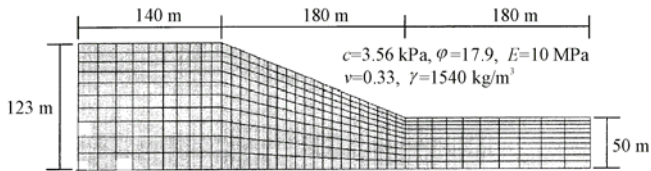
Fig. 1.11 A slope problem
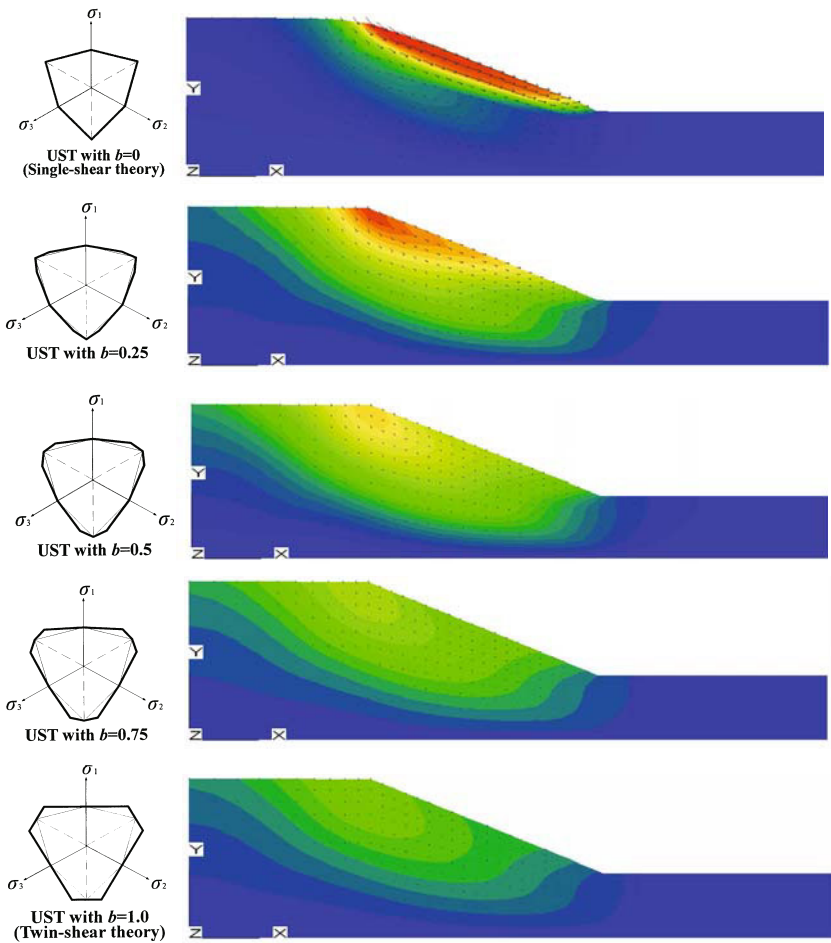
Fig. 1.12 Displacements of the slope with different yield criteria

It is seen that the difference in the results is obvious, however, the result obeying the unified strength theory with *b*=0 and the result obeying the Mohr-Coulomb theory are identical. That is due to the fact that the unified strength theory encompasses the Mohr-Coulomb theory as a special case. On the other hand, the Mohr-Coulomb theory can be deduced from the unified strength theory when *b*=0.

1.5 Historical Review: with Emphasis on the Implementation and Application of Unified Strength Theory

Finite element methods originated in the field of structural analysis and were widely developed and exploited in civil structures and aerospace industries during the 1950s and 1960s. Such methods are firmly established in civil and aeronautical engineering.

Strength theory (yield criterion and failure criterion, or the material model) as one of the most important constitutive relations has been implemented in various computational codes, especially nonlinear computer codes based on the finite element method (FEM). Elasto-plastic programs have been used for many years around the world. In general, these material models are the Tresca-Mohr-Coulomb single-shear series and the Huber-von Mises-Drucker-Prager three-shear series of strength theories. A reference book on the topic is available (Brebbia, 1985). Several excellent textbooks and monographs devoted to computational plasticity have been published. Related books and a brief history of nonlinear finite elements before 2000 were described by Belytschko, Liu and Moran (2000).

The form of yield surfaces of the single-shear series of strength theories is angular in the π-plane. However, the flow vector of the plastic strain is not uniquely defined at the corners of the Tresca and Mohr-Coulomb criteria and the direction of the plastic strain there is indeterminate. Koiter (1953) has provided limits within which the incremental plastic strain vector must lie. These singularities give rise to constitutive models that are difficult to implement numerically. To avoid such singularity, Drucker and Prager (1952) introduced an indented Huber-von Mises criterion in which the ridge corners have been rounded. The Drucker-Prager criterion has been widely implemented in nonlinear FEM codes and is widely used for geomechanics and in geotechnical engineering. Unfortunately, this gives a very poor approximation to the real failure conditions (Humpheson and Nayalor, 1975; Zienkiewicz and Pande, 1977; Chen, 1985, Chen and Baladi, 1985).

Therefore, a lot of smooth ridge models were proposed. They include the Gudehus-Argyris criterion, William-Warnke criterion, Lade-Duncan criterion, Matsuoka-Nakai criterion, Dafalias criterion, Burd criterion, Menetrey-Willam criterion, Zhao-Song criterion, JJ Jiang criterion and others. Most of them are of the octahedral-shear type (J2 theory) function expressed by three shear stresses. Various forms of smooth models were summarized in Chapter 3 of this monograph

and Chapter 11 of another monograph (Yu, 2004).

At the same time, the singularities of the Tresca and Mohr-Coulomb yield criteria can also be overcome by rounding off the corners of the surface or by employing a simple mathematical artifice in the numerical procedure (Owen, 1980). The accurate treatments of corners in yield surfaces were studied by Marques (1984), Ortiz et al. (1985; 1987; 1994), Yin (1984), Yin and Zhou (1985), Sloan and Booker (1986), de Borst (1987; 1989), Simo et al. (1988), Runesson et al. (1988), Pramono and Willam (1989), Pankaj and Bicanic (1991), Khan and Huang (1995), Larsson and Runesson (1996), Jeremic and Sture (1997) and others. So single-shear-type yield criteria are easy to use and easily implemented in computational codes. The singularity of Tresca plasticity at finite strains was studied by Peric and de Neto (1999).

A course on "Advanced Numerical Applications and Plasticity in Geomechanics" was held by the International Centre for Mechanical Sciences (Le Centre International des Sciences et Mecaniques (CISM) in Udine, Italy). Eight papers were edited by Griffiths and Gioda in 2000. The material spans a remarkable range of topics, from theoretical developments involving novel algorithms and constitutive models to practical applications involving prediction of stresses and deformations in tunnel linings.

A monograph on the "Introduction to Computational Plasticity" was given by Dunne and Petrinic (2005). A range of plasticity models including those for superplasticity, porous plasticity, creep, cyclic plasticity and thermo-mechanical fatigue are introduced. Microplasticity and continuum plasticity, the implementation of constitutive equations, and associated material Jacobian into finite element software are addressed. The Huber-von Mises yield criterion implemented in the commercial code ABAQUS is described. In the Proceedings of Computational Plasticity: Models, Software and Applications, which was edited by Owen et al. (1989), 101 papers were presented.

The yield criteria have been implemented in the most current commercial FEM systems, such as ABAQUS, ADINA, ANSYS, ASKA, ELFEN (Univ. of Wales Swansea), MSC-NASTRAN, MARC, NonSAP and AutoDYN, DYNA and DYPLAS (Dynamic Plasticity). In some systems, only the Huber-von Mises criterion, Drucker-Prager criteria, Mohr-Coulomb criterion and some other single curve criteria were implemented. The functions and the applied fields of many powerful commercial FEM codes were limited to the choice of failure criteria. More effective and systematic models of materials under complex stress are needed.

As pointed out by Humpheson and Naylor (1975), Zienkiewicz and Pande (1977), and Chen (1982, 1984), there is basically a shortcoming in the Drucker-Prager surface in connection with rock-soil strength modeling: the independence of τ_8 on the angle of similarity θ. It is known that the trace of the failure surface on the deviatoric planes is not circular (Chen, 1982; 1984; 1994).

To facilitate the choice of a model and to determine in an organized way the parameter values based on all the performed tests in a constitutive driver (i.e., a computer program containing a library of models where the tests can be simulated on the constitutive level and where parameter optimization can be performed), four

soil plasticity models have been proposed by Mattsson et al. (1999). These models have, so far, been included in the constitutive driver. The main idea was that the concept could be used for constructing constitutive drivers as a supplement to commercial programs with their constitutive models, as well as for researchers verifying and developing such models. A practical finite element code for plane and axisymmetric modeling of soil and rock plasticity, called PLAXIS, was provided by Vermeer (1998).

The twin-shear strength theory has been implemented in some special finite element programs. such as An and Yu (1991) for solving the hydropower structure, Yu and Li (1991), Yu et al. (1992) for a mechanical structure, Shen (1993) for studying soil mechanics problems, Yu and Meng (1992; 1993) for studying the stability of the ancient city wall in Xi'an, China; Li, et al. (1994) for composite, Li and Ishii (1998) for the structural analysis of a dam, etc. The elasto-visco-plastic finite element analysis of a self-enhanced thick cylinder using the twin-shear strength theory was given by Liu et al. (1994). The twin-shear yield criterion and the twin-shear strength theory have been implemented in three commercial FEM codes by Quint Co. (1993; 1994). The twin-shear strength theory was implemented in an FEM code and applied to analyze the stability of the high slopes of the Three-Gorges Lock by the Yangzhi River Science Academy, China.

3D finite element numerical modeling of large underground caves and the stability of the excavated rock mass of the Tai'an Pumped Storage Hydraulic Plant was done by Professors Sun, Shang, Zhang et al. at Zhejiang University, Hangzhou, China and East China Investigation and Design Institute, the State Power Corporation of China (Sun et al., 2004a; 2004b).

Unified strength theory was also used for dynamic response and blast-resistance analysis of a tunnel subjected to blast loading by Zhejiang University (Liu and Wang, 2004). A new failure criterion introduced from unified strength theory when the strength parameter $b=1/2$, was used by professor Liu for a railroad tunnel. It was also used for the analysis of the stability of a slope (Bai, 2005), the failure analysis of a concrete road (Liang, 2004) and 3D failure process analysis of rock and associated numerical tests by Liang (2005) at Northeastern University, China.

Recently, analysis on textural stress and rock failure in diversion tunnels using the twin-shear strength theory was given by Yang and Zhang (2008; 2009). The twin-shear theory is also used for studying the sudden-crack phenomenon and simulation of the surrounding rock mass in a diversion tunnel (Yang et al., 2008). The adaptive arithmetic of arch dam cracking analysis using the twin-shear strength theory was given by Yang et al. (2009). The singularity has been overcome, and it is easy to use. The twin-shear yield criterion and the twin-shear strength theory have been implemented in three commercial FEM codes by Quint Co. (1993; 1994) in Tokyo, Japan

The unified yield criterion and the unified strength theory have been implemented and applied to some plasticity and engineering problems (Yu et al., 1992; Yu and Zeng, 1994; Yu et al., 1997; 1999). The singularities at the corners of the single-shear series of strength theory, twin-shear series of strength theory and unified strength theory have been overcome using a unified numerical procedure,

i.e., UEPP Code (Yu et al., 1993; Yu and Zeng, 1994; Yu et al., 1997; 1999; Yu, 1998).

Unified strength theory was used to study structural reliability analysis by Wang et al. (2008) at Sichuan University, Sichuan Province, China. It was also used for nonlinear finite element analysis of an RC plate and shell by Wang (1998) at Nanyang Technological University, Singapore.

Unified strength theory is also implemented in the general commercial code, such as ABAQUS and AutDYN by Fan and Qiang (2001) and Zhang et al. (2001) at Griffith University, Australia, for research on the punch of concrete and dynamic problems. Normal high-velocity impact on concrete slabs was simulated using unified strength theory (Fan and Qiang, 2001). Unified strength theory was implemented in non-linear FEM at Nanyang Technological University, Singapore, by Zhou (2002) for the numerical analysis of reinforced concrete subjected to dynamic load. Recently, the secondary development and application of unified strength theory and associated elastoplastic constitutive model to ABAQUS were presented by the North China Electric Power University, Beijing, China and the Institute of Water Resources and Hydropower Research of China (Wang and Lu, 2009) as well as by Tongji University (Pan et al., 2010).

Based on the finite element theoretical scheme of a unified elastoplastic constitutive model, and according to the UMAT interface requirement of ABAQUS, the corresponding UMAT codes are programmed, which will be called the main analytical module of ABAQUS. Adopting a degenerative model of the unified strength ($b=0$, Mohr-Coulomb model) and the built-in Mohr-Coulomb model of ABAQUS, the uniaxial tests and circular chamber are analyzed to verify the correctness and efficiency of the developed material subroutine. Finally, considering the general form of the unified elastoplastic constitutive model ($b \neq 0$) and the hard condition of yield surface, which are not available in ABAQUS software, a circular chamber is simulated and the variational discipline of the stress field is obtained. The basic procedures provided and the programming essentials of UMAT redefined in ABAQUS are universal and can offer a reference for other developers (Pan et al., 2010).

Unified strength theory was used to study topology optimization of evolutionary structures by Li et al. (2008). The abstract of the paper shows that: "Based on the traditional evolutionary structural optimization method and considering wide applications of unified strength theory for all kinds of engineering structures, this paper presents a bi-directional evolutionary structural topology optimization method based on the unified strength criterion. It can be used not only for isotropic materials, but also for many kinds of anisotropic materials. Finally, some numerical examples are given and the results show that this method has wide use in topology optimization design for structures of fragile materials, anisotropic material processing and design fields".

Recently, two papers concerning the applications of the three-parameter unified strength theory to an FEM program, and the Monte-Carlo 3D nonlinear stochastic FEM model for structure reliability analysis were constructed by Wang, et al. (2008a; 2008b). The three-parameter and five parameter unified strength theory are

used for the load bearing capability of a concrete-filled steel tube component considering the effect of intermediate principal stress and plastic seismic damage of a concrete structure by Shao and Qian (2007) and Shao et al. (2007).

UST (unified strength theory) and slip line field theory are also implemented in ANSYS by Li and Chen (2010). The results can be employed to analyze the differences in safety factors and the positions of the critical slip surfaces for unified yield criteria.

A new effective three-dimensional finite difference method (FDM) computer program, FLAC-3D (Fast Lagrangian Analysis of Continua in 3D) was presented (FLAC-3D, 1997). Stability analysis on the high slopes of the Three Gorges Lock using FLAC-3D was given (Kou et al., 2001). It is a pity, however, that only two failure criteria, the Mohr-Coulomb criterion and the Drucker-Prager criterion were implemented in FLAC-3D code.

Unified strength theory is implemented in FLAC-3D by Zhang et al. (2008) for the analysis of structures at the National Key Laboratory of Geomechanics and Geotechnical Engineering, Institute of Rock and Soil Mechanics, Chinese Academy of Science. The abstract of the paper of Zhang, et al. (2008) shows that: "Unified strength theory is a new theory system which can almost describe the strength characteristics of most geomaterials and has been applied widely. And FLAC-3D is an excellent geotechnical program. If the former can be integrated into the later, many complex problems in engineering will be settled. So, according to this problem, the numerical scheme for an elastoplastic unified constitutive model in FLAC-3D was studied. And the numerical format of the elastoplastic constitutive model based on the unified strength theory was derived….The merits of unified strength theory and the FLAC-3D program will be utilized well in geo-engineering after their combination."

In-situ stress measurement and stability analysis based on unified strength theory in large scale underground caverns was presented at Beijing Scientific and Technical University (Li, 2008). Unified strength theory was also implemented in FLAC-3D for stability analysis in large scale underground caverns. Recently, unified strength theory was implemented in FLAC by Hohai University for the dynamic analysis of the 500 kV underground transformer substation for Shanghai World EXPO (Fen and Du, 2010).

Table 1.1 gives some applications of yield criteria in FEM codes.

These implementations and applications can be classified in three types, as follows:

(1) A special elasto-plastic FE program referred as the UEPP—Unified Elasto-Plastic Program. The first version of UEPP was used by Yu's research group at Xi'an Jiaotong University in 1990-1991. The third version of UEPP was used in 1998. WB Zheng, GW Ma, SY Yang, Y Wang, LN He, and N Lu made their contributions to UEPP. At the same time, the twin-shear failure criterion was implemented in several FE codes by ZJ Shen (1989), Yu and Li (1991), An et al. (1991), Yu and Meng (1992), Quint Co. (1993; 1994), Liu et al. (1994), Li and Ishii (1998).

(2) Implementation in several nonlinear FE codes written by researchers at some universities.

(3) Implementation in several commercial nonlinear FE codes by researchers.

Table 1.1 Some applications of yield criteria in FEM codes

Yield criteria	FEM codes														
	1	2	3	4	5	6	7	8	9	10	11	12	13	14	15
Tresca criterion	√	√	√	√	√		√	√					√		√
Mises criterion	√	√	√	√	√		√	√		√			√		√
Mohr-Coulomb	√	√	√	√	√	√	√	√	√	√			√		√
Drucker-Prager	√		√		√	√									√
Twin-shear criterion for Non-SD materials	√	√			√	√	√		√	√			√		√
Twin-shear strength theory for SD materials	√	√			√	√	√	√	√	√			√		√
Unified yield criterion for Non-SD materials	√				√	√	√	√			√	√		√	√
Unified strength theory	√					√	√	√			√	√		√	√
Others	√	√	√	√	√	√	√	√	√	√	√	√	√	√	√

Notes:

1—HAJIF (The Aircraft Strength Research Institute of China)

2—COMPMAT and STAMPS (Quint Co., Japan)

3—MARC (USA)

4—NASTRAN (USA)

5—ANSYS used in Xi'an Jiaotong University and Hohai University, Nanjing, China

6—FLAC-3D used in Beijing Sci. Tech. University and Xi'an Jiaotong University, as well as Wuhan Rock-Soil Mechanics Institute of Chinese Academy

7—UEPP(Xi'an Jiaotong U., Xi'an, China)

8—UEPP (Nanyang Technological University, Singapore)

9—Academy of Yangzhi River

10—North-West Institute for Investigation and Research in Hydraulic-Power

11—Zhejiang University and East China Investigation and Design Institute, State Power Corporation of China

12—Griffith University, Australia; Sichuan University, China; North-East University, China

13—Jinan University, Jinan, Shandong Province, China

14—Zhejiang University and Railway Co.

15—AutDYN at Nanyang Technological University, Singapore

1.6 Brief Summary
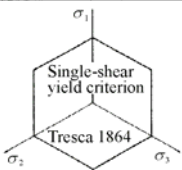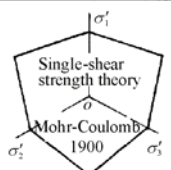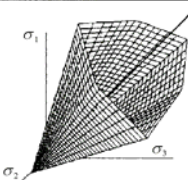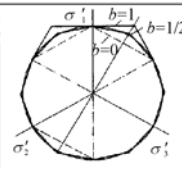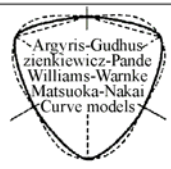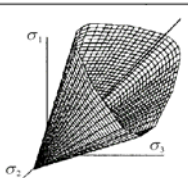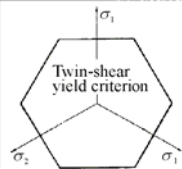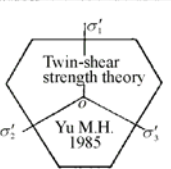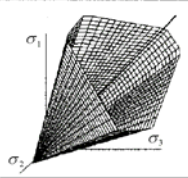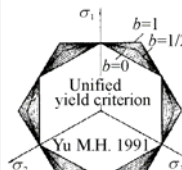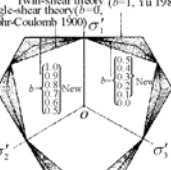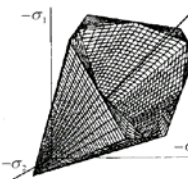
Most materials in structures are acted under the complex stress states, i.e., biaxial and multiaxial stresses. Strength theory provides a yield (or failure) criterion, a limiting stress state for elasticity, or an initial deformation for plasticity. Sometimes it is also used as an associated or non-associated flow rule for plastic constitutive relations.

A series of research works were carried out to show the effects of strength theory on the results of elastoplastic analysis, the load-carrying capacities of structures. The unified yield criterion and unified strength theory provide us with an effective approach to study these effects. Unified strength theory has been implemented in several computational plasticity codes. It is possible for us to adopt a different value of the unified strength theory parameter b to meet the requirements of different materials and structures.

The effects of failure criteria on the analytical results of the slip field for plane strain problems, the characteristic fields of plane stress problems and spatial axisymmetric problems using unified strength theory are researched by Yu et al. Systematic results can be seen in (Yu et al., 2006). The choice of strength theory has a significant influence on these results. Interested readers may refer to the book entitled *Generalized Plasticity* published by Springer in 2006. Comments on the model of Maohong Yu are given by Altenbach and Kolupaev (2008).

Advances in strength theories are briefly summarized in Table 1.2.

Table 1.2 Advance in strength theories

The twin-shear idea was proposed in 1961. Since then, the twin-shear yield criterion for non-SD materials, the generalized twin-shear strength theory for SD materials and the unified strength theory were successfully presented in 1961, 1985 and 1991. It can be seen that the development was very slow, covering 30 years of the development of unified strength theory.

References

American Institute of Aeronautics and Astronautics (1999) Effect of failure criterion used by NASA. Technical Documentation.

An M, Yu MH and Wu X (1991) Applications of generalized twin shear yield criterion in rock mechanics. Rock and Soil Mech., 12(1): 17-26 (in Chinese, English abstract).

Altenbach H and Kolupaev VA (2008) Remarks on Model of Mao-Hong Yu. The Eighth International Conference on Fundamentals of Fracture (ICFF VIII), Zhang TY, Wang B and Feng XQ eds. pp 270-271.

Anandarajah A (2010) Computational Methods in Elasticity and Plasticity: Solids and Porous Media. Springer: New York.

Bai XY (2005) The Application of the Unified Strength Theory for Stability of Slope. Master's Dissertation, Chang'an University.

Bathe KJ (1996) Finite Element Procedures. Prentice Hall of India, New Delhi.

Belytschko T, Liu WK and Moran B (2000) Nonlinear Finite Elements for Continua and Structures. John Wiley, Chichester: New York.

Bonet J and Wood RD (1997) Non-linear Continuum Mechanics for Finite Element Analysis. Cambridge University Press: London.

de Borst R (1987) Integration of plasticity equations for singular yield functions. Comput. Struct., 26: 823-829.

de Borst R (1989) Computational strategies for strongly curved and non-smooth yield criteria with applications to localisation atof deformion. In: Computational Plasticity: Models, Software and Applications, Ed. by Owen, DRJ, Hinton E and Onate E, Pineridge Press Ltd., pp 237-261.

de Borst R, Pankaj and Bićani N (1991) A note on singularity indicators for Mohr-Coulomb type yield criteria. Computers & Structures, 39(1-2): 219-220.

Brebbia CA. ed.(1985) Finite Element Systems (A Handbook), Springer-Verlag: Berlin.

Chen WF (1982) Plasticity in Reinforced Concrete. McGraw-Hill: New York, pp 190-252.

Chen WF and Baladi GY (1985) Soil Plasticity: Theory and Implementation. Elsevier: Amsterdam.

Chen WF and Mizuno E (1990) Nonlinear Analysis in Soil Mechanics: Theory and Implementation. Elsevier: Amsterdam.

Chen WF and Saleeb AF (1994) Constitutive Equations for Engineering Materials.

Vol.1: Elasticity and Modeling, Revised edn. Elsevier: Amsterdam, pp 259-304, 462-489.

Chen WF et al. (1994) Constitutive Equations for Engineering Materials. Vol. 2: Plasticity and modeling. Elsevier: Amsterdam.

Chen WF and Zhang H (1991) Structural Plasticity: Theory, Problems and CAE Software, Springer-Verlag, pp 125-168.

Cook RD, Malkus DS and Plesha ME (1989) Concepts and Applications of Finite Element Analysis,third edition,John Wiley and Sons: New York.

Crisfield M (1991) Non-linear Finite Element Analysis of Solids and Structures. Vol 1: Essentials John Wiley and Sons: Chichester.

Crisfield M (1996) Non-Linear Finite Element Analysis of Solids and Structures. Vol 2:Advanced Topics. John Wiley and Sons: Chichester.

Crisfield M (1997) Non-linear Finite Element Analysis of Solids and Structures. John Wiley and Sons: Chichester.

Davis RO and Selvadurai APS (2002) Plasticity and Geotechnics. Cambridge University Press: Cambridge.

Doltsinis IS ed. (1989) Advances in Computational Nonlinear Mechanics (CISM) Springer-Verlag: Wien.

Desai CS and Gioda G. eds. (1990) Numerical Methods and Constitutive Modeling in Geomechanics, Springer: Wien.

Dixit PM and Dixit US (2008) Modeling of Metal Forming and Machining Processes by Finite Element and Soft Computing Methods. Springer: London.

Dunne FPE and Petrinic N (2005) Introduction to Computational Plasticity. Oxford University Press: Oxford.

Ehlers W (1999) IUTAM Symposium on Theoretical and Numerical Methods in Continuum Mechanics of Porous Materials, Kluwer Academic Publishers: Dordrecht.

Fan SC and Qiang HF 2001 Normal high-velocity impaction concrete slabs- a simulation using the meshless SPH procedures. In: Computational Mechanics–New Frontiers for New Millennium, Valliappan S. and Khalili N. eds. Elsevier Science Ltd, pp 1457-1462.

Fen TG and Du B (2010) Dynamic analysis of the 500kV underground transformer substation for Shanghai World EXPO, to be published.

FLAC-3D (1997) Fast Lagrangian Analysis of Continua in 3-Dimensions , Version 2.0. User's Manual, Itasca Consulting Group, Inc (US).

Frieman PA and Pan J (2000) Effects of plastic anisotropic and yield criteria on prediction of forming limit curves. Int. J. Mech. Sci., 42: 29-48.

Griffiths DV and Gioda Ged (2000) Advanced Numerical Applications and Plasticity in Geomechanics. Springer: Wien.

Haderbache L and Laouami N (2010) The effect of failure criterion on slope stability analysis.The Electronic Journal of Geotechnical Engineering, 15A.

Han W and Reddy BD (1999) Plasticity:Mathematical Theory and Numerical Analysis. Springer: New York.

Haythornthwaite RM (1961) Range of yield condition in ideal plasticity. J. Eng. Mech., 87: 117-133.

Hinton E and Owen DRJ (1979) An Introduction to Finite Element Computations. Pineridge Press: Swansea.

Hopperstad OS, T. Berstad, H. Ilstad et al (1998) Effects of the yield criterion on local deformations in numerical simulation of profile forming. Journal of Materials Processing Technology, 80-81.

Huang XP and Cui WC (2006) Effect of bauschinger effect and yield criterion on residual stress distribution of autofrettaged tube (Gun Tubes Conference, Oxford , 2005). Journal of Pressure Vessel Technology, 128(2): 212-216.

Hughes TRJ (1987) The Finite Element Method. Prentice-Hall, Englewood Cliffs, N.J.

Humpheson C and Naylor DJ (1975) The importance of the form of the failure criterion. C/R/243/75, University of Wales: Swansea, UK.

Inoue T, Kitagawa H and Shima S eds. (1990) Computational Plasticity. Elsevier Appl. Science: London and New York.

Jeremic B and Sture S (1997) Implicit Integrations in Elastoplastic Geotechnics, J. Mechanics of Cohesive-Frictional Materials, 2(2): 165-183.

Jeremić B, Yang ZH, Chen Z et al. (2010) Lectures Notes on Computational Geomechanics: Inelastic Finite Elements for Pressure Sensitive Materials, version 2.1(University of California, Davis).

Khan AS and Huang S (1995) Continuum Theory of Plasticity, John Wiley and Sons Inc:New York.

Khoei AR (2005) Computational Plasticity in Power Forming Processes. Elsevier:Amsterdam.

Kobayashi AS, Oh SI and Altan T (1989) Metal Forming and the Finite Element Method. Oxford University Press: New York.

Koiter WT (1953) Stress-strain relations, uniqueness and variational theorems for elastic-plastic materials with singular yield surface, Quart. Appl. Math., 11: 350-354.

Kojic M and Bathe KJ (2005) Inelastic Analysis of Solids and Structures. Springer:Berlin.

Kotsovos MD and Pavlovic MN (1995) Structural Concrete: Finite Element Analysis for Limit-State Design. Thomas Telford Publ: London, pp 83-103.

Kou XD, Zhou WY, and Ang RQ (2001) Stability analysis on the high slopes of Three-Gorges shiplock using FA\LAC-3D. Chin. J. Rock Mech. Eng., 20(1): 6-10.

Kuroda M and Tvergaard V (2000) Forming limit diagram for anisotropic metal with different yield criteria. Int. J. Solids & Structures, 37: 5037-5059.

Larson R and Runesson K (1996) Implicit integration and consistent linearization for yield criteria of the Mohr-Coulomb type. Mech. Cohesive-Friction Mater, 1: 367-383.

Lewis RW and Schrefler BA (1987) The Finite Element Method in the Deformation and Consolidation of Porous Media. John Wiley & Sons: Chichester.

Fen TG and Du B (2010) Dynamic analysis of the 500kV underground transformer substation for Shanghai World EXPO, to be published.

Li J, Lu XY and Zhao XW (2008) Topology optimization based on bi-directional

evolutionary structure of unified strength. Journal of Shandong Jianzhu University, 23(1): 65-69.

Li K and Chen GR (2010) Finite element analysis of slope stability based on slip line field theory. J. Hohai University (Natural Sciences),38(2): 191-195.

Li Y (2008) In-situ Stress Measurement and Stability Analysis Based on the Unified Strength Theory in Large Scale Underground Caverns Zone. Doctoral Dissertation, Beijing Scientific and Technical University.

Li Y and Qiao L (2012) Stability Analysis of Underground Caverns based on the Unified Strength Theory. In: Computational Plasticity, Zhejiang University Press & Springer Berlin Heidelberg: Heidelberg, pp 369-398.

Li YM, Ishii K, Nakazato C and Shigeta T (1994) Prediction of safety rate and multi-slip direction of slip failure under complex stress state. Advances Eng. Plasticity and its Applications. Xu B.Y and Yang W eds. International Academic Publishers: Beijing, pp 349-354.

Li YM.and Ishii K(1998) The Evaluation of the Elasto-plastic Behavior of Composite Materials under Biaxial Stress with Homogenization Method, Proc. of the Conference on Computational Engineering and Science, 3: 1023-1026. JSCES.

Li YM. and Ishii K(1998) The Evaluation of Strength for Composite Materials. In : Strength Theory, Application, Development and Prospects for 21st Century, Science Press: New York, pp 337-342.

Liang JL (2004) Fracture and Failure Mechanism of Concrete Road and its Applications. Doctoral Dissertation, Changan University, Xi'an, China.

Liang ZZ (2005) Three-Dimensional Failure Process Analysis of Rock and Associated Numerical Tests. Doctoral Dissertation, North-East University, Shenyang, China.

Liu F, Li LY and Mei ZX (1994) Elasto-visco-plastic finite element analysis of self-enhanced thick cylinder. Chinese J. of Appl. Mechanics, 11(3): 133-137 (in Chinese, English abstract).

Liu GH and Wang ZY (2004) Dynamic response and blast—resistance analysis of a tunnel subjected to blast loading. Journal of Zhejiang University (Engineering Science), 38(2): 204-209.

Ma ZY and Liao HJ (2012) Unified strength theory and FLAC-3D. In: Computational Plasticity, Zhejiang University Press & Springer Berlin Heidelberg: Heidelberg, pp 417-446.

Marques,J.M. (1984), Stress computation in elastoplasticity, Engineering Comput., 1:42-51.

Mattsson H, Axelsson K and Klisinski M (1999) On a constitutive driver as a useful tool in soil plasticity. Advances in Engineering Software, 30: 511-528.

Miyoshi T (1985). Foundations of the numerical analysis of plasticity. North-Holland: Amsterdam, New York.

Moin K and Pankaj (1998) Post-peak behavior simulation using different failure theories. Strength Theory: Applications, Developments and Prospects for the 21st Century. Yu MH and Fan SC eds. Science Press: New York, Beijing, pp 1121-1126.

Nakai T and Matsuoka H (1980) In: Proceedings of Society of Japanese Civil En-

gineering Report, No.303, 65-77, and Matsuoka H (2001) Soil Mechanics (Chinese edition). China Hydraulic and Power Press: Beijing, p 142.

Nayak GC and Zienkiewicz CC (1972) Convenient form of stress invariants for plasticity, J. Struct. Div., ASCE, 4: 949-953.

Neto EAS, Periæ D and Owen D.R.J (2009) Computational Methods for Plasticity: Theory and Applications. Wiley: New York.

Nielsen MP (1991) Limit Analysis and Concrete Plasticity. Second Edn. CRC Press: London.

Oden JT (1972) Finite Elements of Nonlinear Continua. McGraw-Hill:New York.

Oñate E and Owen R eds (2007) Computational Plasticity. Springer.

Ortiz M and Popov EP (1985) Accuracy and stability of integration algorithms for elastoplastic constitutive relations. Int. J. Numer. Methods in Eng., 21: 1561-1576.

Ortiz M, Leroy Y and Needleman A (1987) A finite element method for localized failure analysis. Computer Methods Appl. Mech. Eng., 61: 89-124.

Ortiz M and Shih CF eds. (1994) IUTAM Symposium on Computational Mechanics and Materials. J. Modeling and Simulation in Material Sci. and Eng., 2(3A): 421-782.

Owen D.R.J and Hinton E (1980), Finite Elements in Plasticity : Theory and Practice, Pineridge Press Ltd.: Swansea,

Owen DRJ, Hinton E and Onate E (1989) Computational Plasticity: Models, Software and Applications. Pineridge Press Limited, pp 101, 1460.

Owen DRJ, Hinton E and Onate E (1992) Computational Plasticity: Fundamentals and Applications Pineridge Press Ltd.: Swansea

Pan CS (1995) Numerical Method for Tunnel Mechanics. China Railway Engineering Press: Beijing (in Chinese).

Pan XM, Kong J, Yang Z and Liu C (2010) Secondary development and application of unified elastoplastic constitutive model to ABAQUS. Rock and Soil Mechanics, 31(4): 1092-1098.

Pankaj and Bićanić N (1989) On multivector stress returns in Mohr-Coulomb plasticity. In: Second. Int. Conf. Computational Plasticity: Models, Software and Applications, Edited by Owen D.R.J, Hinton E and Onate E. Pineridge Press: Swansea.

Peric D and de Souza Neto EA (1999) A new computational model for Tresca plasticity at finite strains with an optimal parametrization in the principal space. Comput. Methods Appl. Mech. Eng., 171(3-4), 404-489

Pivonka P, Lackner R and Mang HA (2003) Shapes of loading surfaces of concrete models and their influence on the peak load and failure mode in structural analyses. Int. J. Engineering Science, 41(13-14): 1649-1665.

Pramono E and Willam K (1989) Implicit integration of composite yield surface with corners. Engineering Computational, 6: 186-198.

Quint Co. (1993a) COMPMAT-Analysis system for composite materials. FEM codes of Quint Corporation: Japan.

Quint Co. (1993b) COMPMAT-Analysis system for composite materials. FEM codes of Quint Corporation: Japan.

Quint Co. (1994a) PREMAT/POSTMAT-Pre and Post Processor for Composite Materials. FEM Codes of Quint Corporation: Japan.

Quint Co. (1994b) STAMPS-Structural Analysis Program for Civil Engineering. FEM Codes of Quint Corporation: Japan.

Reddy JN (1993) An Introduction to the Finite Element Method, second edition. McGraw-Hill: New York.

Reddy BD ed. (2009) Theoretical Modelling and Computational Aspects of Inelastic Media. Proceedings of IUTAM Symposium, Cape Town, 2008. Springer: Berlin.

Roscoe KH and Poorooshasb HB (1963) A theoretical and experimental study of strains in triaxial compression tests on normally consolidated clays. Geotechnique, 13(1):l2-34.

Roscoe KH, Schofield AN and Thurairajah A (1963) Yielding of clays in states wetter than critical. Geotechnique, 13(3): 211-240.

Roscoe KH and Burland JB (1968) On the generalised stress-strain behaviour of 'wet' clay. In: Engineering Plasticity, Cambridge Univ Press, pp535-609.

Runesson K, Sture S, and Willam K (1988), Integration in computational plasticity. Comput. Struct, 30(1-2): 119-130.

Sakash A, Moondra S and Kinsey, BL. (2006) Effect of yield criterion on numerical simulation results using a stress-based failure criterion. J. Eng. Mater. Technol., 128(3): 436-444.

Scheunemann P 2004 The influence of failure criteria on strength prediction of ceramic components. J. of the European Ceramic Society, 24(8): 2181-2186.

Schofield AN and Wroth CP (1968) Critical State Soil Mechanics. McGraw-Hill: New York.

Shao CJ and Qian YJ (2007) Load bearing capability of concrete-filled steel tube component considering effect of intermediate principal stress. Chinese Journal of Applied Mechanics, 24(03): 396-399.

Shao CJ, Wu YH and Qian YJ (2007) Plastic seismic damage of concrete structure based on five-parameter unified strength theory. Chinese Journal of Applied Mechanics, 24(1): 97-101.

Shen ZJ (1993) Comparison of several yield criteria. Rock and Soil Mechanics, 14(1): 41-50 (in Chinese, English abstract).

Shen ZJ (2000) Theoretical Soil Mechanics. China Hydraulic Power Press: Beijing (in Chinese).

Simo JC and Hughes TJR (1998) Computational Inelasticity. Springer-Verlag: NewYork.

Sloan SW.and Booker JR (1986), Removal of singularities in Tresca and Mohr-Coulomb yield function. Comm. Appl. Num. Meth., 2: 173-179.

Smith DL.ed.(1990) Mathematical Programming Methods in Structural Plasticity. (21 papers, 435 pages) Springer-Verlag: Wien, pp 21, 435.

Smith IM and Griffiths DV (1998) Programming the Finite Element Method, 3rd edition. John Wiley and Sons, Ltd.

Smith IM and Griffiths DV (2004) Programming the Finite Element Method. 4th edition. John Wiley & Sons, Ltd.

Strin E (1993) Progress in Computational Analysis of Inelastic Structures (CISM No.321). Springer-Verlag: Berlin.

Sun HY, Shang YQ, Zhang CS, Ying HP, Li SQ (2004) 3D numerical modeling of possible failure zone with underground excavation. Chinese Journal of Rock Mechanics and Engineering, 23(13): 2192-2196.

Sun HY, Shang YQ and Zhang CS (2004) Numerical modeling analysis for surrounding rockmass stability of large underground cavities. Journal of Zhejiang University (Engineering Science), 38(1): 70-74.

Teodorescu PP (2006) Review of "Unified strength theory and its Applications. Springer, Berlin, 2004". Zentralblatt MATH 2006, Cited in Zbl. Reviews, 1059.74002 (02115115).

Vermeer PA (1998) PLAXIS—Finite Element Code for Soil and Rock Plasticity. Balkema: Rotterdam.

Wagoner RH and Knibloe JR (1989) The importance of constitutive behavior to sheet forming performance. Advance in Constitutive Laws for Eng. Material. Int. Acad Publ: Beijing, pp 154-158.

Wang D, Chen JK, Wang QZ et al. (2008) The New Method of Structural Reliability Analysis by Monte-Carlo Stochastic Finite Element. J. of Sichuan University (Engineering Science Edition), 40(3): 20-26.

Wang D, Chen JK, Wang QZ, Li YL (2008) Structural Reliability Analysis by Monte-Carlo Based on Conditional Expectation Variance Reduction and Antithetic Variable Sampling. China Rural Water and Hydropower, 5: 66-70.

Wang F and Fan SC (1998) Limit pressures of thick-walled tubes using different yield criteria. Strength Theory: Applications, Developments and Prospects for the 21st Century. Yu MH and Fan SC eds. Science Press: New York, Beijing, pp 1047-1052.

Wang F (1998) Nonlinear finite element analysis of RC plate and shell using the unified strength theory. PhD thesis, Nanyang Technological University, Singapore.

Wang JQ and Lu F (2010) Unified strength theory constitutive model embedded software ABAQUS and its application in tunnel engineering. Journal of Yangtze River Scientific Research Institute, 27(2): 68-74 (in Chinese).

Wang JQ and Lu F, (2012) Implementation of the Unified Strength Theory in ABAQUS and its Application for Tunnel Engineering. In: Computational Plasticity, Zhejiang University Press & Springer Berlin Heidelberg: Heidelberg, pp 269-287.

Wang L and Gao Q (2010) Underground Mining. Chapter14 in this monograph.

Wang L and Lee TC (2006) The effect of yield criteria on forming limit curve prediction and deep drawing process simulation. Int. J. of Machine Tools and Manufacture, 46(9): 988-995.

Wunderlich W, Stein E.and Bathe KJ. Eds (1981) Non-linear Finite Element Analysis in Structural Mechanics. Springer-Verlag.

Yang LQ, Zhang SR (2008) Analysis on textural stress and rock failure of diversion tunnels. Chinese J. of Geotechnical Engineering, 30(6): 813-817.

Yang LQ, Li YQ and Chen ZP (2008) Sudden-crack Phenomenon and Simulation

of Surrounding Rock-mass in Diversion Tunnel. China Rural Water and Hydropower, (5): 53-56.

Yang LQ, Zhang SR, Chen ZP.(2009) Adaptive arithmetic of arch dam cracking analysis. J. of Hydraulic Engineering, 40(2): 214-219.

Yin YQ (1984) Loading criteria for a singular yield surface (in Chinese). Acta Mechanica Solida Sinica, 6(2): 282-285.

Yin YQ and Zhou S (1985) Constitutive relation in the singular point of yield criterion for geomaterials. Chinese J. of Rock Mechanics and Eng, 4(1): 33-38.

Yu HS (2006) Plasticity and Geotechnics. Springer: Berlin.

Yu MH (1961a) General behaviour of isotropic yield function. Res. Report of Xi'an Jiaotong University. Xi'an, China (in Chinese).

Yu MH (1961b) Plastic potential and flow rules associated singular yield criterion. Res. Report of Xi'an Jiaotong University. Xi'an, China (in Chinese)

Yu MH (1983) Twin-shear yield criterion. Int. J. Mech. Sci. 25(1): 71-74.

Yu MH (1992) New System of Strength Theory. Xian Jiaotong University Press: Xian, China (in Chinese).

Yu MH (1994) Unified strength theory for geomaterials and its application. Chinese Journal of Geotechinal Engineering, (2): 1-10 (in Chinese, English Abstract).

Yu MH (1998) Twin Shear Theory and Its Applications. The Science Press: Beijing (in Chinese).

Yu MH (2004) Unified Strength Theory and its Applications. Springer: Berlin.

Yu MH and He LN (1991) A new model and theory on yield and failure of materials under complex stress state. In: Mechanical Behavior of Materials-6, Vol. 3, Pergamon Press: Oxford, pp 841-846.

Yu MH and Li YM (1991) Twin shear constitutive theory and its computational implementation. In: Computational Mechanics, Ed. by Cheung YK, Lee JHW and Leung AYT, Balkema: Rotterdam, pp 875-879.

Yu MH and Meng XM (1992) Twin shear elasto-plastic model and its application in geotechnical engineering. Chinese J. Geotech. Eng., 14(3): 71-75 (in Chinese, English abstract).

Yu MH, He LN and Zeng WB (1992) A new unified yield function : Its model, computational implementation and engineering application. Computational Methods in Engineering: Advances and Applications. Tay AAO and Lam KY eds. World Scientific: Singapore, pp 157-162.

Yu MH and Meng XM (1993) Researches in the stability of ancient city wall in Xi'an (in English). Researches in the City Wall in Xi'an. Yu MH, Zhang XP and Fang TP eds. Xi'an Jiaotong University Press: Xi'an, China, pp 168-174 (in Chinese).

Yu MH, Meng XM and Xie S (1993) Researches in the protection and utilization of ancient city wall in Xi'an (in Chinese). Researches in the City Wall in X'ian. Yu MH, Zhang XP and Fang TP eds. Xi'an Jiaotong University Press: Xi'an, China, pp 94-126.

Yu MH et al. (1993, 1998) UEPP User's Manual, Version 3.0, Research Division of Structural Strength, Dept. of Civil Eng., Xi'an Jiaotong University: Xi'an, China.

Yu MH and Zeng WB (1994) New theory of engineering structural analysis and its application. J. Eng. Mech. 11(1): 9-20 (in Chinese, English abstract).

Yu MH, Yang SY, Fan SC, et al (1997) Twin shear unified elasto-plastic constitutive model and its applications. Chin. J. Geotech Eng., 21(6): 9-18 (in Chinese, English abstract).

Yu MH et al. (2006) Generalized Plasticity. Springer: Berlin.

Yu MH, Ma GW and Li JC (2009) Structural Plasticity: Limit, Shakedown and Dynamic Plastic Analyses of Structures. ZJU Press and Springer: Hangzhou and Berlin.

Yu MH and Meng XM (1992) Twin shear elasto-plastic model and its application in geotechnical engineering. Chinese J. Geotech. Eng., 14(3): 71-75 (in Chinese, English abstract).

Yu MH, Zeng WB (1993) Mesomechanical simulation of failure criterion for a composite material. Macro-Meso-Micro Mechanical Properties of Materials. Tokuda M, Xu BY eds. Mie Academic Press: Mie, Japan, pp 571-576.

Yu MH, Yang SY, Fan SC, et al. (1997) Twin shear unified elasto-plastic constitutive model and its applications. Chin. J. Geotech Eng., 21(6): 9-18 (in Chinese, English abstract).

Yu MH, Yang SY, Fan SC, Ma GW (1999) Unified elasto-plastic associated and non-associated constitutive model and its engineering applications. Int. J. of Computers & Structures, 71: 627-636.

Yu MH, Wei XY, Yoshimine M, et al. (2001) Effect of failure criterion on elasto-plastic FEM analysis. Invited paper present at the First Asian-Pacific Congress on Computational Mechanics, In: Computational Mechanics–New Frontiers for New Millennium. Valliappan S and Khalili N eds. Elsevier: Amsterdam, pp 1155-1165.

Zhang CQ (2005) Study on method of safety evaluation for rock engineering based on failure approach index. Doctoral Dissertation of Chinese Academy of Sciences, Institute of Rock & Soil Mechanics.

Zhang CQ, Zhou H, Feng XT (2008) Numerical format of elastoplastic constitutive model based on the unified strength theory in FLAC~(3D) Rock and Soil Mechanics, 29(3): 596-602 (in Chinese, English Abstract).

Zhang XS, Guan H, Yew-Chaye Loo (2001) UST failure criterion for punching shear analysis of reinforcement concrete slab-column connections. In: Computational Mechanics–New Frontiers for New Millennium, Valliappan S. and Khalili N. eds. Elsevier Science Ltd, pp 299-304.

Zhou XQ (2002) Numerical Analysis of Reinforced Concrete using Multi-surface Strength Model. Doctoral thesis of Nanyang Technological University, Singapore.

Zhou XQ (2012) 3D Simulation of normal and oblique penetration and perforation. In: Computational Plasticity, Zhejiang University Press & Springer Berlin Heidelberg: Heidelberg, pp 321-331.

Zhou XQ, Qiang HF and Fan SC (2012) 2D simulation of normal penetration using the unified strength theory. In: Computational Plasticity, Zhejiang University Press & Springer Berlin Heidelberg: Heidelberg, pp 289-320.

Zienkiewicz (1971) The Finite Element Method in Engineering Science. McGraw-Hill: London.

Zienkiewicz OC and Pande GN (1977) Some useful forms of isotropic yield surfaces for soil and rock mechanics. Finite Elements in Geomechanics. Gudehus G. ed. Wiley: London, pp 179-190.

Zienkiewicz OC and Taylor RL (l989) The Finite Element Method, vol. l, 4th edn, McGraw-Hill: London, New York.

2

Stress and Strain

2.1 Introduction

In applied mechanics and engineering, materials and structures are generally regarded as continua. This permits us to describe the behaviour and consequences of the use of materials and structures by means of continuous functions. A material is a point (element), and a structure is a body. The structure may be considered as a partly ordered set of material elements (points) filling a structure (body). The cube is often used as an element.

An element that can fill a space without gaps and overlapping is called spatial equipartition. Various polyhedra used in continuum mechanics result in spatial equipartition, such as cubic elements and regular hexagonal elements. The dodecahedron element, orthogonal octahedron element (twin-shear model) and pentahedron element will be described in this chapter.

It is assumed that the reader is familiar with the basic concepts of the mechanics of materials and the theory of elasticity, including the definitions of stress and strain. We shall, however, briefly review some of these basic concepts. In addition, some new concepts are also described in this chapter.

2.2 Stress at a Point, Stress Invariants

A general state of stress at a point can be determined by a stress tensor σ_{ij}, which stands for nine components, as shown in Fig. 2.1, and can be expressed as

$$\sigma_{ij} = \begin{bmatrix} \sigma_x & \tau_{xy} & \tau_{xz} \\ \tau_{yx} & \sigma_y & \tau_{yz} \\ \tau_{zx} & \tau_{zy} & \sigma_z \end{bmatrix} \qquad (2.1)$$
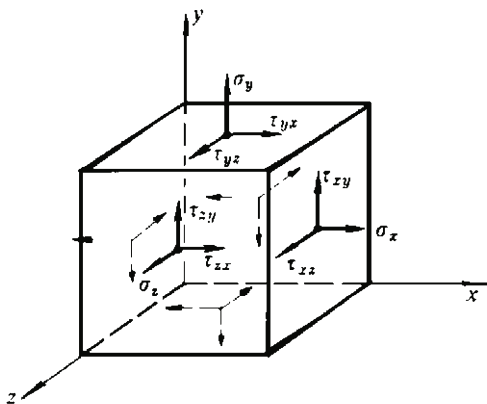
Fig. 2.1 Nine stresses on element

Stress and strain are second-order tensors. The concepts of tensor and tensor notation are useful in derivations and in the proof of theorems.

It can be seen in the course of elasticity, mechanics of solids or plasticity, using three-dimensional transformations, that there exists a coordinate system σ_1, σ_2, σ_3 where the state of stress at the same point can be described by the following:

$$\sigma_i = \begin{bmatrix} \sigma_1 & 0 & 0 \\ 0 & \sigma_2 & 0 \\ 0 & 0 & \sigma_3 \end{bmatrix} \qquad (2.2)$$

The stresses σ_1, σ_2, σ_3 are referred to as the principal stresses, as shown in Fig. 2.2.
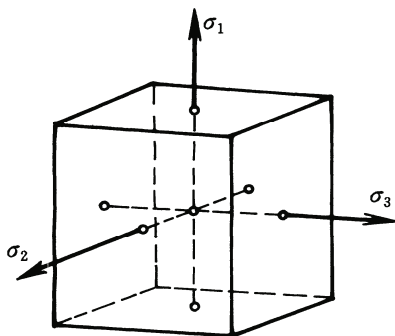
Fig. 2.2 Principal stress element

An element of material subjected to principal stresses σ_1, σ_2 and σ_3 acting in mutually perpendicular directions (Fig. 2.2) is said to be in a state of triaxial stress or three-dimensional stress. If one of the principal stresses equals zero, this is referred to as the plane stress state or biaxial stress state. The triaxial stress and biaxial stress are called the polyaxial stresses, multiaxial stresses or complex stress. The principal planes are the planes on which the principal stresses occur on mutually perpendicular planes.

The principal stresses are the three roots of the equation:

$$\sigma^3 - (\sigma_x + \sigma_y + \sigma_z)\sigma^2 + (\sigma_x\sigma_y + \sigma_y\sigma_z + \sigma_z\sigma_x - \tau_{xy}^2 + \tau_{yz}^2 + \tau_{zx}^2)\sigma$$
$$-(\sigma_x\sigma_y\sigma_z + 2\tau_{xy}\tau_{yz}\tau_{zx} - \sigma_x\tau_{yz}^2 - \sigma_y\tau_{zx}^2 - \sigma_z\tau_{xy}^2) = 0 \tag{2.3}$$

which can be rewritten as

$$\sigma^3 - I_1\sigma^2 + I_2\sigma - I_3 = 0 \tag{2.4}$$

where I_1, I_2, I_3 are

$$I_1 = \sigma_x + \sigma_y + \sigma_z$$
$$I_2 = \sigma_x\sigma_y + \sigma_y\sigma_z + \sigma_z\sigma_x - \tau_{xy}^2 - \tau_{yz}^2 - \tau_{zx}^2 \tag{2.5}$$
$$I_3 = \sigma_x\sigma_y\sigma_z + 2\tau_{xy}\tau_{yz}\tau_{zx} - (\sigma_x\tau_{yz}^2 + \sigma_y\tau_{zx}^2 + \sigma_z\tau_{xy}^2)$$

The quantities I_1, I_2 and I_3 are independent of the direction of the axes chosen. They are called the first, second and third invariants of the stress at a point (or invariant quantities).

If we choose the principal directions as the directions of the coordinate axes, then the three stress invariants take on the simple form

$$I_1 = \sigma_1 + \sigma_2 + \sigma_3$$
$$I_2 = \sigma_1\sigma_2 + \sigma_2\sigma_3 + \sigma_3\sigma_1 \tag{2.6}$$
$$I_3 = \sigma_1\sigma_2\sigma_3$$

The three invariants I_1, I_2 and I_3 are three independent quantities which specify the state of stress just as well as the three principal stresses σ_1, σ_2 and σ_3.

2.3 Deviatoric Stress Tensor and its Invariants

It is convenient in the study of strength theory and plasticity to split the stress tensor into two parts, one called the deviatoric stress tensor S_{ij} and the other the spherical stress tensor p_{ij}. The relation is

$$\sigma_{ij} = S_{ij} + p_{ij} = S_{ij} + \sigma_m \delta_{ij} \tag{2.7}$$

The spherical stress tensor is the tensor whose components are $\sigma_m \delta_{ij}$, where σ_m is the mean stress, i.e.,

$$p_{ij} = \sigma_m \delta_{ij} = \sigma_m \begin{bmatrix} 1 & 0 & 0 \\ 0 & 1 & 0 \\ 0 & 0 & 1 \end{bmatrix} = \begin{bmatrix} \sigma_m & 0 & 0 \\ 0 & \sigma_m & 0 \\ 0 & 0 & \sigma_m \end{bmatrix} \tag{2.8}$$

where

$$\sigma_m = (\sigma_x + \sigma_y + \sigma_z)/3 = (\sigma_1 + \sigma_2 + \sigma_3)/3 = I_1/3 \tag{2.9}$$

It is apparent that σ_m is the same for all possible orientations of the axes. Hence σ_m is named spherical stress. Also, since σ_m is the same in all directions, it can be considered to act as a hydrostatic stress or hydrostatic pressure, denoted by p. It is equal to one-third of the first invariant, $p = \sigma_m = I_1/3$.

The deviatoric stress tensor S_{ij} can be determined as

$$S_{ij} = \sigma_{ij} - p_{ij} = \sigma_{ij} - \sigma_m \delta_{ij} = \begin{bmatrix} \sigma_x - \sigma_m & \tau_{xy} & \tau_{xz} \\ \tau_{yx} & \sigma_y - \sigma_m & \tau_{yz} \\ \tau_{zx} & \tau_{zy} & \sigma_z - \sigma_m \end{bmatrix} \tag{2.10}$$

The invariants of the deviatoric stress tensor are denoted by J_1, J_2, J_3 and can be obtained as follows:

$$J_1 = S_1 + S_2 + S_3 = 0, \quad J_2 = \frac{1}{2} S_{ij} S_{ij} = \frac{2}{3}(\tau_{13}^2 + \tau_{12}^2 + \tau_{23}^2)$$

$$J_3 = |S_{ij}| = S_1 S_2 S_3 = \frac{1}{27}(\tau_{13} + \tau_{12})(\tau_{21} + \tau_{23})(\tau_{31} + \tau_{32}) \tag{2.11}$$

The invariants of the deviatoric stress tensor J_2, and J_3 can be written in terms of the principal stresses

$$J_2 = \frac{1}{6}\left[(\sigma_1 - \sigma_2)^2 + (\sigma_2 - \sigma_3)^2 + (\sigma_3 - \sigma_1)^2\right]$$

$$J_3 = (\sigma_1 - \sigma_m)(\sigma_2 - \sigma_m)(\sigma_3 - \sigma_m) \tag{2.12}$$

2.4 Stresses on the Oblique Plane

If the three principal stresses σ_1, σ_2, σ_3 are acting on three principal planes, respectively, at a given point, we can determine the stresses acting on any plane through this point. This can be done by consideration of the static equilibrium of an infinitesimal tetrahedron formed by this plane and the principal planes, as shown in Fig. 2.3. In this figure, we have shown the principal stresses acting on the three principal planes. These stresses are assumed to be known. We wish to find the stresses σ_α and τ_α acting on the oblique plane whose normal direction cosines are l, m and n.
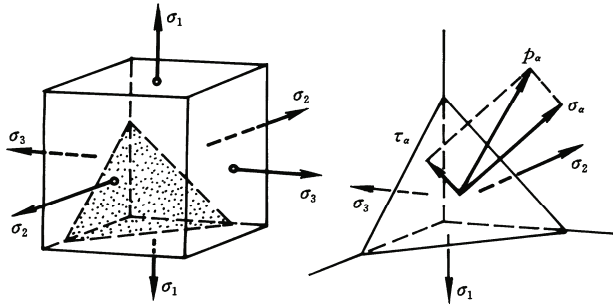
Fig. 2.3 Stress on an infinitesimal tetrahedron

2.4.1 Stresses on the Oblique Plane

The normal stress σ_α and shear stress τ_α acting on this plane can be determined as follows:

$$\sigma_\alpha = \sigma_1 l^2 + \sigma_2 m^2 + \sigma_3 n^2$$
$$\tau_\alpha = \sigma_1^2 l^2 + \sigma_2^2 m^2 + \sigma_3^2 n^2 - (\sigma_1 l^2 + \sigma_2 m^2 + \sigma_3 n^2) \qquad (2.13)$$
$$\boldsymbol{p_\alpha} = \boldsymbol{\sigma_\alpha} + \boldsymbol{\tau_\alpha}$$

2.4.2 Principal Shear Stresses

The three principal shear stresses τ_{13}, τ_{12} and τ_{23} can be obtained as

$$\tau_{13} = \frac{1}{2}(\sigma_1 - \sigma_3), \quad \tau_{12} = \frac{1}{2}(\sigma_1 - \sigma_2), \quad \tau_{23} = \frac{1}{2}(\sigma_2 - \sigma_3) \qquad (2.14)$$

The maximum shear stress acts on the plane bisecting the angle between the largest and smallest principal stresses and is equal to half of the difference between

these principal stresses

$$\tau_{max} = \tau_{13} = \frac{1}{2}(\sigma_1 - \sigma_3) \tag{2.15}$$

The corresponding normal stresses σ_{13}, σ_{12} and σ_{23} acting on the sections where τ_{13}, τ_{12} and τ_{23} are acting, respectively, are

$$\sigma_{13} = \frac{1}{2}(\sigma_1 + \sigma_3), \quad \sigma_{12} = \frac{1}{2}(\sigma_1 + \sigma_2), \quad \sigma_{23} = \frac{1}{2}(\sigma_2 + \sigma_3) \tag{2.16}$$

The three principal shear stresses τ_{13}, τ_{12} and τ_{23} and corresponding normal stresses σ_{13}, σ_{12} and σ_{23} acting on the principal shear stresses sections form a rhomboidal- dodecahedron (τ_{13}, τ_{12}, τ_{23}; σ_{13}, σ_{12}, σ_{23}), as shown in Fig. 2.4.
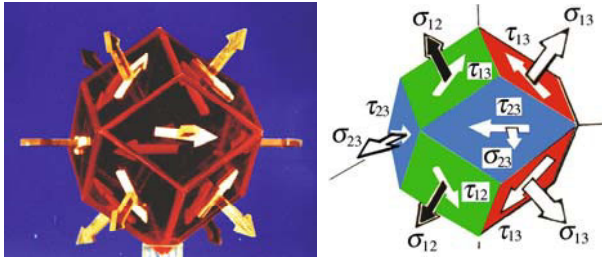
Fig. 2.4 Dodecahedron multi-shear model (τ_{13}, τ_{12}, τ_{23}; σ_{13}, σ_{12}, σ_{23})

The three principal stresses, three principal shear stresses and the three normal stresses acting on the principal shear stresses sections can be illustrated by three stress circles. This is referred to as the Mohr circle, as shown in Fig. 2.5.
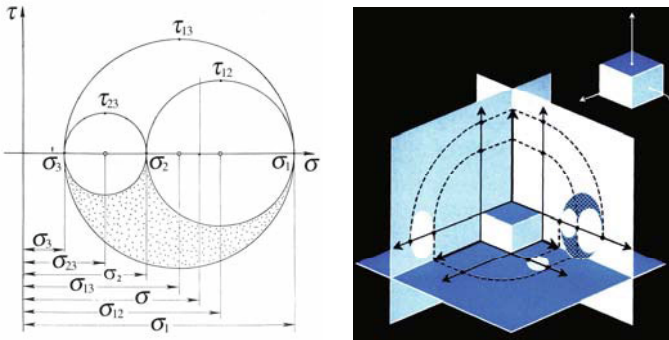
Fig. 2.5 The principal stresses, principal shear stresses and stress circles

The magnitude of the normal and shear stresses of any plane are equal to the distance of the corresponding stress point on the stress circle. The three principal

shear stresses are evidently equal to the radius of the three Mohr circles. A detailed description of the stress circle can be found in Johnson and Mellor (1962), Kussmaul (1981), Chakrabarty (1987), Davis and Selvadurai (2002) and others. Figure 2.6 shows the relations between the stress circles and different planes, where the stresses are acted on.
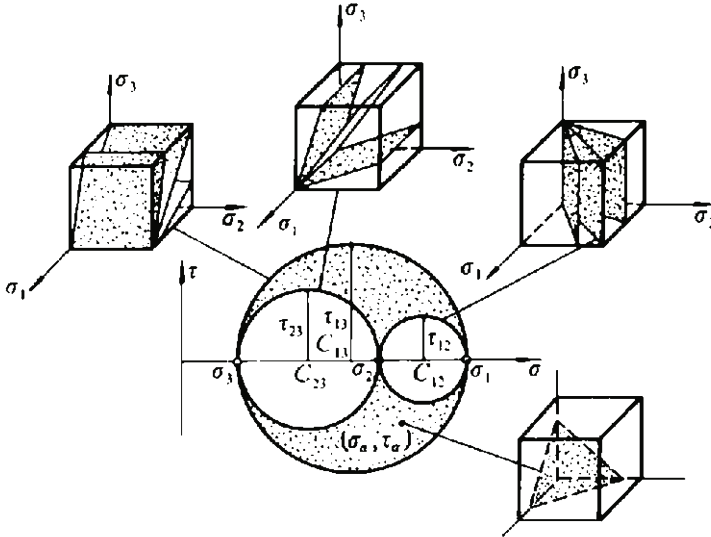
Fig. 2.6 Relations between the stress circles and different planes

2.4.3 *Octahedral Shear Stress*

If the normal of the oblique plane makes equal angles with all the principal axes, and

$$l=m=n=\pm\frac{1}{\sqrt{3}} \tag{2.17}$$

then these planes are called the octahedral plane and the shear stresses acting on it are called the octahedral shear stresses. The normal stress, called the octahedral normal stress σ_8 (or σ_{oct}), acting on this plane equals the mean stress

$$\sigma_8=\frac{1}{3}(\sigma_1+\sigma_2+\sigma_3)=\sigma_m \tag{2.18}$$

A tetrahedron similar to this one can be constructed in each of the four quadrants above the x–y plane and in each of the four quadrants below the x–y plane. On the oblique face of each of these eight tetrahedra the condition $l^2=$

$m^2=n^2=1/3$ will apply. The difference between the tetrahedra will be in the signs attached to *l*, *m* and *n*. The eight tetrahedra together form an isoclinal octahedron element, as shown in Fig. 2.7, and each of the eight planes form the face of this octahedron.
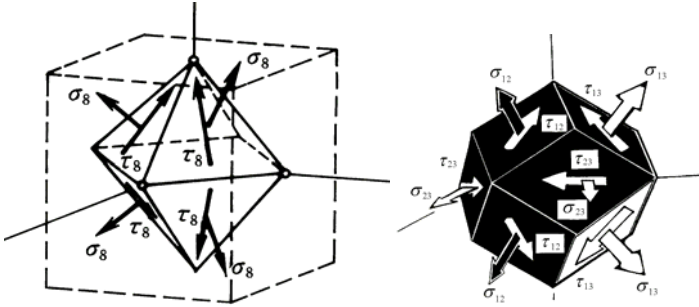
Fig. 2.7 Isoclinal octahedron element and dodecahedron element

The octahedral normal stress is given by Eq. (2.18) and the octahedral shear stress τ_8 (sometimes denoted as τ_{oct}) acting on the octahedral plane is

$$
\begin{aligned}
\tau_8 &= \frac{1}{3}[(\sigma_1 - \sigma_2)^2 + (\sigma_2 - \sigma_3)^2 + (\sigma_3 - \sigma_1)^2]^{1/2} \\
&= \frac{1}{\sqrt{3}}[(\sigma_1 - \sigma_m)^2 + (\sigma_2 - \sigma_m)^2 + (\sigma_3 - \sigma_m)^2]^{1/2}
\end{aligned}
\tag{2.19}
$$

The direction cosines *l*, *m* and *n* of principal planes, principal shear stress planes and the octahedral plane, as well as the normal stresses and shear stresses, are listed in Table 2.1.

Table 2.1 Direction cosines of the principal planes, the principal shear stress planes and the octahedral planes

	Principal plane			Principal shear stress planes			Octa. plane
l	± 1	0	0	$\pm\dfrac{1}{\sqrt{2}}$	$\pm\dfrac{1}{\sqrt{2}}$	0	$\dfrac{1}{\sqrt{3}}$
m	0	± 1	0	$\pm\dfrac{1}{\sqrt{2}}$	0	$\pm\dfrac{1}{\sqrt{2}}$	$\dfrac{1}{\sqrt{3}}$
n	0	0	± 1	0	$\pm\dfrac{1}{\sqrt{2}}$	$\pm\dfrac{1}{\sqrt{2}}$	$\dfrac{1}{\sqrt{3}}$
σ	σ_1	σ_2	σ_3	$\sigma_{12}=\dfrac{\sigma_1+\sigma_2}{2}$	$\sigma_{13}=\dfrac{\sigma_1+\sigma_3}{2}$	$\sigma_{23}=\dfrac{\sigma_2+\sigma_3}{2}$	σ_8
τ	0	0	0	$\tau_{12}=\dfrac{\sigma_1-\sigma_2}{2}$	$\tau_{13}=\dfrac{\sigma_1-\sigma_3}{2}$	$\tau_{23}=\dfrac{\sigma_2-\sigma_3}{2}$	τ_8

2.5 From Single-Shear Element to Twin-Shear Element

The cubic element (σ_1, σ_2, σ_3), i.e. the principal stress element, is commonly used. The three principal stresses σ_1, σ_2, σ_3 act on this element, as shown at the top of Fig. 2.8. According to the concept of stress state, various polyhedral elements can be drawn.
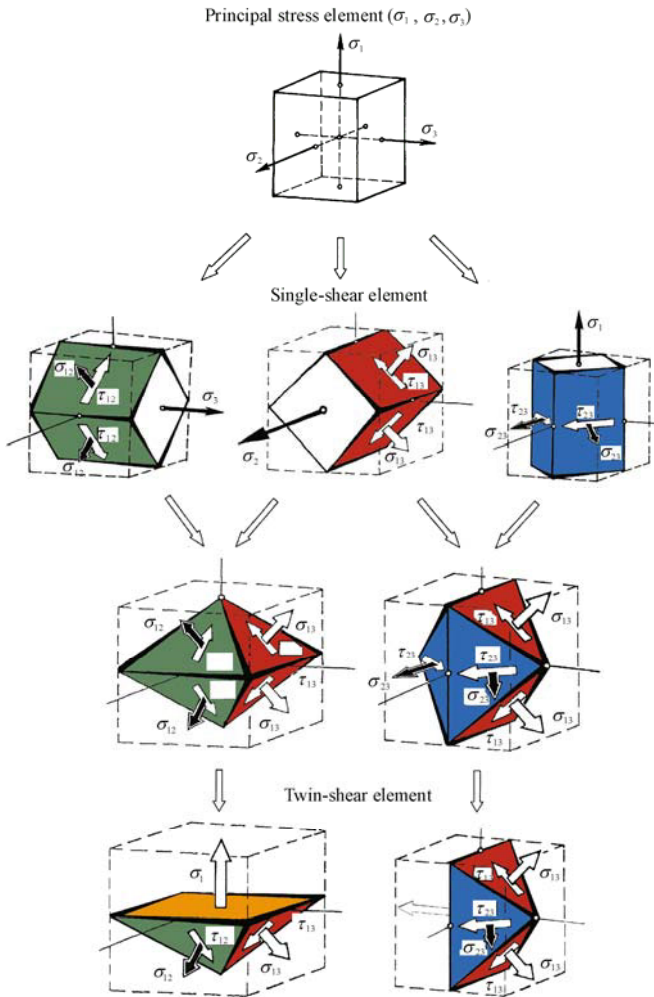
Fig. 2.8 From single-shear element to twin-shear element

Three quadrangular prism elements can be obtained from the cubic element, as shown in Fig. 2.8. The single shear stresses, τ_{13}, τ_{12}, or τ_{23}, act respectively.This may be referred to as the single-shear element. The first single-shear element is the maximum shear stress element in which the maximum shear stress τ_{13} and respective normal stress σ_{13}, as well as the intermediate principal stress σ_2, act on this element. Another single-shear element is the quadrangular prism element (τ_{12}, σ_{12}, σ_3 when $\tau_{12} \geq \tau_{23}$). The intermediate principal shear stress element, the intermediate principal shear stress τ_{12} and the respective normal stress σ_{12}, as well as the minimum principal stress σ_3 act on this element. Other one is the quadrangular prism element (τ_{23}, σ_{23}, σ_1, when $\tau_{12} \geq \tau_{23}$). The minimum principal shear stress element, the minimum principal shear stress τ_{23} and the respective normal stress σ_{23}, as well as the maximum principal stress σ_1 act on this element.

Two orthogonal octahedron elements (τ_{13}, τ_{12}; σ_{13}, σ_{12}) and (τ_{13}, τ_{23}; σ_{13}, σ_{23}) can be obtained from the single-shear element, as shown in Fig. 2.8 This may be referred to as the twin-shear element. The principal shear stresses τ_{13}, τ_{12} and the respective normal stresses σ_{13}, σ_{12} act on the first twin-shear element. The principal shear stresses τ_{13}, τ_{23} and the respective normal stresses σ_{13}, σ_{23} act on the second twin-shear element. These two twin-shear elements form a spatial equipartition in continuum mechanics.

2.6 Stress Space

The stress point $P(\sigma_1, \sigma_2, \sigma_3)$ in stress space can be expressed in other forms, such as $P(x, y, z)$, $P(r, \theta, \xi)$ or $P(J_2, \theta, \xi)$. The geometrical representation of these transfers can be seen in Fig. 2.9.

For the straight line OZ passing through the origin and making the same angle with each of the coordinate axes, the equation is

$$\sigma_1 = \sigma_2 = \sigma_3 \qquad (2.20)$$

The equation for the π_0-plane is

$$\sigma_1 + \sigma_2 + \sigma_3 = 0 \qquad (2.21)$$

The stress tensor σ_{ij} can be divided into the spherical stress tensor and deviatoric stress tensor. The stress vector σ can also be divided into two parts, the hydrostatic stress vector σ_m and the mean shear stress vector τ_m.

$$\sigma = \sigma_m + \tau_m \qquad (2.22)$$
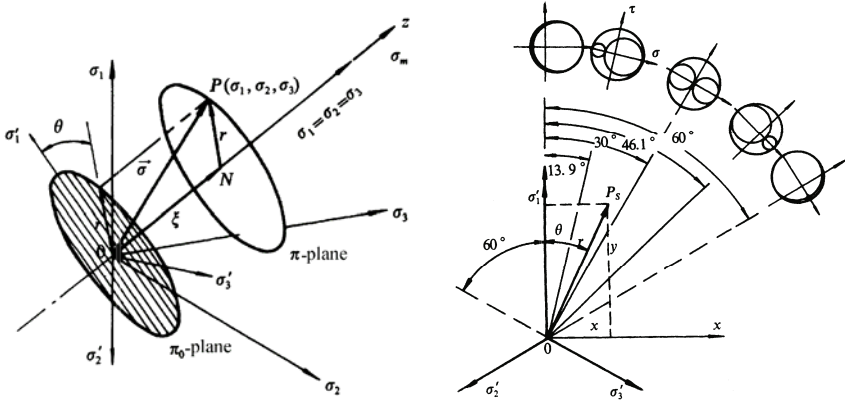
Fig. 2.9 Cylindrical coordinates and stress state in the π-plane

Their magnitudes are given by

$$\xi = \frac{1}{\sqrt{3}}(\sigma_1 + \sigma_2 + \sigma_3) \tag{2.23}$$

$$r = \sqrt{\frac{1}{3}\left[(\sigma_1 - \sigma_2)^2 + (\sigma_2 - \sigma_3)^2 + (\sigma_3 - \sigma_1)^2\right]} \tag{2.24}$$

$$\tau_m = \sqrt{\frac{\tau^2_{13} + \tau^2_{12} + \tau^2_{23}}{3}} = \sqrt{\frac{1}{12}\left[(\sigma_1 - \sigma_2)^2 + (\sigma_2 - \sigma_3)^2 + (\sigma_3 - \sigma_1)^2\right]} \tag{2.25}$$

The π-plane is parallel to the π_0-plane and is given by

$$\sigma_1 + \sigma_2 + \sigma_3 = C \tag{2.26}$$

where C is a constant. The spherical stress tensor σ_m is the same for all points in the π-plane of the stress space and

$$\sigma_m = \frac{C}{3} \tag{2.27}$$

The projections of the three principal stress axes σ_1, σ_2, σ_3 in the stress space are σ_1', σ_2', σ_3'. The relationship between them is

$$\sigma_1' = \sigma_1 \cos\beta = \sqrt{\frac{2}{3}}\sigma_1, \sigma_2' = \sigma_2 \cos\beta = \sqrt{\frac{2}{3}}\sigma_2, \sigma_3' = \sigma_3 \cos\beta = \sqrt{\frac{2}{3}}\sigma_3 \tag{2.28}$$

where β is the angle between $O'A$, $O'B$, $O'C$ and the three coordinates, as shown in

Fig. 2.10.
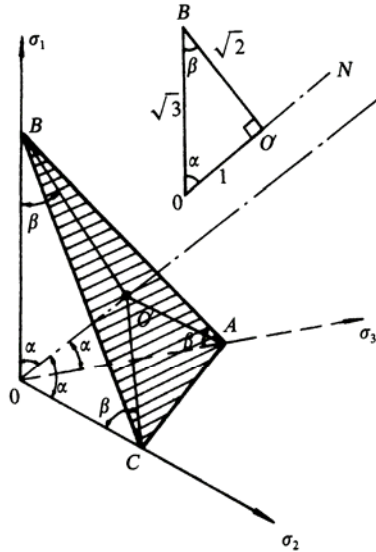
Fig. 2.10 Deviatoric plane

In the following, we will introduce Relationship between $(\sigma_1, \sigma_2, \sigma_3)$ and (x, y, z)
The relationship between the coordinates of the deviatoric plane and the principal stresses are

$$x = \frac{1}{\sqrt{2}}(\sigma_3 - \sigma_2), \ y = \frac{1}{\sqrt{6}}(2\sigma_1 - \sigma_2 - \sigma_3), z = \frac{1}{\sqrt{3}}(\sigma_1 + \sigma_2 + \sigma_3) \qquad (2.29)$$

$$\sigma_1 = \frac{1}{3}(\sqrt{6}y + \sqrt{3}z), \qquad (2.30)$$

$$\sigma_2 = \frac{1}{6}(2\sqrt{3}z - \sqrt{6}y - 3\sqrt{2}x)$$

$$\sigma_3 = \frac{1}{6}(3\sqrt{2}x - \sqrt{6}y + 2\sqrt{3}z)$$

The relationship between the cylindrical coordinates (ξ, r, θ) and the principal stresses $(\sigma_1, \sigma_2, \sigma_3)$ are

$$\xi = |ON| = \frac{1}{\sqrt{3}}(\sigma_1 + \sigma_2 + \sigma_3) = \frac{I_1}{3} = \sqrt{3}\sigma_m \qquad (2.31)$$

$$r = |NP| = \frac{1}{\sqrt{3}}\left[(\sigma_1 - \sigma_2)^2 + (\sigma_2 - \sigma_3)^2 + (\sigma_3 - \sigma_1)^2\right]^{\frac{1}{2}}$$

$$= \left(S_1^2 + S_2^2 + S_3^2\right)^{\frac{1}{2}} = \sqrt{2J_2} = \sqrt{3}\tau_8 = 2\tau_m \qquad (2.32)$$

$$\theta = \tan^{-1}\left(\frac{x}{y}\right) \tag{2.33}$$

From Eq. (2.25) and Eq. (2.28) we can obtain

$$\cos\theta = \frac{y}{r} = \frac{\sqrt{6}S_1}{\sqrt{2J_2}} = \frac{\sqrt{3}}{2}\frac{S_1}{\sqrt{J_2}} = \frac{2\sigma_1 - \sigma_2 - \sigma_3}{2\sqrt{3}\sqrt{J_2}} \tag{2.34}$$

The second and third invariants of the deviatoric stress tensor are

$$J_2 = -(S_1 S_2 + S_2 S_3 + S_3 S_1) \tag{2.35}$$
$$J_3 = S_1 S_2 S_3 \tag{2.36}$$

Three principal deviatoric stresses can be deduced

$$S_1 = \frac{2}{\sqrt{3}}\sqrt{J_2}\cos\theta, \ \ S_2 = \frac{2}{\sqrt{3}}\sqrt{J_2}\cos\left(\frac{2\pi}{3}-\theta\right), \ \ S_3 = \frac{2}{\sqrt{3}}\sqrt{J_2}\cos\left(\frac{2\pi}{3}+\theta\right) \tag{2.37}$$

These relationships are suitable for the conditions $\sigma_1 \geq \sigma_2 \geq \sigma_3$ and $0 \leq \theta \leq \pi/3$. The limit loci in the π-plane have threefold symmetry, so if the limit loci in the range of 60° are given, the limit loci in the π-plane can be obtained.

The three principal stresses can be expressed as

$$\sigma_1 = \frac{1}{\sqrt{3}}\xi + \sqrt{\frac{2}{3}}r\cos\theta$$

$$\sigma_2 = \frac{1}{\sqrt{3}}\xi + \sqrt{\frac{2}{3}}r\cos(\theta - 2\pi/3) \tag{2.38}$$

$$\sigma_3 = \frac{1}{\sqrt{3}}\xi + \sqrt{\frac{2}{3}}r\cos(\theta + 2\pi/3)$$

The principal stresses can also be expressed in terms of the first invariant I_1 of the stress tensor and the second invariant of the deviatoric stress J_2, as

$$\sigma_1 = \frac{I_1}{3} + \frac{2}{\sqrt{3}}\sqrt{J_2}\cos\theta$$

$$\sigma_2 = \frac{I_1}{3} + \frac{2}{\sqrt{3}}\sqrt{J_2}\cos(\theta - \frac{2\pi}{3}) \tag{2.39}$$

$$\sigma_3 = \frac{I_1}{3} + \frac{2}{\sqrt{3}} \sqrt{J_2} \cos(\theta + \frac{2\pi}{3})$$

The principal shear stresses can also be obtained

$$\tau_{13} = \sqrt{J_2} \sin\left(\theta + \frac{\pi}{3}\right) = \sqrt{2}\tau_m \sin\left(\theta + \frac{\pi}{3}\right)$$

$$\tau_{12} = \sqrt{J_2} \sin\left(\frac{\pi}{3} - \theta\right), \quad \tau_{23} = \sqrt{J_2} \sin(\theta)$$

(2.40)

2.7 Stress State Parameters

The stress state at a point (element) is determined by the combination of the three principal stresses (σ_1, σ_2, σ_3). Based on the characteristics of the stress state and by introducing a certain parameter, it can be divided into several types. Lode (1926) introduced a stress parameter μ_σ as

$$\mu_\sigma = (2\sigma_2 - \sigma_1 - \sigma_3)/(\sigma_1 - \sigma_3)$$

(2.41)

μ_σ is referred to as the Lode stress parameter. The Lode parameter can be expressed in terms of principal shear stress as

$$\mu_\sigma = \frac{2\sigma_2 - \sigma_1 - \sigma_3}{\sigma_1 - \sigma_3} = \frac{\tau_{23} - \tau_{12}}{\tau_{13}}$$

(2.42)

In fact, there are three principal shear stresses τ_{13}, τ_{12} and τ_{23} in the three-dimensional principal stress state. However, the three principal shear stresses τ_{13}, τ_{12} and τ_{23} are not independent and only two principal shear stresses are dependent variables, because the maximum principal shear stress τ_{13} is equal to the sum of the other two shear stresses. This relationship is expressed as

$$\tau_{13} = \tau_{12} + \tau_{23}$$

(2.43)

Hence, the twin-shear idea was proposed by Yu (1961). The twin-shear function can be established as (Yu, 1983; Yu and He, 1983; 1985)

$$f = \tau_{13} + \tau_{12}$$

(2.44)

$$f' = \tau_{13} + \tau_{23}$$

(2.45)

Subsequently, Yu (1991; 1992) introduced the "twin shear stress" concept into the analysis of the stress state and offered two twin-shear stress parameters as

$$\mu_\tau = \frac{\tau_{12}}{\tau_{13}} = \frac{\sigma_1 - \sigma_2}{\sigma_1 - \sigma_3} = \frac{S_1 - S_2}{S_1 - S_3} \qquad (2.46a)$$

$$\mu'_\tau = \frac{\tau_{23}}{\tau_{13}} = \frac{\sigma_2 - \sigma_3}{\sigma_1 - \sigma_3} = \frac{S_2 - S_3}{S_1 - S_3} \qquad (2.46b)$$

$$\mu_\tau + \mu'_\tau = 1, \quad 0 \le \mu_\tau \le 1, \ 0 \le \mu'_\tau \le 1 \qquad (2.46c)$$

The twin-shear stress parameters are simpler and have an explicit physical meaning. They can reflect the state of the intermediate principal stress and can represent the status of the stress state.

The twin-shear stress parameters have nothing to do with the hydrostatic stress. They instead represent the status of the deviatoric stress state and the stress angle on the deviatoric plane in the stress space, as shown in Fig. 2.12. Five different stress states are shown in Fig. 2.12. They are

1) $\theta=0°$ ($\mu_\tau=1$);
2) $\theta=13.9°$ ($\mu_\tau=3/4$, $\mu_\tau'=3/$);
3) $\theta=30°$ ($\mu_\tau=\mu_\tau'=0.5$);
4) $\theta=46.1°$ ($\mu_\tau=1/4$, $\mu_\tau'=3/4$) ;
5) $\theta=60°$ ($\mu_\tau=0$, $\mu_\tau'=1$).

According to the meaning of the twin-shear stress parameters, we know that if $\mu_\tau=1$ ($\mu_\tau'=0$, stress angle equals $\theta=0°$), the stress states include the three following cases:

1) $\sigma_1>0$, $\sigma_2=\sigma_3=0$, uniaxial tension stress state;
2) $\sigma_1=0$, $\sigma_2=\sigma_3<0$, equal biaxial compression stress state;
3) $\sigma_1>0$, $\sigma_2=\sigma_3<0$, uniaxial tension, equal biaxial compression stress state.

If $\mu_\tau=\mu_\tau'=0.5$ (stress angle equals $\theta=30°$), the corresponding stress states are as follows:

1) $\sigma_2=(\sigma_1+\sigma_3)/2=0$, pure shear stress state;
2) $\sigma_2=(\sigma_1+\sigma_3)/2>0$, biaxial tension and uniaxial compression stress state;
3) $\sigma_2=(\sigma_1+\sigma_3)/2<0$, uniaxial tension and biaxial compression stress state.

If $\mu_\tau=0$ ($\mu_\tau'=1$, stress angle equals $\theta=60°$), then the corresponding stress states are as follows:

1) $\sigma_1=\sigma_2=0$, $\sigma_3<0$, uniaxial compression stress state;
2) $\sigma_1=\sigma_2>0$, $\sigma_3=0$, equal biaxial tension stress state;
3) $\sigma_1=\sigma_2>0$, $\sigma_3<0$, equal biaxial tension and uniaxial compression stress state.

According to the twin-shear stress parameters and the magnitude of the two smaller principal shear stresses, the stress state can be divided into three kinds of conditions as follows:

1) Extended tension stress state, $\tau_{12} > \tau_{23}$, $0 \le \mu_\tau' < 0.5 < \mu_\tau \le 1$. The stress state (uniaxial tension and biaxial compression) can be expressed by deviatoric stress, and the absolute magnitude of the tensile stress is a maximum, so it can be called the

extended tension stress state. When the intermediate principal stress σ_2 equals the minimum principal stress σ_3, then $\mu_\tau=1$ ($\mu_\tau'=0$). If $\sigma_2=\sigma_3=0$, the extended tension stress state becomes the uniaxial tension stress state.

2) Extended shear stress state, $\tau_{12}=\tau_{23}$, $\sigma_2=(\sigma_1+\sigma_3)/2$. The two smaller stress circulars are equal, the second deviatoric stress $S_2=0$ and the magnitude of the other two deviatoric stresses are identical, but one is tensile and the other is compressive. The two twin-shear stress parameters are identical, $\mu_\tau=\mu_\tau'=0.5$. If $\sigma_2=(\sigma_1+\sigma_3)/2=0$, the extended shear stress state becomes the pure shear stress state.

3) Extended compression stress state, $\tau_{12}<\tau_{23}$, $0\leq\mu_\tau<0.5<\mu_\tau'\leq1$. If $\sigma_1=\sigma_2=0$, $\sigma_3<0$, this stress state becomes the uniaxial compression stress state.

The twin-shear parameters simplify the Lode parameter and have a clear physical meaning. Their relationships are

$$\mu_\tau = \frac{1-\mu_\sigma}{2}=1-\mu_\tau', \quad \mu_\tau' = \frac{1+\mu_\sigma}{2}=1-\mu_\tau \tag{2.47}$$

Some types of stress states and stress state parameters including the Lode parameter and the twin-shear stress parameters are summarized in Table 2.2.

Table 2.2 Principal stresses, shear stresses and stress state parameters

Stress state		Principal stress	Principal shear stress	Deviatoric stress	Stress angle	Parameter of stress state		
						μ_τ	μ_τ'	μ_σ
Extended tension	Pure tension, Equal Biaxial compression	$\sigma_2=\sigma_3$	$\tau_{12}=\tau_{13}$ $\tau_{23}=0$	$S_2=S_3$ $S_1=S_2+S_3$	$0°$	1	0	-1
	$\tau_{23}=\dfrac{\tau_{12}}{3}$, $\tau_{13}=4\tau_{23}$	$\sigma_2<\dfrac{\sigma_1+\sigma_3}{2}$	$\tau_{12}>\tau_{23}$	$S_1=S_2+S_3$	$13.9°$	$\dfrac{3}{4}$	$\dfrac{1}{4}$	$\dfrac{-1}{2}$
Pure shear		$\sigma_2=\dfrac{\sigma_1+\sigma_3}{2}$	$\tau_{12}=\tau_{23}$	$S_1=\lvert S_3\rvert$ $S_2=0$	$30°$	0.5	0.5	0
Extended compression	$\tau_{12}=\dfrac{\tau_{23}}{3}$, $\tau_{13}=4\tau_{12}$	$\sigma_2>\dfrac{\sigma_1+\sigma_3}{2}$	$\tau_{12}<\tau_{23}$	$\lvert S_3\rvert=S_1+S_2$	$46.1°$	$\dfrac{1}{4}$	$\dfrac{3}{4}$	$\dfrac{1}{2}$
	Pure compression equal biaxial compression	$\sigma_2=\sigma_1$	$\tau_{12}=0$ $\tau_{23}=\tau_{13}$	$S_1=S_2$ $\lvert S_3\rvert=S_1+S_2$	$60°$	0	1	$+1$

The relationships between various shear stresses are listed in Table 2.3. It is convenient to compare various textbooks on plasticity. Different symbols or expressions may be used on different courses.

Table 2.3 Relationships between various shear stresses and J_2

	q_τ	τ_8	τ_s	$\tau_\pi = r$	J_2	S_{ij}
Generalized shear stress q_τ	q_τ	$\dfrac{3}{\sqrt{2}}\tau_8$	$\sqrt{3}\tau_s$	$\sqrt{\dfrac{3}{2}}\tau_\pi$	$\sqrt{3J_2}$	$\sqrt{\dfrac{3}{2}S_{ij}S_{ij}}$
Octahedral shear stress τ_8	$\dfrac{\sqrt{2}}{3}q_\tau$	τ_8	$\sqrt{\dfrac{2}{3}}\tau_s$	$\dfrac{1}{\sqrt{3}}\tau_\pi$	$\sqrt{\dfrac{2}{3}J_2}$	$\sqrt{\dfrac{1}{3}S_{ij}S_{ij}}$
Pure shear stress τ_s	$\dfrac{1}{\sqrt{3}}q_\tau$	$\sqrt{\dfrac{3}{2}}\tau_8$	τ_s	$\dfrac{1}{\sqrt{2}}\tau_\pi$	$\sqrt{J_2}$	$\sqrt{\dfrac{1}{2}S_{ij}S_{ij}}$
Shear stress on deviatoric plane $\tau_\pi=r$	$\sqrt{\dfrac{2}{3}}q_\tau$	$\sqrt{3}\tau_8$	$\sqrt{2}\tau_s$	τ_π	$\sqrt{2J_2}$	$\sqrt{S_{ij}S_{ij}}$
Second invariant J_2 of deviatoric stress	$\dfrac{1}{3}q_\tau^2$	$\dfrac{3}{2}\tau_8^2$	τ_s^2	$\dfrac{1}{2}\tau_\pi^2$	J_2	$\dfrac{1}{2}S_{ij}S_{ij}$

2.8 Strain Components

When a continuum is deformed, a generic point experiences a displacement $\{U\}$ with components u, v, w, with respect to Cartesian orthogonal axes x, y, z, respectively. For very small strains, the axial strains ε_x, ε_y, ε_z and shear strains γ_{xy}, γ_{yz}, γ_{zx} can be expressed by the displacement differentiation as follows

$$\varepsilon_x = \frac{\partial u}{\partial x}, \quad \varepsilon_y = \frac{\partial v}{\partial y}, \quad \varepsilon_z = \frac{\partial w}{\partial z} \tag{2.48}$$

$$\gamma_{xy} = \frac{\partial u}{\partial y} + \frac{\partial v}{\partial x}, \quad \gamma_{yz} = \frac{\partial v}{\partial z} + \frac{\partial w}{\partial y}, \quad \gamma_{xz} = \frac{\partial u}{\partial z} + \frac{\partial w}{\partial x} \tag{2.49}$$

The six strain components ε_x, ε_y, ε_z, γ_{xy}, γ_{yz}, γ_{zx} can describe completely the state of strain at the considered point. Similar to the stress tensor, there also exist principal strains ε_1, ε_2, ε_3 with the companion shear strains equal to zero. For a plane strain state, the third principal strain ε_3 vanishes and the principal strains can be expressed as follows

$$\varepsilon_1 = \frac{\varepsilon_x + \varepsilon_y}{2} + \sqrt{\frac{1}{4}(\varepsilon_x - \varepsilon_y)^2 + (\gamma_{xy}/2)^2}$$
$$\varepsilon_2 = \frac{\varepsilon_x + \varepsilon_y}{2} - \sqrt{\frac{1}{4}(\varepsilon_x - \varepsilon_y)^2 + (\gamma_{xy}/2)^2} \tag{2.50}$$

The principal direction is given by

$$\tan 2\alpha = -\frac{\gamma_{xy}}{\varepsilon_x - \varepsilon_y} \tag{2.51}$$

Equation (2.51) still holds when $\varepsilon_z \equiv \varepsilon_3 \neq 0$, provided ε_z is a principal strain.

2.9 Equations of Equilibrium

The following three differential equations of equilibrium in the direction of the coordinate axes are

$$\frac{\partial \sigma_x}{\partial x} + \frac{\partial \tau_{xy}}{\partial y} + \frac{\partial \tau_{xz}}{\partial z} + X = 0$$

$$\frac{\partial \tau_{xy}}{\partial x} + \frac{\partial \sigma_y}{\partial y} + \frac{\partial \tau_{yz}}{\partial z} + Y = 0 \tag{2.52}$$

$$\frac{\partial \tau_{xz}}{\partial x} + \frac{\partial \tau_{yz}}{\partial y} + \frac{\partial \sigma_z}{\partial z} + Z = 0$$

where X, Y, Z are the components of the body force per unit volume. For a body in an equilibrium state, the variation in stresses is governed by the above equations of equilibrium.

2.10 Generalized Hooke's Law

Equations relating to stress, strain, stress-rate (increase in stress per unit time) and strain-rate are called   constitutive equations, which are determined by the material properties under consideration. In the case of elastic solids, the constitutive equations take the form of the generalized Hooke's law, which involves stress and strain instead of the stress-rate and strain-rate.

In a general three-dimensional stress state, the generalized Hooke's law has the form of

$$\varepsilon_x = \frac{1}{E}[\sigma_x - v(\sigma_y + \sigma_z)] \tag{2.53a}$$

$$\varepsilon_y = \frac{1}{E}[\sigma_y - v(\sigma_x + \sigma_z)] \tag{2.53b}$$

$$\varepsilon_z = \frac{1}{E}[\sigma_z - v(\sigma_x + \sigma_y)] \tag{2.53c}$$

$$\gamma_{xy} = \frac{1}{G}\tau_{xy}, \quad \gamma_{yz} = \frac{1}{G}\tau_{yz}, \quad \gamma_{xz} = \frac{1}{G}\tau_{xz} \tag{2.53d}$$

where E and v are the modulus of elasticity and the Poisson's ratio, respectively. G is the modulus of rigidity. Only two of them are independent and there is

$$G = \frac{E}{2(1+v)}$$

Equations (2.53a)–(2.53d) may be rewritten conversely as

$$\begin{aligned}
\sigma_x &= 2G\varepsilon_x + \lambda(\varepsilon_x + \varepsilon_y + \varepsilon_z) \\
\sigma_y &= 2G\varepsilon_y + \lambda(\varepsilon_x + \varepsilon_y + \varepsilon_z) \\
\sigma_z &= 2G\varepsilon_z + \lambda(\varepsilon_x + \varepsilon_y + \varepsilon_z) \\
\tau_{xy} &= G\gamma_{xy}, \quad \tau_{yz} = G\gamma_{yz}, \quad \tau_{zx} = G\gamma_{zx}
\end{aligned} \tag{2.54}$$

where the constants G and λ are called Lame's constants and

$$\lambda = \frac{vE}{(1+v)(1-2v)} \tag{2.55}$$

Another important elastic constant is called the bulk modulus of elasticity K, which defines the dilatation (volumetric strain) ε_v as the unit change in volume

$$\varepsilon_v = \varepsilon_x + \varepsilon_y + \varepsilon_z \tag{2.56}$$

with the hydrostatic component of stress, or spherical component of stress σ_m,

$$\sigma_m = \frac{1}{3}(\sigma_x + \sigma_y + \sigma_z) \tag{2.57}$$

As such

$$\varepsilon_v = \frac{1}{K}\sigma_m \tag{2.58}$$

From the generalized Hooke's law, K is derived as

$$K = \frac{E}{[3(1-2v)]} \tag{2.59}$$

2.11   Compatibility Equations

Equations (2.48) and (2.49) implicitly show that the strain components are functions of the three displacement components. Differentiate the first equation within Eq. (2.48) twice with respect to y and the second equation within Eq. (2.48) with respect to x and add the results,

$$\frac{\partial \varepsilon_x^2}{\partial y^2} + \frac{\partial \varepsilon_y^2}{\partial x^2} = \frac{\partial^3 u}{\partial y^2 \partial x} + \frac{\partial^3 v}{\partial x^2 \partial y} \tag{2.60}$$

Differentiating the first equation within Eq. (2.20) with respect to x and y yields

$$\frac{\partial \gamma_{xy}^2}{\partial x \partial y} = \frac{\partial^2}{\partial x \partial y}\left(\frac{\partial u}{\partial y} + \frac{\partial v}{\partial x}\right) \tag{2.61}$$

And since the order of differentiation for single-value, continuous functions is immaterial

$$\frac{\partial \varepsilon_x^2}{\partial y^2} + \frac{\partial \varepsilon_y^2}{\partial x^2} = \frac{\partial^2 \gamma_{xy}}{\partial x \partial y}$$

Similarly, we can derive the following additional equations

$$\frac{\partial \varepsilon_x^2}{\partial y^2} + \frac{\partial \varepsilon_y^2}{\partial x^2} = \frac{\partial^2 \gamma_{xy}}{\partial x \partial y} \tag{2.62a}$$

$$\frac{\partial \varepsilon_y^2}{\partial z^2} + \frac{\partial \varepsilon_z^2}{\partial y^2} = \frac{\partial^2 \gamma_{yz}}{\partial y \partial z} \tag{2.62b}$$

$$\frac{\partial \varepsilon_z^2}{\partial x^2} + \frac{\partial \varepsilon_x^2}{\partial z^2} = \frac{\partial^2 \gamma_{zx}}{\partial z \partial x} \tag{2.62c}$$

$$2\frac{\partial^2 \varepsilon_x}{\partial y \partial z} = \frac{\partial}{\partial x}\left(-\frac{\partial \gamma_{yz}}{\partial x} + \frac{\partial \gamma_{xz}}{\partial y} + \frac{\partial \gamma_{xy}}{\partial z}\right) \tag{2.62d}$$

$$2\frac{\partial^2 \varepsilon_y}{\partial z \partial x} = \frac{\partial}{\partial y}\left(\frac{\partial \gamma_{yz}}{\partial x} - \frac{\partial \gamma_{xz}}{\partial y} + \frac{\partial \gamma_{xy}}{\partial z}\right) \tag{2.62e}$$

$$2\frac{\partial^2 \varepsilon_z}{\partial x \partial y} = \frac{\partial}{\partial z}\left(\frac{\partial \gamma_{yz}}{\partial x} + \frac{\partial \gamma_{xz}}{\partial y} - \frac{\partial \gamma_{xy}}{\partial z}\right) \qquad (2.62f)$$

Equations (2.62a)–(2.62f) are called Saint-Venant compatibility equations, or compatibility equations in terms of strain.

In total, there are fifteen governing equations, including three equilibrium equations (Eqs. (2.52)), six strain displacement relations (Eq. (2.48) and Eq. (2.49)), and six stress-strain relations (Eqs. (2.53)) for solving the fifteen variables (the six stress components σ_x, σ_y, σ_z, τ_{xy}, τ_{yz} and τ_{xz}, the six strain components ε_x, ε_y, ε_z, γ_{xy}, γ_{yz} and γ_{xz}, and the three displacements u, v, w). The compatibility equations are derived from the strain-displacement equations and, therefore, cannot be counted as governing equations. The compatibility equations will be satisfied automatically if the fifteen governing equations are satisfied.

2.12 Governing Equations for Plane Stress Problems

For plane stress problems, the stress components are simplified as

$$\sigma_x = \sigma_x(x,y), \quad \sigma_y = \sigma_y(x,y), \quad \tau_{xy} = \tau_{xy}(x,y) \qquad (2.63a)$$

$$\tau_{xz} = \tau_{yz} = \sigma_z = 0 \qquad (2.63b)$$

The equilibrium equations become

$$\frac{\partial \sigma_x}{\partial x} + \frac{\partial \tau_{xy}}{\partial y} + X = 0 \qquad (2.64a)$$

$$\frac{\partial \tau_{xy}}{\partial x} + \frac{\partial \sigma_y}{\partial y} + Y = 0 \qquad (2.64b)$$

where the body forces X and Y are functions of x and y only, and Z equals zero. The strain-stress relations take the form of

$$\varepsilon_x = \varepsilon_x(x,y) = \frac{1}{E}[\sigma_x - v\sigma_y] \qquad (2.65a)$$

$$\varepsilon_y = \varepsilon_y(x,y) = \frac{1}{E}[\sigma_y - v\sigma_x)] \qquad (2.65b)$$

$$\varepsilon_z = \varepsilon_z(x,y) = \frac{1}{E}[-v(\sigma_x + \sigma_y)] \qquad (2.65c)$$

$$\gamma_{xy} = \gamma_{xy}(x,y) = \frac{1}{G}\tau_{xy} \tag{2.65d}$$

The two shear strains γ_{xz} and γ_{yz} and the normal strain ε_z vanish. Finally, the strain-displacement relations are simplified as

$$\varepsilon_x = \frac{\partial u}{\partial x}, \quad \varepsilon_y = \frac{\partial v}{\partial y}, \quad \gamma_{xy} = \frac{\partial u}{\partial y} + \frac{\partial v}{\partial x} \tag{2.66}$$

There are eight equations in total to correlate the eight unknown quantities of σ_x, σ_y, τ_{xy}, ε_x, ε_y, γ_{xy}, u and v. Again, the governing equations can only be solved with specific stress and displacement boundary conditions.

2.13   Governing Equations in Polar Coordinates

For analysis of a circular ring and plate, rotating disk, curved bars of a narrow rectangular cross section with a circular axis, etc., it is advantageous to use polar coordinates. If the external forces are also rotationally symmetric, the stress state can be assumed to be the plane stress independent of the z-axis which is perpendicular to the polar coordinates plane. The position of a point in the middle plane of a plate is then defined by the distance from the origin O and the angle θ between r and a certain axis O_x fixed in the plane. Denoting σ_r and σ_θ as the normal stress components in the radial and circumferential directions, respectively, and $\tau_{r\theta}$ as the shear stress component, the equation of equilibrium takes the form of

$$\frac{\partial \sigma_r}{\partial r} + \frac{1}{r}\frac{\partial \tau_{r\theta}}{\partial \theta} + \frac{\sigma_r - \sigma_\theta}{r} + R = 0 \tag{2.67a}$$

$$\frac{1}{r}\frac{\partial \sigma_\theta}{\partial \theta} + \frac{\partial \tau_{r\theta}}{\partial r} + \frac{2\tau_{r\theta}}{r} + S = 0 \tag{2.67b}$$

where R and S are the components of body force per unit volume in the radial and tangential directions, respectively.

The corresponding stress components are derived as

$$\sigma_r = \frac{A}{r^2} + B(1 + 2\log r) + 2C \tag{2.68a}$$

$$\sigma_\theta = -\frac{A}{r^2} + B(3 + 2\log r) + 2C \tag{2.68b}$$

$$\tau_{r\theta} = 0 \tag{2.68c}$$

A, B and C are constants that can be determined by boundary conditions.

Denoting the displacements in the radial and tangential directions as u_r and u_θ, respectively, the strain components in the polar coordinates are derived as

$$\varepsilon_r = \frac{\partial u_r}{\partial r}, \quad \varepsilon_\theta = \frac{u_r}{r} + \frac{1}{r}\frac{\partial u_\theta}{\partial \theta} \quad \text{and} \quad \gamma_{r\theta} = \frac{1}{r}\frac{\partial u_r}{\partial \theta} + \frac{\partial u_\theta}{\partial r} - \frac{u_\theta}{r} \tag{2.69}$$

The generalized Hooke's law is then expressed by

$$\varepsilon_r = \frac{1}{E}(\sigma_r - v\sigma_\theta) \tag{2.70a}$$

$$\varepsilon_\theta = \frac{1}{E}(\sigma_\theta - v\sigma_r) \tag{2.70b}$$

$$\gamma_{r\theta} = \frac{1}{G}\tau_{r\theta} \tag{2.70c}$$

Thus, based on the equilibrium equations, the strain-displacement relations, the compatibility equations and Hooke's law plus relative boundary conditions, the stress and displacement fields of the rotational symmetrical body can be solved. Detailed derivations can be referred to in *Theory of Elasticity* by Timoshenko and Goodier (1970) and in *Elasticity: Tensor, Dynamic and Engineering Approaches* by Chou and Pagano (1967).

2.14 Brief Summary

This chapter presents the fundamentals of solid mechanics. Some basic concepts with respect to the stress tensors, stress tensor invariants, deviatoric stress tensors, deviatoric stress tensor invariants, octahedral shear and normal stresses, principal stresses and principal shear stresses, strain components, and some new concepts regarding twin-shear stresses, the twin-shear element and the twin-shear stress parameter are introduced. They are used in the following chapters.

Stress states can be studied on many courses, such as elasticity, plasticity, mechanics of solids, rock mechanics and soil mechanics. The basic formulae are only given here.

The relationships between various shear stresses and J_2 are listed in Table 2.3. Different notations may be used in different textbooks. It is useful to refer to other textbooks.

Governing equations for general stress state solids, plane stress solids and rotationally symmetrical solids are given.

It should be mentioned that only the governing equations in the elastic range of solids are considered. Based on the elastic solutions, by adopting proper yield criterion, the elastic limit load of the solid body can be derived. For elasto-plastic analysis and plastic limit analysis, a yield criterion and a relevant flow law should be applied. The following two chapters will introduce conventional yield criteria

and a unified strength theory developed by Yu (1991; 1992; 2004).

References

Chakrabarty J (1987) Theory of Plasticity. McGraw-Hill: New York.

Chou PC and Pagano NJ (1967) Elasticity: Tensor, Dynamic and Engineering Approaches. Van Nostrand, Princeton: New Jersey.

Davis RO and Selvadurai APS (2002) Plasticity and Geotechnics. Cambridge University Press:Cambridge.

Johnson W and Mellor PB (1962) Plasticity for Mechanical Engineers. D.Van Nostrand Co.: London.

Kussmaul Karl (1981) Festigkeitslehre I. MPA Stuttgart, University Stuttgart.

Timoshenko SP and Goodier JN (1970) Theory of Elasticity. McGraw-Hill: New York.

Yu MH (1961a) General behariour of isotropic yield function. Res. Report of Xi'an Jiaotong University. Xi'an, China (in Chinese).

Yu MH (1961b) Plastic potential and flow rules associated singular yield criterion. Res. Report of Xi'an Jiaotong University. Xi'an, China (in Chinese).

Yu MH (1983) Twin shear stress criterion of plastic deformation in metals. Chinese Science Bulletin (English edition), 28(8): 1141.

Yu MH and He LN (1983) Non-Schmid effect and twin shear stress criterion of plastic deformation in crystals and polycrystalline metals. Acta Metallurgica Sinica, 19(5): B190–196 (in Chinese, English abstr.).

Yu MH, He LN and Song LY (1985) Twin shear stress theory and its generalization. Scientia Sinica (Sciences in China), English edn. Series A, 28(11): 1174-1183.

Yu MH and He LN (1991) A new model and theory on yield and failure of materials under complex stress state. In: Mechanical Behaviour of Materials-6, Vol. 3, Pergamon Press: Oxford, pp 841-846.

Yu MH (1992) A new system of strength theory. Xian Jiaotong University Press: Xi'an, China (In Chinese).

Yu MH (1998) Twin-Shear Theory and its Applications. Science Press: Beijing (in Chinese).

Yu MH (2004) Unified Strength Theory and its Applications. Springer: Berlin.

3

Material Models in Computational Plasticity

3.1 Introduction

The material model in computational plasticity poses an important basic problem. Much research has been devoted to the study of this interesting topic (Zyczkowski, 1981; Chen and Saleeb, 1994; Chen et al., 1994; Harris, 1992). A report on "Formulation and Computational Aspects of Plasticity and Damage Models with Application to Quasi-Brittle Materials" was submitted to the Sandia National Laboratories (Chen and Schreyer, 1995). Material models for non-SD materials and SD materials with the emphasis on the yield criteria of materials under complex stress states, multi-parameter criteria for geomaterials and two bounds of the convex yield criteria will be discussed in this chapter.

The stress-strain curve of a mild steel under uniaxial stress (Fig. 3.1) shows that there exist a tensile yield point and a compressive yield point at which the material will begin to deform plastically. In this case the stress is uniaxial and the magnitudes of the tensile yield point σ_{yt} and the compressive yield point σ_{yc} are identical, $\sigma_{yt}=\sigma_{yc}=\sigma_y$.

Material behaviour is elastic if stress $\sigma < \sigma_y$. This yield stress can readily be determined. What if, however, there are several stresses acting on an element with biaxial stress or triaxial stress? What combination of these stresses will cause yielding? We will now extend the definition for yielding from the uniaxial concept of a yield stress σ_y to a general three-dimensional state of stress.

The criteria for deciding what combination of multiaxial stresses will cause yielding are called the yield criteria. A yield criterion is a function of the stress state and the material parameters. Sometimes, it is a hypothesis concerning the limit of elasticity under any possible combination of stresses. The suitability of any proposed yield criterion must be checked by experiment.
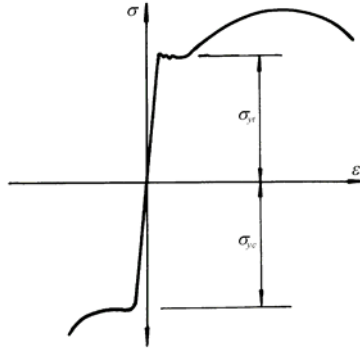
Fig. 3.1 Stress-strain curve of mild steel in uniaxial stress

In the most general case, the yield criterion will depend on the complete state of stress at the point under consideration and will therefore be a function of the nine components of stress at the point (element). Since the stress tensor is symmetric, we can reduce this function to a function with six independent components of the stress tensor. This yield criterion for a material is then essentially extended from the single yield point of the uniaxial tensile test to the six-component stress tensor. The yield criterion can be expressed mathematically by a yield function

$$f(\sigma_{ij}, \sigma_y) = 0 \quad \text{or} \quad f(\sigma_{ij}) = 0 \tag{3.1}$$

Material behaviour will be elastic if the yield function $f(=\sigma_{ij}) < 0$.

For isotropic materials, the orientation of the principal stresses is immaterial, and the values of the three principal stresses σ_1, σ_2 and σ_3 suffice to uniquely describe the state of stress. A yield criterion, therefore, can be expressed in the form of

$$f(\sigma_1, \sigma_2, \sigma_3) = 0 \tag{3.2}$$

or

$$f(I_1, I_2, I_3) = 0 \tag{3.3}$$

where I_1, I_2 and I_3 are the three invariants of the stress tensor σ_{ij}. The yield criterion can be also expressed by other forms.

Another conclusion stemming from isotropy is that the yield function f should not change if the axes are interchanged, so that axis 2 becomes axis 1, and so on.

This means that the yield function is a symmetric function of the principal stresses σ_i ($i = 1, 2, 3$). The yield function is threefold symmetric.

3.2 Material Models for Non-SD Materials (Metallic Materials)

The yield functions of non-SD materials have the following general behaviour

3.2.1 Hydrostatic Stress Independence

This behaviour shows that hydrostatic pressure does not affect the yield deformation behaviour of a wide range of metals. It implies that the yield function must satisfy the following condition:

$$f(\sigma_i) = f(\sigma_i \pm \sigma_m) = f(S_i) = f(S_1, S_2, S_3) \tag{3.4}$$

or

$$\frac{\partial f}{\partial \sigma_i} = 0 \tag{3.5}$$

or

$$f(\sigma_1, \sigma_2, \sigma_3) = f(\sigma_1 \pm \sigma_m, \sigma_2 \pm \sigma_m, \sigma_3 \pm \sigma_m) = f(S_1, S_2, S_3) \tag{3.6}$$

where σ_m is the hydrostatic stress or mean stress and S_1, S_2, S_3 are the deviatoric stresses. On the purely mathematical level, that hydrostatic or volumetric stress does not affect yielding is equivalent to saying that the first invariant I_1 of the stress tensor σ_{ij} is of no physical importance as regards yield. The yield function (3.3′) therefore can be expressed in the form of

$$f(I_2, I_3) = 0 \tag{3.7}$$

In the isotropic case we can use the deviatoric stress invariants instead of the principal deviatoric stresses above. Noting that by definition $J_1 \equiv 0$, the yield function (3.3) or (3.8) reduces to the form

$$f(J_2, J_3;\ \sigma_y) = 0 \quad \text{or} \quad f(J_2, J_3) = 0 \tag{3.8}$$

where J_2, J_3 are the second and third invariants of the deviatoric stress tensor.

$$J_1 = S_{ii} = S_1 + S_2 + S_3 = 0$$

$$J_2 = \frac{1}{2}(S_1^2 + S_2^2 + S_3^2) = \frac{1}{6}\left[(\sigma_1 - \sigma_3)^2 + (\sigma_1 - \sigma_2)^2 + (\sigma_2 - \sigma_3)^2\right] \tag{3.9}$$

$$J_3 = S_1 S_2 S_3 = S_1 + S_2 + S_3 = \frac{1}{3}(S_1^3 + S_2^3 + S_3^3) \tag{3.10}$$

3.2.2   The Tensile Yield Stress Equals the Compressive Yield Stress

It is shown in Fig. 3.1 that the yield stresses in tension and compression are identical. To ensure that the yield stress is the same both in tension and in compression, it is necessary to impose the further restriction that

$$f(-\sigma_i)=f(\sigma_i) \tag{3.11}$$

or

$$f(-\sigma_1,-\sigma_2,-\sigma_3)=f(\sigma_1,\sigma_2,\sigma_3) \tag{3.12}$$

It requires the value of the yield function to remain unchanged when the signs of all stresses are changed.

The second invariant of deviatoric stress J_2 is always positive, and the third invariant of deviatoric stress J_3 reverses in sign if the signs of all the stresses are changed. Condition (3.10) thus requires that in Eq. (3.9) this sign reversal be suppressed, by expressing Eq. (3.9) as an even function of J_3 (e.g., in terms of the square of J_3). The yield function can be written in the form of

$$f(J_2,J_3{}^2)=0 \tag{3.13}$$

3.2.3   Sixfold Symmetry of the Yield Function

For an isotropic material, the yield function $f(\sigma_i, \sigma_y)=0$ is a symmetric function of the principal stresses σ_i ($i=1, 2, 3$). So, the yield function is threefold symmetric for three axes $\sigma_1, \sigma_2, \sigma_3$. In addition, if the yield stresses in tension and compression are identical, the yield function must have sixfold symmetry to three axes $\sigma_1, \sigma_2, \sigma_3$ in the π-plane (Fig. 3.2).
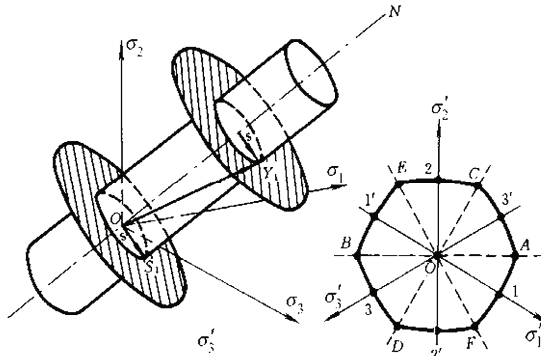
Fig. 3.2 Yield surface in the principal stress space

3.2.4 Convexity of the Yield Function

According to the Drucker postulate, the yield surface in the stress space must have a convex surface. For a smooth function, $f(\sigma)$ is convex if the following inequality holds

$$\lambda f(\sigma_{ij}) + (1-\lambda) f(\sigma_{ij}^{*}) < f[\lambda \sigma_{ij} + (1-\lambda) \ \sigma_{ij}^{*}] \tag{3.14}$$

where $f(\sigma_{ij})$ and $f(\sigma_{ij}^{*})$ are two points in the stress space; λ is real and $0<\lambda<1$.

The geometric meaning of this definition is illustrated in Figs.3.3 and 3.4 for the one dimensional case.

The definition of convexity:

The origin of coordinates or the coordinate axis is taken as the reference. As can be seen, the definition of convexity and the understanding of the word 'non-concave' are the same.

But it must be specified that convex (or concave) have different frames of reference. For example, in Fig. 3.3 of the convex function, from the following axis looking up, it is convex; but from above looking down the curves, it is concave. For consistency, we use the coordinates of the origin or axis as a reference system, as shown in Fig. 3.4.
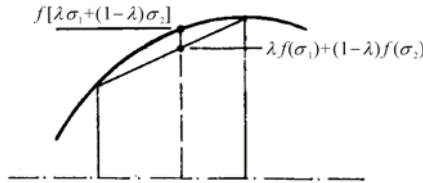
Fig. 3.3 Convexity of yield surface

(a) $y''<0$ (b) $y''>0$
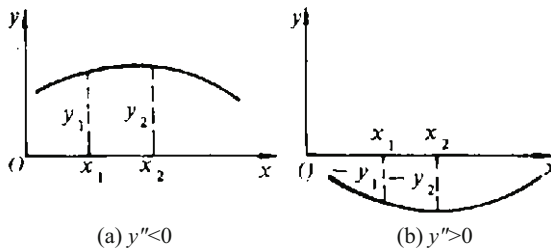
Fig. 3.4 Convexity and coordinate axis

A more general example of the convex yield surface is shown in Figs. 3.5 and 3.6(b). In order to coordinate the origin as a reference, the figure of the yield surface

is convex everywhere. The yield surface at any stress point should meet the yield condition $f(\sigma_{ij})=0$. Drawing a tangent for the yield surface at any stress point σ_{ij}, all possible stress points σ_{ij}^* within or on the yield surface must be on the side of the tangent AA, namely the yield surface is convex. It can also be interpreted that a line linking any two points within the convex yield surface is still within this surface.
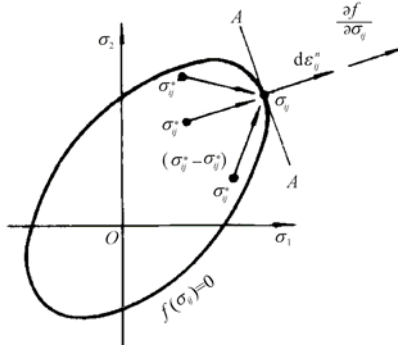
Fig. 3.5 Convex smooth yield surface

(a)   (b)
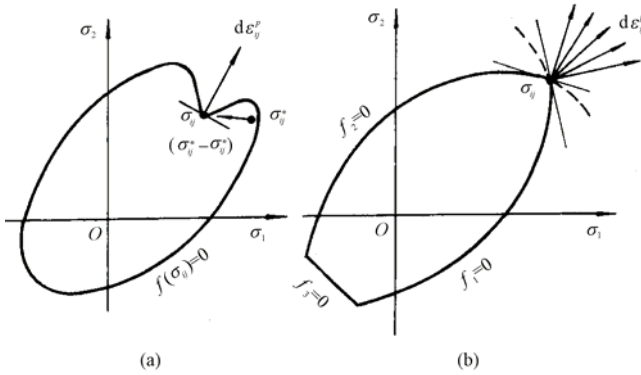
Fig. 3.6 Non-convex and convex yield surfaces

The general behaviour of the yield function may be regarded as a restriction on the yield function. The yield criterion may be expressed in the form of principal shear stresses as

$$f(\tau_{13}, \tau_{12}, \tau_{23}; \sigma_y) = 0 \tag{3.15}$$

3.2.5   *Bounds of the Yield Function for Non-SD Materials*

According to convexity, the yield surface must be convex. Two bounds of the yield

criteria for isotropic materials with the same yield stresses in tension and compression are shown in Fig. 3.7. The inner (lower) bound is the yield locus of the single-shear yield criterion (Tresca criterion, 1864). The outer (upper) bound is the yield locus of the twin-shear yield criterion (Yu, 1961a), or the maximum deviatoric stress criterion (Haythornthwaite, 1961). The circle of the Huber-von Mises criterion circumscribes the inner bound and inscribes the outer bound. Most of the experimental results are situated between these two bounds.
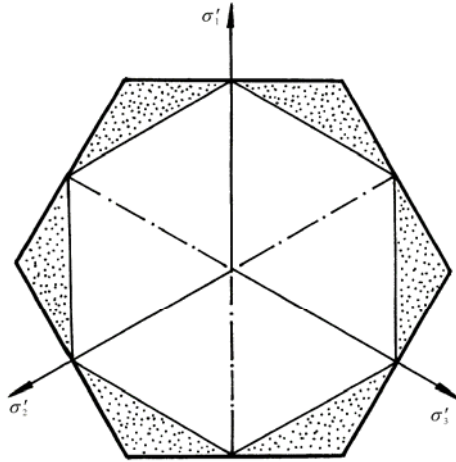
Fig. 3.7 Bounds and region of the convex yield loci for non-SD materials

The intermediate principle stress σ_2 was not taken into account at the single-shear yield criterion (Tresca criterion), only a single shear stress is taken into account. Many studies were devoted to the research of the effect of the intermediate principle stress for non-SD materials (Schmidt, 1932; Ishlinsky, 1940; Hill, 1950; Haythornthwaite, 1961: Yu, 1961;1983).

A shape change yield criterion was proposed by Schmidt in 1932 and later, independently, by Ishlinsky in 1940 as follows (Pisarenko and Lebedev, 1976; Chinese edition, 1983; Zyczkowski, 1981). The shape change of the element is assumed as the yield criterion

$$\gamma_1 = \varepsilon_1 - \theta$$

where θ as the volume change of element $\theta = (\varepsilon_1 + \varepsilon_2 + \varepsilon_3)/3$,

$$\gamma_1 = \frac{(1+\nu)}{E} S_1 = \frac{1+\nu}{E}(\sigma_1 - \sigma_m) = \frac{1+\nu}{3E}(2\sigma_1 - \sigma_2 - \sigma_3) = C \qquad (3.16)$$

The shape change yield criterion is then obtained as

$$f = 2\sigma_1 - (\sigma_2 + \sigma_3) = 2\sigma_y \qquad (3.17)$$

Hill also suggested a linear yield criterion to approximate the Huber-von Mises criterion in 1950 as

$$f = \sigma_1 - \frac{1}{2}(\sigma_2 + \sigma_3) = m\sigma_y \qquad (3.18)$$

The yield locus of Hill's criterion intersects the yield locus of the Huber-von Mises criterion. It is equal to the maximum deviatoric yield criterion when $m=1$. The maximum deviatoric stress criterion was given later, independently, by Haythornthwaite in 1961 as

$$f = S_{max} = \sigma_1 - \frac{1}{3}(\sigma_1 + \sigma_2 + \sigma_3) = \sigma_y \qquad (3.19)$$

Another new idea was proposed by Yu in 1961. The intermediate principle stress σ_2 was taken into account through the consideration of the intermediate principle shear stress τ_{12} or τ_{23} by Yu in 1961.

There are three principal shear stresses τ_{13}, τ_{12} and τ_{23} in the three-dimensional principal stress state. Only two principal shear stresses, however, are independent variables among τ_{13}, τ_{12}, τ_{23}, because the maximum principal shear stress equals the sum of the other two, that is $\tau_{13} = \tau_{12} + \tau_{23}$. According to this formula the twin-shear idea came into being in 1961 (Yu, 1961a; 1961b). The mathematical modeling of the twin-shear stress yield criterion is expressed as follows:

$$f = \tau_{13} + \tau_{12} = C \qquad \text{when} \qquad \tau_{12} \geq \tau_{23} \qquad (3.20a)$$
$$f' = \tau_{13} + \tau_{23} = C \qquad \text{when} \qquad \tau_{12} \leq \tau_{23} \qquad (3.20b)$$

where $\tau_{13} = \dfrac{\sigma_1 - \sigma_3}{2}$, $\tau_{12} = \dfrac{\sigma_1 - \sigma_2}{2}$, $\tau_{23} = \dfrac{\sigma_2 - \sigma_3}{2}$, C is the material parameter.

The twin-shear yield criterion was then obtained by Yu in 1961 as

$$f = \sigma_1 - \frac{1}{2}(\sigma_2 + \sigma_3) = \sigma_y \qquad \text{when} \quad \sigma_2 \leq \frac{1}{2}(\sigma_1 + \sigma_3) \qquad (3.21a)$$

$$f' = \frac{1}{2}(\sigma_1 + \sigma_2) - \sigma_3 = \sigma_y \qquad \text{when} \quad \sigma_2 \leq \frac{1}{2}(\sigma_1 + \sigma_3) \qquad (3.21b)$$

The concept of the twin-shear theory is as clear as the single-shear theory. Moreover, the concept of the twin-shear can be generalized for SD materials by considering the effect of the normal stress acting on the same section in which the

shear stresses are considered. The mathematical modeling of the generalized twin-shear criterion was developed by Yu in 1985 as

$$F = \tau_{13} + \tau_{12} + \beta(\sigma_{13} + \sigma_{12}) = C, \quad \text{when} \quad \tau_{12} + \beta\sigma_{12} \geq \tau_{23} + \beta\sigma_{23} \qquad (3.22a)$$

$$F' = \tau_{13} + \tau_{23} + \beta(\sigma_{13} + \sigma_{23}) = C, \quad \text{when} \quad \tau_{12} + \beta\sigma_{12} \leq \tau_{23} + \beta\sigma_{23} \qquad (3.22b)$$

The expressions of the generalized twin-shear theory for SD materials can be obtained as

$$F = \sigma_1 - \frac{\alpha}{2}(\sigma_2 + \sigma_3) = \sigma_t, \text{ when } \sigma_2 \leq \frac{\sigma_1 + \alpha\sigma_3}{1+\alpha}, \quad \alpha = \sigma_t / \sigma_c \qquad (3.23a)$$

$$F' = \frac{1}{2}(\sigma_1 + \sigma_2) - \alpha\sigma_3 = \sigma_t, \text{ when } \sigma_2 \geq \frac{\sigma_1 + \alpha\sigma_3}{1+\alpha} \qquad (3.23b)$$

where $\alpha = \sigma_t / \sigma_c$ is a strength ratio of material in tension and compression. The generalized twin-shear criterion for SD materials will be described in the next section.

The advances in yield loci in the π-plane of non-SD materials from the lower bound (1864) to the median (1904-1913), from the median to the upper bound (1961), and from a single criterion to a unified criterion (a series of criteria) are shown in Fig. 3.8. The unified yield criterion will be described in detail in the next chapter.

Numerous experiments on metallic materials under complex stresses have been carried out. The experimental data are summarized in Table 3.1. Some data before 1975 are taken from the historical survey article of Michino and Findley (1976). The ratio τ_y/σ_y of the shear yield strength τ_y with tensile yield strength σ_y is also given. All the references regarding the yield criterion and experimental studies are available in Yu (2002; 2004a).

Advances in yield criteria	Yield loci in deviatoric plane	Yield loci in plane stress
Single-shear theory (1864) (inner bound)	Single-shear yield criterion Tresca 1864	Single Shear Stress Yield Criterion
Three-shear theory (1904-1913) (octahedral stress theory)	Huber-Mises 1904-1913	Unified yield criterion with $b=1/2$
Twin-shear theory (1961) (outer bound)	Twin-shear yield criterion	Twin-Shear Yield Criterion Unified yield criterion with $b=1$
Unified theory (1991)	Unified yield criterion Yu M.H. 1991	Unified yield criterion Yu M.H. 1991

Fig. 3.8 Advances in yield criterion for non-SD materials

Table 3.1 Summary and comparison of the yield criteria with experimental results

Researcher	Materials	Specimen	Strength parameters		Researcher
			τ_y/σ_y	b	
Guest, 1900	Steel, brass, etc.	Tubes	0.474,0.727	≈ 0 >1	Tresca,
Hancock, 1906; 1908	Mild steel		0.50–0.82	0, >1	
Scoble, 1906	Mild steel	Solid rods	0.45–0.57	≈ 0 0.366	Tresca
Smith, 1909	Mild steel	Solid rods	0.55–0.56	0.36	> Tresca
Turner, 1909; 1911	Annealed steel	Tubes	0.460–0.572	0-	
Turner, 1909; 1911	Steels	Review work	0.55–0.65	0.3-1	
Mason, 1909	Mild steel	Tubes	0.64	0.9	
Scoble, 1910	Steel	–	0.38–0.45	<0	

(Table 3.1)

Researcher	Materials	Specimen	Strength parameters		Researcher
			τ_y/σ_y	b	
Becker, 1916	Mild steel	Tubes	–		
Seeley & Putnam, 1919	Steels	Bars & tubes	0.6	0.5	>.Mises
Seigle & Cretin, 1925	Mild steel	Solid bars	0.45–0.49	≈0	Tresca
Lode, 1926	Iron, mild steel, nickle, copper	Tubes	–	≈0.4	Mises
Ros & Eichinger, 1926	Mild steel	Tubes	–	≈0.4	Mises
Taylor & Quinney, 1931	Aluminum, copper	Tubes	–	≈0.4	Mises
Taylor & Quinney, 1931	Mild steel	Tubes	–	≈1.0	near Twin shear
Marin, 1936	Mild steel	Review work	–		
Morrison, 1940; 1948	Mild steel	Tubes	–		
Davis et al., 1945	Copper, steel	Tubes	–	≈0.4	Mises
Osgood, 1947	Aluminum alloy	Tubes	–	≈0.4	Mises
Cunningham et al., 1947	Magnesium alloy	Tubes	–	≈0.4	Mises
Bishop and Hill, 1951	Polycrystals	Tubes	0.54	≈0.4	Mises
Fikri and Johnson, 1955	Mild steel	Tubes	–	0.5	> Mises
Marin and Hu, 1956	Mild steel	Tubes		≈0.4	Mises
Naghdi et al., 1958	Aluminum alloy	Tubes	–	0.5	> Mises
Hu and Bratt, 1958	Aluminum alloy	Tubes	–	≈0.4	Mises
Ivey, 1961	Aluminum alloy	Tubes	o.66	1.0	Twin shear
Bertsch and Findley, 1962	Aluminum alloy	Tubes	–	≈0.4	Mises
Mair and Pugh, 1964	Copper	Tubes	–	0.4-1.0	Mises Twin shear
Miastkowski, 1965	Brass	–	–	≈0.4	Mises
Rogan, 1969	Steel	tubes	0.5	0	Tresca
Pisarenko et al., 1969	Copper, Cr-steel	Low temperature	–	≈0.4	Mises
Dawson, 1970	Polycrystals	–	0.64	0.9	near Twin shear
Phillips et al., 1970; 1972	Aluminum	Elevated temperature	0.53	≈0.2	between Tresca and Mises
Deneshi et al., 1976	Aluminum, Copper	Low temperature	0.6	0.5	> Mises
Winstone, 1984	Nickel alloy	Elevated temperature	0.7	>1	Twin shear
Ellyin, 1989	Titanium	Tubes	0.66	≈1.0	Twin shear
Wu and Yeh, 1991	Aluminum stainless steel	Tubes	0.58 0.66–0.7	0.366 1.0 ≈1.0	Mises Twin shear
Ellyin, 1993	Titanium	Tubes	0.62–0.7	0.6-1.0	–
Ishikawa, 1997	Stainless steel	Tubes	0.6–0.63	0.5–0.55	> Mises

It is very interesting that most experimental results are situated between the lower bound (single-shear criterion) and upper bound (twin-shear criterion). The ratio τ_y/σ_y of the shear yield strength τ_y with tensile yield strength σ_y is situated between $0.5 \leqslant \tau_y/\sigma_y \leqslant 0.667$.

Interesting experimental results were reported by Winstone in 1984. He presented new research results using the acoustic emission technique, which provides an accurate and sensitive method for determining yield surfaces. Combined tension and torsion tests were carried out on a servohydraulic testing machine capable of applying a maximum tensile load of 50 kN and a maximum torque of 200 Nm. The testing was undertaken using constant rates of tension and torsion. An acoustic emission transducer was used. All the yield surface tests used tubular test pieces.

The sequence of a typical test to determine the initial yield surface of the cast nickel superalloy Mar-M002 at 750°C was given by Winstone in the UK, as shown in Fig. 3.9(a). This material is usually used for gas turbine blades. The yield surface was obtained by probing the plastic region under various combinations of tensile and torsional loads (Winstone, 1984). The yield loci of the Tresca yield criterion and the von Mises yield criterion are also shown. The dotted line shows the Tresca yield criterion and the broken line shows the Huber-von Mises yield criterion. The deviations of the experimental result from the Tresca yield criterion and the Huber-von Mises yield criterion are significant.

Three other initial yield surfaces were obtained by Winstone in the research on the yield surfaces, as shown in Figs. 3.9(b), (c) and (d).

The following can be seen:

1). All the initial yield surfaces are identical. The four initial yield surfaces for nickel alloy at a high temperature of 750 °C are plotted together in Fig. 3.10. They lie within a tight scatter band. The ratio of shear yield stress τ_y to the tensile yield stress σ_y is $\tau_y/\sigma_y = 0.7$. Winstone pointed out that this value was surprisingly high when compared with the values of $\tau_y/\sigma_y = 0.58$ and $\tau_y/\sigma_y = 0.5$ expected from the Huber-von Mises yield criterion and the Tresca yield criterion respectively. Clearly, neither of these criteria can accurately model the yield behavior of this material.

2). These results are close to the value of the twin-shear stress yield criterion. The ratio of shear yield stress τ_y to the tensile yield stress σ_y for the twin-shear yield criterion is $\tau_y/\sigma_y = 0.667$.

The initial yield surfaces of the cast nickel superalloy Mar-M002 indicated a ratio of shear yield stress to tensile yield stress of 0.7. The comparisons of this experimental result with the three yield criteria are as follows. The deviations are:

Tresca yield criterion: $\dfrac{0.7 - 0.5}{0.5} = 40\%$;

von Mises yield criterion: $\dfrac{0.7 - 0.577}{0.577} = 21\%$;

Twin-shear yield criterion: $\dfrac{0.7-0.667}{0.667}=4.9\%$.

The twin-shear yield criterion is better for matching the experimental result of nickel superalloy Mar-M002.
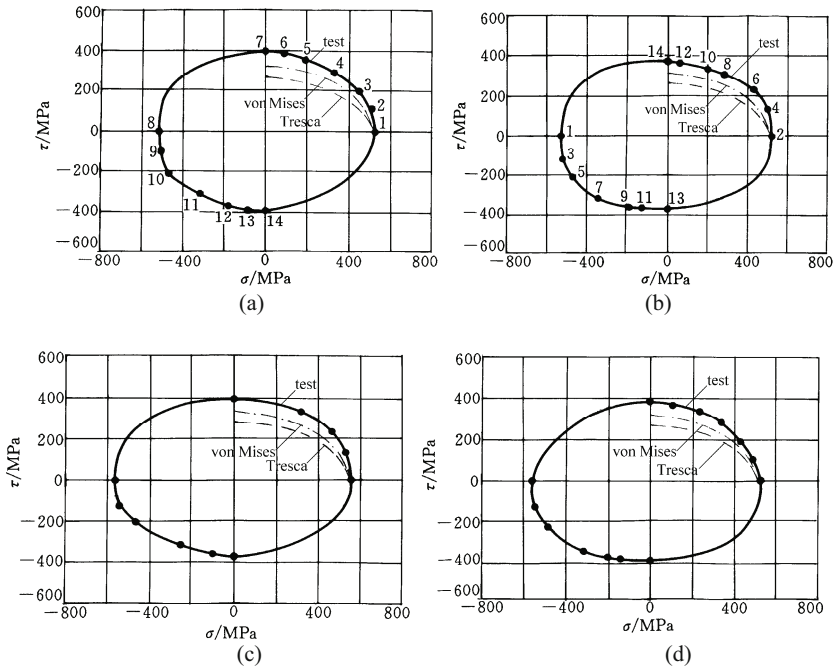
Fig. 3.9 Initial yield surface of Mar-M002 alloy at 750˚C (Winstone, 1984)
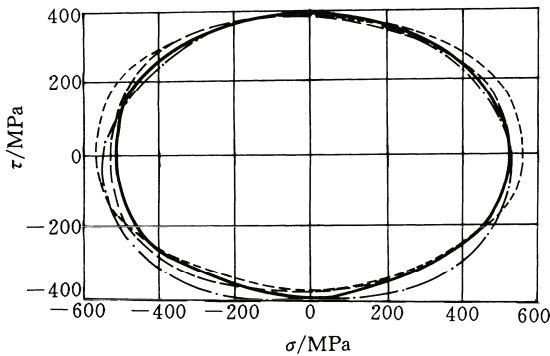
Fig. 3.10 Initial yield surface of Mar-M002 alloy (Winstone, 1984)

3.3   Material Models for SD Materials

3.3.1   General Behavior of Yield Function for SD Materials

The yield functions of SD materials have the following general behaviors.

3.3.1.1   Six Basic Experimental Points for SD Materials

The yield locus for SD materials on the π plane has to meet simultaneously through the six basic experimental points in tension and in compression. The vector lengths of the tensile point and compressive point are r_t and r_c, their ratio is $K= r_t/ r_c$. The relation between K, tensile yield stress σ_t, compressive yield stress σ_c and strength ratio $\alpha=\sigma_t/\sigma_c$ may be expressed as

$$K = \frac{1+2\alpha}{2+\alpha} \tag{3.24}$$

As the strength ratio $\alpha =\sigma_t/\sigma_c$ ranges between $0<\alpha\leqslant 1$，the vector ratio K should be

$$\frac{1}{2} < K \leq 1 \tag{3.25}$$

In general, $r_t\neq r_c$, the shape of the yield loci on the π plane should not be a circle,as shown in Fig. 3.11. Only in a few conditions for non-SD material, $r_t= r_c$, may the shape of yield loci on a plane be a circle.

3.3.1.2   Threefold Symmetry of the Yield Function

The yield loci of SD materials on the π plane should be threefold symmetry, as shown in Fig. 3.12. A possible shape of the yield locus is plotted as shown on the dotted line in Fig. 3.12. It is an equilateral hexagon and consistent with the threefold symmetry. Although a circle shown in Fig. 3.12 also meets this condition, the circle cannot meet the requirement $r_t\neq r_c$, as shown in Fig. 3.11.
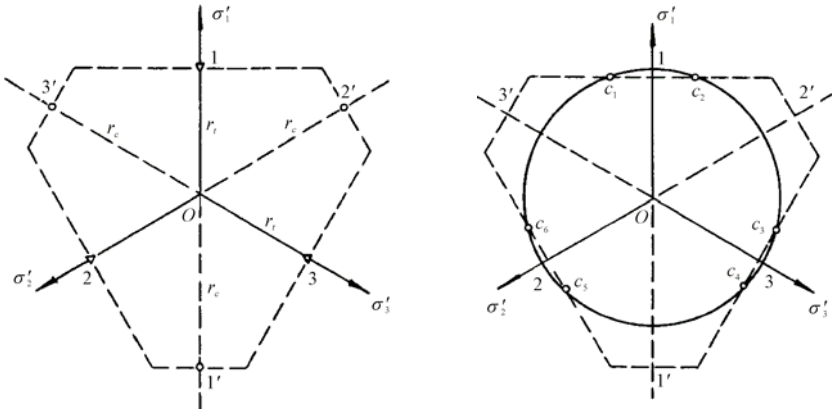
Fig. 3.11 Six basic experimental points   **Fig. 3.12** Threefold symmetry of yield loci on π plane

3.3.1.3   Convexity of the Yield Function

The convexity for SD materials is the same as for non-SD materials. The yield surface cannot be concave, but it can be sub-smooth yield function so as to form a yield surface and allow the formation of corner points, as shown in Fig. 3.12.

In addition, because of the change in the stress state within the yield surface, the material is elastic and, therefore, the yield locus is simply connected. It means that the stress vector from the starting coordinates at the origin cannot be intersected by the yield locus twice.

3.3.2   Three Basic Models for SD Materials

Three kinds of material models are presented. They are the single-shear series criteria, the three-shear series criteria and the twin-shear series criteria.

The expressions of the single-shear theory are

$$F = \tau_{13} + \beta\sigma_{13} = C, \quad \text{or} \quad F = \sigma_1 - \alpha\sigma_3 = \sigma_t, \quad \alpha = \sigma_t / \sigma_c \tag{3.26}$$

It is a two-parameter criterion, the famous Mohr-Coulomb theory.
The expressions of the three-shear theory are

$$F = \tau_8 + \beta\sigma_8 = C \tag{3.27}$$

The expressions of the generalized twin-shear criterion can be obtained by

considering the effect of the normal stress acting on the shear stress section as follows

$$F = \tau_{13} + \tau_{12} + \beta(\sigma_{13} + \sigma_{12}) = C, \quad \text{when} \quad \tau_{12} + \beta\sigma_{12} \geq \tau_{23} + \beta\sigma_{23} \quad (3.28a)$$

$$F' = \tau_{13} + \tau_{23} + \beta(\sigma_{13} + \sigma_{23}) = C, \quad \text{when} \quad \tau_{12} + \beta\sigma_{12} \leq \tau_{23} + \beta\sigma_{23} \quad (3.28b)$$

The generalized twin-shear criterion assumes that the yielding of materials begins when the sum of the two larger principal shear stresses and the corresponding normal stress function reach a magnitude C. Where β is the coefficient that represents the effect of the normal stress on the yield, C is a strength parameter of the material, τ_{13}, τ_{12} and τ_{23} are the principal shear stresses and σ_{13}, σ_{12} and σ_{23} are the corresponding normal stresses acting on the sections where τ_{13}, τ_{12} and τ_{23} acted. They are defined as

$$\tau_{13} = \frac{1}{2}(\sigma_1 - \sigma_3), \quad \tau_{12} = \frac{1}{2}(\sigma_1 - \sigma_2), \quad \tau_{23} = \frac{1}{2}(\sigma_2 - \sigma_3)$$

$$\sigma_{13} = \frac{1}{2}(\sigma_1 + \sigma_3), \quad \sigma_{12} = \frac{1}{2}(\sigma_1 + \sigma_2), \quad \sigma_{23} = \frac{1}{2}(\sigma_2 + \sigma_3) \quad (3.29)$$

The magnitude of parameters β and C can be determined by experimental results of the uniaxial tension strength σ_t and uniaxial compression strength σ_c. The experimental conditions are

$$\sigma_1 = \sigma_t, \quad \sigma_2 = \sigma_3 = 0$$

$$\sigma_1 = \sigma_2 = 0, \quad \sigma_3 = -\sigma_c \quad (3.30)$$

So the material constants β and C can be determined as

$$\beta = \frac{\sigma_c - \sigma_t}{\sigma_c + \sigma_t} = \frac{1 - \alpha}{1 + \alpha}, \quad C = \frac{2\sigma_c\sigma_t}{\sigma_c + \sigma_t} = \frac{2}{1 + \alpha}\sigma_t; \quad \alpha = \sigma_t / \sigma_c \quad (3.31)$$

Substituting β and C into the Eqs. (3.28a) and (3.28b), the generalized twin-shear criterion is now obtained. It can be expressed in terms of principal stresses as

$$F = \sigma_1 - \frac{\alpha}{2}(\sigma_2 + \sigma_3) = \sigma_t, \text{ when } \sigma_2 \leq \frac{\sigma_1 + \alpha\sigma_3}{1 + \alpha}, \quad (3.32a)$$

$$F' = \frac{1}{2}(\sigma_1 + \sigma_2) - \alpha\sigma_3 = \sigma_t, \text{ when } \sigma_2 \geq \frac{\sigma_1 + \alpha\sigma_3}{1 + \alpha}, \quad (3.32b)$$

It is interesting that the expression of the generalized twin-shear criterion for

SD materials is very simple and similar to the expression of the twin-shear yield criterion for non-SD materials Eqs. 3.21(a) and 3.21(b). The twin-shear yield criterion is a special case of the generalized twin-shear criterion when $\alpha = \sigma_t / \sigma_c = 1$.

The limit surface and limit loci in the deviatoric plane of the single-shear theory (Mohr-Coulomb strength theory), three-shear theory (octahedral shear stress theory) and the twin-shear theory were always consistent with a threefold-symmetry hexagonal pyramid failure surface, as shown in Figs. 3.13, 3.14 and 3.15.
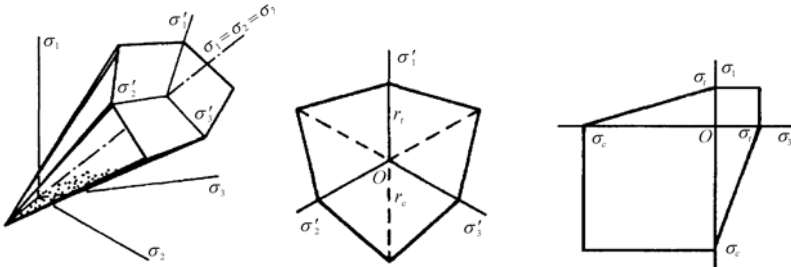
Fig. 3.13 Limit surface and limit loci on π-plane of the single-shear theory
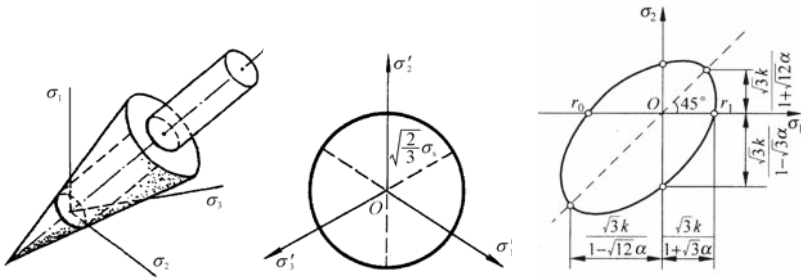
Fig. 3.14 Limit surface and limit loci on π-plane of the three-shear theory
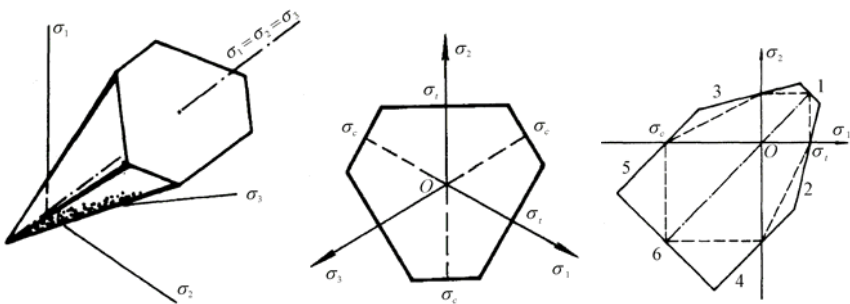
Fig. 3.15 Limit surface and limit loci on π-plane of the twin-shear theory

Single-shear strength theory (Mohr-Coulomb, 1900) forms the lower (inner)

bound for all the possible convex failure surfaces coinciding with the Drucker postulation on the deviatoric plane in the stress space. The disadvantage of the Mohr-Coulomb theory is that the intermediate principal stress σ_2 is not taken into account. Substantial departures from the predictions of the Mohr-Coulomb theory were observed by many researchers. The failure locus of twin-shear theory on the π-plane (deviatoric plane) has outer hexagonal threefold symmetry (upper bound).

3.4 Multi-Parameter Criteria for Geomaterials

Nonlinear Mohr-Coulomb criteria are used in rock mechanics and rock engineering. All the references regarding the multi-parameters are available in Yu (2002; 2004a).

3.4.1 Multi-Parameter Single-Shear Failure Criterion

Various forms of multi-parameter single-shear failure criteria are expressed as

$$\sigma_1 - \sigma_3 = \sigma_c + a\sigma_3 b \qquad \text{(Hobbs criterion)} \qquad (3.33)$$

$$F = \tau_{13} + \lambda\sigma^n_{13} = 0 \qquad \text{(Murrell criterion)} \qquad (3.34)$$

$$F = \left(\frac{\sigma_1 - \sigma_3}{2c}\right)^n = 1 - \frac{\sigma_1 + \sigma_3}{2t} \qquad \text{(Ashton et al. criterion)} \qquad (3.35)$$

$$\sigma_1 - \sigma_3 = a\,(\sigma_1 + \sigma_3)b \qquad \text{(Franklin criterion)} \qquad (3.36)$$

$$F = (\sigma_1 - \sigma_3) + \sqrt{m\sigma_1 - c} = 0$$

or $\tau = A(\sigma_0 + B)^C$ (Hoek-Brown criterion 1980)   (3.37)

$$F = \left[(1-k)\frac{\sigma_1^2}{\sigma_c^2} + \frac{\sigma_1 - \sigma_3}{\sigma_c}\right]^2 + k^2 m\frac{\sigma_1}{\sigma_c} = k^2 c \quad \text{(Pramono-Willam criterion)} \quad (3.38)$$

in which $k \in (0,1)$ is the normalized strength parameter and c and m are the cohesive and frictional parameters.

A hydrostatic type single-shear failure criterion was proposed by Sandel in 1919 in Stuttgart (Mohr, 1928). Sandle's expression is

$$(\sigma_1 - \sigma_3) + m\,(\sigma_1 + \sigma_2 + \sigma_3) = \sigma_s \qquad (3.39)$$

Sandel's expression can be modified into

$$(\sigma_1 - \alpha\sigma_3) + m(\sigma_1 + \sigma_2 + \sigma_3) + n(\sigma_1 + \sigma_2 + \sigma_3)a = \sigma_0 \tag{3.40}$$

$$\sigma_1 - \sigma_2 = \alpha K(q)(\sigma_1 + \sigma_2 + \sigma_3)^\beta \quad \text{(Yoshinaka and Yamabe, 1980)} \tag{3.41}$$

A modification of the Coulomb-Mohr theory with tension cut-off was suggested by Paul (1961). Paul's mode features a vertical branch for the tension cut-off. Chen and Drucker (1969) proposed a modified Mohr-Coulomb failure criterion with a small tension cut-off for the bearing capacity of concrete blocks or rock. The Chen-Drucker model features a circular cap for the tension cut-off. Page (1978) proposed a similar failure criterion surface for mortar joints in masonry panels. Page's mode has an inclined branch for tension cut-off.

A Mohr-Coulomb failure surface with spherical cap was proposed by Drucker et al. (1957). A multi-surface interface model combined with the Mohr-Coulomb surface with a compressive cap was proposed and used for masonry structures and reinforced soils by Lourenco and Rots (1997), Yu and Sloan (1997) and Sutcliffe et al. (2001). A piece-wise linear assemblage of the yield surfaces (a Mohr-Coulomb linear yield surface with a tension cut-off) was presented by Paul (1968) and Maier (1970).

3.4.2 Multi-Parameter Three-Shear Failure Criterion

The first effective formulation of such a condition in a general form was given by Burzynski in 1928 (Zyczkowski, 1981). The general function of a three-parameter criterion is expressed as

$$A\tau_8 + B\sigma_8^2 + C\sigma_8 - 1 = 0 \quad \text{or} \quad A\tau_8^2 + B\sigma_8^2 + C\sigma_8 - 1 = 0 \tag{3.42a}$$

It is equivalent to

$$AJ_2^{1/2} + BI_1^2 + CI_1 - 1 = 0 \tag{3.42b}$$

The general Eq. (3.42) and its variations or particular cases were later proposed more or less independently by many authors (Zyczkowski, 1981). For instance, the three parameter expression $F = \tau_8 + b\sigma_8 + a\sigma_{82} = C$ is the same as Eq. (3.42). All the failure criteria in terms of τ_8 can be expressed by three principal shear stresses τ_{13}, τ_{12} and τ_{23}. So, these kinds of strength theories may also be referred to as the three-shear strength theory.

A formulation of plasticity models for isotropic soils, granular materials and intact jointed rock was presented by Harris in the spirit of the theory of constitutive equations (Harris, 1992).

The multi-parameter three-shear failure criterion contains many curvilinear models and three, four and five-parameter failure criteria used in concrete me-

chanics. Many empirical formulae, typically fitted with different functions, were proposed around the 1980s to cater for various engineering materials. Among these are curvilinear models and many multi-parametric criteria as

$$\sigma_1 = B\sigma_3^{\ b} + \sigma_3 \ \text{ or } \ r = K_2 \sigma_n^{\ 2} \qquad \text{(Beinlawski, 1974)} \qquad (3.43)$$

$$F = \frac{3}{2}\tau_8^2 + \frac{1}{3}A\sigma_8 = C \qquad \text{(Chen-Chen criterion)} \qquad (3.44)$$

$$F = \frac{3}{2}\tau_8^2 - \frac{1}{6}\sigma_8^2 + \frac{1}{3}A\sigma_8 = C \qquad \text{(Chen-Chen concrete criterion)} \qquad (3.45)$$

$$F = a\tau_8^2 + b\tau_8 + c\sigma_1 + d\sigma_8 = 1 \qquad \text{(Chen criterion)} \qquad (3.46)$$

$$\frac{\sigma_1 - \sigma_3}{\sigma_1 + \sigma_3} = -2(m-1)^2 K\left\{1 + \frac{2K}{\sigma_1 + \sigma_3}\left[\left(\frac{m-1}{2}\right)^2 - l\right]\right\}$$

$$\text{when } m(2m-1)\sigma_1 + \sigma_3 < 0 \qquad \text{(Desai and Satami, 1987)} \qquad (3.47)$$

$$f_2 = [\frac{\alpha}{\alpha 0}(I_1)^n + \gamma \cdot I_1^{\ 2}](1 - \beta S_r)^m \qquad \text{(Desai and Satami, 1987)} \qquad (3.48)$$

$$\sigma_1 = K, \ \text{ when } m(2m-1)\sigma_1 + \sigma_3 \geq 0 \ \text{(Fairhurst, 1964)} \qquad (3.49)$$

$$g(\theta) = \frac{2k}{(1+K) - (1-K)\sin 3\theta} \qquad \text{(Gudehus-Argyris criterion)} \qquad (3.50)$$

$$F = \tau_8 + a^2\tau_8^2 + b\tau_8 + d\sigma_1 = C \qquad \text{(Hsieh et al., criterion)} \qquad (3.51)$$

$$\frac{\sigma_1}{\sigma_c} = (\frac{M}{B}\frac{\sigma_1}{\sigma_c} + 1)^B \qquad \text{(Johnston, 1985)} \qquad (3.52)$$

$$\left[\frac{I_1^3}{I_3} - 27\right](\frac{I_1}{P_a})^m = \eta_1 \qquad \text{(Kim and Lade, 1984)} \qquad (3.53)$$

$$F = \tau_8 + a(\sigma_8 + b)^n = C \qquad \text{(Kotsovos criterion)} \qquad (3.54)$$

$$F = J_3 + cJ_2 - (1-\eta)c^3 = 0, \qquad \text{(Krenk criterion)} \qquad (3.55)$$

$$F = \frac{I_1^3}{I_3} = C \qquad \text{(Lade-Duncan criterion)} \qquad (3.56)$$

$$F = \left(\frac{I_1^3}{I_3} - 27\right)\left(\frac{I_1}{p_a}\right)^m = C \qquad \text{(Lade criterion)} \qquad (3.57)$$

$$g(\theta) = r_c \frac{2k(c_1 + c_2 \cos 3\theta)}{(c_3 + k) + (c_3 - k)\cos 3\theta} \qquad \text{(Lin-Bazant criterion)} \qquad (3.58)$$

$$F = \frac{I_1 I_2}{I_3} = C \qquad \text{(Matsuoka-Nakai criterion)} \qquad (3.59)$$

$$F = (a\tau_8)^2 + m\left[b\tau_8 p(\theta, \lambda) + c\sigma_8\right] = C \quad \text{(Menetrey-Willam criterion)} \qquad (3.60)$$

$$\ln(\frac{q^2}{f_0^2}+a_1P\frac{q}{f_0}+a_2P^2) = a_4 \ln[\frac{2q/(pf_0)+a_1-a_3}{2q/(pf_0)+a_1+a_3}]+\ln a_5 \quad \text{(Michelis, 1987)} \quad (3.61)$$

$$F = \tau_8 + a\tau_8^2 + b\sigma_8 = C \qquad \text{(Ottosen criterion)} \qquad (3.62)$$

$$F = \tau_8^2 + c_1P(\theta)\tau_8 + c_2\sigma_8 = C \qquad \text{(Podgorski criterion)} \qquad (3.63)$$

where $P = \cos[1/3\arccos(\cos 3\theta)-\beta]$.

The elliptic function proposed by Willams and Warnke (1975) is

$$g(\theta)=\frac{(1-K^2)(\sqrt{3}\cos\theta-\sin\theta)+(2K-1)\sqrt{(2+\cos 2\theta-\sqrt{3}\sin 2\theta)(1-K^2)+5K^2-4K}}{(1-K^2)(2+\cos 2\theta-\sqrt{3}\sin 2\theta)+(1-2K)^2}$$

$$(3.64)$$

$$g(\theta)=\frac{(7+2k)-2(1-k)\sin 3\theta}{9} \qquad \text{(Yang-Shi criterion)} \qquad (3.65)$$

$$F = \tau_8 + r(\theta)(C+\frac{1}{\sqrt{3}}\frac{\sigma_8}{\tau_8}) = 0 \qquad \text{(William-Warnke criterion)} \qquad (3.66)$$

$$F = \tau_{8t} + a_1\sigma_8 + a_2\sigma_8^2 = C_1 \quad (\theta = 60°)$$

$$F' = \tau_{8c} + b_1\sigma_8 + b_2\sigma_8^2 = C_2 \quad (\theta = 0°) \quad \text{(Willam-Warnke criterion)} \qquad (3.67)$$

$$F = \alpha\sigma_m^2 + \beta\sigma_m + \gamma + (\tau_8/g(\theta))^2 = 0 \quad \text{(Zienkiewicz-Pande criterion)} \qquad (3.68)$$

where $g(\theta)$ is the shape function. Various functions were proposed as follows and some other failure criteria were proposed by Chinese scholars:

$$F = \frac{\sqrt{3}}{\sqrt{2}}\tau_8 - k(1-3\sigma_8/\sigma_{ttt})-(3\sigma_8/\sigma_{ccc})\beta = 0 \qquad \text{(Yu BZ criterion)} \qquad (3.69)$$

where α and β are the shape functions, $0 \le \alpha \le 1$ and $0 \le \beta \le 1$.

$$F = \tau_8 + \alpha(1-\lambda)\left(\frac{\sigma_8+b}{\sigma_8+2a}\right)^\alpha + a\lambda\left(\frac{\sigma_8+b}{\sigma_8+3a}\right)^\beta \qquad \text{(Qu criterion)} \qquad (3.70)$$

where $\lambda = (\sin\frac{3}{2}\theta)^{\left(0.8+\frac{3}{2+\theta}\right)}$.

$$F = \frac{1}{\sqrt{2}}\left[\left(\frac{\tau_{12}}{\sigma_{12}}\right)^2+\left(\frac{\tau_{13}}{\sigma_{13}}\right)^2+\left(\frac{\tau_{23}}{\sigma_{23}}\right)^2\right]^{1/2} = C \qquad \text{(Shen ZJ criterion)} \qquad (3.71)$$

$$F = J_2 - a + bI_1J_3^{1/3} = C, \qquad \text{(Yin criterion)} \qquad (3.72)$$

$$F = \tau_8 + a \left(\frac{b - \sigma_8}{c - \sigma_8} \right)^d \qquad \text{(Guo-Wang criterion)} \qquad (3.73)$$

where $c = c_t (\cos 3\theta / 2)^{1.5} + c_c (\sin 3\theta / 2)^{1.5}$.

$$F = a\tau_8^{1.5} + b\tau_8 \cos\theta + a\sigma_8 = C \qquad \text{(Zhang-Huang criterion)} \qquad (3.74)$$

$$F = a\tau_8^2 + (b + c\cos\theta)\tau_8 + d\sigma_8 = C \qquad \text{(Jiang JJ criterion)} \qquad (3.75)$$

$$F = \tau_{8t} + a_1\sigma_8 + b_1\sigma_8^2 = C_1, \quad (\theta = 0°) \quad F' = \tau_{8c} + a_2\sigma_8 + b_2\sigma_8^2 = C_2, \quad (\theta = 60°)$$
$$\text{(Song-Zhao criterion)} \quad (3.76)$$

where $\tau_8(\theta) = \tau_8 \cos^2(3\theta / 2) + \tau_8 \sin^2(3\theta / 2)$.

$$F = A_2 \left(\frac{\rho_c}{f_c} \right)^2 + A_1 \frac{\rho_c}{f_c} = A_0 \quad (\theta = 60°)$$

$$F = B_2 \left(\frac{\rho_t}{f_t} \right)^2 + B_1 \frac{\rho_t}{f_t} = B_0 \quad (\theta = 0°) \quad \text{(Kuang-Jiang criterion)} \ (3.77)$$

where $\rho(\theta) = \rho_t + (\rho_c - \rho_t)\sin^4 \dfrac{3\theta}{2}$.

3.4.3 *Multi-Parameter Twin-Shear Failure Criterion*

The twin-shear strength theory has been extended into various multiple parameter criteria for more complex conditions (Yu and Liu, 1988; 1990; Yu, 2002; 2004). Several multi-parameter twin-shear failure criteria can be given by considering the effect of hydrostatic stress σ_m

$$F = \tau_{13} + \tau_{12} + \beta_1(\sigma_{13} + \sigma_{12}) + A_1\sigma_m + B_1\sigma_m^2 = C \qquad (3.78a)$$

$$F' = \tau_{13} + \tau_{23} + \beta_2(\sigma_{13} + \sigma_{23}) + A_2\sigma_m + B_2\sigma_m^2 = C \qquad (3.78b)$$

where β, A, B, C are material parameters. This is the nonlinear twin-shear criterion. A simple three parameter twin-shear criterion can be expressed as follows:

$$F = (\tau_{13} + \tau_{12}) + \beta_1(\sigma_{13} + \sigma_{12}) + A\sigma_m = C \qquad (3.79a)$$

$$F' = (\tau_{13} + \tau_{23}) + \beta_2(\sigma_{13} + \sigma_{23}) + A\sigma_m = C \qquad (3.79b)$$

or

$$F = (\tau_{13} + \tau_{12})^2 + \beta_1(\sigma_{13} + \sigma_{12})^2 + A\sigma_m = C \tag{3.80a}$$

$$F' = (\tau_{13} + \tau_{23})^2 + \beta_2(\sigma_{13} + \sigma_{23})^2 + A\sigma_m = C \tag{3.80b}$$

The hyperbolic function based on twin-shear modeling can be obtained (Yu and Liu, 1988; 1990a) as

$$g(\theta) = \frac{2(1-K^2)\cos\theta + (2K-1)\sqrt{4(1-K^2)\cos^2\theta + 5K^2 - 4r_t}}{4(1-K^2)\cos^2\theta + (K-2)^2}$$

$$g(\theta) = \frac{2(1-K^2) + (K-2)\sqrt{4(K^2-1) + (5-4K)\sec^2(\theta - \pi/3)}}{4(1-K^2) - (K-2)^2 \sec^2(\theta - \pi/3)} r_t \sec(\theta - \pi/3) \tag{3.81}$$

The single-shear series of strength theories forms the lower bound of the strength theory. The twin-shear series of strength theories forms the upper bound of the strength theory. The three-shear series of strength theories lies between the two bounds of the strength theory.

Interested readers are referred to the literature review by Chen (1994), Kolymbas (2000), Belytschko et al. (2000), and Yu (2002b; 2004a). The mu lti-par ameter criterion of three-shear theory takes the three principal stresses and the hydrostatic stress into account. It is very interesting that the failure surfaces of most multi-parameter criteria of three-shear theory are the curvilinear failure surfaces that are situated between the failure surface of the single-shear strength theory and the failure surface of the twin-shear strength theory. Twin-shear strength theory was proposed and developed by Yu from 1961 to 1990. Subsequently, the unified strength theory was established in 1991 based on the twin-shear mechanical model.

3.5 **Bounds and the Region of the Convex Yield Function**

There are hundreds of yield and failure criteria that can be seen. Various yield criteria and failure criteria have been proposed in the past; however, all of them must be situated between the two bounds if the convexity is considered, as shown in Fig. 3.16(a).

The lower bound is a piece-wise linear yield loci of the single-shear strength theory (the Mohr-Coulomb strength theory) and the single-shear yield criterion (the Tresca yield criterion).

The upper bound is another piece-wise linear yield loci of the twin-shear strength theory (Yu et al., 1985) and the twin-shear yield criterion (Yu, 1961a), or the maximum deviatoric stress criterion (Haythornthwaite, 1961). Other yield criteria, including the curvilinear criteria and piece-wise linear criteria are situated between these two bounds. The three-shear theory (octahedral shear stress theory or OS theory) is always a median criterion between the two bounds, as shown in

Fig. 3.16(b).

(a) Two bounds and region   (b) Three kinds of yield criteria
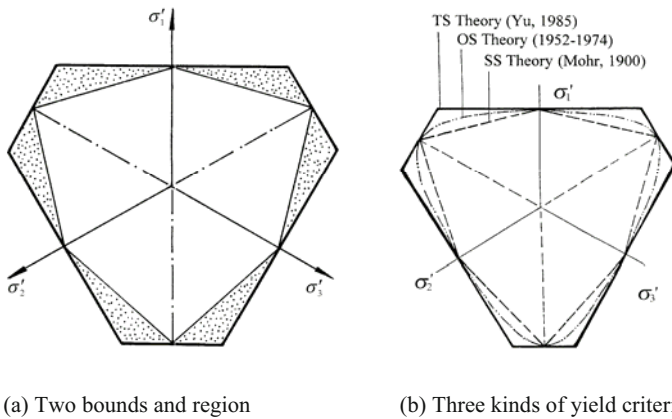
Fig. 3.16 Two piece-wise linear bounds and a curve criterion between two bounds

The yield loci of SD materials in the π plane must have three-fold symmetry to the three axes σ_1, σ_2, σ_3 so the yield locus can be illustrated by a one-third locus, as shown in Fig.3.17. The advances in the failure criterion from single-shear theory to twin-shear theory and from single criterion to unified theory are expressed in Fig. 3.18. The unified strength theory proposed by Yu in 1991 will be described in detail in the next chapter.
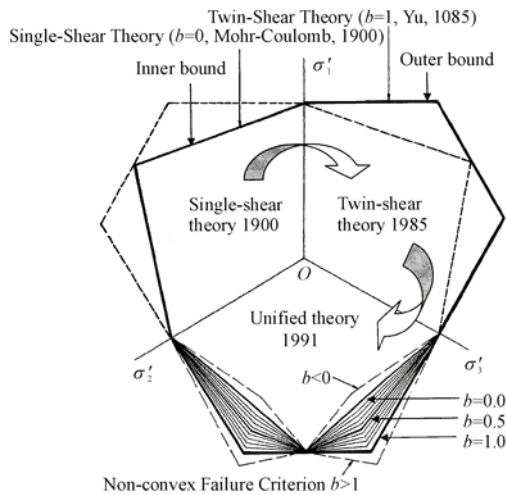
Fig. 3.17 From single-shear theory to twin-shear theory to unified theory

3.6 Brief Summary

A considerable number of failure criteria were proposed in the past century. Over fifty yield criteria are summarized in this chapter. The single-shear theory (Tresca-Mohr-Coulomb strength theory), three-shear theory (octahedral shear stress theory, Huber-von Mises criterion and its extension) and the twin-shear theory (twin-shear yield criterion and generalized twin-shear criterion) are described. The literature can be seen in detail in Zyczkowski (1981), Michino and Findley (1976) and Yu (2002b; 2004a).

The advances in yield loci in the π-plane of non-SD materials and SD materials from the lower bound to the median and from the median to the upper bound are shown in Fig. 3.18. The advance in yield criterion from a single criterion to a unified theory (a series of criteria) is also given in Fig. 3.18. The unified strength theory will be described in detail in the next chapter.
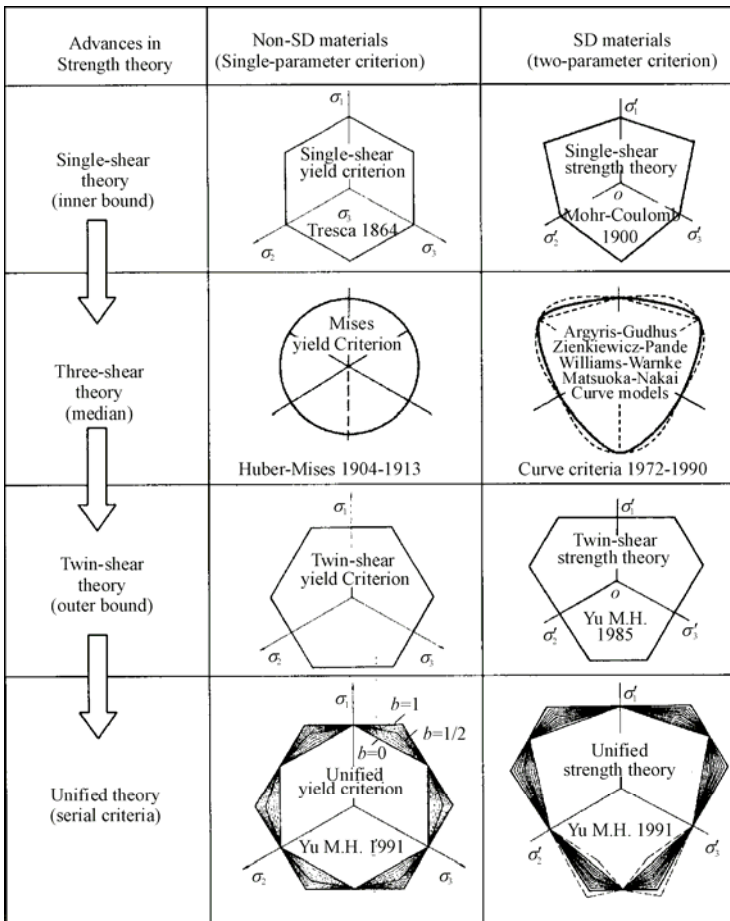
Fig. 3.18 Advances in yield criterion

References

Belytschko T, Liu WK and Moran B (2000) Nonlinear Finite Elements for Continua and Structures. John Wiley: Chichester, New York.

Chen WF and Saleeb AF (1994) Constitutive Equations for Engineering Materials. Vol.1: Elasticity and Modeling, Revised edn. Elsevier: Amsterdam, pp259–304, pp 462-489.

Chen WF et al. (1994) Constitutive Equations for Engineering Materials. Vol. 2: Plasticity and modeling. Elsevier: Amsterdam.

Chen Z and Schreyer HL (1995) Formulation and Computational Aspects of Plasticity and Damage Models with Application to Quasi-Brittle Materials. Contractor Report, SAND95-0329 Sandia National laboratories.

Haythornthwaite RM (1961) Range of yield condition in ideal plasticity. J. Eng. Mech. ASCE, 87(6): 117-133.

Harris D (1992) Plasticity models for soils, granular and jointed rock materials. J. Mech, Phys. Solids, 40(2): 273-290.

Hill R (1950) Philosophisical Magazine (London), 41:733-744 (See: Zyczkowski M 1981, P.100).

Ishlinsky AY (1940) Hypothesis of strength of shape change. Uchebnye Zapiski Moskovskogo Universiteta, Mekhanika, 46 (in Russian, from Zyczkowski, 1981, pp100；and Pisarenko and Lebedev 1976, Chinese edition 1983, pp 70-71.

Kolymbas D ed. (2000) Constitutive Modelling of Granular Materials. Springer: Berlin.

Michino MJ and Findley WN (1976) An historical perspective of yield surface investigation for metals. Int. J. Non-linear Mechanics, 11: 59-82.

Pisarenko GS and Lebedev AA (1976) Deformation and strength of material under complex stressed state. Naukova Dumka, Kiev (in Russian; Chinese edition 1983).

Schmidt R (1932) Uber den Zusammenhang von Spannungen und Formaenderungen im Verfestigungsgebiet, IA 3: 215-235 (in German, from Zyczkowski, 1981, p 100).

Winstone MR (1984) Influence of prestress on the yield surface of the cast nickel superalloy Mar-M002 at elevated temperature. Mechanical Behavior of Materials-4 (ICM-4), Carlsson J and Ohlson NG eds. Pergamon Press: Vol. 1, pp 199-205.

Yu MH (1961a) General behavior of isotropic yield function. Res. Report of Xi'an Jiaotong University. Xi'an, China (in Chinese).

Yu MH (1961b) Plastic potential and flow rules associated singular yield criterion. Res. Report of Xi'an Jiaotong University. Xi'an, China (in Chinese).

Yu MH (1983) Twin shear stress yield criterion. Int. J. Mech. Sci., 25(1): 71-74.

Yu MH, He LN and Song LY (1985) Twin shear stress theory and its generalization. Scientia Sinica (Sciences in China), English edn. Series A, 28(11): 1174-1183.

Yu MH and Liu FY (1988) Twin shear three-parameter criterion and its smooth ridge model. China Civil Engng. J., 21(3): 90-95 (in Chinese, English abstract).

Yu MH and He LN (1991) A new model and theory on yield and failure of materials under complex stress state. In: Mechanical Behavior of Materials-6, Vol. 3, Pergamon Press: Oxford, pp 841-846.

Yu MH (1992) A New system of strength theory. Xian Jiaotong University Press: Xi'an (In Chinese).

Yu MH (1994) Unified strength theory for geomaterials and its application. Chinese J. of Geotech. Eng., 16(2): 1-10 (in Chinese, English Abstract).

Yu MH (1998) Twin-shear Theory and Its Applications. Science Press: Beijing (in Chinese).

Yu MH (2002a) Concrete Strength Theory and Its Applications. Higher Education Press: Beijing, (in Chinese).

Yu MH (2002b) Advances in strength theories for materials under complex stress state in the 20th Century. Applied Mechanics Reviews ASME, 55(3): 169-218.

Yu MH (2004a) Historical reviews. Chapter 11 In: Unified Strength Theory and Its Applications, Springer: Berlin, pp 293-405.

Yu MH (2004b) Unified Strength Theory and its Applications. Springer: Berlin.

Zyczkowski M (1981) Combined Loadings in the Theory of Plasticity. Polish Scientific Publishers: PWN and Nijhoff.

4

Unified Strength Theory and its Material Parameters

4.1 Introduction

Great effort has been devoted to the formulation of strength theories, failure criteria and yield criteria. Many versions of these were presented during the past 100 years. The single-shear criterion Maximum shear criterion (Tresca, 1864), the Huber-von Mises criterion (1904; 1913) and the twin-shear criterion (Yu 1961a; 1983) can be suitable for those materials that have identical strength both in tension and compression. For these materials the shear yield stresses are $\tau_y=0.5\sigma_y$, $\tau_y=0.577\sigma_y$ and $\tau_y=0.667\sigma_y$, respectively, where τ_y is the shear yield strength and σ_y is the uniaxial yield strength of materials. The Drucker-Prager criterion contradicts the experimental results of geomaterials. The single-shear theory (Mohr-Coulomb strength theory, 1900) and the twin-shear strength theory (Yu, 1985) are two bounds of the convex strength theory. Each one mentioned above is suitable for only a certain kind of material.

What is the relationship between various strength theories? Can we propose a unified strength theory that is adapted to more kinds of materials?

Before the study, we should discuss the general behavior of yield functions of materials under a complex stress state.

For an isotropic material, the yield function can generally be expressed in terms of the three principal stresses or stress invariants as

$$F(\sigma_1, \sigma_2, \sigma_3) = 0, \qquad \text{or} \qquad F(I_1, J_2, J_3) = 0 \tag{4.1}$$

The general yield function can also be expressed in terms of cylindrical coordinates (Haigh-Westgaard coordinates) as

$$F(\xi, \rho, \theta) = 0 \tag{4.2}$$

It is evident that all the effects of the three components σ_1, σ_2, σ_3 must be included in the general yield function. It means that the three stress invariants I_1, J_2, J_3 have to be incorporated into the expressions of the general yield function. In other words, the general mathematical expression of the yield function must include all three components both of σ_1, σ_2, σ_3 and I_1, J_2, J_3.

The basic characteristics of material under complex stress have been summarized in Chapter 3. The following general behaviors must be considered in the yield function:

1) SD effect (Strength Difference of material in tension and in compression).
2) Hydrostatic stress effect.
3) Normal stress effect.
4) Effect of the intermediate principal stress.
5) Effect of intermediate principal shear stress or effect of the twin-shear stresses.
6) Three-fold symmetry of the yield surface for SD materials and six-fold symmetry of yield surface for non-SD materials.

The mathematical expression of a yield function for isotropic materials $F(\sigma_1, \sigma_2, \sigma_3)=0$ is a symmetric function of the principal stresses σ_i (i=1, 2, 3). So, the yield surface of the yield function is three-fold symmetry.

The yield function may be also expressed in the form of the principal shear stresses as follows:

$$f(\tau_{13}, \tau_{12}, \tau_{23}) = 0 \quad \text{or} \quad f(\tau_{13}, \tau_{12}, \tau_{23}; \sigma_{13}, \sigma_{12}, \sigma_{23}) = 0 \tag{4.3}$$

4.2 Mechanical Model of Unified Strength Theory

Mechanical model and mathematical modelling are powerful means for establishing and understanding the development of a new theory. Mechanical modelling is an abstraction, a formation of an idea or ideas that may involve the subject with special configurations. Mathematical modelling may involve relationships between continuous functions of space, time and other variations (Meyer, 1985; Tayler, 1986; Besseling and van der Liesen, 1994; Wu et al., 1999).

To express the general nature of strength theory, the cubic element is often used. It is clear that there are three principal stresses σ_1, σ_2 and σ_3 acting on the cubic element. The proposition to introduce the regular octahedral element to the Huber-von Mises yield criterion was made by Ros-Richinger-Nadai (1926-1931, see: Zyczkowski, 1981). Other elements were studied by Yu in 1961-1985. Figures 4.1(a), 4.1(b), 4.1(c) show the single-shear element, twin-shear element and the three-shear element. The Tresca-Mohr-Coulomb strength theory can be introduced from the single-shear element. However, the effect of the intermediate

principal stress σ_2 and the effect of the intermediate principal shear stress (τ_{12} or τ_{23}) are not taken into account in the single-shear theory (Tresca-Mohr-Coulomb strength theory).

The twin-shear stress element and multi-shear element were proposed by Yu (1983; 1985; 1992). The principal stress state (σ_1, σ_2, σ_3) can be converted into the principal shear-stress state (τ_{13}, τ_{12}, τ_{23}) as shown in Fig. 4.1(c).

(a)   (b)   (c)
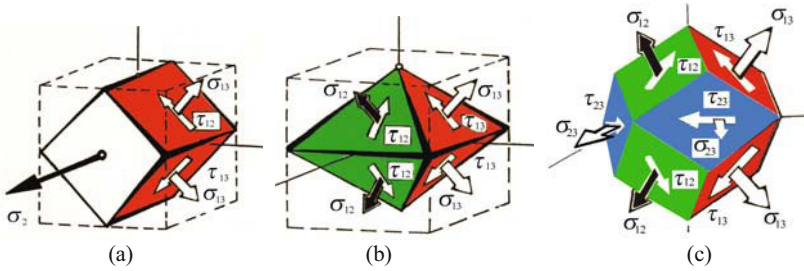
Fig. 4.1 Single-shear element, Twin-shear element and Three-shear element (Yu, 1985)

It is clear that there are three principal shear stresses τ_{13}, τ_{12} and τ_{23} in the three-dimensional principal stress state σ_1, σ_2 and σ_3. However, only two principal shear stresses are independent variables among τ_{13}, τ_{12}, τ_{23} because the maximum principal shear stress equals the sum of the other two. That is

$$\tau_{13} = \tau_{12} + \tau_{23} \tag{4.4}$$

Since there are only two independent principal shear stresses, the shear stress state can also be converted into the twin-shear stress state (τ_{13}, τ_{12}, σ_{13}, σ_{12}) or (τ_{13}, τ_{23}, σ_{13}, σ_{23}). This stress state corresponds to the model shown in Fig. 4.2(a). The eight sections that two groups of shear stress act on consist of the orthogonal octahedral elements, so the twin-shear mechanical model can be obtained as shown in Figs. 4.2(a) and 4.2(b).
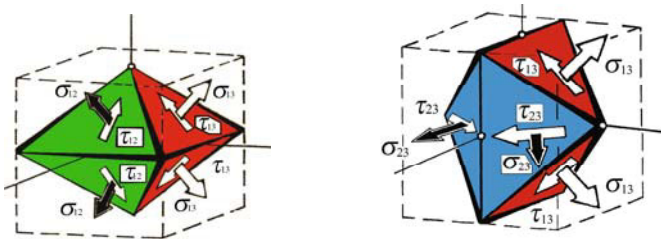
(a) Twin-shear stress state (τ_{13}, τ_{12}, σ_{13}, σ_{12})   (b) Twin-shear stress state (τ_{13}, τ_{23}, σ_{13}, σ_{23}).

Fig. 4.2 Twin-shear model of the unified strength theory (orthogonal octahedral element)

By removing half of the orthogonal octahedral model, we can obtain a new pentahedron element, as shown in Figs. 4.3(a) and 4.3(b). The relationship

between the twin-shear stress and the principal stress σ_1 or σ_3 can be deduced from this element. Based on the orthogonal octahedral element and pentahedron element, a new unified strength theory (yield criterion) can be developed (Yu, 1991; 2004).
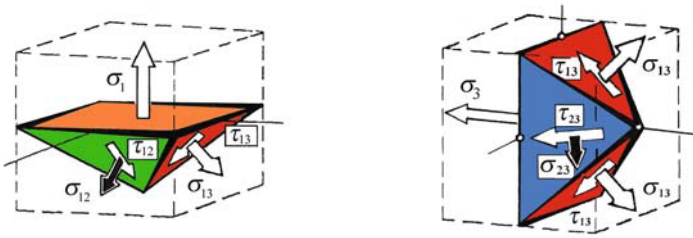
(a) Twin-shear stress state (τ_{13}, τ_{12}, σ_{13}, σ_{12})   (b) Twin-shear stress state(τ_{13}, τ_{23}, σ_{13}, σ_{23}).

Fig. 4.3 Twin-shear model of the unified strength theory (pentahedron element)

The twin-shear orthogonal octahedral model is different from the regular octahedral model. The orthogonal octahedral model consists of two groups of four sections that are perpendicular to each other and are acted on by the maximum shear stress τ_{13} and the intermediate principal shear stress τ_{12} or τ_{23}.

It is worth noticing that the orthogonal octahedral model can be subjected to an affinity deformation but remains a parallehedron, which fills the space without gaps or overlapping. The orthogonal octahedral model, like the cubic element, is also a spatial equipartition, which consists of completely filling a volume with polyhedra of the same kind. The combination of many orthogonal octahedral models can be used as a continuous body (Fig. 4.4(a)). Obviously, the twin-shear pentahedron element is also a spatial equipartition as shown in Fig.4.4(b). The effect of intermediate principal shear-stress (τ_{12} or τ_{23}) can be taken into account naturally in the mathematical modelling of strength theory.
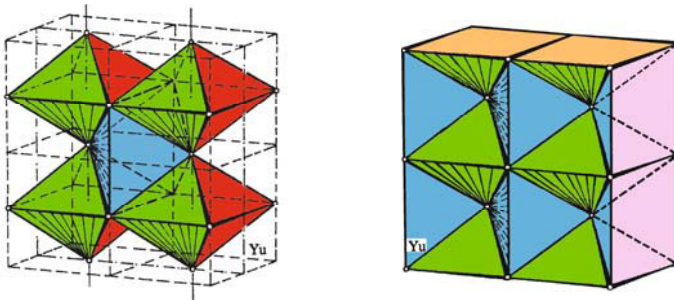
(a) Orthogonal octahedral element   (b) Pentahedron element

Fig. 4.4 Spatial equipartition of twin-shear model

4.3 Mathematical Modelling and the Determination of the Material Parameters of the Unified Strength Theory

Considering all the stress components acting on the twin-shear element and the different effects of various stresses on the yield of materials, the mathematical modelling of the unified strength theory was proposed by Yu in 1991. It can be expressed as (Yu and He, 1991b; Yu, 1992a; 2004)

$$F = \tau_{13} + b\tau_{12} + \beta(\sigma_{13} + b\sigma_{12}) = C, \quad \text{when} \quad \tau_{12} + \beta\sigma_{12} \geq \tau_{23} + \beta\sigma_{23}$$
$$\text{(Extended tension stress state)} \quad (4.5a)$$

$$F' = \tau_{13} + b\tau_{23} + \beta(\sigma_{13} + b\sigma_{23}) = C, \quad \text{when} \quad \tau_{12} + \beta\sigma_{12} \leq \tau_{23} + \beta\sigma_{23}$$
$$\text{(Extended compression stress state)} \quad (4.5b)$$

$$F'' = \sigma_1 = \sigma_t, \qquad\qquad \text{when} \quad \sigma_1 > \sigma_2 > \sigma_3 > 0 \qquad (4.5c)$$

The unified strength theory assumes that the yielding of materials begins when the sum of the two larger principal shear stresses and the corresponding normal stress function reach a magnitude C. Where b is a parameter that reflects the influence of the intermediate principal shear stress τ_{12} or τ_{23} on the yield of material, β is the coefficient that represents the effect of the normal stress on the yield, C is a strength parameter of the material, τ_{13}, τ_{12} and τ_{23} are principal shear stresses and σ_{13}, σ_{12} and σ_{23} are the corresponding normal stresses acting on the sections where τ_{13}, τ_{12} and τ_{23} act. They are defined as

$$\tau_{13} = \frac{1}{2}(\sigma_1 - \sigma_3), \quad \tau_{12} = \frac{1}{2}(\sigma_1 - \sigma_2), \quad \tau_{23} = \frac{1}{2}(\sigma_2 - \sigma_3)$$
$$\sigma_{13} = \frac{1}{2}(\sigma_1 + \sigma_3), \quad \sigma_{12} = \frac{1}{2}(\sigma_1 + \sigma_2), \quad \sigma_{23} = \frac{1}{2}(\sigma_2 + \sigma_3) \quad (4.6)$$

The magnitude of parameters β and C can be determined by experimental results of uniaxial tension strength σ_t and uniaxial compression strength σ_c. The experimental conditions are

$$\sigma_1 = \sigma_t, \ \sigma_2 = \sigma_3 = 0 \,; \quad \sigma_1 = \sigma_2 = 0, \ \sigma_3 = -\sigma_c \qquad (4.7)$$

So the material constants β and C can be determined from Eqs. (4.5a), (4.5b) and (4.7) as

$$\beta = \frac{\sigma_c - \sigma_t}{\sigma_c + \sigma_t} = \frac{1-\alpha}{1+\alpha}, \quad C = \frac{2\sigma_c\sigma_t}{\sigma_c + \sigma_t} = \frac{2}{1+\alpha}\sigma_t \qquad (4.8)$$

4.4 **Mathematical Expression of the Unified Strength Theory**

Substituting β and C into Eqs. (4.5a) and (4.5b), the unified strength theory is now obtained. It can be expressed in terms of the three principal stresses as

$$F = \sigma_1 - \frac{\alpha}{1+b}(b\sigma_2 + \sigma_3) = \sigma_t, \text{ when } \sigma_2 \leq \frac{\sigma_1 + \alpha\sigma_3}{1+\alpha}, \qquad (4.9a)$$

$$F' = \frac{1}{1+b}(\sigma_1 + b\sigma_2) - \alpha\sigma_3 = \sigma_t, \text{ when } \sigma_2 \geq \frac{\sigma_1 + \alpha\sigma_3}{1+\alpha}, \qquad (4.9b)$$

$$F'' = \sigma_1 = \sigma_t, \qquad \text{when } \sigma_1 > \sigma_2 > \sigma_3 > 0 \qquad (4.9c)$$

Equation (4.9c) is used only in the three tensile stress state. It is similar to the Mohr-Coulomb theory with tension cutoff suggested by Paul in 1961. The unified strength theory with tension cutoff can be used for geomaterials.

Equations (4.9a) and (4.9b) are the mathematical formulae of the unified strength theory. b is a choice parameter of the yield criteria. It may be referred to as the unified strength theory parameter. b is also a parameter reflecting the effect of the intermediate principal stress σ_2. The relationship between shear strength τ_0, the uniaxial tensile strength σ_t, uniaxial compressive strength σ_c and unified strength theory parameter b can be determined as

$$b = \frac{(1+\alpha)\tau_0 - \sigma_t}{\sigma_t - \tau_0} = \frac{1+\alpha - B}{B-1}, \; \alpha = \frac{\sigma_t}{\sigma_c}, \; B = \frac{\sigma_t}{\tau_0} = \frac{1+b+\alpha}{1+b} \qquad (4.10)$$

For non-SD materials, Eq. (4.10) can be simplified to

$$b = \frac{2\tau_0 - \sigma_t}{\sigma_t - \tau_0} = \frac{2-B}{B-1}, \; B = \frac{\sigma_t}{\tau_0} = \frac{2+b}{1+b} \qquad (4.10')$$

The ratio of shear strength to tensile strength of materials can be introduced from the unified strength theory as

$$\alpha_\tau = \frac{\tau_0}{\sigma_t} = \frac{1+b}{1+b+\alpha} \qquad (4.11)$$

It is shown that

1) The ratio of shear strength to tensile strength $\alpha_\tau = \tau_0/\sigma_t$ of brittle materials ($\alpha_\tau < 1$) is lower than that of ductile materials ($\alpha_\tau = 1$). This agrees with the experimental data.

2) The yield surface may be non-convex when the ratio of shear strength to tensile strength is $\alpha_\tau < 1/(1+\alpha)$ or $\alpha_\tau > 2/(2+\alpha)$.

3) The shear strength of the material is lower than the tensile strength of the material. This is true for non-SD materials. It needs, however, further study for SD materials.

4.5 Special Cases of the Unified Strength Theory

4.5.1 Special Cases of the Unified Strength Theory (Varying b)

The unified strength theory contains a series of yield criteria for metal materials ($\alpha=1$) and for other materials ($\alpha \neq 1$).

It is worth pointing out that the parameter b is an important parameter in the unified strength theory.

b is a parameter of intermediate principal shear stress τ_{12} or τ_{23} in Eq. (4.8). It reflects the influence of the intermediate principal shear stress on the failure of a material.

b is also a parameter of intermediate principal stress σ_2 in Eq. (4.12). It also reflects the influence of the intermediate principal stress σ_2 on the failure of a material.

We can see below that b is also the parameter that determines the formulation of a failure criterion. A series of convex failure criteria can be obtained when the parameter varies in the range of $0 \leq b \leq 1$. The parameter b has a clear meaning and important significance. The unified strength theory gives us a possibility to choose a reasonable yield criterion for research and applications.

The five typical failure criteria with the values of $b=0$, $b=1/4$, $b=1/2$, $b=3/4$ and $b=1$ are introduced from the unified strength theory. In addition, the unified strength theory can also introduce a family of non-convex failure criteria when $b<0$ or $b>1$.

● **b=0**

The Mohr-Coulomb strength theory can be deduced from the unified strength theory with $b=0$ as

$$F = F' = \sigma_1 - \alpha\sigma_3 = \sigma_t \qquad (4.12)$$

●*b*=1/4

A new failure criterion is deduced from the unified strength theory with *b*=1/4 as

$$F = \sigma_1 - \frac{\alpha}{5}(\sigma_2 + 4\sigma_3) = \sigma_t, \quad \sigma_2 \le \frac{\sigma_1 + \alpha\sigma_3}{1+\alpha}$$

(Extended tension stress state)   (4.13a)

$$F' = \frac{1}{5}(4\sigma_1 + \sigma_2) - \alpha\sigma_3 = \sigma_t, \quad \sigma_2 \ge \frac{\sigma_1 + \alpha\sigma_3}{1+\alpha}$$

(Extended compression stress state)   (4.13b)

●*b*=1/2

A new failure criterion is deduced from the unified strength theory with *b*=1/2 as

$$F = \sigma_1 - \frac{\alpha}{3}(\sigma_2 + 2\sigma_3) = \sigma_t, \quad \sigma_2 \le \frac{\sigma_1 + \alpha\sigma_3}{1+\alpha}$$

(Extended tension stress state)   (4.14a)

$$F' = \frac{1}{3}(2\sigma_1 + \sigma_2) - \alpha\sigma_3 = \sigma_t, \quad \sigma_2 \ge \frac{\sigma_1 + \alpha\sigma_3}{1+\alpha}$$

(Extended compression stress state)   (4.14b)

Since the Drucker-Prager criterion cannot match the practice for geomaterials, this criterion is more reasonable and can be substituted for the Drucker-Prager criterion.

●*b*=3/4

A new failure criterion is deduced from the unified strength theory with *b*=3/4 as

$$F = \sigma_1 - \frac{\alpha}{7}(3\sigma_2 + 4\sigma_3) = \sigma_t, \quad \sigma_2 \le \frac{\sigma_1 + \alpha\sigma_3}{1+\alpha}$$

(Extended tension stress state)   (4.15a)

$$F = \frac{1}{7}(4\sigma_1 + 3\sigma_2) - \alpha\sigma_3 = \sigma_t, \quad \sigma_2 \ge \frac{\sigma_1 + \alpha\sigma_3}{1+\alpha}$$

(Extended compression stress state)   (4.15b)

● *b=1*

A new failure criterion is deduced from the unified strength theory with *b*=1. The mathematical expression is

$$F = \sigma_1 - \frac{\alpha}{2}(\sigma_2 + \sigma_3) = \sigma_t, \quad \text{when} \quad \sigma_2 \leq \frac{\sigma_1 + \alpha\sigma_3}{1+\alpha}$$

(Extended tension stress state)   (4.16a)

$$F' = \frac{1}{2}(\sigma_1 + \sigma_2) - \alpha\sigma_3 = \sigma_t, \quad \text{when} \quad \sigma_2 \geq \frac{\sigma_1 + \alpha\sigma_3}{1+\alpha}$$

(Extended compression stress state)   (4.16b)

This is the generalized twin-shear strength model proposed by Yu in 1983 (Yu, 1983; Yu et al., 1985).

4.5.2 Special Cases of the Unified Strength Theory (Varying α)

● *α=1*, The Unified Yield Criterion for Non-SD Materials

When the tensile strength and the compressive strength are identical, the tension–compressive strength ratio $\alpha = \sigma_t/\sigma_c$ equals 1. A unified yield criterion can be deduced from the Yu unified strength theory. The mathematical expression of the unified yield criterion is expressed as follows. It also contains a series of yield criteria.

$$F = \sigma_1 - \frac{1}{1+b}(b\sigma_2 + \sigma_3) = \sigma_s, \qquad \sigma_2 \leq \frac{\sigma_1 + \sigma_3}{2}$$

(Extended tension stress state)   (4.17a)

$$F' = \frac{1}{1+b}(\sigma_1 + b\sigma_2) - \sigma_3 = \sigma_s, \qquad \sigma_2 \geq \frac{\sigma_1 + \sigma_3}{2}$$

(Extended compression stress state) (4.17b)

in which *b* is a parameter that reflects the influence of the intermediate principal shear stress τ_{12} or τ_{23} on material strength. It can be determined from the shear yield strength τ_y and the tensile strength σ_y of the materials.

In the general case, the unified yield criterion can be expressed by 12 equations as follows:

$$f = \sigma_1 - \frac{1}{1+b}(b\sigma_2 + \sigma_3) = \pm\sigma_y \; ; \quad f = \sigma_1 - \frac{1}{1+b}(\sigma_2 + b\sigma_3) = \pm\sigma_y$$

$$f = \sigma_2 - \frac{1}{1+b}(b\sigma_1 + \sigma_3) = \pm\sigma_y \; ; \quad f = \sigma_2 - \frac{1}{1+b}(\sigma_1 + b\sigma_3) = \pm\sigma_y \qquad (4.18)$$

$$f = \sigma_3 - \frac{1}{1+b}(b\sigma_2 + \sigma_1) = \pm\sigma_y \; ; \quad f = \sigma_3 - \frac{1}{1+b}(\sigma_2 + b\sigma_1) = \pm\sigma_y$$

The single-shear criterion (Tresca yield criterion) and the twin-shear yield criterion are special cases of the unified yield criterion when $b=0$ and $b=1$, respectively. The Huber-von Mises criterion can be approximated by the unified yield criterion by letting $b=0.5$. In fact, the unified yield criterion contains a series of yield criteria that vary the parameter b. The unified yield criterion with $b=0$, $b=1/4$, $b=1/2$, $b=3/4$ and $b=1$ can be adapted to most kinds of metallic materials whose tensile strengths are the same as their compressive strength.

The relations between the tensile yield stress σ_y, shear yield stress τ_y and the parameter b in the unified yield criterion ($\alpha=1$) can be determined from the ratio of shear yield stress to tensile yield stress

$$b = \frac{2\tau_y - \sigma_y}{\sigma_y - \tau_y}, \qquad (4.19)$$

or

$$\tau_y = \frac{b+1}{b+2}\sigma_y$$

Inversely, the ratio of shear yield stress to tensile yield stress can be given as

$$\alpha_\tau = \frac{\tau_y}{\sigma_y} = \frac{b+1}{b+2} \qquad (4.20)$$

Some conclusions for non-SD materials can be made from this condition:

1) The shear yield stress is lower than tensile yield stress for metallic materials.

2) Yield surfaces are convex when $0 \le b \le 1$ or $1/2 \le \alpha_\tau \le 2/3$.

3) Yield surfaces are nonconvex when $b<0$ and $b>1$, or the ratio of shear yield stress to tensile yield stress is $\alpha_\tau = \tau_y/\sigma_y < 1/2$ and $\alpha_\tau = \tau_y/\sigma_y > 2/3$.

For example, if the ratio of the shear yield stress to the tensile yield stress of the material is $\alpha_\tau = \tau_y/\sigma_y = 0.45$, it can be determined from Eq. (4.19) that the parameter $b = -1/6$. This means that the yield criterion is nonconvex.

● α=1/2, New Series of Failure Criteria

The main disadvantage of the unified yield criterion is that it is only suitable for metallic materials having the same strength both in tension and in compression. It cannot adapt to those materials that have a different strength in tension and compression, or in cases where the strength is pressure dependent, such as iron, high-strength steels, polymers and geomaterials. This can be solved by using the unified strength theory with $0<\alpha<1$. A series of failure criteria can be obtained from the unified strength theory with $0<\alpha<1$ (Fig. 4.5). For an example, we take $\alpha=1/2$. A new series of failure criteria can be obtained as

$$F = \sigma_1 - \frac{1}{1+b}(b\sigma_2 + \sigma_3) = \sigma_t, \quad \text{when} \quad \sigma_2 \le \frac{\sigma_1 + \alpha\sigma_3}{1+\alpha}$$

$$\text{(Extended tension stress state)} \qquad (4.21a)$$

$$F' = \frac{1}{1+b}(\sigma_1 + b\sigma_2) - \frac{1}{2}\sigma_3 = \sigma_t, \quad \text{when} \quad \sigma_2 \ge \frac{\sigma_1 + \alpha\sigma_3}{1+\alpha}$$

$$\text{(Extended compression stress state)} \qquad (4.21b)$$
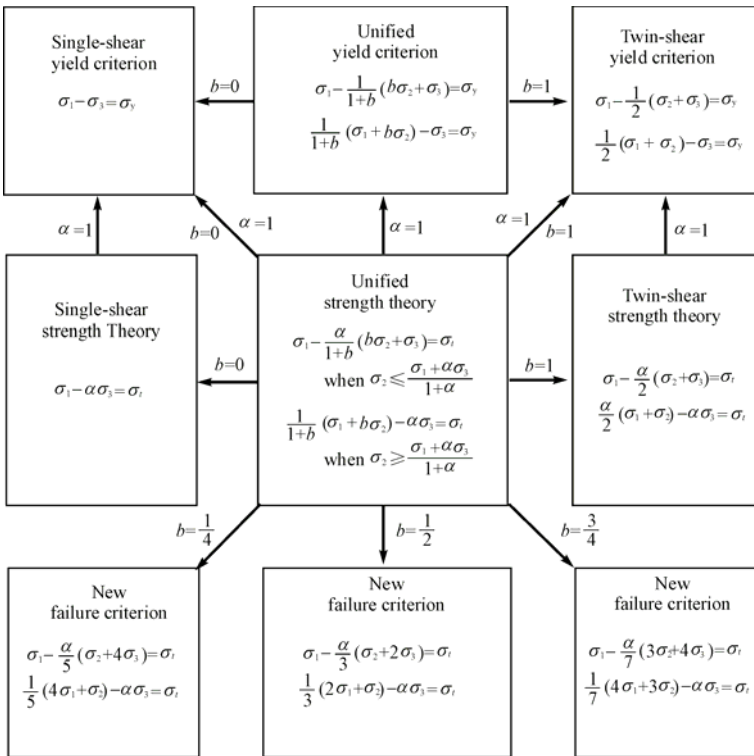
Fig. 4.5 Unified strength theory and its special cases

Figure 4.5 shows the relationship between the unified yield criterion, the unified strength theory, the single-shear yield criterion (the Tresca yield criterion), the single-shear strength theory (the Mohr-Coulomb strength theory), the twin-shear yield criterion (Yu, 1961), the twin-shear strength theory (Yu, 1985) as well as some new failure criteria. A great number of new failure criteria can be introduced from the Yu unified strength theory. Three new failure criteria are introduced from the Yu unified strength theory when $b=1/4$, $b=1/2$ and $b=3/4$, as shown in the third range in Fig. 4.5.

4.6 Other Formulations of the UST and Material Parameters

The use of a yield function is always connected to the material parameter. These parameters are required to be simple and easy to obtain. The uniaxial tensile strength σ_y is used for the material parameter in the Tresca yield criterion (1864), the Huber-von Mises yield criterion (1904; 1913) and the twin-shear yield criterion (Yu, 1961). It is the same for the unified strength theory in the case of $\alpha=1$. The Tresca criterion, the Huber-von Mises criterion and the twin-shear stress criterion can be suitable for those materials that have identical strength both in tension and compression and have the ratio $\alpha_\tau=\tau_y/\sigma_y=0.5$, $\alpha_\tau=\tau_y/\sigma_y=0.577$ and $\alpha_\tau=\tau_y/\sigma_y=0.667$.

The uniaxial tensile strength σ_t and the ratio of tension strength and compression strength α are used for the Mohr-Coulomb strength theory, the Drucker-Prager criterion and the twin-shear strength theory. They are two-parameter criteria. The two parameters in the unified strength theory are the same as these two material parameters. The other material parameters are also used in different applications. It needs some transfer of the mathematical expressions of the yield function.

The unified strength theory expressed in terms of principal stresses has been described in Eq. (4.9). The materials parameters are uniaxial tensile strength σ_t and the ratio of tension strength and compression strength α. Other material parameters can also be used.

4.6.1   *UST with Principal Stress and Compressive Strength*
$$F(\sigma_1, \sigma_2, \sigma_3, \alpha, \sigma_c)$$

In soil and rock mechanics and engineering, the compressive strength σ_c is often adopted. Rewriting Eqs. (4.9a) and (4.9b) in terms of the principal stress and compressive strength σ_c, we have

$$F = \frac{1}{\alpha}\sigma_1 - \frac{1}{1+b}(b\sigma_2 + \sigma_3) = \sigma_c \ , \quad \text{when} \quad \sigma_2 \le \frac{\sigma_1 + \alpha\sigma_3}{1+\alpha} \qquad (4.24a)$$

$$F' = \frac{1}{\alpha(1+b)}(\sigma_1 + b\sigma_2) - \sigma_3 = \sigma_c , \quad \text{when} \quad \sigma_2 \ge \frac{\sigma_1 + \alpha\sigma_3}{1+\alpha} \qquad (4.24b)$$

The unified strength theory can also be expressed in terms of another material parameter *m* as follows:

$$\sigma_1 - \frac{1}{m(1+b)}(b\sigma_2 + \sigma_3) = \sigma_t \qquad (\sigma_2 \le \frac{m\sigma_1 + \sigma_3}{m+1}) \qquad (4.25a)$$

$$\frac{1}{1+b}(\sigma_1 + b\sigma_2) - \frac{\sigma_3}{m} = \sigma_t \qquad (\sigma_2 \ge \frac{m\sigma_1 + \sigma_3}{m+1}) \qquad (4.25b)$$

where $m = \sigma_c/\sigma_t$ is the compressive-tensile strength ratio of the material. The ratio *m* is an index of the material strength difference effect and $m \ge 1$ in general. The unified strength theory can also be expressed by other terms.

4.6.2 UST with Stress Invariant and Tensile Strength $F(I_1, J_2, \theta, \sigma_t, \alpha)$

The principal stress state (σ_1, σ_2, σ_3) can be converted into the principal shear stress state (τ_{13}, τ_{12}, τ_{23}), invariates of stress tensor (I_1, I_2, I_3) or invariates of stress tensor (I_1, I_2, I_3). The principal shear stress state can be described in terms of the stress invariant.

The unified strength theory can also be expressed in terms of stress invariant $F(I_1, J_2, \theta)$ and materials σ_t, α as

$$F = (1-\alpha)\frac{I_1}{3} + \frac{\alpha(1-b)}{1+b}\sqrt{J_2}\sin\theta + (2+\alpha)\sqrt{\frac{J_2}{3}}\cos\theta = \sigma_t, 0° \le \theta \le \theta_b \quad (4.26a)$$

$$F' = (1-\alpha)\frac{I_1}{3} + \left(\alpha + \frac{b}{1+b}\right)\sqrt{J_2}\sin\theta + \left(\frac{2-b}{1+b}+\alpha\right)\sqrt{\frac{J_2}{3}}\cos\theta = \sigma_t, \theta_b \le \theta \le 60° (4.26b)$$

where I_1 is the first stress invariant (hydrostatic pressure), J_2 is the second deviatoric stress invariant and θ is the stress angle corresponding to the twin-shear parameter $\mu_\tau = \tau_{12}/\tau_{23}$ or $\mu_\tau' = \tau_{23}/\tau_{13}$. The stress angle at the corner θ_b can be determined by the condition $F = F'$.

$$\theta_b = \text{arctg} \frac{\sqrt{3}(1+\beta)}{3-\beta}, \quad \beta = \frac{1-\alpha}{1+\alpha} \tag{4.27}$$

4.6.3   UST with Stress Invariant and Compressive Strength $F(I_1, J_2, \theta, \alpha, \sigma_c)$

The unified strength theory can also be expressed in terms of stress invariant $F(I_1, J_2, \theta)$ and materials α, σ_c as

$$F = \frac{1-\alpha}{3\alpha} I_1 + \frac{1-b}{1+b}\sqrt{J_2}\sin\theta + \frac{2+\alpha}{\alpha\sqrt{3}}\sqrt{J_2}\cos\theta = \sigma_c, \quad 0° \le \theta \le \theta_b \tag{4.28a}$$

$$F' = \frac{1-\alpha}{3\alpha} I_1 + \frac{\alpha+\alpha b+b}{\alpha(1+b)}\sqrt{J_2}\sin\theta + \frac{2+\alpha+\alpha b-b}{\alpha\sqrt{3}(1+b)}\sqrt{J_2}\cos\theta = \sigma_c, \theta_b \le \theta \le 60° \tag{4.28b}$$

4.6.4   UST with Principal Stress and Cohesive Parameter $F(\sigma_1, \sigma_2, \sigma_3, C_0, \varphi)$

In Eqs. (4.9a) and (4.9b), we adopt the material constants σ_t and the tension-compression ratio α. In geotechnical engineering, the cohesion C_0 and the friction angle coefficient φ reflecting the material properties are used. The relationships between the tensile strength σ_t, the tension-compression ratio α, the material parameter C_0 and φ can be obtained as

$$\sigma_t = \frac{2C_0 \cdot \cos\varphi}{1+\sin\varphi}, \qquad \alpha = \frac{1-\sin\varphi}{1+\sin\varphi} \tag{4.29}$$

By substituting Eq. (4.29) into Eqs. (4.9a) and (4.9b), the Yu unified strength theory can be expressed in terms of C_0 and φ as

$$F = \sigma_1 - \frac{1-\sin\varphi}{(1+b)(1+\sin\varphi)}(b\sigma_2 + \sigma_3) = \frac{2C_0\cos\varphi}{1+\sin\varphi},$$

$$\text{when} \quad \sigma_2 \le \frac{1}{2}(\sigma_1 + \sigma_3) - \frac{\sin\varphi}{2}(\sigma_1 - \sigma_3) \tag{4.30a}$$

$$F' = \frac{1}{1+b}(\sigma_1 + b\sigma_2) - \frac{1-\sin\varphi}{1+\sin\varphi}\sigma_3 = \frac{2C_0\cos\varphi}{1+\sin\varphi},$$

$$\text{when } \sigma_2 \geq \frac{1}{2}(\sigma_1 + \sigma_3) - \frac{\sin\varphi}{2}(\sigma_1 - \sigma_3) \qquad (4.30\text{b})$$

4.6.5 UST with Stress Invariant and Cohesive Parameter $F(I_1, J_2, \theta, C_0, \varphi)$

The unified strength theory can be also expressed by the stress invariant, stress angle and material parameters cohesion C_0 and friction angle φ.

$$F = \frac{2I_1}{3}\sin\varphi + \frac{2\sqrt{J_2}}{1+b}\left[\sin\left(\theta + \frac{\pi}{3}\right) - b\sin\left(\theta - \frac{\pi}{3}\right)\right] + \frac{2\sqrt{J_2}}{(1+b)\sqrt{3}} \times$$

$$\left[\sin\varphi\cos\left(\theta + \frac{\pi}{3}\right) + b\sin\varphi\cos\left(\theta - \frac{\pi}{3}\right)\right] = 2C_0\cos\varphi, \quad 0° \leq \theta \leq \theta_b \quad (4.31\text{a})$$

$$F' = \frac{2I_1}{3}\sin\varphi + \frac{2\sqrt{J_2}}{1+b}\left[\sin\left(\theta + \frac{\pi}{3}\right) - b\sin\theta\right]$$

$$+ \frac{2\sqrt{J_2}}{(1+b)\sqrt{3}}\left[\sin\varphi\cos(\theta + \frac{\pi}{3}) + b\sin\varphi\cos\theta\right] = 2C_0\cos\varphi, \quad \theta_b \leq \theta \leq 60° \quad (4.31\text{b})$$

4.7 Other Material Parameters of the Unified Strength Theory

The unified strength theory in terms of three principal stresses, Eq. (4.9), is introduced from the mathematical modeling equation, Eq. (4.5) as

$$F = \tau_{13} + b\tau_{12} + \beta(\sigma_{13} + b\sigma_{12}) = C, \quad \text{when} \quad \tau_{12} + \beta\sigma_{12} \geq \tau_{23} + \beta\sigma_{23}$$

$$\text{(Extended tension stress state)} \qquad (4.5\text{a})$$

$$F' = \tau_{13} + b\tau_{23} + \beta(\sigma_{13} + b\sigma_{23}) = C, \quad \text{when} \quad \tau_{12} + \beta\sigma_{12} \leq \tau_{23} + \beta\sigma_{23}$$

$$\text{(Extended compression stress state)} \qquad (4.5\text{b})$$

The material parameters β and C are determined by experimental results of the uniaxial tension strength σ_t and uniaxial compression strength σ_c. The experimental conditions are

$$\sigma_1 = \sigma_t, \ \ \sigma_2 = \sigma_3 = 0 \ \ \text{(uniaxial tension)}$$
$$\sigma_1 = \sigma_2 = 0, \ \ \sigma_3 = -\sigma_c \ \ \text{(uniaxial compression)} \tag{4.32}$$

So the material constants β and C can be determined.

The material parameters β and C can be determined also by other experimental results. A lot of experimental results may be used for the determination of the material parameter in the unified strength theory.

4.7.1   Material Parameters β and C are Determined by Experimental Results of Uniaxial Tension Strength σ_t and Shear Strength τ_0

The material parameters β and C of the unified strength theory can be determined by experimental results of uniaxial tension strength σ_t and pure shear strength τ_0. The experimental conditions are

$$\sigma_1 = \sigma_t, \ \ \sigma_2 = \sigma_3 = 0 \ \ \text{(uniaxial tension)}$$
$$\sigma_1 = -\sigma_3 = 0, \ \ \sigma_2 = \tau_0 \ \ \text{(pure shear)} \tag{4.33}$$

4.7.2   Material Parameters β and C are Determined by Experimental Results of Uniaxial Compressive Strength σ_c and Shear Strength τ_0

The material parameters β and C of the unified strength theory can be determined by experimental results of the uniaxial compressive strength σ_c and pure shear strength τ_0. The experimental conditions are

$$\sigma_1 = \sigma_2 = 0, \ \ \sigma_3 = -\sigma_c \ \ \ \text{(uniaxial compression)}$$
$$\sigma_1 = -\sigma_3 = 0, \ \ \sigma_2 = \tau_0 \ \ \ \text{(pure shear)} \tag{4.34}$$

4.7.3 Material Parameters β and C are Determined by Experimental Results of Uniaxial Compressive Strength σ_c and Biaxial Compressive Strength σ_{cc}

The material parameters β and C of the unified strength theory can be determined by experimental results of the uniaxial tension strength σ_t and biaxial compressive strength σ_{cc}. The experimental conditions are

$$\sigma_1 = \sigma_2 = 0, \ \sigma_3 = -\sigma_c \quad \text{(uniaxial compression)}$$
$$\sigma_1 = 0, \ \sigma_2 = \sigma_3 = \sigma_{cc} \quad \text{(biaxial compression)} \tag{4.35}$$

4.7.4 Material Parameters β and C are Determined by Experimental Results of Uniaxial Compressive Strength σ_c and Biaxial Compressive Strength σ_{cc}

The material parameters β and C of the unified strength theory can be determined by experimental results of the uniaxial tension strength σ_t and biaxial compressive strength σ_{cc}. The experimental conditions are

$$\sigma_1 = \sigma_t, \ \sigma_2 = \sigma_3 = 0 \quad \text{(uniaxial tension)}$$
$$\sigma_1 = 0, \ \sigma_2 = \sigma_3 = \sigma_{cc} \quad \text{(biaxial compression)} \tag{4.36}$$

4.7.5 Material Parameters β and C are Determined by Experimental Results of Uniaxial Compressive Strength σ_c and Biaxial Compressive Strength σ_{cc}

The material parameters β and C of the unified strength theory can be determined by experimental results of the pure shear strength τ_0 and biaxial compressive strength σ_{cc}. The experimental conditions are

$$\sigma_1 = -\sigma_3 = 0, \ \sigma_2 = \tau_0 \quad \text{(pure shear)} \tag{4.37}$$
$$\sigma_1 = 0, \ \sigma_2 = \sigma_3 = \sigma_{cc} \quad \text{(biaxial compression)} \tag{4.38}$$

4.8 Three-Parameter Unified Strength Theory

The unified strength theory can be generalized as a three-parameter unified strength criterion. The mathematical modeling equation for the three-parameter unified strength criterion is

$$F = \tau_{13} + b\tau_{12} + \beta(\sigma_{13} + b\sigma_{12}) + A\sigma_m = C,$$

when $\tau_{12} + \beta\sigma_{12} \geq \tau_{23} + \beta\sigma_{23}$ (4.39a)

$$F' = \tau_{13} + b\tau_{23} + \beta(\sigma_{13} + b\sigma_{23}) + A\sigma_m = C,$$

when $\tau_{12} + \beta\sigma_{12} \leq \tau_{23} + \beta\sigma_{23}$ (4.39b)

where b is a parameter that reflects the influence of the intermediate principal shear stress τ_{12} or τ_{23} on the failure of the material; β is the coefficient that represents the effect of the normal stress on failure; σ_m is average stress; A is the coefficient that represents the effect of the average stress on failure; C is a strength parameter of the material; τ_{13}, τ_{12} and τ_{23} are principal shear stresses and σ_{13}, σ_{12} and σ_{23} are the corresponding normal stresses acting on the sections where τ_{13}, τ_{12} and τ_{23} act.

Another kind of three parameters criterion of the unified strength theory can be obtained by using the different parameters β_a and β_b. The mathematical modeling equation of this kind of three-parameter unified strength criterion is

$$F = \tau_{13} + b\tau_{12} + \beta_a(\sigma_{13} + b\sigma_{12}) = C, \quad \text{when} \quad \tau_{12} + \beta\sigma_{12} \geq \tau_{23} + \beta\sigma_{23} \quad (4.40a)$$

$$F' = \tau_{13} + b\tau_{23} + \beta_b(\sigma_{13} + b\sigma_{23}) = C, \quad \text{when} \quad \tau_{12} + \beta\sigma_{12} \leq \tau_{23} + \beta\sigma_{23} \quad (4.40b)$$

The three material parameters β, C and A or β_a, β_b and C can be determined by three experimental conditions. Interested readers can refer to the recent book (Yu, 2004).

4.9 Stress Space and Yield Loci of the UST

The yield criterion is a function of three principal stresses $\sigma_1, \sigma_2, \sigma_3$ as follows:

$$F = F(\sigma_1, \sigma_2, \sigma_3, K_1, K_2) = 0 \quad (4.41)$$

It can be interpreted for an isotropic material in terms of a geometrical representation of the stress state obtained by taking the principal stresses as coordinates, as shown in Fig. 4.6. The yield surface in a three-dimensional principal stress space was introduced by Haigh and Westergaard in 1920.

Sometimes it is called the Haigh-Westergaard space. The advantage of such a space lies in its simplicity and visual presentation.

The three-dimensional principal stresses (σ_1, σ_2, σ_3) can be regarded as a three-dimensional space of principal stresses. If we take the tensile stress as positive while taking the compressive stress as negative, the stress state may combine the space stresses into various magnitudes and signs of stress combinations. The stress point $P(\sigma_1, \sigma_2, \sigma_3)$ of different signs could combine up to eight quadrants of $(+ + +)$, $(+ + -)$, $(+ - +)$, $(+ - -)$, $(- + +)$, $(- + -)$, $(- - +)$ and $(- - -)$. A stress point could be situated anywhere within the three-dimensional space of the principal stresses.

In stress space the yield criterion defines a surface that is generally referred to as the yield surface. If a stress point is situated in the yield surface, it means the yield function $f < 0$ and the material will be elastic; if a stress point reaches the yield surface, it means the yield function $f = 0$ and yield of the material will occur.

The state of stress at any point in a body or a structure may be represented by a vector emanating from the origin O (Fig. 4.6). The isoclinic axis ON is equally inclined to the three axes and its direction cosines are $(1/\sqrt{3}, 1/\sqrt{3}, 1/\sqrt{3})$. The stress vector Or, whose stress components are (σ_1, σ_2, σ_3), may be resolved into a vector OO' along isoclinic axis ON and a vector Or_0 in a plane that is perpendicular to ON and passes through the origin. The vector OO' is of magnitude $\sqrt{3}\sigma_m$ and represents the hydrostatic stress with components (σ_m, σ_m, σ_m). The vector Or_0 represents the deviatoric stress with components $f(S_1, S_2, S_3)$ and magnitude $\sqrt{2J_2}$. For any given state of stress, the deviatoric stress vector will lie in the plane passing through O and perpendicular to ON. This plane is known as the deviatoric plane in stress space or the π_0-plane. Its equation is $\sigma_1 + \sigma_2 + \sigma_3 = 0$ in the principal stress space. The planes that are parallel to the π_0-plane are called the π-planes and are given by $\sigma_1 + \sigma_2 + \sigma_3 = C$, where C is a constant.

If a hydrostatic stress has no effect on yielding, it follows that yielding can depend only on the magnitude and the direction of the deviatoric stress vector Or_0 in the π_0-plane or the deviatoric stress vector $O'r$ in the π-plane. The yield surfaces are therefore regarded as a prismatic surface whose generators are perpendicular to the deviatoric plane. Any stress state in which the stress point lies on the prismatic surface corresponds to a state of yielding. Any point inside the prismatic surface represents an elastic state of stress.

The general shape of a yield surface in a three-dimensional stress space for metallic materials with the same strength both in tension and in compression can best be determined by its cross-sectional shapes in the deviatoric planes, because the shapes on any π-plane are identical. The cross sections of the yield surface are the intersection of the yield surface with the deviatoric plane, called the yield locus.
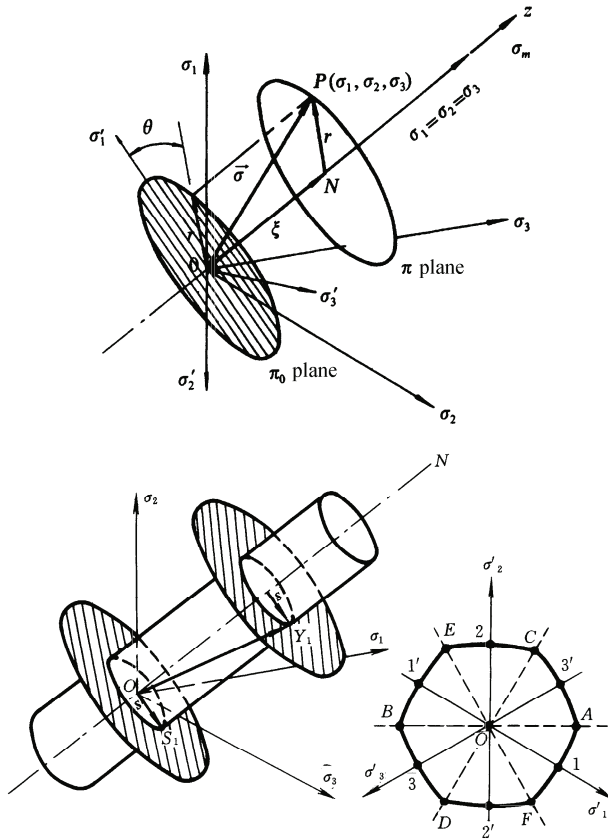
Fig. 4.6 Cylindrical coordinates and a yield surface for metal in principal stress space

Considering the yield locus together with the orthogonal projections of the stress axes on the deviatoric plane, the yield locus is symmetrical with respect to the projections of the σ_1, σ_2, σ_3 axes. The yield locus, therefore, is threefold symmetric. The yield loci on the deviatoric plane, the axes x, y and projections of the stress axes σ_1', σ_2', σ_3' are taken in the plane of the paper (Fig. 4.6).

The relationship between the coordinates of the deviatoric plane and hydrostatic stress axis z with the principal stresses are

$$x = \frac{1}{\sqrt{2}}(\sigma_3 - \sigma_2), \quad y = \frac{1}{\sqrt{6}}(2\sigma_1 - \sigma_2 - \sigma_3), \quad z = \frac{1}{\sqrt{3}}(\sigma_1 + \sigma_2 + \sigma_3) \qquad (4.42)$$

$$\sigma_1 = \frac{1}{3}(\sqrt{6}y + \sqrt{3}z), \quad \sigma_2 = \frac{1}{6}(2\sqrt{3}z - \sqrt{6}y - 3\sqrt{2}x),$$

$$\sigma_3 = \frac{1}{6}(3\sqrt{2}x - \sqrt{6}y + 2\sqrt{3}z) \qquad (4.43)$$

The ratio between the tensile radius and the compressive radius in π plane is given by

$$K = \frac{r_t}{r_c} = \frac{1+2\alpha}{2+\alpha} = \frac{3-\sin\phi}{3+\sin\phi} \tag{4.44}$$

By substituting Eq. (4.49) into the unified strength theory Eq. (4.25a) and (4.25b), the equations of the unified strength theory in the deviatoric plane can be obtained.

$$F = -\frac{\sqrt{2}(1-b)}{2(1+b)}ax + \frac{\sqrt{6}(2+\alpha)}{6}y + \frac{\sqrt{3}(1-\alpha)}{3}z = \sigma_t \tag{4.45a}$$

$$F' = -(\frac{b}{1+b}+\alpha)\frac{\sqrt{2}}{2}x + (\frac{2-b}{1+b}+\alpha)\frac{\sqrt{6}}{6}y + \frac{\sqrt{3}(1-\alpha)}{3}z = \sigma_t \tag{4.45b}$$

A great number of new failure criteria can be generated from the unified strength theory by changing α and b. The shape and size of yield loci of the unified strength theory are changed with α, b and hydrostatic stress axis z. The shape of yield loci is similar for certain values of α and b, but the size of the yield loci is changed with hydrostatic stress σ_m.

The variation in the unified strength theory with b is shown in Fig. 4.7. Ten special cases with values of $b=0$, $b=0.1$, $b=0.2$, $b=0.3$, $b=0.4$, $b=0.5$, $b=0.6$, $b=0.7$, $b=0.8$, $b=0.9$ and $b=1$ are given.

The two bounds of convex yield loci are the Mohr-Coulomb theory and the twin-shear strength theory proposed by Yu in 1985. The yield locus of the twin-shear strength theory is the upper bound of the convex yield loci, as shown in Fig. 4.7(a).
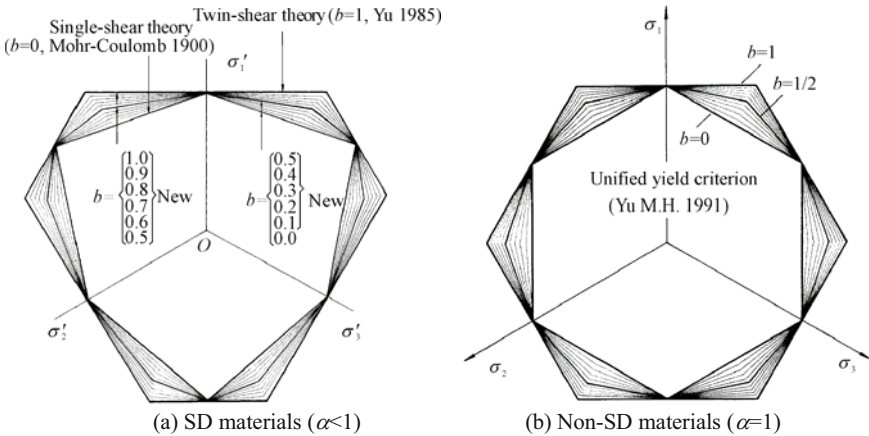

(a) SD materials ($\alpha<1$)   (b) Non-SD materials ($\alpha=1$)

Fig. 4.7 A serial yield loci of the unified strength theory (Yu, 1992)

The single-shear strength theory, the twin-shear strength theory and a series of new failure criteria can be obtained from the unified strength theory in the range of $0 \leq b \leq 1$, $0 \leq \alpha \leq 1$. The smooth-ridge models can also be approximated by the unified strength theory when $b = 1/2$ or $b = 3/4$.

The convex failure criteria can be obtained by varying the value of α ($\alpha < 1$) and b ($0 \leq b \leq 1$).

If $\alpha = \sigma_t / \sigma_c = 1$, that is the tensile strength equals the compression strength, then the radii r of the yield locus of the unified strength theory on the axes σ_1, σ_2, σ_3 and $-\sigma_1$, $-\sigma_2$, $-\sigma_3$ are identical. The ratio between the tensile radius and the compressive radius is given by

$$K = \frac{1+2\alpha}{2+\alpha} = \frac{3-\sin\phi}{3+\sin\phi} = 1$$

which means that the irregular dodecahedron is converted to a regular dodecahedron, and the yield surfaces of the unified yield criterion for $\alpha = \sigma_t / \sigma_c = 1$ materials change to a series of infinite prisms.

A new unified yield criterion can be deduced from Eqs. (4.45a) and (4.45b). The equations of the unified yield criterion for $\alpha = \sigma_t / \sigma_c = 1$ materials on the deviatoric plane can be obtained as follows.

$$F = -\frac{\sqrt{2}(1-b)}{2(1+b)}x + \frac{\sqrt{6}}{2}y = \sigma_t \qquad (4.46a)$$

$$F' = -\frac{\sqrt{2}(1+2b)}{2(1+b)}x + \frac{\sqrt{6}}{2(1+b)}y = \sigma_t \qquad (4.46b)$$

A series of yield loci for $\alpha = \sigma_t / \sigma_c = 1$ materials with $b=0$, $b=0.1$, $b=0.2$, $b=0.3$, $b=0.4$, $b=0.5$, $b=0.6$, $b=0.7$, $b=0.8$, $b=0.9$ and $b=1$ on the deviatoric plane can be obtained as shown in Fig. 4.7(b).

4.10 Yield Surfaces of the UST in Principal Stress Space

The yield surfaces in the stress space of the unified strength theory are usually a semi-infinite hexagonal cone with unequal sides and a dodecahedron cone with unequal sides, as shown in Fig. 4.8. The shape and size of the yield hexagonal cone depends on the parameter b and on the tension-compression strength ratio α. The 3D computer images of the yield surface for the unified strength theory in the stress space were provided by Zhang (2005), as shown in Fig. 4.8 and Fig. 4.9.
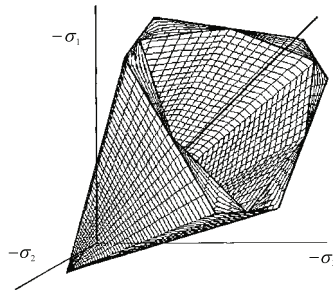
Fig. 4.8 Yield surfaces of the unified strength theory in stress space

In engineering practice, the compressive strength of materials σ_c is often much greater than the tensile strength σ_t, since a region in tension becomes smaller, while it becomes larger in compression. Assuming the compressive strength is positive, the yield surfaces of the UST (unified strength theory) with different values of b are shown in Fig. 4.8. Figure 4.9 shows the three typical yield surfaces of the unified strength theory with $b=0$, $b=1/2$, and $b=1$, respectively. The latter is the yield surface of the twin-shear strength theory (Yu, 1985).

(a) $b=0$ (lower bound)

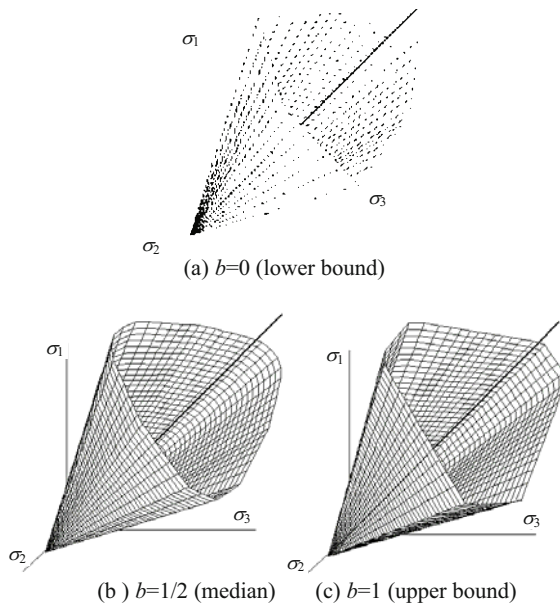(b) $b=1/2$ (median)   (c) $b=1$ (upper bound)

Fig. 4.9 Three typical yield surfaces of the unified strength theory

A unified yield criteria can be deduced from the unified strength theory when $\alpha=1$ as follows.

$$f = \sigma_1 - \frac{1}{1+b}(b\sigma_2 + \sigma_3) = \sigma_y , \quad \text{when} \quad \sigma_2 \leq \frac{\sigma_1 + \sigma_3}{2} \quad (4.47a)$$

$$f' = \frac{1}{1+b}(\sigma_1 + b\sigma_2) - \sigma_3 = \sigma_y , \quad \text{when} \quad \sigma_2 \geq \frac{\sigma_1 + \sigma_3}{2} \quad (4.47b)$$

Their yield loci of the unified yield criterion for $\alpha = \sigma_t / \sigma_c = 1$ materials in the π-plane have been shown in Fig. 4.8.

Five typical yield surfaces and yield loci in the π-plane for metallic materials can be obtained from the unified yield criterion Eqs. (4.17a) and (4.17b) when α =1 and b=0, b=1/4, b =1/2, b =3/4 and b =1 as shown in Figs. 4.10(a), 4.10(b), 4.11(a), 4.12(a), 4.12(b). The yield surfaces and yield loci in the π-plane of the Huber-von Mises criterion are also given in Fig. 4.11(b).
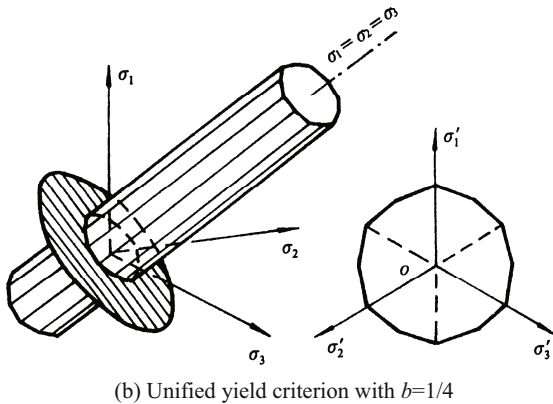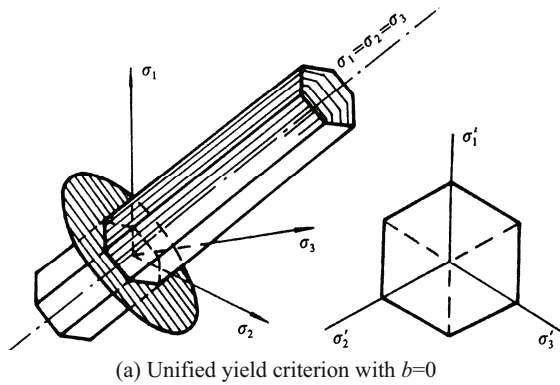

(a) Unified yield criterion with b=0

(b) Unified yield criterion with b=1/4

Fig. 4.10 Yield surfaces and yield loci of two cases of UYC with b=0 and b=1/4

(a) Unified yield criterion with $b=1/2$
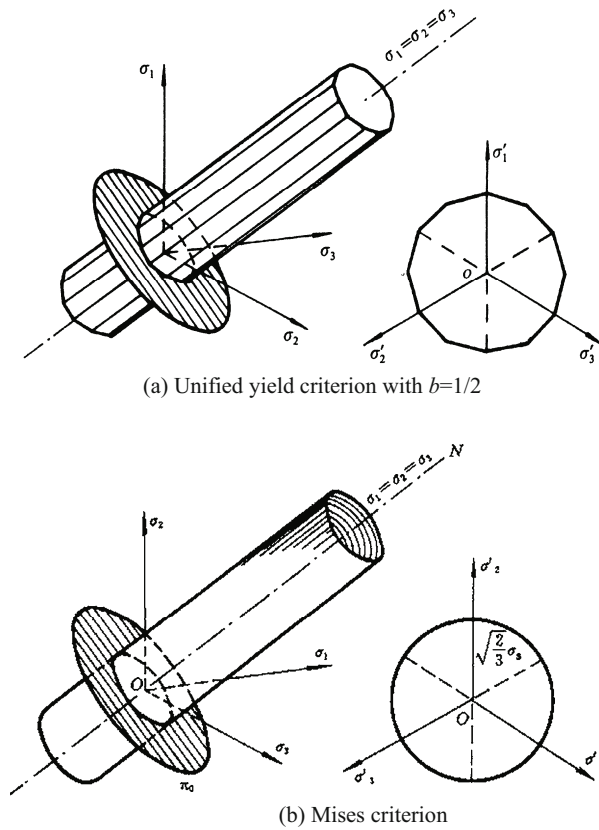
(b) Mises criterion

Fig. 4.11 Yield surfaces and yield loci of UYC with $b=1/2$ and the Mises criterion

Obviously, the middle yield surface and yield locus in the π-plane of the unified yield criterion with $b=1/2$ approximates to the yield surface and yield locus in the π-plane of the Huber-von Mises yield criterion. These two criteria are equivalent in engineering applications.

The middle yield surface and yield locus ($b=1/2$) are the new yield surface and locus, which intersect the yield surface and locus of the Huber-von Mises yield criterion. It may be referred to as the linear Huber-von Mises yield. The comparison of the linear von Mises yield loci ($b=1/2$) with the Huber-von Mises yield criterion in the π-plane is shown in Fig. 4.13.

(a) Unified yield criterion with b=3/4
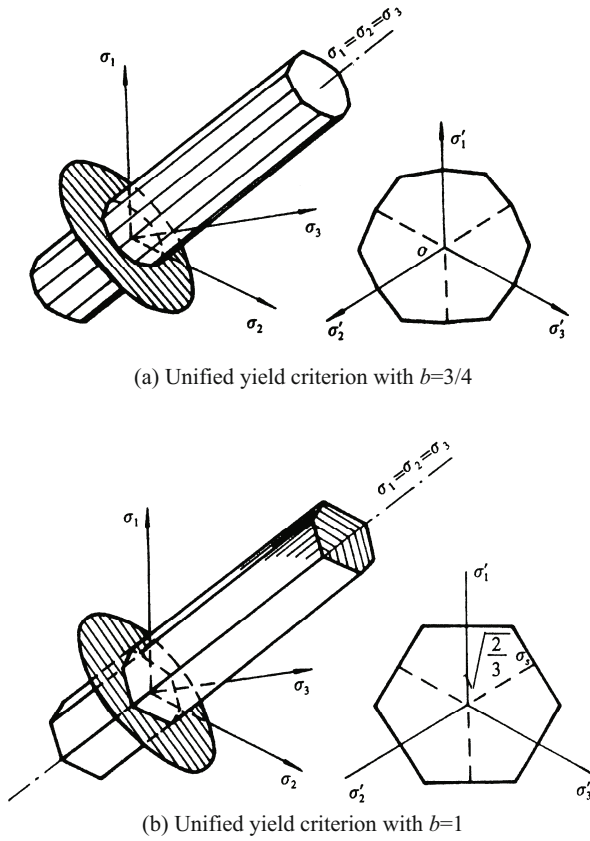

(b) Unified yield criterion with b=1

Fig. 4.12 Yield surfaces and yield loci of UYC with b=3/4 and b=1
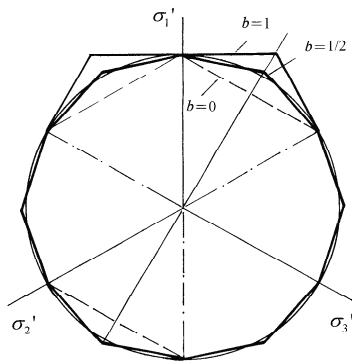

Fig. 4.13 Linear approximation to the Huber-von Mises yield criterion with the unified yield criterion when b=1/2

The variation of yield surfaces of the unified strength theory (UST) in the deviatoric plane with α and $k = \sqrt{3}\,\dfrac{1+b}{1+b+\alpha}$ is given by Kolupaev and Altenbach (2009), as shown in Fig. 4.14.
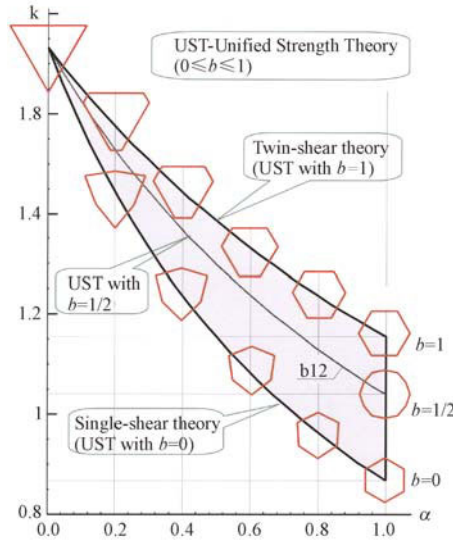

Fig. 4.14 Variation of the shape of yield loci of the unified strength theory with parameters b and α

The lower bound is provided by the single-shear strength theory (the Mohr-Coulomb strength theory, or the unified strength theory with $b=0$). The upper bound is given by the generalized twin-shear strength theory (Yu et al., 1985), or the unified strength theory with $b=1$. The median is a new series of yield criteria deduced from UST with $b=1/2$. Other series of new yield criteria can also be deduced from UST with $b=1/4$ or $b=3/4$, as shown in Fig. 4.7. All the convex yield surfaces are situated between two bounds of the twin-shear theory and the single-shear theory, as shown in Fig. 4.14 (Kolupaev and Altenbach, 2009; Yu et al., 2009).

4.11 Extend of UST from Convex to Non-Convex

The unified strength theory can be extended from convex loci to non-convex loci. The yield loci of UST are convex when the yield criterion parameter b ($0 \le b \le 1$) and the yield loci of UST are non-convex, when the yield criterion parameter $b < 0$

or $b>1$, as shown in Fig. 4.15. This behavior, however, has not been studied so far. It may be of mathematical significance.
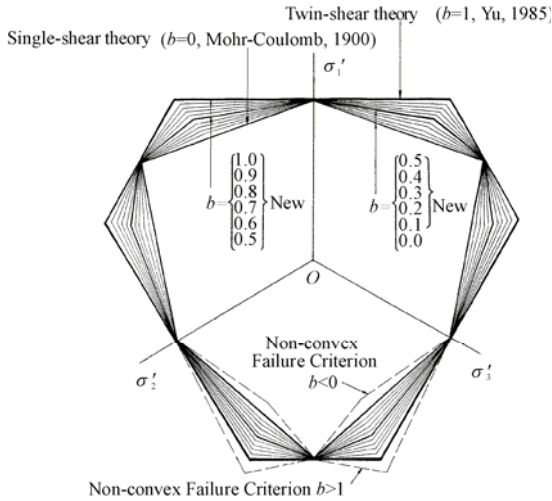
Fig. 4.15 Convex and non-convex yield loci of UST

4.12 Yield Loci of the UST in Plane Stress State

The yield loci of the unified strength theory in the plane stress state form the intersection line of the yield surface in the principal stress space and the σ_1-σ_2 plane. The shape and size depend on the values of b and α. This will be transformed into a hexagon when $b=0$ or $b=1$, and into a dodecagon when $0<b<1$.

The equations of the 12 yield loci of the unified strength theory in the plane stress state can be given as follows. A series of new failure criteria and new yield loci in the plane stress state can be obtained from the unified strength theory.

The yield loci of the unified strength theory (UST) in the plane stress state with different values of b are shown in Fig. 4.16(a) (for $\alpha=1/2$ material) and Fig. 4.16(b) (for $\alpha=1$ materials).

$$\sigma_1 - \frac{\alpha b}{1+b}\sigma_2 = \sigma_t \qquad\qquad \frac{\alpha}{1+b}(\sigma_1 + b\sigma_2) = \sigma_t$$

$$\sigma_2 - \frac{\alpha b}{1+b}\sigma_1 = \sigma_t \qquad\qquad \frac{\alpha}{1+b}(\sigma_2 + b\sigma_1) = \sigma_t$$

$$\sigma_1 - \frac{\alpha}{1+b}\sigma_2 = \sigma_t \qquad\qquad \frac{1}{1+b}\sigma_1 - \alpha\sigma_2 = \sigma_t$$

$$(4.48)$$

$$\sigma_2 - \frac{\alpha}{1+b}\sigma_1 = \sigma_t \qquad\qquad \frac{1}{1+b}\sigma_2 - \alpha\sigma_1 = \sigma_t$$

$$\frac{\alpha}{1+b}(b\sigma_1 + \sigma_2) = -\sigma_t \qquad\qquad \frac{b}{1+b}\sigma_1 - \alpha\sigma_2 = \sigma_t$$

$$\frac{\alpha}{1+b}(b\sigma_2 + \sigma_1) = -\sigma_t \qquad\qquad \frac{b}{1+b}\sigma_2 - \alpha\sigma_1 = \sigma_t$$

(a) $\alpha = 1/2$ material
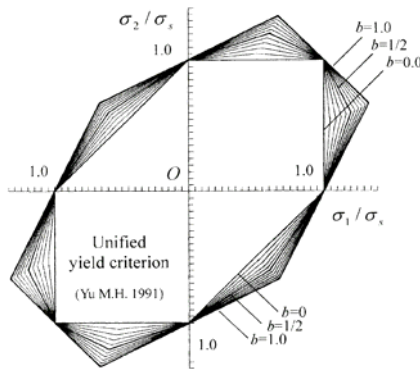
(b) $\alpha = 1$ material

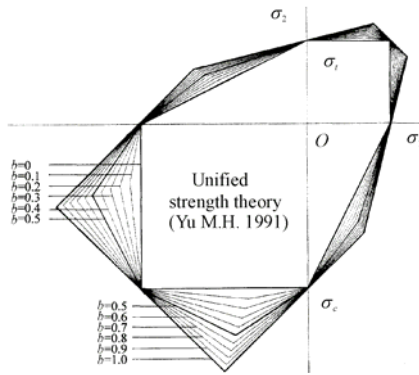**Fig. 4.16** Yield loci of the UST in the plane stress state

Various yield loci of the unified strength theory in the plane stress state are shown in Fig. 4.17. The unified yield criterion, the Mohr-Coulomb strength theory, the twin-shear strength theory and a series of new failure criteria, as well as the non-convex failure loci, can be obtained from the unified strength theory.

If the tensile strength is identical to the compressive strength, the unified strength theory will be transformed into the unified yield criterion. Its yield surfaces are described in Figs. 4.10, 4.11 and 4.12.

In the general case, the unified yield criterion for $\alpha = \sigma_t/\sigma_c = 1$ materials in the plane stress state (σ_1, σ_2) can be expressed by 12 equations as follows:
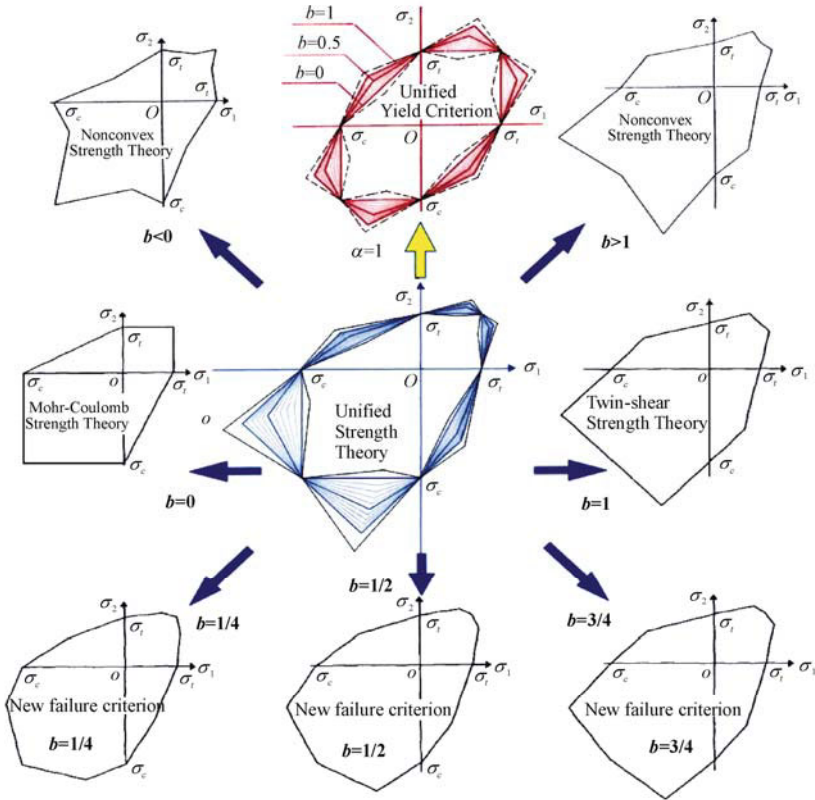
Fig. 4.17 Variation of the UST in the plane stress state

$$f_1 = \sigma_1 - \frac{b}{1+b}\sigma_2 = \pm\sigma_y; \qquad f_2 = \frac{b}{1+b}\sigma_1 - \sigma_2 = \pm\sigma_y$$

$$f_3 = \frac{1}{1+b}\sigma_1 + \frac{b}{1+b}\sigma_2 = \pm\sigma_y; \quad f_4 = \frac{b}{1+b}\sigma_1 + \frac{1}{1+b}\sigma_2 = \pm\sigma_y$$

$$f_5 = \sigma_1 - \frac{1}{1+b}\sigma_2 = \pm\sigma_y \;; \quad f_6 = \frac{1}{1+b}\sigma_1 - \sigma_2 = \pm\sigma_y \tag{4.49}$$

The yield loci of the unified yield criterion ($\alpha=1$) in the plane stress state with different values of b are shown in Fig. 4.18. A series of the yield loci of the unified yield criterion when $\alpha = \sigma_t/\sigma_c = 1$ in the plane stress state can be given, respectively. These yield loci cover all the regions of the convex yield criteria and also include the nonconvex yield criteria, which have never been formulated before. Varieties of the yield loci of the unified yield criterion in the plane stress states can be seen in Fig. 4.18.

Fig. 4.18 Varieties of the UST for $\alpha = \sigma_t/\sigma_c = 1$ materials in plane stress

4.13   Unified Strength Theory in Meridian Plane
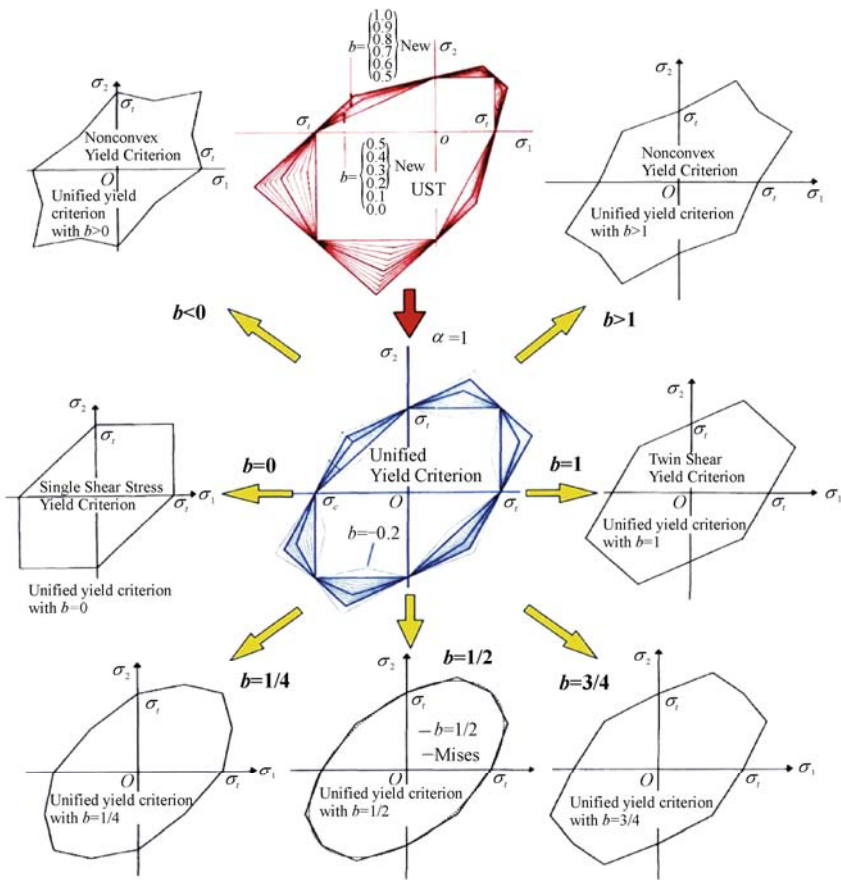
The unified strength theory can also be expressed in other terms, such as by the octahedral normal stress σ_8 and octahedral shear stress τ_8 in plasticity, or by the generalized normal stress σ_g and the generalized shear stress τ_g (or q) in soil mechanics and geomechanics.

The relationships between the three principal stresses σ_1, σ_2, σ_3 and the cylindrical polar coordinates ξ, r, θ in the principal stress space are

$$\begin{Bmatrix} \sigma_1 \\ \sigma_2 \\ \sigma_3 \end{Bmatrix} = \frac{1}{\sqrt{3}}\xi + \sqrt{\frac{2}{3}}r \begin{Bmatrix} \cos\theta \\ \cos(\theta - 2\pi/3) \\ \cos(\theta + 2\pi/3) \end{Bmatrix} \tag{4.50}$$

in which ξ is the major coordinate axis in the stress space and r is the length of the stress vector in the π-plane. They are shown as

$$\begin{aligned} \xi &= \frac{1}{\sqrt{3}}(\sigma_1 + \sigma_2 + \sigma_3) \\ r &= \frac{1}{\sqrt{3}}\sqrt{(\sigma_1 - \sigma_2)^2 + (\sigma_2 - \sigma_3)^2 + (\sigma_3 - \sigma_1)^2} \end{aligned} \tag{4.51}$$

The relationship among the various variables is

$$\begin{aligned} \xi &= \frac{1}{\sqrt{3}}I_1 = \sqrt{3}\sigma_8 = \sqrt{3}p = \sqrt{3}\sigma_m \\ r &= \sqrt{2J_2} = \sqrt{3}\tau_8 = \sqrt{\frac{2}{3}}q = 2\tau_m \end{aligned} \tag{4.52}$$

The principal stress can be expressed as

$$\begin{Bmatrix} \sigma_1 \\ \sigma_2 \\ \sigma_3 \end{Bmatrix} = \frac{1}{3}I_1 + \frac{2}{\sqrt{3}}\sqrt{J_2} \begin{Bmatrix} \cos\theta \\ \cos(\theta - 2\pi/3) \\ \cos(\theta + 2\pi/3) \end{Bmatrix};$$

$$\begin{Bmatrix} \sigma_1 \\ \sigma_2 \\ \sigma_3 \end{Bmatrix} = p + \frac{2}{3}q \begin{Bmatrix} \cos\theta \\ \cos(\theta - 2\pi/3) \\ \cos(\theta + 2\pi/3) \end{Bmatrix};$$

$$\begin{Bmatrix} \sigma_1 \\ \sigma_2 \\ \sigma_3 \end{Bmatrix} = \sigma_8 + \sqrt{2}\tau_8 \begin{Bmatrix} \cos\theta \\ \cos(\theta - 2\pi/3) \\ \cos(\theta + 2\pi/3) \end{Bmatrix};$$

or

$$\begin{Bmatrix} \sigma_1 \\ \sigma_2 \\ \sigma_3 \end{Bmatrix} = \sigma_m + \frac{2\sqrt{2}}{\sqrt{3}} \tau_m \begin{Bmatrix} \cos\theta \\ \cos(\theta - 2\pi/3) \\ \cos(\theta + 2\pi/3) \end{Bmatrix} \tag{4.53}$$

Substituting the above equations into the expression of the unified strength theory, the unified strength theory can then be expressed in other terms. Figure 4.19 shows the yield loci of the unified strength theory in the meridian plane with $\theta=0°$ and $\theta=60°$

The yield meridian loci with $\theta=0°$ and $\theta=60°$ are also called the tension yield meridian locus and the compression yield meridian locus, respectively. It is useful to understand the relationship for various kinds of equations, figures and tables.
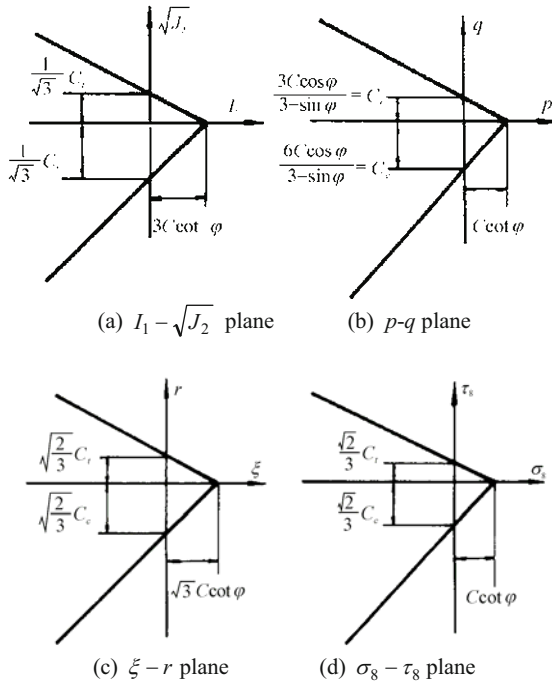

(a) $I_1 - \sqrt{J_2}$ plane　　(b) p-q plane

(c) $\xi - r$ plane　　(d) $\sigma_8 - \tau_8$ plane

Fig. 4.19 Yield loci of the UST in the meridian plane

In some books on soil mechanics and geomechanics, $(\sigma_1-\sigma_3)$ is often used as coordinate. Then the figure $(\sigma_1-\sigma_3)\sim p$ can be drawn. In the case of triaxial confined pressure experiments, the stress state is axisymmetric, i.e., $\sigma_2=\sigma_3$. The generalized shear stress q is

$$q = \sqrt{\frac{1}{2}[(\sigma_1 - \sigma_2)^2 + (\sigma_2 - \sigma_3)^2 + (\sigma_3 - \sigma_1)^2]} = \sigma_1 - \sigma_3 \qquad (4.54)$$

The $q\sim p$ coordinate and the $(\sigma_1-\sigma_3) \sim p$ coordinate are identical in the case of triaxial confined pressure. It is worth noting, however, that they are not identical in other cases.

4.14   Extend of UST from Linear to Non-Linear UST

The unified strength theory can also be extended into various multiple–parameter criteria for more complex conditions. The expressions are

$$F = \tau_{13} + b\tau_{12} + \beta_1(\sigma_{13} + b\sigma_{12}) + A_1\sigma_m + B_1\sigma_m^2 = C \qquad (4.55a)$$
$$F' = \tau_{13} + b\tau_{23} + \beta_2(\sigma_{13} + b\sigma_{23}) + A_2\sigma_m + B_2\sigma_m^2 = C \qquad (4.55b)$$

or

$$F = (\tau_{13} + \beta\sigma_{13})^2 + b(\tau_{12} + \beta\sigma_{12})^2 + A_1\sigma_m^2 = C \qquad (4.56a)$$
$$F' = (\tau_{13} + \beta\sigma_{13})^2 + b(\tau_{23} + \beta\sigma_{23})^2 + A_2\sigma_m^2 = C \qquad (4.56b)$$

Equations (4.55a) and (4.55b) can be simplified to the unified strength theory when $A_1=A_2=0$, $B_1=B_2=0$ and $\beta_1=\beta_2$. In this case, it becomes the single-shear strength theory (Mohr-Coulomb strength theory) when $b=0$, or the twin-shear strength theory when $b=1$.

When $A_1=A_2=0$, $B_1=B_2=0$ and $\beta_1=\beta_2=0$, Eqs. (4.55a) and (4.55b) are simplified to the unified yield criterion. In this case, the single-shear yield criterion (the Tresca yield criterion) and the twin-shear yield criterion are introduced when $b=0$ and $b=1$, respectively.

Equations (4.55a), (4.55b) and (4.56a), (4.56b) are nonlinear equations. It is not convenient for analytical solution in plasticity and engineering applications.

These formulations are the nonlinear unified strength theory. The non-linear yield surfaces of the three special cases ($b=0$, $b=1/2$, and $b=1$) of the unified strength theory can be drafted by computer. The 3D computer images of the yield surface for the unified strength theory in the stress space were given by Zhang (2005). These three special cases of the unified strength theory are the lower bound, the upper bound and the median criterion in entire convex criteria. They may be considered as the three basic criteria, as shown in Figs. 4.20, 4.21 and 4.22.

(a) Linear surface   (b) Non-linear surface
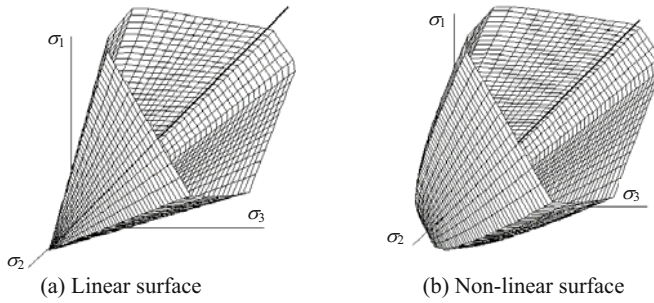
Fig. 4.20 Twin-shear strength theory (unified strength theory with *b*=1)

(a) Linear surface   (b) Non-linear surface

Fig. 4.21 Unified strength theory with *b*=1/2
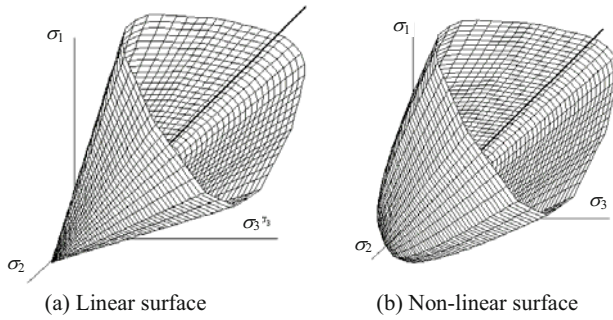
(a) Linear surface   (b) Non-linear surface

Fig. 4.22 Single-shear strength theory (unified strength theory with *b*=0, Mohr-Coulomb theory)

The comparison of the yield surfaces of the nonlinear unified strength theory with the linear unified strength theory are shown in Figs. 4.20, 4.21 and 4.22. The yield surface of the linear unified strength theory with $b=1$ (twin-shear strength theory, linear pressure sensitive) and the yield surface of the nonlinear twin-shear strength theory (nonlinear pressure sensitive) are shown in Fig. 4.20(a). It is a special case as shown in Fig. 4.20(b).
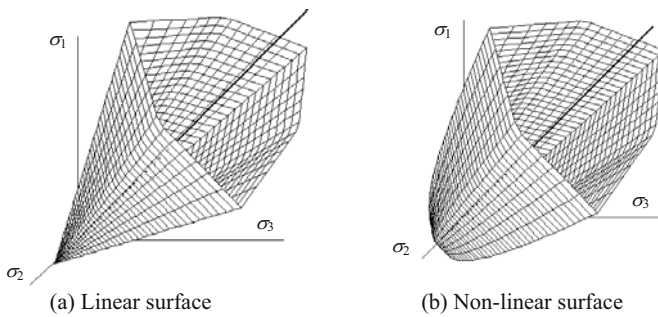
The yield surface of the linear unified strength theory with $b=1/2$ (linear pressure sensitive) and yield surface of the non-linear unified strength theory (nonlinear pressure sensitive) are shown in Figs. 4.21(a) and 1.21(b). The yield surface of the linear unified strength theory with $b=0$ (linear pressure sensitive) and yield surface of the non-linear unified strength theory (nonlinear pressure sensitive) are shown in Figs. 4.22(a) and 4.22(b).

4.15   Equivalent Stress of the Unified Strength Theory

A quantity called the equivalent stress is commonly used in solid mechanics and engineering computational codes. The definition of equivalent stress is very important for the calculation of elasto-plastic theory because the mathematical expression of yield criterion is usually same as the equivalent stress. When the equivalent stress σ^{eq} is less than the yield strength of material under uniaxial stress σ_y, i.e. $\sigma^{eq} < \sigma_y$ the material is elastic; when the equivalent stress σ^{eq} reaches or exceeds the yield strength of material under uniaxial stress, i.e. $\sigma^{eq} \geq \sigma_y$ the material yielding.

The introduction of the equivalent stress gives the possibility to compare multi-axial stress states with a uni-axial one. Unlike stress components, however, the equivalent stress has no direction. It is fully defined by magnitude with stress units. It is always to calculate the elastic limit and the factors of safety at different points. It provides adequate information to assess the safety of the design for many materials and structures. It is also convenient to use the equivalent stress in FE codes and computational plasticity. Application of finite element equivalent stress method is always used to analyze the strength of various structures.

The familiar equivalent stress is the von Mises equivalent stress σ^{eq}_{Mises}, it is also called the von Mises yield criterion, which states that a material starts to yield at a point when the equivalent stress of a three-shear stress function reaches the yield strength of the material, i.e. $\sigma^{eq}_{Mises}=\sigma_y$. However, the equivalent stress at a point does not uniquely define as the von Mises stress, a great of equivalent stresses for non-SD materials and SD materials have been proposed in the past. Several typed equivalent stresses are described below.

4.15.1 Equivalent Stresses for Non-SD Materials

Three typed equivalent stresses for non-SD materials are expressed as follows.
   1) Single-shear equivalent stress (Tresca equivalent stress)

$$\sigma^{eq}{}_{\text{Tresca}} = \sigma_1 - \sigma_3 \tag{4.57}$$

   2) Three-shear equivalent stress (Mises equivalent stress)

$$\sigma^{eq}{}_{\text{Mises}} = \frac{1}{\sqrt{2}} \left[(\sigma_1 - \sigma_3)^2 + (\sigma_1 - \sigma_2)^2 + (\sigma_2 - \sigma_3)^2 \right]^{1/2} \tag{4.58}$$

   3) Twin-shear equivalent stress (twin-shear yield criterion)

$$\sigma^{eq}{}_{\text{Twin-shear}} = \begin{cases} \sigma_1 - \dfrac{1}{2}(\sigma_2 + \sigma_3), & \text{when } \ \sigma_2 \le \dfrac{\sigma_1 + \sigma_3}{2} \\[2mm] \dfrac{1}{2}(\sigma_1 + \sigma_2) - \sigma_3, & \text{when } \ \sigma_2 \ge \dfrac{\sigma_1 + \sigma_3}{2} \end{cases} \tag{4.59}$$

4.15.2 Equivalent Stresses for SD Materials

Lower and upper bounds of equivalent stresses for SD materials are
   1) Lower bound: Single-shear equivalent stress (Mohr-Coulomb equivalent stress)

$$\sigma^{eq}{}_{\text{M–C}} = \sigma_1 - \alpha\sigma_3 \tag{4.60}$$

   2) Upper bound: Twin-shear equivalent stress (Twin-shear strength theory)

$$\sigma^{eq}{}_{\text{Twin–shear}} = \begin{cases} \sigma_1 - \dfrac{\alpha}{2}(\sigma_2 + \sigma_3), & \text{when } \ \sigma_2 \le \dfrac{\sigma_1 + \alpha\sigma_3}{1+\alpha} \\[2mm] \dfrac{1}{2}(\sigma_1 + \sigma_2) - \alpha\sigma_3, & \text{when } \ \sigma_2 \ge \dfrac{\sigma_1 + \alpha\sigma_3}{1+\alpha} \end{cases} \tag{4.61}$$

4.15.3 Equivalent Stresses of the Unified Yield Criterion

Three typed equivalent stresses for non-SD materials expressed in Eqs. (4.57), (4.58), (4.59) can be unified in an equivalent stress of unified yield criterion as

$$\sigma^{eq}_{\text{Unified}} = \begin{cases} \sigma_1 - \dfrac{1}{1+b}(b\sigma_2 + \sigma_3), & \text{when} \quad \sigma_2 \leq \dfrac{\sigma_1 + \sigma_3}{2} \\ \dfrac{1}{1+b}(\sigma_1 + b\sigma_2) - 1\sigma_3, & \text{when} \quad \sigma_2 \geq \dfrac{\sigma_1 + \sigma_3}{2} \end{cases} \tag{4.62}$$

The equivalent stress of unified yield criterion encompassed most well-known equivalent stresses as special cases or linear approximation.

1) $b=0$, deduced to single-shear equivalent stress (Tresca equivalent stress)

2) $b=1$, deduced to twin-shear equivalent stress (Twin-shear yield criterion)

3) $b=0.5$, deduced to a new median equivalent stress (median yield criterion), it is a linear approximation for the three-shear equivalent stress (Mises yield criterion)

4.15.4 Equivalent Stress of the Unified Strength Theory

The general expression of the equivalent stress of the unified strength theory is

$$\sigma^{eq}_{\text{Unified}} = \begin{cases} \sigma_1 - \dfrac{\alpha}{1+b}(b\sigma_2 + \sigma_3), & \text{when} \quad \sigma_2 \leq \dfrac{\sigma_1 + \alpha\sigma_3}{1+\alpha} \\ \dfrac{1}{1+b}(\sigma_1 + b\sigma_2) - \alpha\sigma_3, & \text{when} \quad \sigma_2 \geq \dfrac{\sigma_1 + \alpha\sigma_3}{1+\alpha} \end{cases} \tag{4.62}$$

Equivalent stress of the unified strength theory is a serial formula of equivalent stress. It encompassed most well-known equivalent stresses as special cases. Most equivalent stresses can be deduced from the equivalent stress of the unified strength theory.

4) $\alpha=1$ and $b=0$, deduced to single-shear equivalent stress (Tresca equivalent stress);

5) $b=0$, deduced to single-shear equivalent stress (Mohr-Coulomb equivalent stress);

6) $\alpha=b=1$, deduced to twin-shear equivalent stress (Twin-shear yield criterion);

7) $b=1$, deduced to twin-shear equivalent stress (Twin-shear strength theory);

8) $\alpha=1$ and $b=0.5$, approximated to three-shear equivalent stress (Mises equivalent stress);

9) $b=0.5$, deduced to a new median equivalent stress (median strength theory).

The equivalent stress of the unified strength theory can be used for elastic analysis, elastic limit analysis, elasto-plastic analysis of structures in solid mechanics, FE method, computational plasticity and machine design. A simple example is illustrated as follows.

A part of rocket, tail hood, is analyzed. Three-dimension elastic analysis and the maximum equivalent stresses of UYC (equivalent stress of unified yield criterion) are shown in Table 4.1.

Table 4.1 Maximum equivalent stresses of tail hood

Load q (MPa)	Equivalent stress of UYC (MPa)		
	σ^{eq}_{Tresca} UYC with $b=0$	σ^{eq}_{Mises} UYC with $b=0.4$	$\sigma^{eq}_{Twin-shear}$ UYC with $b=1$
2.4	366.72	327.89	315.81
3.3	427.21	385.05	373.75
3.6	457.34	412.41	400.86

It can be seen that the application of the equivalent stress of unified yield criterion or equivalent stress of unified strength theory is very simple, convenient and useful.

4.16 Examples

Example 4.1

Consider a metallic material with the same yield stress both in tension and in compression. If its shear yield stress is $\tau_y = 0.63\sigma_y$ and Poisson's ratio is $\nu = 0.3$, find an available yield criterion and draw its yield loci in the deviatoric plane, plane stress state and plane strain state.

Solution

The Tresca yield criterion (single-shear yield criterion) predicts the shear yield stress is $\tau_y = 0.5\sigma_y$ and the Huber-von Mises yield criterion (octahetral shear stress yield criterion) predicts the shear yield stress is $\tau_y = 0.577\sigma_y$. Obviously, these two yield criteria do not fit this kind of material with $\tau_y = 0.63\sigma_y$.

According to the unified yield criterion Eqs. (4.21a) and (4.21b), the parameter b in the unified yield criterion can be determined as

$$b = \frac{2\tau_y - \sigma_y}{\sigma_y - \tau_y} = \frac{2 \times 0.63 - 1}{1 - 0.63} = 0.7$$

Substituting $b=0.7$ into Eqs. (4.17a) and (4.17b), a new available yield criterion is obtained as

$$f = \sigma_1 - \frac{1}{1.7}(0.7\sigma_2 + \sigma_3) = \sigma_y, \quad \text{if } \sigma_2 \le \frac{1}{2}(\sigma_1 + \sigma_3)$$

$$f' = \frac{1}{1.7}(\sigma_1 + 0.7\sigma_2) - \sigma_3 = \sigma_y, \quad \text{if } \sigma_2 \ge \frac{1}{2}(\sigma_1 + \sigma_3)$$

The yield locus of this yield criterion ($b=0.7$) in the deviatoric plane and plane stress state are shown in Fig. 4.23.
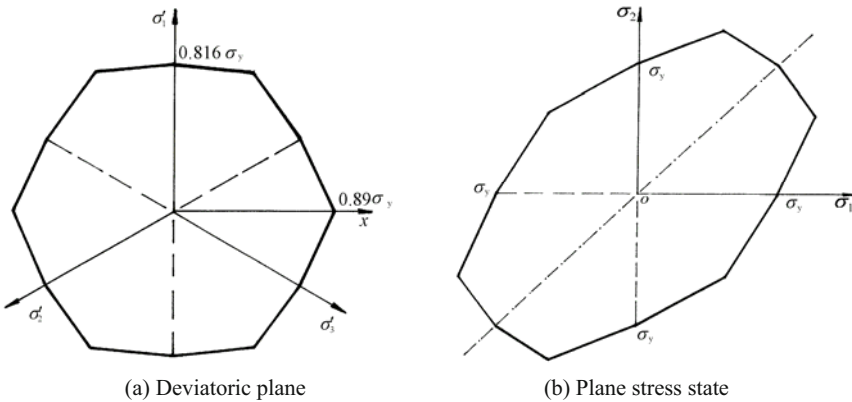

(a) Deviatoric plane   (b) Plane stress state

Fig. 4.23 Yield locus of a new yield criterion ($b=0.7$)

Example 4.2

Introduce an available yield criterion and draw its yield loci in the deviatoric plane, plane stress state and plane strain state when the shear yield stress is $\tau_y = 0.59\sigma_y$ and the Poisson's ratio is $\nu = 0.2$.

Solution

The parameter b in the unified yield criterion can be determined by using the relationship

$$b = \frac{2\tau_y - \sigma_y}{\sigma_y - \tau_y} = \frac{2 \times 0.59 - 1}{1 - 0.59} = 0.44 \qquad (4.64)$$

Substituting $b=0.44$ into Eqs. (4.17a) and (4.17b), an available yield criterion is obtained.

$$f = \sigma_1 - \frac{1}{1.44}(0.44\sigma_2 + \sigma_3) = \sigma_y, \quad \text{if } \sigma_2 \le \frac{1}{2}(\sigma_1 + \sigma_3) \qquad (4.65a)$$

$$f' = \frac{1}{1.44}(\sigma_1 + 0.44\sigma_2) - \sigma_3 = \sigma_y, \quad \text{if } \sigma_2 \ge \frac{1}{2}(\sigma_1 + \sigma_3) \qquad (4.65b)$$

The yield loci of this yield criterion in the deviatoric plane and plane stress state are illustrated in Figs. 4.25 and 4.26.
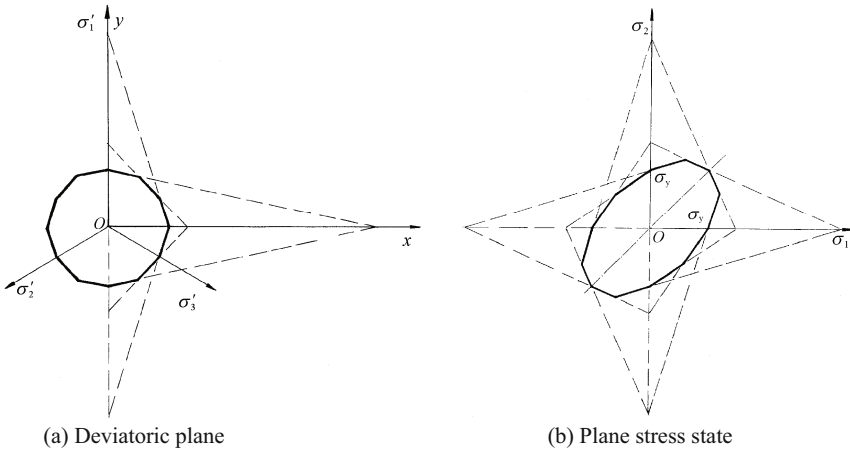

(a) Deviatoric plane   (b) Plane stress state

Fig. 4.24 Yield locus of a new yield criterion ($b=0.44$)

Example 4.3

A yield surface of the unified strength theory with $b=0.5$ in stress space is illustrated by Zhang et al. (2008), as shown in Fig. 4.25.
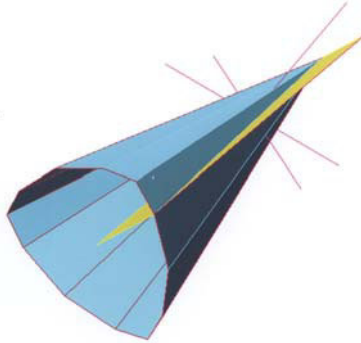
Fig. 4.25 A yield surface of the unified strength theory with *b*=0.5 (Zhang et al., 2008)

4.17 Summary

Based on the the twin-shear model and multi-shear model, a new unified strength theory was proposed by Yu in 1991 (Yu and He, 1991; Yu, 1992). This unified strength theory (unified strength theory) is not a single yield criterion suitable only for one kind of material, but a completely new system. It embraces many well-established criteria as its special or approximate cases, such as the Tresca yield criterion, the Huber-von Mises yield criterion and the Mohr-Coulomb strength theory, as well as the twin-shear yield criterion (Yu, 1961a), the generalized twin-shear strength theory (for SD materials, Yu et al., 1985) and the unified yield criterion (for non-SD materials). The unified strength theory forms an entire spectrum of convex and nonconvex criteria, which can be used to describe many kinds of engineering materials. The unified strength theory has a unified mechanical model and a simple and unified mathematical expression, which can be adapted to the various experimental data. It is easy to use in both research and engineering.

The advances in strength theories are briefly illustrated in Fig. 4.26. This shows the development from single-shear theory to three-shear theory, then from twin-shear theory to the unified strength theory (a set of the serial criteria).
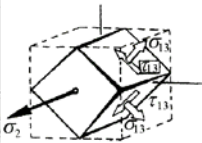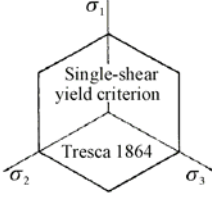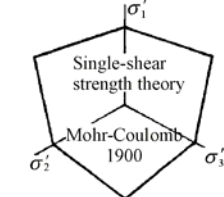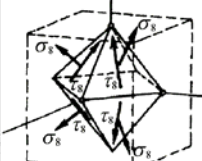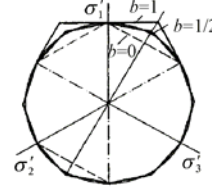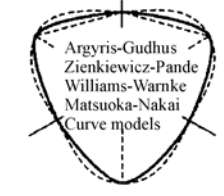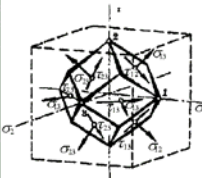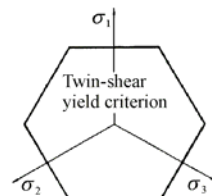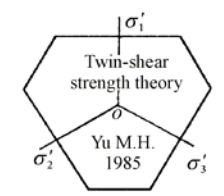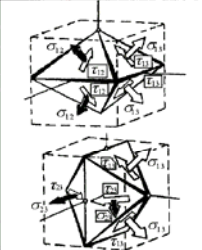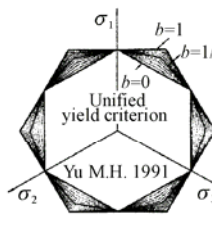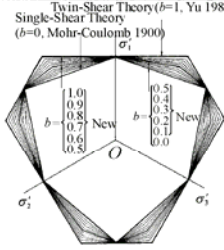
Fig. 4.26 Advances in strength theories

The unified strength theory establishes very clear and simple relations among the various yield criteria, as show in Fig. 4.27. It also provides a method for choosing the appropriate yield criterion.
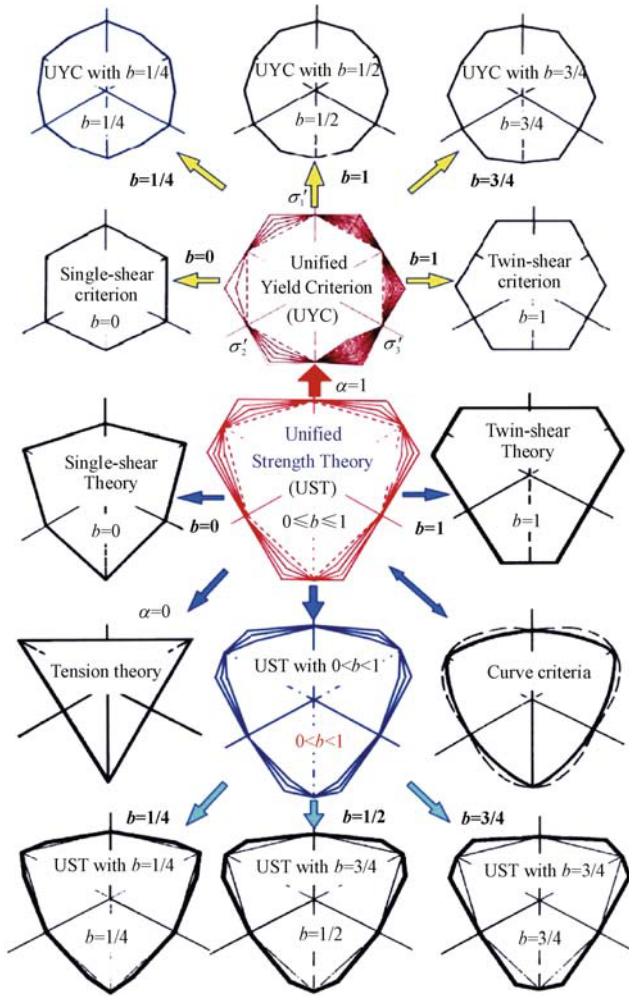
Fig. 4.27 Variation of the unified strength theory and the relationships among the criteria

The SD effect, hydrostatic stress effect, normal stress effect, effect of the intermediate principal stress, the effect of intermediate principal shear stress and the effect of the twin-shear stresses are all taken into account in the unified strength theory.

The unified strength theory is a completely new theory system. The significance of the Yu unified strength theory is summarized as follows:

1) It is suitable for more kinds of isotropic materials.

2) It contains various spread strength theories and forms a new system of yield criteria and failure criteria. It provides a relationship between the single-shear criterion, the twin-shear criterion and a series of new criteria.

3) It gives good agreement with experimental results for various materials.

4) A series of new results can be obtained by using the unified strength theory.

5) The unified strength theory is easy to use for analytical solutions of plastic problems. The applications of the unified strength theory are described in the next chapters. It is suitable for plastic analysis of structures.

The mathematical expression of the unified strength theory can be given in various forms. More than ten kinds of expressions are discussed in this chapter.

The parameters of unified strength theory are the same as the parameters used in the Mohr-Coulomb strength theory (1900), Drucker-Prager criterion (1952), the twin-shear strength theory (Yu et al., 1985) and other two-parameters criteria. Tensile strength σ_t, compressive strength σ_c (or σ_t, α) or friction angle φ and cohesion C_0 are the most used material parameters in engineering.

The yield function can be interpreted for an isotropic material in terms of a geometrical representation of the stress state obtained by taking the principal stresses as coordinates. The advantage of such a space lies in its simplicity and visual presentation.

The yield surface of the unified strength theory in stress space and yield loci on plane stress, the deviatoric plane and meridian plane are illustrated in this chapter. Unified strength theory embraces many well-established yield surfaces and yield loci as its special or asymptotic cases, such as yield surfaces of the Tresca yield criterion, the Huber-von Mises yield criterion and the Mohr-Coulomb strength theory, as well as the twin-shear yield criterion (Yu, 1961a), the twin-shear strength theory and the unified yield criterion. The unified strength theory forms an entire spectrum of convex and nonconvex criteria, which can be used to describe many kinds of engineering materials.

The yield surfaces and yield loci of the unified yield criterion, the twin-shear strength criterion, the twin-shear yield criterion, the single-shear strength criterion (Mohr-Coulomb theory), the single-shear yield criterion (Tresca yield criterion) and many empirical failure criteria are special cases or linear approximations of the yield surface of the unified strength theory. A series of new yield surfaces and yield loci can also be drawn based on the unified strength theory.

A paper entitled "Remarks on Model of Mao-Hong Yu" was written by Altenbach and Kolupaev (2008). Reviews of "Unified Strength Theory and its Applications" were made by Shen (2004) and Teodorescu (2006). Comments on the unified strength theory were made by and Fan and Qiang (2001) and Zhang et al. (2001).

References

Altenbach H and Kolupaev VA (2008) Remarks on Model of Mao-Hong Yu. The Eighth International Conference on Fundamentals of Fracture (ICFF VIII), Tong Yi Zhang, Biao Wang and Xi-Qiao Feng eds, pp 270-271.

Besseling JF and van der Giessen E (1994) Mathematical Modelling of Inelastic Deformation. Chapman & Hall: London. Chen WF (1982) Plasticity in

Reinforced Concrete. McGraw-Hill: New York.

Chen WF and Saleeb AF (1994) Constitutive Equations for Engineering Materials. Vol.1: Elasticity and Modeling, Revised edn. Elsevier: Amsterdam. pp 259-304, 462-489.

Chen W.F et al. (1994) Constitutive Equations for Engineering Materials. Vol. 2: Plasticity and Modeling. Elsevier: Amsterdam.

Chen WF (1998) Concrete Plasticity: Past, Present and Future. In: Strength Theory: Application, Development and Prospects for 21st Century. Science Press: Beijing, New York,1998, pp 7-48.

Drucker D.C and Prager W (1952) Soil mechanics and plastic analysis for limit design. Quart. Appl. Math., 10: 157-165.

Fan SC and Qiang HF (2001) Normal high-velocity impact concrete slabs- a simulation using the meshless SPH procedures. Computational Mechanics–New Frontiers for New Millennium. Valliappan S and Khalili N eds. Elsevier: Amsterdam, pp 1457-1462.

Fan SC, Yu MH and Yang SY (2001) On the unification of yield criteria. J. of Applied Mechanics, ASME, 68: 341-343.

Haythornthwaite RM (1961) Range of yield condition in ideal plasticity. J. Eng. Mech. ASCE, 87(6): 117-133.

Haigh BT (1920) The strain energy function and the elastic limit. Engineering, 109: 158-160.

Hencky H (1925) Ueber das Wesen der plastischen Verformung (The nature of plastic deformation). Zeitschrift des Vereines Deutscher Ingenieure, 69(20), May 16-Sept 26 (in German)

Huber MT (1904) Przyczynek do podstaw wytorymalosci. Czasopismo Technizne, 22:81, (Lwow, 1904; Pisma, 2, PWN, Warsaw, 1956).

Kolupaev V, A and Altenbach H, Considerations on the Unified Strength Theory due to Mao-Hong Yu, Forschung im Ingenieurwesen (to be published) (in German).

Meyer WJ (1985) Concepts of Mathematical Modeling. McGraw-Hill Book Company.

von Mises R (1913) Mechanick der festen Körper im plastisch deformablen Zustand. Nachrichten von der Königlichen Gesellschaft der wissenschaften zu Göettinger. Mathematisch-Physikalische Klasse, pp 582-592.

Mohr O (1900) Welche Umstande bedingen die Elastizitatsgrenze und den Bruch eines Materials. Zeitschrift des Vereins deutscher Ingenieure, 44: 1524-1530; 1572–1577.

Mohr O (1905) Abhandlungen aus den Gebiete der Technischen Mechanik. Verlag von Wilhelm Ernst and Sohn, 1905, 1913, Third edn. 1928.

Nadai A (1931) Plasticity. McGraw-Hill: New York.

Paul B (1961) A modification of the Coulomb–Mohr theory of fracture. J. Appl. Mech, 28: 259-268.

Pisarenko GS and Lebedev AA (1976) Deformation and strength of material under complex stressed state. Naukova Dumka, Kiev (in Russian).

Shen ZJ (2004) Reviews to "Unified Strength Theory and Its Applications". Advances in Mechanics, 34(4):562-563. (in Chinese)

Tayler AB (1986) Mathematical Models in Applied mechanics. Clarendon Press: Oxford.

Teodorescu PP (2006) Review of Unified strength theory and its Applications. Springer, Berlin, 2004". Zentralblatt MATH 2006, Cited in Zbl. Reviews, 1059.74002 (02115115).

Tresca H (1864) Sur l'ecoulement des corps solides soumis a de fortes pression. Comptes Rendus hebdomadaires des Seances de l'Academie des Sciences, Rend, 59: 754-758.

Westergaard HM (1920) On the resistance of ductile materials to combined stresses. J. Franklin Inst.,189: 627-640.

Wu KKS, Lahav O and Rees MJ (1999) The large-scale smoothness of the Universe. Nature, 397: 225-230.

Yu MH (1961a) General behaviour of isotropic yield function. Res. Report of Xi'an Jiaotong University. Xi'an, China(in Chinese):

Yu MH (1961b) Plastic potential and flow rules associated singular yield criterion (in Chinese). Res. Report of Xi'an Jiaotong University. Xi'an, China.

Yu MH (1983) Twin shear stress yield criterion. Int. J. Mech. Sci., 25(1): 71-74.

Yu MH, He LN and Song LY (1985) Twin shear stress theory and its generalization. Scientia Sinica (Sciences in China), English edn. Series A, 28(11): 1174-1183.

Yu MH and Liu FY (1988) Twin shear three-parameter criterion and its smooth ridge model. China Civil Engng. J., 21(3): 90-95 (in Chinese, English abstract).

Yu MH and He LN (1991) A new model and theory on yield and failure of materials under complex stress state. In: Mechanical Behariour of Materials-6, Vol. 3: Pergamon Press: Oxford, pp 841-846.

Yu MH (1992a) A new system of strength theory. Xian Jiaotong University Press: Xi'an (in Chinese).

Yu MH (1994) Unified strength theory for geomaterials and its application. Chinese J. of Geotech. Eng., 16(2): 1-10 (in Chinese, English Abstract).

Yu Mao-hong. (1998) Twin-shear Theory and Its Applications. Science Press: Beijing (in Chinese).

Yu MH (2002a) Concrete Strength Theory and Its Applications. Higher Education Press: Beijing.

Yu MH (2002b) Advances in strength theories for materials under complex stress state in the 20th Century. Applied Mechanics Reviews ASME, 55(3): 169-218.

Yu MH, Zan YW, Zhao J and Yoshimine M (2002) A unified strength criterion for rock. Int. J. of Rock Mechanics and Mining Science, 39: 975-989.

Yu MH (2004) Unified Strength Theory and its Applications. Springer: Berlin.

Yu MH, Xia GY, Kolupaev VA (2009) Basic characteristics and development of yield criteria for geomaterials. Journal of Rock Mechanics and Geotechnical Engineering, 1(1): 71-88.

Zhang CQ, Zhou H, Feng XT (2008) Numerical format of elastoplastic constitutive model based on the unified strength theory in FLAC~(3D). Rock and Soil Mechanics, 29(3): 596-602 (in Chinese, English Abstract).

Zhang LY (2005) The 3D images of geotechnical constitutive models in the stress space. Chinese J. of Geotechnical Engineering, 27(1):64-68.

Zhang XS, Guan H, Loo YC (2001) UST failure criterion for punching shear analysis of reinforcement concrete slab-column connections. Computational Mechanics–New Frontiers for New Millennium. Valliappan S and Khalili N eds. Elsevier: Amsterdam, pp 299-304.

Zienkiewicz OC and Pande GN (1977) Some useful forms of isotropic yield surfaces for soil and rock mechanics. Finite Elements in Geomechanics. Gudehus G ed. Wiley: London, pp 179-190.

Zyczkowski M (1981) Combined Loadings in the Theory of Plasticity. Polish Scientific Publishers: PWN and Nijhoff.

5

Non-Smooth Multi-Surface Plasticity

5.1 Introduction

Most materials in structures are acted under the complex stress states, i.e., biaxial and multiaxial stresses. Strength theory provides a yield (or failure) criterion, a limiting stress state for elasticity, or an initial deformation for plasticity. Sometimes it is also used as an associated or non-associated flow rule for plastic constitutive relations.

The previous chapters described the yield functions and the corresponding yield surfaces that characterize the initial yielding of materials. The post-yielding, loading and unloading behavior of the materials is related to the stress-strain relation for plastically deformed solids, namely the constitutive relations for plastic deformation of engineering materials. Classical plasticity theory discusses plastic flow rules such as Levy-Mises and Prandtl-Reuss equations, Drucker's stability postulate, isotropic, kinematic and combined hardening rules, and derives general stress-strain relations for plastic deformation of different materials. The general description on plasticity can be seen in Hill (1950), Johnson and Mellor (1962), Mendelson (1968), Martin (1975), Owen and Hinton (1980), Chakrabarty (1981), Khan (1995), Belytschko et al. (2000), and Dunne and Petrinic (2005).

Non-smooth multi-surface plasticity, where the yield surface consists of several smooth yield surfaces, is studied and described by Simo and Tarloy (1998). The non-smooth multi-surface is shown in Fig. 5.1(a). Non-smooth multi-surface plasticity, where the yield surface consists of several linear yield surfaces, is studied and described by Yu (1992; 1998; 2004), as shown in Fig. 5.1(b). It is the piece-wise linear yield surface, which was studied by Koiter (1953). Sometimes the non-smooth multi-surface is referred to as the singular yield surface.

In this chapter, the non-smooth multi-surface yield criterion or piece-wise linear yield functions are developed and used to describe the fundamental problem of

plasticity. For solving the singularity of piece-wise linear yield functions, the associated flow rule and incremental constitutive relations for unified strength theory will be mainly developed.

(a) Consisting of some smooth surfaces   (b) Consisting of some smooth linear surfaces
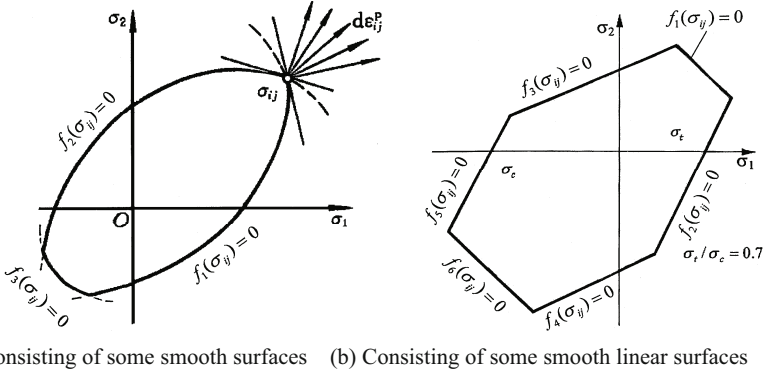
Fig. 5.1 Non-smooth multi-surface yield criterion

5.2 Plastic Deformation in Uniaxial Stress State

For a stress-strain curve shown in Fig. 5.2 of an elasto-plastic material, the behavior can be characterized as an elastic region with an elastic modulus E until yielding commences at the axial yield stress σ_Y, and at a plastic region with a continually varying local tangent E_T to the curve. E_T is the elasto-plastic tangent modulus. The hardening law $k = k(\kappa)$ can be readily derived in terms of the plastic work achieved for the material.

In the elastic region, the stress-strain relation has a linear form,

$$\sigma = E\varepsilon \tag{5.1}$$

In the plastic region, the total strain increment in the uniaxial stress state is the sum of the elastic strain increment and the plastic strain increment, i.e.

$$d\varepsilon = d\varepsilon^e + d\varepsilon^p \tag{5.2}$$

Assuming that the plastic deformation is rate insensitive, the stress increment is linearly related to the elastic strain increment in the plastic region and can be expressed by

$$d\sigma = Ed\varepsilon^e = E(d\varepsilon - d\varepsilon^p) \tag{5.3}$$
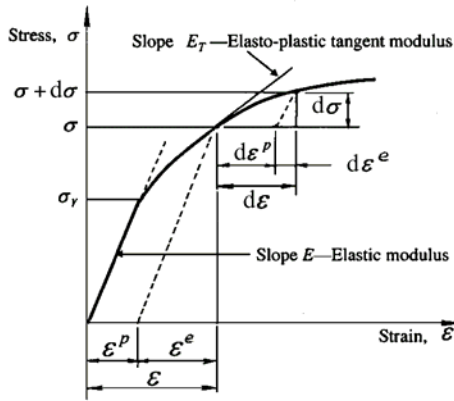
Fig. 5.2 Uniaxial elasto-plastic stress strain curve

The initial yield point σ_Y differentiates the elastic and plastic regions. The stress in the plastic region can be determined by a hardening rule,

$$\sigma = \sigma_Y(\kappa) \tag{5.4}$$

where κ is a hardening parameter. In the uniaxial stress state, the plastic strain ε^p is usually used for the hardening parameter, i.e. $\kappa = \varepsilon^p$. The plastic strain ε^p is history or path dependent. It can be calculated by

$$\varepsilon^p = \int d\varepsilon^p \tag{5.5}$$

Considering the strain decomposition Eq. (5.2), we can derive

$$d\varepsilon^p = d\varepsilon - d\varepsilon^e = \frac{d\sigma}{E_T} - \frac{d\sigma}{E} = \left(\frac{1}{E_T} - \frac{1}{E}\right) d\sigma \tag{5.6}$$

The tangent modulus E_T is considered to be a function of stress and plastic strain ε^p,

$$E_T = E_T(\sigma, \varepsilon^p) \tag{5.7}$$

which should be determined experimentally from a simple uniaxial yield test. Based on Eqs. (5.6) and (5.7), an incremental constitutive relation of the material can thus be derived.

The constitutive relation differs for plastic loading and elastic loading or unloading. It is necessary to identify the process as belonging to plastic loading or

elastic unloading. Loading and unloading represent a deformation process that starts from a plastic state, continues to deform plastically and then returns to the elastic region. A previous plastic state is always implied. The loading and unloading criterion in the uniaxial stress state can be represented as

$$\sigma d\sigma \geq 0 \quad \text{for loading} \tag{5.8}$$

$$\sigma d\sigma < 0 \quad \text{for unloading} \tag{5.9}$$

It can be seen that the fundamental elements of the plastic deformation include initial yielding of the material, strain hardening and subsequent yielding, the incremental constitutive equation and loading and unloading criterion, etc. In the three-dimensional case, the constitutive equations can be represented in tensor notation, which will be discussed in the following sections.

5.3 Three-Dimensional Elastic Stress-Strain Relation

Plastic theory in the uniaxial stress can be extended to the three-dimensional case. The elastic stress-strain relationship in the three-dimensional case can be given by the generalized Hooke's law in the Cartesian coordinate system for isotropic materials. In tensor notation, it has the form of

$$\varepsilon_{ij} = \frac{\sigma_{ij}}{2G} - \frac{3v}{E} p\delta_{ij} \tag{5.10}$$

where σ_{ij} is the Kronecker delta and $p=\sigma_{kk}/3$ is the mean stress or hydrostatic pressure in the material. E, G and v are the elastic modulus, the shear modulus and the Poisson's ratio, respectively. They have the following relationship,

$$G = \frac{E}{2(1+v)} \tag{5.11}$$

Equation (5.10) can be rewritten as

$$\begin{aligned}
\varepsilon_{ij} &= \frac{1}{E}\left[(1+v)\sigma_{ij} - 3v\,p\delta_{ij}\right] \\
&= \frac{1}{E}\left[(1+v)\delta_{ik}\delta_{jl} - v\delta_{ik}\delta_{kl}\right]\sigma_{kl} \\
&= M_{ijkl}\sigma_{kl}
\end{aligned} \tag{5.12}$$

where $M_{ijkl} = \dfrac{1}{E}\left[(1+v)\delta_{ik}\delta_{jl} - v\delta_{ik}\delta_{kl}\right]$. The elastic stress tensor can then be deduced from Eq. (5.12) as

$$
\begin{aligned}
\sigma_{ij} &= \frac{E}{1+v}\left[\frac{3v}{1-2v}\varepsilon_m\delta_{ij} + \varepsilon_{ij}\right] \\
&= \frac{E}{1+v}\left[\delta_{ik}\delta_{il} + \frac{v}{1-2v}\delta_{ij}\delta_{kl}\right]\varepsilon_{kl} \\
&= C_{ijkl}\varepsilon_{kl}
\end{aligned}
\tag{5.13}
$$

in which C_{ijkl} is the stiffness tensor of the fourth order, $\varepsilon_m = \varepsilon_{kk}/3$ is the mean strain and

$$
C_{ijkl} = \frac{E}{1+v}\left[\delta_{ik}\delta_{il} + \frac{v}{1-2v}\delta_{ij}\delta_{kl}\right]
\tag{5.14}
$$

The stiffness tensor C_{ijkl} has 21 independent components for anisotropic materials. The components depend on two independent constants only for isotropic materials.

The stress tensor can also be written using the Lame constantas

$$
\sigma_{ij} = 2G\varepsilon_{ij} + \lambda\varepsilon_{kk}\delta_{ij}
\tag{5.15}
$$

where λ is the Lame constant and can be expressed in terms of E and v as

$$
\lambda = \frac{Ev}{(1+v)(1-2v)}
\tag{5.16}
$$

The elastic stress strain relation can also be expressed in an incremental form, i.e.

$$
d\varepsilon_{ij} = M_{ijkl}d\sigma_{ij}
\tag{5.17}
$$

or

$$
d\sigma_{ij} = C_{ijkl}d\varepsilon_{ij}
\tag{5.18}
$$

5.4 Plastic Work Hardening and Strain Hardening

The total strain increments in the three-dimensional case can be generalized as

$$\mathrm{d}\varepsilon_{ij} = \mathrm{d}\varepsilon_{ij}^{e} + \mathrm{d}\varepsilon_{ij}^{p} \qquad (5.19)$$

where $\mathrm{d}\varepsilon_{ij}{}^{e}$ is the elastic strain increment and $\mathrm{d}\varepsilon_{ij}{}^{p}$ is the plastic strain increment. The decomposition is correct for cases of infinitesimal strain, only that in the case of finite strain there will be geometrical elasto-plastic coupling between the elastic and plastic strain measures so that Eq. (5.19) will lose its conventional physical meaning.

After initial yielding, the stress level at which further plastic deformation occurs may be dependent on the current degree of plastic straining. Such a phenomenon is termed work hardening or strain hardening. Thus, the yield surface will vary at each stage of the plastic deformation, with the subsequent yield surfaces being dependent on the plastic strains in some way. Due to its dissipation feature the plastic deformation process is history or path dependent. In other words, there will not be a one-to-one correspondence between stress-strain during plastic deformation. Some alternative models which describe strain hardening in a material are illustrated in Fig. 5.3. A perfect plastic material means that the yield stress level does not depend in any way on the degree of plastic deformation. If the subsequent yield surfaces are a uniform expansion of the original yield curve, without translation, the strain hardening model is said to be isotropic. On the other hand, if the subsequent yield surfaces preserve their shape and orientation but translate in the stress space as a rigid body, kinematic hardening is said to take place. Such a hardening model gives rise to the experimentally observed Bauschinger effect on cyclic loading.
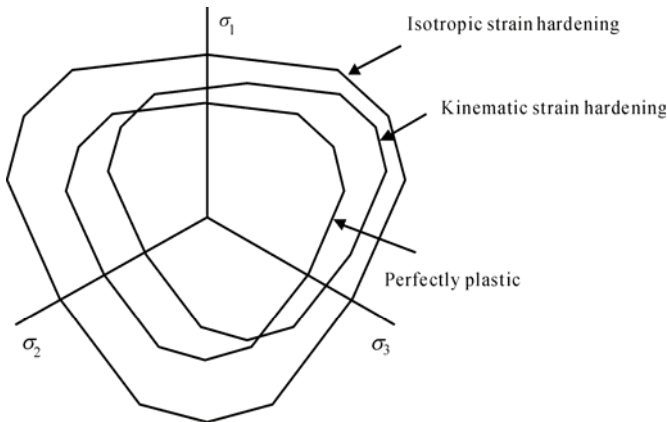

Fig. 5.3 Representation of Strain Hardening Behavior

The progressive development of the yield surface can be defined by relating the yield stress k to the plastic deformation by means of the hardening parameter κ. This can be postulated to be a function of the total plastic work W_p only. Plastic deformation can also be associated with the dissipation of energy so that it is

irreversible. Then

$$\kappa = W_p \qquad (5.20)$$

where

$$W_p = \int \sigma_{ij}(d\varepsilon_{ij}^p) \qquad (5.21)$$

in which $d\varepsilon_{ij}^p$ are the plastic components of strain occurring during a strain increment. Alternatively, κ can be related to a measure of the total plastic deformation termed the effective, generalized or equivalent plastic strain which is defined incrementally as

$$d\bar{\varepsilon}_p = \sqrt{\frac{2}{3}}\left[(d\varepsilon_{ij}^p)(d\varepsilon_{ij}^p)\right]^{\frac{1}{2}} \qquad (5.22)$$

A physical insight of this definition is proven where uniaxial yielding is considered. For situations where the assumption that yielding is independent of any hydrostatic stress is valid, $d\varepsilon_{ij}^p = 0$ and hence $d\varepsilon_{ij}'^p = d\varepsilon_{ij}^p$, where $d\varepsilon_{ij}'^p$ is the deviatoric plastic strain increment. Consequently, the above equation can be rewritten as

$$d\bar{\varepsilon}_p = \sqrt{\frac{2}{3}}\left[(d\varepsilon_{ij}'^p)(d\varepsilon_{ij}'^p)\right]^{\frac{1}{2}} \qquad (5.23)$$

Then the hardening parameter k is assumed to be defined as

$$\kappa = \bar{\varepsilon}_p \qquad (5.24)$$

where $\bar{\varepsilon}_p$ is the result of integrating $d\bar{\varepsilon}_p$ over the strain path. This behavior is termed strain hardening.

Strain states for which $f=k$ represent plastic states, while elastic behavior is characterized by $f<k$. In a plastic state, $f=k$, the incremental change in the yield function due to an incremental stress change is

$$df = \frac{\partial f}{\partial \sigma_{ij}}d\sigma_{ij} \qquad (5.25)$$

Then, if

$df<0$ elastic unloading occurs and the stress point returns inside the yield surface.

$df=0$ neutral loading and the stress point remains on the yield surface.

$df>0$ plastic loading for a strain hardening material.

5.5 Plastic Flow Rule

The general mathematical treatment of the constitutive equation for plastic deformation or flow was proposed by von Mises in 1928. In elastic theory the strain tensor was related to the stress tensor through an elastic potential function, the complementary strain energy U such that

$$\varepsilon_{ij} = \frac{\partial U}{\partial \sigma_{ij}} \tag{5.26}$$

By extending this idea to plasticity theory, Mises proposed that there existed a plastic potential function $Q(\sigma_{ij})$, and the plastic strain increments $d\varepsilon_{ij}^p$ can be derived similar to Eq. (5.26),

$$d\varepsilon_{ij}^p = d\lambda \frac{\partial Q}{\partial \sigma_{ij}} \tag{5.27}$$

where $d\lambda$ is a proportional positive scalar factor. To determine $d\lambda$, the yield function should be used. The plastic flow rule shown in Eq. (5.27) is called plastic potential theory. The plastic potential $Q(\sigma_{ij})=C$, or a constant, represents a surface in the six-dimensional stress space, and the plastic strain $d\varepsilon_{ij}^p$ can be represented by a vector which is perpendicular to the surface $Q(\sigma_{ij})=C$.

A common approach in plasticity theory is to assume that the plastic potential function $Q(\sigma_{ij})$ is the same as the yield function $F(\sigma_{ij})$,

$$Q(\sigma_{ij}) = F(\sigma_{ij}) \tag{5.28}$$

Equation (5.23) can then be rewritten as

$$d\varepsilon_{ij}^p = d\lambda \frac{\partial F}{\partial \sigma_{ij}} \tag{5.29}$$

and the plastic flow vector is normal to the yield surface. This is called the associated flow rule. On the other hand, if $Q \neq F$, the flow rule is called non-associated.

The association of Q with F is based on an assumption whose validity can be verified empirically. Experimental observations show that the plastic deformation of metals can be characterized quite well by the associated flow rule, but for some porous materials such as rocks, concrete and soils, the non-associated flow rule may provide a better representation of their plastic deformation. Mathematically it can be proved by using Drucker's stability postulate that if the material is stable in Drucker's sense, the flow vector must be associated.

The Prandtl-Reuss equation is a special case of the associated flow rule. Indeed, applying the Huber-von Mises yield criterion gives

$$\frac{\partial J_2}{\partial \sigma_{ij}} = S_{ij} \qquad (5.30)$$

where S_{ij} is the deviatoric stress tensor. Eq. (5.29) then gives

$$d\varepsilon_{ij}^p = d\lambda \frac{\partial F}{\partial \sigma_{ij}} = d\lambda S_{ij} \qquad (5.31)$$

which is the Prandtl-Reuss equation, or the Levy-Mises equation if the elastic strain rate is ignored. Thus, within the general framework of the plastic potential theory, the Prandtl-Reuss or the Levy-Mises equation implies the Huber-von Mises yield function and the associated flow rule.

The complete incremental relationship between stress and strain for elasto-plastic deformation is found to be

$$d\varepsilon_{ij} = \frac{1}{E}\left[(1+\nu)\delta_{ik}\delta_{jl} - \nu\delta_{ik}\delta_{kl}\right]d\sigma_{kl} + d\lambda \frac{\partial Q}{\partial \sigma_{ij}} \qquad (5.32)$$

5.6 Drucker's Postulate – Convexity of the Loading Surface

Drucker (1951) proposed a unified approach based on his stability postulate to establish the general plastic stress-strain relations. One major consequence of Drucker's posulate is that the flow rule for stable materials is associated (i.e., $Q=F$). For a stable material, it can be proved that the yield surface must be convex (Drucker, 1952; Mendelson, 1968). The proof of convexity of the yield surface by Mendelson is described as follows.

Considering a material element in equilibrium with a given state of stress σ_{ij}^0 inside the loading surface, as shown in Fig. 5.4, first it is necessary to define a stress cycle or a closed loading-unloading path in stress space. Let some external agency add stresses along some arbitrary path inside the surface. Only elastic changes have taken place so far. Now suppose the external agency to add a very small outward pointing stress increment $d\sigma_{ij}$, which produces small plastic strain increments $d\varepsilon_{ij}^P$ as well as elastic increments. The external agency then releases the $d\sigma_{ij}^P$ and the state of stress is returned to σ_{ij}^0 along an elastic path.
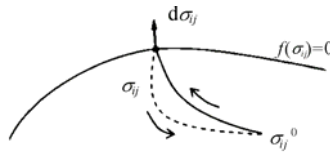
Fig. 5.4 A closed loading-unloading path

The work done by the external agency over the cycle is

$$\delta W = (\sigma_{ij} - \sigma_{ij}^0)\mathrm{d}\varepsilon_{ij}^p + \mathrm{d}\sigma_{ij}\mathrm{d}\varepsilon_{ij}^p \tag{5.33}$$

If the plastic strain coordinates are superimposed on the stress coordinates as in Fig. 5.5, δW may be interpreted as the scalar product of the vector $(\sigma_{ij} - \sigma_{ij}^0)$ and the vector $\mathrm{d}\varepsilon_{ij}^p$ plus the scalar product of $\mathrm{d}\sigma_{ij}$ and $\mathrm{d}\varepsilon_{ij}^p$. Now, from the strain-hardening definition, we have

$$\mathrm{d}\sigma_{ij}\mathrm{d}\varepsilon_{ij}^p \geq 0 \tag{5.34}$$

or

$$\left|\mathrm{d}\sigma_{ij}\right|\left|\mathrm{d}\varepsilon_{ij}^p\right|\cos\theta \geq 0 \tag{5.35}$$
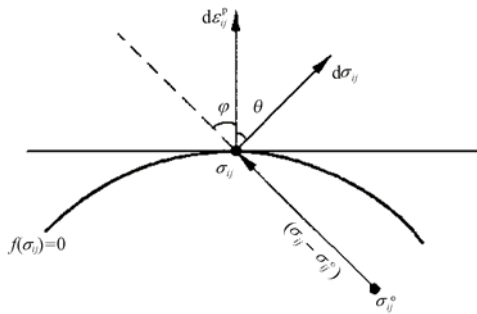
and $-\pi/2 \leq \theta \leq \pi/2$.

Fig. 5.5 Stress and plastic strain increment vectors

It means that the vector $\mathrm{d}\sigma_{ij}$ and $\mathrm{d}\varepsilon_{ij}^p$ form an acute angle with each other. Since the magnitude of $(\sigma_{ij} - \sigma_{ij}^0)$ can always be made larger than the magnitude of $\mathrm{d}\sigma_{ij}$, it follows that

$$(\sigma_{ij} - \sigma_{ij}^0)\mathrm{d}\varepsilon_{ij}^p \geq 0 \tag{5.36}$$

or

$$\left|\sigma_{ij} - \sigma_{ij}^0\right|\left|d\varepsilon_{ij}^p\right|\cos\varphi \geq 0 \tag{5.37}$$

Hence

$$-\pi/2 \leq \varphi \leq \pi/2$$

Thus the vector $(\sigma_{ij} - \sigma_{ij}^0)$ forms an acute angle with the vector $d\varepsilon_{ij}^p$ for all choices of σ_{ij}^0. Therefore, all points σ_{ij}^0 must lie on one side of a plane perpendicular to $d\varepsilon_{ij}^p$ and, since $d\varepsilon_{ij}^p$ is normal to the yield surface, this plane will be tangent to the yield surface. This must be true for all points σ_{ij} on the yield surface, so that no vector $(\sigma_{ij} - \sigma_{ij}^0)$ can pass outside the surface intersecting the surface twice or more, as shown in Fig. 5.6. The yield surface must therefore be convex. The yield surface shown in Fig. 5.6 is non-convex (from the view of the yield surface interior it is concave). On the non-convex yield surface several vectors $(\sigma_{ij} - \sigma_{ij}^0)$ can make $\sigma_{ij} - \sigma_{ij}^0 \, d\varepsilon_{ij}^p < 0$ and the inequality (5.36) is violated. The vector $(\sigma_{ij} - \sigma_{ij}^0)$ can pass outside the surface that intersects the surface thirdly, as shown in Fig. 5.7.
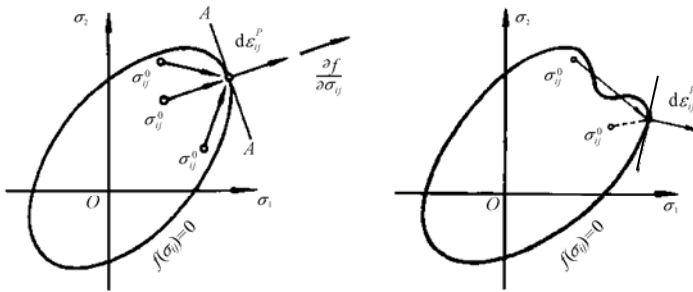

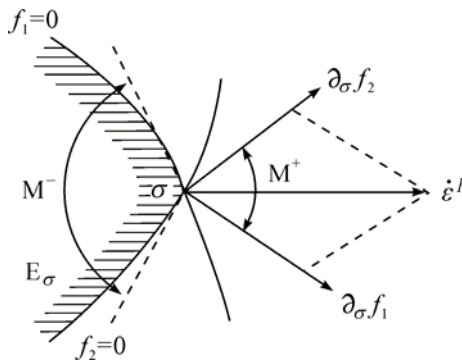**Fig. 5.6** Convex yield surface and Non-convex yield surface

Fig. 5.7 Illustration of the geometry at a singular point (Simo and Hughes, 1991; 1998)

The convex yield surface may be a single function, or piece-wise functions consisting of some smooth functions, in which two convex functions $f_1(\sigma_{ij})$ and

$f_2(\sigma_{ij})$ or $f_1(\sigma_{ij})$ and $f_3(\sigma_{ij})$ intersect non-smoothly as shown in Figs. 5.7 and 5.8. Fig. 5.7 is an illustration of the geometry at a singular point, the intersection of two yield surfaces (Simo and Hughes, 1991; 2000).

Figure 5.9 is a family of piece-wise linear functions. It is interesting that the two bounds of the convex yield surface are piece-wise linear. It is the same as the yield surface of the unified strength theory illustrated in Figs. 4.16 and 4.17 in Chapter 4. The inner bound (dotted line) and the outer bound are consisted of six linear functions.
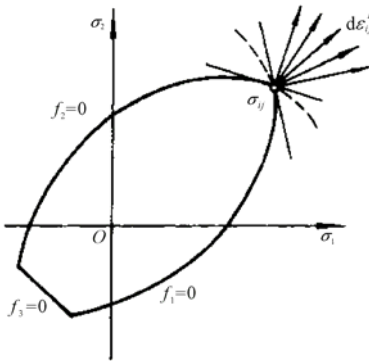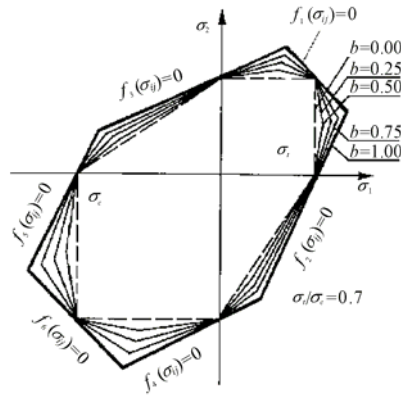

Fig. 5.8 Piece-wise yield function   Fig. 5.9 Piece-wise-linear yield functions

The associate plastic flow rule implies that the yield surface has a unique gradient. It may happen, however, that the yield surface has vertices or corners where the gradient is not defined. For example, the Tresca hexagon has no unique normal at the corners, where two of the stresses are equal. Such points are called singular points or singular yield conditions, as shown in Fig. 5.10. Figure 5.11 shows the singularity of the single-shear theory and the twin-shear theory. The process of the singularity of the yield functions will be discussed in Sections 5.10 −5.13.

The yield loci (elastic boundaries) of the single-shear theory (Tresca criterion and the Mohr-Coulomb criterion) are composed of several linear yield loci. Sometimes the yield loci may be composed of several smooth loci. They are the non-smooth yield surface. The singularity at the corners or singular points and non-smooth multi-surface plasticity were investigated by many researchers. The details can be seen in the books of Owen and Hinton (1980), and the book of Simo and Hughes (1998). The process of corners were also described in the books of Owen et al. (1989) and Smith and Griffiths (2004). Removal of singularities in the Tresca and Mohr-Coulomb yield function was studied by Sloan and Booker (1986). The corners on the Tresca surface and on the Mohr-Coulomb surface were processed by rounding off the yield surface corners. The method used in the programs to overcome this singularity is to replace the hexagonal surface by a

smooth conical surface at the local corner. The detailed research of non-smooth multi-surface plasticity can be seen in Simo et al. (1988) and in Chapter 7 of Owen and Hinton (1980), chapter 5 of Simo and Hughes (1998) and Chapter 6 of Smith and Griffiths (2004).
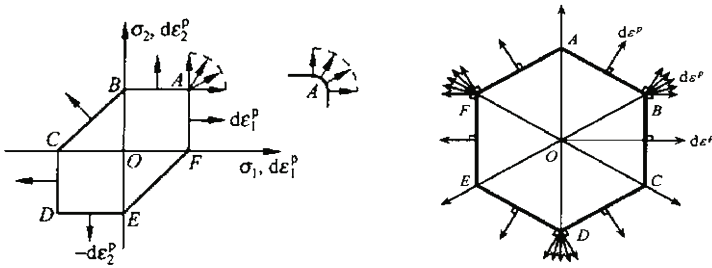

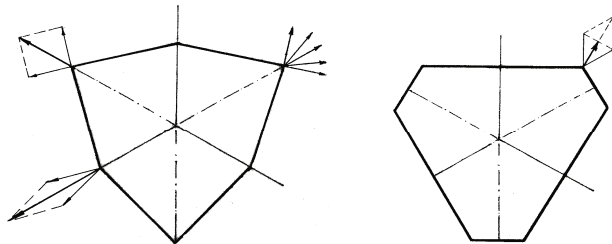**Fig. 5.10** Tresca yield function and its singularity at corners

Fig. 5.11 Singularity at corners of the single-shear and twin-shear theories

5.7 Incremental Constitutive Equations in Matrix Formulation

For various engineering materials, a yield criterion indicating the stress level at which plastic flow commences must be postulated. A relationship between stress and strain must be developed for post-yield behavior, i.e. when the deformation is made up of both elastic and plastic components. The yield surface separates the plastic region from the elastic region. The change in the stress state from the yield surface toward its interior will cause elastic unloading. Plastic loading will occur only if the increment of the stress is directed toward the outside of the yield surface.

The yield function can be represented by

$$F(\sigma_{ij}, k) = 0 \quad \text{or} \quad f(\sigma_{ij}) = k \tag{5.38}$$

where k is a material parameter. It can be determined experimentally. It can be a function of a few material strength coefficients or a constant for elastic-perfect-plastic material. The term k can be defined a function of a hardening

parameter κ. Thus the yield function can be extended to describe the post-yield of the material, or $k = k(\kappa)$.

For simplicity, the yield function in Eq. (5.38) can be rewritten in terms of the three principal stressesas.

$$F(\sigma_1, \sigma_2, \sigma_3, k) = 0 \tag{5.39}$$

For isotropic material, the yield function is independent of the orientation of the coordinate system employed. Therefore, it is usually presented by a function of the three invariants, i.e.,

$$F(I_1, J_2, J_3, k) = 0 \tag{5.40}$$

where I_1 is the first invariant of the stress tensor, J_2 and J_3 are respectively the second and the third invariants of the deviatoric stress tensor. Alternatively, the above yield function is represented as

$$F(I_1, J_2, \theta, k) = 0 \tag{5.41}$$

in which θ is a Haigh-Westergaard coordinate or Lode angle, as used in geotechnical engineering.

For elasto-perfect-plastic material, the parameter k in the yield functions is a constant. It means that the yield surface is independent of the plastic strain, thus the geometry and the size of the yield surface will not change with the successive deformation of the material. The post-yielding surface is exactly the initial one. When the stress point is retained at the yield surface, this means under loading conditions, and when the stress point moves into the inside of the yield surface, this implies unloading. For plastic hardening material, k can be defined by a work-hardening or strain-hardening parameter κ. The post-yielding surface is thus different from the initial yielding surface.

The equation is termed the normality condition since $\dfrac{\partial F}{\partial \sigma_{ij}}$ is a vector directed normal to the yield surface at the stress point under consideration.

Differentiating a hardening yield function, it has

$$dF = \frac{\partial F}{\partial \sigma_{ij}} d\sigma_{ij} + \frac{\partial F}{\partial k} dk = \frac{\partial F}{\partial \sigma_1} d\sigma_1 + \frac{\partial F}{\partial \sigma_2} d\sigma_2 + \frac{\partial F}{\partial \sigma_3} d\sigma_3 + \frac{\partial F}{\partial k} d\kappa = 0 \quad (5.42)$$

Introducing a parameter A, where $A = -\dfrac{1}{d\lambda} \dfrac{\partial F}{\partial k} dk$, the above equation can be rewritten in a matrix form as

$$\frac{\partial F}{\partial \sigma_{ij}} \mathrm{d}\sigma_{ij} - A\mathrm{d}\lambda = 0 \tag{5.43}$$

Converting Eq. (5.43) to a vector form by denoting

$\{\sigma\}^{\mathrm{T}} = \{\sigma_x, \sigma_y, \sigma_z, \tau_{xy}, \tau_{yz}, \tau_{zx}\}$, it has

$$\{a\}^{\mathrm{T}} = \frac{\partial F}{\partial \{\sigma\}} = \left\{ \frac{\partial F}{\partial \sigma_x}, \frac{\partial F}{\partial \sigma_y}, \frac{\partial F}{\partial \sigma_z}, \frac{\partial F}{\partial \tau_{xy}}, \frac{\partial F}{\partial \tau_{yz}}, \frac{\partial F}{\partial \tau_{zx}} \right\} \tag{5.44}$$

where $\{a\}$ is termed the flow vector. Thus,

$$\{a\}^{\mathrm{T}} \mathrm{d}\{\sigma\} - A\mathrm{d}\lambda = 0 \tag{5.45}$$

The strain increments can then be derived as

$$\mathrm{d}\{\varepsilon\} = [D]^{-1} \mathrm{d}\{\sigma\} + \{a\} \mathrm{d}\lambda \tag{5.46}$$

where $[D]$ is the usual matrix of elastic constants. Pre-multiplying both sides of Eq. (5.46) by $\{a\}^{\mathrm{T}}[D]$.

$$\{a\}^{\mathrm{T}}[D]\mathrm{d}\{\varepsilon\} = \{a\}^{\mathrm{T}} \mathrm{d}\{\sigma\} + \mathrm{d}\lambda\{a\}^{\mathrm{T}}[D]\{a\} = A\mathrm{d}\lambda + \mathrm{d}\lambda\{a\}^{\mathrm{T}}[D]\{a\} \tag{5.47}$$

The plastic multiplier is then obtained as

$$\mathrm{d}\lambda = \frac{\{a\}^{\mathrm{T}}[D]\mathrm{d}\{\varepsilon\}}{A + \{a\}^{\mathrm{T}}[D]\{a\}} \tag{5.48}$$

Substituting $\mathrm{d}\lambda$ into Eq. (5.46), the complete elasto-plastic incremental stress-strain relation can be derived to be

$$\mathrm{d}\{\sigma\} = [D]_{ep}\mathrm{d}\{\varepsilon\} \tag{5.49}$$

in which the elasto-plastic stiffness matrix $[D]_{ep}$ is

$$[D]_{ep} = [D] - \frac{[D]\{a\}\{a\}^{\mathrm{T}}[D]^{\mathrm{T}}}{A + \{a\}^{\mathrm{T}}[D]\{a\}} \tag{5.50}$$

It now remains to determine the explicit form of the scalar term *A*. *A* is a

function of the hardening parameter κ. Employing the work hardening hypothesis and the normality condition,

$$\mathrm{d}\kappa = \{\sigma\}^{\mathrm{T}} \mathrm{d}\{\varepsilon^{p}\} = \{\sigma\}^{\mathrm{T}} \mathrm{d}\lambda\{a\} = \mathrm{d}\lambda\{a\}^{\mathrm{T}}\{\sigma\} \tag{5.51}$$

For the uniaxial case, $\sigma = \bar{\sigma} = \sigma_Y$, $\mathrm{d}\varepsilon_p = \mathrm{d}\bar{\varepsilon}_p$, $\bar{\sigma}$ and $\bar{\varepsilon}_p$ are respectively the effective stress and plastic strain.

$$\mathrm{d}\kappa = \sigma_Y \mathrm{d}\bar{\varepsilon}_p = \mathrm{d}\lambda\{a\}^{\mathrm{T}}\{\sigma\} \tag{5.52}$$

The effective stress $\bar{\sigma}$ is a function of $\bar{\varepsilon}_p$, i.e. $\bar{\sigma} = H(\bar{\varepsilon}_p)$. Differentiating it, we obtain

$$\frac{\mathrm{d}\bar{\sigma}}{\mathrm{d}\bar{\varepsilon}_p} = \frac{\mathrm{d}\sigma_Y}{\mathrm{d}\bar{\varepsilon}_p} = H' \tag{5.53}$$

Using Euler's theorem applicable to all homogeneous functions of order one, we have

$$\{a\}^{\mathrm{T}}\{\sigma\} = \sigma_Y \tag{5.54}$$

Substituting Eqs. (5.53) and (5.54) into Eq. (5.52), we obtain

$$\mathrm{d}\lambda = \mathrm{d}\bar{\varepsilon}_p \quad \text{and} \quad A = H' \tag{5.55}$$

The parameter A is determined by the local slope of the uniaxial stress strain curve as

$$H' = \frac{E_T}{1 - E_T / E} \tag{5.56}$$

5.8　Determination of Flow Vector for Different Yield Functions

For the convenience of numerical simulation implementation, the yield functions in Eqs. (5.39)~(5.41) are often used (Nayak and Zienkiewicz, 1972; Owen and Hinton, 1980). The principal stresses can be calculated by

$$
\left\{ \begin{matrix} \sigma_1 \\ \sigma_2 \\ \sigma_3 \end{matrix} \right\} = \frac{2\sqrt{J_2}}{\sqrt{3}} \left\{ \begin{matrix} \cos\theta \\ \cos\left(\theta - \dfrac{2\pi}{3}\right) \\ \cos\left(\theta + \dfrac{2\pi}{3}\right) \end{matrix} \right\} + \frac{I_1}{3} \left\{ \begin{matrix} 1 \\ 1 \\ 1 \end{matrix} \right\}
\tag{5.57}
$$

with $\sigma_1 \geq \sigma_2 \geq \sigma_3$ and $0 \leq \theta \leq \pi/3$.

The flow vector can thus be expressed as

$$
\{a\}^{\mathrm{T}} = \frac{\partial F}{\partial \{\sigma\}} = \frac{\partial F}{\partial I_1}\frac{\partial I_1}{\partial \{\sigma\}} + \frac{\partial F}{\partial \sqrt{J_2}}\frac{\partial \sqrt{J_2}}{\partial \{\sigma\}} + \frac{\partial F}{\partial \theta}\frac{\partial \theta}{\partial \{\sigma\}}
\tag{5.58}
$$
$$
= C_1\{a_1\} + C_2\{a_2\} + C_3\{a_3\}
$$

where

$$
C_1 = \frac{\partial F}{\partial I_1}
\tag{5.59a}
$$

$$
C_2 = \left(\frac{\partial F}{2\sqrt{J_2}} + \frac{\cot 3\theta}{\sqrt{J_2}}\frac{\partial F}{\partial \theta} \right)
\tag{5.59b}
$$

$$
C_3 = -\frac{\sqrt{3}}{2\sin 3\theta \sqrt{J_2^3}}\frac{\partial F}{\partial \theta}
\tag{5.59c}
$$

$$
\{a_1\}^{\mathrm{T}} = \frac{\partial I_1}{\partial \{\sigma\}} = \{1,1,1,0,0,0\}
\tag{5.60a}
$$

$$
\{a_2\}^{\mathrm{T}} = \frac{\partial \sqrt{J_2}}{\partial \{\sigma\}} = \frac{1}{2\sqrt{J_2}}\{\sigma'_x,\sigma'_y,\sigma'_z,2\tau_{yz},2\tau_{zx},2\tau_{xy}\}
\tag{5.60b}
$$

$$
\{a_3\}^{\mathrm{T}} = \frac{\partial J_3}{\partial \{\sigma\}}
$$
$$
= \left\{ \left(\sigma'_y\sigma'_z - \tau_{yz}^2 + \frac{J_2}{3} \right), \left(\sigma'_x\sigma'_z - \tau_{xz}^2 + \frac{J_2}{3} \right), \left(\sigma'_x\sigma'_y - \tau_{xy}^2 + \frac{J_2}{3} \right), \right.
\tag{5.60c}
$$
$$
\left. 2(\tau_{xz}\tau_{xy} - \sigma'_x\tau_{yz}), (\tau_{xy}\tau_{yz} - \sigma'_y\tau_{xz}), (\tau_{yz}\tau_{xz} - \sigma'_z\tau_{yz}) \right\}
$$

And

$$
\frac{\partial \theta}{\partial \{\sigma\}} = \frac{\sqrt{3}}{2\sin 3\theta}\left[\frac{1}{\sqrt{J_3^2}}\frac{\partial J_3}{\partial \{\sigma\}} - \frac{3J_3}{J_2^2}\frac{\partial \sqrt{J_2}}{\partial \{\sigma\}} \right]
\tag{5.61}
$$

For different yield functions, the vectors $\{a_1\}$, $\{a_2\}$, and $\{a_3\}$ are consistent and only the constants C_1, C_2 and C_3 need to be determined. In Table 5.1, the constants for six different yield functions are given.

Table 5.1 Parameters C_1, C_2 and C_3 for 6 different yield functions

Yield function		C_1	C_2	C_3
Tresca		0	$2\left[\sin\left(\theta+\dfrac{\pi}{3}\right)+\cos\left(\theta+\dfrac{\pi}{3}\right)\cot 3\theta\right]$	$-\dfrac{\sqrt{3}\,\cos\left(\theta+\dfrac{\pi}{3}\right)}{J_2\,\sin 3\theta}$
Mises		0	$\sqrt{3}$	0
Yu $\alpha=1$ $b=1$	$\theta\le\theta_b$	0	$\sqrt{3}\,\sin\theta\,(\cot\theta-\cot 3\theta)$	$\dfrac{3\sin\theta}{2J_2\,\sin 3\theta}$
	$\theta\ge\theta_b$	0	$\sqrt{3}\left[\cos\left(\theta-\dfrac{\pi}{3}\right)-\sin\left(\theta-\dfrac{\pi}{3}\right)\cot 3\theta\right]$	$\dfrac{3\sin\left(\theta-\dfrac{\pi}{3}\right)}{2J_2\,\sin 3\theta}$
Mohr-Coulomb		$\dfrac{\sin\varphi}{3}$	$\left(\dfrac{\sin\varphi}{\sqrt{3}}+\cot 3\theta\right)\cos\left(\theta+\dfrac{\pi}{3}\right)$ $+\left(1-\dfrac{1}{\sqrt{3}}\cot 3\theta\,\sin\varphi\right)\sin\left(\theta+\dfrac{\pi}{3}\right)$	$\dfrac{\sin\left(\theta+\dfrac{\pi}{3}\right)\sin\varphi-\sqrt{3}\cos\left(\theta+\dfrac{\pi}{3}\right)}{2J_2\,\sin 3\theta}$
Drucker-Prager		α	1	0
Yu $\alpha\ne1$ $b=1$	$\theta\le\theta_b$	$\dfrac{2\sin\varphi}{3}$	$\dfrac{1}{\sqrt{3}}(3+\sin\varphi)\sin\theta\,(\cot\theta-\cot 3\theta)$	$\dfrac{(3+\sin\varphi)\sin\theta}{2J_2\,\sin 3\theta}$
	$\theta\ge\theta_b$	$\dfrac{2\sin\varphi}{3}$	$\dfrac{1}{\sqrt{3}}(3-\sin\varphi)\sin\left(\theta-\dfrac{\pi}{3}\right)$ $\cdot\left[\cot\left(\theta-\dfrac{\pi}{3}\right)-\cot 3\theta\right]$	$\dfrac{(3-\sin\varphi)\sin\left(\theta-\dfrac{\pi}{3}\right)}{2J_2\,\sin 3\theta}$

5.9   Singularity of Piecewise-Linear Yield Functions

The plastic flow vector has singular points for piecewise-linear yield functions, such as the single-shear theory (the Tresca yield function and the Mohr-Coulomb yield function), twin-shear theory and the unified strength theory. The flow vector at the corners is not unique when the normality condition is applied. Some smooth corner models have been proposed to eliminate the singularity of plastic flow for piecewise-linear yield functions. These smooth corner models can be divided into two categories (Koiter, 1953; Nayak and Zienkiewicz, 1972; Zienkiewicz and Pande, 1977; Owen and Hinton, 1980).

One category is that the projection on the deviatoric plane of the yield surface is

simply approximated by a circle (the Huber-von Mises and Drucker-Prager criteria fall into this category). It assumes the same tensile and compressive meridians, thus cannot agree the experimental results for geomaterials which always give different vector lengths for different meridians with a different angle on the deviatoric plane ($r_c \neq r_t$), as shown in Fig. 5.12.

The other category is a kind of smoothening model, which smoothens the corners using very complex mathematical models. It lacks a physical concept and is not convenient for use in analytical and numerical derivations. The following will introduce some convenient ways to solve the corner singularity problem for piecewise-linear yield functions, which can be readily implemented into elasto-plastic finite element analysis.

Considering the associated flow rule, the flow vector is normal to the yield surface. At the corners of the piecewise-linear yield functions, the flow vectors from different sides are thus not consistent. For unified strength theory, there are three corners on the deviatoric plane as shown in Fig. 5.13, i.e. $\theta = 0°$ (point A), $\theta = \theta_b$ (point C) and $\theta = 60°$ (point B). At the corners, the derivative of the yield function does not exist, the value and the direction of the plastic strain increment vector of the corner cannot be determined directly from the plastic flow rule.
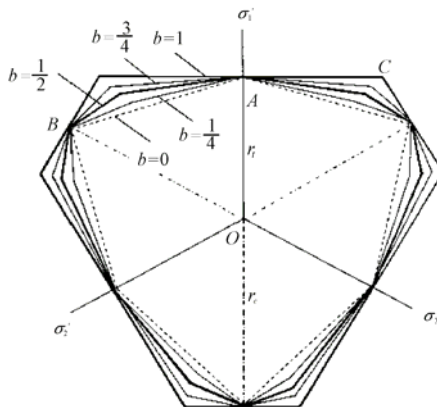

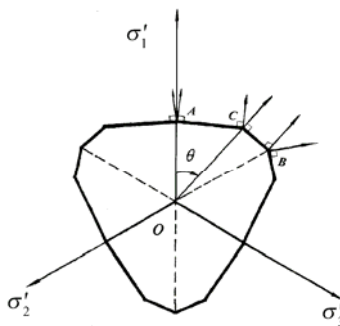**Fig. 5.12** Different vector lengths of yield loci

Fig. 5.13 Singular points of linear piece-wise yield surface

The process of the singularity includes
1) Vector summation method (Koiter, 1953). Its mathematical expression is

$$d\varepsilon_{ij}{}^{p} = d\lambda_1 \frac{\partial F_1}{\partial \sigma_{ij}} + d\lambda_2 \frac{\partial F_2}{\partial \sigma_{ij}} \tag{5.62}$$

2) Partially smoothening method (Nayak and Zienkiewicz, 1972). When dealing with the singularity of the Tresca and the Mohr-Coulomb functions, Nayak and Zienkiewicz (1972) expressed the yield function as $F = F(I_1, J_2, \theta, k)$, where I_1 is the first stress invariant, J_2 is the second partial stress invariant, θ is the angle of the deviatoric plane. The plastic strain increment of the corner ($\theta = \theta_0$) can be expressed as

$$d\varepsilon_{ij}{}^{p} = d\lambda \left(\frac{\partial F_{\theta=\theta_0}}{\partial I_1} \frac{\partial I_1}{\partial \sigma_{ij}} + \frac{\partial F_{\theta=\theta_0}}{\partial \sqrt{J_2}} \frac{\partial \sqrt{J_2}}{\partial \sigma_{ij}} + \frac{\partial F_{\theta=\theta_0}}{\partial \theta} \frac{\partial \theta}{\partial \sigma_{ij}} \right) \tag{5.63}$$

The third item of Eq. (5.63) is simply set to 0.
3) Linear combination method, i.e.

$$d\varepsilon_{ij}{}^{p} = \mu d(\varepsilon_{ij}{}^{p})_1 + (1-\mu)d(\varepsilon_{ij}{}^{p})_2 = \mu d\lambda_1 \frac{\partial f_1}{\partial \sigma_{ij}} + (1-\mu)d\lambda_2 \frac{\partial f_2}{\partial \sigma_{ij}} \tag{5.64}$$

where $0 \le \mu \le 1$, the direction of $d\varepsilon_{ij}^p$ is between $d(\varepsilon_{ij}^p)_1$ and $d(\varepsilon_{ij}^p)_2$.

These three methods can eliminate the singularity of the yield surface in some cases; however, each of them has some drawbacks and sometimes may introduce additional errors. For method (1), when the piecewise-linear function is the special case $F_1 = F_2$, the plastic strain increment is two times the real value, which is not unreasonable. An average of the vector summation is suggested to solve the problem by Yu et al. (1994; 2004). Method (2) eliminates the singularity of $\dfrac{\partial \theta}{\partial \sigma_{ij}}$, but it made the assumption that $\left.\dfrac{\partial F}{\partial \theta}\right|_{\theta=\theta_0} = 0$. Thus its application is limited. Method (3) introduced an uncertain parameter μ and from a practical analysis this method cannot eliminate the singularity in some cases. Besides, Zienkiewicz (1972) and Zienkiewicz and Pande (1977) proposed a smooth corner model to replace the piecewise-linear yield function.

Invariant expressions of the unified yield theory have the following form

$$F = \left(1 + \frac{\alpha}{2}\right) \frac{2}{\sqrt{3}} J_2{}^{1/2} \cos\theta + \frac{\alpha(1-b)}{1+b} J_2{}^{1/2} + \frac{I_1}{3}(1-\alpha) = \sigma_t \tag{5.65a}$$

$$F' = \left(\frac{2-b}{1+b}+\alpha\right)\frac{1}{\sqrt{3}}J_2^{1/2}\cos\theta + \left(\alpha+\frac{b}{1+b}\right)J_2^{1/2}\sin\theta + \frac{I_1}{3}(1-\alpha) = \sigma_t \quad (5.65b)$$

The projection curve on the deviatoric plane of Eqs. (5.62a) and (5.62b) is shown in Fig. 5.11. From $F=F'$, it gives

$$\theta_b = \arctan\frac{\sqrt{3}}{2\alpha+1}. \qquad (5.66)$$

According to the symmetrical condition, only the singularity of the three points A, B, and C should be discussed. For the Tresca criterion and the Mohr-Coulomb criterion, there are two singular points A, B only.

Using the plastic flow vector defined in Eq. (5.58), when $F \geq F'$, or $0 \leq \theta \leq \theta_b$, it gives

$$C_1 = \frac{1}{3}(1-\alpha) \qquad (5.67a)$$

$$C_2 = \left(1+\frac{\alpha}{2}\right)\frac{2}{\sqrt{3}}\cos\theta + \frac{\alpha(1-b)}{1+b}\sin\theta$$

$$+ \cot 3\theta\left[-\left(1+\frac{\alpha}{2}\right)\frac{2}{\sqrt{3}}\sin\theta + \frac{\alpha(1-b)}{1+b}\cos\theta\right] \qquad (5.67b)$$

$$C_3 = -\frac{\sqrt{3}}{2J_2\sin 3\theta}\left[-\left(1+\frac{\alpha}{2}\right)\frac{2}{\sqrt{3}}\sin\theta + \frac{\alpha(1-b)}{1+b}\cos\theta\right] \qquad (5.67c)$$

When $F<F'$, or $\theta_b < \theta \leq \pi/3$, it gives

$$C_1' = \frac{1}{3}(1-\alpha) \qquad (5.68a)$$

$$C_2' = \left(\frac{2-b}{1+b}\right)\frac{1}{\sqrt{3}}\cos\theta + \left(\alpha+\frac{b}{1+b}\right)\sin\theta$$

$$+ \cot 3\theta\left[-\left(\frac{2-b}{1+b}\right)\frac{1}{\sqrt{3}}\sin\theta + \left(\alpha+\frac{b}{1+b}\right)\cos\theta\right] \qquad (5.68b)$$

$$C_3' = -\frac{\sqrt{3}}{2J_2\sin 3\theta}\left[-\left(\frac{2-b}{1+b}+\alpha\right)\frac{1}{\sqrt{3}}\sin\theta + \left(\alpha+\frac{b}{1+b}\right)\cos\theta\right] \qquad (5.68c)$$

On the two lines AC and BC except for the corners, C_1, C_2, C_3 or C_1', C_2', C_3' have a unique value, and the plastic strain increment is unique. The singularity at the three corner points A, B, C is discussed separately below.

Point A   The corresponding stress state is $\sigma_1 \geq \sigma_2 = \sigma_3$, and $\theta=0$.
When $b \neq 1$

$$\sin\theta = 0, \cos\theta = 1, \cot 3\theta \to \infty \tag{5.69}$$

So, $C_2 \to \infty$, $C_3 \to \infty$, the plastic vector is a singular function.
When $b=1$

$$C_1 = \frac{1}{3}(1-\alpha), \lim_{\theta \to (\pi/3)} C_2 = \frac{2}{3\sqrt{3}}(2+\alpha), \lim_{\theta \to (\pi/3)} C_3 = \frac{1}{6J_2}(2+\alpha) \tag{5.70}$$

then

$$C_2\big|_{\theta=0} = \frac{2}{3\sqrt{3}}(2+\alpha), C_3\big|_{\theta=0} = \frac{1}{6J_2}(2+\alpha) \tag{5.71}$$

So, when $b=1$, there is no singularity for point A.
Point B   The stress state is $\sigma_1 \geq \sigma_2 = \sigma_3$, and $\theta=\pi/3$.
When $b \neq 1$,

$$\sin\left(\theta - \frac{\pi}{3}\right) = 0, \cos\left(\theta - \frac{\pi}{3}\right) = 1, \cot 3\theta \to \infty \tag{5.72}$$

So with $C'_2 \to \infty$, $C'_3 \to \infty$, there is singularity for the plastic flow.
When $b=1$,

$$C'_1 = \frac{1}{3}(1-\alpha), \lim_{\theta \to (\pi/3)} C'_2 = \frac{2}{3\sqrt{3}}(2\alpha+1), \lim_{\theta \to (\pi/3)} C'_3 = -\frac{1}{6J_2}(2\alpha+1) \tag{5.73}$$

so that

$$C'_2\big|_{\theta=\pi/3} = \frac{2}{3\sqrt{3}}(2\alpha+1), C'_3\big|_{\theta=\pi/3} = -\frac{1}{6J_2}(2\alpha+1) \tag{5.74}$$

So, when $b=1$, there is no singularity for point B.
Point C $F = F', \theta = \theta_0 = \arctan\dfrac{\sqrt{3}}{2\alpha+1}$
When $b \neq 0$,

$$C_1 = C'_1, C_2 \neq C'_2, C_3 \neq C'_3 \tag{5.75}$$

There is singularity for the plastic flow.

When $b = 0$, $F = F'$, it is the Mohr-Coulomb criterion,

$$C_1 = C_1', C_2 = C_2', C_3 = C_3' \tag{5.76}$$

and there is no singularity for the plastic flow.

So, for the three singular points A, B, C, when $b=1$ there is no singularity for points A, B; when $b = 0$, there is no singularity for point C.

5.10 Process of Singularity of the Plastic Flow Vector

The three different methods discussed in Section 5.9 are first adopted to solve the singularity at the three points A, B, C.

Point A If method (1) is used,

$$C_1^{\ I} = \frac{2}{3}(1 - \alpha) \tag{5.77a}$$

$$C_2^{\ I} = \lim_{\theta \to 0^+} C_2 + \lim_{\theta \to 0^-} C_2 = \frac{4}{3\sqrt{3}}(2 + \alpha) \tag{5.77b}$$

$$C_3^{\ I} = \lim_{\theta \to 0^+} C_3 + \lim_{\theta \to 0^-} C_3 = \frac{1}{3J_2}(2 + \alpha) \tag{5.77c}$$

When $b=1$, there is no singularity for point A. When $b \to 1$, $C_1^{\ I}$, $C_2^{\ I}$, $C_3^{\ I}$ should be equal to $C_1|_{\substack{b=0 \\ \theta=0}}$, $C_2|_{\substack{b=0 \\ \theta=0}}$, $C_3|_{\substack{b=0 \\ \theta=0}}$. However, $C_1^{\ I} = 2C_1|_{\substack{b=0 \\ \theta=0}}$, $C_2^{\ I} = 2C_2|_{\substack{b=0 \\ \theta=0}}$, $C_3^{\ I} = 2C_3|_{\substack{b=0 \\ \theta=0}}$, so method (1) is actually unreasonable.

If method (2) is used it gives

$$C_1^{\ II} = \frac{1}{3}(1 - \alpha) \tag{5.78a}$$

$$C_2^{\ II} = \frac{4}{3}(2 + \alpha) \tag{5.78b}$$

$$C_3^{\ II} = 0 \tag{5.78c}$$

i.e., $C_1^{\ II} = C_1|_{\substack{b=1 \\ \theta=0}}$, $C_2^{\ II} \neq C_2|_{\substack{b=1 \\ \theta=0}}$, $C_3^{\ II} \neq C_3|_{\substack{b=1 \\ \theta=0}}$, so method (2) is also unreasonable.

If method (3) is used it gives

$$C_1^{\text{III}} = \frac{1}{3}(1-\alpha) \tag{5.79a}$$

$$C_2^{\text{III}} = \mu \lim_{\theta \to 0^+} C_2 + (1-\mu) \lim_{\theta \to 0^-} C_2 \tag{5.79b}$$

$$C_3^{\text{III}} = \mu \lim_{\theta \to 0^+} C_3 + (1-\mu) \lim_{\theta \to 0^-} C_3 \tag{5.79c}$$

When $\mu=1/2$, $C_1^{\text{III}} = C_1\big|_{\substack{b=1\\\theta=0}}$, $C_2^{\text{III}} = C_2\big|_{\substack{b=1\\\theta=0}}$, $C_3^{\text{III}} = C_3\big|_{\substack{b=1\\\theta=0}}$. So the singularity of point A is eliminated. When $\mu \neq 1/2$, $C_2^{\text{III}} \to \infty$, $C_3^{\text{III}} \to \infty$, the singularity of point A cannot be eliminated. So method (3) is not suitable in some instances.

Point B After some derivation, the following can be obtained:

$$C_1'^{\text{I}} = \frac{2}{3}(1-\alpha) \quad C_2'^{\text{I}} = \frac{4}{3\sqrt{3}}(2\alpha+1) \quad C_3'^{\text{I}} = -\frac{1}{3J_2}(2\alpha+1) \tag{5.80a}$$

$$C_1'^{\text{II}} = \frac{1}{3}(1-\alpha) \quad C_2'^{\text{II}} = \frac{1}{\sqrt{3}}(2\alpha+1) \quad C_3'^{\text{II}} = 0 \tag{5.80b}$$

$$C_1'^{\text{III}} = \frac{1}{3}(1-\alpha), \quad C_2'^{\text{III}} = \mu \lim_{\theta \to (\pi/3)^+} C_2' + (1-\mu) \lim_{\theta \to (\pi/3)^-} C_2',$$

$$C_3'^{\text{III}} = \mu \lim_{\theta \to (\pi/3)^+} C_3' + (1-\mu) \lim_{\theta \to (\pi/3)^-} C_3'' \tag{5.80c}$$

It can achieve similar conclusions to point A.

Point C If method (1) is used it gives

$$C_1^{\text{I}} = \frac{2}{3}(1-\alpha) \tag{5.81a}$$

$$C_2^{\text{I}} = C_2\big|_{\theta=\theta_0} + C_2'\big|_{\theta=\theta_0} \tag{5.81b}$$

$$C_3^{\text{I}} = C_3\big|_{\theta=\theta_0} + C_3'\big|_{\theta=\theta_0} \tag{5.81c}$$

It can be seen that $\lim_{b \to 0} C_1^{\text{I}} = 2C_1\big|_{b=0}$, $\lim_{b \to 0} C_2^{\text{I}} = 2C_2\big|_{b=0}$, $\lim_{b \to 0} C_3^{\text{I}} = 2C_3\big|_{b=0}$. However, when $b=0$, there is no singularity for point C, so method (1) is unreasonable.

If method (2) is used

$$C_1^{\text{II}} = C_1'^{\text{II}} = \frac{1}{3}(1-\alpha) \tag{5.82a}$$

$$C_2^{\text{II}} = \left(1+\frac{\alpha}{2}\right)\frac{2}{\sqrt{3}}\cos\theta_0 + \left(\frac{\alpha(1-b)}{1+b}\right)\sin\theta_0 \tag{5.82b}$$

$$C_2'^{\text{II}} = \left(\frac{2-b}{1+b} + \alpha\right)\frac{1}{\sqrt{3}}\cos\theta_0 + \left(\alpha + \frac{b}{1+b}\right)\sin\theta_0 \tag{5.82c}$$

$$C_3^{\text{II}} = C_3'^{\text{II}} = 0 \tag{5.82d}$$

For $C_2^{\text{II}} \neq C_2'^{\text{II}}$ $(b \neq 0)$, so method (2) cannot eliminate the singularity at Point C.

If method (3) is used it gives

$$C_1^{\text{III}} = \frac{1}{3}(1-\alpha) \tag{5.83a}$$

$$C_2^{\text{III}} = \mu C_2|_{\theta=\theta_0} + (1-\mu)C_2'|_{\theta=\theta_0} \tag{5.83b}$$

$$C_3^{\text{III}} = \mu C_3|_{\theta=\theta_0} + (1-\mu)C_3'|_{\theta=\theta_0} \tag{5.83c}$$

This method can eliminate the singularity of point C and $\lim\limits_{b\to 0} C_2^{\text{III}} = C_2|_{b=0}$, $\lim\limits_{b\to 0} C_3^{\text{III}} = C_3|_{b=0}$.

5.11   Suggested Methods

From the above discussion, methods (1) and (2) are unreasonable, method (3) cannot eliminate the singularity in some cases. Two simple methods are suggested to eliminate the singularity for the piecewise-linear yield functions (Yu, 1994; 1998; 2004).

Method (4) uses the average method of flow vectors, i.e. assuming $\mu = 1/2$ in method (3).

At point A it gives

$$C_1^{(A)} = \frac{1}{3}(1-\alpha),\ C_2^{(A)} = \frac{1}{6J_2}(2+\alpha),\ C_3^{(A)} = \frac{1}{6}(1-\alpha) \tag{5.84}$$

At point B the constants are

$$C_1'^{(A)} = \frac{1}{3}(1-\alpha),\ C_2'^{(A)} = \frac{1}{3\sqrt{3}}(2\alpha+1),\ C_3'^{(A)} = \frac{1}{6J_2}(2\alpha+1) \tag{5.85}$$

They are equal to the corresponding parameters when $b = 1$.

At point C the constants become

$$C_1^{(A)} = \frac{1}{2}\left(C_1\big|_{\theta=\theta_0} + C_1'\big|_{\theta=\theta_0}\right) = \frac{1}{3}(1-\alpha)$$

$$C_2^{(A)} = \frac{1}{2}\left(C_2\big|_{\theta=\theta_0} + C_2'\big|_{\theta=\theta_0}\right) \tag{5.86}$$

$$C_3^{(A)} = \frac{1}{2}\left(C_3\big|_{\theta=\theta_0} + C_3'\big|_{\theta=\theta_0}\right)$$

And it satisfies $C_1^{(A)} = C_1\big|_{b=0}$, $\lim\limits_{b\to 0} C_2^{(A)} = C_2\big|_{b=0}$, $\lim\limits_{b\to 0} C_3^{(A)} = C_3\big|_{b=0}$. The constants based on method (4) are reasonable because they can be degraded to that of the special cases when $b=1$ at corners A and B, and when $b=0$ at corner C. **Method (5)** simply uses the constants of the case where $b=1$ for points A and B and the constants of $b=0$ for point C.

For point A it gives

$$C_1^{(B)} = \frac{1}{3}(1-\alpha), \ \ C_2^{(B)} = \frac{1}{3\sqrt{3}}(2+\alpha), \ \ C_3^{(B)} = \frac{1}{6J_2}(2+\alpha) \tag{5.87}$$

For point B the constants are

$$C_1'^{(B)} = \frac{1}{3}(1-\alpha),$$

$$C_2'^{(B)} = \frac{1}{3\sqrt{3}}(2\alpha+1), \tag{5.88}$$

$$C_3'^{(B)} = \frac{1}{6J_2}(2\alpha+1)$$

For point C they are

$$C_1^{(B)} = \frac{1}{3}(1-\alpha)$$

$$C_2^{(B)} = \left(1+\frac{\alpha}{2}\right)\frac{2}{\sqrt{3}}\cos\theta_0 + \alpha\sin\theta_0 \tag{5.89}$$

$$C_3^{(B)} = -\frac{\sqrt{3}}{2J_2\sin 3\theta_0}\left[-\left(1+\frac{\alpha}{2}\right)\frac{2}{\sqrt{3}}\sin\theta_0 + \alpha\cos\theta_0\right]$$

These two methods are shown in Figs. 5.14 and 5.15. The average method of flow vectors for the piecewise-linear yield function is used for method (4), as shown in Fig. 5.14; the corner of the yield function is 'cut' by using method (5), as

shown in Fig. 5.15.
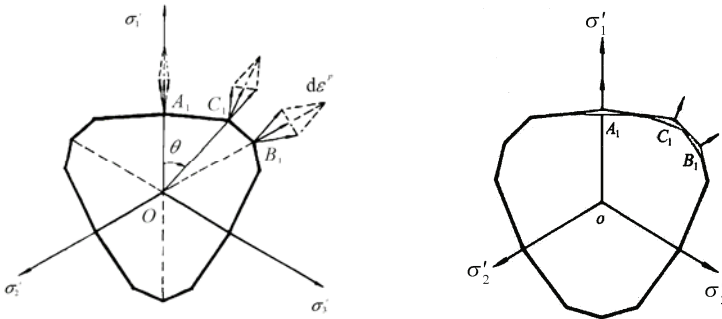
Fig. 5.14 Process of singular points (method 4)   **Fig. 5.15** Process of singular points (method 5)

Table 5.2 shows the values of the parameters C_1, C_2, C_3 for different methods. From the table, we can be find the parameters C_1, C_2, C_3 of points A, B for method (4) and method (5). These two methods are more reasonable than method (1) and method (2) and more applicable than method (3). It is very simple. The physical concept of the average method of flow vectors is clear.

Table 5.3 shows the parameters of methods (4) and (5) when α, b are given different values. From this table, it can be found that method (5) is independent of the parameter b, and is close to method (4) when b is near 0.

Table 5.2 Values of the parameters

Method	Point A			Point B		
	C_1	C_2	C_3	C_1	C_2	C_3
(1)	$\frac{2}{3}(1-\alpha)$	$\frac{4}{3\sqrt{3}}(2+\alpha)$	$\frac{1}{3J_2}(2+\alpha)$	$\frac{2}{3}(1-\alpha)$	$\frac{4}{3\sqrt{3}}(2\alpha+1)$	$-\frac{1}{3J_2}(2\alpha+1)$
(2)	$\frac{1}{3}(1-\alpha)$	$\frac{1}{\sqrt{3}}(2+\alpha)$	0	$\frac{1}{3}(1-\alpha)$	$\frac{1}{\sqrt{3}}(2\alpha+1)$	0
(3)	$\frac{1}{3}(1-\alpha)$	$\mu \neq \frac{1}{2}, \infty$ $\mu = \frac{1}{2}$ $\frac{2}{3\sqrt{3}}(2+\alpha)$	$\mu \neq \frac{1}{2}, \infty$ $\mu = \frac{1}{2}$ $\frac{1}{6J_2}(2+\alpha)$	$\frac{1}{3}(1-\alpha)$	$\mu \neq \frac{1}{2}, \infty$ $\mu = \frac{1}{2}$ $\frac{2}{3\sqrt{3}}(2\alpha+1)$	$\mu \neq \frac{1}{2}, \infty$ $\mu = \frac{1}{2}$ $-\frac{1}{6J_2}(2\alpha+1)$
(4)	$\frac{1}{3}(1-\alpha)$	$\frac{2}{3\sqrt{3}}(2+\alpha)$	$\frac{1}{6J_2}(2+\alpha)$	$\frac{1}{3}(1-\alpha)$	$\frac{2}{3\sqrt{3}}(2\alpha+1)$	$-\frac{1}{6J_2}(2\alpha+1)$
(5)	$\frac{1}{3}(1-\alpha)$	$\frac{2}{3\sqrt{3}}(2+\alpha)$	$\frac{1}{6J_2}(2+\alpha)$	$\frac{1}{3}(1-\alpha)$	$\frac{2}{3\sqrt{3}}(2\alpha+1)$	$-\frac{1}{6J_2}(2\alpha+1)$

Table 5.3 Comparison of the parameters

α	Method (5)		Method (4)									
	$0 \le b \le 1$		$b = 0$		$b = 0.25$		$b = 0.5$		$b = 0.75$		$b = 1$	
	C_2	$C_3 \cdot J_2$	C_2	$C_3 \cdot J_2$	C_2	$C_3 \cdot J_2$	C_2	$C_3 \cdot J_2$	C_2	$C_3 \cdot J_2$	C_2	$C_3 \cdot J_2$
$\alpha = 1$	2	0	2	0	1.8	0	1.67	0	1.6	0	1.5	0
$\alpha = 0.75$	1.81	0.26	1.8	0.26	1.62	0.21	1.5	0.17	1.4	0.15	1.3	0.13
$\alpha = 0.5$	1.78	0.58	1.8	0.58	1.58	0.47	1.44	0.39	1.4	0.33	1.3	0.29
$\alpha = 0.25$	2.32	1.31	2.3	1.31	1.98	1.05	1.76	0.88	1.6	0.75	1.5	0.66

5.12   Unified Process of the Corner Singularity

From the above analysis, the following can be found:

The expression of the piece-linear yield function is simple and easy to use. It can be adopted for various close-form analyses of various classical elasto-plastic problems. However, the singularity of plastic flow for the piecewise-linear yield function may cause some troubles in elasto-plastic flow vector calculation. Process of singular points for the piece-wise functions is necessary.

1) Traditional methods used to eliminate singularity are unreasonable or cannot be used in all cases. There exist obvious errors and drawbacks.

2) The two suggested methods are easy for handling the singularity problem and can be used conveniently to eliminate the singularity of the present piecewise-linear yield function plastic flow.

3) Using the unified strength theory as the yield potential function and adopting the suggested unified process of the flow vector singularity can solve the singularity of all kinds of corners, which improves the calculation efficiency. The processing method of the singularity problem can be implemented into a computer program conveniently and in a unified form.

Different results for the single yield function can be obtained as follows:

5.12.1 Tresca Yield Criterion

When $\theta = 0°$, $\theta = 60°$, it gives

$$f = \sqrt{3}\sqrt{J_2} - \sigma_s = 0 \tag{5.90}$$

With the derivation in Eqs. (5.69)~(5.71), it gives

$$C_1 = 0, \ C_2 = \sqrt{3}, \ C_3 = 0 \tag{5.91}$$

Compared with Table 5.1, it can be found that in the corner of Tresca criterion, this result is the same as the one of Huber-von Mises.

5.12.2 Mohr-Coulomb Yield Criterion

$$\theta = 0°, F = \frac{1}{3} I_1 \sin\varphi + \frac{1}{2}\sqrt{\frac{J_2}{3}}(3 + \sin\varphi) - C_0 \cos\varphi = 0$$

$$\theta = 60°, F = \frac{1}{3} I_1 \sin\varphi + \frac{1}{2}\sqrt{\frac{J_2}{3}}(3 - \sin\varphi) - C_0 \cos\varphi = 0 \tag{5.92}$$

With the derivation in Eqs. (5.69)~(5.71), it gives

$$\theta = 0°, C_1 = \frac{1}{3}\sin\varphi, C_2 = \frac{1}{2\sqrt{3}}(3 + \sin\varphi), C_3 = 0$$

$$\theta = 60°, C_1 = \frac{1}{3}\sin\varphi, C_2 = \frac{1}{2\sqrt{3}}(3 - \sin\varphi), C_3 = 0 \tag{5.93}$$

5.12.3 Twin-Shear Yield Criterion

At the corner

$$\theta_b = \arctan\frac{\sqrt{3}}{3} = \frac{\pi}{6} \tag{5.94}$$

$$f = f' = \frac{3}{2}\sqrt{J_2} - \sigma_3 = 0 \tag{5.95}$$

Then

$$C_1 = 0, C_2 = \sqrt{3}, C_3 = 0 \tag{5.96}$$

5.12.4 Generalized Twin-Shear Yield Criterion

The corner is not at $\theta = \pi/6$ for the generalized twin-shear stress yield criterion. From $F = F'$, the angle can be obtained as in Figs. 5.10 and 5.11.

$$\theta_b = \arctan\left(\frac{\sqrt{3}(1 + \sin\varphi)}{3 - \sin\varphi}\right) \tag{5.97}$$

At the corner

$$F = F' = \frac{2}{3} I_1 \sin\varphi + \sqrt{\frac{J_2}{3}} (3 + \sin\varphi) \cos\theta_b - 2C_0 \cos\varphi \qquad (5.98)$$

Using Eqs. (5.69)~(5.71), it gives

$$C_1 = \frac{2}{3} \sin\varphi, C_2 = \frac{1}{\sqrt{3}} (3 + \sin\varphi) \cos\theta_b, C_3 = 0 \qquad (5.99)$$

After the handling of the generalized twin-shear yield criterion, the direction and relative value of the plastic flow vector on the deviatoric plane are shown in Fig. 5.16.

From the above singularity process, we can obtain a certain value of the flow vector for any single criterion. For the unified strength theory, the constants can be derived with a unified solution. The constant C_i of the unified strength theory is shown in Table 5.4.
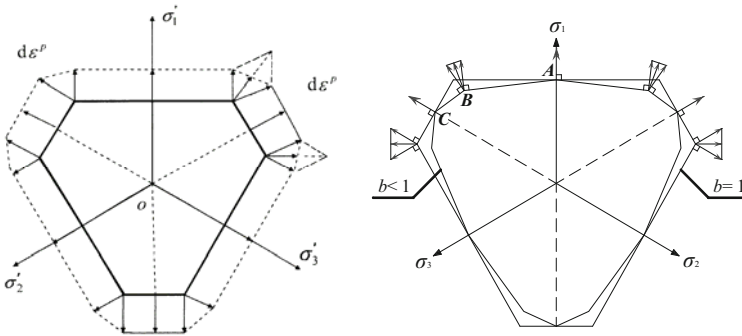
Fig. 5.16 Plastic flow of the unified strength theory

Table 5.4 Parameters for the unified strength theory

θ	b	C_1	C_2	C_3
0	$b=1$	$\frac{1}{3}(1-\alpha)$	$\frac{2}{3\sqrt{3}}(2+\alpha)$	$\frac{1}{6J_2}(2+\alpha)$
	$0 \le b < 1$	$\frac{1}{3}(1-\alpha)$	$\frac{1}{\sqrt{3}}(2+\alpha)$	0
60	$b=1$	$\frac{1}{3}(1-\alpha)$	$\frac{2}{3\sqrt{3}}(2\alpha+1)$	$-\frac{1}{6J_2}(2+\alpha)$
	$0 \le b < 1$	$\frac{1}{3}(1-\alpha)$	$\frac{1}{\sqrt{3}}(1+2\alpha)$	0
θ_b	$0 < b \le 1$	$\frac{1}{3}(1-\alpha)$	$\dfrac{\dfrac{(2+\alpha)}{\sqrt{3}}\cos\theta}{-\dfrac{(2+\alpha)\cos 3\theta}{\sqrt{3}(3\cos^2\theta - \sin^2\theta)}}$	$\dfrac{(2+\alpha)}{2J_2(3\cos^2\theta - \sin^2\theta)}$

The direction and the relative value of the plastic flow vector for the unified strength theory are shown in the solid lines of Fig. 5.17. It can be seen that the singularity processing method can lead to a reasonable, uniformly and continually variable flow vector on the yield surface.
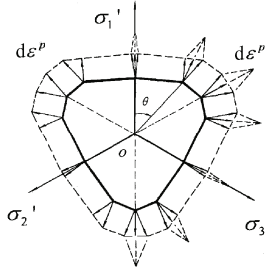
Fig. 5.17 Plastic strain increments of the unified strength theory with $b=1/2$

5.13 Brief Summary

The plastic stress-strain relationship as an important part of plasticity is described in this chapter. The plastic flow vector has singular points for the piecewise yield functions and the piecewise-linear yield functions. The Tresca yield function, the Mohr-Coulomb yield function, the twin-shear yield function and the unified strength theory are all piecewise-linear yield functions. The flow vector at the corners is not unique when the normality condition is applied. A simple and unified method is suggested for solving the singularity.

The associated flow rule and the incremental constitutive relations for the unified strength theory are given. Some methods have been proposed to eliminate the singularity of plastic flow for piecewise-linear yield functions. The plastic strain increments of the unified strength theory in the whole region are shown in Fig. 5.16 and Fig. 5.17. The suggested method can also be applied to nonsmooth multisurface plasticity and viscoplasticity.

Now the singularity of the plastic flow of piecewise-linear yield functions is not a problem for computational plasticity, but a characteristic of piecewise-linear yield functions. The Tresca criterion, the Mohr-Coulomb criterion, the twin-shear yield criterion, the generalized twin-shear criterion and unified strength theory are successfully applied in elasto-plasticity analysis of structures, computational mechanics and numerical analysis in mechanical engineering, geotechnical engineering and other fields.

References

Belytschko T, Liu WK and Moran B (2000) Nonlinear Finite Elements for Continua and Structures. John Wiley: Chichester, New York.

Chakrabarty J (1987) Theory of Plasticity. McGraw-Hill: New York.

Drucker DC (1952) A more fundamental approach to plastic stress-strain relations, 1st U.S. Congress of Applied Mechanics, ASME, New York, pp 116-126.

Dunne F and Petrinic N (2005) Introduction to Computational Plasticity. Oxford University Press: Oxford and New York.

Hill R (1950) The Mathematical Theory of Plasticity. Clarendon: Oxford.

Johnson W and Mellor PB (1962) Plasticity for Mechanical Engineers. Van Nostrand: London and New York.

Khan AS (1995) Continuum Theory of Plasticity. John Wiley & Sons: New York.

Koiter WT (1953) Stress-strain relations, uniqueness and variational theorems for elastic-plastic materials with singular yield surface. Quart. Appl. Math., 11: 350-354.

Martin J.B (1975) Plasticity: Fundamentals and General Results. The MIT Press.

Mendelson A (1968) Plasticity: Theory and Application. Macmillan: New York.

Nayak GC and Zienkiewicz OC (1972) Convenient form of stress invariants for plasticity. Journal of the Structure Division, Proc. Of ASCE, 949-953.

Owen DRJ and Hinton E (1980) Finite Elements in Plasticity: Theory and Practice. Pineridge Press Limited: Swansea, UK.

Owen DRJ, Hinton E and Onate E (1989) Computational Plasticity: Models, Software and Applications. Pineridge Press Limited, pp 1460.

Simo JC and Hughes TJR (1998) Computational Plasticity. Springer: Berlin.

Simo JC, Kennedy JG and Govindjee S (1988) Non-smooth multisurface plasticity and viscoplasticity, loading/unloading conditions and numerical algorithms. Int. J. for Numerical Methods in Engineering, 26: 2162-2185.

Sloan,S.W.and Booker,J.R. (1986), Removal of singularities in Tresca and Mohr-Coulomb yield function. Comm. Appl. Num. Meth., 2: 173-179.

Smith DL ed. (1990), Mathematical Programming Methods in Structural Plasticity. (21 papers, 435 pages) Springer-Verlag: Wien.

Smith IM and Griffiths DV (2004) Programming the Finite Element Method. 4th edition John Wiley & Sons, Ltd.

Yu MH (1983) Twin shear stress yield criterion, Int. J. Mech. Sci., 25(1): 71-74.

Yu MH, He LN and Song LY (1985) Twin shear stress strength theory and its generalization. Scientia Sinica (Sciences in China), series A, 28 (11): 1174-1183.

Yu MH and He LN (1991) A new model and theory on yield and failure of materials under the complex stress state. Mechanical Behavior of Materials-6: Pergamon Press: Oxford, vol.3, pp 841-846.

Yu MH and Li YM (1991) Twin shear constitutive theory and its computational implementation. In: Computational Mechanics, Ed. by Cheung YK, Lee JHW and Leung AYT. Balkema: Rotterdam, pp 875-879.

Yu MH and Zeng WB. (1994) New theory of engineering structural analysis and its

application. J. Eng. Mech., 11(1): 9-20 (in Chinese, English abstract).

Yu Mao-hong (1998) Twin-shear Theory and Its Applications. Science Press: Beijing (in Chinese)

Yu MH, Yang SY and Fan SC (1999) Unified elasto-plastic associated and non-associated constitutive model and its application. Computers and Structures,71(6): 627-636.

Yu MH (2004) Unified Strength theory and Its Applications. Springer: Berlin.

Yu MH et al. (2006) Generalized Plasticity. Springer: Berlin.

Zienkiewicz OC and Pande GN (1977) Some useful forms of isotropic yield surfaces for soil and rock mechanics, Finite Elements in Geomechanics, ed. Gudehus. John Wiley & Sons Ltd, pp 179-190.

6

Implementation of the Unified Strength Theory into FEM Codes

6.1 Introduction

The yield criteria and various material models have been implemented into elasto-plastic programs and most current commercial FEM systems. In some systems, only the Huber-von Mises criterion, Drucker-Prager criterion and the Mohr-Coulomb criterion were implemented. Sometimes, the multi-parameters criteria for geomaterials and concrete structures are also used. The twin-shear strength theory has been implemented into special finite element programs since 1990 (Yu and Meng, 1990; Yu and Li, 1991; Yu, 1992; Yu et al., 1992). Only some single models, however, are used in several programs, and only one result can be obtained by using the single material model, which can be adopted only for one kind of material. Such models as the Tresca model can be used only for non-SD materials (those materials with the same strength both in tension and in compression), and the shear strength equals half of the tensile strength $\tau_y = 0.5\sigma_y$. The Huber-von Mises model can be used for non-SD materials with the shear strength $\tau_y = 0.577\sigma_y$. The twin-shear yield criterion (Yu, 1961) or the maximum deviatoric stress criterion (Haythornthwaite, 1961), the shape distortion criterion (Schmidt-Ishilinsky, 1932-1940), or the matched circular criterion (Hill, 1950) can be used only for non-SD materials, and with the shear strength $\tau_y = 0.667\sigma_y$. There is no relationship between these material models.

The unified yield criterion and the unified strength theory have been implemented and applied to several plasticity and engineering problems (Yu et al., 1992; Yu et al., 1993; Yu and Zeng, 1994; Yu et al., 1997; 1999). The singularities at the corners of the single-shear series of strength theory, twin-shear series of strength theory and the singularity of the unified strength theory have been overcome by using a unified numerical procedure.

Yu and his research group wrote a special elasto-plastic FEM program. It is called the UEPP-Unified Elasto-Plastic Program (Yu et al., 1993; Yu et al., 1992; Yu and Zeng, 1994; Yu and Lu, 1994; Yu and Yang, 1997; Yu et al., 1999). The feature of the UEPP is that the unified strength theory was implemented into the finite element method code. UEPP includes two codes, i.e. UEPP-2D for plane stress, plane strain and axial-symmetric problems and UEPP-3D for three-dimensional problems. The material models are increasing and forming a series of systematical and effective constitutive relations for practical use. A detailed description of the unified strength theory and UEPP can be seen in the books "New System of Strength Theory" (Yu, 1992, in Chinese) and "Twin-Shear Theory and its Applications" (Yu, 1998, in Chinese). Some examples can be found in the papers in English (Yu et al., 1992; Yu and Zeng, 1993; Yu et al., 1994, Yu et al., 1999; Yu, 2001; Yu et al., 2001) and Chinese papers (Yu and Zeng, 1994; Yu and Lu, 1994; Yu et al., 1997).

Recently, the unified strength theory was also implemented into the general FEM code, such as ABAQUS, AutDYN and FLAC-3D at Nangyang Technological University, Singapore; Griffith University in Australia, the National Key Laboratory of Geomechanics and Geotechnical Engineering, Institute of Rock and Soil Mechanics, Chinese Academy of Science; Beijing Sci. and Tech. University, Sichuan University, Jinan University in China. The work was conducted by Shen (1993), Quint Co. (1993; 1994), Li and Ishii (1994; 1998), Liu et al. (1994), Wang (1998), Fan and Qiang (2001), Zhang et al. (2001), Zhou (2002), Zhang CQ (2005), Shao and Qian (2007), Shao et al. (2007), Yang (2008), Li et al. (2008), Li (2008), Wang et al. (2008), Zhang et al. (2008). The details can be seen in chapter 1. Table 1.1 gives some cases of yield criteria in FEM codes

The unified strength theory can be applied and implemented into various elasto-plastic programs. It is worth showing that most parts of the elasto-plastic program are the same as the conventional program, only the subroutine of yield criteria (subroutine "INVAR" to calculate equivalent stresses), the subroutine of flow vector and the subroutine of the corner (subroutine "YIELD" and "FOLWPL" to calculate flow vector) are different. The details of the finite element method in plasticity can be seen in Hinton and Owen (1977), Owen and Hinton (1980), Lewis and Schrefler (1987), Owen et al., (1989), Smith and Griffiths (2004). An elasto-plastic program in 2D and an elasto-viscoplastic program in 2D are presented in chapter 7 and chapter 8 of the book by Owen and Hinton (1980). A 2D non-linear thermo-elastoplastic consolidation program, PLASCON, is described in detail in chapter 9 by Majorana in the book of Lewis and Schrefler (1987). The unified strength theory is easy to implement in these programs.

A series of results can be obtained by using the unified strength theory for various problems. It can be applied in various materials such as metal, plastic,rock, soil and concrete. Therefore, it can not only be employed in strength calculation of metal structures and machine parts in mechanical engineering, electrical engineering, chemical engineering, aeronautical engineering and railway

engineering, but can also be used in elastic and plastic analysis of geological and concrete structures in civil engineering, geological engineering and hydraulic engineering. In the meantime, it can be applied in the computer-aided teaching of courses such as mechanics of materials, plasticity, plastic ultimate analysis of structures, finite element methods and geomechanics.

It contains:
1) Elastic limit analysis;
2) Elasto-plastic analysis of structures;
3) Plastic limit analysis of structures;
4) Elasto-visco-plastic analysis;
5) Eigenvalue analysis;
6) Elasto-plastic transient analysis;
7) Earthquake response analysis.

6.2 Bounds of the Single Criteria for Non-SD Materials

The stress state of an arbitrary infinitesimal element can be described in three principal stresses. We call the two or three principle stresses state the complex stress state. The strength of material under the complex stress state is an important and complicated problem. A large amount of research was conducted by researchers all over the world, and various yield or failure criteria were proposed. The three main yield criteria for metal materials with the same tensile and compressive strength are:

1). Single-shear yield criterion (Tresca, 1864) used for those materials: $\tau_y = 0.5\sigma_y$;

2). Three-shear yield criterion (Huber-von Mises, 1904-1913), used for those materials: $\tau_y = 0.577\sigma_y$;

3). Twin-shear yield criterion (Yu, 1961) or maximum deviatoric stress criterion (Haythornthwaite, 1961) used for those materials: $\tau_y = 0.667\sigma_y$

These three yield loci in π-plane are shown in Fig. 6.1.

The intermediate principle stress σ_2 was not taken into account in the Tresca yield criterion. Many studies were devoted to the research of the effect of the intermediate principle stress. The intermediate principle stress σ_2 was taken into account through the consideration of the intermediate principle shear stress by Yu Maohong in 1961. The mathematical modeling of the twin-shear stress yield criterion is as follows:

$$f = \tau_{13} + \tau_{12} = C \qquad \text{when} \quad \tau_{12} \geq \tau_{23} \qquad\qquad (6.1a)$$
$$f' = \tau_{13} + \tau_{23} = C \qquad \text{when} \quad \tau_{12} \leq \tau_{23} \qquad\qquad (6.1b)$$
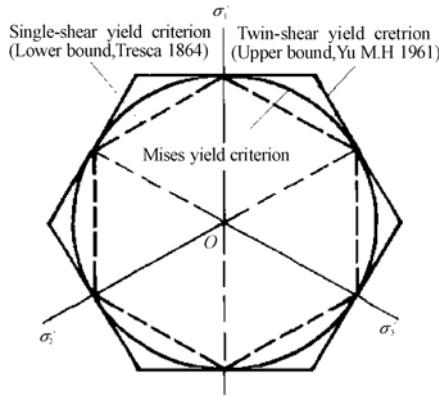
Fig. 6.1 Three yield loci in π plane (for non-SD materials)

where $\tau_{13} = \dfrac{\sigma_1 - \sigma_3}{2}$, $\tau_{12} = \dfrac{\sigma_1 - \sigma_2}{2}$, $\tau_{23} = \dfrac{\sigma_2 - \sigma_3}{2}$, C is material parameter.

The twin shear yield criteria can be represented in principal stresses $\sigma_1, \sigma_2, \sigma_3$:

$$f = \sigma_1 - \frac{1}{2}(\sigma_2 + \sigma_3) = \sigma_y \qquad \text{when} \quad \sigma_2 \leq \frac{1}{2}(\sigma_1 + \sigma_3) \qquad (6.2a)$$

$$f' = \frac{1}{2}(\sigma_1 + \sigma_2) - \sigma_3 = \sigma_y \qquad \text{when} \quad \sigma_2 \leq \frac{1}{2}(\sigma_1 + \sigma_3) \qquad (6.2b)$$

Here σ_y is the yield stress under tension and compression. Single-shear yield criterion, three-shear yield criterion and the twin-shear yield criterion are suitable for materials with the same strength both in tension and in compression. Only one parameter is needed for such materials.

6.3 Bounds of the Failure Criteria for SD Materials

There are four kinds of failure criteria for SD materials. They are suitable for materials with different strengths in tension and in compression such as rocks and concrete. i.e.

(1) Single-shear failure criterion (Mohr, 1900; Coulomb, 1773) is the lower bound of the convex criteria.

(2) Twin-shear failure criterion (Yu, 1983) is the upper bound of the convex criteria.

(3) Drucker-Prager criterion (1952) is a circle.

(4) Curved criteria.

Actually, Mohr-Coulomb's single-shear criterion and the Drucker-Prager

criterion are the generalizations of the Tresca criterion and Huber-von Mises criterion. It is shown that the Mohr-Coulomb single-shear criterion only considers two principle stresses σ_1 and σ_3, the intermediate principle stress σ_2 is not taken into account. In the meantime, the Drucker-Prager criterion is not in good agreement with experiments for geomaterials. Yu (1983) generalized Eq. (6.1a) and (6.1b) and applied them to SD materials. The mathematical modeling of the generalized twin-shear criterion is

$$F = \tau_{13} + \tau_{12} + \beta\left(\sigma_{13} + \sigma_{12}\right) = C, \quad \text{when } \tau_{12} + \beta\sigma_{12} \geq \tau_{23} + \beta\sigma_{23} \qquad (6.3a)$$

$$F' = \tau_{13} + \tau_{23} + \beta(\sigma_{13} + \sigma_{23}) = C, \quad \text{when } \tau_{23} + \beta\sigma_{23} \leq \tau_{23} + \beta\sigma_{23} \qquad (6.3b)$$

The mathematical formulae in terms of the three principal stresses are

$$F = \sigma_1 - \frac{\alpha}{2}\left(\sigma_2 + \sigma_3\right) = \sigma_t, \qquad \text{when } \sigma_2 \leq \frac{\sigma_1 + \alpha\sigma_3}{1+\alpha} \qquad (6.4a)$$

$$F' = \frac{1}{2}\left(\sigma_1 + \sigma_2\right) - \alpha\sigma_3 = \sigma_t, \quad \text{when } \sigma_2 \geq \frac{\sigma_1 + \alpha\sigma_3}{1+\alpha} \text{ 时} \qquad (6.4b)$$

where $\sigma_{13} = \dfrac{\sigma_1 + \sigma_3}{2}$, $\sigma_{12} = \dfrac{\sigma_1 + \sigma_2}{2}$, $\sigma_{23} = \dfrac{\sigma_2 + \sigma_3}{2}$, β and C are material constants. The comparison of failure loci in the π plane of twin-shear strength theory (TS theory) and Mohr-Coulomb criterion (Single-shear strength theory, SS theory), three-shear theory (Octahedral-shear theory, OS theory) is shown in Fig. 6.2.
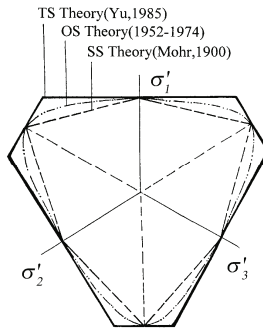
Fig. 6.2 Yield loci of three main theories in π plane (SD materials)

It can be seen that two parameters are needed for the SD material. It is noted that only some materials can be applied for each of the yield criteria.

6.4 Unification of the Yield Criteria for Non-SD Materials and SD Materials

The mathematical modeling of the unified strength theory can be expressed as follows:

$$F = \tau_{13} + b\tau_{12} + \beta\left(\sigma_{13} + b\sigma_{12}\right) = C, \quad \text{when} \quad \tau_{12} + \beta\sigma_{12} \geq \tau_{23} + \beta\sigma_{23} \qquad (6.5a)$$

$$F' = \tau_{13} + b\tau_{23} + \beta\left(\sigma_{13} + b\sigma_{23}\right) = C, \quad \text{when} \quad \tau_{12} + \beta\sigma_{12} \leq \tau_{23} + \beta\sigma_{23} \qquad (6.5b)$$

The mathematical expression of the unified strength theory in terms of principal stresses σ_1, σ_2 and σ_3 is:

$$F = \sigma_1 - \frac{\alpha}{1+b}\left(b\sigma_2 + \sigma_3\right) = \sigma_t, \quad \text{when} \quad \sigma_2 \leq \frac{\sigma_1 + \alpha\sigma_3}{1+\alpha} \qquad (6.6a)$$

$$F' = \frac{\alpha}{1+b}\left(\sigma_1 + b\sigma_2\right) - \alpha\sigma_3 = \sigma_t, \quad \text{when} \quad \sigma_2 \geq \frac{\sigma_1 + \alpha\sigma_3}{1+\alpha} \qquad (6.6b)$$

where b is the unified strength theory parameter, the limit loci of the unified strength theory in the π plane is shown in Fig. 6.3. The figure of the yield loci shows the eleven special cases of the unified yield criterion.

There are some special cases of Eqs. (8.5) and (8.5′) as follows:

(a) $b = 1$, $\beta \neq 0\ (\alpha \neq 1)$, Yu twin-shear strength theory (1983);

(b) $b = 0$, $\beta \neq 0\ (\alpha \neq 1)$, Mohr-Coulomb single-shear strength theory (1900);

(c) $b = 1, \beta = 0\ (\alpha = 1)$, Twin-shear yield criterion (Yu, 1961), or the maximum deviatoric stress criterion (Haythornthwaite, 1961), or the sharp distortion criterion (Schmidt, 1932; Ishilinski, 1940);

(d) $b = 0, \beta = 0\ (\alpha = 1)$, Tresca single-shear yield criterion (1864);

(e) $b = (\sqrt{3} - 1)/2,\ \beta = 0\ (\alpha = 1)$, Approximated Huber-von Mises criterion (1913).

It can be seen that all the commonly used strength criteria are special cases of the unified strength theory. There is a series of yield criteria suitable for non-SD materials when b varies from 0 to 1. These criteria lie between the Mohr-Coulomb single-shear theory and Yu Mao-hong (1985) twin-shear strength theory.
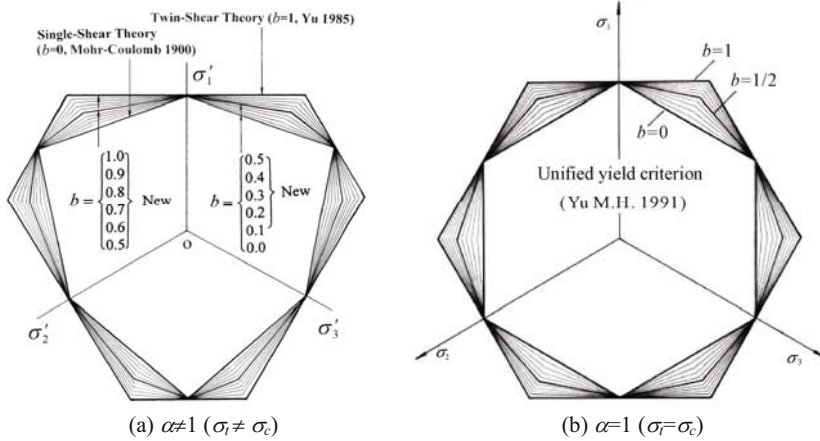
Fig. 6.3   Limit loci of unified strength theory in π-plane

Yield loci of the unified strength theory in the plane stress state (σ_1-σ_2 plane) are shown in Fig. 6.4.
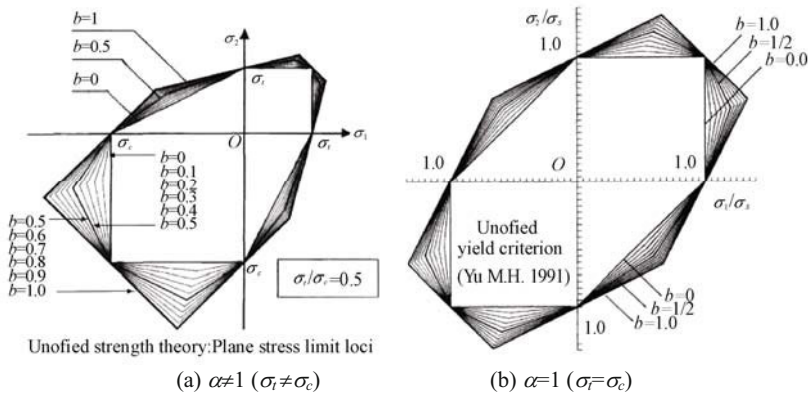
Fig. 6.4   Limiting loci of the unified strength theory in plane stress state (σ_1-σ_2 plane)

It is shown that the unified strength theory has a relatively clear physical meaning and simple mathematical formulae. The frequently used criteria are its special cases or approximation forms. The theory is suitable for most material and is readily used in engineering. The material models of unified strength elasto-plastic programs are based on the unified strength theory.

6.5 Material Models

The material models can be implemented and used as follows.

1) Tresca yield criterion (single-shear criterion) is equal to the unified yield criterion with $b=0$.

2) Huber-von Mises yield criterion (three-shear criterion) is equivalent to the unified yield criterion with $\alpha=1$ and $b=0.366$.

3) Twin-shear yield criterion (twin-shear criterion) is equal to the unified yield criterion with $b=1$.

4) Mohr-Coulomb failure criterion (single-shear theory) is equal to the unified strength theory with $b=0$.

5) Drucker-Prager failure criterion (three-shear theory)

6) Twin-shear failure criterion (twin-shear theory) is equal to the unified strength theory with $b=1$.

7) UST (unified strength theory) with any α, b, $0 \leqslant \alpha \leqslant 1$, $0 \leqslant b \leqslant 1$.

8) UST with $\alpha=1$, $b=0$ is equal to the Tresca criterion.

9) UST with $\alpha=1$, $b=0.25$ is a new one.

10) UST with $\alpha = 1, b = (\sqrt{3}-1)/2$ is equal to the Huber-von Mises criterion.

11) UST with $\alpha=1$, $b=0.5$ is equivalent to the Huber-von Mises criterion.

12) UST with $\alpha=1$, $b=0.75$ is a new one.

13) UST with $\alpha=1$, $b=1$ is equal to the twin-shear yield criterion, or maximum deviatoric stress yield criterion.

14) UST with any α and $b=0$ is equal to the single-shear theory (the Mohr-Coulomb theory).

15) UST with any α and $b=1/4$ is a new one.

16) UST with any α and $b=1/2$ is a new one.

17) UST with any α and $b=3/4$ is a new one.

18) UST with any α and $b=1$ is equal to the twin-shear strength theory.

19) Twin-shear three parameter criterion.

20) Three parameter unified strength theory.

21) Others.

The yield loci of the five typical criteria of the unified yield criterion with $\alpha=1$ and $b=0$, $b=1/4$, $b=1/2$, $b=3/4$ and $b=1$ for non-SD materials (material models 8, 9, 11, 12 and 13) are illustrated in Fig. 6.5. The yield loci of the five typical criteria of the unified strength theory with $b=0$, $b=1/4$, $b=1/2$, $b=3/4$ and $b=1$ for SD materials (material models 14 to 18) are illustrated in Fig. 6.6.
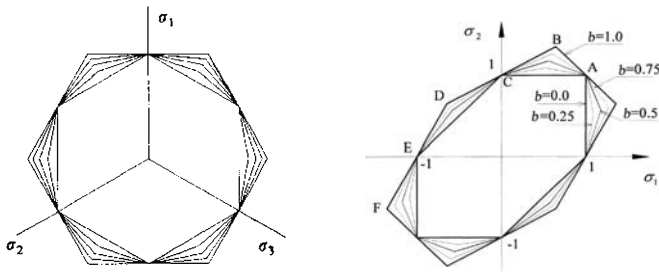
Fig. 6.5   Yield loci of the five typical criteria of the unified yield criterion for non-SD materials
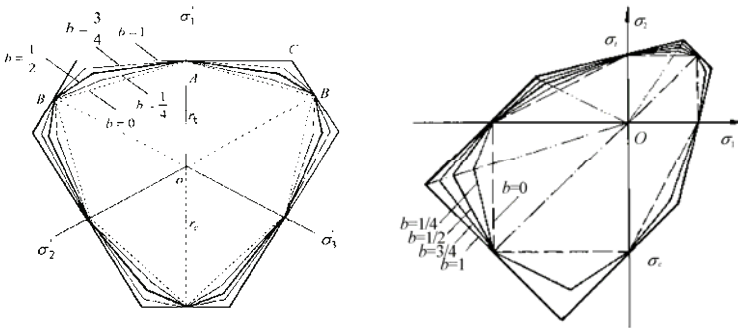
Fig. 6.6   Yield loci of five typical criteria of the unified strength theory for SD materials
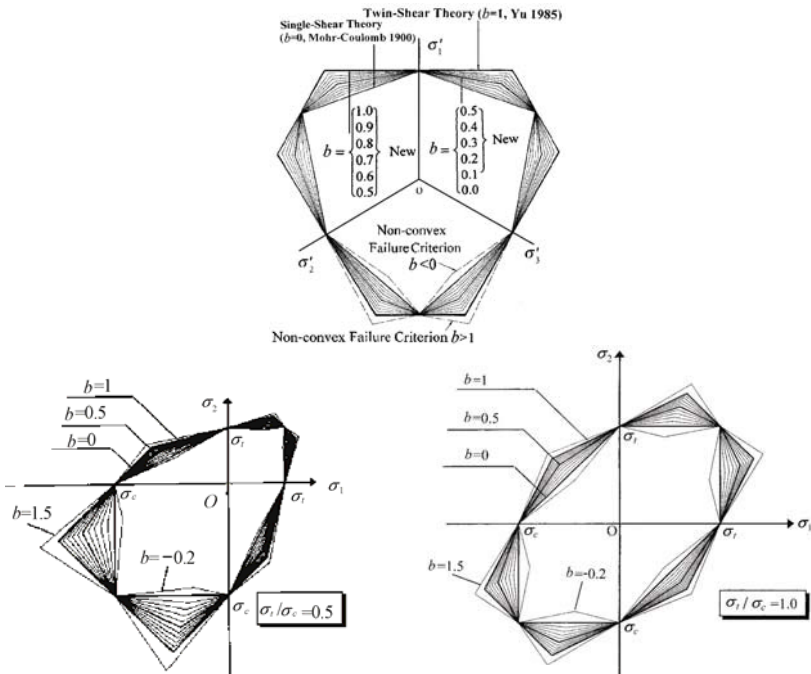
Fig. 6.7   Convex yield loci extend to non-convex yield loci of the unified strength theory

6.6   Program Structure and its Subroutines Relating to the Unified Strength Theory: INVARY, YIELDY, FLOWVP

The flow chart for calculating the elasto-plastic problems is shown in Fig. 6.8.
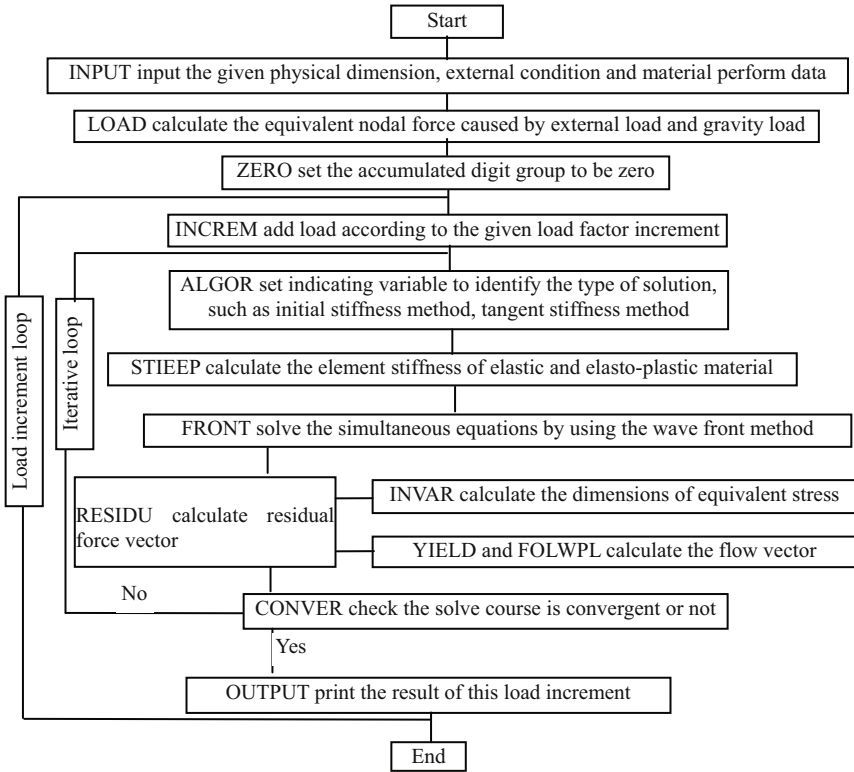
Fig. 6.8   The flow chart for calculating the elasto-plastic problems

Several subroutines about the unified strength theory and its flow vector will be introduced in this section, including INVAR, INVARY, YIELDY and CRITEN. When these subroutines are implemented in any elasto-plastic programs, the unified strength elasto-plastic analysis can be conducted. Therefore, a series of ordered results can be obtained.

6.6.1 Subroutine "Invar"

The purpose of this subroutine is to calculate the stress functions which indicate whether it is the initial or succeeding plastic deformation when considering

various yield criteria. The yield criteria include various criteria such as Huber-von Mises, Drucker-Prager, Tresca, Mohr-Coulomb and a series of the yield criteria introduced from the unified strength theory.

```
SUBROUTINE   "INVAR" (LPROP,NCRIT,PROPS,STEFF,SMEAN,NPROP,THETA,
VARJ2,VARJ3,YIELD,IND,IELEM,GASH,MATNO)
C*************************************************************
C***   EVALUATES THE STRESS INVARIANTS AND THE CURRENT VALUE
C*************************************************************
IMPLICIT REAL*8(A-H,O-Z)
COMMON/CMN01/NELEM,NPOIN,NVFIX,NMATS,NDOFN,
.                NGAUS, NGAS2,NALGO,NINCS,NTOTV,
.                NTOTG,NSTRE, NSTR1,NTYPE,NREST
COMMON/CMN06/FACTDP
DIMENSION NCRIT(NMATS),PROPS(NMATS,NPROP),MATNO(NELEM,3)
PI=3.1415926535
ROOT3=1.73205080757
STEFF=DSQRT(VARJ2)
IF(STEFF.EQ.0.0) GO TO 31
COST3=3.0*ROOT3*VARJ3/(2.0*VARJ2*STEFF)
GO TO 20
31      COST3=0.0
20      CONTINUE
IF(COST3.LT.-1.0) COST3=-1.0
IF(COST3.GT.1.0) COST3=1.0
THETA=DACOS(COST3)/3.0
NCRT1=NCRIT(LPROP)
NTMP=MATNO(IELEM,2)/10
IF((NTMP.EQ.3).OR.(NTMP.EQ.4)) GO TO 1
YIELD=DSQRT(GASH)
RETURN
C
C*** VON MISES
C
1       IF(NCRT1.EQ.2) THEN
YIELD=ROOT3*STEFF
RETURN
ENDIF
C
C*** DRUCKER-PRAGER
C
IF(NCRT1.EQ.5) THEN
PHIRA=PROPS(LPROP,7)*0.017453292
SNPHI=DSIN(PHIRA)
C*** COMPRESSIVE CONE
C          YIELD=6.0*SMEAN*SNPHI/(ROOT3*(3.0-SNPHI))+STEFF
C*** TENSILE CONE
YIELD=6.0*SMEAN*SNPHI/(ROOT3*(3.0+FACTDP*SNPHI))+STEFF
RETURN
ENDIF
```

```
C
C*** CALL UNIFIED TWINSHEAR STRESS CRITERION
C
IF(NCRT1.LE.18) THEN
BTWIN=PROPS(LPROP,8)
ARLFA=PROPS(LPROP,7)/PROPS(LPROP,5)
SMEAM=SMEAN*(1.0-ARLFA)
CALL INVARY(SMEAM,ARLFA,STEFF,THETA,BTWIN,IND,YIELD)
RETURN
ENDIF
IF(NCRT1.EQ.19) THEN
BTWIN=PROPS(LPROP,8)
CTWIN=(1.0+BTWIN)*PROPS(LPROP,5)*PROPS(LPROP,7)/
.     (PROPS(LPROP,5)+PROPS(LPROP,7))
ATWIN=CTWIN*(PROPS(LPROP,9)-PROPS(LPROP,5))/(PROPS(LPROP,5)*
.     PROPS(LPROP,9))
BEITA=2.0*(CTWIN/PROPS(LPROP,7)-ATWIN)/(1.0+BTWIN)-1.0
ARLFA=(1.0-BEITA)/(1.0+BEITA)
SMEAM=((1.0-ARLFA)+3.0*(1.0+ARLFA)*ATWIN/(1.0+BTWIN))*SMEAN
CALL INVARY(SMEAM,ARLFA,STEFF,THETA,BTWIN,IND,YIELD)
RETURN
ENDIF
IF(NCRT1.GE.20) CALL USERINVR(LPROP,NCRIT,PROPS,SMEAN,
.                 NPROP,NMATS,THETA,VARJ2,VARJ3,YIELD,IND)
END
```

6.6.2 Subroutine "Invary"

The aim of this subroutine is to calculate the invariants of the unified strength
theory.

```
SUBROUTINE INVARY(SMEAM,ARLFA,STEFF,THETA,BTWIN,IND,YIELD)
C**************************************************************
C
C***   EVALUATES THE STRESS INVARIANTS AND THE CURRENT VALUE OF
C***   THE UNIFIED STRENGTH THEORY
C
C**************************************************************
IMPLICIT REAL*8(A-H,O-Z)
PI=3.1415926535
ROOT3=1.73205080757
TWINB=1.0/(1.0+BTWIN)
VARJA=2.0*STEFF/ROOT3
F1=SMEAM+VARJA*(DCOS(THETA)-ARLFA*TWINB*BTWIN*DCOS(THETA-2.0*P
I/3.0)-ARLFA*TWINB*DCOS(THETA+2.0*PI/3.0))
F2=SMEAM+VARJA*(TWINB*DCOS(THETA)+TWINB*BTWIN*DCOS(THETA-2.0*
PI/3.0)-ARLFA*DCOS(THETA+2.0*PI/3.0))
YIELD=F1
IND=1
```

```
IF(F1.LT.F2) YIELD=F2
IF(F1.LT.F2) IND=2
IF(DABS(F1-F2).LE.1.0E-6) IND=3
RETURN
END
```

6.6.3 Subroutine "Yieldy"

The aim of this subroutine is to conduct the corner point process for the Tresca criterion, the Mohr-Coulomb criterion and the unified strength theory.

```
SUBROUTINE YIELDY(THETA,IND,ARLFA,VARJ2,LPROP,PROPS,CONS2,CONS3)
C************************************************************
C
C***   EVALUATES CONSTANTS OF FLOW VECTORS OF UNIFIED STRENGTH
THEORY
C
C************************************************************
IMPLICIT REAL*8(A-H,O-Z)
COMMON/CMN01/NELEM,NPOIN,NVFIX,NMATS,NDOFN,
.              NGAUS, NGAS2,NALGO,NINCS,NTOTV,
.              NTOTG,NSTRE, NSTR1,NTYPE,NREST
COMMON/CMN02/MBUFA,MFRON,MSTIF,NPROP
DIMENSION PROPS(NMATS,NPROP)
ROOT3=1.73205080757
PI=3.1415926535
BTWIN=PROPS(LPROP,8)
TWINB=1.0/(1.0+BTWIN)
ATATH=1.0/DTAN(THETA)
SINTH=DSIN(THETA)
COSTH=DCOS(THETA)
SINT3=DSIN(3.0*THETA)
IF(IND.EQ.1.OR.IND.EQ.3) THEN
ABTHE=THETA*57.29577951308
IF(ABTHE.LT.0.1) THEN
CONA3=(1.0+0.5*ARLFA)/VARJ2
CONA2=4.0*(1.0+0.5*ARLFA)/3.0/ROOT3
ELSE
ATAT3=1.0/DTAN(3.0*THETA)
C1=2.0*(1.0+0.5*ARLFA)/ROOT3
C2=ARLFA*(1-BTWIN)/(1.0+BTWIN)
CONA2=C1*COSTH+C2*SINTH+ATAT3*(-C1*SINTH+C2*COSTH)
CONA3=-0.5*ROOT3*(-C1*SINTH+C2*COSTH)/(VARJ2*SINT3)
ENDIF
ENDIF
IF(IND.EQ.2.OR.IND.EQ.3) THEN
ABTHE=THETA*57.29577951308
IF(ABTHE.GT.59.9) THEN
CONA3=(0.5+ARLFA)/VARJ2
```

```
CONA2=4.0*(0.5+ARLFA)/3.0/ROOT3
ELSE
ATAT3=1.0/DTAN(3.0*THETA)
C1=(ARLFA+(2.0-BTWIN)/(1.0+BTWIN))/ROOT3
C2=(ARLFA+BTWIN/(1.0+BTWIN))
CONB2=C1*COSTH+C2*SINTH+ATAT3*(-C1*SINTH+C2*COSTH)
CONB3=-0.5*ROOT3*(-C1*SINTH+C2*COSTH)/(SINT3*VARJ2)
ENDIF
ENDIF
IF(IND.EQ.1) THEN
CONS2=CONA2
CONS3=CONA3
ELSE IF(IND.EQ.2) THEN
CONS2=CONB2
CONS3=CONB3
ELSE
CONS2=(CONA2+CONB2)/2.0
CONS3=(CONA3+CONB3)/2.0
ENDIF
RETURN
END
```

6.6.4 Subroutine "Criten"

The aim of this subroutine is to calculate the flow vectors for various yield criteria. For Tresca, Mohr-Coulomb and unified strength theories, invoke YIELDY to conduct the corner point process.

```
SUBROUTINE CRITEN(LPROP,NCRIT,PROPS,THETA,SMEAN,VARJ2,
.                  VARJ3,CONS1,CONS2,CONS3,IND)
C***********************************************************
C
C**** THIS SUBROUTINE EVALUATES THE FLOW VECTOR
C
C***********************************************************
IMPLICIT REAL*8(A-H,O-Z)
COMMON/CMN01/NELEM,NPOIN,NVFIX,NMATS,NDOFN,
.             NGAUS, NGAS2,NALGO,NINCS,NTOTV,
.             NTOTG,NSTRE, NSTR1,NTYPE,NREST
COMMON/CMN02/MBUFA,MFRON,MSTIF,NPROP
COMMON/CMN06/FACTDP
DIMENSION PROPS(NMATS,NPROP),NCRIT(NMATS)
ROOT3=1.73205080757
NCRT1=NCRIT(LPROP)
FRICT=PROPS(LPROP,7)
C
C*** VON MISES
C
IF(NCRT1.EQ.2) THEN
```

```
CONS1=0.0
CONS2=ROOT3
CONS3=0.0
GO TO 40
ENDIF
C
C*** DRUCKER-PRAGER
C
IF(NCRT1.EQ.5) THEN
SNPHI=DSIN(FRICT*0.017453292)
C*** COMPRESSIVE CONE
C          CONS1=2.0*SNPHI/(ROOT3*(3.0-SNPHI))
C*** TENSILE CONE
CONS1=2.0*SNPHI/(ROOT3*(3.0+FACTDP*SNPHI))
CONS2=1.0
CONS3=0.0
GO TO 40
ENDIF
C
C*** TWIN SHEAR STRESS ALSO TRESCA MOHR-COULOMB
C
IF(NCRT1.LE.18) THEN ARLFA=PROPS(LPROP,7)/PROPS(LPROP,5)
CONS1=(1.0-ARLFA)/3.0
CALL YIELDY(THETA,IND,ARLFA,VARJ2,LPROP,PROPS,CONS2,CONS3)
GO TO 40
ENDIF
C
C***   TWIN SHEAR
C
IF(NCRT1.EQ.19) THEN
BTWIN=PROPS(LPROP,8)
CTWIN=(1.0+BTWIN)*PROPS(LPROP,5)*PROPS(LPROP,7)/
.          (PROPS(LPROP,5)+PROPS(LPROP,7))
ATWIN=CTWIN*(PROPS(LPROP,9)-PROPS(LPROP,5))/(PROPS(LPROP,5)*
.          PROPS(LPROP,9))
BEITA=2.0*(CTWIN/PROPS(LPROP,7)-ATWIN)/(1.0+BTWIN)-1.0
ARLFA=(1.0-BEITA)/(1.0+BEITA)
CONS1=(1.0+ARLFA)*ATWIN/(1.0+BTWIN)+(1.0-ARLFA)/3.0
CALL YIELDY(THETA,IND,ARLFA,VARJ2,LPROP,PROPS,CONS2,CONS3)
GO TO 40
ENDIF
IF(NCRT1.GE.20) CALL USERCRIT(LPROP,NCRT1,PROPS,THETA,SMEAN,
VARJ2,VARJ3,NPROP,NMATS,CONS1,CONS2,CONS3,IND)
40      CONTINUE
RETURN
END
```

6.7 Brief Summary

The unified strength theory and its associated flow rule are implemented in finite element codes UEPP, which are described in this chapter. Most parts of the elasto-plastic program are the same as the conventional elasto-plastic program, only the **subroutine** of yield criteria (subroutine "INVAR" to calculate equivalent stresses), **subroutine** flow vector and the **subroutine** of the corner (subroutine "YIELD" and "FOLWPL" to calculate flow vector) are different. Several subroutines for the unified strength theory and its flow vector are given, including INVAR, INVARY, YIELDY and CRITEN. When these subroutines are implemented in any elasto-plastic programs, the unified strength elasto-plastic analysis can be conducted. Therefore, a series of ordered results for elasto-plastic analysis of structures can be obtained.

The unified strength theory is also implemented into several commercial FEM codes, and used for engineering problems (Shen, 1993; Quint Co., 1993; 1994; Li and Ishii, 1994; 1998; Liu et al., 1994; Wang, 1998; Fan and Qiang, 2001; Zhang et al., 2001; Zhou, 2002; Sun et al., 2004a; 2004b; Liu and Wang, 2004; Zhang et al., 2005; Shao and Qian, 2007; Shao et al., 2007; Yang, 2008; Li et al., 2008; Li, 2008; Wang et al., 2008; Zhang et al., 2008; Yang and Zhang, 2008; 2009; Wang and Lu, 2009; Fen and Du, 2010; Li and Chen, 2010; Li and Qiao, 2010; Ma and Liao, 2010; Pan et al., 2010). Serial results are obtained that can be adapted for more materials and structures.

References

Belytschko T, Liu WK and Moran B: (2000) Nonlinear Finite Elements for Continua and Structures. John Wiley, Chichester: New York

Fan SC and Qiang HF (2001)Normal high-velocity impaction concrete slabs- a simulation using the meshless SPH procedures. In: Computational Mechanics–New Frontiers for New Millennium, Valliappan S. and Khalili N. eds. Elsevier Science Ltd, pp 1457-1462.

Hinton E and Owen DRJ (1977) Finite Elements Programming. Academic Press: London.

Lewis RW and Schrefler BA (1987) The Finite Element Method in the Deformation and Consolidation of Porous Media. John Wiley & Sons: Chichester.

Fen TG and Du B (2010) Dynamic analysis of the 500 kV underground transformer substation for Shanghai World EXPO, to be published.

Li J, Lu XY and Zhao XW (2008) Topology optimization based on bi-direction evolutionary structural of unified strength. Journal of Shandong Jianzhu

University, 23(1): 65-69.

Li K and Chen GR (2010) Finite element analysis of slope stability based on slip line field theory. Journarl of Hohai University (Natural Sciences),38(2): 191-195.

Li Y (2008) In-situ Stress Measurement and Stability Analysis Based on the Unified Strength Theory in Large Scale Underground Caverns Zone. Doctoral Dissertation, Beijing Scientific and Technical University.

Li Y and Qiao L (2010) Stability Analysis of Underground Caverns based on the Unified Strength Theory, Chapter16 in this monograph.

Li YM, Ishii K, Nakazato C and Shigeta T (1994) Prediction of safety rate and multi-slip direction of slip failure under complex stress state. Advances Eng. Plasticity and its Applications. Xu BY and Yang W eds. International Academic Publishers: Beijing, pp 349-354.

Li YM and Ishii K (1998) The Evaluation of the Elasto-plastic Behavior of Composite Materials under Biaxial Stress with Homogenization Method, Proc. of the Conference on Computational Engineering and Science, 3: 1023-1026. JSCES.

Li YM. and Ishii K(1998) The Evaluation of Strength for the Composite Materials. In : Strength Theory: Application, Development and Prospect for 21st Century, Yu MH and Fan SC eds. Science Press: New York and Beijing, pp 337-342.

Liu F, Li LY and Mei ZX (1994) Elasto-visco-plastic finite element analysis of self-enhanced thick cylinder. Chinese J. Appl. Mechanics, 11(3): 133-137 (in Chinese, English abstract).

Liu GH and Wang ZY (2004) Dynamic response and blast-resistance analysis of a tunnel subjected to blast loading. Journal of Zheiiang University (Engineering Science), 38(2):204-209 (In Chinese).

Ma ZY and Liao HJ (2010) Unified strength theory and FLAC-3D. Chapter 18 in this monograph.

Owen DRJ and Hinton E (1980)Finite Elements in Plasticity: Theory and Practice. Pineridge Press: Swansea.

Owen DRJ, Hinton E and Onate E (1989) Computational Plasticity: Models, Software and Applications. Pineridge Press Limited, pp 1460.

Pan XM, Kong J, Yang Z and Liu C (2010) Secondary development and application of unified elastoplastic constitutive model to ABAQUS. Rock and Soil Mechanics, 31(4): 1092-1098.

Quint Co. (1993a)   COMPMAT-Analysis system for composite materials. FEM codes of Quint Corporation: Japan.

Quint Co. (1993b)   COMPMAT-Analysis system for composite materials. FEM codes of Quint Corporation, Japan.

Quint Co. (1994a) PREMAT/POSTMAT-Pre and Post Processor for Composite Materials. FEM Codes of Quint Corporation, Japan.

Quint Co. (1994b) STAMPS-Structural Analysis Program for Civil Engineering. FEM Codes of Quint Corporation, Japan.

Shao CJ and Qian YJ (2007) Load bearing capability of concrete-filled steel tube component considering effect of intermediate principal stress. Chinese Journal

of Applied Mechanics, 24(03): 396-399.

Shao CJ, Wu YH and Qian YJ (2007) Plastic seismic damage of concrete structure based on five-parameter unified strength theory. Chinese Journal of Applied Mechanics**,** 24(1): 97-101.

Shen ZJ (1993) Comparison of several yield criteria. Rock and Soil Mechanics, 14(1): 41-50 (in Chinese, English abstract).

Smith IM and Griffiths DV (2004) Programming the Finite Element Method, 4th edition. John Wiley & Sons，Ltd.

Sun HY, Shang YQ, Zhang CS, Ying HP, Li SQ (2004)   3D numerical modeling of possible failure zone with underground excavation. Chinese Journal of rock mechanics and engineering, 23(13): 2192- 2196.

Sun HY, Shang YQ and Zhang CS (2004) Numerical modeling analysis for surrounding rockmass stability of large underground cavities. Journal of Zheiiang University (Engineering Science), 38(1): 70-74.

UEPP User's Manual, Version 3.0, Research Division of Structural Strength, Dept. of Civil Eng., Xi'an Jiaotong University.

Wang D, Chen JK, Wang QZ, Chen Y, Huang Y (2008) The new method of structural reliability analysis by Monte-Carlo stochastic finite element. Journal of Sichuan University (Engineering Science Edition), 40(3): 20-26.

Wang D, Chen JK, Wang QZ, Li YL (2008) Structural Reliability Analysis by Monte-Carlo Based on Conditional Expectation Variance Reduction and Antithetic Variable Sampling**.** China Rural Water and Hydropower, (5):66-70.

Wang F and Fan SC (1998) Limit pressures of thick-walled tubes using different yield criteria. Strength Theory: Applications, Developments and Prospects for the 21st Century. Yu MH and Fan SC eds. Science Press: New York, Beijing, pp 1047-1052.

Wang F (1998) Nonlinear finite element analysis of RC plate and shell using the unified strength theory. PhD thesis, Nanyang Technological University, Singapore.

Wang JQ and Lu F (2010) Unified strength theory constitutive model embedded software ABAQUS and its application in tunnel engineering. Journal of Yangtze River Scientific Research Institute, 27(2): 68-74 (in Chinese).

Wang JQ and Lu F, (2010) Implementation of the Unified Strength Theory into ABAQUS and its Application for Tunnel Engineering. Chapter11 in this monograph.

Yang LQ, Zhang SR (2008) Analysis of textural stress and rock failure of diversion tunnels. Chinese Journal of Geotechnical Engineering, 30(6): 813-817.

Yang LQ, Li YQ and Chen ZP (2008) Sudden-crack Phenomenon and Simulation of Surrounding Rock-mass in Diversion Tunnel**.** China Rural Water and Hydropower, (5):53-56.

Yang LQ, Zhang SR, Chen ZP. (2009) Adaptive arithmetic of arch dam cracking analysis**.** Journal of Hydraulic Engineering, 40(2): 214-219.

Yu-MH, He LN, Song LY (1985) Twin shear strength theory with extension research, Sciences in China (Series.A), 28(11): 1113-1120 (English Edn);

28(12): 1174-1183(Chinese Edn).

Yu MH and Meng XM (1990) Research in the protection and utilization of ancient city wall in Xi'an (in Chinese). Research Report of   Xian Jiaotong University, pp 90-338, In: Fourth Symposium of Ancient Architecture and Gardens of China, Xi'an China.

Yu MH and Li YM (1991) Twin shear constitutive theory and its computational implementation. In: Computational Mechanics, Ed. by CheungYK LeeJ,H,W. and LeungA.Y.T. Balkema: Rotterdam, pp 875-879.

Yu MH (1992) New System of Strength Theory. Xian Jiaotong University Press: Xian, China (in Chinese).

Yu MH, He LN and Zeng WB (1992) A new unified yield function : Its model, computational implementation and engineering application. Computational Methods in Engineering: Advances and Applications. Tay AAO and Lam KY eds. World Scientific: Singapore, pp 157-162.

Yu MH, He LN, Liu CY (1992) Generalized twin shear yield criteria with extension research. Bulletin of Science, 37(2):182-186.

Yu MH and Meng XM (1992) Twin shear elasto-plastic model and its application in geotechnical engineering. Chin. J. Geotech. Eng., 14(3): 71-75 (in Chinese, English abstract).

Yu MH and Meng XM (1993) Researches on the stability of ancient city wall in Xi'an (in English). Research in the City Wall in Xi'an. Yu MH, Zhang XP and Fang TP eds. Xi'an Jiaotong University Press: Xi'an China, pp 168-174.

Yu MH, Meng XM and Xie S (1993) Research on the protection and utilization of ancient city wall in Xi'an (in Chinese). Research on the City Wall in Xian. Yu MH, Zhang XP and Fang TP eds. Xian Jiaotong University Press: Xi'an, China, pp 94-126.

Yu MH and Zeng WB (1993) Mesomechanical simulation of failure criterion for a composite material. Macro-Meso-micro Mechanical Properties of Materials. Tokuda M and Xu BY eds. Mie Academic Press: Mie, Japan, pp 571-576.

Yu MH and Zeng WB (1994) New theory of engineering structural analysis and its application. J. Eng. Mech., 11(1): 9-20 (in Chinese, English abstract).

Yu MH, Zeng WB, Ma GW, Yang SY, Wang F and Wang Y (1993) Unified Elasto-Plastic Program—UEPP. Xian Jiaotong University, English version.

Yu MH, Zeng WB, Ma GW, Yang SY, Wang F and Wang Y (1993) Unified Elasto-Plastic Program—UEPP. Xian Jiaotong University, Chinese version.

Yu MH (1994) Unified strength theory for geomaterials and its application. Chinese J. Geotech. Eng., 16(2): 1-9 (in Chinese, English abstract).

Yu MH and Zeng WB (1994) New theory of engineering structural analysis and its application. J. Eng. Mech., 11(1): 9-20 (in Chinese, English abstract).

Yu MH, Yang SY, Fan SC, et al. (1997) Twin shear unified elasto-plastic constitutive model and its applications. Chin. J. Geotech Eng., 21(6): 9-18 (in Chinese, English abstract).

Yu MH (1998) Twin Shear Theory and its Applications. The Science Press: Beijing (in Chinese).

Yu MH, Yang SY, Fan SC and Ma GW (1999) Unified elasto-plastic associated

and non-associated constitutive model and its engineering applications. Int.Journal of Computers & Structures, 71: 627-636.

Yu MH (2004) Unified Strength Theory and its Applications. Springer: Berlin.

Yu MH, Ma GW et al. (2006) Generalized Plasticity. Springer: Berlin.

Yu MH, Ma GW and Li JC (2009) Structural Plasticity: Limit, Shakedown and Dynamic Plastic Analyses of Structures. ZJU Press and Springer: Hangzhou and Berlin.

Zhang CQ (2005) Study on method of safety evaluation for rock engineering based on failure approach index. Doctoral Dissertation of Chinese Academy of Sciences, Institute of Rock & Soil Mechanics.

Zhang CQ, Zhou H and Feng XT (2008) Numerical format of elastoplastic constitutive model based on the unified strength theory in FLAC~(3D). Rock and Soil Mechanics, 29(3): 596-602 (in Chinese, English Abstract).

Zhang XS, Guan H, Yew-Chaye Loo (2001) UST (Unified Strength Theory) failure criterion for punching shear analysis of reinforcement concrete slab-column connections. In: Computational Mechanics–New Frontiers for New Millennium, Valliappan S. and Khalili N. eds. Elsevier Science Ltd, pp 299-304.

Zhou XQ (2002) Numerical Analysis of Reinforced Concrete using Multi-surface Strength Model. Doc. thesis of Nanyang Technological University, Singapore.

7

Examples of the Application of Unified Elasto-Plastic Constitutive Relations

7.1 Introduction

The unified strength theory, its singularity and the process of the piece-wise linear yield criterion, the implementation of the unified strength theory, and the subroutine of yield criteria (subroutine "INVAR" to calculate equivalent stresses), the subroutine of flow vector and the subroutine of the corner (subroutine "YIELD" and "FOLWPL" to calculate flow vector) have been introduced in previous chapters. Some simple examples including the plane stress, plane strain and spatial axial-symmetry problems will be described in this chapter. It is easy for the reader to find out about the possibility of adding new functions to the procedure (Yu, 1992; Yu et al., 1992; 1994; UEPP User's Manual, 1998).

(a) Plane stress problem   (b) Plane strain problem   (c) Spatial axisymmetric problem
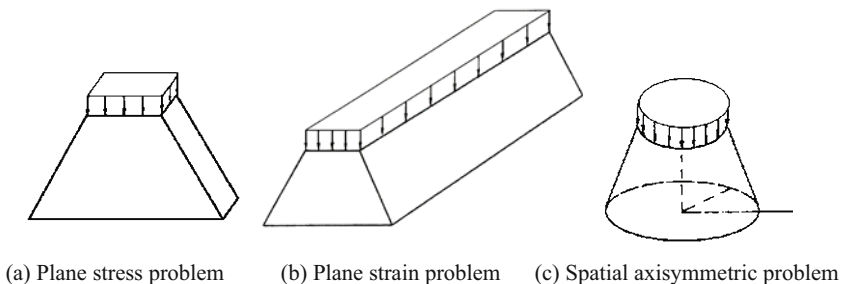
Fig. 7.1   Three kinds of engineering structures

Plane stress, plane strain and spatial axisymmetric problems are three important problems in plasticity and engineering. Figure 7.1 shows an example of these three kinds of structures. Figure 7.1(a) is a plane stress structure with a

uniform thickness of thin lamina, deformed under the action of the force which lies in its median plane. Figure 7.1(b) is a plane strain problem with zero strain in the z direction (length) in a structure of very great thickness. Figure 7.1(c) is a spatial axisymmetrical problem which is symmetrical in terms of geometry, boundary conditions and external loading about an axis.

These three kinds of structure shown in Fig. 7.1 have an identical section, a trapezoid, but different stress states. The stresses normal to the solution domain σ_z in the plane stress state are zero principal stress and nonzero principal stress in the plane strain; the hoop stress σ_θ in special axisymmetrical problems is also a principal stress.

Several examples are calculated using the UEPP (Yu et al., 1992; Yu et al., 1993; Yu and Zeng, 1994; UEPP User's Manual, 1998) based on the unified strength theory (for SD materials) or the unified yield criterion (for non-SD materials) with $b=0$, $b=1/2$ and $b=1$ in this chapter. Some examples are the same as the previous examples presented in the literature, for comparison. These three special cases of the unified strength theory are three basic criteria, which are the lower criterion, the upper criterion and the median criterion for all the convex criteria. So, three basic results can be obtained.

Sometimes, five types of criteria of the unified strength theory with $b=0$, $b=1/4$, $b=1/2$, $b=3/4$ and $b=1$ are used. Eleven results can be obtained using the unified strength theory with $b=0$, $b=0.1$, $b=0.2$, $b=0.3$, $b=0.4$, $b=0.5$, $b=0.6$, $b=0.7$, $b=0.8$, $b=0.9$ and $b=1$, if needed.

7.2 Plane Stress Problems

7.2.1 Elasto-Plastic Analysis of a Cantilever Beam

A plastic analysis of a simple, plane stress, cantilever beam can be seen in the book by Zienkiewicz in 1971. Ideal plasticity behaviour of a Huber von Mises material model was assumed. The spread of plastic zones for different ratios of q/q_p when q_p is calculated as from plastic beam theory (q_p = collapse load) is shown in Fig. 7.2. The loads are given in terms of the collapse load estimated on the basis of elementary plastic hinge theory.
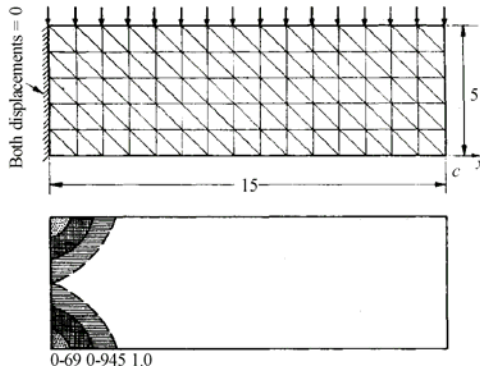
Fig. 7.2 The spread of plastic zones for cantilever beam (Zienkiewicz, 1971)

Figure 7.3 shows the increase in displacements with load. As the collapse load is approached progressively, larger numbers of iterations are required and indeed at $P/P_p=1$ no convergence was achieved (Zienkiewicz, 1971). Thus, although the non-linear solution allows a lower bound in collapse load to be found (by satisfying equilibrium and yield conditions) the actual collapse load cannot be found by incrementing the loads. To obtain a better picture of collapse behavior it is simpler to apply specified displacements at the load point and to increment these until no further increase in the reaction at that point is achieved.
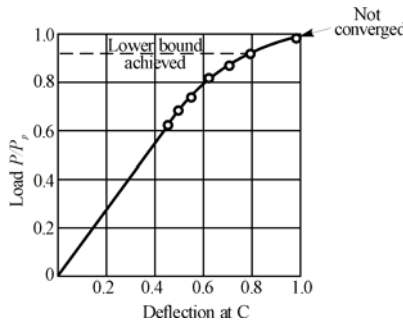
Fig. 7.3 Displacements versus load P/P_p
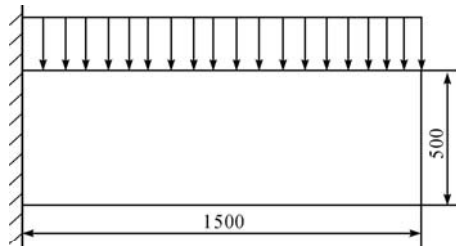
Fig. 7.4 A similar cantilever beam (Zienkiewicz, 1971)

A similar cantilever beam under the act of a uniform load shown in Fig. 7.4 is studied again in terms of the unified strength theory and UEPP (Yu, 1993). In Fig. 7.4 the mechanical behaviour of material is $E=2.1\times10^5$ MPa, $v=0.3$, ideal plasticity, yield stress $\sigma_y=240$ MPa. Calculate the elastic limit of the beam, the plastic region and the load-displacement relationship using the unified yield criterion with different parameter b.

The beam is considered as a plane stress problem. The configuration and the division into 40 isoparametric elements are shown in Fig. 7.5. An 8-nodes isoparametric element is used. The number of the nodes is 147. After the first iteration the elastic limits of the cantilever beam in terms of the unified yield criterion with different value of b ($b=0$, $b=1/2$, $b=1$) are obtained respectively, as follows.

(a) $b=0$

(b) $b=0.5$

(b) $b=1$
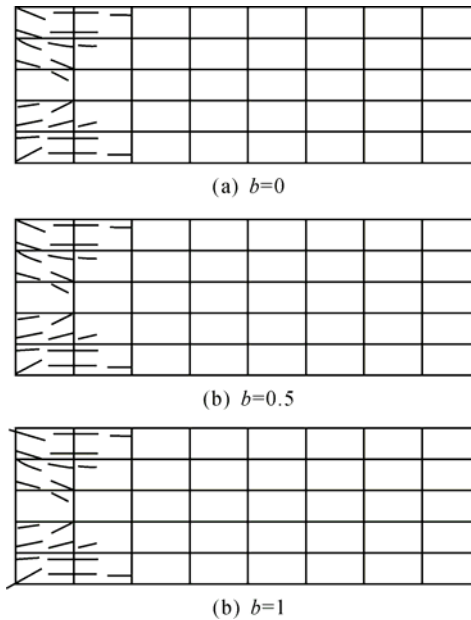
Fig. 7.5　Plastic zones of cantilever beam under the same load $w_e=15$ N/mm^2

1) $q_e=9.03$ N/mm^2 (unified yield criterion with $b=0$, single-shear criterion, i.e. the single-shear yield criterion or the Tresca criterion);

2) $q_e=9.36$ N/mm^2 (unified yield criterion with $b=1/2$, linear Mises criterion);

3) $q_e=9.54$ N/mm^2 (unified yield criterion with $b=1$, twin-shear criterion).

The plastic zones for different values of the unified yield criterion parameter b under the same load $w_e=15$ N/mm^2 are different, as shown in Fig. 7.5. Figure 7.5(a) is the plastic zone of the unified yield criterion with $b=0$. It is also the plastic zone of the single-shear criterion or the Tresca yield criterion. Figure 7.5(b) is the plastic zone of the unified yield criterion with $b=1/2$ It approximates to the plastic zone of the Huber-von Mises yield criterion. Figure 7.5(c) is the plastic zone of the unified yield criterion with $b=1$. It is the plastic zone of the twin-shear yield

criterion.

The increase in displacements with load in terms of different values of the unified strength theory parameter b is displayed in Fig. 7.6. It requires a large number of iterations of non-linear computation, until no further increase in the reaction at that point is achieved (furthermore, the numerical solution process will be divergent). The plastic limit load is approached progressively to the point where no convergence is achieved, as shown in Fig. 7.3 and Fig. 7.6. The convergent results using the three basic criteria can be obtained respectively, as shown in Fig. 7.6.
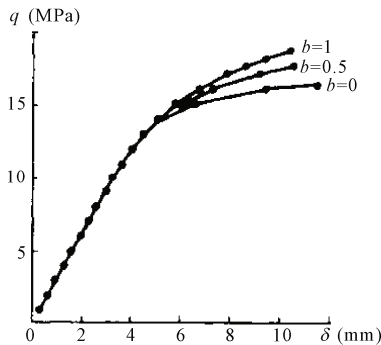
Fig. 7.6   Increase of displacements with load for different yield criteria

The numerical results achieved by using the unified strength theory with $b=0$ are very close to the results of Zienkiewicz (1971). Some new results, moreover, are obtained by using the unified strength theory.

7.2.2 Elasto-Plastic Analysis of a Trapezoid Structure under Uniform Load

The trapezoid structure is an important structure in engineering. It can be processed as a unified problem in FEM-2D codes.

On a symmetrical trapezoidal plate, the vertex angle formed by the extension line of its two bevels is 2ξ ($\xi=45°$), the upper side of the trapezoidal plate (Fig. 7.7) exerts a uniform pressure q. The parameters of the material are elastic modulus, $E=2.06\times10^4$ MPa, Poisson's ratio $\mu=0.167$. The uniaxial tensile strength of the material is $\sigma_t=2.4$ MPa, the uniaxial compressive stress is $\sigma_c=24$ MPa, i.e. the strength ratio of extension to compression is $\alpha=0.1$. Then calculate the elastic limit load and plastic limit load by using the unified yield criterion with different parameter b.

This problem can be considered as a plane stress problem. We analyze a half of the trapezoidal structure because of the symmetry. The isoparametric elements can be chosen as eight nodes and a quadrilateral, as shown in Fig. 7.8. And there are 128 element and 433 nodes in total. The elastic limit can be calculated under different yield criteria.

The elastic limit of a trapezoidal plate in terms of the unified yield criterion with a different value of b ($b=0$, $b=0.5$, $b=1$, i.e. different yield criteria) under plane stress state can be obtained as follows.

1) $q_e=23.9$ MPa (unified strength theory with $b=0$, single-shear theory, i.e. the Mohr-Coulomb theory);

2) $q_e=25.2$ MPa (unified strength theory with $b=1/2$, a new criterion);

3) $q_e=28.1$ MPa (unified strength theory with $b=1$, i.e. Twin-shear theory).
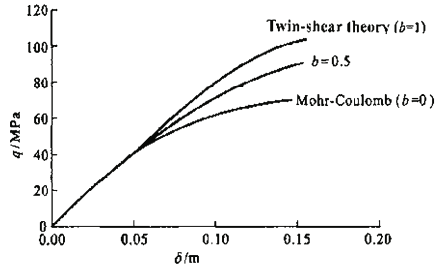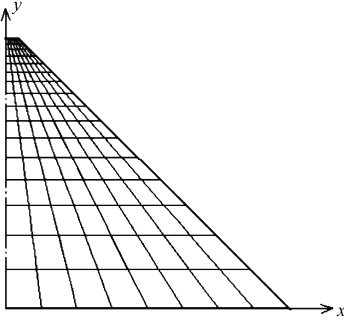
Fig. 7.7   Mesh of a half-trapezoidal structure   **Fig. 7.8**   load-displacement relations

As shown in Fig. 7.8, the load-displacement curve of node 2 in the middle of the plate can be obtained by increasing the uniform load step-by-step. The solution is obtained until the limit load is reached. The limit load is approached progressively. A larger number of iterations are required until no convergence is achieved.

The solution is convergent when $q=70$ MPa (for single-shear theory or the unified strength theory with $b=0$), $q=92$ MPa (for the unified strength theory with $b=1/2$), $q=104$ MPa (for the unified strength theory with $b=1$). Increase the load again and the solution process will be divergent; therefore three kinds of limit load can be obtained, respectively.

The plastic limit of a trapezoidal structure in terms of the unified yield criterion with different values of b ($b=0$, $b=0.5$, $b=1$) under plane stress state are

1) $q_p=70$ MPa (unified strength theory with $b=0$, single-shear theory, i.e. the Mohr-Coulomb theory);

2) $q_p=92$ MPa (unified strength theory with $b=1/2$, a new criterion);

3) $q_p=104$ MPa (unified strength theory with $b=1$, twin-shear theory).

7.3 Plane Strain Problems

Figure 7.9 shows a typical structure in railway and high road engineering and the city wall in Xi'an, China. It can be simplified to a plane strain problem. The uniform distributed load is applied on the top. A symmetrical trapezoidal structure

with a top angle 2ξ and the slip line field of the trapezoid structure are also shown in Fig. 7.9. The slip line field was constructed as shown in Fig. 7.9 (Yu et al.). The stability of the city wall in Xi'an, China, can be seen in Chapter 18.
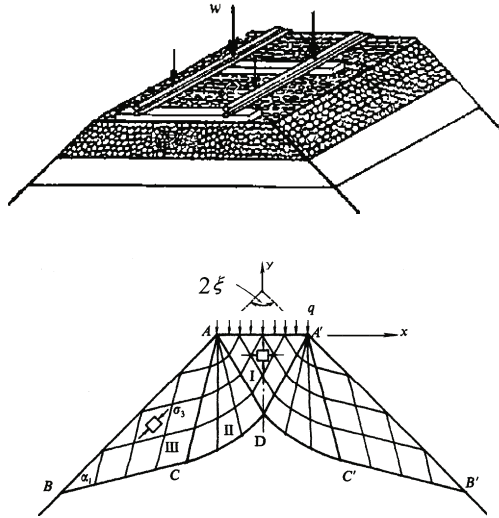
Fig. 7.9   Base of a railroad and the plane strain problem

The mesh of a trapezoidal structure under plane strain is identical to the mesh of a plane stress problem shown in Fig. 7.8. The isoparametric elements with eight nodes and a quadrilateral are used.

The elastic limit of a symmetrical trapezoidal structure in terms of the unified yield criterion with different values of b ($b=0$, $b=0.5$, $b=1$) under plane strain state can be obtained as follows.

1) $q_e=28.8$ MPa （unified strength theory with $b=0$, single-shear theory, i.e. the Mohr-Coulomb theory);

2) $q_e=33.1$ MPa (unified strength theory with $b=1/2$, a new criterion);

3) $q_e=35.8$ MPa (unified strength theory with $b=1$, twin-shear theory).

The load-displacement relation of node 2 in the middle of the trapezoidal structure under plane strain condition using the three yield criteria can be obtained, as shown in Fig. 7.10.
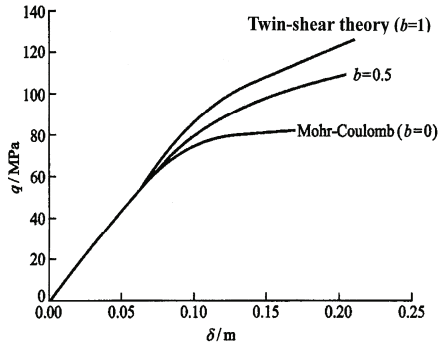
Fig. 7.10   Load-displacement relation of a trapezoidal structure under plane strain condition

The convergent result can be obtained when q=81.8 MPa (unified strength theory with b=0, i.e. the Mohr-Coulomb single-shear theory), q=109 MPa (unified strength theory, b=0.5), q=125.8 MPa (unified strength theory, b=1). Increasing the loads further, the numeric solution process will be divergent. Then the limit load can be obtained by using the three yield criteria respectively.

The plastic limit of a trapezoidal structure in terms of the unified yield criterion with different values of b (b=0, b=0.5, b=1) under the plane strain state can be obtained as follows.

1) q_p=81.8 MPa (unified strength theory with b=0, single-shear theory, i.e. the Mohr-Coulomb theory);

2) q_p=109 MPa (unified strength theory with b=1/2, a new criterion);

3) q_p=125.8 MPa (unified strength theory with b=1, twin-shear theory).

7.4 Spatial Axisymmetric Problems

7.4.1 Analysis of Plastic Zone for Thick-Walled Cylinder

Another example of using the unified strength theory is a thick-walled cylinder shown in Fig. 7.11 and Fig. 7.12. When the internal pressure exceeds p_e, a plastic zone will begin at the inner surface and spread outwards toward the outer surface. The elastic–plastic boundary at any stage has a radius r_c. In the elastic region, ($r_c \leq r \leq r_b$), the radial and circumferential stresses are obtained from Lame's equations using the boundary condition σ_r=0 at r=r_b and the fact that the material at r=r_c is stressed to the yield point. The pressure reaches its maximum value when the plastic zone reaches the outer surface of the thick-walled tube.

The elastic part of the elastic-plastic thick-walled tube may be considered as a new tube with inner radius r_c and outer radius r_b, with an internal pressure p_e. The stress distribution in the elastic region for an incompressible material is easily obtained.
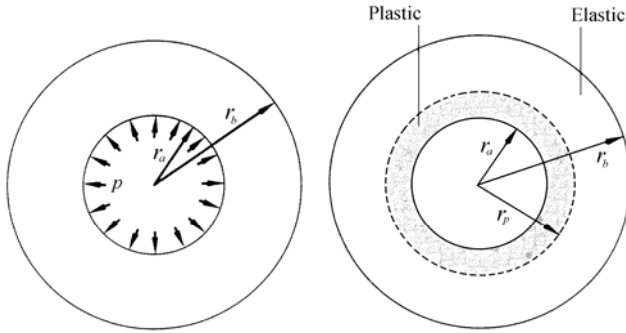
Fig. 7.11 Thick-walled cylinder

Due to symmetry, only a quarter of the thick-walled cylinder is shown. The cylinder has an inner radius r_a=100 mm, and an outer radius r_b=200 mm. The elastic modulus is E =2.1×10^5 MPa, Poisson ratio μ=0.3, tensile yield stress σ_y =240 MPa. This example is the same as the example in Chapter 7 of the book (Owen and Hinton, 1980) for comparison.
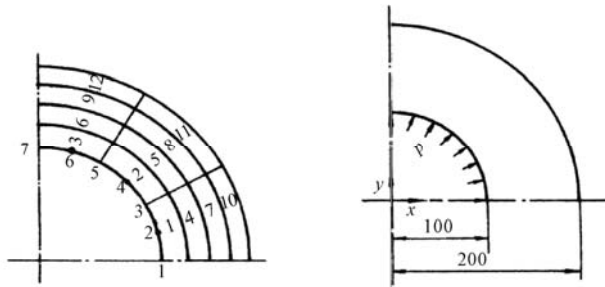
Fig. 7.12 Thick-walled cylinder and finite element mesh

Four elastic limit pressures using different yield criteria are obtained as follows.
1) p_e=97.9 MPa (unified yield criterion with b=0, single-shear criterion or the Tresca criterion);

2) p_e=111.0 MPa (unified yield criterion with b=1/(1+$\sqrt{3}$), a new criterion);
3) p_e=111.6 MPa (Huber-von Mises yield criterion);
4) p_e=125.8 MPa (unified yield criterion with b=1, twin-shear yield criterion).
Figure 7.13 shows the distribution of the circumferential stress in a thick-walled cylinder with the twin-shear yield criterion (b=1), the Huber-Mises criterion (b =1/(1+$\sqrt{3}$)) and the Tresca criterion (b=0) respectively. The curves are the analytical solution and the dots are the numerical solution. The third curve in Fig. 7.13 agrees with the previous result (Johnson and Mellor, 1962; Mendelson, 1968; Chakrabarty, 1987).
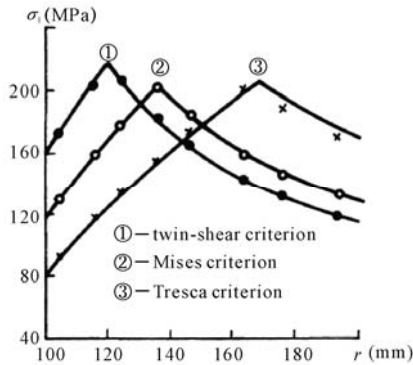
Fig. 7.13   Distribution of circumferential stress in cylinder with different yield criteria

The distributions of circumferential stresses with different yield criteria in the elasto-plastic thick-walled cylinder subjected to internal pressure p=160 MPa are shown in Fig. 7.13. Three curves are drawn according to the analytical solutions in terms of the unified strength theory (Yu, 2004). The points are obtained from the numerical calculations of the thick-walled cylinder that obey the unified yield criterion with b=0, $b = 1/(1+\sqrt{3})$ and b=1, respectively.

The plastic zones in a thick-walled cylinder with different yield criteria under the same load are shown in Fig. 7.14. The radius of the plastic zone with the unified yield criterion when b=0 (Tresca yield criterion) is larger than that obtained from $b = 1/(1+\sqrt{3})$ and b=1. As a comparison, the distribution of circumferential stress σ_θ in the elasto-plastic thick-walled cylinder obeying the Huber-von Mises yield criterion is also shown in Fig. 7.14(c).

It is seen that the results obeying the Huber-von Mises yield criterion and the unified yield criterion with $b = 1/(1+\sqrt{3})$ are identical both in analytical solution and numerical calculation.
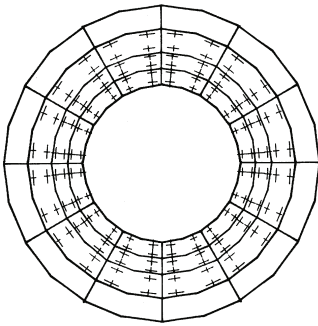
(a) UST with b=0 (Single-shear criterion,)
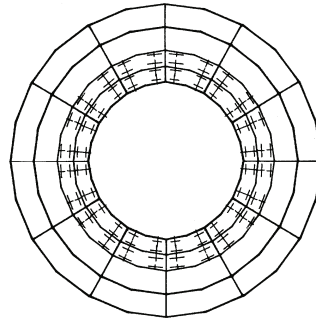
(b) UST with $b = 1/(1+\sqrt{3})$
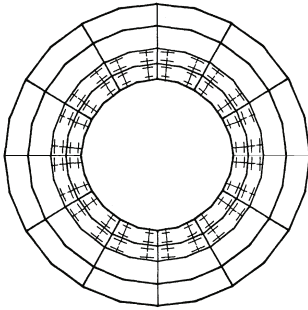
(c)   Huber-von Mises criterion
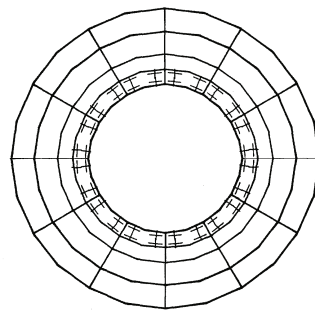
(d) UST with b=1 (Twin-shear criterion)

Fig. 7.14   Distribution of plastic zone in thick-walled cylinder with different parameter b

7.4.2 Analysis for Limit-Bearing Capacity of a Circular Plate

The numerical result of a simply supported circular plate can be seen in the book of Owen and Hinton (1980) in terms of the Huber-von Mises criterion. A uniformly loaded simply supported circular plate and finite element (FE) mesh are shown in Fig. 7.15. Only one-half of the plate is analyzed due to the symmetry. The plate is modeled by five axisymmetric elements and loading takes the form of a progressively increasing uniformly distributed load. The isoparametric element with eight nodes in the element family of UEPP is chosen for analysis. It is the same as in Owen and Hinton (1980).
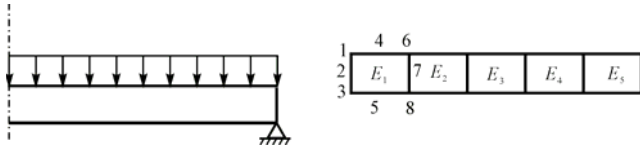
Fig. 7.15   Simply supported plate and finite element mesh of plate

The elastic limit of the simply supported circular plate in terms of different values of b of the unified yield criterion (i.e. different yield criteria) are obtained by using the unified strength theory as follows.

1) $b=0$ (Tresca criterion), $q_e=2.2707$ N/mm^2;
2) $b=1/2$ (linear Mises criterion), $q_e=2.2733$ N/mm^2;
3) $b=1$ (twin-shear criterion), $q_e=2.2747$ N/mm^2.

It is worth noting that the three elastic limits of a simply supported circular plate for different yield criteria are identical. This is because the maximum stress point is situated at the centre point of the plate, which has a special stress state, i.e. $\sigma_r = \sigma_\theta$. All the three yield loci of the Tresca criterion, Huber-von Mises criterion and the twin-shear criterion cross at the same point A, as shown in Fig. 7.16.
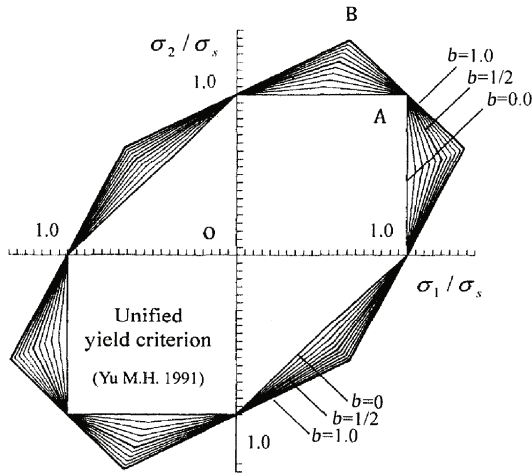
Fig. 7.16   Yield loci of the unified yield criterion in plane stress state

The plastic zone spreads from the centre point to the neighboring area around the centre point of the simply supported circular plate after a further increase in the load, in which the two stresses are not equal, i.e. $\sigma_r \neq \sigma_\theta$. The yield point at the yield loci spreads from A to other points, where the yield states of the three yield criteria are not identical.

The elasto-plastic load-displacement curves at the center of the plate with different yield criteria are shown in Fig. 7.17. Ideal plastic behaviour with a different parameter b of the unified yield criterion is assumed. The median elasto-plastic load-deflection curve of the plate is the same as that of Owen and

Hinton (1980).

The plastic limit of a uniform loading simply supported circular plate using the three basic criteria, i.e., the unified yield criterion with $b=0$, $b=1/2$ and $b=1$, can be obtained as follows.

1) $b=0$ (Tresca criterion), $q_p=2.7$ N/mm^2;
2) $b=1/2$ (a new criterion), $q_p=3.0$ N/mm^2;
3) $b=1$ (twin-shear criterion), $q_p=3.18$ N/mm^2.
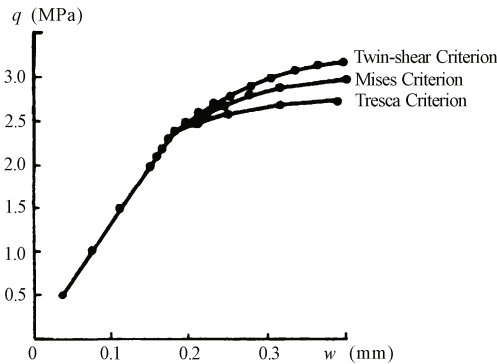
Fig. 7.17 Load-deflection curve of plate with the unified yield criterion

The differences between the three curves show the effect of the yield criterion on the plastic limit bearing capacity of circular plates. The limit-bearing capacity of a plate with the twin-shear criterion (unified yield criterion when $b=1$) is the maximum, and the limit-bearing capacity with the single-shear criterion (Tresca criterion or the unified yield criterion when $b=0$) is the minimum. The limit-bearing capacity with the Huber-von Mises criterion is median. The median result is equivalent to the result obeying the unified yield criterion with $b=1/2$ or $b=1/(1+\sqrt{3})$. The numerical results using the UEPP are very close to the analytical results described in (Yu, Ma and Li JC, 2009)

7.4.3 *Truncated Cone under the Uniform Load on the Top*

A truncated cone under the uniform load on the top is shown in Fig. 7.18(a). Similar to the plane stress problem and plane strain problem, this spatial symmetric structure has the identical section with the plane problem as shown in Fig. 7.18(b).

(a) Spatial symmetric problem   (b) FEM mesh
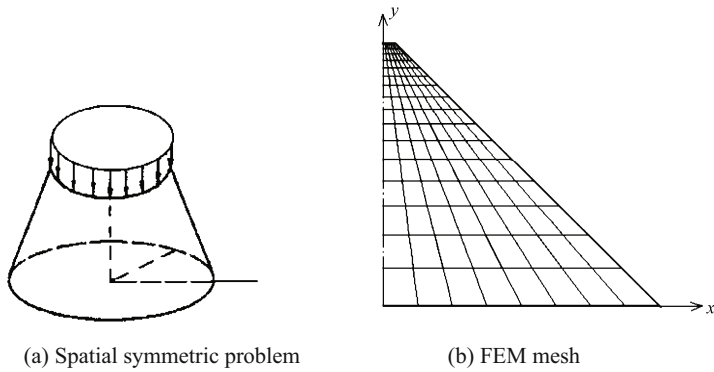
Fig. 7.18   Truncated cone and its FEM mesh

The elastic limit of the truncated cone in terms of the unified yield criterion with three basic values of b ($b=0, b=0.5, b=1$)in a spatial axisymmetric stress state can be obtained as follows.

1) $q_e = 33.6$ MPa (unified strength theory with $b=0$, single-shear theory, i.e. the Mohr-Coulomb theory);

2) $q_e = 40.6$ MPa (unified strength theory with $b=1/2$, a new criterion);

3) $q_e = 43.0$ MPa (unified strength theory with $b=1$, the twin-shear theory).

The load-displacement relationship of node 2 in the middle of the truncated cone structure under uniform load on the top, using the unified strength theory with three parameters b ($b=0, b=0.5, b=1$), is obtained as shown in Fig. 7.19.
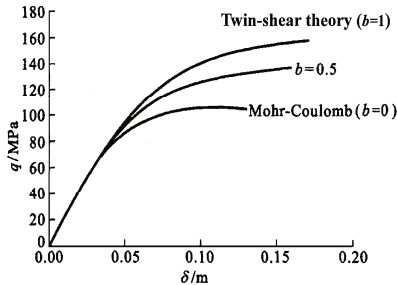
Fig. 7.19   Load-displacement relation of a truncated cone

The convergent result can be obtained when $q=105$ MPa   (unified strength theory with $b=0$, i.e., the Mohr-Coulomb single-shear theory), $q=136$ MPa (unified strength theory, $b=0.5$), $q=158.1$ MPa (unified strength theory, $b=1$). Increasing the loads further, the numeric solution process will be divergent. Then the limit load can be obtained by using the unified strength theory with three parameters respectively.

The plastic limit of a cone in terms of the unified yield criterion with three basic values of b ($b=0, b=0.5, b=1$) under the plane strain state can be obtained as follows.

1) q_p=105 MPa (unified strength theory with b=0, the single-shear theory, i.e. the Mohr-Coulomb theory);

2) q_p=136 MPa (unified strength theory with b=1/2, a new criterion);

3) q_p=158.1 MPa (unified strength theory with b=1, the twin-shear theory).

7.5 Brief Summary

The unified strength theory has been implemented in a non-linear FE program. Several examples are calculated by using the unified strength theory and associated flow rule. A series of results can be obtained for every example, which may be adapted for most materials and structures.

Plane stress, plane strain and spatial axisymmetric problems are three important problems in plasticity and engineering. Some typical examples, described in textbooks and monographs relating to computational plasticity are calculated again for comparison.   The results show that the result of the unified strength theory with b=0 is in good agreement with the result using the Mohr-Coulomb theory. The result of the unified strength theory with α=1 and b=0 is in good agreement with the result using the Tresca criterion. The result of the unified strength theory with α=1 and b=1/2 is equivalent to the result using the Huber-von Mises criterion. The result of the unified strength theory with b=1 is in good agreement with the result using the twin-shear theory and the result of the unified strength theory with α=1 and b=0 is in good agreement with the result using the twin-shear yield criterion, or the maximum deviatoric stress criterion. A series of new results can be also obtained by using the unified strength theory. The Tresca-Mohr–Coulomb single-shear strength theory, the twin-shear strength theory and a new median criterion can be deduced from the unified strength theory when b=0, b=1 and b=1/2. They are all piecewise linear yield criteria. The lower bound, upper bound and the median criterion situated between these two bounds may be considered as three basic criteria for SD materials (α≠1) and non-SD materials (α=1). The yield loci of the three criteria are shown in Fig. 7.20.

(a) SD materials   (α≠1)   (b)   Non-SD materials (α=1)
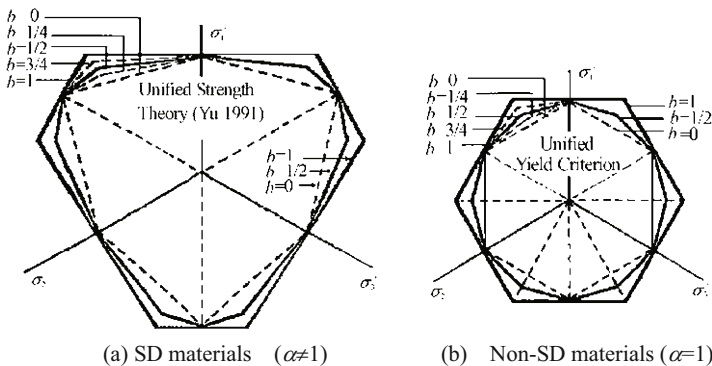
Fig. 7.20   Yield loci of several typical criteria of the unified strength theory

The numerical results obtained by using the unified strength theory are in good agreement with the results of the unified solution described in (Yu et al., 2009).

The unified strength theory and associated flow rule have also been implemented in several commercial non-linear FE codes and applied to engineering problems, which will be described in the next chapters.

References

Chakrabarty J (1987) Theory of Plasticity. McGraw-Hill: New York.

Johnson W and Mellor PB (1962) Plasticity for Mechanical Engineers. Van Nostrand: London and New York.

Mendelson A (1968) Plasticity: Theory and Application. Macmillan: New York.

Owen DRJ and Hinton E (1980) Finite Elements in Plasticity : Theory and Practice. Pineridge Press Ltd: Swansea.

UEPP User's Manual, Version 3.0(1998) Research Division of Structural Strength, Dept. of Civil Eng., Xi'an Jiaotong University.

Yu MH and Li YM (1991) Twin shear constitutive theory and its computational implementation. In: Computational Mechanics, Ed. by Cheung YK, Lee JHW and Leung AYT, Balkema, Rotterdam, pp 875-879.

Yu MH (1992) New System of Strength Theory. Xian Jiaotong University Press: Xian, China (in Chinese).

Yu MH, He LN and Zeng WB (1992) A new unified yield function : Its model, computational implementation and engineering application. Computational Methods in Engineering: Advances and Applications. Tay AAO and Lam KY eds. World Scientific: Singapore, pp 157-162.

Yu MH and Zeng WB (1994) New theory of engineering structural analysis and its application. J. Eng. Mech., 11(1): 9-20. (in Chinese, English abstract).

Yu MH, Zeng WB, Ma GW, Yang SY, Wang F and Wang Y (1993) Unified Elasto-Plastic Program-UEPP. Xian Jiaotong University, English version.

Yu MH (2004) Unified Strength Theory and Its Applications. Springer: Berlin.

Yu MH et al. (2006) Generalized Plasticity. Springer: Berlin.

Yu MH, Ma GW and Li JC (2009) Structural Plasticity: Limit, Shakedown and Dynamic Plastic Analyses of Structures. Springer and Zhejiang University Press.

Zienkiewicz (1971) The Finite Element Method in Engineering Science. McGraw-Hill: London.

8

Strip with a Circular Hole under Tension and Compression

8.1 Introduction

Elasto-plastic analysis of a strip with a hole under tension is a classical problem in computational plasticity. It was studied experimentally by Theocaris and Marketos (1964) and was first analyzed using finite element methods by Marcal and King (1967) and Zienkiewicz, Valliappan and King (1969). This problem was also studied by Narisawa (1991) and Yu and Zeng (Yu, 1998). The results were described by many authors, such as Zienkiewicz (1971), Zienkiewicz and Taylor (2000; 2009) and Yu (1998; 2004). The Huber-von Mises criterion for non-SD materials was used before 1994. The results can be adopted only for those materials which have identical strength both in tension and compression and the shear strength equals $\tau_y = 0.577\sigma_y$. It cannot be used for most materials, especially geomaterials. The twin-shear strength theory was used for elasto-plastic analysis of a strip with a hole under tension and compression for non-SD materials and SD materials by Yu and Zeng (Yu, 1998). The unified yield criterion was studied for elasto-plastic analysis of a strip with a hole under tension for non-SD materials by Yu (Yu, 2004). The analytical results obtained using various yield criteria are very different. The shape and size of the plastic zone as well as the slip angle are influenced strongly by the choice of the yield criterion. It is necessary to use a new efficient criterion. The effect of the yield criterion on analytical results in plasticity were observed by Humpheson and Naylor (1975), Zienkiewicz and Pande (1977), Mean and Hutchinson (1985), Tvergaard (1987), Narisawa (1991), Lee and Ghosh (1996), Hopperstad et al. (1998), Moin and Pankaj (1998), Wang and Fan (1998), Frieman and Pan (2000), Kuroda and Tvergaard (2000).

The unified strength theory and its implementation in a computer code provides us with a very effective approach for studying the effect of yield criterion for various engineering problems. A series of new computational results can be obtained by using the unified strength theory (see Chapter 5). These serial results can be adapted for more materials and structures.

Elasto-plastic analysis of a strip with a circular hole for non-SD materials (having identical strength both in tension and compression), SD materials (strength difference in tension and compression) and concrete plates are described in this chapter. A simple experimental method is used for comparison. The analytical and experimental results clearly show the difference in plastic regions of a strip with a circular hole between tension and compression when SD materials are involved.

8.2   Plastic Analysis of a Strip with a Circular Hole for Non-SD Material

The finite element mesh and spread of the plastic zone using the Huber-von Mises criterion was given by Zienkiewicz (1971), as shown in Fig. 8.1.
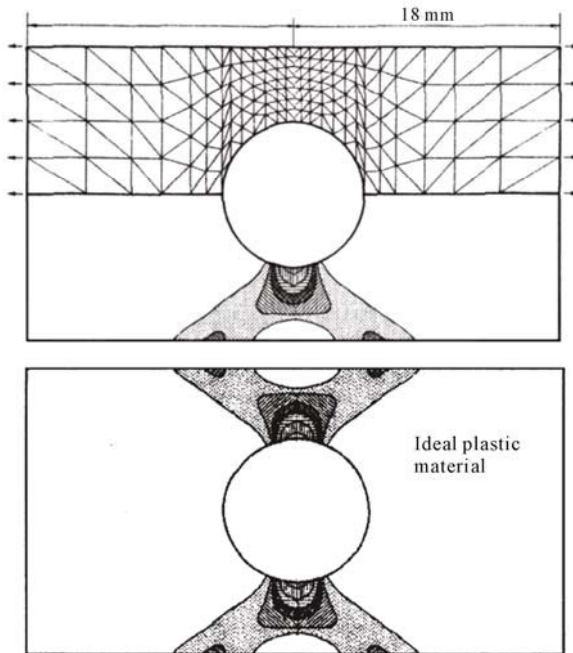
Fig. 8.1   FEM mesh and plastic zone of a strip with a hole (Zienkiewicz, 1971)

The growth in yielding around a circular hole of polymer alloys material was studied by Narisawa (1991). The spread of the plastic zone using FEM plasticity is shown in Fig. 8.2. It is obtained also by using the Huber-von Mises criterion. The shear yielding grows toward a region near $\theta=45°$, as shown in Fig. 8.2. The extension of the plastic zone is the same as in Fig. 8.1.
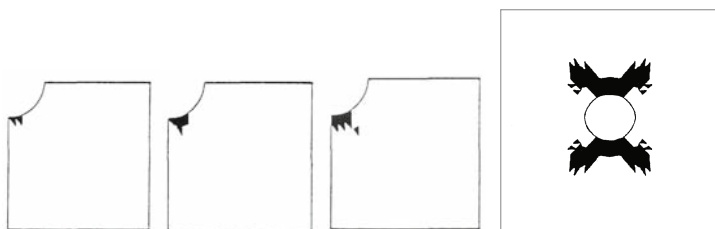
Fig. 8.2   The onset and growth of yielding around the circular hole (Narisawa, 1991)

A similar problem was also analyzed by Yu and Zheng based on the unified strength theory for comparison, as shown in Fig. 8.3. The material behaviour is $E=7\times10^4$ MPa, $\mu=0.2$, yield stress $\sigma_s=243$ MPa. The strip is considered as a plane stress problem.
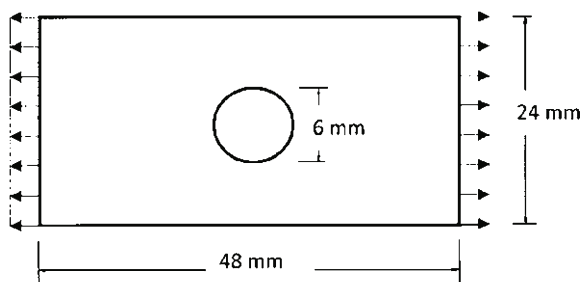
Fig. 8.3   A strip with a circular hole under tension

The configuration and the division into 96 isoparametric elements are shown in Fig. 8.4, in which the 4-nodes isoparametric element is used. The number of the nodes is 119. The elastic limit of a strip with a circular hole in terms of the unified yield criterion can be obtained after the first iteration. It requires a large number of iterations of non-linear computation for the plastic limit, until no further increase in the reaction at that point is achieved (furthermore, the numerical solution process will be divergent). The plastic limit load is approached progressively until that limit point where no convergence is achieved. The strip with a circular hole reaches the plastic limit in terms of the unified yield criterion with $b=0$ (i.e. the Tresca criterion) when $p=140$ MPa.

The size and shape of the plastic zone is of importance to the understanding of the failure of structures. The spread figures of plastic zones with a different parameter b of the unified yield criterion (i.e. different criteria) at a same load $p=140$MPa for a strip with a circular hole are shown in Figs. 8.4(a)~8.4(e).

Figure 8.4(a) shows the spread of the plastic zone obeying the unified yield criterion when $b=0$ and $\alpha=\sigma_t/\sigma_c=1$, i.e. the single-shear yield criterion or the Tresca yield criterion. Fig. 8.4(b) shows the spread of the plastic zone obeying the unified

yield criterion when $b=1/4$ and $\alpha= \sigma_t/\sigma_c=1$; this is a new yield criterion introduced from the unified yield criterion. Figure 8.4(c) shows the spread of the plastic zone obeying the unified yield criterion when $b=1/2$ and $\alpha= \sigma_t/\sigma_c=1$; this is a new yield criterion introduced from the unified yield criterion. Figure 8.4(d) shows the spread of the plastic zone obeying the unified yield criterion when $b=3/4$ and $\alpha= \sigma_t/\sigma_c=1$; this is a new yield criterion introduced from the unified yield criterion. Figure 8.4(e) shows the spread of the plastic zone obeying the unified yield criterion when $b=1$ and $\alpha=\sigma_t/\sigma_c=1$, i.e. the twin-shear yield criterion (Yu, 1961; 1983).
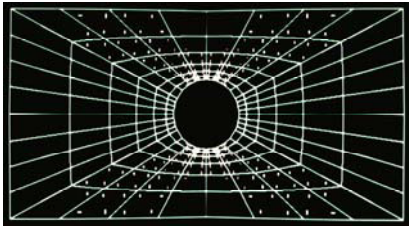
(a) UST with $b=0$ and $\alpha =1$(Single-shear; criterion, Tresca criterion)
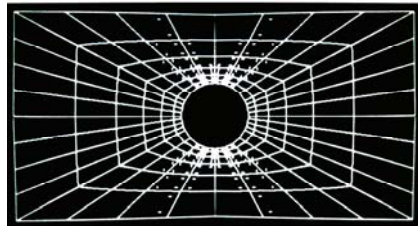
(b) UST with $b=1/4$ and $\alpha =1$ (New criterion introduced from the unified yield criterion)
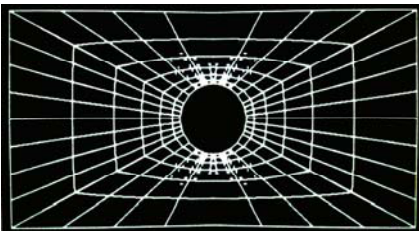
(c) UST with $b=1/2$ and $\alpha =1$ (New criterion introduced from the unified yield criterion)
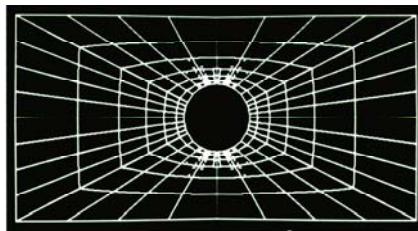
(d) UST with $b=3/4$ and $\alpha =1$ (New criterion introduced from the unified yield criterion)
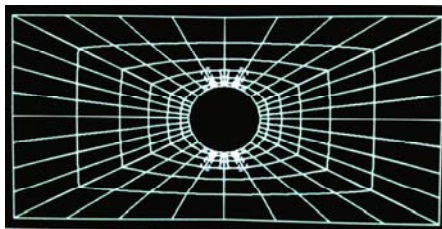
(e) UST with $b=1$ and $\alpha =1$ (Twin-shear criterion)

Fig. 8.4   Distribution of plastic zone around a circular hole with different yield criteria

It is of interest to note that the spread of the plastic region is different under the same load for different yield criteria. It means the effect of the yield criterion on the spread of the plastic zone is evident. The plastic zone of twin-shear material (the unified yield criterion with $b=1$) is smallest. The plastic zone of single-shear material (the unified yield criterion with $b=0$), i.e. the Tresca yield criterion, is largest, as shown in Fig. 8.4. Obviously, the plastic zone of the unified yield criterion with $b=1/4$ is the median between the plastic zone of the unified yield criterion with $b=0$ and $b=1/2$. The plastic zone of the unified yield criterion with $b=3/4$ is the median between the plastic zone of the unified yield criterion with $b=1/2$ and $b=1$.

The unified yield criterion with $b=1/2$ and $\alpha=\sigma_t/\sigma_c=1$ may be regarding as a linear approximation to the Huber-von Mises yield criterion. The result of the unified yield criterion with $b=1/2$ and $\alpha=\sigma_t/\sigma_c=1$ is equivalent to the result of the Huber-von Mises criterion.

8.3   Elasto-Plastic Analysis of a Strip with a Circular Hole for SD Material under Tension

A similar example is examined by using the unified strength theory (Yu, 1991) and associated flow rule for a pressure sensitive material (SD material, $\sigma_t \neq \sigma_c$). Material parameters are chosen for the comparison with experimental materials. The experimental material is a hard blue polymer, the color of which can change to white when it reaches the plastic state. Material parameters are as follows: tensile yield stress σ_t=5.89 kN/cm^2, compressive yield stress σ_c=7.58 kN/cm^2, the ratio of tensile strength to compressive strength is $\alpha = \sigma_t/\sigma_c$=0.777.

The plastic zones of a strip with a circular hole for SD material under tension were also tested and calculated using the unified strength theory and unified elasto-plastic constitutive rule (Yu, 1998). The plastic zone based on the unified strength theory with $b=0$ (single-shear theory, i.e. the Mohr-Coulomb theory) is shown in Fig. 8.5. The plastic zone based on the unified strength theory with $b=1$ (twin-shear theory) is illustrated in Fig. 8.6. The plastic zones are different for single-shear material and twin-shear material.

UST with b=1.0
(Single-shear theory)

Fig. 8.5   Plastic zone based on the unified strength theory with b=0 (Single-shear theory)
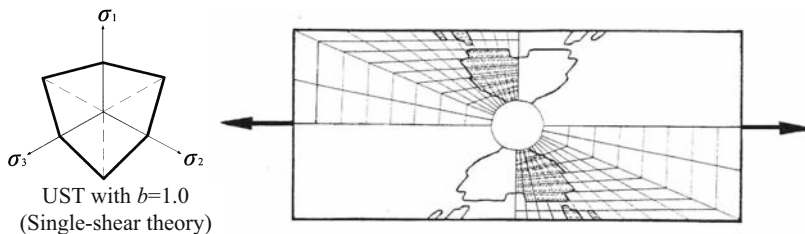
UST with *b*=1.0
(Twin-shear theory)
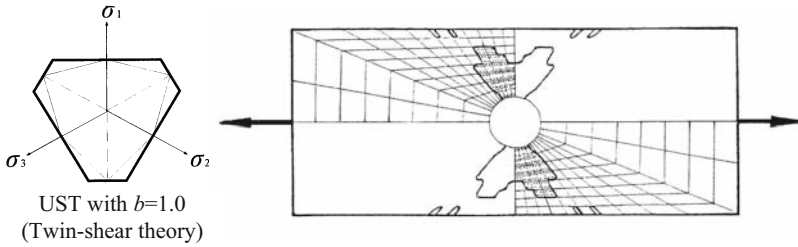
Fig. 8.6   Comparison of plastic zones of strip in tension with *b*=1 (Twin-shear theory)

The test results of two specimens are shown in Fig. 8.7. It can also be seen that the point of the plastic zone in the test result is close to the result of twin-shear theory.

(a)   Smaller circular hole

(b) Bigger circular hole
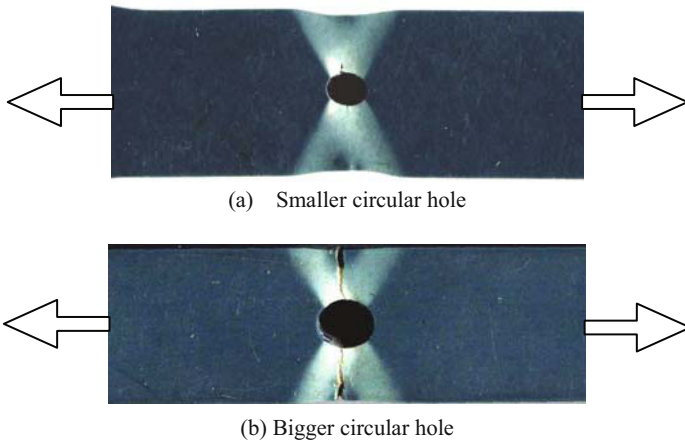
Fig. 8.7   Test result of plastic zones of strip with two different circular holes under tension

The experimental results also present the difference in plastic zones under tension and under compression.

8.4   Plastic Zone of a Strip with a Circular Hole for SD Material under Compression

The plastic zones of a strip with a circular hole for SD material under compression were calculated by using the unified strength theory and the unified elasto-plastic constitutive rule. The plastic zone based on the unified strength theory with *b*=0 (single-shear theory, i.e. the Mohr-Coulomb theory, 1900) and *b*=1 (twin-shear strength theory (Yu, 1985)) are illustrated in Fig. 8.8. It can be seen that the plastic zones of a strip with a circular hole under compression are different for single-shear material and twin-shear material.
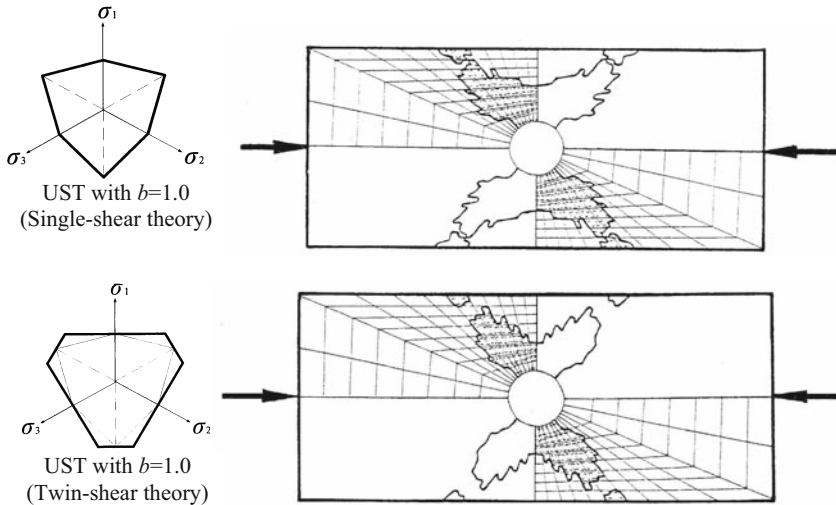
Fig. 8.8   Comparison of plastic zones of strip under compression using two theories

8.5   Comparison of Numerical Analysis with Experiments

As can be seen, the plastic zones under tension and compression are different for SD (strength difference in tension and in compression) materials. Figure 8.9 shows the computational results of the spread of the plastic zone of a strip using the twin-shear strength theory under tension. Figure 8.10 shows the computational results of the spread of the plastic zone of a strip using the twin-shear strength theory under compression.

An experimental study using polymer and computer image techniques was carried out by Yu et al. (1992). A strip with a circular hole subjects a tensile load, as show in Fig. 8.9 and Fig. 8.10. Sometimes deformation is accompanied by a change in color; the material deforms and changes color when it reaches a plastic state. The different colors and patterns of a strip in different regions show up clearly, which can be seen in Fig. 8.8. The plastic zone begins at the edge of the hole and spreads in four directions, as show in Fig. 8.9 and Fig. 8.10. The plastic zones are similar to the calculated results using the unified strength theory with $b=1$ (Twin-shear strength theory). In general, the slip angle is a compromise between the two angles of   single-shear theory and twin-shear theory. Obviously, the slip angle is close to that of twin-shear theory, as shown in Fig. 8.6.
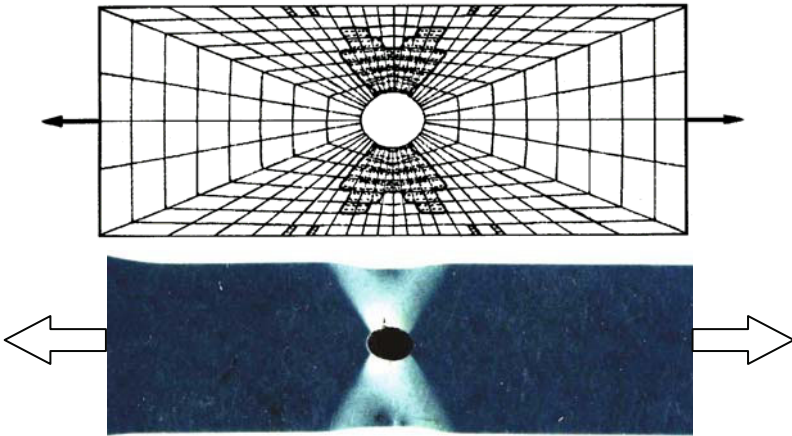
Fig. 8.9 Comparison of the computational results with experiments on plastic
Zones under tension

A strip with a circular hole subjecting a load to compression is shown in Fig.
8.12. The plastic zone begins at the edge of circular hole and spreads in four
directions, as shown in Fig. 8.12. The plastic zones are similar to the calculated
results of a strip under compression using the unified strength theory with $b=1$
(Twin-shear strength theory).
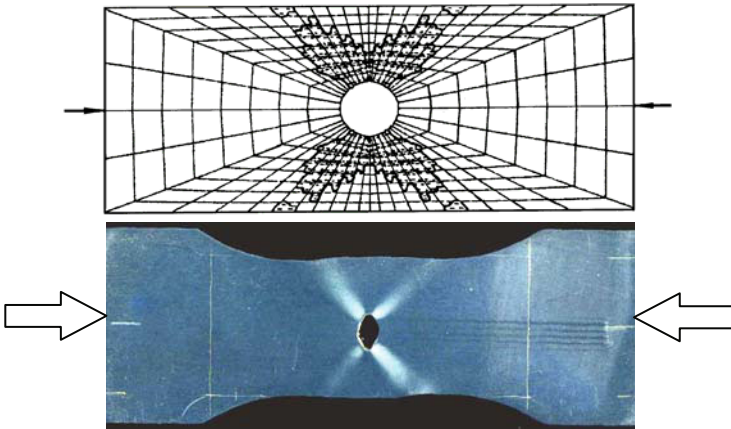
Fig. 8.10 Comparison of computational results with experiments on plastic zones
under compression

The analytical result can be obtained by unified slip line field theory (Yu et
al., 1997; Yu et al., 2006). The computational results are very close to those
results obtained from the experiments and from slip line theory.

8.6 Elasto-Plastic Analysis of a Strip with a Circular Hole for a Special SD Material: Concrete

Concrete is an SD material. The compressive strength is much larger than the tensile strength. A concrete plate with a circular hole under pressure q is shown in Fig. 8.11. The thickness of the plate is 6cm, so it is considered to be a plane stress problem. The material parameters are: σ_t=2.7 MPa, σ_c=27 MPa, E=2.65×10^4 MPa, ν=0.19.

The single-shear theory (Mohr-Coulomb strength theory) and the twin-shear strength theory are used as the yield criteria for concrete (This analysis was done by Zheng in 1990). Due to symmetry, only a quarter of the plate is considered. The beginning and the spread of the plastic zone for single-shear material under q=228.6 kg/cm and q=400 kg/cm are shown in Fig. 8.11.

(a) q=228.6 kg/cm   (b) q=400 kg/cm
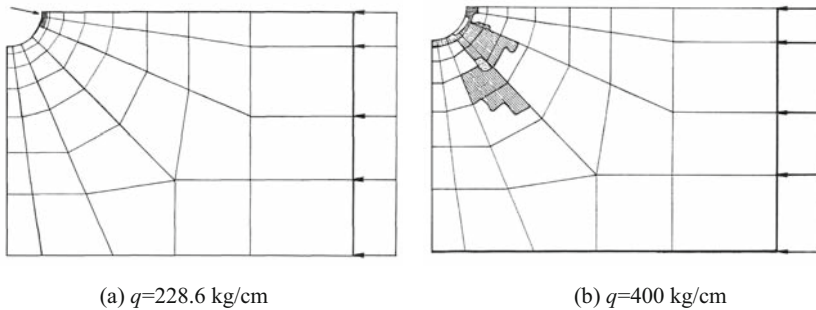
Fig. 8.11 Spread of plastic zones for Mohr-Coulomb material

According to the twin-shear theory, no plastic zone occurs when q=228.6 kg/cm. The spread of the plastic zone for twin-shear material under q=400 kg/cm and q=571.4 kg/cm is shown in Fig. 8.12.

(a) q=400 kg/cm   (b) q=571.4 kg/cm
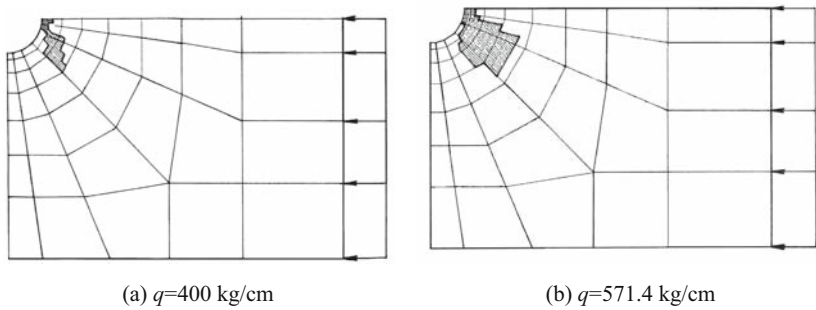
Fig. 8.12 Spread of plastic zones for twin-shear material

Figure 8.13 shows the comparison between the two computational results for single-shear material and twin-shear material under the same load. It is shown that the plastic zone of the twin-shear material is smaller than that of single-shear material under the same load. The bearing capacity of twin-shear material is higher than that for single-shear material.

(a) Single-shear material   (b) Twin-shear material
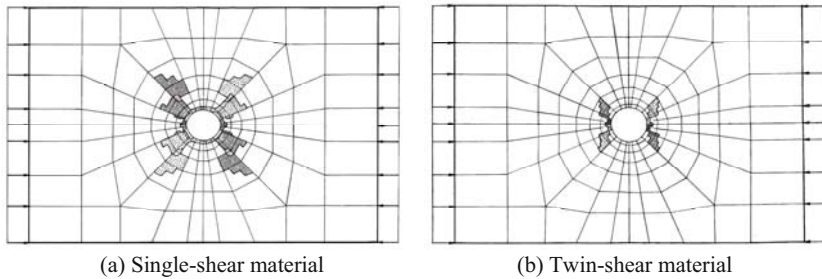
Fig. 8.13 Comparison of the spread of plastic zones for a concrete plate with a circular hole using the single-shear criterion and the twin-shear criterion under the same load

8.7 Brief Summary

The shape and size of the plastic zone, as well as the slip angle, are influenced strongly by the choice of the yield criterion. This can be seen from the tension and compression of a strip with a circular hole, as shown in Fig. 8.14 and Fig. 8.15. These results are also different for SD materials for the same strip under tension and under compression. The single-parameter criterion can only be used for non-SD materials. SD materials, however, have to use the two-parameters criterion.

The computational results for a strip under compression and the experimental results are summarized in Fig. 8.14. The comparisons show that the results for twin-shear theory are closer to the experimental results than the results for single-shear theory.

The computational results for a strip under tension and the experimental results are summarized in Fig. 8.15. The comparisons show that the results for twin-shear theory are closer to the experimental results than the results for single-shear theory.

It is very important how we choose a reasonable strength theory (yield criteria or material model in FEM code) in research and design. We have to determine the bounds and region of the failure criteria before the research. The two bounds are important. The two bounds and region of the yield loci for non-SD materials and SD materials are shown in Fig. 8.16. The lower bound (inner bound) is the yield locus of the single-shear theory, and the upper bound (outside bound) is the twin-shear theory.
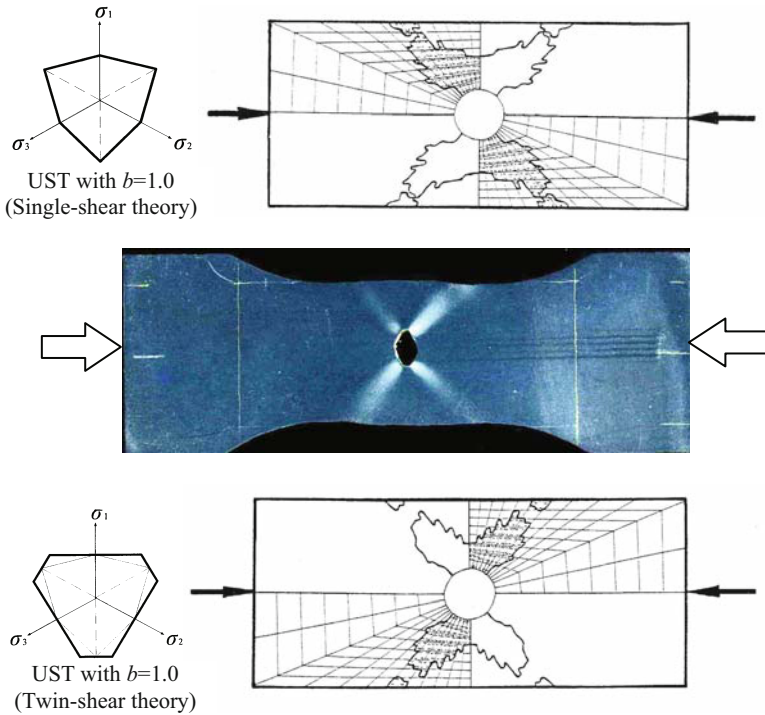
Fig. 8.14   Plastic zones of a strip with a circular hole under compression based on single-shear theory and twin-shear theory

The results of research and design depend strongly on the choice of strength theory in most cases. The selection of the correct strength theory becomes even more important than the calculations, as indicated by Sturmer, Schulz and Wittig (1991) and others. The bearing capacity of structures, the forming limit of FEM simulations, the size of plastic zones, the orientation of the shear band and plastic flow localization *etc*. will be much affected by the application of strength theory. More experimental results regarding the strength of materials in a complex stress state and a more precise choice of the strength theory applied are necessary in research and engineering applications.

As use of FEM and other numerical analysis expands in engineering design with increased access to computers, it becomes important that strength theory (yield criterion, failure criterion) related stress be carefully chosen. In adopting a criterion for use it is important that at least as much concern be directed to the physics of the problem and to the limitation of the criteria. When it becomes necessary to adopt a criterion for use, it is important to experimentally check the criterion, or to investigate the experimental data in the literature. If this is not done, then very exact numerical procedures or commercial codes can lead to completely worthless results (Hopperstad et al., 1998).

The unified yield criterion and the unified strength theory provide us with systematic yield criteria, an effective approach and a powerful tool for studying these effects. More results can be obtained using strength theory and the associated flow rule, which can be adapted for different materials and structures.

UST with *b*=1.0
(Single-shear theory)

UST with *b*=1.0
(Twin-shear theory)
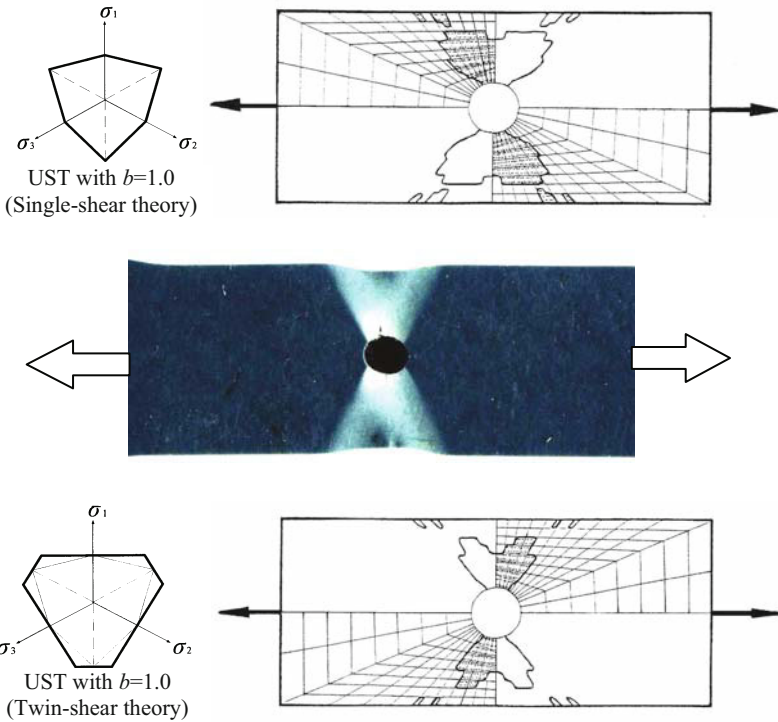
Fig. 8.15   Plastic zones of a strip with a circular hole under tension based on single-shear theory and twin-shear theory

(a) For non-SD materials   (b) For SD materials
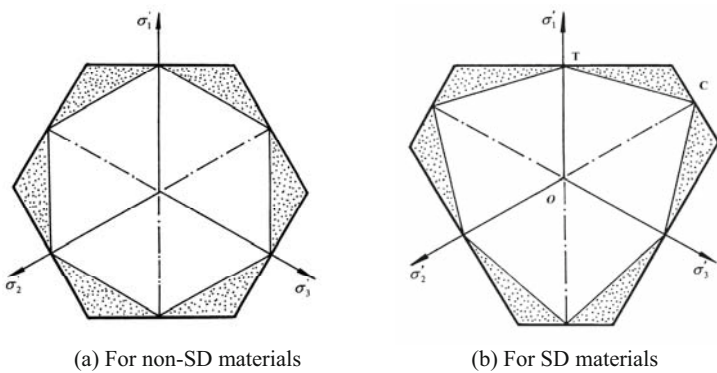
Fig. 8.16   Bounds and region of yield loci

References

Frieman PA and Pan J (2000) Effects of plastic anisotropic and yield criteria on prediction of forming limit curves. Int. J. Mech. Sci., 42: 29-48.

Hopperstad OS, Berstad T, Listad H and Lademo OG (1998) The effects of different yield criteria on local deformations in numerical simulation of profile forming. J. Materials Processing Technology, pp 80-81, 551-555.

Humpheson C and Naylor DJ (1975) The importance of the form of the failure criterion. C/R/243/75, University of Wales: Swansea, UK.

Kuroda M and Tvergaard V (2000) Forming limit diagram for anisotropic metal with different yield criteria. Int. J. Solids Structures, 37: 5037-5059.

Lee YK and Ghosh J (1996) The significance of J_3 to the prediction of shear bands. Int. J. of Plasticity, 12(9): 1179-1197.

Marcal P.V and I. P King (1967) Elastic-plastic analysis of two dimensional stress systems by the finite element method. Int. J. Mech. Sci., 9: 143-55.

Mean ME and Hutchinson JW (1985) Influence of yield surface curvature on flow localization in dilatant plasticity. Mechanics of Materials, 4: 395-407.

Moin K and Pankaj (1998) Post-peak behavior simulation using different failure theories. Strength Theory: Applications, Developments and Prospects for the 21st Century. Yu MH and Fan SC eds. Science Press: New York, Beijing, pp 1121-1126.

Narisawa I (1991) Crazing and shear deformation of polymer alloys. In: Jono M and Inoue T eds, Mechanical Behaviour of Materials-VI, 3: 311-318.

Sturmer G, Schulz A and Wittig S (1991) Life time prediction for ceramic gas turbine components. ASME–Paper, 91-GT-96.

Theocaris P S and E. Marketos (1964) Elastic-plastic analysis of perforated thin strips of a strain hardening material．J．Mech．Phys. Solids, 12: 377-90.

Tvergaard V (1987) Effect of yield surface curvature and void nucleation on plastic flow localization. J. Mech. Phys. Solids, 35: 43-60.

Wang F and Fan SC (1998) Limit pressures of thick-walled tubes using different yield criteria. Strength Theory: Applications, Developments and Prospects for the 21st Century. Yu MH and Fan SC eds. Science Press: New York, Beijing, pp 1.

Yu MH (1983) Twin shear stress yield criterion. Int. J. Mech. Sci., 25(1): 71-74.

Yu MH, He LN and Song LY (1985) Twin shear stress theory and its generalization. Scientia Sinica (Sciences in China), English edn. Series A, 28(11): 1174-1183.

Yu MH et al (1992) Computer image analysis of the plastic zone of structure. J. of Xi'an Jiaotong University, 26(2): 121-123 (in Chinese).

Yu MH et al (1998) Constitutive model: from single shear to tri-shear to twin-shear to unification. Chinese Journal of Rock Mechanics and Engineering, 17 (Suppl.) 739-743 (in Chinese, English abstract).

Yu MH (1998) Twin-shear Theory and its Applications. Science Press: Beijing. (in Chinese).

Yu MH (2004) Unified Strength Theory and its Applications. Springer: Berlin.

Yu MH et al.(2006) Generalized Plasticity. Springer: Berlin.

Zheng SJ (1990) Research on the Static and Fatigue Strength of Concrete under Combined Stresses. Master's Dissertation of Xi'an Jiaotong University, Xi'an, China (in Chinese).

Zienkiewicz OC, Valliappan S and King IP (1969) Elasto-plastic solution of engineering problems. Initial-stress, finite element approach. Int. J. Num. Meth. in Eng., 1: 75-100.

Zienkiewicz OC (1971) The Finite Element Method in Engineering Science. McGraw-Hill: London.

Zienkiewicz OC and Pande GN (1977) Some useful forms of isotropic yield surfaces for soil and rock mechanics. Finite Elements in Geomechanics. Gudehus G ed. Wiley: London, pp 179-190.

Zienkiewicz OC and Taylor RL (2000) The Finite Element Method. Fifth Ed.Butterworth Heinemann.

Zienkiewicz OC and Taylor RL (2009) The Finite Element Method for Solid and Structural Mechanics. Sixth edn.Elsevier: Amsterdam and Elsevier: Singapore Pte Ltd.

9

Plastic Analysis of Footing Foundation Based on the Unified Strength Theory

9.1 Introduction

Bearing capacity of soils and settlement of strip foundations and circular foundation are an important and classical problem. Loads from a structure are transferred to the underlying soil through a foundation such as a footing. The foundation and soils must not collapse or become unstable under any conceivable loading.

Prandtl indicated that the metallic material will be deformed below a rigid plate, as shown in Fig. 9.1(a). Terzaghi applied Prandtl's theory to a strip footing with the assumption that the soil is a semi-infinite, homogeneous, isotropic, weightless rigid-plastic material, as shown in Fig. 9.1(b). The systematic description of bearing capacity of shallow foundations can be seen in Chen and McCarron (1991).

The solutions of footing foundation were generalized to a unified solution introduced from the unified slip field theory (Yu et al., 1997; 2006). A series of solutions can be obtained by using the unified slip field theory. The unified solutions for plane strain, plane stress and spatial axial-symmetric problems have been summarized in (Yu, 2006).

(a) Non-SD materials   (b) SD materials
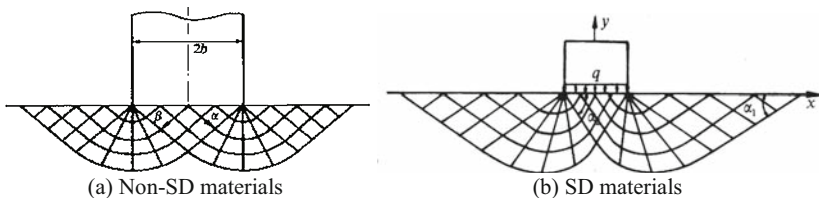
Fig. 9.1   Slip field of footing foundation

Numerical method is also applied to geomechanics and geotechnological engineering (Chen, 1975; de Borst and Vermeer, 1984; Chen and Mizuno, 1990; Verruijt, 1995; 2009; Potts and Zdravkovic, 1999; 2001; Contractor and Desai, 2001; Griffiths and Gioda, 2001; Davis and Selvadurai, 2002; Kolymbas, 2003; Bull, 2003; Pastor and Tamagnini, 2004; Yu, 2006; Chan and Shiomi, 2006; Pietruszczak, 2010). Recently, special Lecture Notes on Computational Geomechanics: Inelastic Finite Elements for Pressure Sensitive Materials are presented by Jeremić et al. (2010).

A series of international conference of IACMAG are organized by the International Association for Computer Methods and Advances in Geomechanics about every three years. Serial proceedings on Computer Methods and Advances in Geomechanics are published. Another series of International Symposium on Numerical Models in Geomechanics are held since 1982. Relating Proceedings of International Symposium on Numerical Models in Geomechanics (NUMOG) were published (Pande and van Impe, 1986; Pietruszczak and Pande, 1989; Pande and Pietruszczak, 1992; 1995; 1997; 1999; 2002; 2004; 2007). The serial conferences on Numerical Methods in Geotechnical Engineering were organized by the European Regional Technical Committee ERTC7 (Numerical Methods in Geotechnical Eng.) under the auspices of the International Society for Soil Mechanics and Geotechnical Engineering (ISSMGE). One of the first conferences of this series was held in 1986 in Stuttgart, Germany and continued every four years (Santander, Spain, 1990; Manchester, United Kingdom, 1994; Udine, Italy, 1998; Paris, France, 2002; Graz, Austria, 2006). The Seventh European Conference on Numerical Methods in Geotechnical ngineering has been held in Trondheim, Norway 2010.

Numerical method is used for studying of footing foundation. Various finite element analyses for elastoplastic deformation and bearing capacity of strip footing and circular foundation have been reported in the literature. The development of plastic zone in soil under a strip footing foundation was studied by Nayak and Zienkiewicz (1972), Humpheson and Naylor (1975), Zienkiewicz and Pande (1977), de Borst and Vermeer (1984), Chen and Mizuno (1990), Moore and Rowe (1991), Ehlers (1995), Wunderlich et al. (2001), Otani et al. (2001) and others. The results show the spread of plastic zone at various footing penetrations, the final slip surface, and soil materials collapses with a mechanism are similar to that of Prandtl for perfectly plastic materials. Many researchers have investigated numerically the bearing capacity of shallow foundations on cohesionless soil that obeys the Mohr-Coulomb failure criterion. Two velocity fields for strip footing foundation are shown in Figs. 9.2(a) and 9.2(b). The mesh effect and failure mechanism of footing by using the Drucker-Prager criterion with size-adjustment on Mohr-Coulomb theory was given by Zimmermann and Commend (2001), as shown in Fig. 9.2(b).

The Mohr-Coulomb model or the Drucker-Prager criterion is always used for numerical simulation of strip footing and circular foundation. Only one result is given by using of the Mohr-Coulomb model or the Drucker-Prager criterion, which is adapted only for one kind of material.

(a) Moore and Rowe(1991)   (b) Zimmermann and Commend (2001)
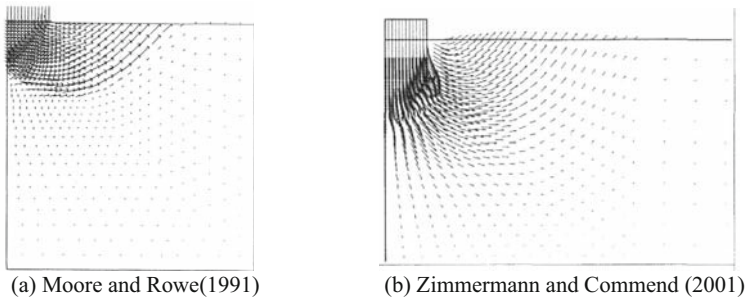
Fig. 9.2   Simulations for velocity fields

The similar results were also obtained by other researchers. A real-life problem in geomechanics were investigated by Wunderlich et al. (2001) using a six parameters criterion. The plastic strains of strip foundation by using the Ehlers single-surface yield criterion was giver by Ehlers (1995), as shown in Fig. 9.3.
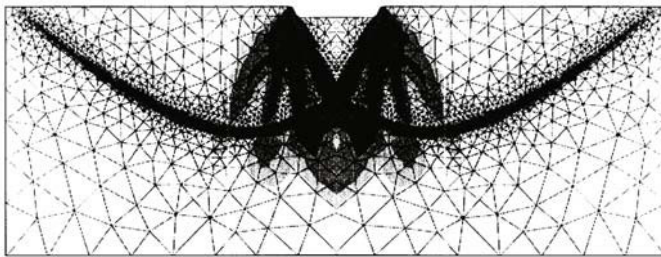
Fig. 9.3   Numerical Simulations of plastic strains for strip foundation (Ehlers, 1995)

Bearing capacity of strip and circular footings in sand following the Mohr-Coulomb failure criterion are given by Loukidis and Salgado (2009). Collapse mechanisms as depicted by contours of the plastic maximum shear strain increment compared against the mechanism yielded by Martin's ABC program (Martin, 2003; 2005) for strip footings on weightless soil with surcharge are presented (Loukidis and Salgado, 2009).

Two- and three-dimensional bearing capacity of footings in sand are studied by Lyamin et al. (2007). A 3D rigid plastic finite element analysis for strip footing was solved by using of the Drucker-Prager criterion (Otani et al., 2001). Finite element mesh and 3D velocity field for strip footing are shown in Fig. 9.4.
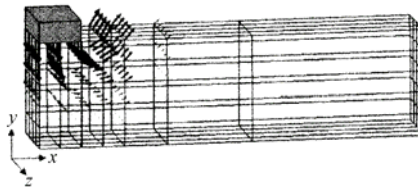
Fig. 9.4   Simulation of velocity field for strip footing (Otani et al., 2001)

The shape of velocity field roughly resembles the Prandtl mechanism for perfectly plastic materials, although only part of the solid material in motion is responding plastically, with both the block of material directly under the rigid footing and much of the solid within the "passive motion" behaving elastically. The shape is also similar the results obtained by the unified slip field theory for plane strain problem and unified characteristics line field of spatial axisymmetry problems (Yu and Li, 2001; Yu et al., 2006).

9.2 Effect of Yield Criterion on the Limit Analysis of Footing

The limit analysis of strip footing foundation was studied by Nayak and Zienkiewicz (1972), Humpheson and Naylor (1975), Zienkiewicz and Pande (1977). Great difference among the different solutions using different yield criteria is obvious. It has been shown in Fig. 1.8 in Chapter 1. Similar result is also given by Chen and Mizuno (1990). The load-displacement curves by the Drucker-Prager models with different radius of yield circles (different material constants) are different.

As indicated by Chen and Mizuno, the analysis using material constants matched with the compressive meridian of the Mohr-Coulomb criterion in three-dimensional space results in a collapse load (365 psi or 2520 kPa) which is almost twice that of the other analyses (158, 190 psi or l090, 1310 kPa). This load-displacement curve is characterized by linear elastic response to approximately l50 psi and nonlinear elastic-plastic response to the collapse load. On the other hand, the Drucker-Prager criterion with material constants matched with the tensile meridian of the Mohr-Coulomb criterion predicts a collapse load (190 psi) which is somewhat higher than that of l75 psi given by Tetzaghi. Further, the collapse load (158 psi) predicted by the Drucker-Prager criterion matched with the Mohr-Coulomb criterion in the plane strain condition is, as expected., almost the same as that of l52 psi predicted by the Mohr-Coulomb criterion (Zienkiewicz et al., 1975; 1999). This load is close to the loads (l75 psi and 143 psi) given by the Terzaghi and Prandtl solutions.

As a result the analysts with the material constants of compressive meridian of the Mohr-Coulomb criterion for the Drucker-Prager criterion does not agree with the well-known Terzaghi and Prandtl solutions. The important point to be noted here in using the Drucker-Prager model is the careful selection of material constants. In order for this criterion to represent a proper generalization of the Mohr-Coulomb or modified Mohr-Coulomb criteria under multi-dimensional stress states. Its material constants must be properly defined. These constants should not be treated as fixed expressions for all types of applications. Rather, their choice depends on the particular problems to be solved (Chen and Mizuno, 1990). The limit loci of extension circular cones give a very poor approximation to the real failure conditions.

The influence of different forms of yield surfaces on load-bearing capacity is

obvious. Most of the limit surfaces of different failure criteria are cones in stress space. The limit loci in the meridian plane are linear. This means that the strength of materials is linearly dependent on the hydrostatic stress, as has been demonstrated in a number of tests, in which the hydrostatic stress is not high. The differences between the limit loci of various failure criteria in the deviatoric plane have been shown in Fig. 1.8 in Chapter 1.

Obviously, various circular cones of Drucker-Prager criterion, i.e. extension cone, compromise cone, compression cone and the Drucker-Prager criterion (inscribed cone of the Mohr-Coulomb semi-infinite hexagonal cone with unequal sides) cannot match with the six experimental points, as shown in Fig. 9.5(a). The Tresca regular hexagon cannot also match the six points as shown in Fig. 9.5(b). According to the convexity, all the yield loci must be situated between the two bounds, as shown in Fig. 9.6. Three basic criteria of the unified strength theory with $b=0$, $b=1/2$ and $b=1$ for SD materials shown in Fig. 9.6(b) are recommended.

(a) Circle match   (b) Regular hexagon match
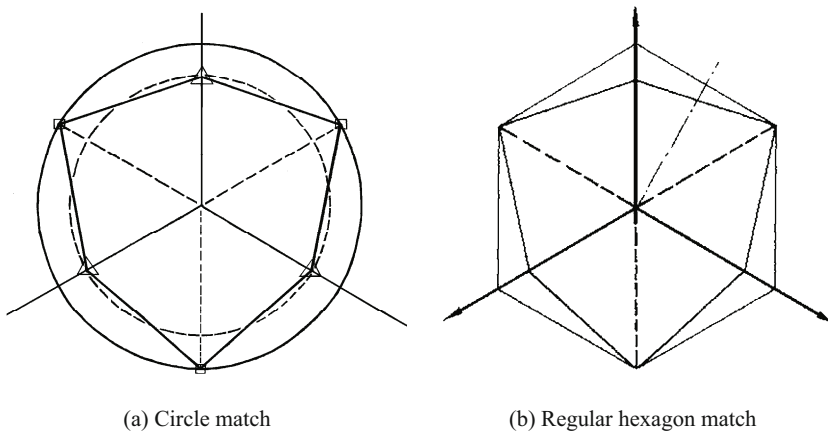
Fig. 9.5   Circles loci and regular hexagon loci

(a) Two bounds and region of yield loci   (b) Three or five basic criteria for SD materials
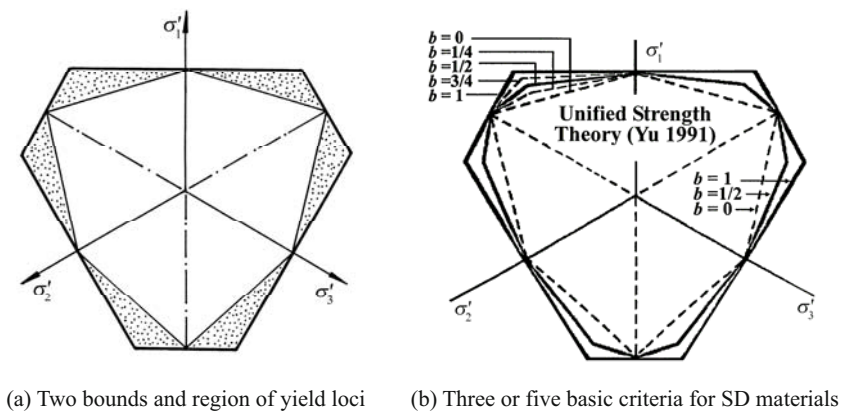
Fig. 9.6   Two bounds and three basic criteria for SD materials

The lower bound and upper bound solutions of plastic limit load for various structure can be given when $b=0$ and $b=1$ respectively. The limit loci on the deviatoric section of experimental results published in the literature are convex and lie in these two bounds. It means that the unified strength theory parameter b will be ranged at $0 \le b \le 1$.

9.3   Elasto-Plastic Analysis of Foundation Using UST

Elasto-plastic analysis of strip footing for weightless soil under a plane strain strip load is studied again by Yu et al. (2001). The unified strength theory and associated flow rule (Yu et al., 1993; UEPP User's Manual, 1993; 1998) are used. The velocity field and displacement field are similar to the previous results in literatures, as shown in Fig. 9.7.
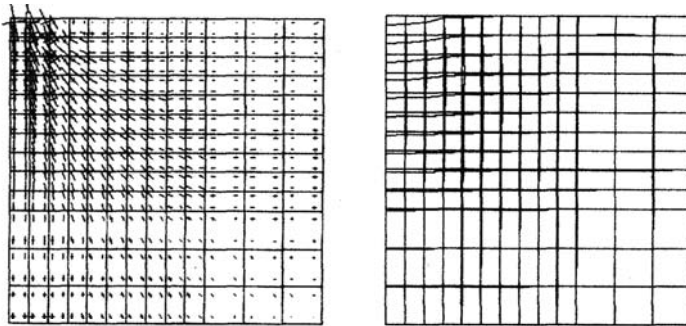
Fig. 9.7   Velocity and displacement field

The unified strength theory and associated flow rule are implemented in a special FE program: UEPP (Unified Elasto-Plastic Program). It is used for the studying of the effect of the yield criteria on limit capacity of strip footing. Three basic criteria of the unified strength theory with $b=0$, $b=1/2$ and $b=1$ are applied to elasto-plastic analysis of strip footing. The complete load-displacement curves obtained by using the unified strength theory with three parameters b ($b=0$, $b=0$ 5 and $b=1$) are shown in Fig. 9.8 where the applied load is plotted versus the centerline displacement directly beneath the footing for each case.

A series of results using the unified strength theory with parameter $0 \le b \le 1$ can be obtained. However, only three results with $b=0$, $b=1/2$ and $b=1$ are given here. It is similar to such which we hoped for, the unified strength theory with $b=0$ gives the minimum result, the unified strength theory with $b=1$ gives the maximum result and the unified strength theory with $b=1/2$ gives the median result, as shown in Fig. 9.8 (Yu et al., 2001).

Velocity fields respective to the three basic yield criteria ($b=0$, $b=0.5$ and $b=1$)

under a same load are shown in Fig. 9.9.
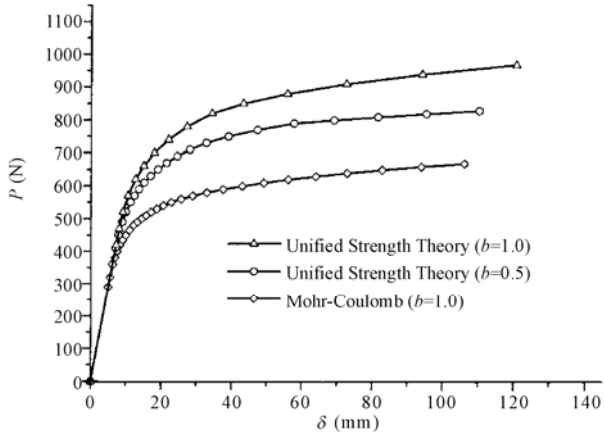
Fig. 9.8   Bearing capacity of strip footing with the three basic criteria

(a)UST with $b=0$ (b) UST with $b=0.5$ (c) UST with $b=1$
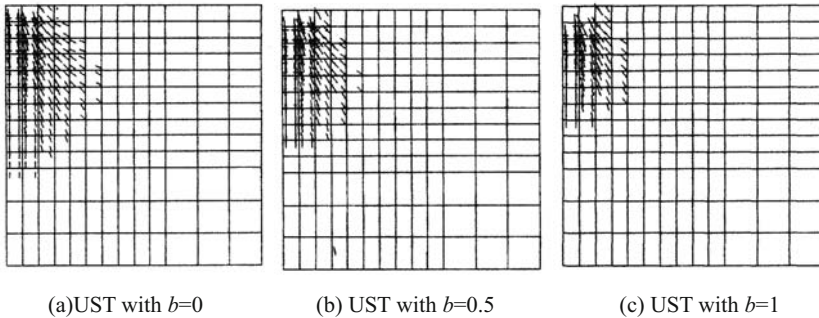
Fig. 9.9   Velocity fields respective to three basic yield criteria under the same load

Another example of foundation was studied by Wang. The color figures of effective stress also demonstrate the differences between the results obtained by using of the three basic yield criteria, as shown in Fig. 9.10. They give us the lower bound, upper bound and a median result. More results can be given when unified strength theory parameter b equals to $0 \leq b \leq 1$.

(a) UST with b=0   (b) UST with b=0.5   (c) UST with b=1.0
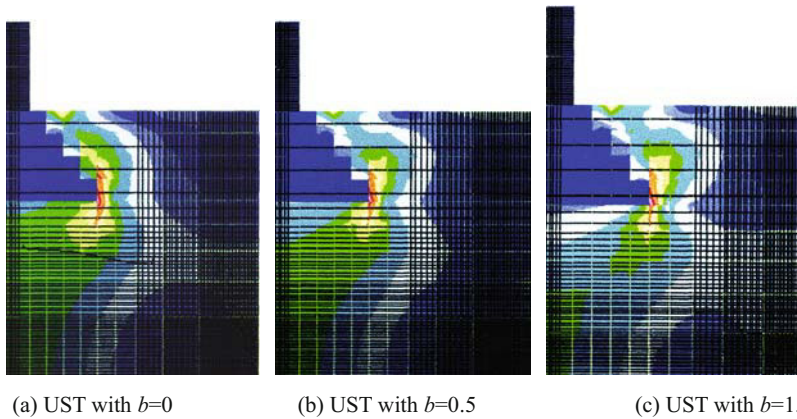
Fig. 9.10   Configuration of effective stress of the three basic yield criteria under the same load

9.4   Plastic Analysis of Strip Foundation Using UST

The bearing capacity of strip foundation is a basic and important problem in solid mechanics and soil mechanics. The analysis solution can be found in the textbook of plasticity or soil mechanics. It is always a single solution adapted for only one kind of material. The unified analysis solution has been presented in the monograph "Generalized Plasticity" that is the first monograph of serial plasticity published by Springer in 2004 and 2006 (Yu, 2004; 2006) and Springer and ZJU Press in 2009 (Yu et al., 2009). The slip-line field is shown in Fig. 9.11.
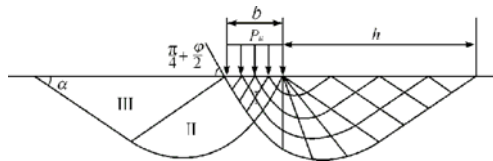
Fig. 9.11   Slip-line field of footing foundation

The unified solution of limit bearing capacity for footing foundation can be expressed as

$$P_{\text{unified}} = C_{\text{unified}} \cdot \text{ctg}\,\varphi_{\text{unified}} \left[\frac{1+\sin\varphi_{\text{unified}}}{1-\sin\varphi_{\text{unified}}} \exp(\pi \cdot \tan\varphi_{\text{unified}}) - 1 \right] \quad (9.1)$$

where φ_0 is friction angle of material; φ_{unified} and C_{unified} are unified material parameters obtained from the unified slip line field theory proposed by Yu in 1997 (Yu et al., 1997; 2006). The two unified material parameters can be expressed as

$$\sin \varphi_{\text{unified}} = \frac{2(b+1)\sin \varphi_0}{2 + b(1 + \sin \varphi_0)}$$ (9.2)

$$C_{\text{unified}} = \frac{2(b+1)\cos \varphi_0}{2 + b(1 + \sin \varphi_0)} \cdot \frac{C_0}{\cos \varphi_{\text{unified}}}$$ (9.3)

The numerical simulation of strip footing by using of the unified strength theory is calculated by Dr. Ma ZY. Material parameters are: cohesion $C_0 = 1.0$ kPa, friction angle $\varphi_0 = 20°$, $E = 10.0$ MPa, $v = 0.32$. The mesh of trip foundation is shown in Fig. 9.12. Only the half of mesh is shown in Fig. 9.12 owing to the symmetry (Liao et al., 2010; Ma and Liao, 2010).
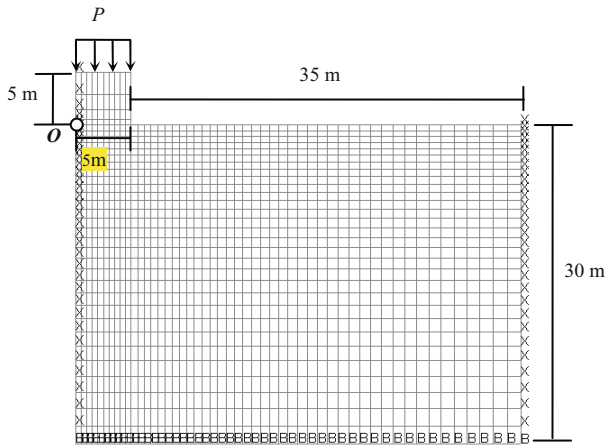
Fig. 9.12 Model and meshing of strip footing

The generalized shear strain contours obeying three yield criteria are shown in Fig. 9.13. The displacement vector fields obeying three yield criteria are shown in Fig. 9.14.
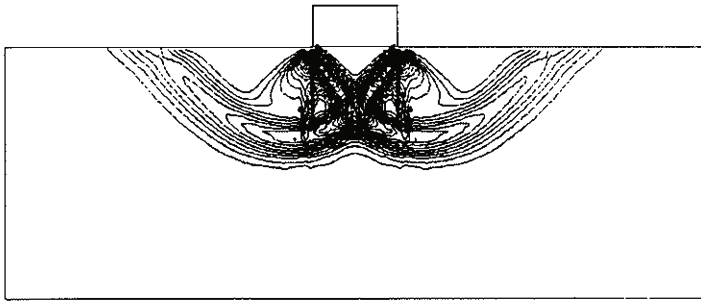
(a) UST with *b*=0.0 (Single-shear theory)
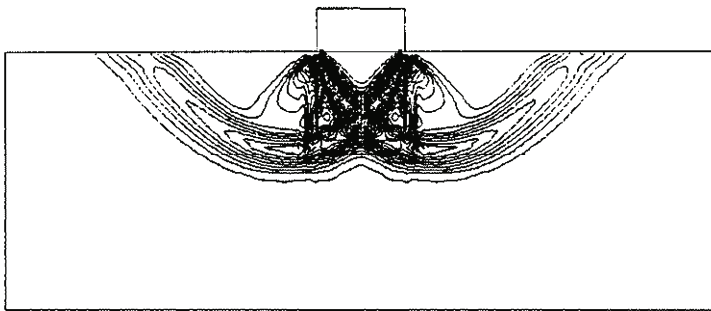
(b) UST with *b*=0.5 (New criterion)
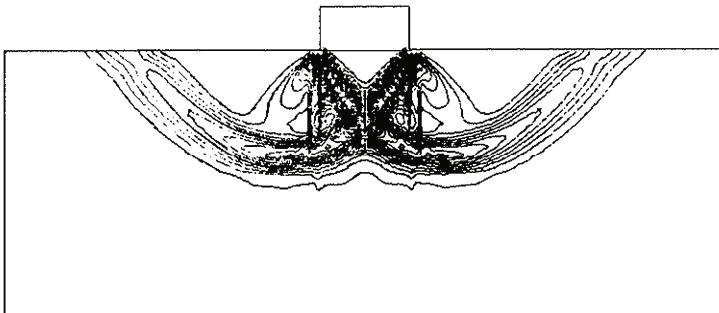
(c) UST with *b*=1.0 (Twin-shear theory)

Fig. 9.13   Generalized shear strain contour of foundation under limit state
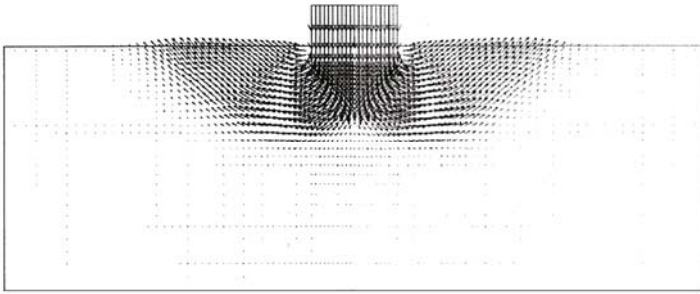
(a)   UST with *b*=0.0 (Single-shear theory)
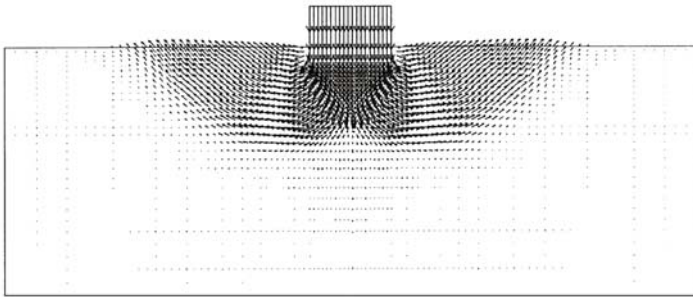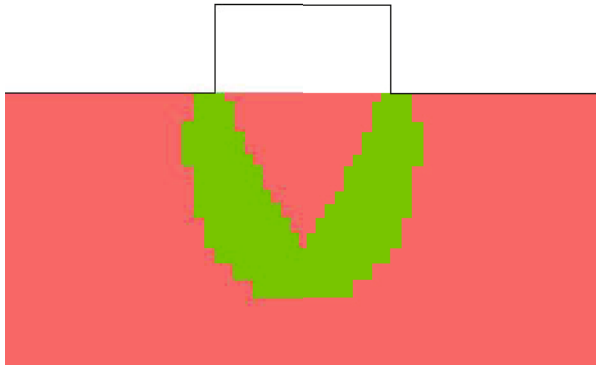

(b) UST with *b*=0.5 (New criterion)
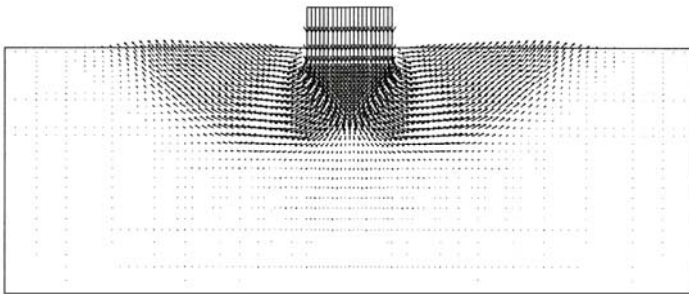
(c) UST with *b*=1.0 (Twin-shear theory)

**Fig. 9.14**   Displacement vector fields obeying three yield criteria

The limit loads obeying different yield criteria are obtained. The relations between length of plastic zones and the UST (unified strength theory) parameter *b* and relations between limit load and the UST parameter *b* are shown in Fig. 9.15 and Fig. 9.16. The solution of slip-line theory for different UST parameter *b* are also given for comparison, as shown in Fig. 9.16 (Liao et al., 2010; Ma and Liao, 2010).
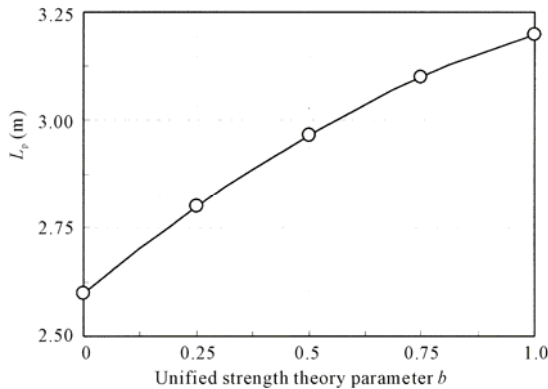
Fig. 9.15   Relations between length of plastic zones and the UST parameter *b*
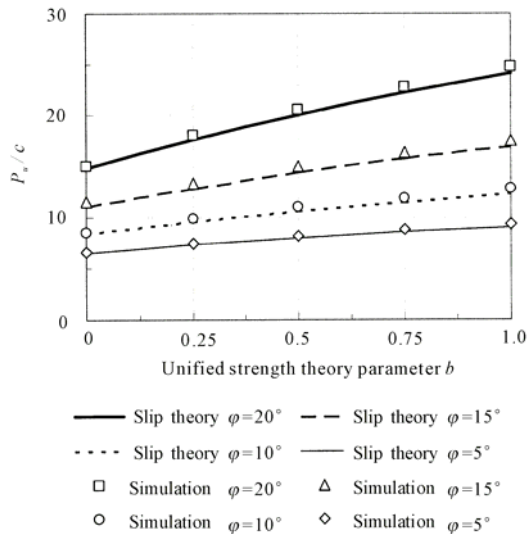
Fig. 9.16   Relations between limit load and the UST parameter *b*

It can be seen that

1) A number of results can be obtained by using of the unified strength theory and associated flow rule. It can be adapted for more materials and structures.

2) Three basic results are given by using of the unified strength theory with three basic yield criteria (*b*=0, *b*=0.5 and *b*=1). They are the lower, median and upper results, if necessary; five results (*b*=0, *b*=0.25, *b*=0.5, *b*=0.75 and *b*=1) can also be given as shown in Fig. 9.15 and Fig. 9.16.

3) The generalized shear strain contour and displacement vector fields for different yield criteria are similar; however, the limit loads and the size of plastic zones are different.

4) The unified strength theory with *b*=0 (single-shear theory) gives the lower limit load and smaller plastic zone at limit state, as shown in Fig. 9.15 and 9.16

(Attention: The unified strength theory with b=0 gives the larger plastic zone, and the unified strength theory with b=1 gives the smaller plastic zone under the same load).

5) The unified strength theory with b=1 (twin-shear theory) gives the upper limit load and larger plastic zone at limit state, as shown in Fig. 9.13 and 9.16. The unified strength theory with b=1 (twin-shear theory) also gives the lenient length of plastic zones at limit state, as shown in Fig. 9.13 and Fig. 9.16. It means that more materials in structure are contributed for the bearing capacity of structure when the unified strength theory parameter b>0, and the highest limit load can be obtained when the UST parameter b=1 is used. It is why the higher limit load can be obtained with the use of the unified strength theory. It is advantageous in the material and energy saving, and also advantageous in the environment protection.

The difference of the generalized shear strain for these three yield criteria in the unified strength theory can be seen clearly in the color figures as shown in Fig. 9.17 (Calculated by Dr. Ma ZY in 2010).

(a) UST with b=0.0 (Single-shear theory)

(b) UST with b=0.5 (New criterion)

(c) UST with b=1.0 (Twin-shear theory)

Fig. 9.17   Spread of the generalized shear strain for three yield criteria at limit states

9.5 Plastic Analysis of Circular Foundation Using UST

9.5.1 Unified Characteristics Line Field of Spatial Axisymmetric Problem

A semi-infinite body under the circular foundation pressure q on the free surface is a spatial axisymmetric problem (Shield, 1955; Cox, 1961; Tani and Craig, 1995). The Mohr-Coulomb model was used.

An example with radium of the foundation pressure region is 2 m is shown in Fig. 9.18. The soil parameters are that $c_0=0.3$ MPa and $\varphi_0=15°$.
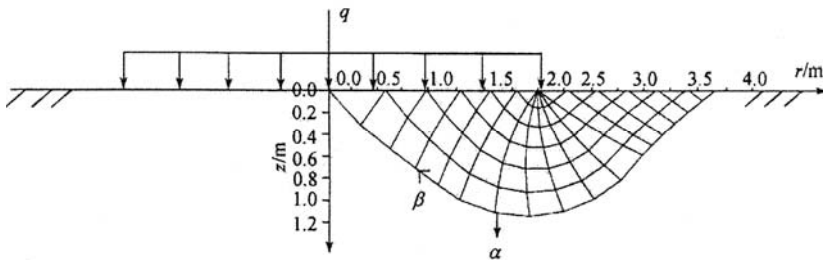
Fig. 9.18   Semi-infinite body under the circular foundation compression and the characteristics line field
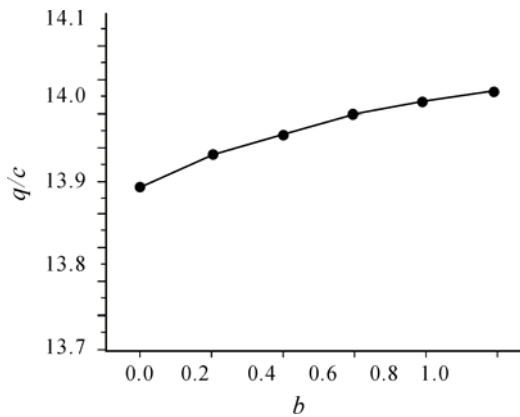
Fig. 9.19   The relation between the limit loading q and the UST parameter b

The right part of the characteristics line field is shown in Fig. 9.18 when $b=1$ (the twin-shear strength theory (Yu, 1985)). The relations between q/c_0 and b has been obtained (Yu and Li, 2001), as shown in Fig. 12.19. It is obtained by using of the unified characteristics line field theory (Yu et al., 2006). The solution at $b=0$ ($q/c_0=13.9$) in Fig. 9.19 is the complete solution of Cox (Chen, 1975), which is based on the Haar von-Karman condition and the Mohr-Coulomb strength theory.

A series of results can be introduced for the SD materials with the different tensile-compression strength ($\varphi_0 \neq 0$) and the non-SD materials with same tensile-compression strength ($\varphi_0 \neq 0$) by the unified characteristics line field theory. The solutions of the Mohr-Coulomb material and Tresca material are special cases of the solutions of the unified characteristics line theory (Yu and Li, 2001; Yu, 2006).

9.5.2 Numerical Simulation of Spatial Axisymmetric Problem

Numerical analysis of bearing capacity of circular footings has been studied widely, such as Potts and Zdravkovic (1999; 2001), Erickson and Drescher (2002), Loukidis and Salgado (2009) Collapse mechanisms as depicted by contours of the plastic maximum shear strain increment compared against the mechanism yielded by Martin's ABC program for circular footings on weightless soil with surcharge are presented by Erickson and Drescher (2002).

The Mohr-Coulomb model is always used for numerical simulation of strip footing and circular foundation. Only one result is given by using of the Mohr-Coulomb model, which is adapted only for one kind of material. The numerical simulation of circular foundation by using of the unified strength theory is calculated by Dr. Ma ZY. Material parameters are: cohesion C_0=1.0 kPa, friction angle φ_0=20°, E=10.0 MPa, v=0.32. The mesh of trip foundation is shown in Fig. 9.20. Only the half of mesh is shown in Fig. 9.20 owing to the symmetry. Displacement vector fields obeying the UST with b=0, b=1/2 and b=1 are shown in Fig. 9.21.
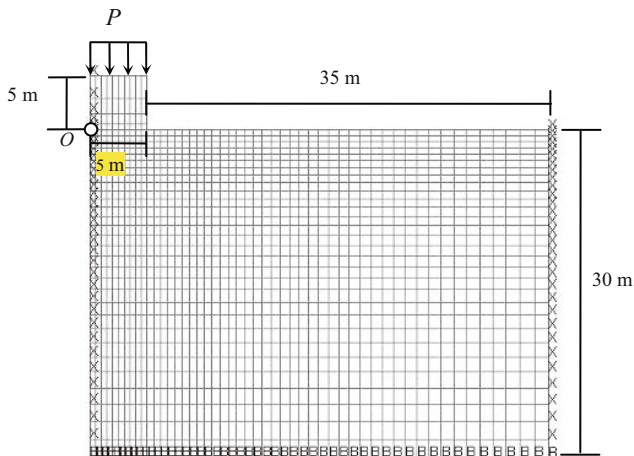
Fig. 9.20 Model and meshing of circular foundation
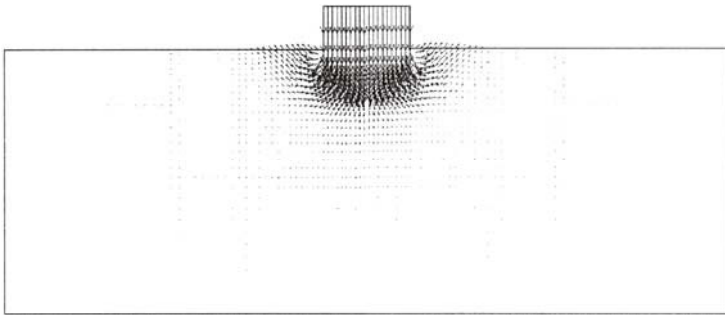
(a) UST with b=0.0 (Single-shear theory)
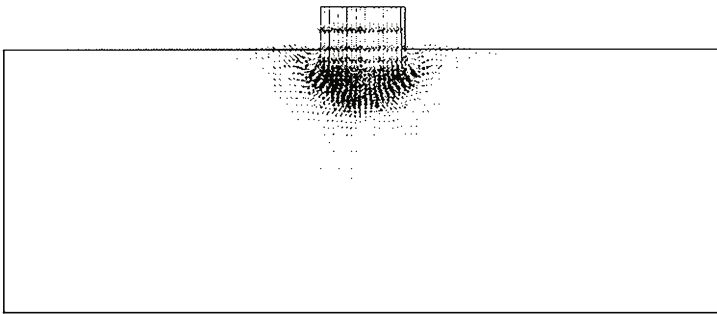
(b) UST with b=0.5 (New criterion)
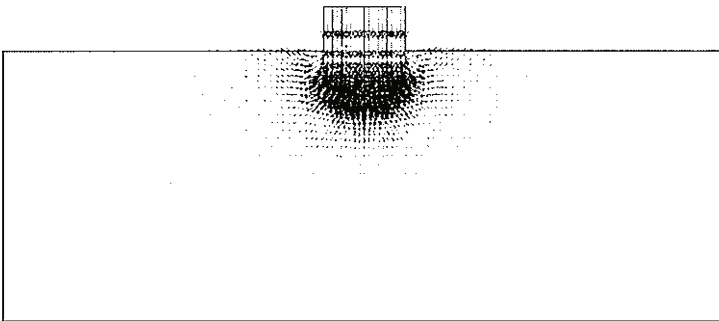
(c) UST with b=1.0 (Twin-shear theory)

Fig. 9.21   Displacement vector fields obeying the UST

UST with b=0.0 (Single-shear theory)
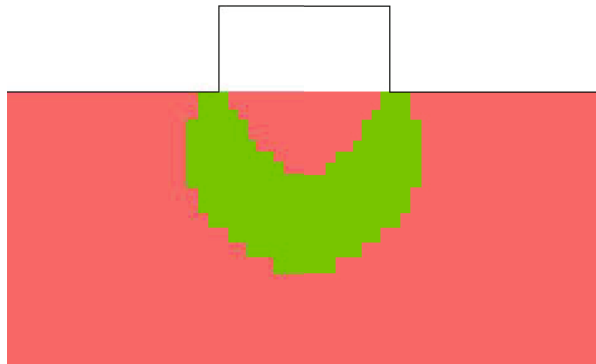
(b) UST with b=0.5 (New criterion)
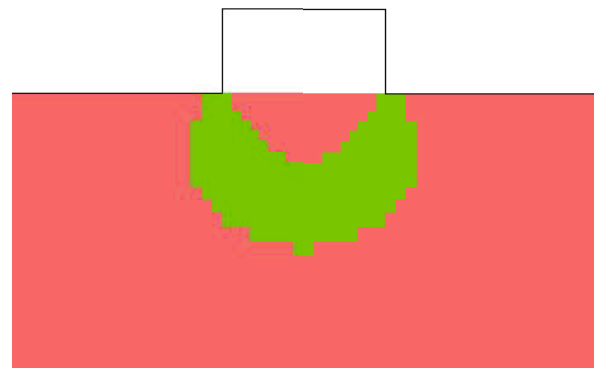
(c) UST with b=1.0 (Twin-shear theory)

Fig. 9.22   Plastic zones of circular foundation

The plastic zones of a circular foundation under uniform load are shown in Fig. 9.20, in which three different shapes and sizes of plastic zones are displayed. It is seen that the depth of the plastic zone of the single-shear theory (UST with b=0) is deepest, the depth of the plastic zone of the twin-shear theory (UST with b=1) is shallowest.

9.5.3 *Effect of UST Parameter φ on the Spread of Shear Strain*

More results can be obtained by using of the unified strength theory. The effect of UST parameter b (effect of yield criterion) on the calculated result has been studied above. The effect of UST parameter φ (friction angle of materials) on calculated results can be also given by using of the unified strength theory. A series of new interesting results are obtained by using of the unified strength theory with different parameters b and φ.

Generalized shear strain of circular foundation for different material strength parameter φ are shown in Fig. 9.23. The results are obtained using the different cohesive strength of materials with φ=0°, φ=10°, φ=30°, φ=60° and the same shear strength c=1.0 kPa and b=1. The cohesive strength of material φ=0° means this material is non-SD material; the others are SD materials (φ>0°).

It is interesting that the shape and the direction of the spread of generalized shear strain are strongly depended on the variation of material strength parameters φ. The larger parameter φ means the smaller ratio of material strength in tension and in compression $\alpha=\sigma_t/\sigma_c$. These figures are also depended on the UST parameter b.

(a) UST with b=1 and φ=0°

Fig. 9.23   Generalized shear strain of circular foundation for different strength parameter φ
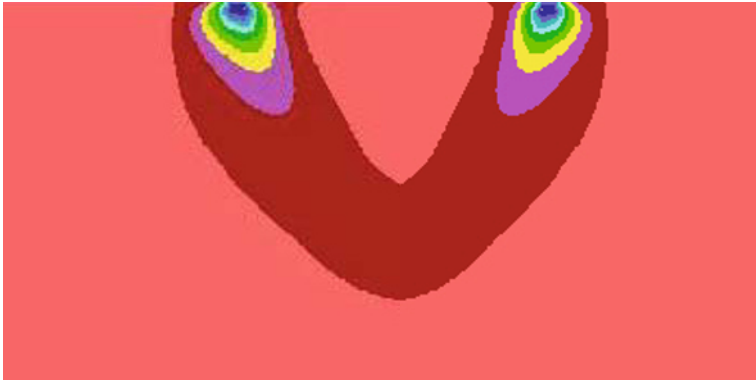
(b) UST with $\varphi=10°$

(c) UST with $b=1$ and $\varphi=30°$

(d) UST with $b=1$ and $\varphi=60°$

Fig. 9.23 Continued

9.6 Effect of UST Parameter *b* and φ on the Spread of Shear Strain

The generalized shear strain of strip foundation using UST with different parameter *b* and φ are shown in Figs. 9.24, 9.25 and 9.26. Only half figures are displayed owing to the symmetry (calculated by Dr. Ma ZY).

| *b*=0.0 | *b*=0.5 | *b*=1.0 |
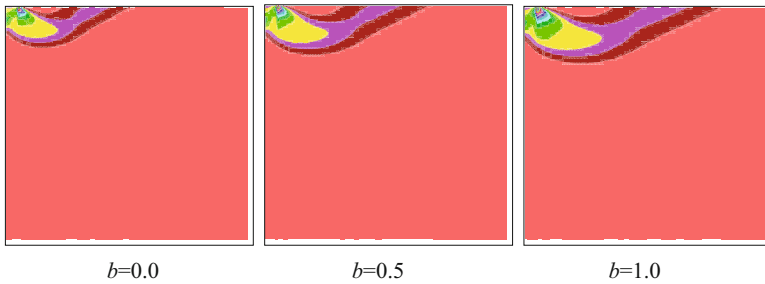
Fig. 9.24   Generalized shear strain of strip foundation at limit state for strength parameter φ=30°

| *b*=0.0 | *b*=0.5 | *b*=1.0 |
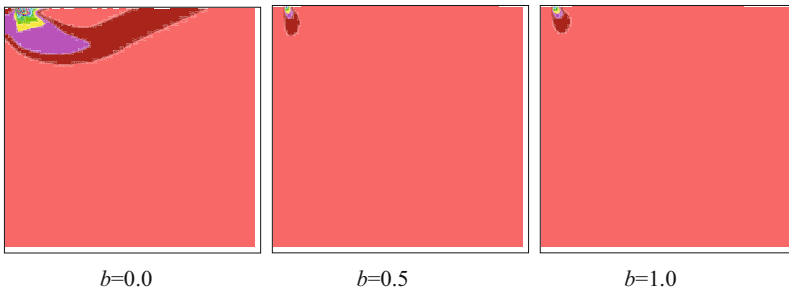
Fig. 9.25   Generalized shear strain of strip foundation at limit state for strength parameter φ=40°

| *b*=0.0 | *b*=0.5 | *b*=1.0 |
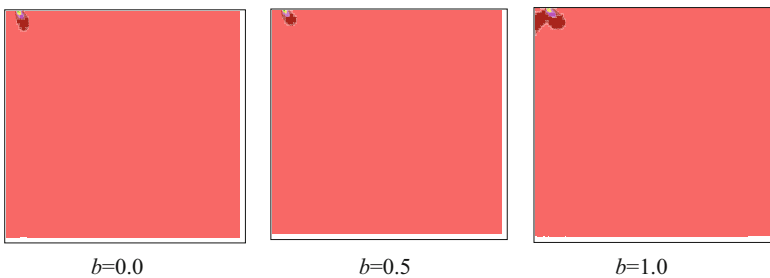
Fig. 9.26   Generalized shear strain of strip foundation at limit state for strength parameter φ=50°

| b=0.0 | b=0.5 | b=1.0 |
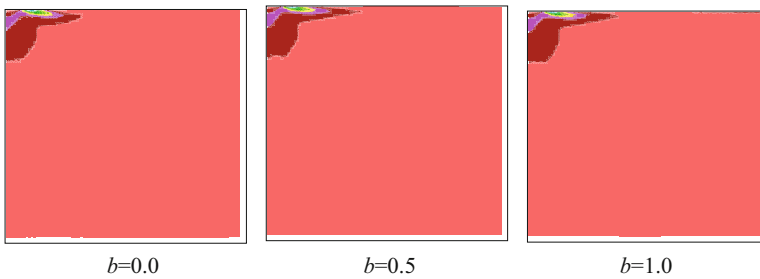
Fig. 9.27   Generalized shear strain of strip foundation at limit state for strength parameter $\varphi=70°$

It is interesting that the shape and size of plastic zone and the spread direction of generalized shear stain are strongly depended on the UST parameters b and φ.

9.7 Brief Summary

The prediction of bearing capacity of structural, shape and size of plastic zones, the spread direction of generalized shear stain is influenced strongly by the choosing of the yield criterion and strength parameter of materials. It is very important that how to known the lower value and the upper value of limit load, and how to choose the reasonable strength theory (yield criteria, failure criterion, or material model in FEM code) in the research and design.

The change in shape and size of the limit surface of various failure criteria is great. We have to determine the bounds and region of failure criteria before the discussion. Two bounds and three basic criteria or five basic criteria introduced from the unified strength theory of convex failure criteria are studied and used for the plastic analysis of strip footing and circular foundation in this chapter.

The results of researches and designs are depended strongly on the choice of strength theory in most cases. The shape of the yield surface is found to have significant effect on the plastic deformations and bearing capacity predicted in the simulations.

The unified strength theory and associated flow rule provide us with systematic yield criteria, an effective approach and a powerful tool to study these effects. Considerable numbers of new and interesting results are obtained by using of the unified strength theory and associated flow rule, which can be adapted for more different materials and structures. Moreover, the application of the unified strength theory is advantageous in the material and energy saving, and also advantageous in the environment protection.

References

Bull JW ed. (2003) Numerical Analysis and Modelling in Geomechanics. Taylor & Francis.

de Borst R and Vermeer PA (1984) Possibilities and limitations of finite elements for limit analysis. Géotechnique, 34 (2): 199-210.

Chan AK and Shiomi T (2006) Practical Programming in Computational Geomechanics: With Special Reference to Earthquake Engineering. John Wiley & Sons.

Chen WF (1975) Limit Analysis and Soil Plasticity. Elsevier: New York,

Chen WF and Mizuno E (1990) Nonlinear Analysis in Soil Mechanics: Theory and Implementation. Elsevier: Amsterdam.

Chen WF and McCarron WO (1991) Bearing capacity of shallow foundations. In: Foundation Engineering Handbook (ed Fang HY), 2nd edn. Chapman & Hall: New York, pp l44-165.

Contractor D and Desai CS eds (2001) Computer Methods and Advances in Geomechanics, Proceedings of the 10th International Conference on Computer Methods and Advances in Geomechanics, Tucson, Arizona, USA, 7-12 January, Taylor & Francis

Cox AD (l961) Axially-symmetric plastic deformation in soil. Ⅱ:Indentation of ponder-able soi1s. Int.J Mech Sci, 4: 371-380.

Davis RO and Selvadurai APS (2002) Plasticity and Geomechanics. Cambridge University Press: Cambridge.

Ehlerhs W (1997) Shear band localization in fluid-saturated granular elasto-plastic porous media. In: Mechanics of Granular and Porous Materials. Ed: Fleck NA and Cocks ACF, A.A.Balkema; Kluwer Acadmic Pub: Boston

Erickson HL and Drescher A (2002) Bearing capacity of circular footings, J Geotech Geoenviron Eng ASCE, 128(1): 38-43.

Griffiths VD and Gioda G eds (2001) Advanced numerical applications and plasticity in geomechanics. Springer: Wien.

Kolymbas D ed(2003) Advanced Mathematical and Computational Geomechanics. (Lecture Notes in Applied and Computational Mechanics) Springer: Wein.

Humpheson C and Naylor DJ (1975) The importance of the form of the failure criterion. C/R/243/75, University of Wales: Swansea, UK.

Jeremić B, Yang ZY, Cheng Z, Jie GZ, Sett K, Taiebat M, Preisig M and Tafazzoli N (2010) Computational Geomechanics: Inelastic Finite Elements for Pressure Sensitive Materials. CompGeoMechUCD Lecture Notes, Google.

Liao HJ, Ma ZY, Ning CM, Liu L and Sassa K (2010) Stability analysis of high loess slope under complex stress state. In: Recent developments of geotechnical engineering, Proceedings of the fourth Japan-China geotechnical symposium, Okinawa Japan.

Loukidis D and Salgado R (2009) Bearing capacity of strip and circular footings in sand using finite elements. Computers and Geotechnics,36(5): 871-879.

Lyamin A, Salgado R, Sloan SW and Prezzi M (2007) Two- and three-dimensional bearing capacity of footings in sand. Géotechnique, 57(8): 647-662.

Ma ZY and Liao HJ (2010) Study on the constitutive model of twin shear unified elasto-plastic and strain hardening/softening based on FLAC^{3D}. To be published in Chinese Journal of Geotechnical Engineering.

Martin CM (2003) User guide for ABC –Analysis of Bearing Capacity, Version 1.0. OUEL Report No. 2261/03. Department of Engineering Science, University of Oxford.

Martin CM (2005) Exact bearing capacity calculations using the method of characteristics. In: Barla G, Barla M, editors. Proceedings of the 11th IACMAG, Vol. 4: 441-450.

Moore ID and Rowe RK (1991) Objective solutions for bearing capacity of strain-softening soils. In: Beer G, Booker JR and Carter JP eds. Computer Methods and Advances in Geomechanics. Rotterdam: A.A.Balkema, 2: 1183-1189.

Nayak GC and Zienkiewicz CC (1972) Convenient form of stress invariants for plasticity, J. Struct. Div., ASCE, 4: 949-953.

Otani J, Hoashi H, Mukunoki T et al. (2001) Evalution of failure in soils under unconfined compression using 3-D rigid plastic finite element analysis. In: Valliappan S and Khalili N eds., Computational Mechanics : New Frontiers for the New Millennium. Elsevier, pp 445-450.

Pande GN and van Impe WF eds (1986) Numerical models in geomechanics, Proceedings of the Second International Conference (NUMOG II), Ghent, 31st. Jackson & Son: England.

Pande GN and Pietruszczak S eds (1992) Numerical Models in Geomechanics NUMOG IV: Proceedings of the Fourth International Symposium on Numerical Models in Geomechanics (NUMOG IV), Swansea. August 1992, Taylor & Francis: Lodon.

Pande GN and Pietruszczak S eds (1995) Numerical Models in Geomechanics NUMOG V: Proceedings of the Fifth International Symposium on Numerical Models in Geomechanics (NUMOG V), Davos, Switzerland. Taylor & Francis: London.

Pande G and Pietruszczak S eds (1997) Numerical Models in Geomechanics NUMOG VI, Proceedings of the Sixth International Symposium on Numerical Models in Geomechanics (NUMOG VI), Montreal, Canada. Taylor & Francis: London.

Pande GN and Pietruszczak S eds (1999) Numerical Models in Geomechanics NUMOG VII: Proceedings of the 7th International Symposium, NUMOG VII, Graz, Austria. Taylor & Francis:London.

Pande GN and Pietruszczak S eds (2002) Numerical Models in Geomechanics NUMOG VIII: Proceedings of the Eighth International Symposium on Numerical Models in Geomechanics (NUMOG V), Rome, Italy. Balkema.

Pande GN and Pietruszczak S eds (2004) Numerical Models in Geomechanics, Proceedings of the Ninth International Symposium on Numerical Models in Geomechanics (NUMOG IX), Ottawa, Canada. Taylor & Francis: London

Pande GN and Pietruszczak S eds (2007) Numerical Models in Geomechanics NUMOG X, Proceedings of the 10th International Symposium on 'Numerical

Models in Geomechanics (NUMOG X), Rhodes, Greece. Taylor & Francis: London.

Pastor M and Tamagnini (2004) Numerical Modelling in Geomechanics. ISTE Publishing Company.

Pietruszczak S and Pande GN eds (1989) Numerical Models in Geomechanics NUMOG III: Proceedings of the Third International Symposium on Numerical Models in Geomechanics (NUMOG III), Routledge.

Pietruszczak S (2010) Fundamentals of Plasticity in Geomechanics. CRC Press.

Potts DM and Zdravkovic L(1999) Finite Element Analysis in Geotechnical Engineering: Theory. Thomas Telford Ltd: London.

Potts DM and Zdravkovic L (2001) Finite Element Analysis in Geotechnical Engineering:Applications. Thomas Telford Ltd: London.

Shield RT (1955) On the plastic flow of metal under conditions of axial symmetry．Proc Roy. Soc., 233A: 267-287.

Tani K and Craig WH (1995) Bearing capacity of circular foundations on soft clay of strength increasing with depth. Soil Found, 35(4):21-35.

UEPP User's Manual, Version 3.0 (1998), Research Division of Structural Strength, Dept. of Civil Eng., Xi'an Jiaotong University.

Verruijt A (1995) Computational Geomechanic. Kluwer Akedamic Pub: The Nertherlands.

Verruijt A (2009) Computational Geomechanic. Springer: The Nertherlands.

Wunderlich, Findeib and Cramer in (2001) Finite element analysis of bearing capacities in geomechanics considering dilatant and contractant constitutive laws. In: Valliappan S and Khalili N eds. Computational Mechanics: New Frontiers for the New Millennium. Elsevier: Amsterdam. pp 509-519.

Yu HS (2006) Plasticity and Geotechnics. Springer:Poston.

Yu MH, He LN and Song LY (1985) Twin shear stress theory and its generalization. Scientia Sinica (Sciences in China), English edn. Series A, 28(11), 1174-1183.

Yu MH and He LN (1991) A new model and theory on yield and failure of materials under the complex stress state. Mechanical Behaviour of Materials-6 (ICM-6). Jono M and Inoue T eds. Pergamon Press: Oxford, Vol 3, pp 841-846.

Yu MH, Zeng WB, Ma GW, Yang SY, Wang F and Wang Y (1993) Unified Elasto-Plastic Program—UEPP. Xian Jiaotong University, English version.

Yu MH et al. (1993) UEPP User's Manual. Deparament of Civil Engineering, Xi'an Jiaotong University, Xi'an, China.

Yu MH, Yang SY, Liu CY and Liu JY (1997) Unified plane-strain slip line theory. China Civil Engrg. J., 30(2): 14-26 (in Chinese, English abstract).

Yu MH and Li JC (2001) Unified characteristics line theory of spatial axisymmetric plastic problem. Science in China (Series E), English Edition, 44(2): 207-215; Chinese Edition: 31(4): 323-331.

Yu MH, Wei XY, Yoshimine M, et al (2001) Effect of failure criterion on the elasto-plastic FEM analysis. Invited paper present at the First Asian-Pacific congress on computational mechanics, In: Computational Mechanics–New Frontiers for New Millennium. Valliappan S and Khalili N eds. Elsevier:

Amsterdam, pp 1155-1165.

Yu MH (2004) Unified Strength Theory and Its Applications. Springer: Berlin.

Yu MH et al. (2006) Generalized plasticity. Springer: Berlin.

Zienkiewicz OC and Pande GN (1977) Some useful forms of isotropic yield surfaces for soil and rock mechanics. Finite Elements in Geomechanics. Gudehus G ed. Wiley: London, pp 179-190.

Zienkiewicz OC, Chan AMC, Pastor M, Schrefler BA and Shiomi T (1999) Computational Geomechanics: with Special Reference to Earthquake Engineering. John Wiley & Sons: Chichester and New York.

Zimmermann T and Commend S (2001) Stabilized finite element applications in geomechanics. In: Valliappan S and Khalili N eds., Computational Mechanics: New Frontiers for the New Millennium. Elsevier: Amsterdam, pp 533-538.

10

Underground Caves, Tunnels and Excavation of Hydraulic Power Station

10.1 Introduction

Underground caves, excavations or underground openings pose fundamental problems in rock mechanics and geotechnical engineering (Brady and Brown, 1985; Goodman, 1989; Wittke, 1990; Hudson and Harrison, 1997; Sun, 1999; Harrison and Hudson, 2000; Zhou and Yang, 2005). Underground opening includes mines, shafts, tunnels (drifts), hydraulic power plants and chambers for the military, for storage of foods, chemical products, oil and natural gas and for other civil, industrial and war applications. Underground excavation breaks the equilibrium of the original stresses in the rock or soil and causes a redistribution of stress in the surrounding rock or soil. The stress state of an underground circular cave or tunnel is shown in Fig. 10.1. The surrounding rock (or soil) is acted upon under the vertical stress σ_y and the horizontal stress σ_x.

According to the Kirsch formula in rock mechanics, the stresses at the element (point M in Fig. 10.1) within the surrounding rock could be calculated from

$$\sigma_r = \frac{\sigma_x + \sigma_y}{2}(1 - \frac{a^2}{r^2}) - \frac{\sigma_y - \sigma_x}{2}(1 - 4\frac{a^2}{r^2} + 3\frac{a^4}{r^4})\cos 2\theta \qquad (10.1a)$$

$$\sigma_\theta = \frac{\sigma_x + \sigma_y}{2}(1 + \frac{a^2}{r^2}) + \frac{\sigma_y - \sigma_x}{2}(1 + 3\frac{a^4}{r^4})\cos 2\theta \qquad (10.1b)$$

$$\tau_{r\theta} = \frac{\sigma_y - \sigma_x}{2}(1 + 2\frac{a^2}{r^2} - 3\frac{a^4}{r^4})\sin 2\theta \qquad (10.1c)$$

where σ_r, σ_θ and $\tau_{r\theta}(\tau_{r\theta} = \tau_{\theta r})$ are radial, tangential and shear stresses at the

element, respectively.
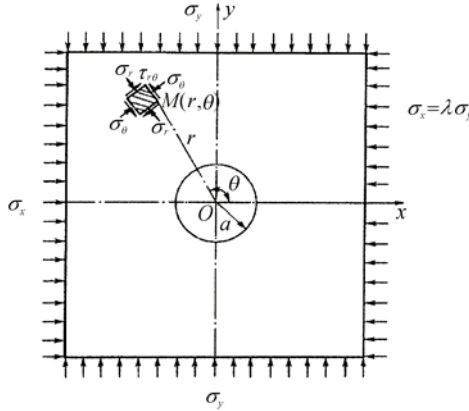
Fig. 10.1   Stress state of an underground circular tunnel

If r is infinite, or $R_0=0$, the expressions of situ stresses in the polar coordinates system are obtained as follows:

$$\sigma_r = \frac{\sigma_x + \sigma_y}{2} - \frac{\sigma_y - \sigma_x}{2}\cos 2\theta \qquad (10.2a)$$

$$\sigma_\theta = \frac{\sigma_x + \sigma_y}{2} + \frac{\sigma_y - \sigma_x}{2}\cos 2\theta \qquad (10.2b)$$

$$\tau_{r\theta} = \frac{\sigma_y - \sigma_x}{2}\sin 2\theta \qquad (10.2c)$$

The finite element method has now become recognized as a general method of wide applicability to geomechanics and rock engineering. The elasto-plastic FEM or non-linear material problem has also been widely accepted. Descriptions and examples of analysis can be seen in the book of Zienkiewicz (1971). The Mohr-Coulomb criterion, the Drucker-Prager criterion and the no-tension material model were usually used.

Some examples are given to show the effect of the failure criteria on the results. The unified strength theory provides us with a very effective approach for studying the effect of failure criterion on various problems. The plastic analysis of an underground circular excavation (cave or tunnel etc.) is described in this chapter.

Many large hydraulic power plants have been constructed on the Yellow River, Yangtze River and in other regions in China. The stability of the underground cave of a large hydraulic power station has been studied by many researchers. The failure of the surrounding rock mass may be caused by the lower strength of the rock mass somewhere. Also, it may be caused by the accumulation of stress at the underground excavation. The local failure of the rock mass caused by stress accumulation during excavation can be forecast by numerical modeling analysis.

The distribution of the weak positions has a certain regularity, but also has some differences due to the difference in the virginal geo-stress field, the form of excavation, the direction of the excavation's axis, the method of excavating and the choice of yield criterion.

Plastic zones analysis for the stability of the underground cave of a large hydraulic power station based on the twin-shear unified strength theory was carried out during excavation engineering by the Investigation and Design Institute of Northwest China Hydroelectric Power (Liu, 1994; 1995; Liu and Wu, 1995; Sun, 1998). The twin-shear unified strength theory and associated flow rule were implemented in FEM codes and used for several large hydraulic engineering and pumped storage hydraulic power station projects (Sun et al., 2004a; 2004b). The twin-shear unified strength theory is also used for dynamic problems. Dynamic response and blast-resistance analysis of a tunnel subjected to blast loading was conducted successfully by professors Liu and Wang (2004) at Zhejiang University, Hangzhou, China, for a railroad tunnel.

10.2   Effect of Yield Criterion on the Plastic Zone for a Circular Cave

Plastic analysis was calculated for a circular cave under the action of a uniform vertical pressure. The spread of plastic zones in terms of the single-shear theory or the Mohr-Coulomb strength theory and the twin-shear strength theory with material parameter C_0=3 MPa were obtained and shown in Fig. 10.2. The difference between the single-shear theory and the twin-shear theory is obvious.

The plastic zones in terms of the single-shear theory or the Mohr-Coulomb strength theory and the twin-shear strength theory with material parameter C_0=2.6 MPa are given as shown in Fig. 10.3. The difference is also displayed.
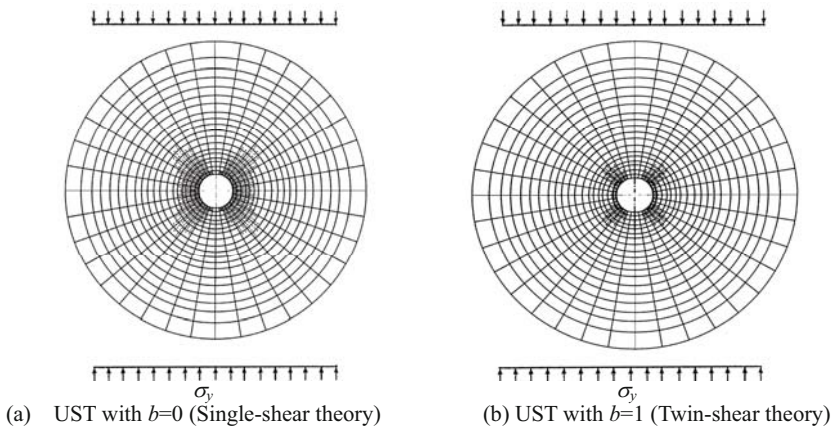
(a)   UST with b=0 (Single-shear theory)   (b) UST with b=1 (Twin-shear theory)
Fig. 10.2   Distribution of plastic zone around circular cave (C_0= 3.0 MPa)

(a) UST with *b*=0 (Single-shear theory)   (b) UST with *b*=1 (Twin-shear theory)
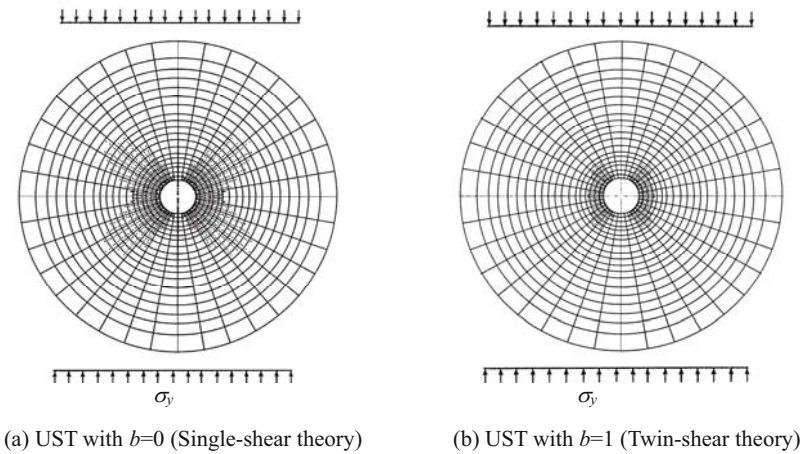
Fig. 10.3   Distribution of plastic zone around circular cave (C_0= 2.6 MPa)

10.3 Plastic Zone for Underground Circular Cave under Two Direction Compressions

An underground circular cave is under vertical stress and horizontal stress, as shown in Fig. 10.4. The structure is considered a plane strain problem. A series of computational results can be obtained by using the unified strength theory. The ratio of load $\lambda=\sigma_x/\sigma_y$ is referred to as the lateral stress coefficient.
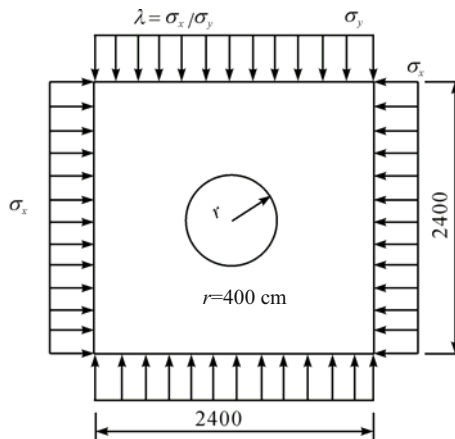
Fig. 10.4   Underground circular cave under vertical stress and horizontal stress

10.3.1 Material Model

Three basic yield criteria of the unified strength theory are chosen for use in geomaterials and geotechnical engineering. They are:

(1) $b=0$, the single-shear theory, or the Mohr-Coulomb strength theory

$$F = F' = \sigma_1 - \alpha\sigma_3 = \sigma_t \qquad (10.3)$$

(2) $b=1$, the twin-shear strength model (Yu, 1985)

$$F = \sigma_1 - \frac{\alpha}{2}(\sigma_2 + \sigma_3) = \sigma_t, \quad \text{when} \ \ \sigma_2 \leq \frac{\sigma_1 + \alpha\sigma_3}{1+\alpha} \qquad (10.4a)$$

$$F' = \frac{1}{2}(\sigma_1 + \sigma_2) - \alpha\sigma_3 = \sigma_t, \quad \text{when} \ \ \sigma_2 \geq \frac{\sigma_1 + \alpha\sigma_3}{1+\alpha} \qquad (10.4b)$$

(3) $b=1/2$, a new yield criterion deduced from the unified strength theory

$$F = \sigma_1 - \frac{\alpha}{3}(\sigma_2 + 2\sigma_3) = \sigma_t, \ \ \sigma_2 \leq \frac{\sigma_1 + \alpha\sigma_3}{1+\alpha} \qquad (10.5a)$$

$$F' = \frac{1}{3}(2\sigma_1 + \sigma_2) - \alpha\sigma_3 = \sigma_t, \ \ \sigma_2 \geq \frac{\sigma_1 + \alpha\sigma_3}{1+\alpha} \qquad (10.5b)$$
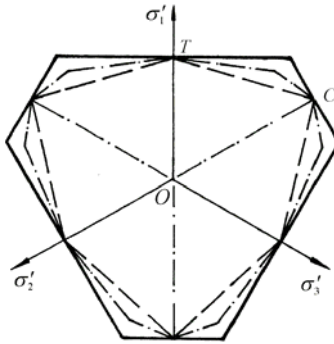
Fig. 10.5   Three fundamental criteria for geomaterials (two bounds and the median)
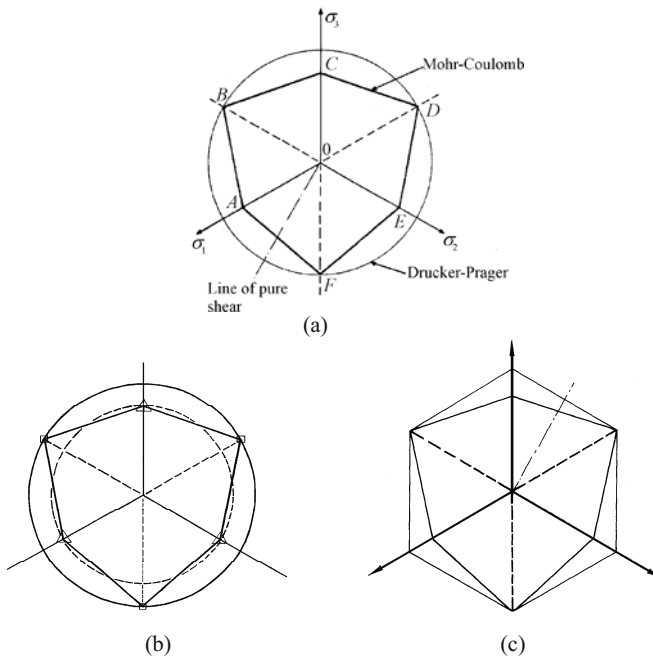
Fig. 10.6   Circle and regular hexagonal cannot match six test points

The Mohr-Coulomb single-shear strength theory, the twin-shear strength theory and this new criterion can be deduced from the unified strength theory when $b=0$, $b=1$ and $b=1/2$, as shown in Fig. 10.5. They are all the piecewise linear yield criteria. The lower bound, upper bound and the median locus situated between these two bounds may be considered as three basic criteria for SD materials.

The circles of the Drucker-Prager criterion cannot match the six experimental points, as shown in Figs. 10.6(a) and 10.6(b). The regular hexagonal also cannot match the six test points, as shown in Fig. 10.6(c).

The new yield criteria given by the unified strength theory with $b=1/2$ is a median yield criterion between two bounds. It maybe becomes a new reasonable yield criterion instead of the circular cone criteria. The stress angle effect on material strength is not taken into account in various circular cone criteria.

Of course, there is still a need for new models. A general, but simple and thereby well suited model for many potential users may be developed.

10.3.2 Elastic Bearing Capacity

The elastic limits of a structure under six cases of load with $\lambda=\sigma_x/\sigma_y=1.0$, $\lambda=0.75$, $\lambda=0.5$, $\lambda=0.3$, $\lambda=0.2$, $\lambda=0$ can be obtained by using the unified strength theory.

The elastic limit in terms of the Drucker-Prager criterion is also given for comparison. The results are listed in Table. 10.1.

Table 10.1   Elastic limit of caves under deferent load obtained from deferent criteria

Yield criterion	Elastic limit (MPa)					
	$\lambda=1$	$\lambda=0.75$	$\lambda=0.5$	$\lambda=0.3$	$\lambda=0.2$	$\lambda=0.0$
UST with $b=0$ (Single-shear theory)	16.31	14.63	13.21	12.25	11.82	11.05
UST with $b=0.5$	17.5l	15,72	14.19	13.16	12.70	11.87
UST with $b=1$ (Twin-shear theory)	18.19	16.32	14.73	13.67	13.19	12.23
Drucker-Prager criterion	17.42	15.63	14.11	13.09	12.63	11.81

   It is shown that the elastic limit of the cave under vertical compression in terms of the unified strength theory with $b=1$ (i.e. twin-shear theory) is the maximum, and the elastic limit of the unified strength theory with $b=0$ (i.e. single-shear theory, Mohr-Coulomb strength theory) is the minimum. The results of using unified strength theory with $b=1/2$ lie between these two limits. It is interesting that the elastic limit of the Drucker-Prager criterion is similar to the elastic limit of the unified strength theory with $b=1/2$.

10.3.3 Lasto-Plastic Analysis

Choose an 8-node quadrilateral element, mesh the structure into 48 elements with a total of 173 nodes, as shown in Fig. 10.7. A series of computational results using the unified strength theory and unified elasto-plastic constitutive relationship can be obtained. When the load coefficient is $\lambda=\sigma_x/\sigma_y=0.2$, $\sigma_y=20$ MPa, by increasing gradually to 30 MPa, then to 34 MPa, the spreads of the plastic zone using the unified strength theory with $b=0$, $b=1/2$, and $b=1$ are shown in Figs. 10.7, 10.8 and 10.9.

(a) $\sigma_y=20$ MPa   (b) $\sigma_y=30$ MPa   (c) $\sigma_y=34$ MPa
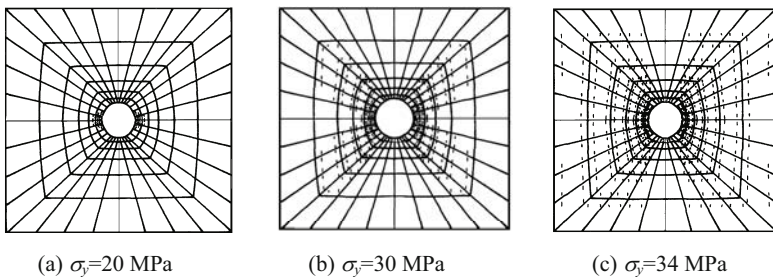
Fig. 10.7   Spread of plastic zone of a cave using UST with $b=0$ (Single-shear theory)

(a) σ_y=20 MPa   (b) σ_y=30 MPa   (c) σ_y=34 MPa
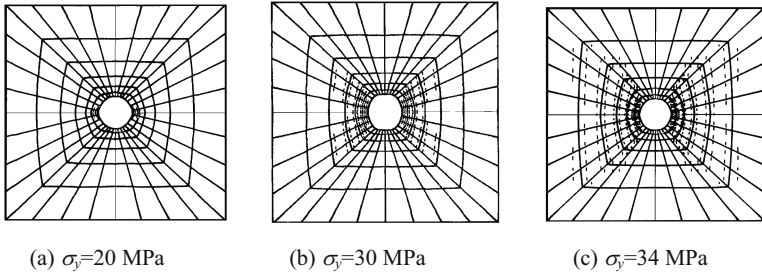
Fig. 10.8   Spread of plastic zone of a cave using UST with b=1/2 (A new criterion)

(a) σ_y=20 MPa   (b) σ_y=30 MPa   (c) σ_y=34 MPa
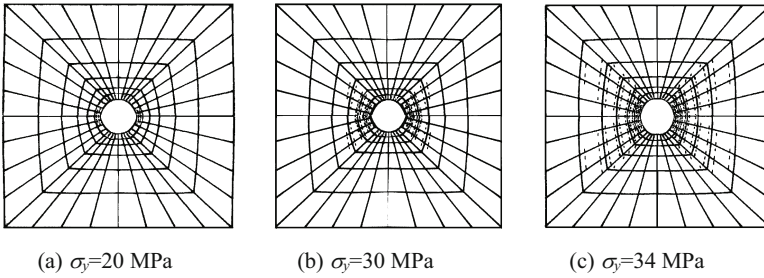
Fig. 10.9   Spread of plastic zone of a cave using UST with b=1 (Twin-shear theory)

10.3.4 Comparison of Different Criteria

For comparison, three cases of load $\lambda=\sigma_x/\sigma_y$=0, λ=0.2 and λ=0.5 are analyzed. The spreads of the plastic zone when σ_y increases gradually from 20 MPa can be obtained. The unified strength theory with b=0, b=1/2 and b=1 and the Drucker-Prager criterion are calculated respectively. The Drucker-Prager criterion is used for comparison

Figures 10.10 and 10.11 are the comparison of the spreads of plastic zones with four criteria when $\lambda=\sigma_x/\sigma_y$=0, i.e. the vertical load only, as σ_y increases from 20 MPa to 24 MPa and 28 MPa.
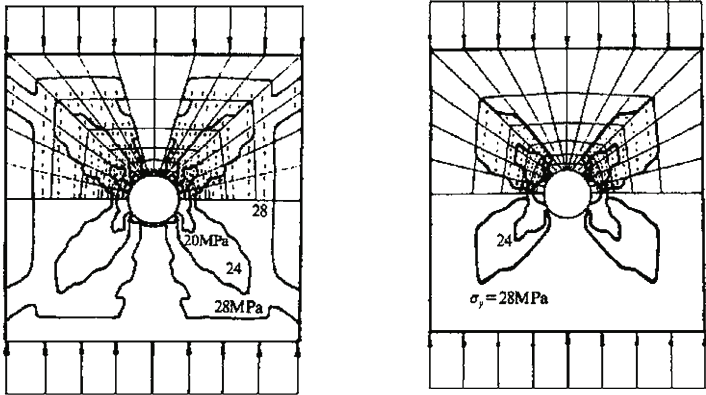
(a) UST with b=0 (Single-shear theory)   (b) UST with b=1/2 (New criterion)

Fig. 10.10   Spread of plastic zone of a cave under vertical load (λ=0)
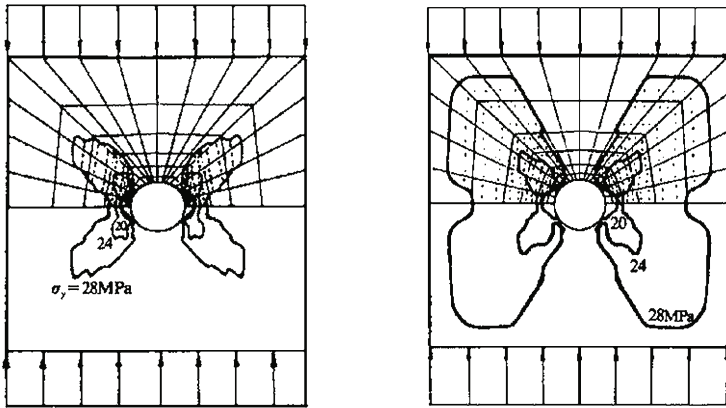
(a) UST with b=1 (Twin-shear theory)   (b) Drucker-Prager criterion

Fig. 10.11   Spread of plastic zone of a cave under vertical stress (λ=0)

Figures 10.12 and 10.13 are the comparison of the plastic zones with four criteria when λ=0.2 and σ_y increases from 20MPa to 30 MPa and 34 MPa.

(a) UST with *b*=0 (Single-shear theory)   (b) UST with *b*=1/2 (New criterion)

Fig. 10.12   Spread of plastic zone of a cave under load λ=0.2

(a) UST with *b*=1 (Twin-shear theory)   (b) Drucker-Prager criterion
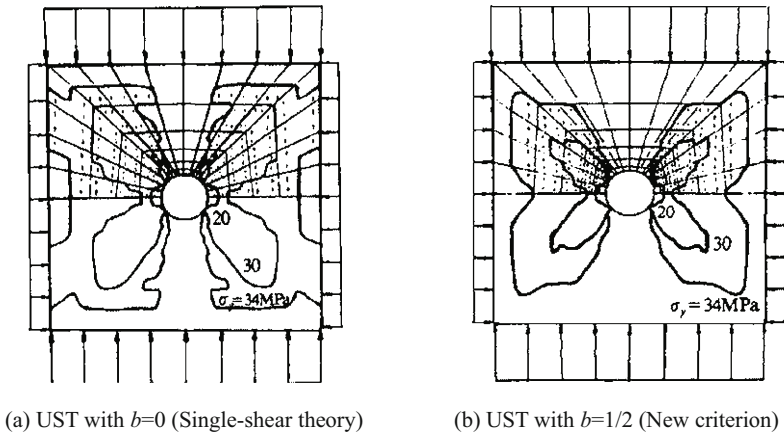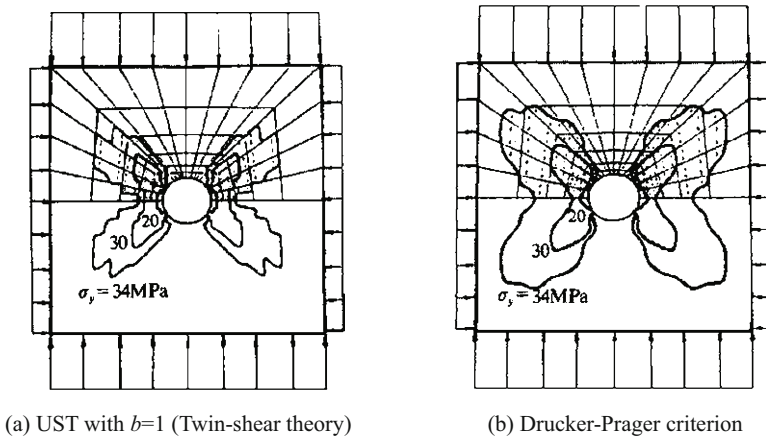
Fig. 10.13   Spread of plastic zone of a cave under load λ=0.2

Figures 10.14 and 10.15 are the comparison of the plastic zones with four criteria when $\lambda=\sigma_x/\sigma_y$=0.5 and σ_y increases from 20 MPa to 36 MPa and 44 MPa.

It is seen from the results above that, under the same load, the spread of the plastic zone of an underground cave strongly depends on the choice of the yield criteria, when the unified strength theory parameter *b*=0, namely single-shear theory (Mohr-Coulomb strength theory), gives the largest plastic zone which has already gone through the periphery of the computational result under σ_y=34 MPa. The unified strength theory with *b*=1, i.e. the twin-shear strength theory, gives the smallest plastic zone. The unified strength theory with *b*=0.5 is a new criterion, which gives the median result. These three typical criteria, i.e. two bounds and the median criterion can be adapted for different materials and structures, respectively.

(a) UST with $b=0$ (Single-shear theory)　　　(b) UST with $b=1/2$ (New criterion)
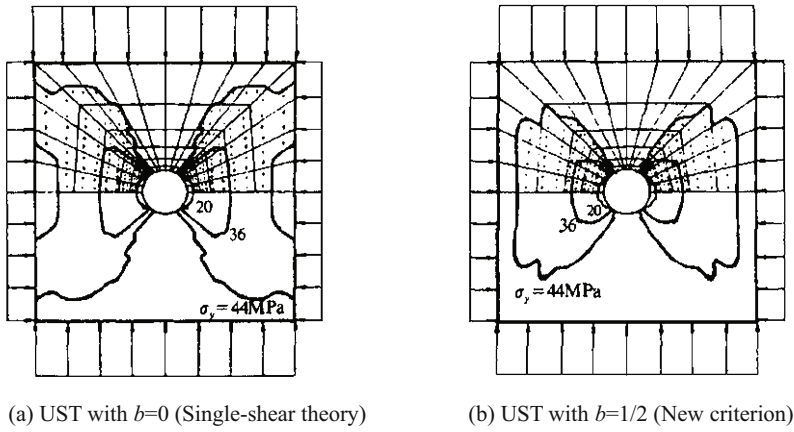
Fig. 10.14　Spread of plastic zone of a cave under load $\lambda=0.5$

(a) UST with $b=1$ (Twin-shear theory)　　　(b) Drucker-Prager criterion
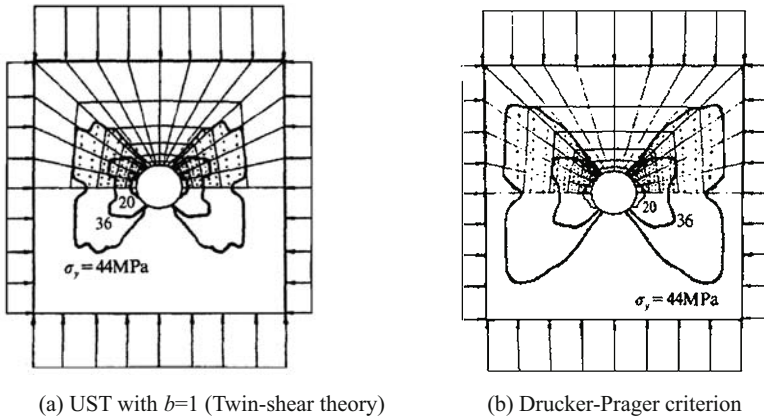
Fig. 10.15　Spread of plastic zone of a cave under load $\lambda=0.5$

10.4　Laxiwa Hydraulic Power Plant on the Yellow River

The Laxiwa Hydraulic Power Station is the largest power station on the Yellow River. The total installed capacity is 4200 MW, the unit capacity 700 MW, the annual power output 10.223 billion kWh. The power crest elevation is 2460 m, the maximum height 250 m and the total reservoir storage capacity is 1.079 billion cubic meters. Figures 10.16 and 10.17 show pictures of the Laxiwa Hydraulic Power Station and the underground powerhouse cavern. A series of research works were done for the Laxiwa Hydraulic Power Station by Northwest China Hydroelectric Power Investigation and Design Institute. A cross section of the caverns containing the hydroturbine-electric generator and transformer is shown in Fig. 10.18.

Fig. 10.16   Laxiwa Hydraulic Power Station on the Yellow River, China

Fig. 10.17   Large cave of Laxiwa Hydraulic Power Station
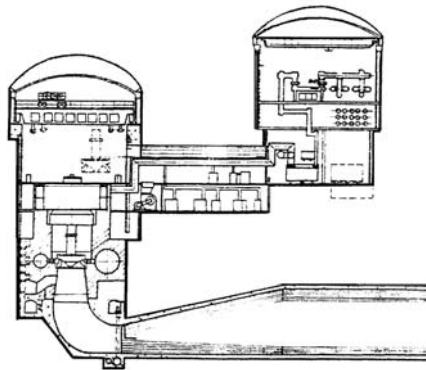
Fig. 10.18   Caverns of hydroturbine electric generator and transformer

Three underground excavations were carried out under the high mountain.

This is a high ground stress area in Laxiwa. The stability of the underground caves is important. So the plastic analysis of the underground excavations were made by An and Hu (1991), Liu and Sun at the Investigation and Design Institute of Northwest China Hydroelectric Power (Liu, 1994; 1995; Liu and Wu, 1995**;** Sun, 1998; Zhang, 1996). Various yield criteria were used for comparison. The results are given to show the effect of the yield criteria on the analysis. The unified strength theory provides us with a very effective theory and approach for studying the effect of failure criterion on various problems.

The numerical simulation of underground excavation with high ground stress in the area of the Laxiwa Hydraulic Power Plant on the Yellow River, China, was carried out by the Northwest China Hydroelectric Power Investigation and Design Institute (An, 1990; Liu, 1994; 1995; Liu and Hu, 1996; Sun 1998). The dimensions of three underground excavations are shown in Table 10.1.

Table 10.1   Dimensions of three underground excavations

Underground excavation	Maximum (m)	Maximum Height (m)	Height of wall (m)	Total length (m)
1	29	67	50	250
2	23	46	40	224
3	20	57	53	157

The ground stresses can be regarded as a combined stress (σ_x, σ_y, τ_{xy}) acting on the rock around the underground excavation where σ_x=15.3 MPa, σ_y=13.1 MPa, τ_{xy}=0.595 MPa. Figure 10.19 shows the finite element mesh. The plane strain condition is assumed in the FEM analysis. Figures 10.20 and 10.21 show the principal stress trajectory and the maximum principal stress σ_1 and principal stress σ_2 around the caves of the underground excavation under the ground stresses. Displacement of rock around the caves is shown in Fig. 10.22**.**
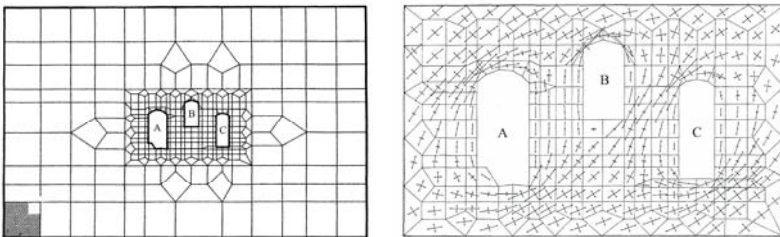
Fig. 10.19   Finite element mesh and principal stress trace around underground excavation
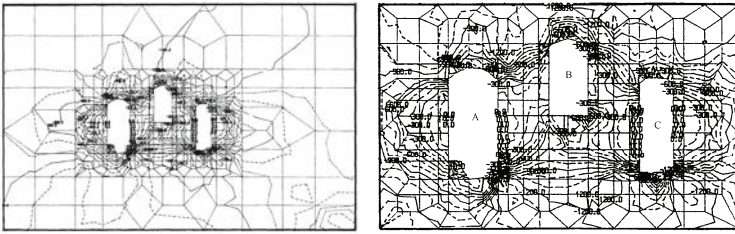
Fig. 10.20   The maximum principal stress σ_1 around the curves
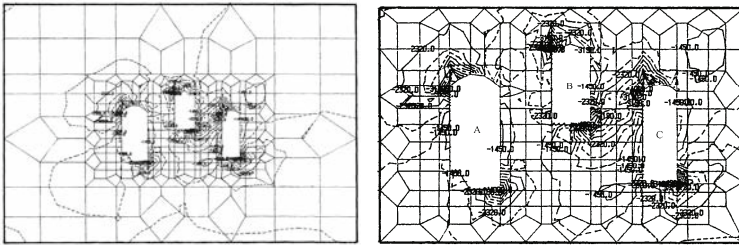
Fig. 10.21   The principal stress σ_2 around the curves
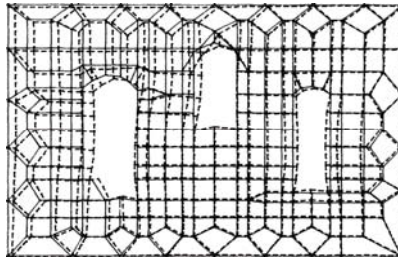
Fig. 10.22   Displacement of rock around the caves

10.5 Plastic Analysis for Underground Excavation at Laxiwa Hydraulic Power Station

10.5.1 Strength of the Laxiwa Granite

The true tri-axial experimental for the Laxiwa granite was made by the Investigation and Design Institute of Northwest China Hydroelectric Power and Wuhan Institute of Rock and Soil Mechanics of the Chinese Academy of Science (Li XC and Xu, 1994). Five groups of experiments on stress angles ($\theta = 0°$, 13.9°, 30°, 46.1°, 60°) were carried out under a hydrostatic pressure of $p=130$ MPa. The test results and limit locus in the π-plane for granite under hydrostatic pressure

p=130 MPa are shown in Fig. 10.23 (Li XC and Xu, 1990).
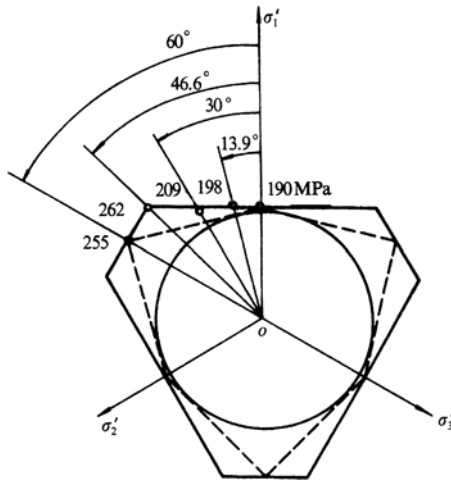
Fig. 10.23   Limit locus in the π-plane for granite (Li and Xu, 1990)

The following can be seen.

1) The length of vector q differs corresponding to different stress angles of θ in the π-plane when the hydraulic pressure p is constant. Granite shows an obvious stress angle effect. There is an obvious distinction between the circular limit loci of the Drucker-Prager criterion and the experimental results.

2) All the experimental points are located outside the limit loci of the Mohr-Coulomb strength theory and they are closer to that of the twin-shear strength theory.

3) In the process of varying the stress angle from θ=0° to θ=60°, the value of q increases and reaches q=262.2 MPa. It then decreases to q=255 MPa. This result agrees with the twin-shear strength theory.

So the twin-shear strength theory was used for the plastic analysis of underground excavation at Laxiwa Hydraulic Power Station. Other criteria are also used for comparison. The results are given to show how they are influenced by the yield criteria. The twin-shear unified strength theory was also used by Sun et al. (2004) at Zhejiang University and the East China Investigation and Design Institute, State Power Corporation of China for the Tai'an Pumped Storage Hydraulic Power Station in Shandong Province, China.

10.5.2 *Plastic Zones Around the Underground Excavation Using the Single-Shear and Twin-Shear Theories*

The spreads of the plastic zones under the ground stresses were obtained by using the Mohr-Coulomb strength theory (unified strength theory with $b=0$) and the twin-shear strength theory (unified strength theory with $b=1$) as shown in Fig. 10.24. It is seen that the area of the plastic zone of the twin-shear strength theory is less than the plastic zone of the Mohr-Coulomb strength theory (single-shear theory or the unified strength theory with $b=0$). According to the calculation made by the Northwest China Hydroelectric Power Investigation and Design Institute, if the area of the plastic zone around the underground excavation obeys the single-shear theory, it is 100% of the total area. Then the area of the plastic zone around the underground excavation that obeys the twin-shear theory is 44% of the total area.
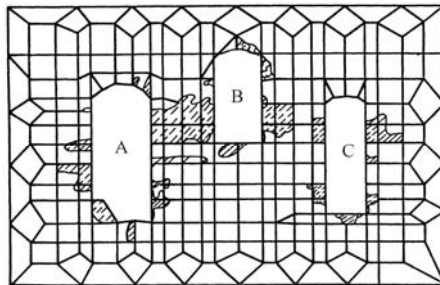
(a) UST with $b=0$ (Single-shear theory)
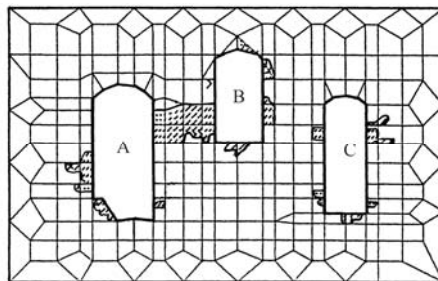
(b) UST with $b=1$ (Twin-shear theory)

Fig. 10.24   lastic zone around underground excavation

According to the convexity of the yield surface, some smooth models and two bounds are shown in Fig. 18.25, in which the limit locus 1 is the Mohr-Coulomb strength theory (1900), locus 2 is the twin-shear strength theory (Yu et al., 1985), locus 3 is the William and Warnke criterion (1975), locus 4 is the twin-shear smooth model (Yu and Liu, 1990a; 1990b) and locus 5 is the Gudehus-Argyris criterion.
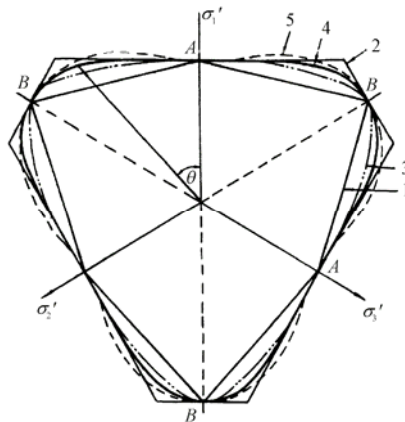
Fig. 10.25 Some smooth yield loci and two bounds of the convex yield loci

The distribution of the plastic zone around the underground excavation with the Gudehus-Argyris yield criterion is shown in Fig. 10.26.
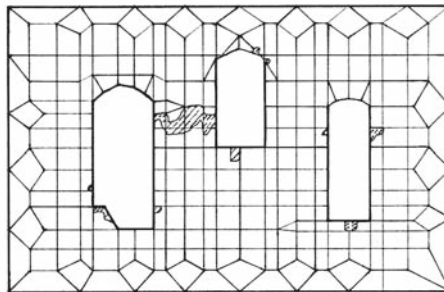
Fig. 10.26 Plastic zone around underground excavation (Gudehus-Argyris criterion)

10.5.3 Plastic Zones Around the Underground Excavation with Four Yield Cone Criteria

The yield loci of four yield cone criteria are shown in Fig. 10.27. They are (a) extended cone; (b) inscribed cone (Drucker-Prager criterion); (c) compromise cone; (d) compressive cone. The plastic zone around the underground excavation with four yield cones is shown in Fig. 10.28.
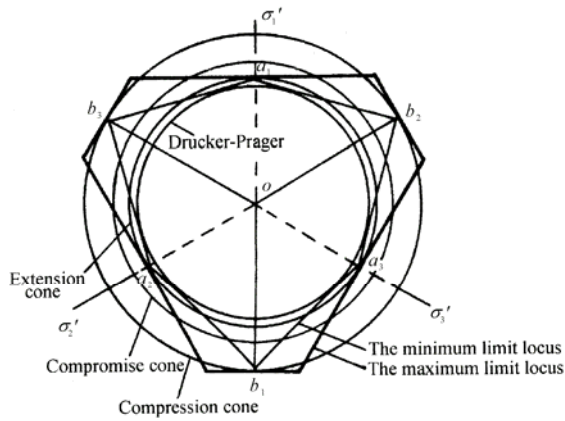
Fig. 10.27   Limit loci of various failure criteria on the deviatoric plane

(a) Extended cone

(b) Inscribed cone (Drucker-Prager criterion)

(c) Compromise cone

(d) Compressive cone
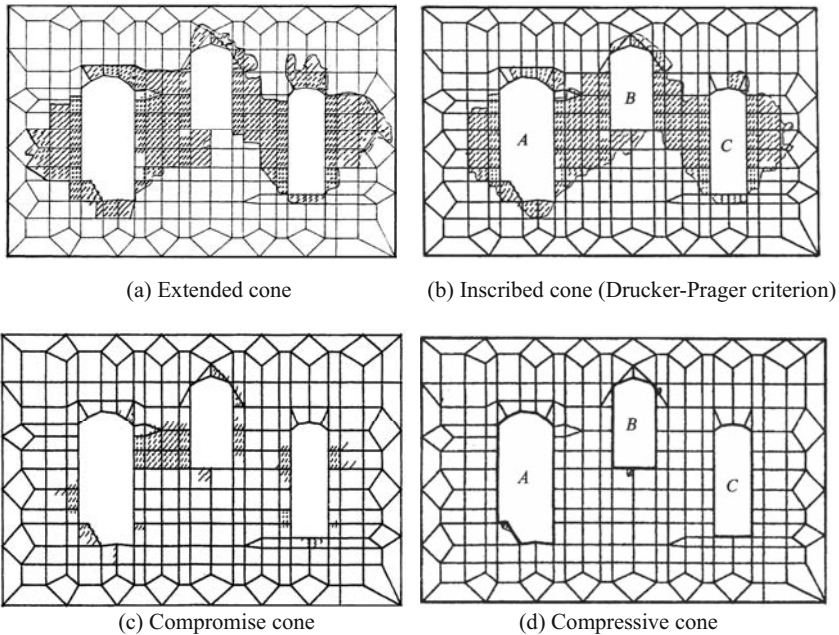
Fig. 10.28   Plastic zone around underground excavation with four yield cones

10.6 The Effect of Failure Criterion on the Plastic Zone of the Underground Excavation

A great deal of research has been dedicated to showing the effects of failure criteria on the analytical results of load-carrying capacities of structures. A famous

example was given by Humpheson and Naylor (1975), and was further studied by Zienkiewicz and Pande (1977). They show a great difference between results obtained by using various failure criteria. Obviously, the question arises as to which one of these results should be preferred, because there is only one reasonable result for a given material and structure.

As pointed out by Zienkiewicz and Pande (1977), the choice of the best limit surface is still in the hands of the analyst who has modeled the strength behaviour in the best possible manner. They also indicated that the Drucker-Prager criterion and the limit loci of circular cones give a very poor approximation to the real failure conditions (Humpheson and Naylor, 1975; Zienkiewicz and Pande, 1977).

Most of the limit surfaces of different failure criteria are cones in the stress space. The limit loci in the meridian plane are linear. This means that the strength of materials is linearly dependent on the hydrostatic stress in the range of lower and median hydrostatic stresses, as has been demonstrated in a number of tests. The differences between the limit loci of various failure criteria in the deviatoric plane are shown in Fig. 10.25 and Fig. 10.27.

The experimental data of true triaxial tests done by the Investigation and Design Institute of Northwest China Hydroelectric Power, Ministry of the Power Industry, Ministry of Water Resources, the China Institute of Rock and Soil Mechanics, are higher than the Mohr-Coulomb single-shear theory and close to the twin-shear theory.

In this example, the twin-shear theory is applied to the plastic analysis of underground excavation at Laxiwa Hydraulic Power Station, because the experimental results for underground rock (granite) at the Laxiwa area obtained by the Investigation and Design Institute of Northwest China Hydroelectric Power and Wuhan Institute of Rock and Soil Mechanics of Chinese Academy of Science agree well with the twin-shear strength theory, as shown in Fig. 10.23 (Liu, 1994; 1995; Liu and Wu, 1995; Sun, 1998). The plastic zone around the underground excavation is shown in Fig. 10.24(b). A conclusion was made therefore by the Investigation and Design Institute of Northwest China Hydroelectric Power that "The area of the plastic zone obeying the twin-shear theory is only 0.44 times the area of the plastic zone obeying the single-shear theory. Using the twin-shear unified strength theory can reduce considerably the amount of support work and save a lot of investment. It will be a significant economic benefit. Preliminary estimates show that up to 15 million RMB Yuan can be saved."

10.7 Three Dimension Numerical Modeling of Underground Excavation for a Pumped-Storage Power Station

A pumped-storage scheme is a type of power station for storing and producing electricity to supply high peak demands by moving water between reservoirs at different elevations. In general, water is channeled from a high-level reservoir to a low-level reservoir, through turbine generators that generate electricity. This is

done when the station is required to generate power. During low-demand periods, such as overnight, the generators are reversed to become pumps that move the water back up to the top reservoir.

The Tai'an Pumped Storage Hydraulic Power Station has been constructed in Shandong Province, China. The upper water reservoir of the storage power station on the top of the mountain is shown in Fig. 10.29. It has a total capacity of 1000 MkW.

Fig. 10.29   Top water reservoir of the Tai'an Pumped Storage Hydraulic Plant

3D finite element numerical modeling of the excavation rock mass of Tai'an Pumped Storage Hydraulic Power Station was done by Professors Sun, Shang, Zhang et al. of Zhejiang University, Hangzhou, China and East China Investigation and Design Institute, State Power Corporation of China (Sun et al., 2004a; 2004b).

The rock mass failure of an underground excavation often begins with local instability (failure of rock).

The initial failure position is the weak part of the surrounding rock mass. It would not take too much money to reinforce the rock mass if the weak position of the rock mass can be found and reinforced reasonably. The failure of the surrounding rock mass may be caused by the lower strength of the rock mass somewhere. Also, it may be caused by the accumulation of stress on the underground excavation. The local failure of the rock mass caused by stress accumulation during excavation can be forecast by numerical modeling analysis.

The weak position may not be located in the middle part of the excavation, but may be located at a certain distance from the end of the excavation. This has been proven by the outcome of the 3D finite element numerical modeling study of the excavated rock mass at the Tai'an Pumped Storage Hydraulic Power Station. Therefore, based on 2D numerical simulation results of the middle part of the excavation, the reinforced design may be unsafe. In order to make a reasonable evaluation of the excavation area, the weak position in the surrounding rock mass should be determined by 3D numerical modeling. In this analysis, the twin-shear unified strength theory proposed by Yu is used (Sun et al., 2004a; 2004b).

The isograms of the major principal stress and minor stress in the middle of the excavation and their variety at elastic range are shown in Figs. 10.30 to 10.32.
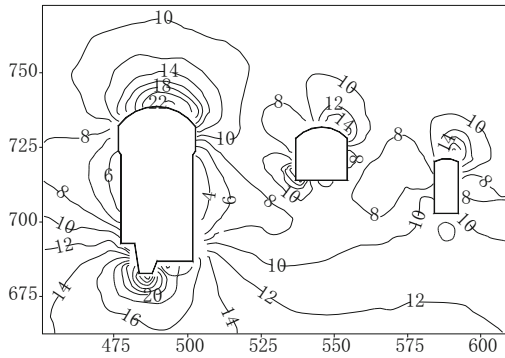
Fig. 10.30   Isograms of major principal stress
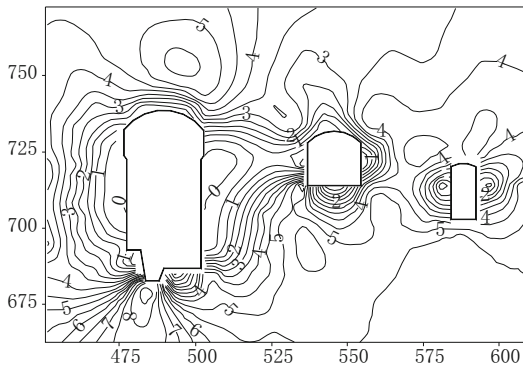
Fig. 10.31   Isograms of minor principal stress

A map of the excavation and analysed section locations is shown in Fig. 10.33. The plastic zones of the underground excavation are calculated in terms of the twin-shear unified strength theory. Three calculated results of the plastic zone of the underground excavation are obtained. The plastic zones of the underground excavation of section *A-A* and section *B-B* are shown in Figs. 10.34 and 10.35, respectively. The failure zone of surrounding rock of *C-C* section is rather small.

(a) At the top of cave

(b) At the wall of cave
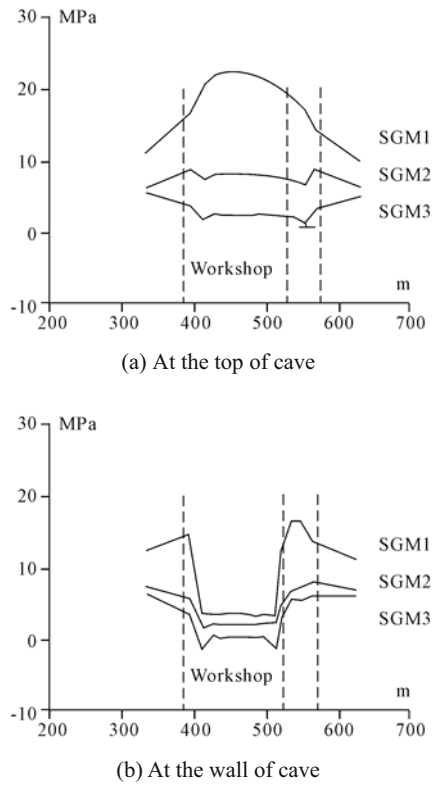
Fig. 10.32   Principal stress variation along the excavation axis
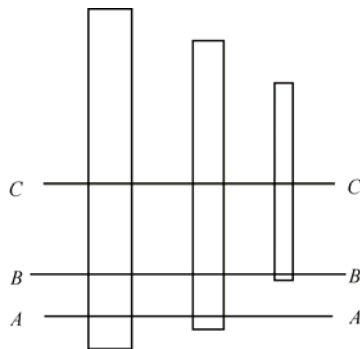
Fig. 10.33   Map of the excavation locations
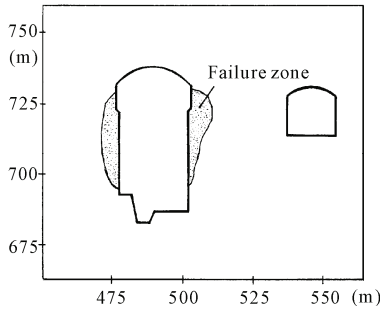
Fig. 10.34   Failure zone of surrounding rock (*A-A* section)
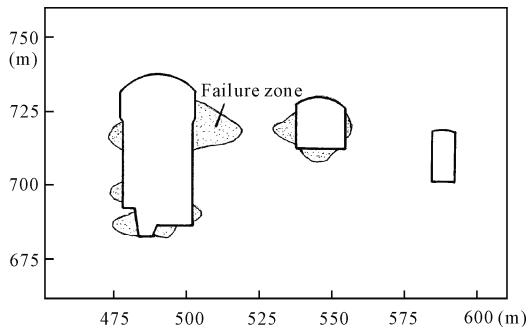
Fig. 10.35   Failure zone of surrounding rock (*B-B* section)

According to the feature of the failure zone of the surrounding rock between the caves, the failure zone of surrounding rock at section *C-C* is very small. The surrounding rock is stable. However, the section to the side of the middle position of the surrounding rock still contains several destructive areas, as shown in Fig. 10.35. Therefore, we should increase the anchor intensity and anchor rod length in these sections to guarantee the stability of the surrounding rock. Several design proposals were presented by Sun et al. (2004).

The research of Professers Sun and Shang was adopted for application at the Tai'an Pumped Storage Hydraulic Power Station. The excavation of underground caves was carried out in six parts, as shown in Fig. 10.36. Distributions of the surrounding rock rupture zone of a typical section after the fifth excavation and sixth excavation are shown in Figs. 10.36 and 10.37 (Sun et al., 2004).
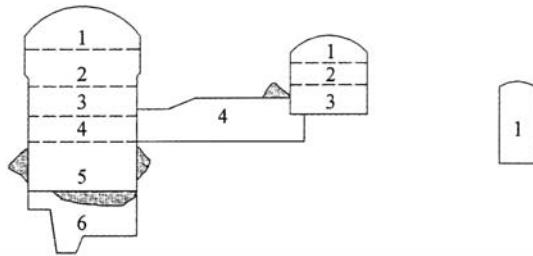
Fig. 10.36 Distribution of surrounding rock rupture zone of typical section after fifth excavation
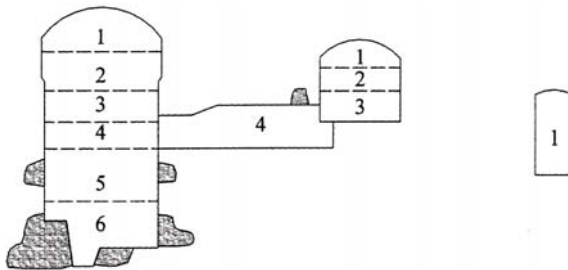
Fig. 10.37   Distribution of surrounding rock rupture zone of typical section after sixth excavation

10.8   Dynamic Response and Blast-Resistance Analysis of a Tunnel Subjected to Blast Loading

This work was done by professors Liu GH and Wang ZY at Zhejiang University, Hangzhou, China, for a railroad tunnel (Liu and Wang, 2004). The twin-shear unified strength theory is also used for dynamic problems.

In recent years, research on the structural characteristics of demolition under the load function has invited widespread interest. Ultra short distance demolition appraisal is one of the research topics in this domain.

The blast with a short distance is harmful to an existing tunnel, which is the key problem in the practical engineering. Dynamic analysis and unified strength theory were applied to develop appropriate methods for evaluating the tunnel's safety and to devise an optimal blasting scheme for nearby blasting by Prof. Liu at Zhejiang University. Blasting dynamic analysis results are used to plot the time-course curves and the frequency spectrum of the structural response. A case study is presented to illustrate the rational benefits of the above theory and method.

Displacement vector fields for a railroad tunnel, when the source of the explosion is 15 m away and explosive charges $Q=32.4$ kg are used, are shown in Fig. 10.38.

(a) Q=32.4 kg, t=5.6 ms   (b) Q=32.4 kg, t=8.2 ms
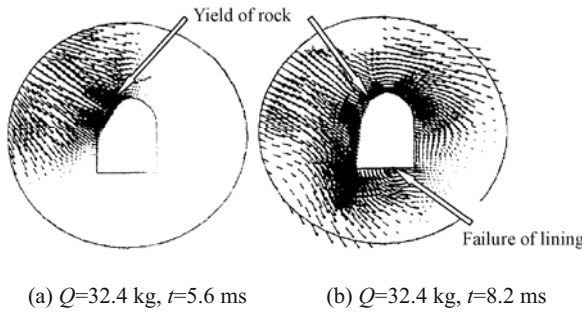
Fig. 10.38   Displacement vector fields of railroad tunnel under all blasting (Q=32.4 kg)

Attenuation of vibration velocity, with the distance between explosion source and the tunnel for an existing tunnel, are shown in Fig. 10.39. If the simulated result of the explosion has a total explosive charge of Q=32.4 kg, the response is great.
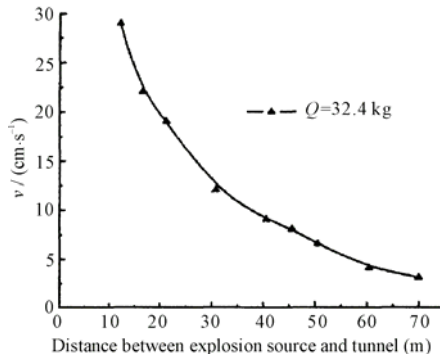
Fig. 10.39   Attenuation of vibration velocity with distance between explosion source and tunnel

When the whole explosion causes adverse vibration effects on the tunnel, the use of a step-blasting technique can effectively reduce the vibration response. Displacement vector fields for a railroad tunnel, when the explosion source is 15m away and step explosive charges of Q=6 kg are used, are shown in Fig. 10.40. The displacement vector fields for a railroad tunnel are shown in Fig. 10.41. Obviously, the dynamic response has decreased significantly. When the whole explosion (32.4 kg) is divided into 7 steps, the dynamic response of step blasting explosives (the largest step explosive amount is 6 kg) in the numerical simulation results is shown in Fig. 10.41.

(a) *Q*=6 kg, *t*=5.6 ms   (b) *Q*=6 kg, *t*=8.2 ms
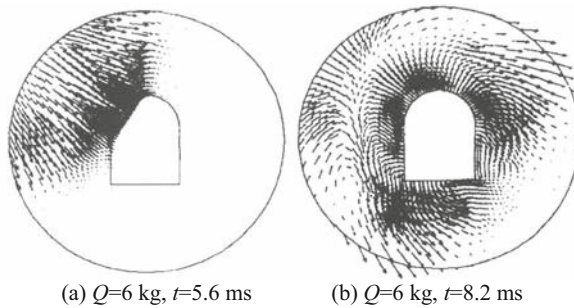
Fig. 10.40   Displacement vector fields of railroad tunnel under step blasting (*Q*=6 kg)
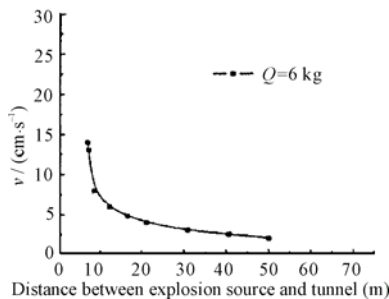
Fig. 10.41   Attenuation of vibration velocity with distance between explosion source and tunnel

Some key dynamic problems of the underground blasting structure were studied by Liu GH and Wang ZY for a railroad tunnel. The blasting safety assessment and optimal selection of construction methods are discussed in detail, in which the twin-shear strength criterion is adopted as the basic theory. The dynamic analysis method with twin-shear strength theory can not only be used for the spectrum characteristics of the dynamic response, but also for the stress analysis and security assessment of tunnel engineering.

We can study the dynamic response and blast-resistance analysis of a tunnel subjected to blast loading based on the stress state of the rock mass and failure criteria, in which the twin-shear strength theory is adopted as a failure criterion. The blasting construction plane, according to this theory and method, are adopted for use in practical railroad engineering.

10.9   Brief Summary

The numerical simulations of the effect of yield criterion on the plastic zone for an underground circular cave under vertical compression and two direction compressions, the stability of surrounding rock of the underground excavation of the Laxiwa Hydraulic Power Station on the Yellow River, 3D numerical

modeling of the underground excavation for a pumped-storage power station, and the dynamic response and blast-resistance analysis of a tunnel subjected to blast loading are described above.

The numerical results show that the prediction of the numerical simulation of structural strength is influenced strongly by the choice of the yield criterion. The effect of the yield criterion on the bearing capacity and the plastic zone of underground caves in the tunneling and excavation of a hydraulic power station is obvious. It is very important to choose a reasonable strength theory (yield criteria or material model in FEM code) in the research and design.

The change in shape and size of the yield surface of various yield criteria is great. The two bounds and region of yield criteria for materials are important. The lower bound, the upper bound and the median yield loci are the three basic yield criteria for convex yield criteria.

The results of research and design are strongly dependent on the choice of strength theory in most cases. The selection of the correct strength theory becomes even more important than anything else. A better choice of strength theory will be demanded in research and engineering applications in future. When it becomes necessary to adopt a criterion for use, it is important to experimentally check the criterion, or to investigate the experimental data in the literature. If this is not done, then very exact numerical procedures or commercial codes may lead to completely worthless results. It is important therefore to facilitate the choice of a model (Zienkiewicz and Taylor, 1989).

A large number of material models have been proposed throughout the years. So far, no general model that can simulate all these variations has been presented. Therefore, several models are normally implemented in commercial programs to allow for simulations of different materials under various conditions. It is obviously of great importance to choose a constitutive model suitable for the material and the problem under consideration, as well as to assign proper values to the parameters included in this model.

The unified strength theory and associated flow rule provide us with systematic yield criteria from the lower bound to upper bound, an effective approach and a powerful tool for computational plasticity. This takes into account the effect of the intermediate principal stress and the effect of the stress angle on the strength of geomaterials. The unified strength theory has a simple mathematical formula; it can not only make better use of the strength of materials than the single-shear strength theory, but is also in wide agreement with the experimental results for different materials. The material parameters of the unified strength theory are the same as the material parameters used in the Mohr-Coulomb criterion.

According to the research results provided by the Investigation and Design Institute of Northwest China Hydroelectric Power, the spreads of the plastic zones under the ground stresses were obtained using the Mohr-Coulomb strength theory (unified strength theory with $b=0$) and the twin-shear strength theory (unified strength theory with $b=1$). It is seen that the area of the plastic zone obeying the twin-shear strength theory is less than the plastic zone of the Mohr-Coulomb

strength theory (single-shear theory or the unified strength theory with b=0). If the area of the plastic zone around the underground excavation that obeys the single-shear theory is 100% of the total area, then the area of the plastic zone around the underground excavation that obeys the twin-shear theory is 44% of the total. Underground excavation engineering involves a large amount of work and has a long construction period. Owing to the experimental results of the true triaxial tests for the surrounding rock (Laxiwa granite) close to the twin-shear theory, The Investigation and Design Institute of Northwest China Hydroelectric Power came to the conclusion that, according to the twin-shear theory, the design will be a significant economic benefit.

References

An M (1990) Elasto-plastic analysis for excavation of a large hydropower station. Master's thesis of Xi'an Jiaotong University, Xi'an, China (in Chinese).

An M, Yu MH and Wu X (1991) Applications of generalized twin-shear yield criterion in rock mechanics. Rock Soil Mech., 12(1): 17-26 (in Chinese, English abstract).

Brady BHG and Brown ET (1985) Rock Mechanics for Underground Mining. London: George Allen&Unwin Ltd.

Dhawan KR, Singh DN, Gupta ID (2002) 2D and 3D finite element analysis of underground openings in an inhomogeneous rock mass. Int. J. Rock Mechanics and Mining Sciences, 39(2): 217-227.

Goodman RE (1989) Introduction to Rock Mechanics. John Wiley & Sons: New York.

Hudson JA and Harrison JP (1997) Engineering Rock Mechanics: An Introduction to the Principles. Elsevier Science.

Harrison JP and Hudson JA (2000) Engineering Rock Mechanics: Illustrative Worked Examples. Elsevier Science.

Humpheson C and Naylor DJ (1975) The importance of the form of the failure criterion. C/R/243/75, University of Wales, Swansea, UK.

Jacnto AC, Ambrosnir D, and Danesir F (2001) Experimental and computational analysis of plates under air blast loading. Int. J. Impact Engineering, 25: 927-947.

Krauthammer T (1999) Blast-resistant structural concrete and steel connections. Int. J. of Impact Engineering, 22: 887-910.

Li XC, Xu DJ, Liu SH and An M (1994) The experimental research of the strength, deformation and failure properties of Laxiwa granite   under the status of true triaxial stresses. Proc. Third Conf. of Chinese Society for Rock Mechanics and Engineering. China Science and Technology Press: Beijing, pp 153-159 (in Chinese, English abstract).

Liu GH and Wang ZY (2004) Dynamic response and blast-resistance analysis of a tunnel subjected to blast loading. Journal of Zhejiang University (Engineering

Science), 38(2): 204-209 (in Chinese).

Liu SH (1994) Study on the stability of surrounding rock of large underground powerhouse caverns of the Laxiwa Hydropower Project in high crustal stress area (Part One). Northwest China Water Power, (4) (Total 50): 39-43 (in Chinese).

Liu SH (1995) Study on the stability of surrounding rock of large underground powerhouse caverns of the Laxiwa Hydropower Project in high crustal stress area (Part Two). Northwest China Water Power, (1) (Total 51): 45-48 (in Chinese).

Liu SH, Wu X (1995) LAXIWA: Upland areas of large underground powerhouse and stability of surrounding rock of large underground caverns. Hydropower (WATER POWER), (3): 17-21 (in Chinese).

Pellet F, Benoit O (1999) 3-D numerical simulation of the behavior of underground structures crossing faults zone. In: Vouille G, Berest P, ed. Proc. 9th Int. Congress on Rock Mechanics. A A Balkema: Rotterdam, pp 213-218.

Sun J (1999) Rheology Theory and Its Engineering Applications. China Building Industry Press: Beijing (in Chinese).

Sun HY, Shang YQ, Zhang CS (2004a) Numerical modeling analysis for the stability of surrounding rockmass of large underground excavations. J. Zhejiang University (Engineering Science), 38(1): 70-74 (in Chinese, English abstract).

Sun HY, Shang YQ, Zhang CS, Ying HP, Li SQ (2004b) 3-D Numerical modeling of possible failure location in underground excavation. Chinese J. Rock Mechanics and Engineering, 23(123): 2192-2196 (in Chinese, English abstract).

Sun ZM (1995) Study on the dam, reservoir water and the dam foundation interaction under static and dynamic force. Northwest Hydropower, (4): 12-24 (in Chinese).

Sun ZM (1998) Dam and reservoir water, as well as dynamic and static analysis of the dam foundation interaction. Hydropower (Water Power), (3): 9-13,6 (in Chinese).

Wittke W (1990) Rock Mechanics: Theory and Applications with Case Histories. Springer-Verlag: Berlin (Germany edn. 1984)

Yan DJ, Qiang IH and Tang DG (2001) Reliability of isolation system under blast shock and vibration. China Civil Engineering Journal, 34(3):23-28 (in Chinese).

Yu MH, He LN and Song LY (1985) Twin shear stress theory and its generalization. Scientia Sinica (Sciences in China), English edn. Series A, 28(11):1174-1183.

Yu MH and He LN (1991) A new model and theory on yield and failure of materials under complex stress state. In: Mechanical Behaviour of Materials-6, Vol. 3. Pergamon Press: Oxford, pp 841-846.

Yu MH (1992a) A new system of strength theory. Xian Jiaotong University Press: Xi'an (in Chinese).

Yu MH (1998) Twin-shear Theory and Its Applications. Science Press: Beijing (in Chinese).

Yu MH (2002) Advances in strength theories for materials under complex stress state in the 20th Century. Applied   Mechanics Reviews ASME, 55(3):169-218.

Yu MH (2004) Unified Strength Theory and its Applications. Springer: Berlin.

Zhang MY (1996) High arch dam: the key scientific and technological research findings. Hydropower (Water Power), 8 (in Chinese).

Zhou WY and Yang Q (2005) Numerical Computational Methods for Rock Mechanics. China Electric Power Press: Beijing.

Zienkiewicz OC (1971) The Finite Element Method in Engineering Science. McGraw-Hill: London.

Zienkiewicz OC and Pande GN (1977) Some useful forms of isotropic yield surfaces for soil and rock mechanics. Finite Elements in Geomechanics. Gudehus G ed. Wiley: London, pp 179-190.

Zienkiewicz OC and Taylor RL (l989) The Finite Element Method, vol. l, 4th edn, McGraw-Hill: London, New York.

11

Implementation of the Unified Strength Theory into ABAQUS and its Application

11.1 Introduction

The software ABAQUS, which is developed and supported by HKS Inc. is currently one of the most powerful nonlinear finite element codes. The ABAQUS Unified FEA product suite offers powerful and complete solutions for both routine and sophisticated engineering problems covering a vast spectrum of industrial applications, which specialize in geometry and material nonlinear problems. Best-in-class companies are taking advantage of ABAQUS Unified FEA to consolidate their processes and tools, reduce costs and inefficiencies, and gain a competitive advantage. ABAQUS includes many different kinds of material models such as the Drucker-Prager criterion, Mohr-Coulomb criterion and Cambridge constitutive models for use in geotechnical problems (Hibbitte et al., 2002; Zhuang, 1988).

The Mohr-Coulomb strength theory is used in geotechnical engineering extensively and many empirical criteria all predict that the intermediate principal stress σ_2 has no effect on the strength of material. The previous experimental results indicated that the intermediate principal stress has remarkable effects on the material. The value of the strength of rock under various increases in σ_2 is greater than that from confined triaxial tests, and the strength of rock is increased by 20%-30% when the effect of the intermediate principal stress is taken into account.

Though some non-linear elastic models are implemented into ABAQUS by

This chapter was contributed by Prof. Wang JQ, North China Electric Power University, Beijing, China and Prof. Lu Feng, Institute of Water Resources and Hydropower Research, Beijing, China.

using a User Subroutine, the non-linear elastic procedure, however, is easy to use though this model cannot consider the effect of the intermediate principal stress. This fact limits the scope of the software to some extent. It is important to develop some constitutive model to consider the intermediate principal stress in ABAQUS so as to execute more powerful numerical analysis.

In this chapter, the unified strength theory and associated constitutive model is implemented in the nonlinear finite element software ABAQUS using the User Subroutine second development function. The numerical test of a thick wall cylinder is completed to verify this implementation, and three dimensional analysis of tunnel excavation is done for practical engineering purposes. All numerical results show that the process of adding this model to ABAQUS enriches the material and heightens the computational efficiency and precision. The present study using the unified strength theory with $b=0$ and the result using the original Mohr-Coulomb criterion in ABAQUS are identical. It is also a verification of the implementation. Meanwhile, the example and the tunnel excavation simulation demonstrate that to consider the influence of the intermediate principal stress in geotechnical engineering can guide engineering practice and reduce investment outlay.

This research was carried out for the Jinping diversion tunnel, a large hydraulic engineering project.

11.2   Basic Theory

11.2.1 Expression of the Unified Strength Theory

The unified strength theory (UST) was proposed by Yu in 1991, and further presented by Yu in 1992 and 1994. It was based on the concept of a multiple slip mechanism and the multi-shear element model. It reflects the fundamental characteristics of materials in a complex stress state. The Mohr-Coulomb strength theory, the twin-shear stress theory, and many other new criteria can also be degenerated from the unified strength theory. The unified strength theory can also be generalized to cover non-convex failure criteria. The SD effect (strength difference in tension and compression) and the effect of the intermediate principal stress can also be presented (Yu, 1991; 1992; 2004).

In terms of the stress invariant, the united strength theory has the mathematical expression

$$F = (1-\alpha)\frac{I_1}{3} + \frac{\alpha(1-b)}{1+b}\sqrt{J_2}\sin\theta + (2+\alpha)\sqrt{\frac{J_2}{3}}\cos\theta = \frac{2c\cos\varphi}{1+\sin\varphi}$$

$$(0° \le \theta \le \theta_b) \quad (11.1a)$$

$$F' = (1-\alpha)\frac{I_1}{3} + (\alpha + \frac{b}{1+b})\sqrt{J_2}\sin\theta + (\frac{2-b}{1+b} + \alpha)\sqrt{\frac{J_2}{3}}\cos\theta = \frac{2c\cos\varphi}{1+\sin\varphi}$$

$$(\theta_b \le \theta \le 60°) \quad (11.1b)$$

where b is a coefficient reflecting the effect of the intermediate principal shear stresses on material strength, I_1 is the first stress invariant (hydrostatic pressure), J_2 is the second deviatoric stress invariant and θ is the stress angle. The Mohr-Coulomb yield criteria can be obtained from the unified strength theory with $b=0$. The stress angle θ corresponding to the twin-shear stress state parameter is

$$\mu_\tau = \frac{\tau_{12}}{\tau_{13}} = \frac{\sigma_1 - \sigma_2}{\sigma_1 - \sigma_3} \quad \text{or} \quad \mu_\tau' = \frac{\tau_{23}}{\tau_{13}} = \frac{\sigma_2 - \sigma_3}{\sigma_1 - \sigma_3} \quad (11.2)$$

The twin-shear stress state parameter is the simplification of the Lode stress parameter

$$\mu_\sigma = \frac{2\sigma_2 - \sigma_1 - \sigma_3}{\sigma_1 - \sigma_3} = \frac{\tau_{23} - \tau_{12}}{\tau_{13}} \quad (11.3)$$

However, twin-shear stress state parameters μ_τ and μ_τ' have a simple equation and simple signification, as described inChapter 2 of this monograph.

The SD effect is considered by the coefficient $\alpha=(1-\sin\varphi)/(1+\sin\varphi)$. The stress angle at the corner θ_b can be determined by using the condition $F=F'$.

$$\theta_b = \text{car}\tan\frac{\sqrt{3}}{1+2\alpha} \quad (11.4)$$

11.2.2 The General Expression of Elastic-Plastic Increment Theory

The loading surface can be considered as a small yield surface F developing to be a bigger yield surface Φ. The first basic assumption in the incremental theory of plasticity is that a loading function exists which depends upon the state of stress and strain and the history of loading. In other words, at each stage of a plastic deformation of unloading, there is some function of stress $F(\{\sigma\})$ such that no additional plastic deformation takes place when F is smaller than some number κ, which also may depend on plastic strain and loading history. Plastic flow of a work-hardening material occurs when F exceeds κ. The loading function is the yield function for the deformed material. At any stage of plastic deformation, the loading function can be represented, geometrically, like the yield function in perfect plasticity, by a surface in a stress space. This surface is called a subsequent

yield surface or a loading surface Φ. It changes its configuration with the plastic flow according to intrinsic, so-called hidden variables, which are expressed in terms of the plastic strain and a hardening parameter κ.

$$\Phi(\{\sigma\},\{\varepsilon_p\},\kappa) = 0 \tag{11.5}$$

A general derivation of the stress-strain relation is given for an elastic work-hardening-plastic material based on the flow rule

$$\{d\sigma\} = \left[D_{ep}\right]\{d\varepsilon\} \tag{11.6}$$

where the elastic-plastic-stiffness tensor has the form

$$\left[D_{ep}\right] = [D] - \frac{[D]\left\{\dfrac{\partial \Phi}{\partial \sigma}\right\}^{\mathrm{T}}\left\{\dfrac{\partial F}{\partial \sigma}\right\}[D]}{A + \left\{\dfrac{\partial \Phi}{\partial \sigma}\right\}^{\mathrm{T}}[D]\left\{\dfrac{\partial F}{\partial \sigma}\right\}} \tag{11.7}$$

it represents the degradation of the material constitution due to plastic flow.

Part of the programming is to calculate $\left\{\dfrac{\partial F}{\partial \sigma}\right\}$ and $\left\{\dfrac{\partial \Phi}{\partial \sigma}\right\}$, and to treat the discontinuities of the singularity corner of the yield surface in the π plane.

11.3   ABAQUS UMAT (User Material)

11.3.1 General Introduction of UMAT

The commercial finite element software ABAQUS offers a powerful solution for non-linear engineering problems. ABAQUS provides an interface from which users can implement their own constitutive models in user subroutine, UMAT. Through UMAT, the user-defined constitutive model can be used with any ABAQUS structural element type.

Several utility routines may help in coding the user subroutine UMAT. Their functions include determining stress invariants for a stress tensor and calculating principal values and directions for stress or strain tensors.

The main objectives of UMAT are as follows:
(1) update the stress state;
(2) obtain Jacobian matrix

$$[D] = \frac{\partial \Delta \sigma}{\partial \Delta \varepsilon} \tag{11.8}$$

A general process for an incremental FEM solution, as in ABAQUS, is given as follows. For a series of given variables (σ, ε, $\Delta \varepsilon$) at the start of the nth step, UMAT is expected to calculate the σ, ε and other state dependent variables, and provide the Jacobian matrix for a global iterative Newson-Raphson solution by using ABAQUS.

11.3.2 Interface and Algorithm of UMAT

User-defined mechanical material behavior, which is called UMAT, communicates with ABAQUS data by its main program interface. In the input file, the keyword "user material" describes user-defined mechanical material behavior.

The user subroutine UMAT is called for each material point at each iteration of every increment. It is provided with the material state at the start of the increment (stress, solution-dependent state variables, temperature and any predefined field variables) and with the increments in temperature, predefined state variables, strain and time.

In addition to updating the stresses and the solution-dependent state variables to their values at the end of the increment, subroutine UMAT must also provide the material Jacobian matrix, $\dfrac{\partial \Delta \sigma}{\partial \Delta \varepsilon}$, for the mechanical constitutive model. This matrix will also depend on the integration scheme used if the constitutive model is in rate form and is integrated numerically in the subroutine. For any nontrivial constitutive model these will be challenging tasks. For example, the accuracy with which the Jacobian matrix is defined will usually be a major determinant of the convergence rate of the solution and, therefore, will have a strong influence on computational efficiency.

It should be noted that the Jacobian matrix only influences the rate of iteration convergence, but not the accuracy of the results. The following describes some issues concerning the elastic-plastic incremental relationship, divided into three sections.

11.3.3 Elastic and Plastic State

The general steps elastic-plastic state is determined as follows (only the isotropic hardening situation is discussed here):

(1) With displacements known at all points within the element, the increment-of-strain vector at any point can be obtained by taking suitable

derivatives of Eq. (11.9). The incremental-strain-displacement relationship can be established as

$$\Delta \varepsilon = B \Delta u \qquad (11.9)$$

with the matrix generally being composed of derivatives of the shape functions.

(2) A set of incremental elastic stresses $\Delta \tilde{\sigma}$ and elastic trial stresses $^{t+\Delta t} \tilde{\sigma}$ is computed by Eq. (11.10) and Eq. (11.11), as

$$\Delta \tilde{\sigma} = D_e \Delta \varepsilon \qquad (11.10)$$

$$^{t+\Delta t} \tilde{\sigma} = {}^t \sigma + \Delta \tilde{\sigma} \qquad (11.11)$$

where ${}^t \sigma$ is the stress at the end of the last step.

(3) Then calculate the state variables $^{t+\Delta t} \sigma$, $^{t+\Delta t} \varepsilon_p$ at this incremental step according to every integration point in the element.

There are three types of conditions after calculating the yield function $F(^{t+\Delta t} \tilde{\sigma}, {}^t \bar{\varepsilon}_p)$. They are:

(a) If the trial stresses do not violate the loading condition, $F(^{t+\Delta t} \tilde{\sigma}, {}^t \bar{\varepsilon}_p) \leq 0$, the behavior of the material is elastic. This is the point of elastic loading or unloading from the plastic state, the hardening parameters remain unchanged and the final stresses at the end of the loading increment are

$$\Delta \sigma = \Delta \tilde{\sigma} \qquad (11.12)$$

(b) If the loading surface is violated by the elastic trial stresses, the element is under plastic loading. At the outset the stress state satisfies

$$F({}^t \tilde{\sigma}, {}^t \bar{\varepsilon}_p) < 0$$

which indicates an elastic state. Because of the finite load increment, a fully elastic stress path would penetrate the yield surface. The condition violates the yield condition and indicates that a transition from elastic to plastic state occurs during this load increment.

$$F(^{t+\Delta t} \tilde{\sigma}, {}^t \bar{\varepsilon}_p) > 0$$

In this case, the load increment is subdivided into two parts, an elastic portion for the path *AC* and a plastic portion governing the behavior after the yield surface has been reached at *C*. This requires determination of the penetration point *C*, which is a geometric problem of intersecting a surface with a line. If we denote ${}^t \tilde{\sigma} + r \Delta \tilde{\sigma}$, which is the portion of the stress increment where the plastic behavior is first encountered, i.e. when

$$F({}^{t}\tilde{\sigma} + r\Delta\tilde{\sigma}, {}^{t}\overline{\varepsilon}_{p}) = 0 \tag{11.13}$$

in principle, at least, the scaling factor m can be determined from Eq. (11.13).

In actual applications, explicit expressions for r can be derived only for simple types of loading functions. The simplest approximate value of m from Eq. (11.11) is determined by a linear interpolation in f, and a better estimate is obtained by the Taylor exploration of the yield surface. The bisection method can be used to achieve r.

(c) The conditions $F({}^{t+\Delta t}\tilde{\sigma}, {}^{t}\overline{\varepsilon}_{p}) > 0$ and $F({}^{t}\tilde{\sigma}, {}^{t}\overline{\varepsilon}_{p}) = 0$ show that the stress state is loading, $r=0$.

Under the two conditions of (b) and (c), the plastic portion of the strain increment can be determined as follows

$$\Delta\varepsilon' = (1 - r)\Delta\varepsilon \tag{11.14}$$

The initial-stress or plastic-stress increment can be calculated as

$$\Delta\sigma' = \int_{0}^{\Delta\varepsilon'} D_{ep}(\sigma, \overline{\varepsilon}_{p}) d\varepsilon \tag{11.15}$$

The computation of the stress trajectory of Eq. (11.15) requires a numerical integration.

The final stresses at the end of this loading increment are approximate,

$$^{t+\Delta t}\sigma = {}^{t}\sigma + r\Delta\tilde{\sigma} + \Delta\sigma' \tag{11.16}$$

$$^{t+\Delta t}\overline{\varepsilon}_{p} = {}^{t}\Delta\overline{\varepsilon}_{p} + \Delta\overline{\varepsilon}_{p} \tag{11.17}$$

11.3.4 Constitutive Relationship Integration (Stress Update Method)

The integration of a constitutive function is called a stress update algorithm. At the elastic forecasting stage, the plastic strain and the inner variable remain unchanged and, at the plastic revised stage, the total strains remain unchanged. The integration method is a sub-incremental method based on explicit integration and tangent forecasting.

(1) Tangent prediction and backward-radial

(2) Tangent prediction is to use the linear relation—Euler method in Eq. (11.15) to gain the stress increment prediction value.

$$\Delta\tilde{\sigma} = D_{ep}({}^{t}\sigma, {}^{t}\overline{\varepsilon}_{p})\Delta\varepsilon \tag{11.18}$$

Then the total stress prediction value is

$$^{t+\Delta t}\tilde{\sigma} = {}^{t}\sigma + \Delta\tilde{\sigma} \tag{11.19}$$

The $\Delta{}^{t}\bar{\varepsilon}_{p}$ will be obtained simultaneously.

Because Eq. (11.18) shows that the algorithm is the explicit Euler method, $D_{ep}({}^{t+\Delta t}\sigma, {}^{t}\bar{\varepsilon}_{p})$ is the original tangent stiffness, so $\Delta\tilde{\sigma}$ is in the tangent direction. The initial yield surface and all subsequent loading surfaces must be convex, so $^{t+\Delta t}\tilde{\sigma}$ is out of the loading surface. But the yield criterion requires any state of stress lying on or inside the loading surface, so the radial backward method is used to get $^{t+\Delta t}\sigma$ satisfy the yield criterion. If we denote

$$^{t+\Delta t}\sigma = r\,{}^{t+\Delta t}\tilde{\sigma} \tag{11.20}$$

where r is the scaling factor, which can be determined from Eq. (11.21)

$$F({}^{t+\Delta t}\sigma, {}^{t+\Delta t}\bar{\varepsilon}_{p}) = 0 \tag{11.21}$$

Though the corrected $^{t+\Delta t}\sigma$ is lying on the yield surface, the strain increment $\Delta\varepsilon$ and the equivalent plastic strain $^{t+\Delta t}\bar{\varepsilon}_{p}$ remain unchanged; the elastic-plastic state is not fully consistent. The inconsistency increases with the incremental step increases. To decrease the error caused by the inconsistency, the above-mentioned method and subdivided increment method could be incorporated to achieve the stress increment.

(3) Subdivided increment method

The subdivided increment method is an approximate method splitting the given strain increment into equal increments and using tangent prediction and the backward-radial method for each of these smaller intervals to gain stress increment. The elastic-plastic state at the end of every sub-increment is the beginning of the sequence increment. The sub-increment method is useful for achieving a more accurate stress increment and for speeding up the iteration convergence velocity.

The sub-increment number N is given by the nearest integer which is less than

$$N = 8 \times \frac{\bar{\sigma}_{y} - \sigma'_{y}}{\sigma_{y}^{0}} + 1 \tag{11.22}$$

where $\bar{\sigma}_{y} - \sigma'_{y}$ gives a measure of the excess stress and σ_{y}^{0} is the initial uni-axial yield, $\bar{\sigma}_{y}$ is the trial equivalent stress and σ'_{y} is the equivalent stress for $^{t+\Delta t}\sigma = {}^{t}\sigma + r\Delta\tilde{\sigma}$.

11.3.5 Tangent Stiffness Method

The implicit backward Euler integration method often uses a consistent tangent stiffness matrix. We use the explicit forward Euler integration method here.

11.3.6 Treatment of the Singular Points on the Yield Surface

There are intersect lines for the yield surface of the united strength theory, so the flow vector is not uniquely defined and the direction of plastic straining is indeterminate because there are singular points on the π plane. There are two methods for solving the numerical difficulties including the smoothness and non-smoothness methods, in which the non-smoothness disposal methods have been widely applied on account of their simple implementation. The plastic strain increment sum method, provided by Koiter, and returning the similarity angle θ to the original yield expression and derivation method are the two general methods.

(1) The vector sum method is used to correspond to $\theta=\theta_b$.

(2) The returning and derivation method is adopted for $\theta=0°$ and $\theta=60°$.

11.4 Typical Numerical Example

11.4.1 Model Conditions

The numerical example is illustrated in Fig. 11.1. The problem studied is that of a thick cylinder subjected to internal pressure p=160 MPa, inner radius a=0.1 m and outer radius b=0.2 m, the elastic modulus E=2.1×10^5 MPa, Poisson's ratio v=0.3, uniaxial yield stress σ_s=240 MPa.

The theoretical results in terms of the Tresca yield criterion can be found in any textbook on plasticity. A series of results using the unified strength theory have been given in Chapter 10 of Yu's monograph "Unified Strength Theory and its Applications" published by Springer in Berlin in 2004 (Yu, 2004). The elastic ultimate pressure and plastic ultimate pressure that obey the Tresca criterion are

$$p_e = \frac{\sigma_s}{2}(1-\frac{a^2}{b^2}) \tag{11.23}$$

$$p_s = \sigma_s \ln\frac{b}{a} \tag{11.24}$$

These two results are special cases of the unified solution for the elastic limit with b=0 and the plastic limit with b=0. Other serial results can be also obtained from the unified solution with $0<b\leq1$ (Yu, 2004)

The solution with p_e=90 MPa and p_s=166.35 MPa is achieved corresponding to the above condition. The subjected pressure is between p_e and p_s, the cylinder is in the elastic-plastic state. The process of illustrating the correctness of the numerical solution obtained by comparing it with the theoretical results is as follows.

11.4.2 Comparison of 2D and 3D Solution from ABAQUS

The 2D and 3D numerical calculations are executed by ABAQUS, which uses the Mohr-Coulomb criterion. There are 12 equal-parameter elements and 51 nodes for the plane strain problem. Four layers are split along the thickness direction and there are 12 block elements and 122 nodes for the 3D model. The FEM meshes are shown in Fig. 11.1.

(a) 2D   (b) 3D
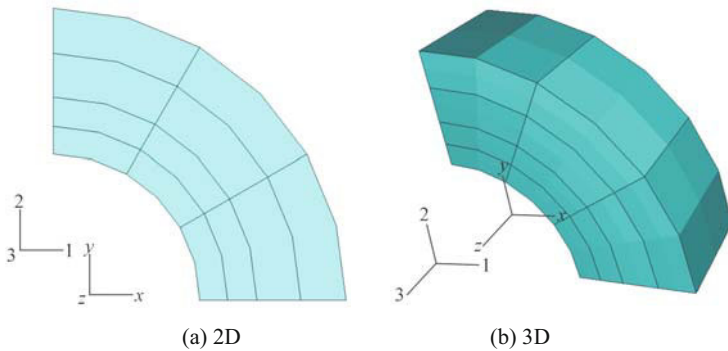
Fig. 11.1   FEM Meshes

The Mohr-Coulomb criterion will degenerate into the Tresca criterion for inner friction angle φ=0°. It is necessary to simulate the Tresca criterion by the Mohr-Coulomb criterion with φ=0.3° and the shearing angle ψ=0° because the friction angle φ cannot be set to 0° in ABAQUS. The results of the 2D and 3D calculations fit totally, which is shown in Table 1 of the radial displacement and stress.

11.4.3 Results from UMAT of the United Strength Theory

(1) Stress and displacement
The united theory strength theory criterion will degenerate into the Tresca criterion for α=1 and b=0. Table 11.1 also shows the circumferential (hoop) stress and radial stress and the displacement distributions for specified points calculated by the UMAT program with UST (Unified Strength Theory). A good agreement

between the ABAQUS and UMAT solutions is evident, which shows the UMAT program is correct and reliable.

Table 11.1 Displacements and stresses of 3-D model along horizontal radial direction

X (mm)	Mohr-Coulomb (ABAQUS)			UST with b=0 (UMAT)		
	U_1 (mm)	σ_{11} (MPa)	Σ_{22} (MPa)	U_1 (mm)	σ_{11} (MPa)	σ_{22} (MPa)
100.	255.813	-169.279	91.0233	255.141	-154.393	86.4583
109.515	232.138	-148.441	111.706	231.628	-142.354	98.5036
119.03	213.253	-127.631	132.38	212.799	-112.096	128.754
129.03	197.367	-109.026	150.709	196.834	-101.376	139.48
139.03	184.798	-90.2334	169.284	184.16	-76.3354	164.514
154.03	170.565	-66.7303	192.545	169.839	-59.2163	181.645
169.03	160.855	-42.9037	214.366	160.148	-30.3002	208.942
184.515	153.591	-24.0713	194.812	152.936	-16.464	184.794
200.	147.99	-5.72096	176.462	147.378	2.64825	171.731

The united strength theory with b=0 or $b = 1/(1+\sqrt{3}) \approx 0.366$ is the linear approximation of the Huber-von Mises criterion, the stress and the displacement distributions achieved by 3D UMAT along the horizontal radial direction are shown in Table 11.2, and the 2D analyzed displacements quoted in (Yu, 1998) are shown simultaneously, which show the agreement is evident. The results of the united strength theory with b=1, that consider the material strength increases, are presented in Table 11.2.

Table 11.2 Displacements and stresses of 3-D model along horizontal radial direction

X (mm)	UST with b=0.366 (UMAT)				UST with b=1 (UMAT)		
	U_1 (mm)	U_1 (mm) Yu 1998	σ_{11} (MPa)	σ_{22} (MPa)	U_1 (mm)	σ_{11} (MPa)	σ_{22} (MPa)
100.	185.1	182.21	-157.16	117.94	159.51	-152.03	168.157
109.515	168.347	165.243	-137.915	139.58	146.15	-137.16	183.912
119.03	155.711	152.535	-107.186	168.66	136.49	-97.305	216.819
129.03	145.684	142.982	-92.4888	183.14	128.60	-82.906	194.998
139.03	138.034	135.676	-65.4417	202.45	122.12	-58.098	177.842
154.03	129.166	127.057	-46.7706	173.93	114.27	-41.362	154.03
169.03	122.336	120.419	-23.4533	157.42	108.23	-20.726	139.318
184.515	116.827	115.203	-12.5755	141.18	103.35	-11.113	124.912
200.	112.58	111.148	2.04003	131.26	99.597	1.8121	116.103

The distribution of the circumferential stress, radial stress and radial displacement that are obtained by ABAQUS and UMAT with b=0, b=0.366 and b=1 are shown in Fig. 11.2. Stresses and displacements of the cylinder obtained by the Mohr-Coulomb criterion in ABAQUS and b=0, b=0.366 and b=1 in the UMAT program, respectively, are compared in Fig. 11.2.

(a) Tangential stress σ_{11}

(b) Radial stress σ_{22}

(c) Radial displacement U_1
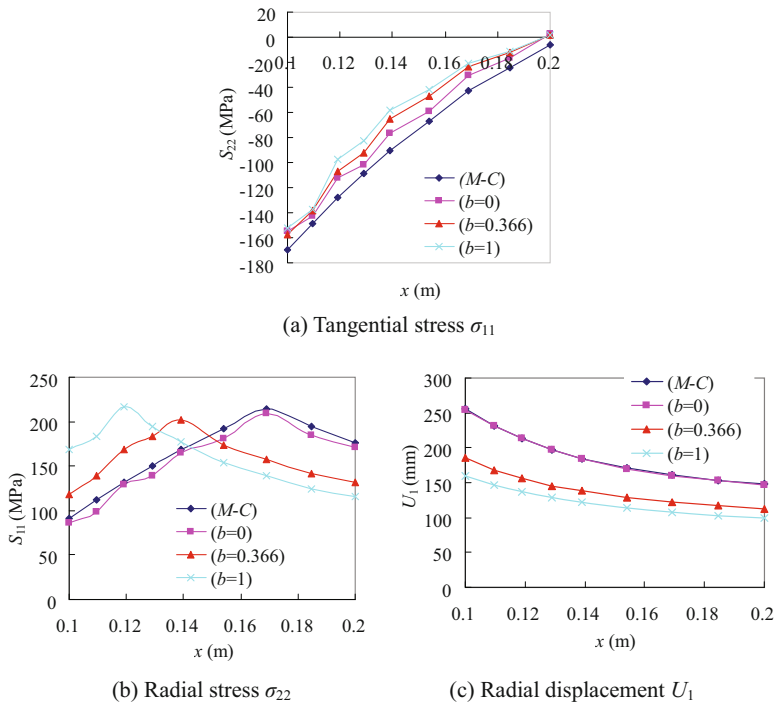
Fig. 11.2   Stresses and displacements of the cylinder obtained by the ABAQUS and UMAT programs

It is found in Fig. 11.2 that the tangential stresses obtained from ABAQUS with Mohr-Coulomb criterion agree well with those gained by UMAT with $b=0$, and the radial displacements coincide. A series of results can be given by UMAT. The maximum value of the circumferential stress is when approaching the inner wall with b increasing, while the radial stresses decrease and the radial displacement decreases also.

(2) Plastic zone

The spread of the plastic zone (an equivalent plastic strain larger than 0.0001) in thick-walled cylinders with different yield criteria is shown in Fig. 11.3. The radius of the plastic zone with the unified yield criterion when $b=0$ (Tresca yield criterion) is larger than that obtained from $b=0.366$ (with two layers of yield elements) and $b=1$ (with one layer of yield elements).
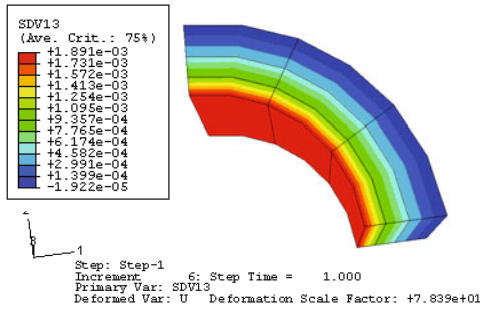
(a) UST with b=0
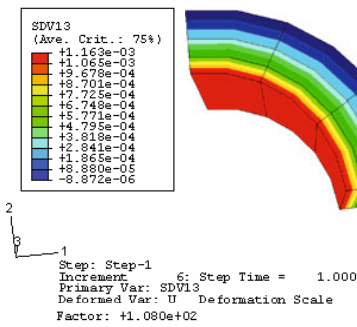
(b) UST with b=0.366
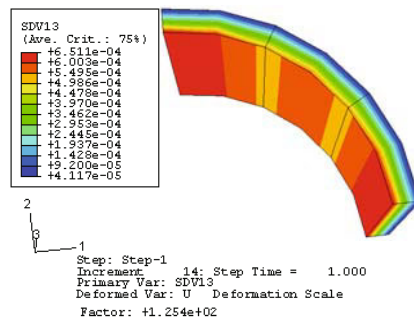
(c) UST with b=1

Fig. 11.3   Distribution of the plastic cylinder zone with the equivalent plastic strain being more than 0.0001

(3) Analysis of results

The unified strength theory and associated constitutive model is implemented into the nonlinear finite element software ABAQUS using the User Subroutine second development function. The numerical test of a thick-walled cylinder is completed and it is shown that UMAT is successful.

11.5   Engineering Applications

11.5.1 Project Background and Material Parameters

The engineering of an underground opening is analyzed. The cave has a diameter D=10.2 m, depth H=620 m, where it is intended to use the TBM construction method, assisted by the drilling and blasting method. The rock in the relevant section is grade II, the rock mass parameters are shown in Table 11.3.

Table 11.3   Values of material parameters

Grade of rock mass	density, ρ (kg/m^3)	E (Pa)	Poisson's ratio, v	Cohesion c (Pa)	Friction angle φ (°)	Dilation angle ψ (°)
II	2450	3e9	0.25	2e6	40	20

11.5.2 FEM Mesh and Boundary Condition

The 3D finite element mesh is shown in Fig. 11.4; a half of the tunnel is considered due to symmetry. To simplify the analysis, the part below ground level (570 m) is substituted by the equivalent surface pressure. Nodes along the vertical boundaries may translate freely along the boundaries but are fixed against displacements normal to these boundaries. The nodes at the base are fixed against displacements in all directions. The tunnel is a one-stage excavation without consideration of the step-by-step incremental excavation and support scheme.
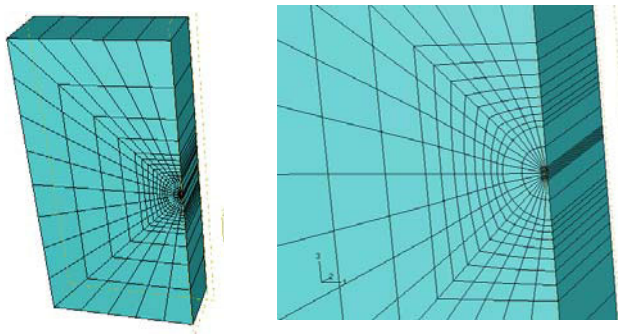
Fig. 11.4   FEM meshes

11.5.3 Results of Analysis

(1) Displacements

The united strength theory can consider the effects of the intermediate principal stress by changing the parameter b, such that it can degenerate to the Mohr-Coulomb criterion when $b=0$. The effects of the intermediate principal stress on the excavation stability are considered with value b changing. The horizontal and vertical displacements are shown in Fig. 11.5 and Fig. 11.6.
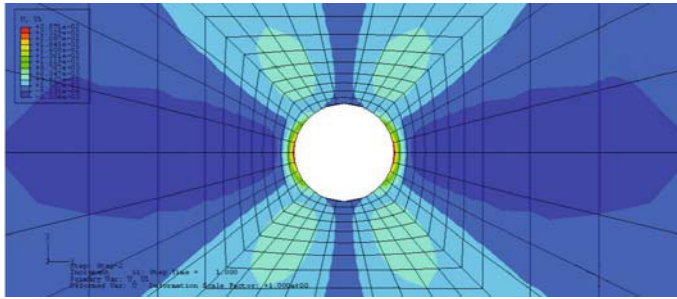
(a) UST with $b=0$
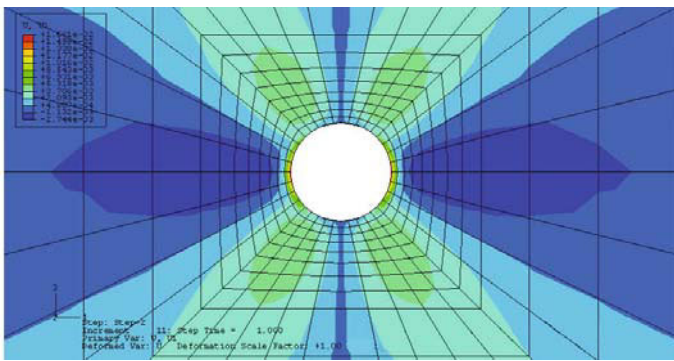
(b) UST with $b=0.366$
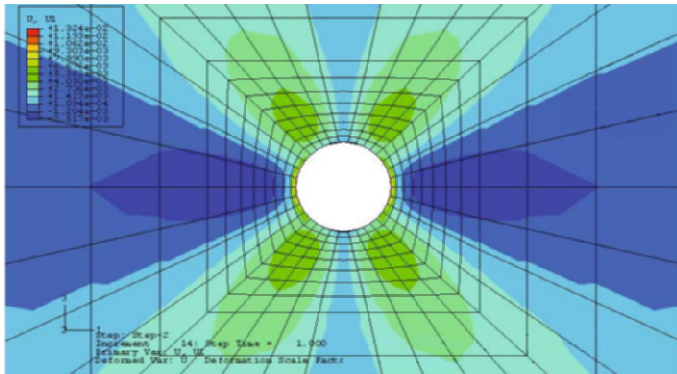
(c) UST with $b=0.8$

Fig. 11.5 Displacement fields in the horizontal direction
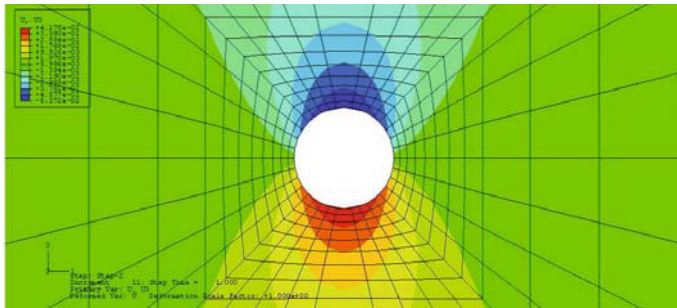
(a) UST with *b*=0
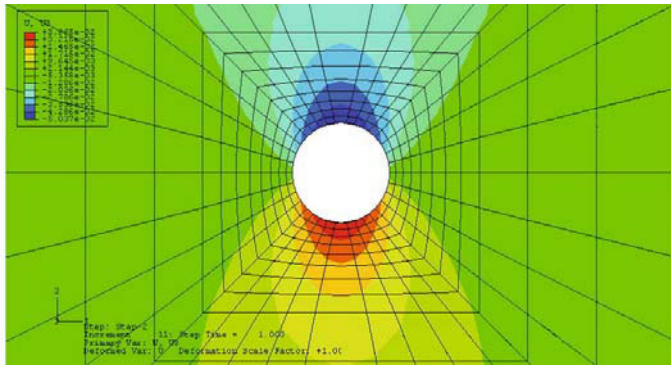
(b) UST with *b*=0.366
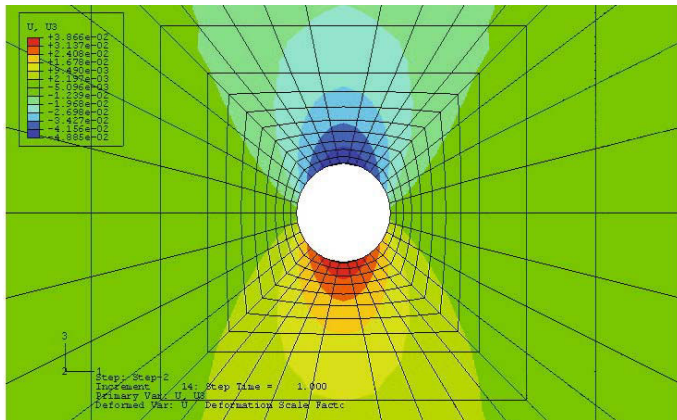
(c) *b*=0.8

Fig. 11.6   Displacement fields in the vertical direction

The variation in radial displacements on the left side of the tunnel, the crown and bottom and the distance from the inner boundary are all shown in Fig. 11.7, 11.8 and 11.9. It is found that the displacements decrease corresponding to increase in the value *b*, and the maximum is about 95% on the lateral wall.
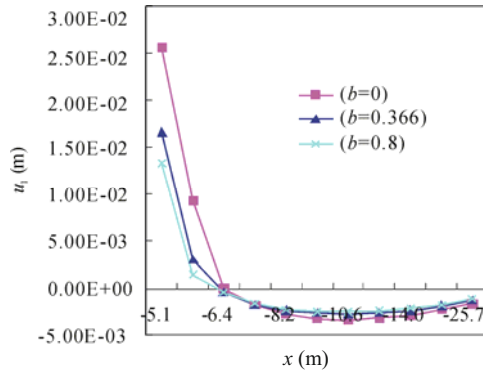
Fig. 11.7 Lateral displacements
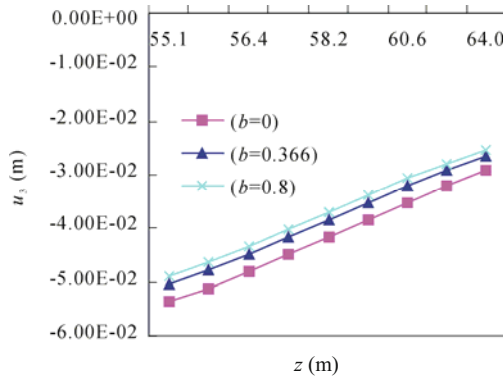
Fig. 11.8 Top displacements
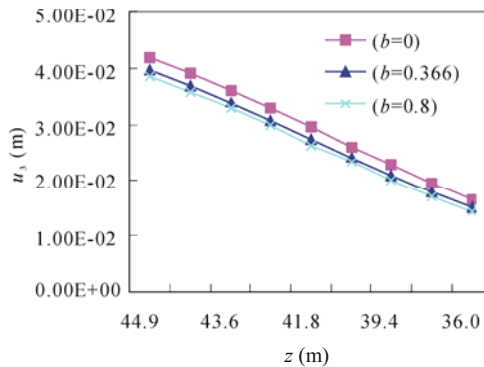
Fig. 11. 9 Comparison of bottom displacements

(2) Plastic zone

Plastic zone distribution is equivalent to the tunnel damage area to a certain extent, which shows the stability conditions of the excavation tunnel. The distribution of the plastic zone (the equivalent plastic strain larger than 0.0001) with different values of b are shown in Fig. 11.10. The plastic zone of the surrounding area

consists of three layers of yield elements with $b=0$ (that means the Mohr-Coulomb criterion is used), the outer layer elements decrease with $b=0.366$, and those become two layers. That is to say, the plastic distribution shrinks as the value b increases.

(a) UST with $b=0$ (b) UST with $b=0.366$ (c) UST with $b=0.8$
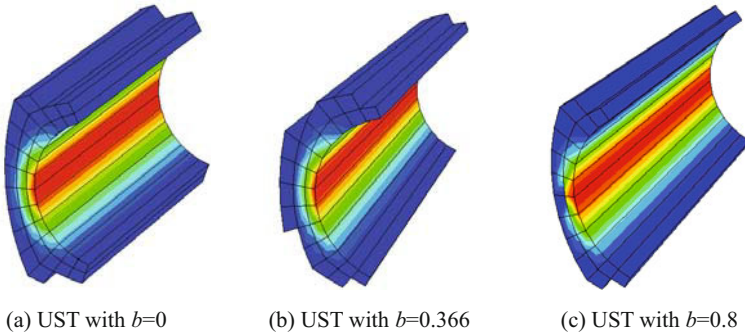
Fig. 11.10   Comparison of plastic zones of the cylinder

(3) Analysis of results

This has been the tunnel excavation example shown in the references, but it is limited in 2D analysis, where the parameter b has a different influence. The engineering example shows that the displacements and the plastic zone shrink as the value b increases. This shows that the actual determination of the value b is important when guiding the support scheme in tunnel construction.

11.6 Conclusions

The implementation of the united strength theory to ABAQUS software is feasible. It is based on the second developing platform of the advanced nonlinear FEM program ABAQUS. The numerical results of a typical example with a closed-form solution show that the precision is perfect. This can expand the practical scope of ABAQUS so as to provide a way to consider the intermediate principal stress in the field of geotechnical engineering. The final numerical verification confirms that the second development of the model is valid. It can be used in real life situations.

All the numerical results of the tunnel excavation example show that the displacements and the plastic zone shrink as the value b increases. These show that the actual determination of the value b is important in guiding the support scheme in tunnel construction. Meanwhile, there are some advantages of faster convergence, higher efficiency, higher precision and more convenient preprocessing and postprocessing. The difficulties in programming the development of soil engineering and maintenance workloads are also greatly decreased.

References

Hibbitte, Karlsson, Sorenson INC (2002). ABAQUS/Standard User's Manual.

Hu QZ, Zhou H and Yang XQ (2009) Effect on plastic strain through the non-smoothness management of corner singularity, Chinese J. Geotechnical Engineering, 31(1): 66-71.

Jiang YJ (1988) Nonlinear finite element method. Beijing Institute of technology Press (in Chinese): Beijing.

Owen DRJ and Hinton E (1980) Finite elements in plasticity. Pineridge Press Limited.

Smith IM and Griffiths DV (1998) Programming the Finite Element Method, third edition. John Wiley ＆ Sons, Inc.

Wang JQ and Lu F (2009) Unified strength theory constitutive model embedded software ABAQUS and its application in tunnel engineering. Journal of Yangtze River Scientific Research Institute, 27(2): 68-74 (in Chinese).

Wang XC (2003) Finite element method. Tsinghua University Press: Beijing. (in Chinese).

Wu TH (1976) Soil Mechanics (second edition). Allyn and Bacon: Boston.

Xu YJ and Wang GQ (2004). Development and implementation of Duncan-Chang constitutive model in ABAQUS. Rock and Soil Mechanics, 25(7): 1032-1036.

Yu MH (1961a) General behaviour of isotropic yield function. Res. Report of Xi'an Jiaotong University. Xi'an, China (in Chinese).

Yu MH (1961b) Plastic potential and flow rules associated singular yield criterion. Res. Report of Xi'an Jiaotong University. Xi'an, China (in Chinese).

Yu MH (1983) Twin-shear yield criterion. Int. J. of Mechanical Science, 25(1): 71-74.

Yu MH and He LN (1991) A new model and theory on yield and failure of materials under complex stress state. In: Mechanical Behaviour of Materials-6, Vol. 3. Pergamon Press: Oxford, pp 841-846.

Yu MH (1992) New System of Strength Theory. Xian Jiaotong University Press: Xi'an, China (in Chinese).

Yu MH (1994) Unified strength theory for geomaterials and its application. Chinese Journal of Geotechinal Engineering, (2): 1-10 (in Chinese, English Abstract).

Yu MH (1998). Twin shear theory and application. Science Press: Beijing (in Chinese).

Yu MH (1999). Engineering Strength Theory. Higher Education Press: Beijing (in Chinese).

Yu MH (2004) Unified Strength Theory and its Applications. Springer: Berlin.

Zhang X, Ding XL and Li SC (2005) Secondary Development of Duncan-Chang Model in ABAQUS Software, J. Yangtze River Scientific Research Institute, 22(4): 45-47 (in Chinese).

Zhuang Z, et al. (1988) Instruction of ABAQUS / Standard. Tsinghua University Press: Beijing (in Chinese).

12

2D Simulation of Normal Penetration Using the Unified Strength Theory

12.1 Introduction

A great deal of researches have been conducted on impact and penetration problems. The penetration studies include various experimental, analytical and computational simulations. "Projectile penetration into a semi-infinite target" by an analytical method using the unified strength theory has been described in (Yu et al., 2009). These studies were done by Li JC (2002), Wei XY (2003) and Wang YB (2004) at Xi'an Jiaotong University, Xi'an China. Systematical results can be obtained by using the unified strength theory. The computational simulation of penetration with Yu's UST (Unified Strength Theory) and AutoDYN for 2D normal penetration, penetration of concrete slabs using UST and SPH (Smoothed Particle Hydrodynamics) methods will be discussed in this chapter. The 3D penetration and perforation will be studied in the next chapter.

In a purpose-built protective building structure, a concrete slab and wall may be required to withstand the effects of missile impact. The impact may be due to a variety of missiles that differ in shape, size and cruising velocity, such as bullets, fragments, tornado-generated missiles, accident generated missiles, etc. Based on the relative deformability between a missile and a target, a missile may be regarded as either a "hard" or "soft" one. For a hard missile, its deformation is considerably smaller than the deformation of the target. Very often, it is regarded as a rigid and non-deformable body. To predict the extent of penetration and/or perforation, there is a wealth of empirical and semi-empirical formulae available. On the other hand, a soft missile deforms considerably compared to the

deformation of the target. The responses of the missile and target are coupled. This renders the prediction more difficult. However, some approximate decoupling methods are available. These methods express the influence of the projectile's deformation as a reduction factor. Most of the empirical methods used in penetration and perforation prediction are solely based on a statistical fit of experimental data.

Nowadays, the investigation of highly dynamic events such as missile impacts and loading by blast waves is supported by numerical calculation. Wave propagation codes or "hydrocodes" have become a valuable tool for analyzing the propagation of stress waves in fluids and solids (Riedel et al., 1999). In general, these hydrocodes are based on well established continuum mechanics principles. The principal advantages of hydrocodes are that they can tackle a wide variety of impact problems, provide detailed information and cope with large displacement. A discrete element model is also used to predict the penetration depth and the perforation caused by a non-deformable missile against a thin reinforced concrete slab (Shui et al., 2009).

In the simulation, the material model plays a vital role. To achieve the accuracy it should be able to capture all major characteristics. On the other hand, a robust numerical procedure should be in place to guarantee the validity and the numerical stability. The Unified Strength Theory (UST) is adopted in defining the material strength effects and constructs dynamic multifold limit/failure surfaces including an elastic limit surface, failure surface and residual failure surface. The proposed model is incorporated into the AutoDYN hydrocode via the user defined subroutine function. The Smooth Particle Hydrodynamics (SPH) procedure seems to offer great promise in making such simulations more practical.

In this chapter, the numerical simulation of concrete against penetration will be described. The UST is implemented into AutoDYN and numerical examples of the penetration of concrete slabs are given. This work was conducted by Dr. Zhou Qiaoqing and Dr. Qiang HF under the supervision of Professor Fan SC at Nanyang Technological University, Singapore. The unified strength theory with parameter b=0.6 is used for simulation of penetration.

A two-dimensional axisymmetric numerical simulation for the projectile-and-target model under high speed impact is also carried out using the Smooth Particle Hydrodynamics (SPH) procedure in this chapter. In the simulation, the available hydrocode AutoDYN is employed with two key enhancements for material modeling. Firstly, an empirical nonlinear equation of state is employed for concrete material. Secondly, the unified strength theory (UST, Yu, 1991; 1992) is adopted in defining the material strength effects, and dynamic multifold limit/failure surfaces including elastic limit surface, failure surface and residual failure surface are constructed. These two enhancements are incorporated into the AutoDYN hydrocode via the user defined subroutine function by Professors Fan and Qiang at Nanyang Technological University, Singapore (Fan and Qiang, 2001; Qiang and Fan, 2002). The results obtained from the numerical simulation are compared with available experimental data. Good agreement is observed. It demonstrates that the proposed model can be used to predict not only the damaged

areas and reduction in velocity of the projectile during the perforation process, but also the debris clouds from the spalling process.

The objectives of this study are:

(1) To develop a new static multi-surface strength material model for static modeling of concrete based on Yu's unified strength theory (Yu's UST).

(2) To calculate some numerical examples on static analysis of a concrete member, and compare the numerical results with the test results.

(3) To develop a dynamic material model for concrete penetration analysis based on Yu's UST and incorporate the developed model into the AutoDYN (2000) through its user's subroutine function.

(4) To simulate the 2D and 3D perforation process of a reinforced concrete slab impacted by a steel projectile.

(5) The 3D simulation of the perforation process and oblique penetration will be described in the next chapter.

12.2 Penetration and Perforation

The physical phenomena associated with a projectile penetrating/perforating a concrete target are very complicated. The nature of the deformations taking place in both the projectile and the target during the penetration process need to be understood. This involves the material properties of both the projectile and the target. It also depends on the impact velocities and the nose shape of the projectile. In the penetration process, the stress waves initiated by the impact play an important role. The subsequent propagation of the stress waves creates a series of events including spalling, scabbing and fracture of the target.

When a projectile hits a target, three types of response can occur. Firstly, the projectile can ricochet, i.e. the projectile rebounds from the impacted surface or it skims the impacted surface with a reduced velocity. Secondly, the projectile can penetrate into the target without completing its passage through the body. Thirdly, perforation can occur when the projectile has sufficient energy to penetrate through the target. Very often, perforation of the target (especially for relatively thin targets) can occur even at an impact velocity well below that required to achieve complete penetration. It is probably due to the scabbing effect, which reduces the effective thickness of the target.

The processes of penetration and perforation of concrete are summarized in Fig. 12.1. Once the initial projectile velocity is large enough to damage the concrete, pieces of its spall from the impact face of the target form a crater, which extends over a considerably greater area than the impact area. As the impact velocity increases, the projectile penetrates deeper and it produces a hole in the concrete with a diameter only slightly greater than that of the projectile diameter. A further increase in the initial projectile velocity results in cracking and then scabbing (ejection) of concrete from the rear surface. The zone of scabbing is generally more extensive but less deep than that of the front spall crater. Since the

ejected concrete pieces (from the rear surface) could themselves constitute a hazard, it is often necessary to define two thicknesses when designing a protective shield: the minimum thickness to prevent perforation and the minimum thickness to prevent scabbing. The Sandia crash test for penetration and perforation of a concrete slab (Zhou, 2002; 2007) is shown in Fig. 12.2.
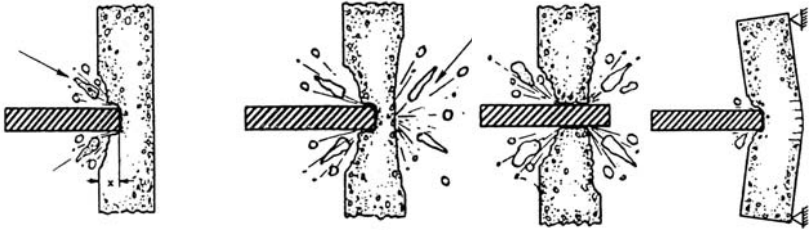
(a) Missile penetration and spalling (b) Target scabbing   (c) Penetration   (d) Overall target response

Fig. 12.1   Penetration and perforation of concrete slabs by non-deforming projectiles (Kennedy, 1976)

Fig. 12.2   A test for penetration and perforation of concrete slab (Sandia crash test)

Plain concrete is generally strong in compression and relatively weak in tension. Therefore, the compressive wave generated in the target does not cause much damage to the target. The failure due to impact is governed by the dynamic tensile strength of the concrete. Spalling occurs at the periphery of the impact area where maximum tensile stress exits (due to the surface stress wave). On the other hand, scabbing is caused by the tensile waves, resulting from the reflection of compressive waves at the free surface. When the compression pulse reaches the rear face of the target, it is reflected as a tensile wave. (This is necessary because the sum of the stresses due to the incident and the reflected waves must vanish at the free surface.) The tensile wave travels back into the target and away from the

rear face. Since the concrete material cannot withstand such large tension, scabbing occurs close to the rear free boundary (Laible, 1980).

The dynamic failure mechanism of concrete is intricate since discontinuities such as cleavage cracks and defects with different shapes and orientations are commonly encountered in concrete and they have significant influence on the deformation and failure characteristics of concrete (Herrmarm, 1969). The initially existing cracks and defects will be nucleated, and will evolve until the material loses strength, when subjected to dynamic loading. The damaged theory has been considered to be more suitable for the cleavage analysis of the concrete material.

How to define the failure criterion of the targets is critical for better analyzing penetration problems (Jonas and Zukas, 1978). The failure criteria such as the Mohr-Coulomb strength theory, the Huber-von Mises criterion and the Tresca yield criterion were often applied to penetration problems, as can be seen from the literature. These criteria do not completely consider all of the stress components in the stress space. The effect of intermediate principal stress is not taken into account in the Tresca criterion and the Mohr-Coulomb strength theory, which are not consistent with the test results of many materials. A unified strength theory, which was suggested by Yu (1991; 1992), considers all of the components in the stress space. It covers a series of strength theories, such as the Mohr-Coulomb's single-shear strength theory and the twin-shear strength theory (Yu, 1985) when the tension and compression strengths of materials are different, as well as the Tresca criterion, the Huber-von Mises criterion and the twin-shear criterion when the tension and compression strengths of materials are identical.

In this research, the unified strength theory is applied to modeling penetration and a unified plasticity-damage penetration model related to the crack density is proposed by Zhou (2002) and Fan-Qiang (2001). The relationship between radial traction and velocity at the cavity-surface can be obtained by analyzing the distributions of stress and velocity of the target material. Based on the cylindrical cavity expansion theory and spatial axisymmetrical unified characteristics line theory (Yu et al., 2001), the attacking capability of a long-rod can be assessed from the derived relation as the rod impacts and penetrates the target with initial velocities of 300~1100 m/s. The results are compared with those of the experiments available in the open literature.

12.3 Constitutive Model of Concrete

The rapid development of computer technology and numerical techniques has provided a powerful tool in the numerical analysis of concrete structures. The material behavior is often expressed by a constitutive law, which should be invoked (Alves, 2000). Once the numerical method is determined, the loading condition and material model are two of the most important points in the numerical simulation. The loading condition subjected to these reinforced concrete (RC) structures can be broadly categorized as two types, static loading and

dynamic loading. According to different loading cases, different numerical simulation methods and different material constitutive models for concrete are required.

In the numerical simulation, putting in place a realistic constitutive model for concrete turns out to be the remaining major obstacle in obtaining a reliable prediction. A lack of adequate models for concrete is one of the major factors hindering the extensive use of numerical methods for reinforced concrete structures. Against this background, the main objective of the present research is to develop a realistic constitutive model for concrete and then implement it in the numerical analysis.

In order to successfully analyze the response of concrete members, the constitutive model for concrete used in the simulation should be appropriate for the characteristics of concrete material under different loading cases. Concrete is a very complex material, consisting of mineral aggregate bound by cement paste containing a large amount of water and voids, which makes the behavior of reinforced concrete material rather complicated. The most important property of concrete material is that it is much weaker in tension compared with its compression strength and thus concrete material easily cracks. Then, cracked concrete shows strong nonlinear behavior. This nonlinear stress, strain behavior in a multiaxial stress state and the post-failure strain-softening behavior are the two most important complexities in modeling concrete material behavior. Because of these complexities, the development of a proper constitutive model describing concrete behavior under all conditions is still a very challenging task facing researchers.

In the constitutive model of concrete material, strength criterion is one of the key points. Although some empirical criteria for concrete such as the Willam-Warnke criterion, Ottosen criterion and Kotsovos-Palovic criterion have proposed practical solutions, a reliable material strength model with sound theoretical background is necessary. The recently developed Yu's unified strength theory (Yu's UST) theory, or twin-shear unified strength theory (TS-UST) (Yu, 1991; 1992; 2004) appeared to be promising. By varying the value of a controlling parameter *b*, Yu's UST theory encompasses many prevailing classic strength criteria as special cases. Though it has a strong mechanics concept, the meridian curve in UST theory is linear, which over-estimates the strength of concrete when it is under high pressure. Against this background, a modified UST theory is developed in the current study. The linear meridians in Yu's UST theory are replaced by empirical curves, meaning Kotsovos' compressive and tensile meridian curves (Kotsovos and Pavlovic, 1995). This logical step leads to a robust semi-empirical, semi·theoretical strength model.

Based on the failure criteria, the concept of a Multi-Surface Strength (MSS) model is developed by Zhou (2002). According to this MSS model, the stress state in concrete can be divided into different stress regions. Inside those regions, different stress-strain relations are constructed accordingly. Based on the concept of the MSS model, both static and dynamic material models for concrete have been developed in the present study.

The mathematical equations of the unified strength theory are

$$F = \sigma_1 - \frac{\alpha}{1+b}(b\sigma_2 + \sigma_3) = \sigma_t, \text{ when } \sigma_2 \leq \frac{\sigma_1 + \alpha\sigma_3}{1+\alpha}, \tag{12.1a}$$

$$F' = \frac{1}{1+b}(\sigma_1 + b\sigma_2) - \alpha\sigma_3 = \sigma_t, \text{ when } \sigma_2 \geq \frac{\sigma_1 + \alpha\sigma_3}{1+\alpha} \tag{12.1b}$$

The three principal stresses can be written in terms of the stress tensor invariant as

$$\begin{Bmatrix} \sigma_1 \\ \sigma_2 \\ \sigma_3 \end{Bmatrix} = \begin{Bmatrix} s_1 \\ s_2 \\ s_3 \end{Bmatrix} + \frac{I_1}{3}\begin{Bmatrix} 1 \\ 1 \\ 1 \end{Bmatrix} = \frac{2\sqrt{J_2}}{\sqrt{3}}\begin{Bmatrix} \cos\theta \\ \cos(\theta - 2\pi/3) \\ \cos(\theta + 2\pi/3) \end{Bmatrix} + \frac{I_1}{3}\begin{Bmatrix} 1 \\ 1 \\ 1 \end{Bmatrix} \tag{12.2}$$

with $\sigma_1 \geq \sigma_2 \geq \sigma_3$.

Therefore, the unified strength theory Eqs. (12.1a) and (12.1b) can be re-written in terms of the invariant notations as

$$F_1 = \frac{I_1}{3}(1-\alpha) + (1+\frac{\alpha}{2})\frac{2}{\sqrt{3}}\sqrt{J_2}\cos\theta + \frac{\alpha(1-b)}{1+b}\sqrt{J_2}\sin\theta = f_t$$

$$\text{when} \quad 0 \leq \theta \leq \theta_b, \tag{12.3a}$$

$$F_2 = \frac{I_1}{3}(1-\alpha) + (\frac{2-b}{1+b}+\alpha)\frac{1}{\sqrt{3}}\sqrt{J_2}\cos\theta + (\alpha + \frac{b}{1+b}r)\sin\theta = f_t$$

$$\text{when} \quad \theta_b \leq \theta \leq 60° \tag{12.3b}$$

where I_1 is the first stress invariant, J_2 is the second deviatoric stress invariant and θ_b is the angle of an angular point of trajectory in the deviatoric plane, which can be calculated from $F_1 = F_2$

$$\theta_b = \arctan\frac{\sqrt{3}}{2\alpha+1} \tag{12.4}$$

The first stress invariant I_1 can be calculated by $I_1 = \sigma_{ii}$, where σ_{ii} is the stress tensor. The second deviatoric stress invariant $J_2 = s_{ij}s_{ij}/2$.

The serial yield loci of the unified strength theory and its special case with $b = 0.6$ are shown in Fig. 12.3.

The yield surface is defined exactly in the same way as the failure surface except that the ultimate tensile strength f_t (in Eqs. (12.3a) and (12.3b)) is replaced by a smaller strength, which defines the elastic limit, namely "yield" strength.
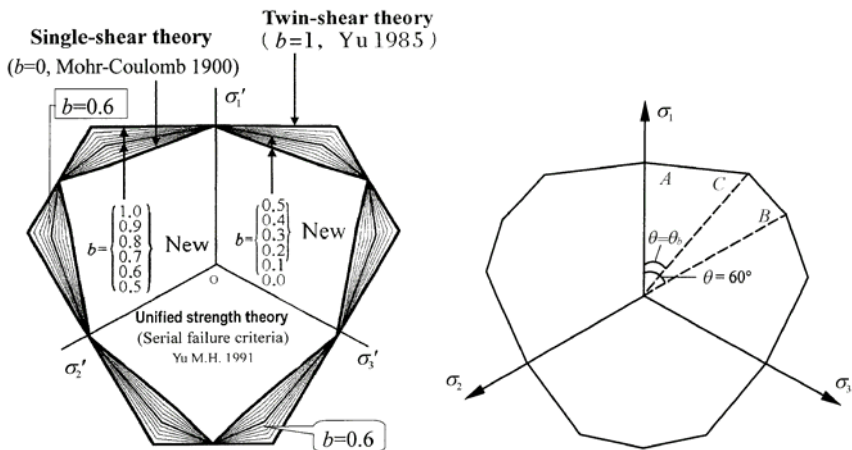
Fig. 12.3   Yield loci of the unified strength theory and its special case with b=0.6

Loading Surface and Work Hardening

Prior to yielding, concrete materials are generally assumed to be in the linear elastic state. Beyond initial yielding, the stress level at which further plastic deformation occurs may be dependent on the current degree of plastic strain. Such a phenomenon is termed 'work hardening' or 'strain hardening'. Therefore, the yield surface will vary at each stage of the plastic deformation and all these subsequent yield surfaces are called "loading surfaces". The progressive development of the loading surfaces can be defined by relating the stresses to the plastic deformation by means of a hardening parameter

$$f(\sigma_{ij}) = K(k) \tag{12.5}$$

where f is a stress function which represents a specific stress level, K is a function of the hardening parameter k and σ_{ij} (i, j=1,2,3) are the components of the stress tensor. Equation (12.5) generates a loading surface in a 3D stress state.

The hardening parameter can be defined in two ways, namely 'work hardening' and 'strain hardening'. In this chapter 'work hardening' is used. The degree of 'work hardening' can be postulated as a function of the total plastic work only. Then

$$k = W_p \tag{12.6}$$

where

$$W_p = \int \sigma_{ij} (d\varepsilon_{ij})_p \tag{12.7}$$

in which $(d\varepsilon_{ij})_p$ are the plastic components of strain occurring during a strain increment. The stress states, when f=k, represent plastic states, while elastic

behavior is characterized by $f<k$. In a plastic state, the incremental change in the yield function due to an incremental stress change is

$$df = \frac{\partial f}{\partial \sigma_{ij}} d\sigma_{ij} \qquad (12.8)$$

Then, if

$f<0$, elastic unloading occurs and the stress point returns inside the yield surface;

$f=0$, means neutral loading and the stress point remains on the yield surface;

$f>0$, means plastic loading and the stress point remains on the expanding yield surface.

Elasto-Plastic Stress-Strain Relation

Beyond initial yielding, the material behavior will be partly elastic and partly plastic. At an increment of stress, the changes in strain are assumed to be decomposed into two components: elastic and plastic components such that

$$d\varepsilon_{ij} = (d\varepsilon_{ij})_e + (d\varepsilon_{ij})_p \qquad (12.9)$$

The elastic strain increment is related to the stress increment. It is assumed that the plastic strain increment is proportional to the stress gradient of the plastic potential g, such that

$$(d\varepsilon_{ij})_p = d\lambda \frac{\partial g}{\partial \sigma_{ij}} \qquad (12.10)$$

where $d\lambda$ is a proportional constant. According to the associated theory of plasticity, it becomes

$$(d\varepsilon_{ij})_p = d\lambda \frac{\partial f}{\partial \sigma_{ij}} \qquad (12.11)$$

where f is the yield function.

Rearranging the yield function Eq. (12.5) leads to

$$F(\sigma_{ij}, \kappa) = f(\sigma_{ij}) - K(\kappa) = 0 \qquad (12.12)$$

Differentiating Eq. (12.12), we have

$$dF = \frac{\partial F}{\partial \sigma_{ij}} d\sigma_{ij} + \frac{\partial F}{\partial \kappa} d\kappa = 0 \qquad (12.13)$$

or

$$\{a\}^{\mathrm{T}} d\sigma_{ij} - A d\lambda = 0 \qquad (12.14)$$

where $\{a\}^{\mathrm{T}}$ is the flow vector, defined as the partial derivative of F with respect to the stress tensor

$$\{a\}^{\mathrm{T}} = \frac{\partial F}{\partial \sigma_{ij}} = [\frac{\partial F}{\partial \sigma_{11}} \frac{\partial F}{\partial \sigma_{22}} \frac{\partial F}{\partial \sigma_{33}} \frac{\partial F}{\partial \sigma_{12}} \frac{\partial F}{\partial \sigma_{23}} \frac{\partial F}{\partial \sigma_{31}}] \qquad (12.15)$$

and

$$A = -\frac{1}{d\lambda} \frac{\partial F}{\partial \kappa} d\kappa \qquad (12.16)$$

Substituting Eq. (12.11) into Eq. (12.9) leads to

$$d\varepsilon_{ij} = [D]^{-1} d\sigma_{ij} + d\lambda \frac{\partial F}{\partial \sigma_{ij}} \qquad (12.17)$$

where [D] is the usual matrix of elastic constants. By pre-multiplying both sides of Eq.(12.17) by $\{a\}^{\mathrm{T}}[D]$ and eliminating $\{a\}^{\mathrm{T}} d\sigma_{ij}$ through Eq.(12.14), the plastic multiplier $d\lambda$ can be obtained as (also Eq. (5.48) in Chapter 5)

$$d\lambda = \frac{1}{A + \{a\}^{\mathrm{T}}[D]\{a\}} \{a\}^{\mathrm{T}}[D] d\{\varepsilon\} \qquad (12.18)$$

Substituting Eq. (12.18) into Eq. (12.17) leads to the complete elasto-plastic incremental stress-strain relation such that

$$d\sigma_{ij} = [D]_{ep} d\varepsilon_{ij} \qquad (12.19)$$

where the matrix of elasto-plastic constants is expressed as (also Eq. (5.50) in Chapter 5)

$$[D]_{ep} = [D] - \frac{[D]\{a\}\{a\}^{\mathrm{T}}[D]^{\mathrm{T}}}{A + \{a\}^{\mathrm{T}}[D]\{a\}} \qquad (12.20)$$

From a thermodynamic viewpoint, the work hardening hypothesis is more general than the strain hardening hypothesis. Therefore, the work hardening

hypothesis is used here,

$$d\kappa = [\sigma]^{\mathrm{T}} d\{\varepsilon\}_p \qquad (12.21)$$

With this hypothesis we can obtain

$$A = H' \qquad (12.22)$$

where H' is the hardening parameter which can be determined experimentally from a simple uniaxial test.

Flow Vector for Numerical Computation and Processing of Corner Singularity

As an alternate form of Eq. (12.15), the flow vector can also be expressed as

$$\{a\} = \frac{\partial F}{\partial \{\sigma\}} = \frac{\partial F}{\partial I_1} \frac{\partial I_1}{\partial \{\sigma\}} + \frac{\partial F}{\partial \sqrt{J_2}} \frac{\partial \sqrt{J_2}}{\partial \{\sigma\}} + \frac{\partial F}{\partial \theta} \frac{\partial \theta}{\partial \{\sigma\}} \qquad (12.23)$$

where

$$\{\sigma\}^{\mathrm{T}} = \{\sigma_{11}\sigma_{22}\sigma_{33}\sigma_{12}\sigma_{23}\sigma_{31}\}$$

When UST theory is used to define the loading surfaces, the flow vector is not uniquely defined at the demarcation points. It occurs at $\theta=0$, $\theta=60°$ and $\theta=\theta_b$. The corresponding points are A, B and C as shown in Fig. 12.4.
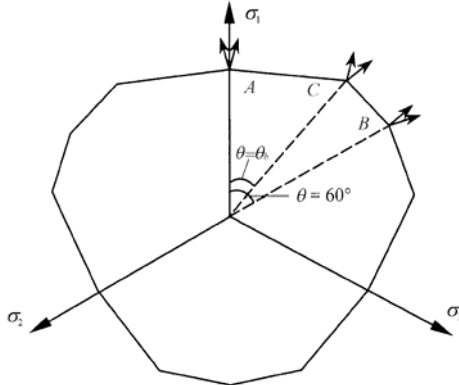
Fig. 12.4 Singular points of UST with $b=0.6$ in the deviatoric plane

It is worth noting that there are two exceptional cases: (1) When b is equal to 1, points A and B are not angular points (see Fig. 12.2). Hence the flow vectors at A and B can be used without any processing. (2) When b is equal to 0, point C is not a singular point (Fig. 12.2) and, accordingly, the corresponding flow vector can be

used without any processing. However, in other cases ($b\neq0$, $b\neq1$), these corner singularities exist. To overcome these, one simple method is to approximate the flow vectors using those in the exceptional cases. That is, the flow vectors at A and B for all cases ($0\leq b\leq1$) are the same as those for $b=1$. Similarly, the flow vectors at C for all cases ($0\leq b\leq1$) are the same as those for $b=0$. The expressions for C_1, C_2, and C_3 for these corners are the same as the description in Chapter 5.

The flow vectors for numerical computation and processing of corner singularity are the same as the processing described in Chapter 5 (Eqs. (5.45) to (5.99)). The corresponding flow vectors are shown in Fig. 12.3.

The UST is generalized to the damage surface study (Zhou, 2002), as shown in Fig. 12.5.
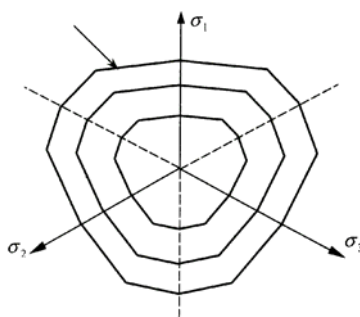
Fig. 12.5   Damage surface based on the UST with $b=0.6$

The dynamic material model for concrete in the present study aims to simulate concrete behavior against penetration. The subject of penetration and perforation has long been of interest in the military field, but it still needs further study because of its complexity. It is a well-known fact that concrete exhibits a rate dependent behavior when subjected to high-speed dynamic loading. As compared with the measured parameters in static tests, it shows a significant increase in dynamic strength and a decrease in non-linearity of the stress-strain response curves. This peculiar behavior is very important under impulsive loading because it dominates the responses of the structure when subjected to impacts (with strain rates $\dot{\varepsilon} > 10^{-2}$ s^{-1}). Observations by others show that the rate-sensitivity is mainly due to the fact that the growth in internal microcracking (for a particular level of strain) is retarded at higher strain-rates. Knowing that the damage to concrete is essentially due to the nucleation and growth of micro voids and micro-cracks, one can deduce that diminishing micro-cracks due to an increasing strain rate will result in a reduction in macroscopic nonlinear behavior and also an increase in dynamic strength (Cervera et al., 1996). Therefore, material models for concrete should be different between the static loading case and dynamic loading case. In other words, the strain rate effect needs to be considered in the dynamic material model for concrete.

In the MSS models developed in the present study, the plastic model and

damage variable are combined to treat the response of concrete at different stress stages. The pre-failure behavior of concrete is modeled by elasto-plastic theory, while the damage model is introduced to treat the post-failure response in order to take account of the degradation of both strength and stiffness. The differences between the static and dynamic versions lie in the definition of the failure surface and the post-failure treatments. In the dynamic version, the strain-rate effect is included in defining the failure surface. In addition, the post-failure behavior follows a kind of isotropic damage model, in which the damage scale is a measure of the accumulated equivalent plain strain. Of course, in the static version no strain-rate effect is considered and the post-failure treatment adopts the Mazars damage model (Mazars, 1986), in which the damage parameter is a measure in the direction of principle stress.

To test and verify Yu's UST-based static models for concrete, some RC beams under static loading are calculated and compared with experimental results. Both two dimensional (2D) and three dimensional (3D) simulations of perforation through a concrete slab are presented to verify the dynamic material model for concrete. These numerical examples show that both the static and the dynamic material models for concrete can be used to simulate the response of a concrete member under different loading cases.

12.4 Penetration and Perforation of Reinforced Concrete Slab

To verify and calibrate the dynamic material model for concrete proposed by Zhou based on the UST and damage theory, numerical simulations were carried out (Zhou, 2002). The specific impact configuration in the experiments set up by Hanchak et al. (1992) was adopted. The target was a 610 mm×610 mm square panel of l78 mm thick reinforced concrete slab. The projectile was an ogival nose shaped 143.7 mm long steel rod having a diameter of 25.4 mm and a 3.0 caliber-radius-head. Hanchack conducted his tests over a range of impact velocities between 300 and 1000 m/s.

Figures 12.6 and 12.7 show the nominal geometric configurations of the steel projectile and the concrete target in Hanchack's tests. An axisymmetric analysis was carried out in the numerical simulation, in which the target is a circular panel of 688.4 mm in diameter. Since the target panel was only lightly reinforced, the effect of the reinforcement would be negligible provided that the projectile impacted on the target somewhere near the center of a space in the reinforcement grid. For this reason, the steel reinforcement bars are not included in the numerical model.
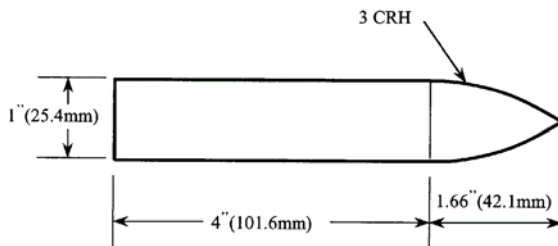
Fig. 12.6   Geometry of the steel projectile
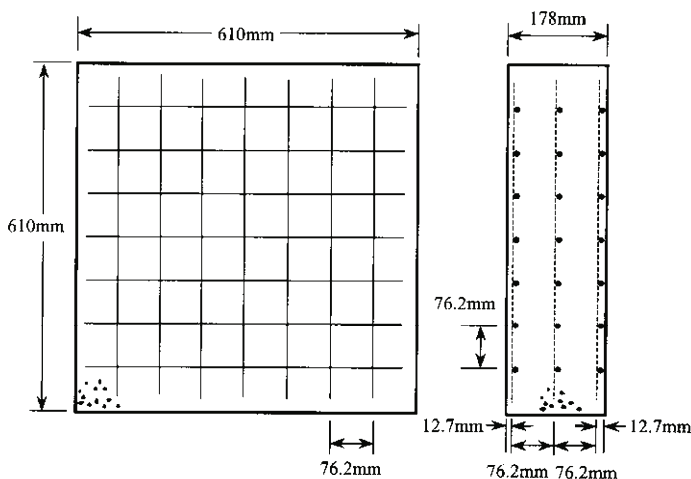
Fig. 12.7   Configuration of concrete target (Zhou, 2002)

The finite element mesh is shown in Fig. 12.8. The mesh for the target has 8000 quadrilateral elements and 8181 nodes. The mesh for the projectile has 504 elements and 559 nodes. Due to symmetry, only half of the target-and-projectile configuration is analyzed.

Post-experimental observations showed little or no damage was inflicted on the projectile. Therefore, as the first-order approximation, the steel projectile was modeled as an elastic-perfectly-plastic material having the following properties (Hanchak et al., 1992): mass density 8020 kg/m^3, bulk modulus 175 GPa, shear modulus 80.8 GPa and yield stress 1.72 GPa. The Huber-von Mises criterion is used as yield criterion for the steel projectile.

Two grades of concrete target were used in the experiments by Hanchak et al. (1992). One set of targets has an unconfined compressive strength of 48.0 MPa while the other set is 140.0 MPa. Only the lower strength concrete target is analyzed here. The material parameters used in the present simulation are shown in Tables 12.1 and 12.2. The piece-wise-linear plastic compaction path for the EOS is defined by five pairs of density to pressure values. Table 12.1 gives the values of these five pairs.

(a) Projectile   (b) Target
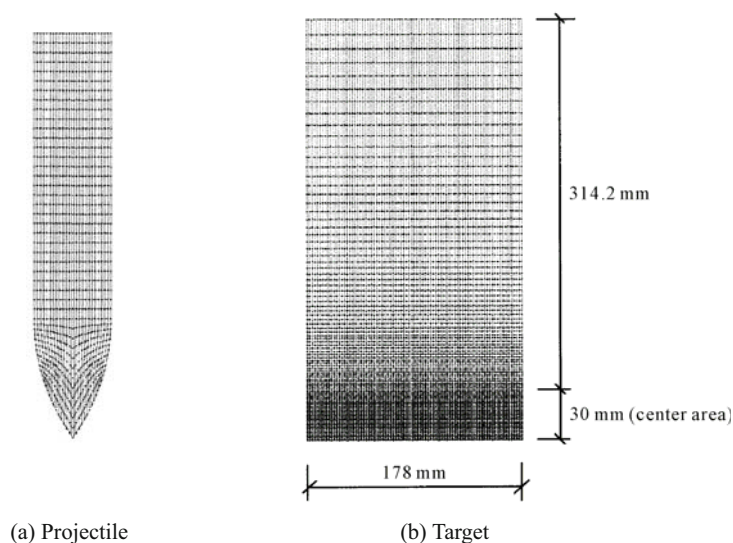
Fig. 12.8   The finite element mesh of the steel projectile and concrete target (Zhou, 2002)

Figure 12.9 shows Hanchack's experimental results of pressure versus volumetric strain and the approximated linearization adopted in Zhou's study (Zhou, 2002).

During the perforation process, some of the Lagrangian elements in the concrete target can become grossly distorted and, unless some remedial actions are taken, can seriously impair the progress of the calculation. To alleviate this problem, a numerical mechanism namely "erosion algorithm" is put in place in the hydrocode Auto-DYNA. A pre-defined strain value is set as the limit strain, beyond which the highly distorted elements will be removed as it progresses. In the present study, erosion is initiated by an incremental geometric strain limit, and a strain value of 300% is set as the limit.

Table 12.1   General material parameters for the concrete target

Parameter	Value	Parameter	Value
Reference density	2430 kg/cm^3	Shear modulus	12.5 GPa
Solid sound speed	2600 m/s	Porous sound speed	2600 m/s
Compressive strength	48 MPa	H'_c	18 GPa
Tensile strength	4 MPa	E	28 GPa
Parameter b of UST	0.6	D_1	0.03
K_{c0}	0.5	D_2	1
K_{t0}	0.9	P_{l0}	40 MPa
H'_t	18 GPa	P_{u0}	55 MPa

Table 12.2   Piece-wise linear porous EOS (pressure versus density)

Density (kg/m^3)	Pressure (MPa)
2305	0
2311.5	30
2321.5	70
2409.1	350
2471.3	644
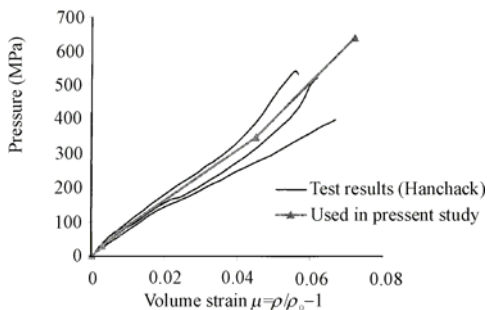
Fig. 12.9   Pressure versus volumetric strain

Hanchack reported his test results with four impact velocities, 1058 m/s, 750 m/s, 434 m/s, 300 m/s. Simulations for these four cases were carried out using Zhou's model i.e. the combination of the UST with $b=0.6$ and damage theory. Figure 12.10 shows the impact velocities versus the residual velocities and compared with Hanchack's results too. Table 12.3 lists the corresponding numerical values. The velocity of the projectile decreases clearly along its path of penetration. The resisting forces arise from the inertia and strength of the target material. Upon perforation, the projectile decouples from the target and its velocity becomes constant. That constant velocity is defined as the residual (or exit) velocity of the projectile. If perforation does not occur, the projectile rests and embeds itself inside the target with zero residual velocity.

Table 12.3   Comparison of exit velocities for perforation of normal RC slab

Impact velocity (m/s)	Exit velocity (m/s) (test result)	Exit velocity (m/s) (numerical result)	Error (%)
300	0	57	——
434	214	219	2.34
750	610	593	2.79
1058	947	920	2.85
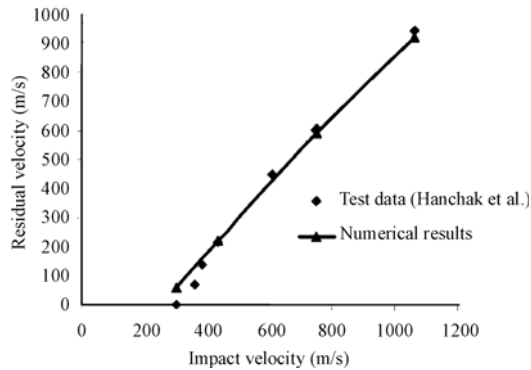
Fig. 12.10   Impact velocity versus residual velocity for test data and numerical results

From Fig. 12.10 and Table 12.3, it can be seen that numerical simulations are in good accord with the experimental results. Apart from the impact velocity of 300 m/s, the relative errors of the numerical results are less than 3%. It is worth noting other details. For illustrative purposes, further details for the case when the impact velocity is 750 m/s are discussed. The detailed procedure of the penetration is also obtained. The contour plots of damage in the concrete target at different time cycles are shown in Fig. 12.11 (Zhou, 2002).

12.5   Perforation of Fibre Reinforced Concrete Slab

Zhou's material model combined with the UST and test data is employed to simulate a fiber-reinforced concrete target. Experiment results are reported by Hansson et al. (2000). The target is a 1.2 m×l.2 m square slab of 0.06 m thick fiber-reinforced concrete, having an unconfined compressive strength of 79.5 MPa and a splitting tensile strength of 7.4 MPa. The modulus of elasticity was taken to be 52.9 GPa and the density 2330 kg/m^3. The projectile is a 43 mm long solid cylinder, having a diameter of 15 mm and a weight of 60 g. It was fabricated from steel SS l4 2541-03 having a 0.2% proof strength of 700 MPa and an ultimate strength between 900 and l 100 MPa. Experimental data are available for two shots fired against the slab at an impact velocity of l637 m/s and l505 m/s respectively.

Since the penetration/perforation process is a highly localized event, it can be simply reduced to a 2D axisymmetrical analysis. As such, the square slab is replaced by a circular plate having a radius of 500 mm. By making use of symmetry, only half of the target-and-projectile section is analyzed. The domain of the target is discretized into 60×100 elements in the finite element model. The size of the element mesh increases gradually and radially away from the center. The projectile is discretized into 44×16 elements. In order to reduce the effect of stress wave reflections from the boundary, a transmissible boundary condition is applied along the peripheral boundaries of the slab.
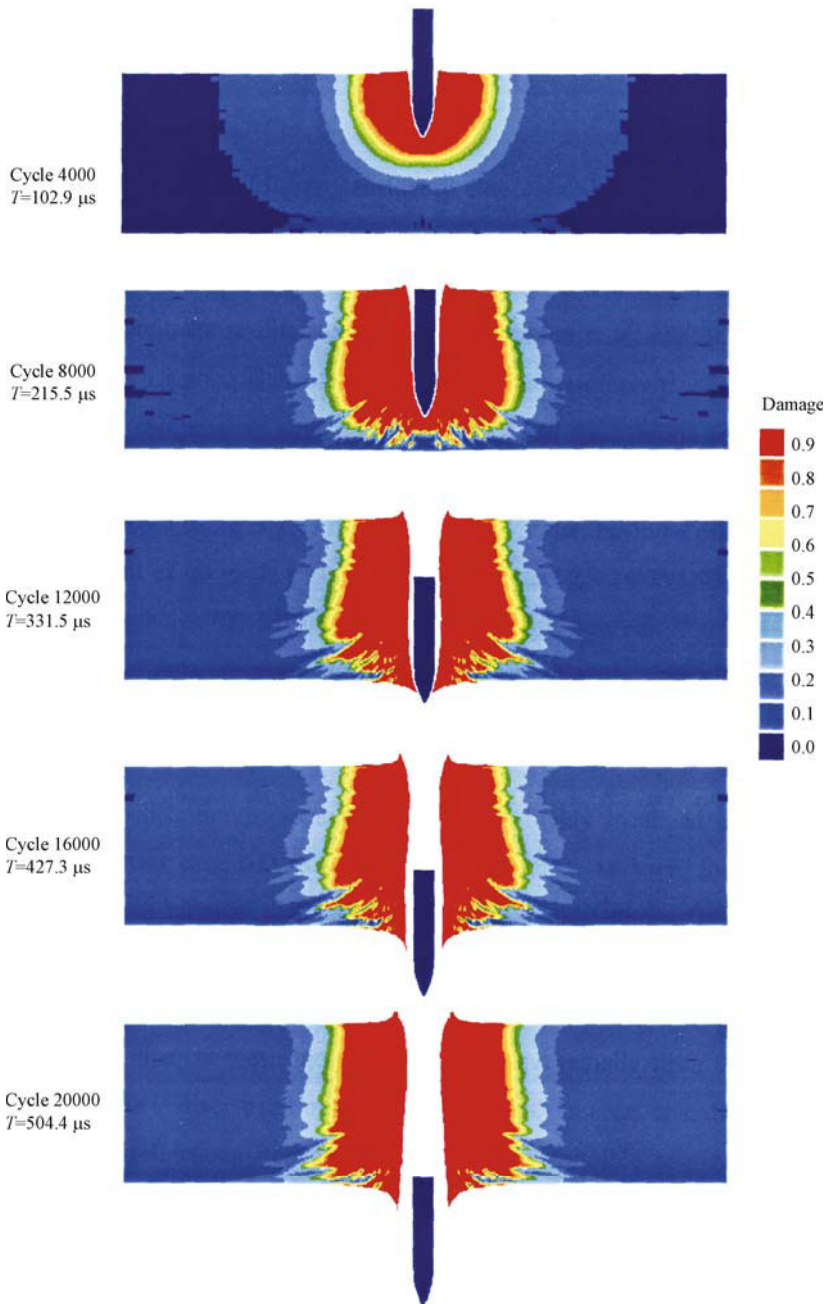
Fig. 12.11   Contour plot of damage at different cycles (v=750 m/s) (Zhou, 2002)

The fiber reinforced concrete is treated as a homogeneous material having similar but slightly different properties, as shown in Table 12.4. The projectile is modeled according to the Johnson & Cook material model for steel. The mechanical properties are based on the typical data for 4340 steel. The material parameters for the steel projectile are shown in Table 12.5 In the simulation, an erosion strain of 500% is adopted.

Table 12.4 General material parameters for the fiber RC target

Parameter	Value	Parameter	Value
Reference density	2410 kg/cm^3	Shear modulus	20.8 GPa
Solid sound speed	2900 m/s	Porous sound speed	2900 m/s
Compressive strength	795 MPa	H'_c	32 GPa
Tensile strength	7.4 MPa	E	50 GPa
UST parameter b	0.6	D_1	0.03
K_{co}	0.5	D_2	1
K_{fo}	0.9	P_{lo}	80 MPa
H'_t	32 GPa	P_{uo}	115 MPa

Table 12.5 Piece-wise linear porous EOS (pressure versus density)

Density(kg/m^3)	Pressure(MPa)
2330	0
2336	20
2346	48
2390	380
2452	650

Simulations are carried out for the two shots having an impact velocity of l503 m/s and l637 m/s. The velocity-history plots for the projectile are shown in Fig. 12.10 and Fig. 12.11, respectively. It can be observed that during the perforation process the velocity of the projectile decreases readily. Upon perforation, the velocity becomes constant. Table 12.6 shows the comparison of exit velocities between the numerical simulations and the test results. Good agreements are observed. Figure 12.12 shows the contour plots of damage at different time steps.
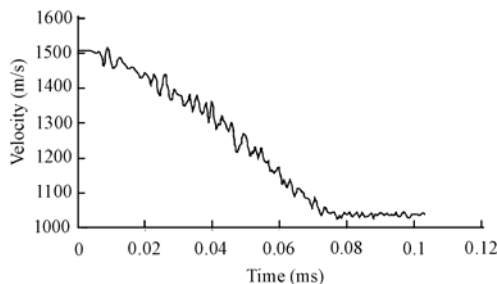
Fig. 12.12 Velocity history of projectile (Fiber RC slab, *v*=1 5 05 m/s)
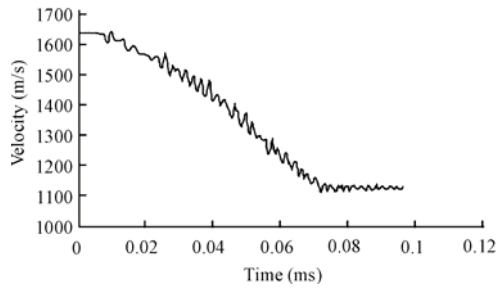
Fig. 12.13   Velocity history of projectile (Fiber RC slab, v=1 637 m/s)
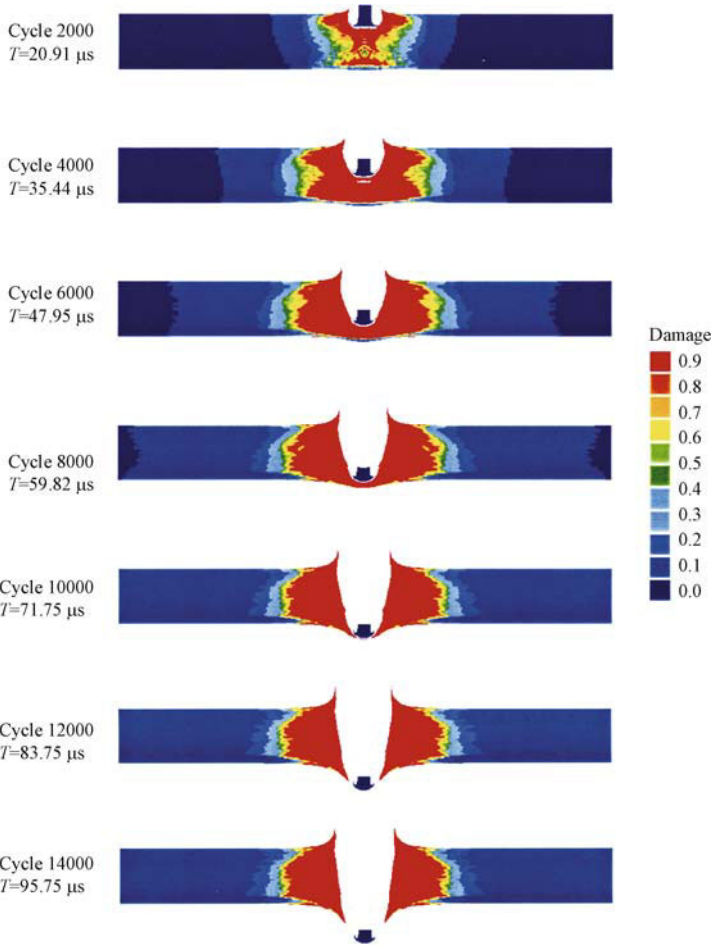
Fig. 12.14   Contour plot of damage at different cycles for fiber RC slab (v=1503 m/s) (Zhou, 2002)

Table 12.6   Material constants for the steel projectile according to Johnson-Coak model

Material constant	Value
Reference density	7830 kg/m^3
Bulk modulus	1 59 GPa
Reference temperature	300 K
Specific heat	477 J/kg
Shear modulus	81.8 GPa
Yield stress	792 MPa
Gardening constant	510 MPa
Hardening exponent	0.26
Strain rate constant	0.014
Thermal softening exponent	1.03
Melting temperature	1793 K

Table 12.7   Comparison of exit velocities for perforation of fiber RC slab

Impact velocity v (m/s)	Exit velocity (m/s)	
	Experimental result	Present simulation
1505	1080	1036
1637	1120	1130

12.6 High Velocity Impact on Concrete Slabs Using UST and SPH Method

The Smoothed Particle Hydrodynamics (SPH) method was first applied by Lucy (1977) to astrophysical problems and was extended by Gingold and Monaghan (1982). Cloutman (1991) has shown that SPH could be used to model hypervelocity impacts. Libersky and Petschek (1991) have shown SPH can be used to model material with strength. Liu et al. (2003) have studied blasting simulation with explosives in fluid media and Liu (2002) has reviewed mesh free methods and introduced this method systematically. In fact, SPH is a gridless Lagrangian technique. The main advantage of the method is to bypass the requirement for a numerical grid to calculate spatial derivatives. This avoids the severe problems associated with mesh tangling and distortion which usually occur in Lagrangian analyses involving large deformation impact and explosive loading events. The grid based methods, such as Lagrange and Euler, assume a connectivity between nodes to construct spatial derivatives. SPH uses a kernel approximation, which is based on randomly distributed interpolation points with no assumptions about which points are neighbours, to calculate spatial derivatives. Here, a dynamic plastic damage model is proposed by Prof. Fan SC and Qiang using UST (Unified Strength theory) and on an RHT concrete model (Riedel et al., 1999). The research was presented by Prof. Fan SC at Sydney, Australia in 2001 (Fan and Qing, 2001) and described below.

12.6.1 Material Model for the Concrete Slab

Dynamic multi-limit surface models based on the unified strength theory are employed here, i.e. the elastic limit surface, failure surface and residual strength surface. The failure surface is a bounding surface, no stress state is allowed to exist beyond it. The shapes of the failure surface could be changed in the stress space during the impact process. However, the loading surface changes its shape non-uniformly from the initial surface to the failure surface with the development of the effective plastic strain. Once the failure surface is reached, the residual strength surface is determined according to the scalar damage value.

Based on this consideration, the dynamic material model is proposed. The main characteristics of this model are:

1) Strain-rate dependent failure surface is considered.
2) UST theory is employed in the failure surface.
3) Linear strain hardening is used to impose the plastic flow consideration.
4) Isotropic damage is used in this model due to increased strain after the stress in the reached failure surface.

12.6.2 The Failure Surface

Amongst the strength models available, UST theory has a clear mechanical concept and simple mathematical formula. The advantage of the UST theory is that it takes account of the second principal stress on the material strength. However, the Huber-von Mises criterion is based on the average principal stresses while the Mohr-Coulomb criterion neglects the intermediate principal stresses. The envelope is then completed by defining a piece-wise linear interpolation function in the deviatoric plane. The beauty of the twin-shear-unified strength theory is its feasibility in defining the convex shape of the surface. Setting the value of the controllable convex parameter b to 0 or 1 yields the lower and upper limit of the convex shape function. For any arbitrary value of b, the shape function can be written in the following form.

$$R_f = \frac{r_t r_c \sin 60°}{r_t \sin\theta + r_c \sin(60°-\theta)}(1-b)+b\frac{r_t}{\cos\theta} \quad \text{when} \quad 0° \leq \theta \leq \theta_b \qquad (12.24a)$$

$$R_f = \frac{r_t r_c \sin 60°}{r_t \sin\theta + r_c \sin(60°-\theta)}(1-b)+b\frac{r_t}{\cos(60°-\theta)} \quad \text{when} \quad \theta_b \leq \theta \leq 60° \qquad (12.24b)$$

where J_2 and J_3 are the second and third stress invariants respectively, r_t and r_c are the tensile and compressive meridians respectively.

$$\theta_b = \arctan\left[\frac{1}{\sqrt{3}}\left(\frac{2r_c}{r_t}-1\right)\right], \cos 3\theta = \frac{3\sqrt{3}}{2}\frac{J_3}{\sqrt{J_2^3}} \tag{12.25}$$

It is worth noting that the unified strength theory parameter b reflects the influence of the intermediate principal stress on the material strength. Besides, it encompasses all prevailing yield or failure criteria. When $b=0$ it can represent the Tresca criterion; when $b=0.5$ it is equivalent to the Huber-von Mises criterion. The shapes represented by different values of b in the deviatoric plane and multi-limit surface in the meridian plane are shown in Fig. 12.15 and Fig. 12.16. In the present investigation, the unified strength theory parameter b is set to $b=0.6$.
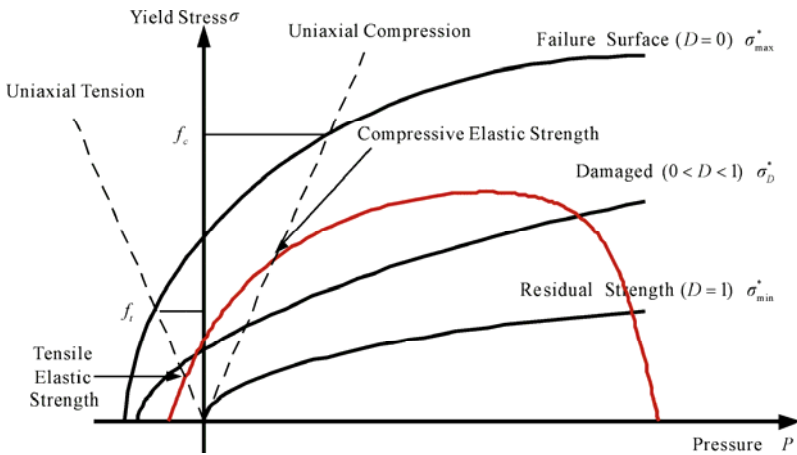
Fig. 12.15 Multi-limit surface in meridian projection
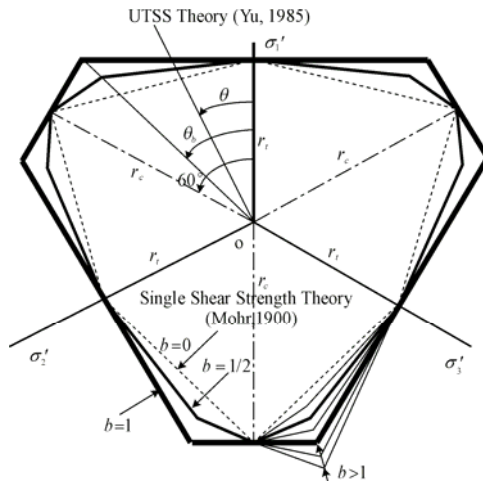
Fig. 12.16 Multi-limit surface in deviatoric projection

The failure surface is defined as a function of pressure P, the Lode stress angle θ and strain rate $\dot{\varepsilon}$.

$$Y_{fail} = Y_{TXC(P)} \cdot R_f \cdot F_{RATE(\dot{\varepsilon})} \tag{12.26}$$

where $Y_{TXC} = f_c \left| A(P^* - P^*_{spall} F_{RATE})^N \right|$, in which f_c is compressive strength; A is failure surface constant; N is failure surface exponent; P^* is pressure normalized by f_c; P^*_{spall} is defined as $P^* (f_t / f_c)$.

$$F_{RATE} = \begin{cases} \left(\dfrac{\dot{\varepsilon}}{\dot{\varepsilon}_0} \right)^D & \text{for} \quad P > \dfrac{1}{3} f_c \quad \text{(compression)} \\[4mm] \left(\dfrac{\dot{\varepsilon}}{\dot{\varepsilon}_0} \right)^a & \text{for} \quad P < \dfrac{1}{3} f_t \quad \text{(tension)} \end{cases}$$

in which D is the compressive strain rate factor exponent; a is the tensile strain factor exponent.

12.6.3 The Elastic Limit Surface

The elastic limit surface is scaled from the failure surface using

$$Y_{elastic} = Y_{fail} \cdot F_{elastic} \cdot F_{CAP(P)} \tag{12.27}$$

where $F_{elastic}$ is the ratio of the elastic strength to failure surface strength. This is derived from two material parameters, tensile elastic strength f_t and compressive elastic strength f_c. $F_{CAP(P)}$ is a function that limits the elastic deviatoric stresses under hydrostatic compression via

$$F_{CAP} = \begin{cases} 1 & \text{for} \quad P \leq P_u \\[3mm] \sqrt{1 - \left(\dfrac{P - P_u}{P_0 - P_u} \right)^2} & \text{for} \quad P_u < P < P_0 \\[3mm] 0 & \text{for} \quad P_0 < P \end{cases} \tag{12.28}$$

12.6.4 Strain Hardening

Linear hardening is used prior to the peak load. During hardening, the current yield surface (Y^*) is scaled between the elastic limit surface and the failure surface via

$$Y^* = Y_{elastic} + \frac{\varepsilon_{pl}}{\varepsilon_{pl(pre\text{-}softening)}} (Y_{failure} - Y_{elastic}) \tag{12.29}$$

where

$$\varepsilon_{pl(pre\text{-}softening)} = \frac{Y_{fail} - Y_{elastic}}{3G} \left(\frac{G_{elastic}}{G_{elastic} - G_{plastic}} \right) \cdot G_{elastic} / (G_{elastic} - G_{plastic})$$

is defined by the user.

12.6.5 Residual Failure Surface

A residual (frictional) failure surface is defined as

$$Y^*_{residual} = BP^{*M} \tag{12.30}$$

where B is the residual failure surface constant; M is the residual failure surface exponent.

12.6.6 Damage Model

Following on from the hardening phase, additional plastic straining of the material leads to damage and strength reduction, as shown in Fig. 12.5. The residual strength is described by a so-called "cumulative damage model" (Persson, 1990). Damage is accumulated via

$$D = \sum \frac{\Delta \varepsilon_{pl}}{\varepsilon_p^{failure}} \tag{12.31}$$

$$\varepsilon_p^{failure} = D_1 (P^* - P^*_{spall})^{D_2} \geq \varepsilon_f^{min} \tag{12.32}$$

where D_1 and D_2 are damage constants; $\varepsilon_f^{\min}$ is the minimum strain to failure.

The post-damaged failure surface is then interpolated via

$$Y_{fractured}^* = (1-D)Y_{failure}^* + DY_{residual}^* \tag{12.33}$$

and the post-damaged shear modulus is interpolated via

$$G_{fractured} = (1-D)G + DG_{residual} \tag{12.34}$$

where $G_{residual}$ is the G^*, the residual shear modulus fraction.

12.7 Numerical Example

To verify and calibrate the present model, a numerical simulation was carried out by Prof. Fan SC and Qiang (2001), which is to illustrate the results of the enhancements incorporated using the SPH method and UST model. It adopts the same configuration and materials used in the tests by Hanchak et al. (1992). The target is a 680 mm×680 mm square of a 178 mm thick reinforced concrete panel. The projectile is an ogival nose shaped 143.7mm long steel rod with a diameter of 25.4 mm and a 3.0 caliber-radius-head. The impact velocities vary between 300 and 1058 m/s. The experimental results are compared with simulation results in the present investigation, and the unconfined compressive strength of concrete is 48 MPa. For other parameters for the material model refer to Riedel et al. (1999).

In the simulation, both the projectile and the target regions are modeled using SPH. In order to simplify it to a 2D axisymmetric analysis, the square panel is approximated by a circular one of radius 303 mm. The target is discretized into 13528 particles while the projectile is represented by 1678 particles. The panel is lightly reinforced. However, Hanchak's results verify that the small amount of reinforcement does not have a major influence on the penetration resistance. Therefore, the steel bars are ignored in the modeling. An evenly spaced particle-model of SPH for concrete target and steel projectile is shown in Fig. 12.17.

The material model for the projectile adopts the linear EOS and the Johnson & Cook strength model. The mechanical properties are based on the AutoDYN's material library for steel 4340: initial density ρ_0=8.1 g/cm^3, bulk modulus K=159 GPa, shear modulus G=81.8 GPa, yield stress f_y=792 MPa etc.
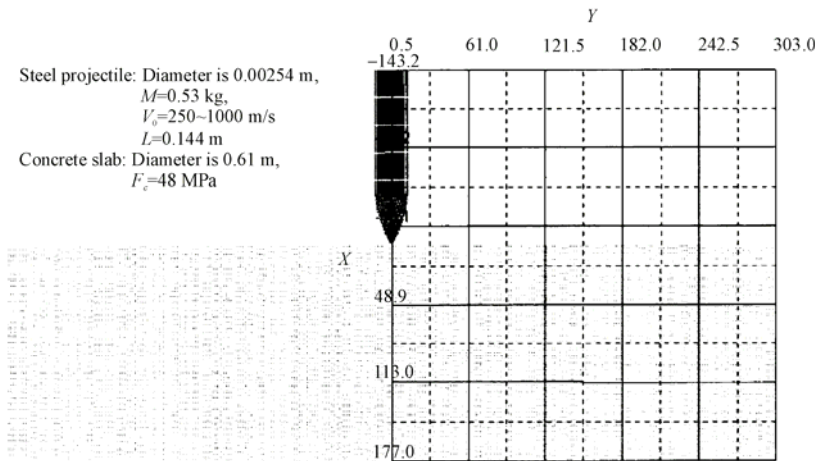
Fig. 12.17 Evenly spaced particle-model of SPH for concrete target and steel projectile

The same EOS is adopted for the concrete slab, only the bulk modulus K is different. The exit velocities and corresponding penetration depths of the projectile are shown in Table 12.8. The decrease in the velocity of the projectile is due to resistance by the target. After perforation (the target is a 680 mm×680 mm square, 178 mm thick), the velocity of the projectile remains constant because the target material can no longer offer any resistance (cases 1 and 2). This constant velocity is defined as the residual (or exit) velocity of the projectile. If perforation did not occur, the projectile would have come to rest and be embedded inside the target with zero residual velocity (case 4). Meanwhile, the reduction in the projectile velocity is recorded over the penetration depth and compared to the residual velocities measured in the normal strength concrete tests (f_c=48 MPa). At high initial velocities, the results of the dynamic constitutive law match the experimental values very closely. A ballistic limit of about 301 m/s is also correctly predicted in the simulation (case 4).

Table 12.8 Comparison of exit velocities and penetration depths

s/n	Impact velocity (m/s)	Exit (residual) velocity (m/s)		Simulation depths (mm)
		Test (Hanchak)	Simulation	
(1)	1058	947	950	178
(2)	749	615	625	178
(3)	360	67	71.5	174
(4)	301	0	0	163

The distribution of the compressive damage for the constitutive theory, with or without its dynamic part, emphasizes the importance of a realistic consideration of the strain-rate effect. In Fig. 12.18 the contour plots of the compressive damage

for time steps during a 750 m/s impact are shown. At the same time, the dynamic constitutive law exhibits a rather homogeneous damage distribution.
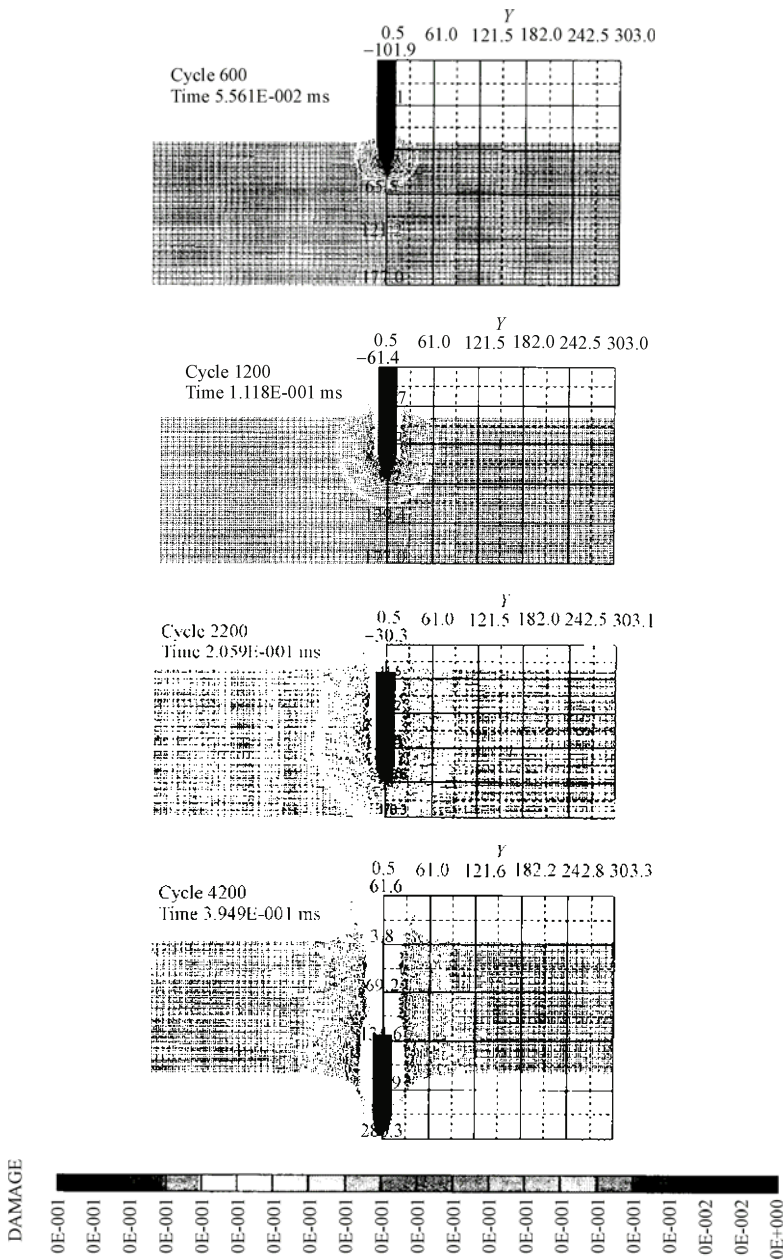
Fig. 12.18   Contour plots at selected time steps (Fan SC and Qiang, 2001)

The SPH procedure is employed by Fan and Qiang (2001) to simulate the impact-penetration process of a hard steel projectile onto/through a concrete target. A nonlinear equation of state and an improved strength criterion for concrete material are incorporated. The strength criterion takes account of the influence of the intermediate principal stress. The SPH procedure does not experience any numerical instability problem. The numerical simulations with the two enhancements yield results in good agreement with the experimental ones. The contour plot at the final step is shown in Fig. 12.19.
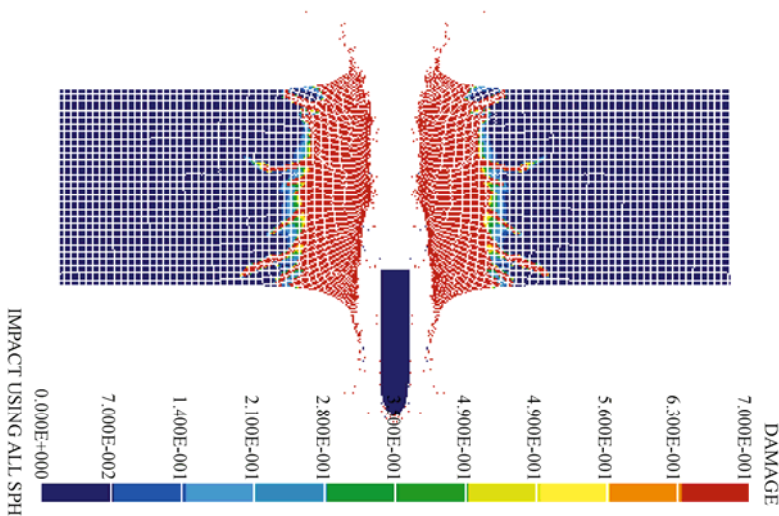
Fig. 12.19   Damaged contour plot at final step (Fan and Qiang, 2001)

12.8   Brief Summary

The UST (Unified Strength Theory) is implemented in AutoDYN and numerical examples of penetration of concrete slabs are given. The unified strength theory with parameter $b=0.6$ is used for simulation of penetration in three examples.

The numerical simulation of the penetration/perforation process of a concrete slab by a cylindrical steel projectile using the FE method and smoothed particle hydrodynamics (SPH) method is studied in this chapter. In the simulation, the available hydrocode AutoDYN-2D is employed with an improved RHT concrete model, in which unified strength theory (UST) or Yu's unified strength theory (Yu UST) is adopted in defining the material strength effects, and dynamic multifold limit/failure surfaces including elastic limit surface, failure surface and residual failure surface are constructed. The proposed model is incorporated into the AutoDYN hydrocode via the user

defined subroutine function. The results obtained from the numerical simulation are compared with available experimental ones. Good agreement is observed. It demonstrates that the proposed model can be used to predict not only the damaged areas and velocity reduction of the projectile during the perforation process, but also the debris clouds from the spalling process.

A multi-limit surface dynamic plastic damage model is developed based on the RHT model using UST theory. The present material model was coded and incorporated into AutoDYN. The numerical simulation was carried out for a case of perforation through a concrete slab by a steel projectile. Numerical results were compared with experimental results by others. They agreed favourably. It demonstrates that the present model could be used to predict not only the damaged areas and the velocity-decrease of the projectile during the perforation process but also the debris clouds from the spalling process, with an acceptable degree of accuracy.

References

Alves M (2000) Material constitutive law for large strain and strain rates. J. Engineering Mechanics, 126(2): 215-218.

AutoDYN (2000) Theory Manual. Century Dynamics Inc.

Cervera M, Oliver J and Manzoli O (1996) A rate dependent isotropic damage model for the seismic analysis of concrete dams. Earthquake Engineering and Structural Dynamics, 25: 987-1010.

Cloutman LD (1991) SPH simulations of hypervelocity impacts. Lawrence Livermore National Laboratory, UCRL-ID-105520.

Fan SC and Qiang HF(2001) Normal high-velocity impaction concrete slabs-a simulation using the meshless SPH procedures. In: Computational Mechanics–New Frontiers for New Millennium, Valliappan S. and Khalili N. eds. Elsevier Science Ltd., pp 1457-1462.

Gingold RA and Monaghan JJ (1982) Kernel estimates as a basis for general particle methods in hydrodynamics. Journal of Computational Physics, 46(4): 429-453.

Hansson H and Agardh L (2000) Experimental and numerical studies of projectile perforation in concrete targets. Structural Failure and Plasticity, Editors：Zhao XL and Grzebieta. Elsevier Science Ltd.115-120.

Hanchak SJ, Forrestal MJ, Young ER and Ehrgott JQ (1992) Perforation of concrete slabs with 40MPa and 140 MPa unconfined compressive strengths. Int. J. of Impact Engineering, 12(1):1-7.

Herrmarm W (1969) Constitutive equation for the dynamic companion of ductile porous material. J. of Applied Physics, 40(6): 2490-2499.

Jonas GH and Zukas JA (1978) Mechanics of penetration: analysis and experiment. Int. J. of Engineering Science, 16: 879-903.

Kennedy RP (1976) Review of procedures for the analysis and design of concrete structures to resist missile impact effects. Nuclear Engineering and Design, 37:183-203.

Kotsovos MD and Pavlovic MN (1995) Structural Concrete, Finite Element Analysis for Limit State Design. Thomas Telford Publications: London.

Laible RC (1980) Ballistic Materials and Penetration Mechanics: Methods and Phenomena. Elsevier: Amsterdam.

Li JC (2001) Investigation of high velocity long rod penetrating semi-infinite concrete target. PhD. Thesis, Xi'an Jiaotong University, Xi'an, China (in Chinese, English abstract).

Libersky LD and Petscheck AG (1991) Smoothed particle hydrodynamics with strength of materials. Proceedings of the Next Free Lagrange Conf. Springer-Verlag: NY, pp 248-257.

Liu MB, Liu GR, Zong Z and Lam KY (2003) Computer simulation of the high explosive explosion using smoothed particle hydrodynamics methodology. Computers & Fluids, 32(3): 305-322.

Liu GR (2002) Mesh Free Methods: moving beyond the finite element method. CRC press: Boca Raton.

Lucy LB (1977) A numerical approach to the testing of the fission hypothesis. The Astronomical Journal, 82(12): 1013-1024.

Mazars J (1986) A description of micro- and macroscale damage of concrete structures. Engineering Fracture Mechanics, 25(5-6): 729-737.

Persson AKE(1990) CMl-A Simple Model for the dynamic deformation and failure properties of brittle materials. Dynamic Research AB Report: Sweden.

Qiang HF and Fan SC (2002) Numerical simulation of perforation of concrete slabs by steel rods using SPH method . The 2nd International Conference on Structural Stability and Dynamics. December 16-18, Singapore.

Riedel W, Thoma K, Hiermaier S and Schmolinske E (1999) Penetration of reinforced concrete by BETA-B-500-Numerical analysis using a new macroscopic concrete model for hydrocodes, Proceedings of 9th Int. Symp. IEMS, Berlin, pp 315-322.

Shiu WJ, Donzé FV and Daudeville L (2009) Influence of the reinforcement on penetration and perforation of concrete targets: A discrete element analysis. Engineering Computations: International Journal for Computer-Aided Engineering and Software, 26(1/2): 29-45.

Wang YB (2003) Research in Structural Impacting Problems based on Unified Strength Theory. PhD. thesis, Xi'an Jiaotong University, Xi'an, China (in Chinese, English abstract).

Wei XY (2002) Investigation of Long Rod Penetrating Target. PhD. thesis, Xi'an Jiaotong University, Xi'an, China (in Chinese, English abstract).

Yu MH, He LN and Song LY (1985) Twin shear stress theory and its generalization. Scientia Sinica (Sciences in China), English Edition, Series A, 28(11): 1174-1183.

Yu MH and He LN (1991) A new model and theory on yield and failure of materials under the complex stress state. In: Mechanical Behavior of

Materials-6, (ICM-6). Jono M and Inoue T ed., Pergamon Press: Oxford, Vol. 3, pp 841-846.

Yu MH (1992) New System for Strength Theory. Xi'an Jiaotong University Press: Xi'an, China (in Chinese).

Yu MH (1998) Twin Shear Theory and its Applications.   Science Press: Beijing (in Chinese).

Yu MH (2002) Concrete Strength Theory and its Applications. Higher Education Press: Beijing (in Chinese).

Yu MH (2002) Advances in strength theories for materials under complex stress state in the 20th Century. Applied Mechanics Reviews, 55(3): 169-218.

Yu MH (2004) Unified Strength Theory and its Applications. Springer: Berlin.

Yu MH, et al (2006) Generalized Plasticity. Springer: Berlin.

Zhou XQ (2002) Numerical Analysis of Reinforcement Concrete Using Multi-Surface Strength Model. Doctoral thesis at Nanyang Technological University, Singapore.

Zhou XQ, Hao H, Li ZX (2007) Numerical simulation of an underground structure under a hypothetic terrorist bombing. Journal of PLA University of Science and Technology (Natural Science Edition), 8(6): 567-572 (in Chinese).

13

3D Simulation of Normal and Oblique Penetration and Perforation

13.1 Introduction

The 2D simulation of normal penetration has been described in Chapter 12. The same problem is re-investigated through 3D simulation using the model proposed by Zhou at Nanyang Technological University (NTU), Singapore, which is the combination of the unified strength theory (Yu, 1998; 2004) and the experimental data.

The 3D simulation of oblique penetration and the perforation process through a concrete slab was also simulated by Zhou XQ at NTU, Singapore in 2002. The unified strength theory with parameter b=0.6 (Fig. 12.3) is implemented in AutDYN (2000) and used again for simulation of the penetration problem.

13.2 Simulation of Normal Impact Process

In this section,the same problem in section 12.3 is investigated through 3D simulation using the present model. Figure 13.1 shows the 3D finite element mesh used in the numerical model. In Fig. 13.1, three front layers of concrete elements are removed to show the reinforcement grid. The structure is modeled by 48×48×14 brick concrete elements and 3 layers of 8×8 beam reinforcement elements.

This chapter is contributed by Prof. Zhou XQ
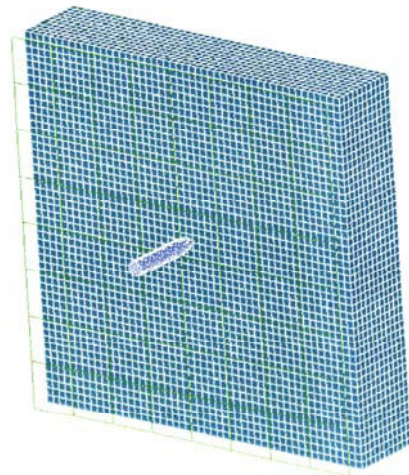
Fig. 13.1   The FE-mesh used in the 3D numerical simulation (Zhou, 2002)

The results of simulation using the UST with b=0.6 are obtained. The material status at different time cycles is shown in Figs. 13.2 to 13.8 (Zhou, 2002).
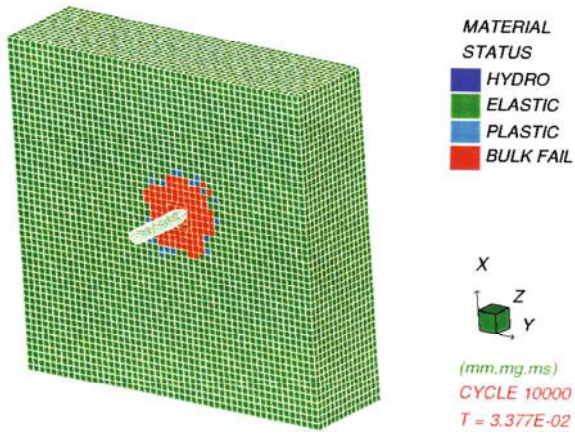
Fig. 13.2   Material status at cycle 10000 (Zhou, 2002)
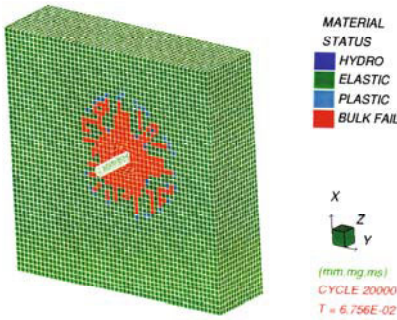
Fig. 13.3   Material status at cycle 20000
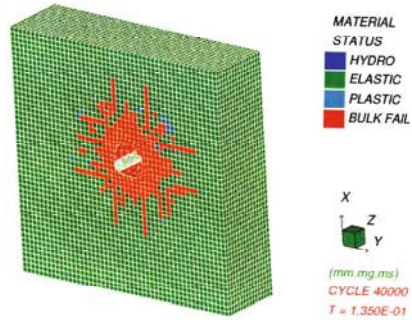
Fig. 13.4   Material status at cycle 40000
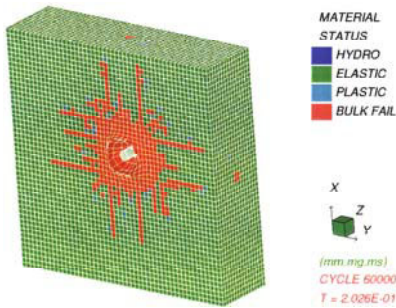
Fig. 13.5   Material status at cycle 60000
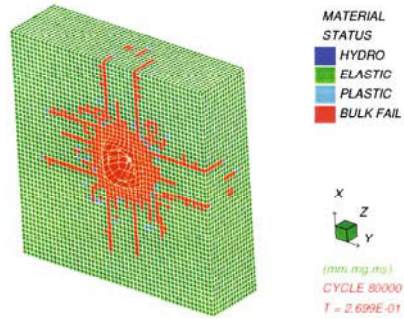
Fig. 13.6   Material status at cycle 80000
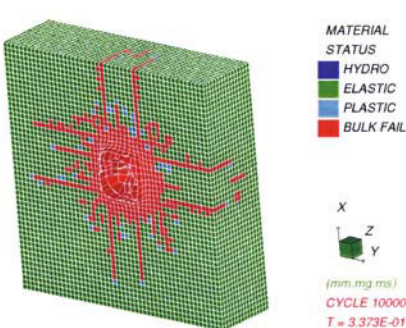
Fig. 13.7   Material status at cycle
100000 (impact surface)
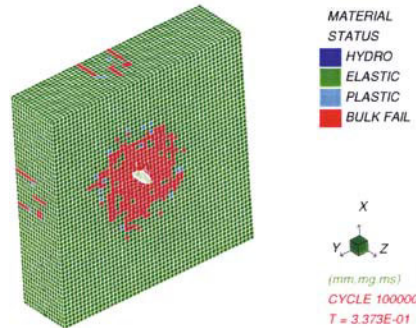
Fig. 13.8   Material status at cycle
100000 (exit surface)

Figures 13.9 and 13.10 reproduce Hanchak's post-test photographs revealing the damage to the front (impact) surface and the rear (exit) surface respectively. By comparing the size of the damaged areas shown in Figs. 13.9 and 13.10 with those in the post-test photographs in Figs. 13.9 and 13.10, the following can be seen.

(1) On the impact surface, the size of the damaged crater obtained by numerical simulation agrees fairly well with that shown in the post-test

photograph (see Figs. 13.7 and 13.9a);

(2) On the exit surface, the size of the damaged crater obtained from numerical simulation is slightly smaller than that shown in the post-test photograph (see Figs. 13.8 and 13.9b).

(a) Impact surface   (b) Rear surface
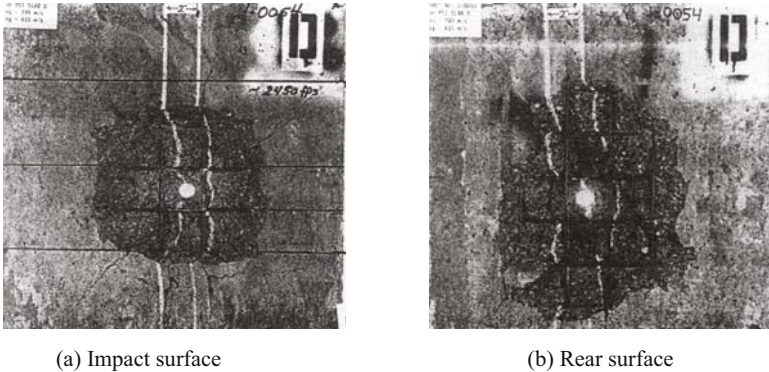
Fig. 13.9   Post-test photograph

The velocity history of the projectile is shown in Fig. 13.10. It can be observed that the exit velocity is about 575 m/s, which is about 5%-6% lower than the experimental result of 610 m/s. Against this background, an alternate 3D simulation with reinforcement omitted was carried out, and the exit velocity becomes 625 m/s (2%-3%higher than 610 m/s). It suggests that the strengthening effect derived from the steel reinforcement bars is over-estimated. This is due to the assumption of perfect bonding between the steel bars and their surrounding concrete (even though they are only pin-jointed at the nodes). However, it shows that the effect of reinforcement bars is minimal.
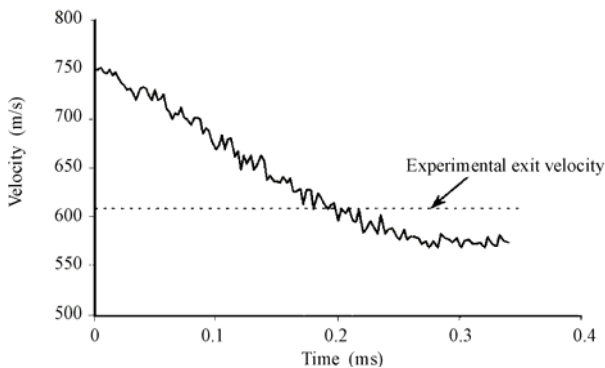
Fig. 13.10   Velocity history of projectile

13.3 Simulation of Oblique Impact Process

The oblique perforation process through a concrete slab has to be a 3D simulation. The impact configurations match those in the experimental tests carried out by Buzaud et al. (1999) in France. The concrete slab is 3000 mm square and has a thickness of 600 mm. The high-strength steel projectile hits the center of the slab at a velocity of 338 m/s with a 30° angle of incidence (measured in the horizontal plane) and a 0° angle of attack (measured in the vertical plane).

Figure 13.11 shows the geometric configurations of the projectile. The projectile was machined out of a 35NCDl6 high strength steel rod with an elasticity limit of l300 MPa. Having a total length of 960 mm and a diameter of l60 mm, its nose is tangent ogive shape with a Caliber Radius Head (CRH) of 6. The thickness of the afterbody is between 17 and 20 mm.
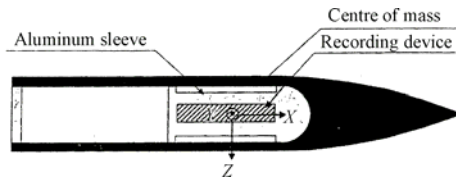
Fig. 13.11   Geometry of the steel projectile

The geometric configuration of the reinforced concrete target is shown in Fig. 13.12. The target is reinforced by a layer of ϕ16 mm high-adherence steel bars at a
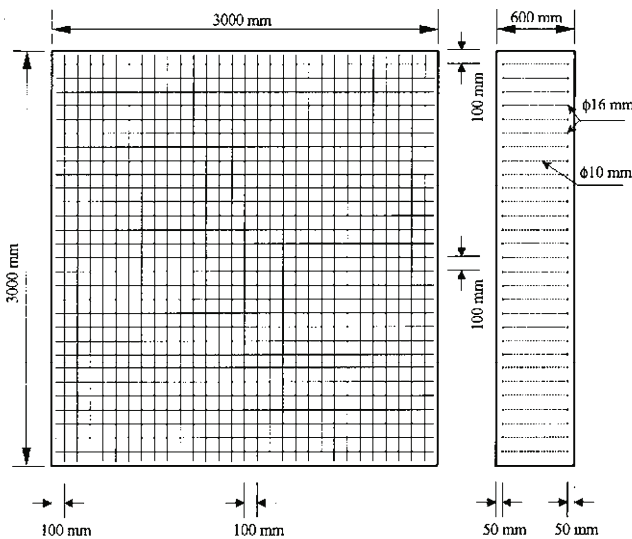
Fig. 13.12   Configuration of concrete target (Zhou, 2002)

distance of 50 mm from the front and another layer at the rear face. The spacing between the ϕ16 mm bars is l00 mm in both directions. The two meshes are bound together by ϕ10 mm high-adherence stirrups at each node. The steel-to-concrete area ratio is 0.67%, which is regarded as light reinforcement to the concrete slab. Against this background, as guided by the experience of previous simulations, the reinforcement bars are not included in the simulation.

Tables 13.1 and 13.2 give the material constants for the concrete. The erosion limit for the incremental geometric strain is set at 150%. It is worth noting that a smaller erosion limit is necessary in 3D simulation. Otherwise, a numerical stability problem may occur and the computation process may stall due to excessive element distortion.

Table 13.1   General material parameters for concrete target

Parameter	Value	Parameter	Value
Reference density	2454.2 kg/m^3	Shear modulus	8.4 GPa
Solid sound speed	2693.17 m/s	Porous sound speed	2693.17 m/s
Compressive strength	43 MPa	H_t'	15 GPa
Tensile strength	4.0 MPa	E	20 GPa
Parameter of the UST, b	0.6	D_1	0.03
K_{co}	0.5	D_2	1.0
K_{t0}	0.9	P_{lo}	40 MPa
H_t'	15 GPa	P_{uo}	55 MPa

Table 13.2   Piece-wise linear porous EOS (pressure versus density)

Density (kg/m^3)	Pressure (MPa)
2368	0
2378	44
2411	180
2446.5	333

Figure 13.13 shows the finite element mesh for the projectile and the target. Figures 13.14–13.21 show the material status at different time cycles (Zhou, 2002).
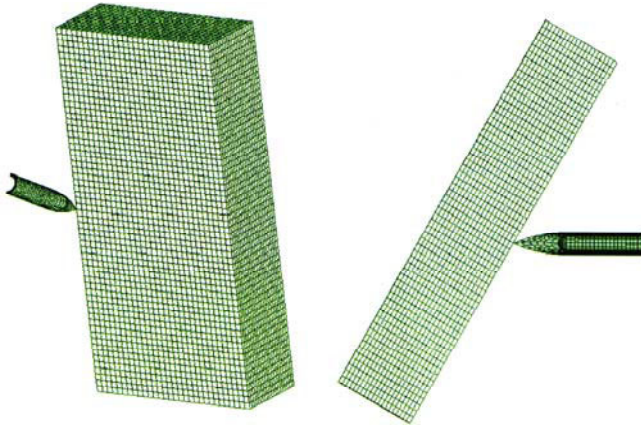
Fig. 13.13 The finite element mesh used in the numerical simulation (Zhou, 2002)
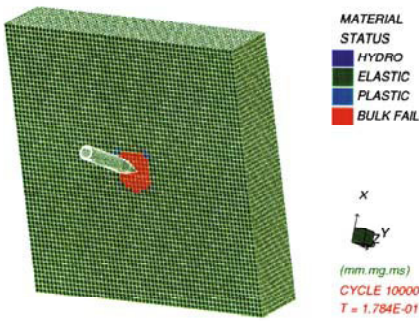
Fig. 13.14 Material status at cycle 10000   **Fig. 13.15** Material status at cycle 50000
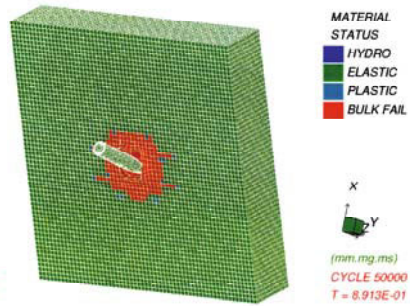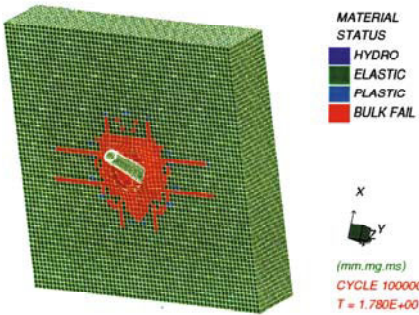
Fig. 13.16 Material status at cycle 100000   **Fig. 13.17** Material status at cycle 20000 (rear surface view)
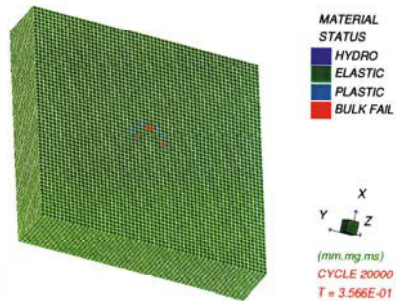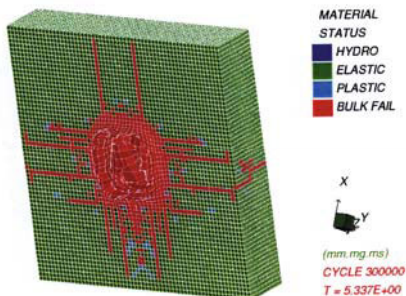
Fig. 13.18   Material status at cycle 30000
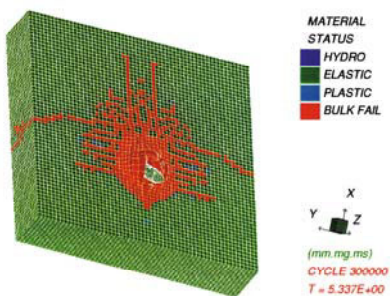
Fig. 13.19   Material status at cycle 300000 (rear surface view)
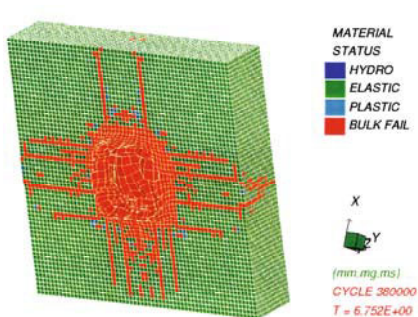
Fig. 13.20   Material status at cycle 380000
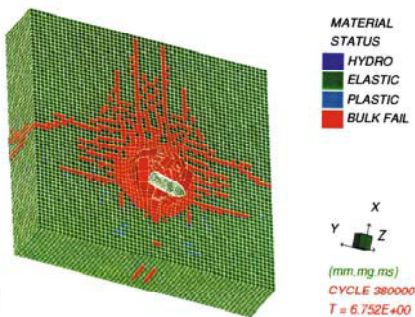
Fig. 13.21   Material status at cycle 380000 (rear surface view)

Figures 13.22 and 13.23 show the experimental results of the residual damaged area appearing on the front and rear face respectively. With regard to the size of the damaged areas on the front (Fig. 13.20) and rear face (Fig. 13.21), comparisons show that the simulation results agree well with the experimental ones (Figs. 13.22 and 13.23). With regard to the initiation point of damage on the rear face and the exit point from the rear face, simulation results (Fig. 13.20 and 13.21), comparisons also show a good accord between the numerical simulation and the experimental results (Fig. 13.23).

The projectile's exit-velocity history is shown in Fig. 13.24. It can be seen that the exit velocity is about 214 m/s, which is slightly higher (~18%) than the experimental result of 180 m/s. It could be partly due to the omission of steel reinforcement bars in the numerical simulation. On the other hand, the pre-defined erosion limit is set lower than 2, which leads to a softer target material and results in a higher exit velocity.
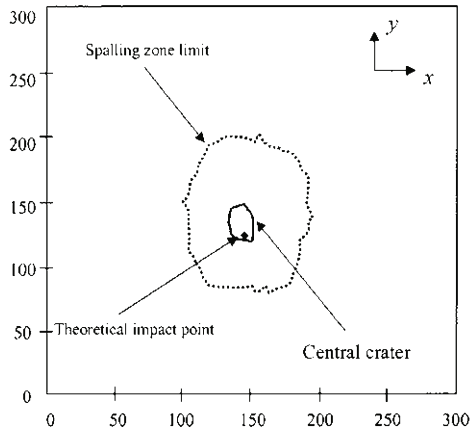
Fig. 13.22   Target residual damage (front face)
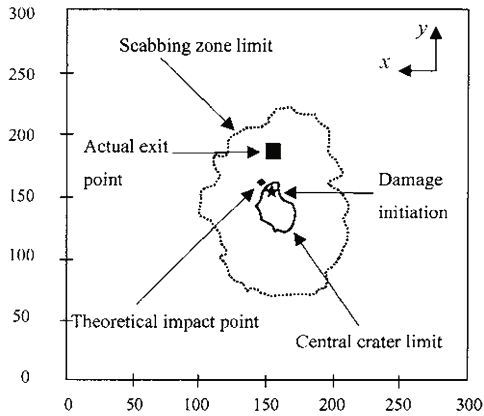
Fig. 13.23   Target residual damage (rear face)
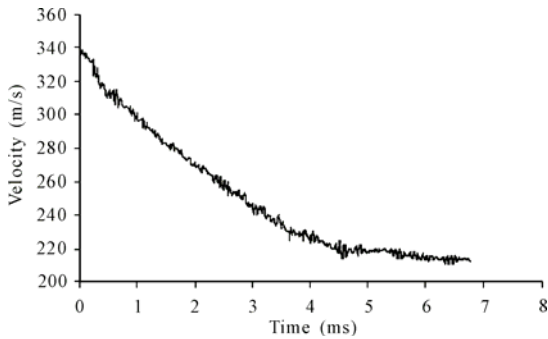
Fig. 13.24   Velocity history of the projectile

13.4 Conclusions

The following conclusions were given by Zhou.

1) Regarding the construction of the strength surface for the failure state of concrete material under triaxial stress condition, most of the available models are empirical criteria based on limited experimental data, such as the Willam-Wamke criterion, Ottosen criterion and Kotsovos-Palovic model (see: Chapter 3). On the other hand, Yu's Unified Twin Shear Stress (UTSS) theory offers a more thorough theoretical insight into the strength criteria. The UTSS clearly defined the role of the intermediate principle shear stress through a contribution factor 'b' ($0 \leq b \leq 1$). Though the UTSS does not provide a complete theoretical strength criterion in the tri-axial stress space (π-space), it is proven to be logical and accurate in the π-space. Against this background, the present study leads to a novel way of constructing the strength surface—a semi-theoretical semi-empirical envelope. Subsequently, it is further developed into a multi-surface strength model for concrete materials. It takes into account the pre-failure elasto-plastic behavior and the post failure damages.

2) The development of the present model evolves from a static version SMl, which follows Yu's UTSS conical failure envelope. An improved static version SMII incorporates Yu's twin-shear criterion in the π-plane with Kotsovos' meridians. The dynamic version is a further development of SMII including the dynamic effects.

3) Construction of the failure envelope in the π-space is the key step. Rules governing the non-linear responses of concrete at different stress stages can be established. The rules for pre-failure behavior follow the elastic-plastic theory, while damage mechanics can be employed to govern the post-failure responses to account for the degradation of both strength and stiffness. The stress states at different stages of the stress path are described with respect to the failure surface. Other surfaces are thus derived to further partition the π-space into sub-zones. The partitioning surfaces demarcate the elastic zone, plastic zone and damage zone.

4) Both static models (UTSS-based SMI and semi-UTSS SMII) can yield reasonably accurate predictions for the ultimate capacity and the overall load-deflection response of RC beams (see Chapter 11). Model SMI leads to results inferior to those from model SMII. In particular, model SMII shows its robustness in the benchmark test for a box beam (see Chapter 11).

5) The dynamic version of the present MSS model, together with other available numerical techniques, are capable of simulating the complicated penetration and perforation process. Not only the velocity history of the projectile, but also the damage zones and the overall performance can be obtained with an acceptable degree of accuracy.

References

AutoDYN (2000) Theory Manual. Century Dynamics Inc.

Buzaud   E, Laurenson R, Darrigade A et al. (1999) Hard target defeat: An analysis of reinforced concrete perforation process. The Ninth Int. Symp. on Interaction of the Effects of Munitions with Structures, Berlin, Germany, 3-7 May, 283-290.

Yu MH (1998) Twin Shear Theory and its Applications. Science Press: Beijing in Chinese).

Yu MH (2004) Unified Strength Theory and its Applications. Springer: Berlin.

Zhou XQ (2002) Numerical Analysis of Reinforcement Concrete Using Multi-Surface Strength Model. Doctoral Thesis at Nanyang Technological University, Singapore.

14

Underground Mining

14.1 Introduction

The mechanical problem in underground mining is that the stope and laneway are always in a state of dynamic evolution, induced by stress adjustment that is caused by excavation and shocks. The dynamic evolution induces a crack field in the wall rock expansion and in the end it caves in. So the mechanics problem in mining is different from other rock engineering problems, such as in powerhouse construction of a hydroelectric power station, traffic tunneling, national defense engineering of rock, etc., which will be firmly supported as soon as they are excavated. However, in mining, the evolution of the crack field and the caving in of the rock are fully used in ore extraction and ground pressure control, such as the mining methods of block caving and long wall mining. In the block caving method, the mining block is undercut near its bottom in order to expose a large free surface near which the ore is in a state of tension, so that cracks in the ore body expand, run through and induce ore caving, as shown in Fig. 14.1 and Fig. 14.2 (Brown, 2003).

In the long wall mining method, see Fig. 14.3 and Fig. 14.4, when the worked-out section is too large, the work face will bear too great a pressure and the sudden rupture of the roof will cause a great shock to the support system. So an ideal mode is that, as the work face advances, the roof caves in bit by bit, which will relief the stress on the work face and avoid the sudden rupture of the roof. It is very necessary in the two mining methods to predict the evolution of the crack field in the wall rock. That is the important mechanical problem in underground mining.
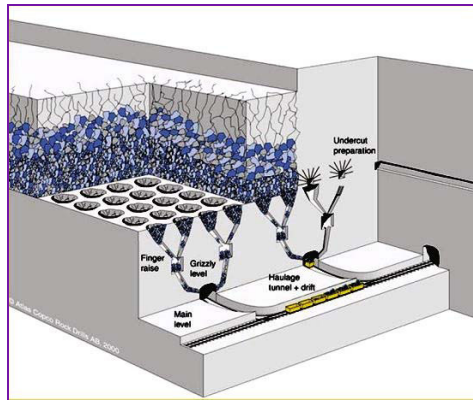
Fig. 14.1   Model of block caving (Brown, 2003)
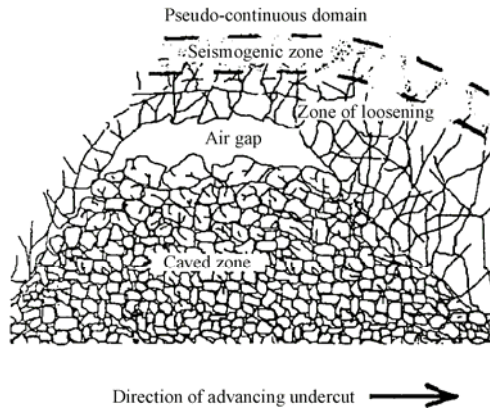
Fig. 14.2   Caving process zone expanding with advancing undercut
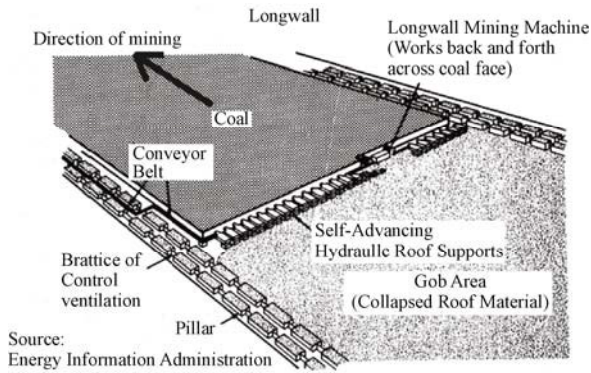
Fig. 14.3   Model of long wall mining
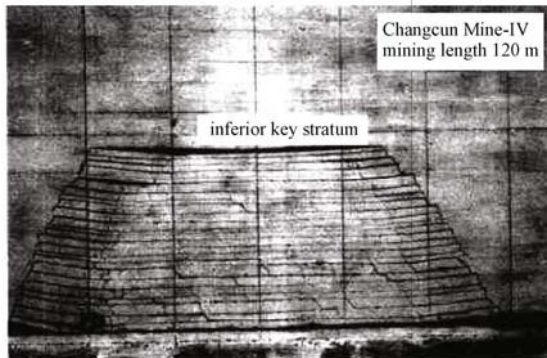
Fig. 14.4 Crack field expanding with extraction advancing

In the calculation of the fracture zone, it is an important problem to select the fracture rule for the rock, which involves choosing a reasonable strength theory. Though strength theory is one of the earliest classic problems in mechanics, it is still progressing. So far, there have been over a hundred mathematics models or criteria proposed. They are divided into single-shear strength theory, twin-shear strength theory and three-shear strength theory under the framework of the unified strength theory. The single strength theory does not consider the effect of intermediate principal stress σ_2, it expresses the stress function of materials with the shear stress and normal stress on the maximum shearing plane, e.g. the Mohr-Columb strength criterion and Tresca strength criterion. Three-shear strength theory is also called octahedral strength theory, e.g. Huber-von Mises criterion and Drucker Prager criterion. Twin-shear theory was proposed by Yu in 1961, 1983 and 1985.

In 1991, Yu presented the unified strength theory in Tokyo and then, in 1992 and in 1994, he gave a further discourse of his theory. The unified strength theory has the advantage that it reflects not only the effects of the intermediate principal stress on material yielding but also the transition from the stress state of generalized tension to that of generalized compression with the intermediate principal stress increasing from $\sigma_2=\sigma_3$ to $\sigma_2=\sigma_1$ in its two expressions (Yu, 1998; 2004).

In this chapter, two examples of the application of the unified strength theory in underground mining are introduced. Block caving and long wall mining are described. In order to reflect the evolution of the crack field in the wall rock, an elastic-brittle damage model has to be established first.

14.2   Elastic-Brittle Damage Model Based on Twin-Shear Theory

14.2.1 Damage Model

The damage variable is defined as

$$D = \left(\frac{\varepsilon}{\varepsilon_s} \right)^n \tag{14.1}$$

where ε_s represents the strain when the material is fully fractured, corresponding to $D=1$; ε is the elastic strain and n is the brittle exponent. The meaning of the damage parameters is shown in Fig. 14.5. They have different values under uniaxial tension and compression.
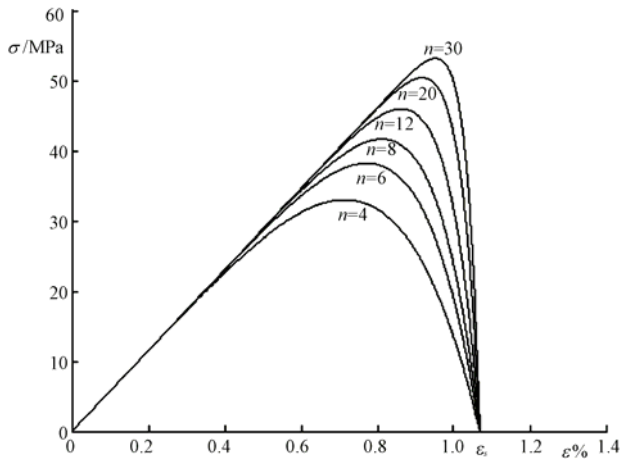
Fig. 14.5   Stress-strain curves of elasto-brittle rock at different n

14.2.2 Three-Dimensional Damage Model

According to twin-shear strength theory (Yu, 1985), the complex stress state can be divided into two kinds of equivalent uniaxial stress states, which are equivalent tension and equivalent compression. The twin-shear strength theory is generalized into a 3D damage model in this research. The twin-shear damage surface equations with principal strains are defined as

$$F' = \left[\varepsilon_1 - \frac{1}{2}(\varepsilon_2 + \varepsilon_3)\right] + \frac{(1-\alpha)(1+v)}{(1+\alpha)(1-v)}\left[\varepsilon_1 + \frac{1}{2}(\varepsilon_2 + \varepsilon_3)\right] = \frac{2(1+v)\varepsilon'_c}{1+\alpha}$$

$$\text{When } \varepsilon_2 \le \frac{\varepsilon_1(1-\alpha v) + \varepsilon_3(\alpha - v)}{(1-v)(1+\alpha)} \quad \text{(generalized tension)} \tag{14.2a}$$

$$F = \left[\frac{1}{2}(\varepsilon_1 + \varepsilon_2) - \varepsilon_3\right] + \frac{(1-\alpha)(1+v)}{(1+\alpha)(1-v)}\left[\frac{1}{2}(\varepsilon_1 + \varepsilon_2) + \varepsilon_3\right] = \frac{2(1+v)\varepsilon'_c}{1+\alpha}$$

$$\text{when } \varepsilon_2 \ge \frac{\varepsilon_1(1-\alpha v) + \varepsilon_3(\alpha - v)}{(1-v)(1+\alpha)} \quad \text{(generalized compression)} \tag{14.2b}$$

where $\alpha = \varepsilon^t_c / \varepsilon^c_c$. ε^c_c, ε^t_c represent the critical value of materials yielding under uniaxial compression or uniaxial tension, they are always positive in the expressions. v is the Poisson rate; the expression to the right of Eqs. (14.2a) and (14.2b) can be simplified into a material parameter C. When the strain state is within the damage surface, that is when $|F|<|C|$ or $|F'|<|C|$, there is no damage evolution. If not, damage evolves. With damage evolution, damage surfaces will shrink because of softened material, so the material parameter C will become small. The 3D damage model can be established by F or F' tracing the 1D damage evolution.

In general compression, with Eqs. (14.1) and (14.2b), the damage variable is

$$D = \left(\frac{|F|}{H\varepsilon_s}\right)^n \tag{14.3a}$$

In general tension, with Eqs. (14.1) and (14.2a), the damage variable is

$$D = \left(\frac{|F'|}{H'\varepsilon'_s}\right)^{n'} \tag{14.3b}$$

in which ε'_s represents the strain when $D=1$ and here

$$H' = \frac{2(1+v)}{1+\alpha}, \quad H = \frac{2\alpha(1+v)}{1+\alpha}$$

The equation of the damage evolution is

$$\dot{D} = \frac{\partial D}{\partial \varepsilon} = \frac{n}{H\varepsilon_s}\left(\frac{|\dot{F}|}{H\varepsilon_s}\right)^{n-1} \quad \text{or} \quad \dot{D} = \frac{\partial D}{\partial \varepsilon} = \frac{n'}{H'\varepsilon'_s}\left(\frac{|\dot{F'}|}{H'\varepsilon'_s}\right)^{n'-1} \tag{14.4}$$

The experimental results of uniaxial and triaxial compression for sand-rock at the Jinchuan mine are shown in Fig. 14.6. The comparison of the calculated results based on the twin-shear damage model with the experimental results shows good agreement.
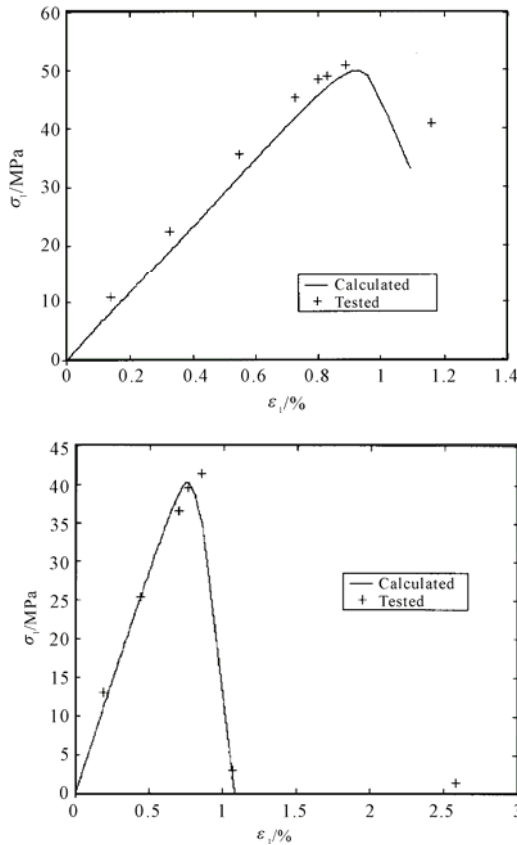
Fig. 14.6   Comparison of the twin-shear damage model with experimental results for sand-rock

14.3   Non-Equilibrium Iteration for Dynamic Evolution

At a certain loading step, damage and fracture of elements result in a decrease in the bearing capacity, which causes redistribution of stress in the structure. As a result, the stress around the damage zones increases. Furthermore, the elements around the damage zones will be damaged and fracture under the increased stress. This is the damage pattern and stress pattern coupling with each other; they are

alternatively expanding and stopping. In the numerical method, the stress redistribution is carried out by non-equilibrium iterations.

At loading step k, the finite element equation is

$$K^{(k)}a^{(k)} = P^{(k)} \tag{14.5}$$

in which $a^{(k)}$ is the displacement array of step k; $P^{(k)}$ is node load array; $K^{(k)}$ is the overall stiffness matrix. It is assembled by the element stiffness matrix

$$K^{(k)} = \sum_e (K^{(e)})^{(k)} = \sum_e \int_{V_e} B^{\mathrm{T}}(D^{(e)})^e B \mathrm{d}V \tag{14.6}$$

in which B is the strain matrix, $(D^{(e)})^{(k)}$ is the element stiffness matrix of step k. It is expressed with the tensor as

$$(D^{(e)}{}_{ijkl})^{(k)} = (2G\delta_{ik}\delta_{jl} + \lambda\delta_{ij}\delta_{kl}) \tag{14.7}$$

in which G λ are Lame constants.

The non-equilibrium load result of element damage is

$$(K^{(k)} - \tilde{K}^{(k)})a^{(k)} = \Delta P^{(k)} \tag{14.8}$$

in which $\tilde{K}^{(k)}$ is the overall stiffness matrix because of damage at step k.

$$\tilde{K}^{(k)} = \sum_e (\tilde{K}^{(e)})^{(k)} = \sum_e \int_{V_e} B^{\mathrm{T}}(\tilde{D}^{(e)})^{(k)} B \mathrm{d}V \tag{14.9}$$

in which $(\tilde{D}^{(e)}_{ijkl})^{(k)}$ is the constitutive matrix of the damaged element. It is written as in tensors

$$(\tilde{D}^{(e)}_{ijkl})^{(k)} = (D^{(e)}{}_{ijkl})^{(k)}(1 - D^{(k)}) \tag{14.10}$$

Keep the load and boundary unchanged, approach equilibrium by iterative calculation and the stress is redistributed as

$$\tilde{K}^{(k)}\Delta a^{(k)} = \Delta P^{(k)} \tag{14.11}$$

The displacements are resolved as $\tilde{a}^{(k)}$

$$\tilde{a}^{(k)} \leftarrow a^{(k)} + \Delta a^{(k)} \tag{14.12}$$

The accumulated displacement is $\tilde{\varepsilon}^{(k)}$

$$\tilde{\varepsilon}^{(k)} = B\tilde{a}^{(k)} \tag{14.13}$$

Use Eqs. (14.2a) or (14.2b) and (14.3a) or (14.3b) for each element and calculate the damage value, then enter Eqs.(14.11)–(14.13). Repeat this course until no damage is produced. Then the step k calculation ends and the program enters the next step calculation.

14.4   Numerical Simulation of Caving Process Zone

14.4.1 Introduction to Block Cave Mining

Block cave mining is a mass mining method that allows for the bulk mining of large, relatively lower grade ore bodies. This method is increasingly being proposed for a number of deposits worldwide such as in Northparkes (Australia), Palabora (South Africa), Questa Mine (New Mexico), Henderson Mine (Colorado) and Freeport (Indonesia). In general terms block cave mining is characterized by caving and extraction of a massive volume of rock which potentially translates into the formation of a surface depression whose morphology depends on the characteristics of the mining, the rock mass and the topography of the ground surface (Fig. 14.1).

A major challenge at the mine design stage is to predict how specific ore bodies will react to block caving depending on the various geometry of the undercut. The scheme of undercut is the most feasible and creative factor because it can directly or indirectly change the cavibility of the ore body and decrease the rate of massive fragments. The caving process zone is the perturbation zone of the ore body above the free surface exposed by the undercut and ore drawing. It includes the caved zone and damaged zone (Fig. 14.2). It represents the dynamic characteristics of rock cracking, fracture and caving. In the chapter, a numerical simulation scheme for block cave mining for the Jinchuan Corp. Mine III (China) is introduced to give an illustration of the application of twin-shear strength theory in underground mining.

14.4.2 Geometry and Undercut Scheme

The experimental block is located in the south of the ore field (Fig. 14.7) and the size of the block and base structure is shown in Fig. 14.8a.
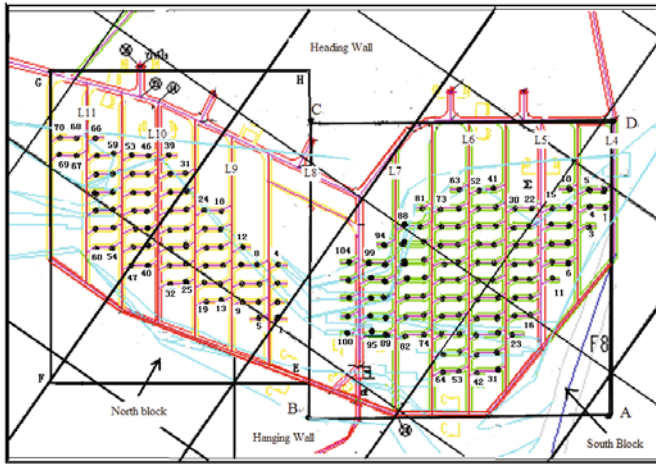
Fig. 14.7   Location of the experimental block (South block) in the ore field

The experimental block has a size of 180 m×140 m×188 m, with the highest level on the earth's surface and with the numerical boundary being 50 m from it. Stability of the base structure is not the aim. The undercut is divided into 6 equal paces which advance in the direction of positive *Y* (Fig. 14.8(b)). The velocity of the advancing undercut is determined by the principle that only if the ore body obtains transient stability at the previous pace will the next pace start.

(a) Geometric model of the block mine   (b) The scheme of undercut
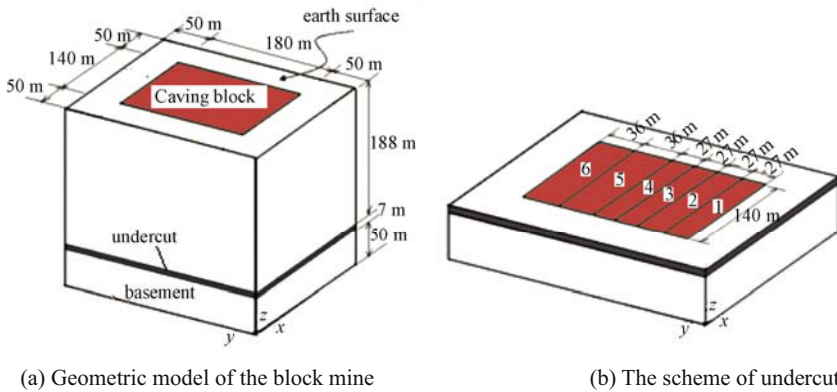
Fig. 14.8   The block and base structure and scheme of undercut

14.4.3 Result of Numerical Simulation

The finite element model is shown in Fig. 14.9, with its displacements set to zero except for the top surface.
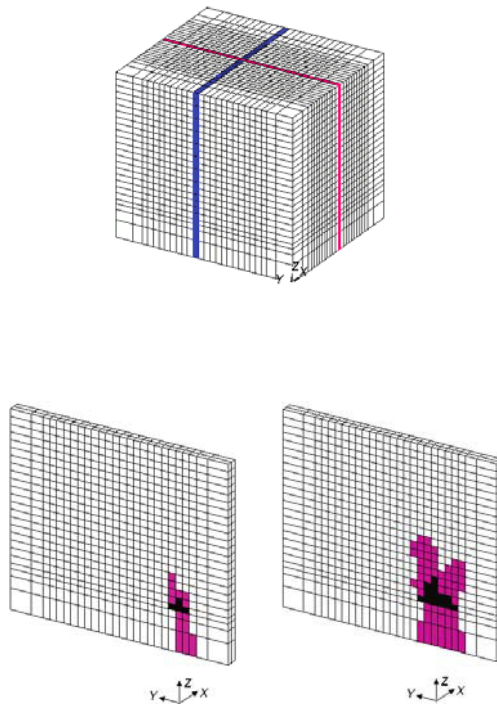
Fig. 14.9   The mesh of the block and undercut 1-1, 1-2

The elements attached to the middle plane of the model in the X direction are selected to show the evolution of the caving process zone, where the black elements represent the caved zone and the purple elements represent the damaged zone (Fig. 14.10). It shows that when the undercut 1 is finished, small caving occurs in the ore body. After the adjustment of stress, the damage zone expands but the caved zone does not, because the undercut pace is too slow. When the undercut 2 is finished, large scale caving occurs and the damage zone also expands much more, even if the undercut does not advance. So, from the undercut 3, the advance of the undercut goes fast and the next undercut should be carried out before the ore body stabilizes at the previous undercut, so that the subsequent undercut is carried out safely. At the end of the undercut, the process zone cannot retain a stable structure and continuous caving happens. Two large shear bands appear on the two sides above the caved zone.

Undercut 2-1   Undercut 2-2   Undercut 2-3

Undercut 3-1   Undercut 3-2   Undercut 5-1

Undercut 6-1   Undercut 6-1 (In *Y*-direction)
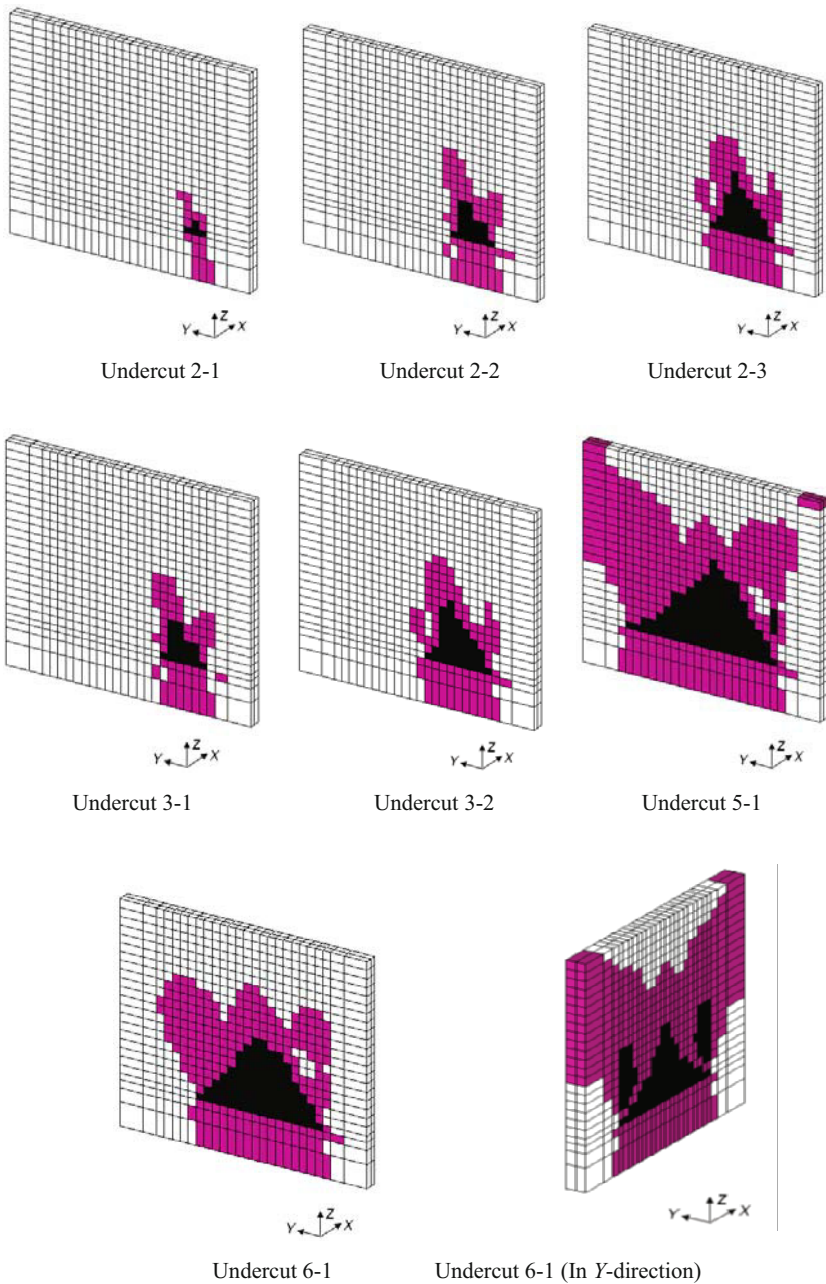
Fig. 14.10   Process zone evolution

14.5 Numerical Simulation for Crack Field Evolution in Long Wall Mining

14.5.1 Geometry and FEM Model

In this section we introduce the application of twin-shear strength theory in numerical simulation for crack field evolution in long wall mining in the Xinyi Coal Mine of the Yi Ma Coal Group in Henan province, China. The aim is to get a foreknowledge of pressure distribution on the workface and crack field evolution in the roof. The mechanical model is a plane strain in which the calculated plane is cross section I-I, as shown in Fig. 14.11 and Fig. 14.12. The FEM model is a fine mesh and rock strata are marked with different colors, as shown in Fig. 14.13.
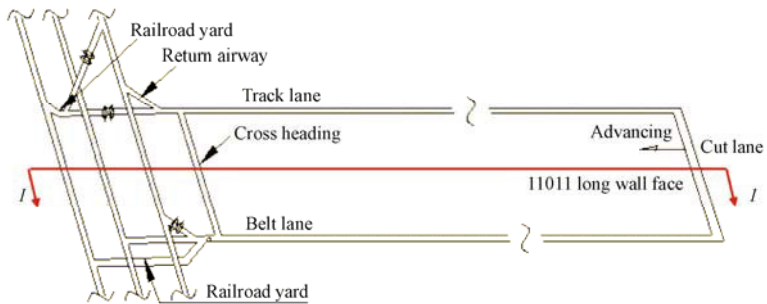
Fig. 14.11   Location of the calculated plane I-I
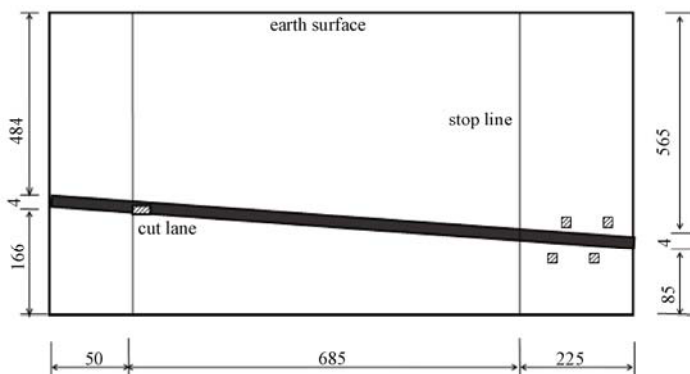
Fig. 14.12   Geometry of the cross section I-I
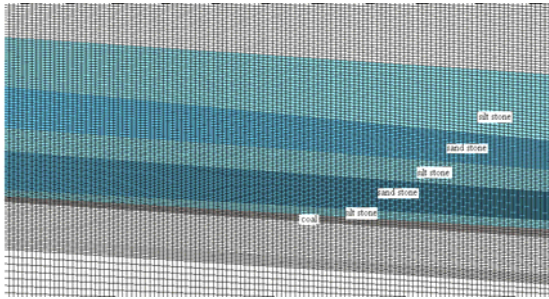
Fig. 14.13   Grid and distribution of rock strata in the calculated field

14.5.2 Evolution of Crack Field in the Roof

Part of the result is shown in Fig. 14.14. The orange color represents the worked-out section in the coal stratum and black represents the cracking zone.
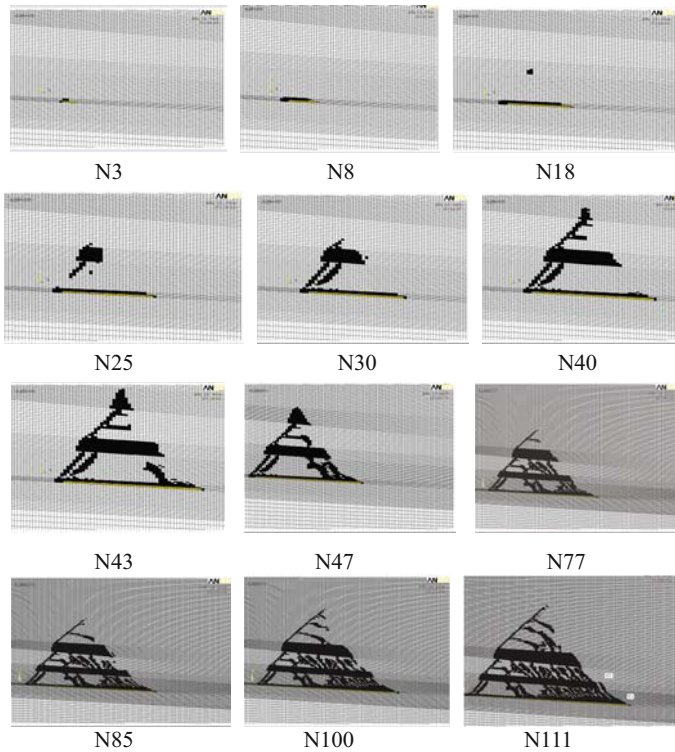
Fig. 14.14   Crack field evolution in roof

14.5.3 Results of Displacement and Stress

Contours of vertical displacement and principal stress σ_3 in the colorful strata are shown in Fig. 14.15. As the mining advances, the roof and the bottom of the worked-out section move oppositely. The largest displacement initially occurs at the main key stratum (K1) before K1 firstly breaks at N47. Then it goes upward as the inferior key stratum (K2) breaks firstly at N69 and, while the two key strata (K1 and K2) break periodically with the advance in the mining, it goes forward. Meanwhile, the zone in a state of tensile stress in the roof initially enlarges and then   disappears. Instead, zero stress occurs and enlarges the roof with the breaking of the roof. The pressure on the two ends of the worked-out section will increase, as shown in Fig. 14.15 and Fig. 14.16.

Disp. Contours at N8 σ_3 Contours at N8

Disp. Contours at N18 σ_3 Contours at N18

Disp. Contours at N47 σ_3 Contours at N47

Disp. Contours at N111 σ_3 Contours at N111
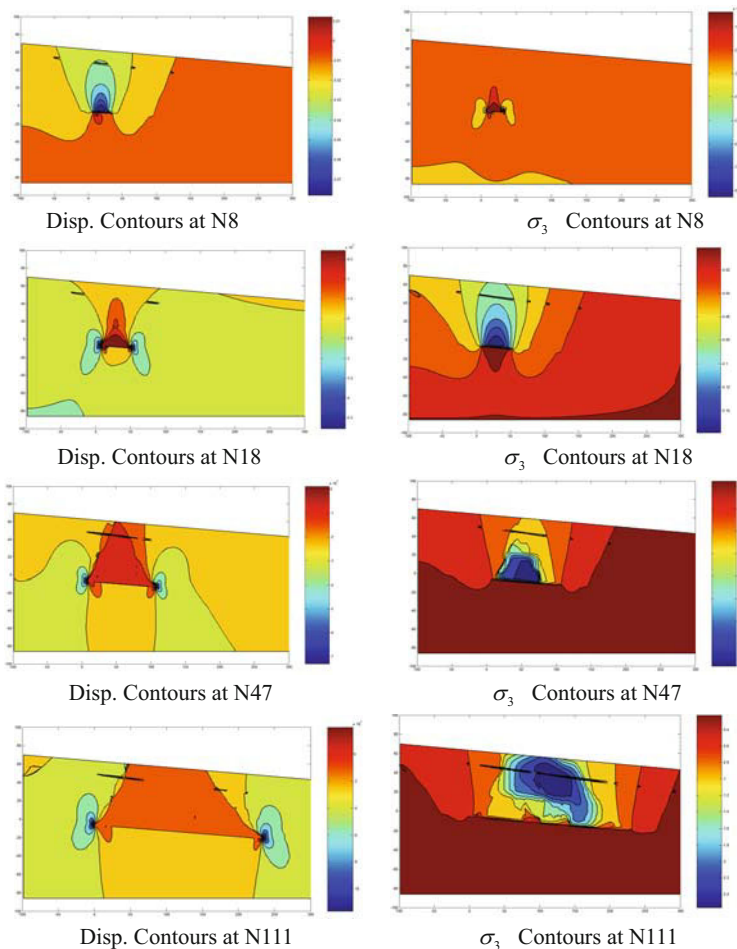
Fig. 14.15   Contours of displacement and stress
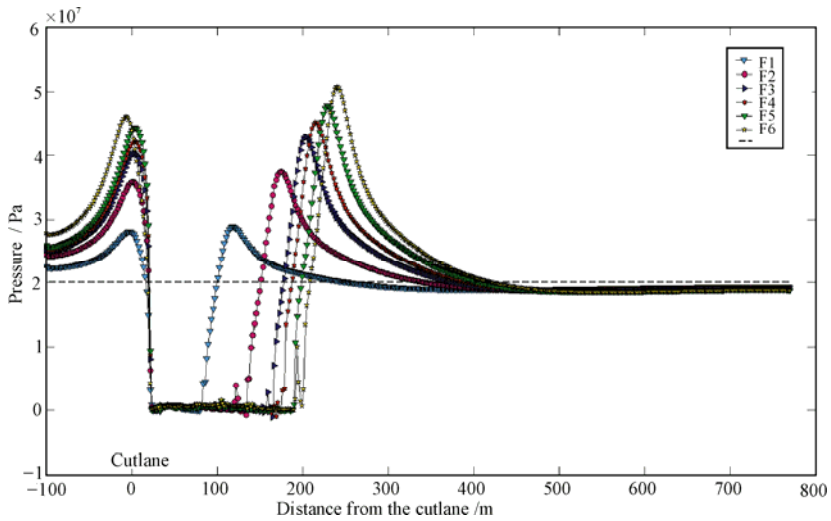
Fig. 14.16   Pressure distribution on the two ends of the worked-out section when K1 is breaking

In fact, with the strata in the roof breaking and caving, the opposite movement of roof and bottom will be prevented by the swelling rock and the zero stress zone will benefit from a supporting effect.
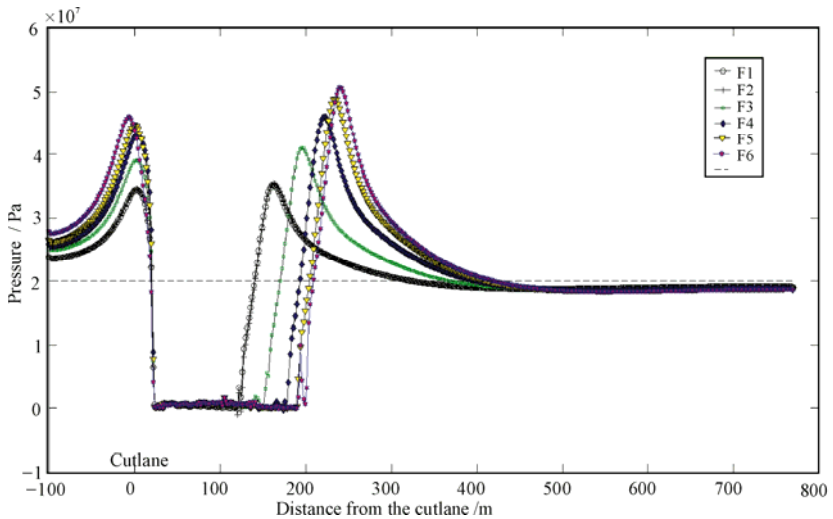
Fig. 14.17   Pressure distribution on the two ends of the worked-out section when K2 is breaking

References

Brown ET (2003) Block caving geomechanics. The international caving study I, 1997-2000. JKMRC monograph series in mining and mineral processing, University of Queensland, vol. 3. Indooroopilly, Australia: JKMRC.

Qian MG, Miu XX ,Xu JL et al. (2000) Key Strata Theory In Ground Control. China Mining and Technology University Press: Xu Zhou, China (in Chinese).

Yu MH, He LN, Song LY (1985) Twin shear stress theory and its generalzation. Scientia Sinica (Science in China, Series A), 28(11): 1174-1183 (English edn.); Chinese edn. ,28(12): 1113-1121.

Yu MH (1994) Unified strength theory for geomaterials and its application. Chinese Journal of Geotechnical Engineering, (2): 1-10 (in Chinese, English Abstract).

Yu MH (1998) Twin-Shear Theory and its Applications. Science Press: Beijing (in Chinese).

Yu MH (2004) Unified Strength Theory and its Applications. Springer: Berlin.

Zhou WY, Shan GR and Yang RQ (1998) Elasto-brittle damage model of rock and its applications. Chinese Journal of Geotechnical Engineering, 20(5): 54-57.

Wang L, Chen YJ and Gao Q (2009) Numerical simulation on caving process zone induced by undercut. Nonferrous Metals (Mining Section), 61(3): 44-48 (in Chinese).

15

Reinforced Concrete Beam and Plate

15.1 Introduction

Concrete plasticity has been described by Chen (1982; 1998) and Nielsen (1984; 1989). Several material models were discussed. Yu's unified strength theory (Yu's UST or UST) and the UEPP (Unified Elasto-Plastic Program) are successfully used for structural analysis, as has been described in Chapters 6, 7 and 8.

The feature of the UEPP is that the unified strength theory was implemented into the finite element method code. UEPP includes two codes, i.e. UEPP-2D for plane stress, plane strain and axial-symmetric problem and UEPP-3D for three-dimensional problems. The material models are increasing and forming a series of systematic and effective constitutive relations for practical use. UEPP provides us with a very effective approach for studying the effect of failure criterion for various problems.

The unified strength theory and unified elasto-plastic constitutive relations are also implemented in some commercial finite element codes and some special finite element codes in China, Japan, Singapore, Australia, Sweden etc. The multi-parameter unified yield criterion has been applied to analyze two groups of reinforced concrete slabs and a parabolic cylindrical shell, by Wang et al., in Singapore. The nonlinear finite-element analysis code for plates and shells written by Huang (1988) and his predecessors (Owen and Hilton, 1980) is modified to incorporate the unified material model for concrete. The unified strength theory with b=0.6 is used. Elasto-plastic analysis for reinforced concrete slabs and high-strength concrete slabs using the unified strength theory was also successfully studied by Wang, Teng and Fan (2001). Various applications of the UST were presented.

The unified strength theory (UST) with tension cutoff is also adopted as the failure criterion for the analysis of punching shear failure of beams and slab-column connections by Zhang et al. at Griffith University, Australia. The

results of applications of UST and UST with tension cutoff criterion and the comparisons with other yield criteria in the literature and experimental data are described in this chapter. These studies are focused on the implementation of the UST for the analysis of failure of reinforced concrete structures. Numerical studies are carried out in an attempt to verify the applicability of the UST. The numerical and published experimental results are compared for several RC (Reinforced Concrete) structures.

The UST is also implemented into FLAC-2D, FLAC-3D, AutoDYNA, AutoDYNA2D, ABQUSE, etc. which has been described in the above chapters.

15.2   Elasto-Plastic Analysis for Reinforced Concrete Beams

At present, some failure criteria are already in use to analyze the punching shear strength of slab-column connections and its associated failure behaviour. Gonzalez-Vidosa et al. (1988) used a failure criterion based on the test data under axisymmetric stress conditions (i.e., two of the three principal stresses are equal) for the axisymmetrical punching shear analysis of reinforced concrete circular slabs. For a similar problem, Zhou and Jiang (1991) adopted Ottosen (1977) criterion in the punching shear failure analysis of reinforced concrete circular slabs under axisymmetrical loading. For a series of half-scale reinforced concrete flat plates with edge and comer column connections, Loo and Guan (1997) have analyzed their flexural failure and punching shear behaviour by means of the Ottosen criterion. The abovementioned failure criteria were developed on the basis of experimental results rather than theoretical derivations.

In addition, such criteria involve a large number of parameters which are rather difficult to determine accurately. When dealing with such a complex stress problem, the appropriate constitutive model and failure criterion for concrete have to be utilized.

15.2.1 Material Modelling

For various materials, Yu (1991; 1992) has suggested a unified strength theory (UST) based on the assumption that the plastic flow is controlled by the combination of the two larger principal shear stresses and their corresponding normal stresses. The UST can be presented by two simple mathematical formulae and a set of piecewise linear yield surfaces. A class of convex criteria can be obtained by varying the coefficient *b* in the UST to suit different materials like metal, concrete, rock and soil, etc.

Based on the orthogonal octahedron of the twin shear element model (Yu, l985), the unified strength theory specifies that material fails when a certain function of the two larger principal shear stresses and the corresponding normal

stresses on their surfaces reach the limiting value. The mathematical modelling of the UST is

$$\tau_{13} + b\tau_{12} + \beta(\sigma_{13} + b\sigma_{12}) = C \quad \text{when} \quad \tau_{12} + \beta\sigma_{12} \geq \tau_{23} + \beta\sigma_{23} \quad (15.1a)$$

$$\tau_{13} + b\tau_{23} + \beta(\sigma_{13} + b\sigma_{23}) = C \quad \text{when} \quad \tau_{12} + \beta\sigma_{12} \leq \tau_{23} + \beta\sigma_{23} \quad (15.1b)$$

where $\tau_{13}, \tau_{12}, \tau_{23}$ are the principal shear stresses defined as $\tau_{13} = (\sigma_1 - \sigma_3)/2$, $\tau_{12} = (\sigma_1 - \sigma_2)/2$, $\tau_{23} = (\sigma_2 - \sigma_3)/2$ and $\sigma_{13}, \sigma_{12}, \sigma_{23}$ are the corresponding normal stresses defined as $\sigma_{13} = (\sigma_1 + \sigma_3)/2$, $\sigma_{12} = (\sigma_1 + \sigma_2)/2$, $\sigma_{23} = (\sigma_2 + \sigma_3)/2$, which are in the stress planes of $(\sigma_1, \sigma_3), (\sigma_1, \sigma_2), (\sigma_2, \sigma_3)$, respectively; $\sigma_1, \sigma_2, \sigma_3$ are the principal stresses and $\sigma_1 \geq \sigma_2 \geq \sigma_3$, C is a material strength parameter; b and β are the coefficients that reflect the influence of the intermediate principal shear stress τ_{12} (or τ_{21}) and the corresponding normal stresses on the strength of the material, respectively.

For concrete, Eqs. (15.1a) and (15.1b) can be rewritten in terms of three principal stresses as

$$\sigma_1 - \frac{\alpha}{1+b}(b\sigma_2 + \sigma_3) = f_t, \quad \text{when} \, \sigma_2 \leq \frac{1}{2}(\sigma_1 + \sigma_3) \quad (15.2a)$$

$$\frac{1}{1+b}(\sigma_1 + +b\sigma_2) - \alpha\sigma_3 = f_t, \quad \text{when} \quad \sigma_2 \geq \frac{1}{2}(\sigma_1 + \sigma_3) \quad (15.2b)$$

where f_t is the tensile strength of concrete, α is the ratio of the tensile strength f_t and the compressive strength f_c of concrete; $b=(\tau_0(1+\alpha)-f_t)/(f_t-\tau_0)$ in which τ_0 is the shear strength of concrete.

Figure 15.1 depicts the limited loci of the UST which also indicates that the unified strength theory represents a group of hexagons on a deviatoric plane. A family of convex yield criteria related to a variety of materials is deduced when b varies from 0 to 1. For instance, UST becomes the Mohr-Coulomb criterion if $b=0$ and the twin-shear yield criterion (Yu, 1983) will be obtained when $b=1$.

The eleven limit loci with parameter $b=0$, $b=0.1$, $b=0.2$, $b=0.3$, $b=0.9$ and $b=1.0$ cover the whole of the convex region, as shown in Fig. 15.1(a); the five typical limit loci with parameters $b=0$, $b=0.1/4$, $b=1/2$, $b=3/4$, and $b=1.0$ and three typical limit loci with parameters $b=0$, $b=1/2$ and $b=1.0$ are as shown in Fig. 15.1(b).

(a) Eleven limit loci cover the whole region   (b) Five and three typical limit loci
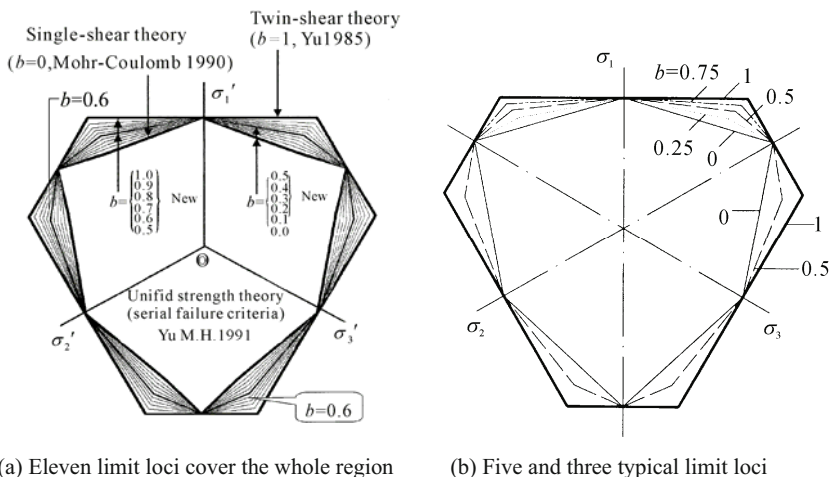
Fig. 15.1   Limited loci of the unified strength theory

15.2.2 Material Modeling of Concrete

In the analysis, the failure of reinforced concrete is considered to be a result of either tension cracking in concrete or plastic yielding, which leads to the crushing of concrete (Loo and Guan, l997). Concrete is assumed to be linear elastic and its behaviour is characterised as isotropic until the specified fracture surface determined by the UST is reached. Numerical modelling of either cracking or crushing of concrete involves the modification of material stiffness and the release of the appropriate stresses partially or completely in the fractured elements.

The tensile type of fracture or cracking is governed by a maximum tensile stress criterion, referred to as the tension cut-off. Cracked concrete is treated as an orthotropic material using a smeared crack approach. After cracking has occurred, the tensile and shear stresses acting on the cracked plane are released and redistributed to the neighboring elements. Under subsequent loading, concrete loses its tensile strength normal to the crack direction, but retains the tensile strength in the directions parallel to the crack plane.

The strain-hardening plasticity approach is used to model the concrete in compression. This approach involves loading surfaces, loading function, normality rule and unloading associated with the UST (Unified Strength Theory). After the compression type of fracture occurs, the concrete material is assumed to lose some, but not all, of its strength and rigidity.

15.2.3 Reinforcing Steel

The reinforcing steel is assumed to be an elastic-plastic uniaxial material．The reinforced bars at a given level in an element are modeled as a smeared steel layer of equivalent thickness.

15.2.4 Structural Modeling

The study of Zhang, Guan and Loo is focused on the implementation of the UST for the analysis of beams and punching shear failure of reinforced concrete slab-column connections, which will be described in the next section. Numerical studies are carried out in an attempt to verify the applicability of this criterion. The numerical and published experimental results are compared for two simply supposed beams and two slab-column connections (next section).

In the study, the layered finite element method developed by Guan and Loo (1997a; 1997b) is adopted to model the structure. In the analysis, eight-node degenerate shell elements with bi-quadratic serendipity shape functions are adopted in conjunction with the layered approach. The model makes use of the transverse shear deformations associated with the Mindlin hypothesis. Five d.o.f are specified at each nodal point. They are the in-plane displacements, u and v, lateral bending displacement w and two independent bending rotations about the x and y axes, i. e.θ_y andθ_x respectively.

In the layered approach, each element is subdivided into a chosen number of layers which are fully bonded together The concrete characteristics are specified individually for each layer over its thickness．On the other hand, each layer of the reinforcing bars is represented by a smeared layer of equivalent thickness. In a nonlinear analysis, the material state at any Gauss point located at the mid-surface of a layer can be elastic, plastic or fractured, according to the loading history. To account for the mechanical change in the materials throughout the incremental loading process, cracking and nonlinear material response are traced layer by layer. By incorporating all the in-plane and out-of-plane stress components in the finite element formulation, inclined cracks can be simulated.

15.2.5 Simply Supported Beams

A series of 12 simply supported, reinforced concrete beams were specially designed and tested by Bresler and Scordelis (1963) to determine the crack loads and the ultimate strength characteristics. Each beam was subjected to a concentrated load applied at the mid-span, as illustrated in Fig. 15.2. The test beams were grouped into four series. The first group, the OA-series (without web

reinforcement), was analysed by Zhang et al. (2001; 2002) at Griffith University, Australia, with dimensional details shown in Fig. 15.2. Other relevant data can be found elsewhere (Bresler and Seordelis, 1963).
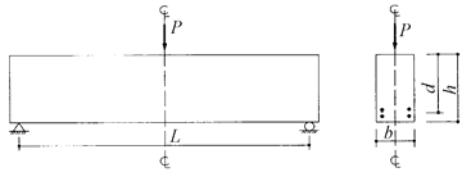
Fig. 15.2   Simply supported beam under central concentrated load

The parameters of the RC beam are: OA1: b=307.3 mm, h=556.3 mm, d=461.0 mm, L=3657.6 mm; OA2: b=304.8 mm, h=561.3 mm, d=466.1 mm, L=4572.0 mm.

The experimental and numerical load-displacement curves are compared in Fig. 15.3. It may be seen that the use of UST is capable of simulating the overall shear failure behavior of the beams without web reinforcement.
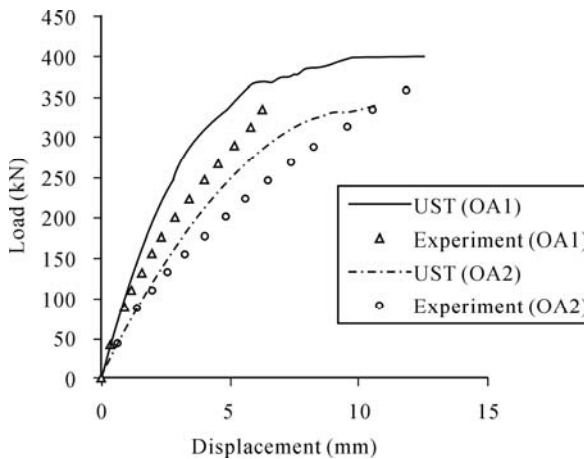
Fig. 15.3   Load versus displacement of beams

The experimental and numerical load-displacement curves are compared in Fig. 15.3. It may be seen that the use of UST (Unified Strength Theory) is capable of simulating the overall shear failure behavior of the beams without web reinforcement.

15.3   Punching Shear Failure Analysis of Flat Slabs by UST

A new analysis of the reinforced concrete slab-column connection was also presented by Zhang, Guan and Loo at Griffith University, Australia, in 2001. The unified strength theory (UST) is adopted as the failure criterion for the analysis of the punching shear failure of slab-column connections. The results described here follow Zhang et al. (2001).

Employing the layered finite element method, both material and geometrical nonlinearities are considered in the analysis. An investigation is carried out on reinforced concrete beams and slab-column connections. The numerical results indicate that the analysis based on UST is capable of simulating the overall failure behavior of slab-column connections.

Punching shear failure is referred to as a local shear failure that could occur around concentrated loads or column heads. In the design of reinforced concrete flat plates, the regions around the columns always pose a critical analysis problem. This is because large bending moments and shear forces are concentrated at the slab-column connections. This in turn complicates the stress distribution at the connections.

15.3.1 Slab-Column Connections

To verify the appropriateness of the UST in predicting the punching shear strength analysis, two typical slab-interior column connections (Slabs A and B) tested by Regan (1986) are analyzed. The dimensions of both slabs were 2 m×2 m×l00 mm; they were simply supported on four sides with l.83m spans and with the comer free to lift up. For each slab, a load was applied through a 200 mm monolithically cast column stub which projected above and below the slab. These two slabs were designed mainly to investigate the effect of the arrangement of flexural reinforcement. Both slabs have the same reinforcement ratios. However, Slab B has a uniform arrangement of flexural reinforcement whereas the steel arrangement in Slab A does not. Figure 15.4 shows the reinforcement details of slab A.
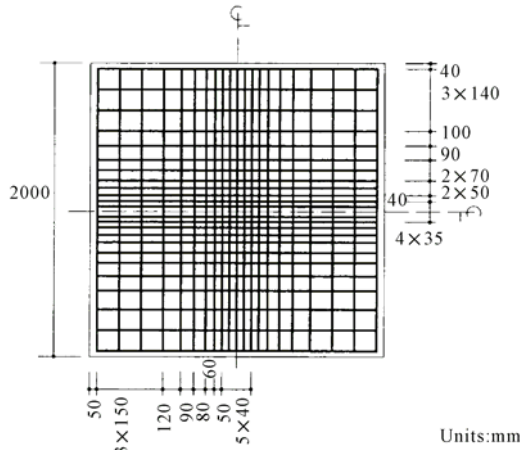
Fig. 15.4   Reinforcement details of slab (Zhang et al., 2001)
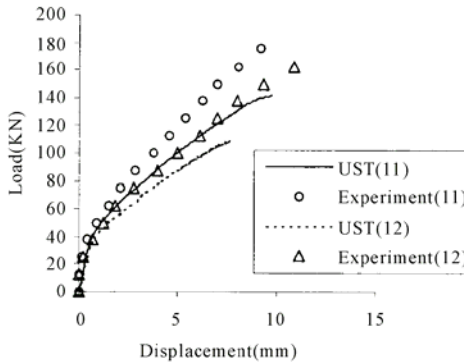
Fig. 15.5   Load versus displacement of slabs (Zhang et al., 2001)

The load-displacement responses shown in Fig. 15.5 demonstrate that the numerical results correlate reasonably well with the experimental outcome except that the numerical analysis somewhat underestimated the punching shear strength of the slab-column connections.

15.3.2 Conclusions

The conclusions of Zhang, Guan and Loo are given as follows:

"The adoption of the unified strength theory (UST) as the failure criterion for the layered finite element shear strength analysis is presented. The capabilities of the UST criterion are checked in a numerical investigation which covers typical

reinforced concrete beams failing in shear, as well as slab-column connections failing in punching shear. Comparisons with published experimental data show that the analysis underestimated the failure loads of the slab-column connections".

   "The UTS (Unified Strength Theory) is advantageous over other failure criteria because it encompasses all other established criteria as special cases. Or, such criteria are merely the linear approximations of the UST. Moreover, the parameters of the UST are easily obtained by experiments."

15.4   Elasto-Plastic Analysis for an Ordinary RC Beam

Yu's UST was implemented into commercial FEM software DIANA through the facility of a user-defined subroutine by Dr. Zhou at Nanyang Technological University in Singapore (Zhou, 2002). UST with parameter $b=0.6$ is the choice. The yield locus of the unified strength theory with $b=0.6$ is shown in Fig. 15.1(a).The descriptions of Zhou are as follows.

   DIANA is a commercial software, which is suitable for treating various kinds of problems in finite element analysis．This program provides some kinds of elements for modeling concrete, steel and also the interfaces between different materials．But there is no strong physical meaning in its material models for concrete, in particular the post-failure behavior. With a user-defined subroutine, any kind of material model is permitted to be added into DIANA. In the subroutine, the previous value of strain tensor ε_{ij}^r, the increment of strain tensor $\Delta\varepsilon_{ij}^{r+1}$ elasticity matrix D, the previous stress σ_{ij}^r, effective stress $\tilde{\sigma}_{ij}^r$, equivalent plastic strain $\overline{\varepsilon}_p^r$ are the input parameters, which can be obtained from the major module. Users are allowed to defined their own constitutive relation and then feed back the current total σ_{ij}^r and the tangent stiffness $[D]_{ep}$ to the main module. The theoretical development outlined in the previous chapter was coded in two subroutines and incorporated into DIANA. In Zhou's study, DIANA release 7.1 is used.

   This example shows the numerical simulation of an ordinary RC beam. The configurations and the loading on the beam are chosen to simulate the experimental tests by Kotsovos and Pavlovic (1995). The beam was subjected to two one- third-point loads and failed in a ductile, flexural manner. Figure 15.6 shows the dimensions of the beam and the reinforcement details.
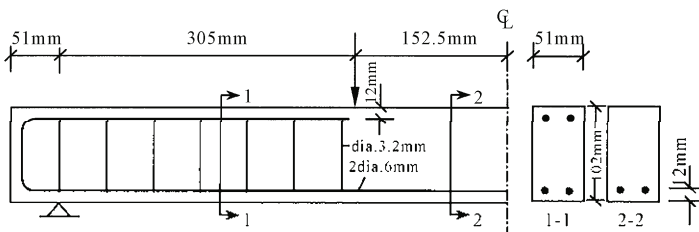
Fig. 15.6   Dimension and details of the RC beam

The ratio of the shear span to the effective depth is equal to 0.33 and the percentage of the longitudinal tension steel is l.2%. Transverse reinforcement was provided within the shear span so as to prevent a shear failure.

The material parameters used in the finite element model are shown in Table 15.1.

Table 15.1   Material parameters of the ordinary RC beam

Parameters	Values
E_c	29100 MPa
E_s	200000 MPa
f_c	37.8 MPa
f_t	3.38 MPa
f_y	417 MPa
v	0.2
UST parameter b	0.6
A_t	1.0
B_t=0.6	50000

Figure 15.7 shows the mesh and loading condition of the beam. Three-node truss elements and twenty-node brick elements are used to model the reinforced bars and the concrete, respectively. The concrete cover to the tension steel is ignored. All the steel elements (truss elements) lie on edges of brick elements (concrete). A perfect bond is assumed throughout this analysis.

With the plastic damage models proposed, the nonlinear response of the beam is calculated and the deflection at the mid-span of the beam is evaluated. Figure 15.8 shows the load-deflection curves obtained from Model I and Model II, which are the combination of UST and Kotsovos's experimental data.
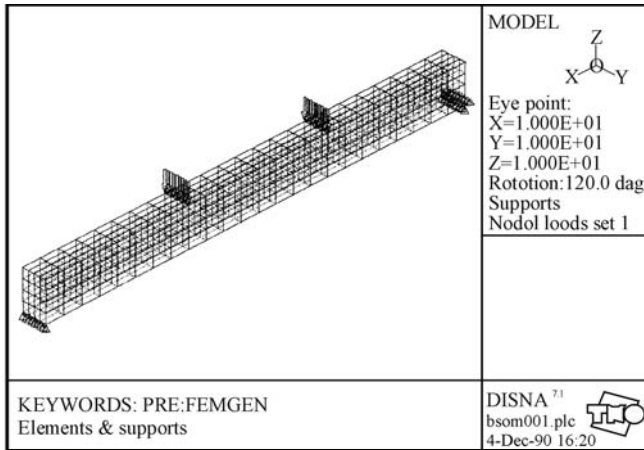
Fig. 15.7 Elements, supports and loading condition of the beam (Zhou, 2002)
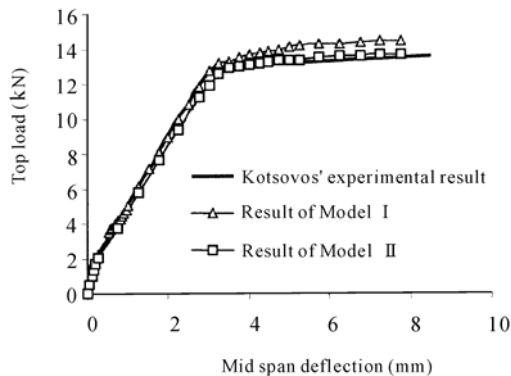
Fig. 15.8 Load-deflection curves of the RC beam (Zhou, 2002)

It can be seen that Model II yields results in very good agreement with the experimental ones, while the results obtained from Model I are inferior to those of Model II. Regarding the ultimate capacity of the beam, the value obtained from the test is 13.6 kN and the analytical values are l4.5 kN for Model I and l3.7 kN for Model II, with an error of 6.6 % and 0.7%, respectively.

15.5 Elasto-Plastic Analysis of an RC Deep Beam

This example shows the numerical simulation of an RC deep beam, which was reportedly tested in the School of Civil and Structural Engineering, Nanyang Technological University, Singapore (Poh and Susanto, 1996). The details of the experimental beam are shown in Fig. 15.9.
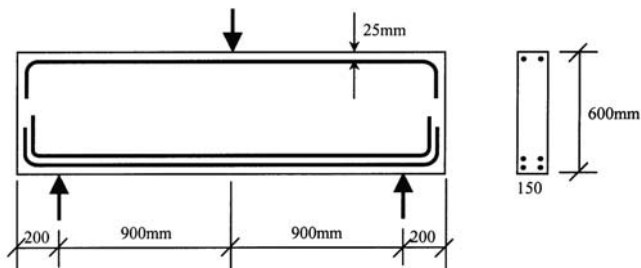
Fig. 15.9   Details of the deep beam (Zhou, 2002)

There is no web reinforcement at all. Only longitudinal reinforcement T22 is provided, 2 numbers near the top surface and 4 numbers near the bottom surface, as can be seen from Fig. 15.7. The material parameters used in the finite element model are listed in Table 15.2.

Table 15.2   Material parameters of the deep beam

Parameters	Values
E_c	29240 MPa
E_s	200000 MPa
f_c	38.2 MPa
f_t	3.40 MPa
f_y	754.08 MPa
v	0.2
UST parameter b	0.6
A_t	1.0
$B_t=0.6$	50000

Figure 15.10 shows the finite element mesh and the loading condition. Two-node truss elements and eight-node brick elements are used to model the steel bars and concrete, respectively. With the two different models (Model I and Model II), the load-deflection curves are obtained and compared with the experimental one in Fig. 15.11.
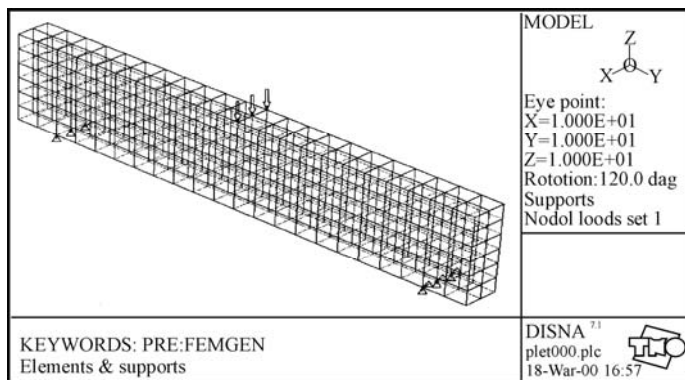
Fig. 15.10   Mesh of the deep beam (Zhou, 2002)
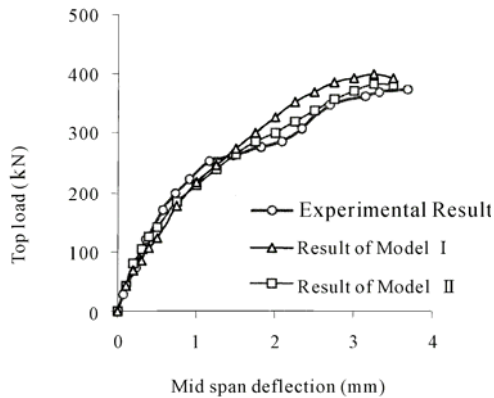
Fig. 15.11   Load-deflection curves of the deep beam (Zhou, 2002)

From this figure, it can be seen clearly that both models give reasonably accurate predictions of the overall response of the beam. Again, the results obtained from Model II are better than those from Model l. In particular for the ultimate capacity of the beam, the experimental value is 375 kN and the analytical values are 399.58 kN for Model I and 384.72 kN for Model II, with an error of 6.55% and 2.59%, respectively.

15.6   Elasto-Plastic Analysis of an RC Box Sectional Beam

From the examples in the previous two sections, we can see that Model II can yield better prediction than Model I for the load-deflection responses. In this section, therefore, Model II is employed to analyze the response of an RC box sectional beam under eccentric loading conditions by Zhou. The box girders tested by Rasmussen and Baker (1999) are analyzed here. The dimensions and the reinforcement layout are depicted in Fig. 15.12.

Three different configurations of anti-symmetric loading are studied, as illustrated in Fig. 15.13. Only point loads were applied at the mid-span. Load cases l and 2 invoke bending，torsion and distortion，while load case 3 invokes only torsion and distortion. It is worth noting that, in load case 2, the upward load is half of the downward load. In the test，the specimens were simply supported but torsionally restrained at both ends.
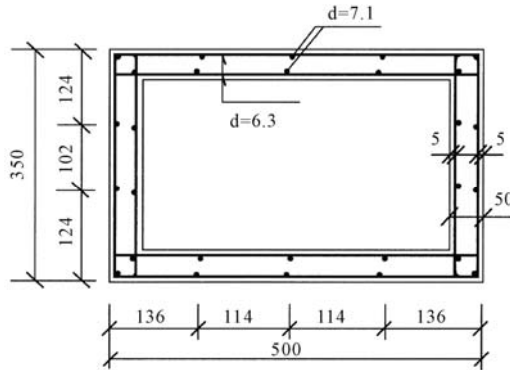
(a) Section A-A
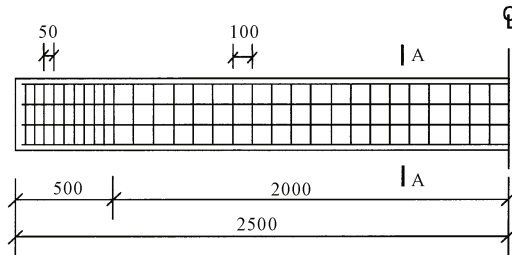
(b) Elevation and reinforcements

Fig. 15.12   Reinforcement layout (dimension in millimeters)
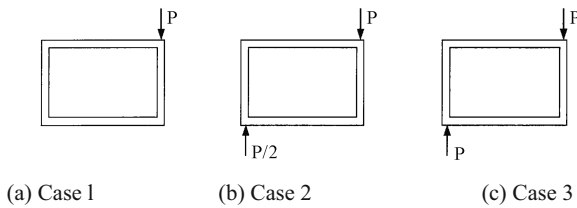
(a) Case 1   (b) Case 2   (c) Case 3

Fig. 15.13   Loading cases in mid-span section (Zhou, 2002)

Figure 15.14(a) shows the finite element mesh used in the calculation. Longitudinally it is divided into 60 segments with respect to the spacing of the stirrups. A two-node truss element and eight-node brick element are used to model the reinforced bars and the concrete, respectively. The concrete cover (5 mm) to the tension steel is ignored，as in the previous analysis. All the steel elements (truss elements) lie on the edges of brick elements (concrete). A perfect bond is assumed in this analysis. The material parameters used in the calculation are shown in Table 15.3.

Table 15.3   Material parameters of the RC box sectional beam

Parameters	Values
E_c	22000 MPa
E_s	200000 MPa
f_c	50.0 Mpa
f_t	4.00 Mpa
f_y	541 Mpa
v	0.2
UST parameter b	0.6
A_t	1.0
B_t=0.6	50000
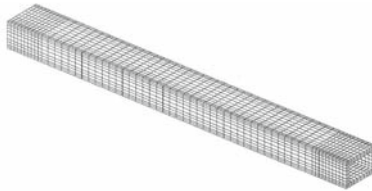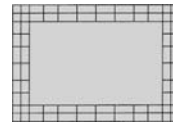
(a) Finite element mesh   (b) Cross section
Fig. 15.14   Finite element mesh used in the calculation

Figure 15.15 compares the numerical and the experimental results in load case
l. Figure 15.l5(a) plots the load versus the vertical deflection and Fig. 15.15(b)
plots the load versus the diagonal distortion. From these figures, it can be seen
clearly that the present model is able to yield good prediction of the overall
response (vertical deflection and diagonal distortion). In particular for the ultimate
capacity of the beam, the experimental value is about 83.0 kN and the analytical
value is 82.37 kN with an error of only 0.8%.
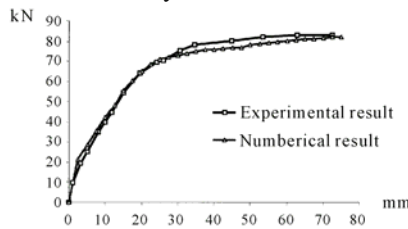
(a) Load versus vertical deflection
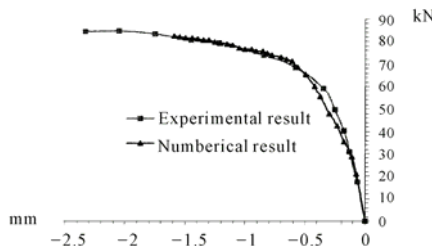
(b) Load versus diagonal distortion
Fig. 15.15   Comparison of numerical results and experimental results for load case 1

Similarly, Fig. 15.16 shows the analytical and experimental results of load versus vertical deflection and load versus diagonal distortion in load case 2.

(a) Load versus vertical deflection

(b) Load versus diagonal distortion
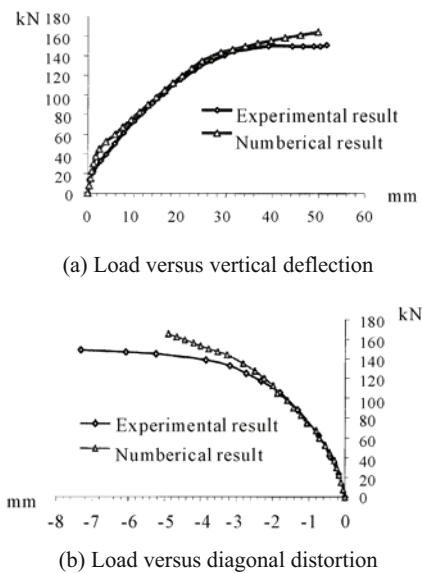
Fig. 15.16   Comparison of numerical results and experimental results for load case 2

Figure 15.17 shows those results in load case 3. From the figures, it can be found that the present model yields accurate predictions of the overall responses except for the near-failure regions, where deviation from experimental results is observed in all load cases, especially in the diagonal distortions. These discrepancies may arise from the differences in the restraint condition at the end supports because, in the test, torsion cannot be strictly restrained at both ends of the beam and end diaphragms were not cast. Nevertheless, the accuracy achieved with the present model can suffice in engineering applications.

(a) Load versus total rotation   (b) Load versus diagonal distortion
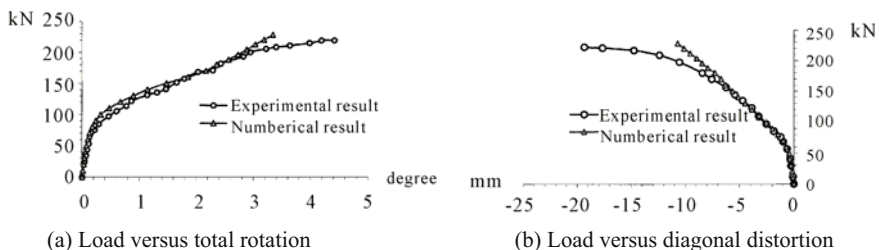
Fig. 15.17   Comparison of numerical results and experimental results for load case 3

On the other hand, the discrepancies may be due to the deviation of the material parameters, in particular the effect of Young's modulus. A sensitivity analysis is performed. Without loss of generality, only load Case 2 is studied here. Figure 15.18 shows the overall response obtained from different values of

Young's modulus. From the figures, it confirms that the variations in Young's modulus can affect the results, to some extent.
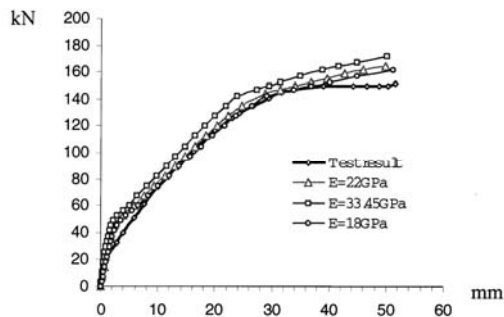
(a) Load versus vertical deflection
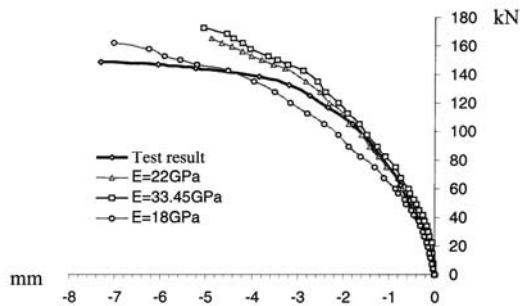
(b) Load versus diagonal distortion

Fig. 15.18 Sensitivity analysis of Young's modulus for load case 2 (Zhou, 2002)

15.7 Summary

Unified strength theory (UST) is also successfully implemented in several commercial FEM codes and finite difference method codes. The unified strength theory (UST) with different parameter b is also adopted as the failure criterion for the analysis of punching shear failure of beams and slab-column connections by Zhang et al. at Griffith University, Australia. Elasto-plastic analysis for reinforced concrete slabs and high-strength concrete slabs using the unified strength theory has also been successfully studied by Zhou and Wang and Fan at Nangyang Technical University in Singapore.

Through comparison of FE simulation results and the experimental data, conclusions can be drawn that the unified strength theory and its associated flow rule, and a new three-dimensional elasto-plastic-damage constitutive model for concrete, can be successfully implemented into non-linear FEM. The derived load-carrying capacities for all the beams and slabs are in good agreement with the

experimental data. Generally, the calculated deflections at different levels of load for all the slabs also reflect the real deformation procedure. The only exception is that the predicted deflections for the high-strength slabs are smaller than for the experimental counterparts, which implies that the high-strength slabs in the simulation are stiffer than the actual slabs. Damage distributions and the reinforcement stress distributions predict well the reinforcement anisotropy of the common concrete slabs and also the failure patterns for the high-strength concrete slabs.

Serial results can be obtained by using the unified strength theory (UST), which can be adopted for more materials. The material models are increasing and forming a series of systematic and effective constitutive relations for practical use. UST and its implementation in computer codes provide us with a very effective base and approach for studying the effect of failure criterion for various problems. It can be used for more materials and more structures. The strength potential of materials may be utilized by using UST with $b>0$.

References

Bresler B and Scordelis AC (1963) Shear strength of reinforced concrete beams. Journal of ACI Proceedings, 60(1): 51-72.

Chen WF (1982) Plasticity in Reinforced Concrete. McGraw–Hill: New York.

Chen WF (1998) Concrete plasticity: past, present and future. In: Strength Theory: Applications, Developments and Prospects for the 21st Century, Yu MH and Fan SC eds. Science Press: Beijing, New York, pp 7-48.

Duddeck H, Griebenow G, and Schaper G (1978) Material and Time-Dependent Nonlinear Behavior of Cracked Slabs. In: Nonlinear Behaviour of Reinforced Concrete Spatial Structures. Vol. 1, Preliminary Report, IASS Smp., Darmstadt. Darmstadt (Mehlhorn G, Ruhle H and Zerna W Eds.). Werner-Verlag: Dusseldorf, pp 101-113.

Fan SC, Wang F (2002) A new strength criterion for concrete. ACI Structural Journal, 99, May-June, 317-326.

Figueigas JA, Owen DRJ (1984) Analysis of Elasto-Plastic and Geometrically Nonlinear Anisotropic Plates and Shells. In: Finite Element Software for Plates and Shells (eds. Hinton E., Owen D.R.J.). Prineridge Press: Swansea, UK, pp 235-326.

Gervera M, and Hinton E (1986) Nonlinear Analysis of Reinforced Concrete Plates and Shells Using a Three Dimensional Model. In: Computational Modeling of Reinforced Concrete Structures (eds. Hinton E. and Owen D.R.J.). Pineridge Press: Swansea, U. K.

Gonzalez-Vidosa, Kotsovos FMD and Pavlovic MN (1988) Symmetrical punching of reinforced concrete slabs：An analytical investigation based on nonlinear finite element modeling.   ACI Structure Journal, 85(5-6): 241-250.

Guan H and Loo YC (1997b) Layered finite element method in cracking and

failure analysis of RC beams and beam-column-slab connections. Structural Engineering and Mechanics, 5(5): 645-662.

Guan H and Loo YC (1997a) Flexural and shear failure analysis of reinforced concrete slabs and flat plates, Advances in Structural Engineering, l(1): 7l-85.

Hinton E, Owen DRJ (1984) Finite Element Software for Plates and Shells. Pineridge Press: Swansea, UK.

Huang HC (1988) Static and Dynamic Analysis of Plates and Shells: Theory Software and Application. Pineridge Press Limited: Swansea, U. K.

Kotsovos MD, Pavlovic MN (1995) Structural Concrete: Finite element analysis for limit-state design. Thomas Tedford Publications, Thomas Telford Services Ltd., 1 Heron Quay, London E14 4JD.

Loo YC and Guan H (1997) Cracking and punching shear failure analysis of RC flat plates. Journal of the Structural Engineering, ASCE, l23(10): 1321-l330.

Marzouk HM, and Hussein A (1991) Experimental Investigation on the Behavior of High-Strength Concrete Slabs. ACI Structural Journal, 88: 701-713.

Nielsen MP (1984, 1999) Limit Analysis and Concrete Plasticity. CRC Press: London.

Ottosen NS (1977) A failure criterion for concrete. ASCE, EM. 4: 103.

Owen DJR, Hinton H (1980) Finite Elements in Plasticity: Theory and Practice. Pineridge Press Limited: Swansea, U. K.

Poh SP and Susanto T (1996) Experimental and analytical investigations on the ultimate strength and serviceability of structural concrete deep beam.   Applied Research Project RP15/92, School of Civil and Structural Engineering, Nanyang Technological University, Singapore, pp 353.

Rasmussen LJ and Baker G (1999) A large-scale experimental investigation of deformable RC box beams. ASCE   Jnl. Struct. Engrg., 125(3): 227-235.

Regan PE (1986) Symmetric punching of reinforced concrete slabs. Magazine of Concrete Research, 38(136):115-128.

Wang F (1998) Nonlinear Finite Element Analysis of RC Plate and Shell Using Unified Strength Theory. Ph.D. Thesis, Nanyang Technological University, Singapore.

Wang F, Teng S; Fan SC (2001) Softened damage model for finite element analysis of structural concrete deep beams, ACI Structural J., 8(1): 27-35.

Yu MH (1983) Twin shear stress yield criterion. Int. J. Mechanical Sciences, 25(1): 71-74.

Yu MH, He LN and Song LY (1985) Twin shear stress theory and its generalization. Scientia Sinica (Sciences in China), English Edition, Series A, 28(11): 1174-1183.

Yu MH and He LN (1991) A new model and theory on yield and failure of materials under the complex stress state. In: Mechanical Behavior of Materials-6, (ICM-6). Jono M and Inoue T ed. Pergamon Press: Oxford, 3: 841-846.

Yu MH (1992) New System for Strength Theory (in Chinese). Xi'an Jiaotong Umiversity Press: Xi'an, China (in Chinese).

Yu MH (2002) Concrete Strength Theory and iIts Applications (in Chinese).

Higher Education Press: Beijing.

Yu MH, Zan YW, Zhao J. Yoshimine M (2002) A unified strength criterion for rock material. Int.J. of Rock Mechanics and Mining Science, 39(6): 975-989.

Yu MH (2004) Unified Strength Theory and Its Applications. Springer: Berlin.

Yu MH et al. (2006) Generalized Plasticity. Springer: Berlin.

Zhang XS, Guan H and Loo YC (2001) UST (Unified Strength Theory) failure criterion for punching shear analysis of reinforcement concrete slab-column connections. In: Computational Mechanics–New Frontiers for New Millennium, Valliappan S. and Khalili N. eds. Elsevier Science Ltd, pp 299-304.

Zhang Bill, Guan H and Loo YC (2002) Unified strength theory for punching shear analyses of edge column-slab connections with stud shear reinforcement. The Second International Conference on Advances in Structural Engineering and Mechanics (ASEM'02), Pusan, Korea, 21-23 August 2002, Eds: Choi, C.K. and Schnobrich, W.C., Techno-Press, CDROM Proceedings, pp 1-8.

Zhou KR and Jiang DH (1991) Imitation of punching failure for reinforced concrete slabs in finite element method. Proc. Computational Mechanics, Hong Kong, pp 221-226.

Zhou XQ (2002) Numerical Analysis of Reinforcement Concrete Using Multi-Surface Strength Model. Ph.D. Thesis at Nanyang Technological University, Singapore.

16

Stability Analysis of Underground Caverns Based on the Unified Strength Theory

16.1 Introduction

In recent years, there has been an increasing interest internationally in the construction of large-scale underground powerhouses. The stability analysis of underground caverns in a hydropower station is often related to the safe operation of the whole station and provides enormous benefits. Due to their large scale, complicated space configurations and reactions between caverns, stability analysis of underground powerhouses is a very difficult and challenging task. Hence, the accurate description of the mechanical behavior of the rock mass and the selection of the rock properties is a very important research topic in underground construction.

The stability of large caverns has been investigated widely. To explore some aspects of the complex geometrical shape, the stress boundary conditions obtained from in-situ stress measurement and constitutive models for the rock mass, large caverns have been studied by Professor Qiao and Li Y. Based on the engineering background of Huanren pumped-storage powerhouse, the unified strength theory as a failure criterion was used in their study to analyze the stability of the main powerhouse and transformer cave and to carry out an investigation of underground excavation and support. The effect of the intermediate principal stress on rock failure and the support design will be discussed in this chapter.

16.2   Huanren Pumped-Storage Powerhouse and Geology

Huanren underground pumped-storage powerhouse is located in Tongtiangou, which is 4 km away from Huanren County, Liaoning Province, China. The project plans to utilize Huanren reservoir as the lower storage reservoir and to construct a dam in Tongtiangou gulley as the upper reservoir. A diversion tunnel is to connect with the underground powerhouse. The pivotal engineering construction mainly consists of the main dam, auxiliary dam of the upper reservoir, diversion tunnel and underground powerhouse. The maximum height of the main dam is 106 m and the length of the dam top is 632 m. The height of the auxiliary dam is 15 m and the length is 403.33 m. The underground powerhouse is located in the middle of the diversion tunnel and is 22.3 m wide, 50 m high and 136.2 m long.

The engineering region is covered with mountains and gullies. The mountain heights are all about 500~700 m and a few of them are over 1000 m high. The volcanic rocks formed in the Jurassic period of the Mesozoic era are widely distributed in the station area and are shaped into cuestas, mesas and all kinds of valleys.

16.2.1 The Powerhouse Region

The powerhouse zone is 136 m long, 22 m wide, 50 m high and 230 m deep. It is located in the interbeds of andesite-tuff and tuff-agglomerate with some tuff-agglomerate rocks near the top. And the direction angle of the axes is NE 15°. The RQD value of the zone is 95%, the acoustic velocity for andesite-tuff is 5.06 km/s, the acoustic velocity for the interbeds is 3.41~5.05 km/s and the associated integrity coefficients are 0.95 and 0.43~0.99.

The rock masses are almost intact, but the lithology of the 16th bed is complicated. In this bed, there are about ten strata of andesite-tuff which are 0.5~5 m thick and show poor properties. The strata will crack and fail when losing water, and have bad stability as well. There is a band standing at a borehole depth of 263 m (elevation of 267 m). The band with bad geological conditions is 15 cm thick, made up of green clay and rock fragments. The angle, measured in the axis of powerhouse tunnel from the band's strike direction, is only 15°~25°, and inclines toward the tunnel. It is very unfavorable for the stabilization of downstream sidewalls. The 15th layer of the tuff rock which is 3 m away from the tunnel's roof causes harm to the stability. In addition, a set of joints which strike NNE is dangerous for sidewall stability too.

16.2.2 *In Situ Stress Measurement in Huanren Pumped Storage Powerhouse*

The in-situ stress measurement involved in this project includes seven measurement sites. The figures obtained during the tests showed the same results.

According to the data obtained by the strain collector, stresses were calculated. An average was introduced when measurements were taken more than two times at one site. The gauge has 12 separate strain gauges, in rosettes of three, and there was some redundancy in the measurements. Thus statistical analysis of the least square method has been made.

16.3   **Comparison of Failure Criteria for Geomaterials**

Failure criteria can be used to understand the materials' response to loads, to determine the failure conditions in different stress states. The selection of failure criteria has a great impact on calculating the results of geotechnical engineering. Because of the differences between geomaterials and general materials in constitutive behavior, it is necessary to choose a suitable yield or failure criterion in engineering applications for purposes of economy and safety.

Various strength criteria have been developed in the past to describe the behavior of rock masses. Of these, the linear Mohr-Coulomb criterion and the nonlinear Hoek-Brown strength criterion are two of the most widely used strength criteria in geotechnical engineering. The Mohr-Coulomb failure criterion can be expressed as

$$\tau_f = c + \sigma \cdot \tan \phi \qquad (16.1)$$

where τ_f is the shear strength, c is the cohesion, ϕ is the friction angle and σ is the normal stress at the shear plane.

Currently, the Mohr-Coulomb strength theory is widely used. It explains that the tensile strength of rocks is much smaller than their shear strength. In addition, a specimen will yield under triaxial constant tension loading conditions and will not fail under triaxial constant compression loading conditions. The Mohr-Coulomb strength theory, however, only considers the effects of two principal stresses σ_1 and σ_3, but ignores the influence of σ_2. Mogi (1967; 1979) and Xu et al. (1985; 1986) and Li and Xu (1990) have proved the effects of σ_2 by using true tri-axial tests. Hence, the Mohr-Coulomb strength theory is an imperfect strength criterion.

The Drucker-Prager criterion is an extension of the Huber von Mises criterion, and is a modification of the Huber-von Mises yield criterion by adding a hydrostatic stress term. Zhu-Jiang Shen calls it a three-shear yield criterion. The expression is

$$F = F(I_1, J_2) = \sqrt{J_2} - \alpha I_1 = k \tag{16.2}$$

or

$$F = F(p, q) = q - 3\sqrt{3}\alpha p = \sqrt{3}k \tag{16.3}$$

where α and k are material parameters which can be deduced from the cohesion and the internal angle of friction.

The intermediate principal stress and the hydrostatic stress are taken into account in the Drucker-Prager criterion. The criterion has been widely used and popularized after it was proposed. However, under some conditions, the criterion contradicts the experimental results. Hence, the criterion has seldom been used in recent years.

The Hoek-Brown failure criterion is an empirical criterion which is derived from experimental data obtained from some triaxial compression tests performed on rocks. Since its first introduction, the criterion has been modified several times. For a jointed rock, the Hoek-Brown failure criterion has been found more suitable than the Mohr-Coulomb criterion. The Hoek-Brown strength parameters can be estimated based on the GSI system, which provides the guidance for the peak strength estimation of rock masses. The latest version of the generalized Hoek-Brown criterion for jointed rock masses is defined by

$$\sigma_1 = \sigma_3 + \sigma_{ci}(m_b \frac{\sigma_3}{\sigma_{ci}} + s)^a \tag{16.4}$$

where σ_3 and σ_{ci} are the minimum principal stress and the uniaxial compressive strength (UCS) of the intact rock, respectively, m_b, s and a are rock mass strength parameters which depend upon the characteristics of the rock mass. The parameters can be determined by using the GSI index and m_i value.

The effect of intermediate principal stress, however, is not taken into account both in the Mohr-Coulomb and the Hoek-Brown strength criteria. Maohong Yu demonstrates that the maximum principal shear stress τ_{13} is always equal to the sum of the other two principal shear stresses τ_{12} and τ_{23}, i.e., $\tau_{13} = \tau_{12} + \tau_{23}$, which means that there are only two independent components in three principal shear stresses. So failure criteria consider the effects of the two relatively larger principal shear stresses. According to the change in the intermediate principal stress, Yu proposed mathematical modeling in the form of twin formulas. Based on the twin-shear criterion (Yu, 1961a; 1985), a parameter related to the effect of intermediate principal stress is considered. The unified strength theory assumes that the materials start to yield when the sum of the two larger principal shear stresses and the corresponding normal stress function reaches a constant value. The mathematical modeling can be expressed as follows:

$$F = \tau_{13} - \beta\sigma_{13} + b(\tau_{12} - \beta\sigma_{12}) = K \quad (\tau_{12} - \beta\sigma_{12} \geq \tau_{23} - \beta\sigma_{23}) \tag{16.5}$$

$$F' = \tau_{13} - \beta\sigma_{13} + b(\tau_{23} - \beta\sigma_{23}) = K \quad (\tau_{12} - \beta\sigma_{12} \leq \tau_{23} - \beta\sigma_{23}) \tag{16.6}$$

where b is a parameter reflecting the influence of the intermediate principal shear stress on the yield of materials. In terms of the convex failure criteria, the value of b ranges from 0 to 1. β is the coefficient representing the effect of the normal stress on the yield and K is a strength parameter of the material. β and K can be expressed as

$$\beta = \frac{1-\alpha}{1+\alpha}, \quad K = \frac{2}{1+\alpha}\sigma_t, \quad \alpha = \frac{\sigma_t}{\sigma_c} \tag{16.7}$$

The shear stresses $\tau_{13}, \tau_{12}, \tau_{23}$ and normal stresses $\sigma_{13}, \sigma_{12}, \sigma_{23}$ can be written by

$$\tau_{13} = \frac{1}{2}(\sigma_1 - \sigma_3), \ \tau_{12} = \frac{1}{2}(\sigma_1 - \sigma_2), \ \tau_{23} = \frac{1}{2}(\sigma_2 - \sigma_3) \tag{16.8}$$

$$\sigma_{13} = \frac{1}{2}(\sigma_1 + \sigma_3), \ \sigma_{23} = \frac{1}{2}(\sigma_2 + \sigma_3), \ \sigma_{12} = \frac{1}{2}(\sigma_1 + \sigma_2) \tag{16.9}$$

The unified strength theory can be used in yield analysis for a wide range of materials, and each proposed strength criterion is just a special type of the unified strength criterion. The unified strength theory consists of twin functions and corresponding limited conditions. The suitable formula should be chosen according to the stress state when the criterion is used. The same strength of materials can be obtained when the two limited conditions are both satisfied simultaneously.

16.4 Determination of Rock Mass Strength Parameters

The effect of intermediate principal stress is not considered in the Mohr-Coulomb and the Hoek-Brown strength criteria, which means that the two strength criteria cannot reasonably reflect the characteristics of variability in rock strength when the intermediate principal stress changes. The unified strength theory incorporates the intermediate principal stress and can choose different parameters according to the data resulting from true triaxial tests on rocks or rock masses. The unified strength theory cannot solve the problem of the yield angle, but this will not affect the deduction of the flow rule used for continuum modeling. The unified yield criterion does not contradict the other strength criteria, while the other criteria are the special cases of the unified strength criterion.

In this study, the unified strength theory is chosen as the failure criterion for the stability analysis of Huanren pumped-storage powerhouse, and the Hoek-Brown criterion is chosen for the determination of parameters from the test data.

For good-quality andesite, Hoek-Brown strength parameters m_b, s and α are estimated to be 1.7, 0.004 and 0.5, respectively, and the uniaxial compressive strength of the intact rock is 70 MPa. Considering the parameters, the criterion can be expressed as

$$F = \sigma_1 - \sigma_3 - \sqrt{1.7 \times 70 \sigma_3 + 0.004 \times 70^2} = 0 \qquad (16.10)$$

It is deduced from Eq. (16.10) that σ_1 is equal to 68.9 MPa when the compressive strength of the rock mass is 4.43 MPa and $\sigma_3 = 20$ MPa. After substituting the parameters mentioned above in Eq. (16.5), we obtain $\beta = 0.53$, $\dfrac{K}{1+b} = 1.034$. Thus $\alpha = 0.31$ can be calculated from Eq. (16.7) and $\sigma_t = \sigma_c \cdot \alpha = 1.36$ MPa from Eq. (16.7). The parameter b will be determined by the experimental results of true tri-axial tests.

16.5 Constitutive Formulation of Unified Strength Theory Used for Fast Lagrangian Analysis

Incremental formulations similar to those of the Mohr-Coulomb model in Flac-3D are used, i.e., only the elastic part of the strain increment will contribute to the stress increment and the elastic behavior is linear. The equations have the forms

$$\Delta \sigma_1 = \alpha_1 \Delta \varepsilon_1^e + \alpha_2 (\Delta \varepsilon_2^e + \Delta \varepsilon_3^e) \qquad (16.11)$$

$$\Delta \sigma_2 = \alpha_1 \Delta \varepsilon_2^e + \alpha_2 (\Delta \varepsilon_1^e + \Delta \varepsilon_3^e) \qquad (16.12)$$

$$\Delta \sigma_3 = \alpha_1 \Delta \varepsilon_3^e + \alpha_2 (\Delta \varepsilon_1^e + \Delta \varepsilon_2^e) \qquad (16.13)$$

where α_1 and α_2 are material constants defined by the shear modulus G, and bulk modulus.

$$\alpha_1 = K + \frac{4}{3} G \qquad (16.14)$$

$$\alpha_2 = K - \frac{2}{3} G \qquad (16.15)$$

The unified form from Eq. (16.11) to Eq. (16.13) can be expressed as

$$\Delta \sigma_i = S_i (\Delta \varepsilon_n^e), \quad (i=1, n) \qquad (16.16)$$

The failure criterion can be written as

$$f(\sigma_n) = 0 \tag{16.17}$$

where f is the yield function based on the unified strength theory. The strain increment can be decomposed into elastic and plastic components from the following equation.

$$\Delta\varepsilon_i = \Delta\varepsilon_i^e + \varepsilon_i^p \tag{16.18}$$

The new stress-vector components must comply with the yield function, which can be expressed as

$$f(\sigma_n + \Delta\sigma_n) = 0 \tag{16.19}$$

A non-associated shear plastic flow rule and an associated tensile plastic flow rule are defined in the Flac-3D model. But the tensile failure is a special case of shear failure according to the unified strength theory, so only a non-associated shear plastic flow rule is used. The form is given by

$$\Delta\varepsilon_i^p = \lambda \frac{\partial g}{\partial\sigma_i} \tag{16.20}$$

From the further expression of the plastic strain increment in the flow rule, the stress increment can be written as

$$\Delta\sigma_i = S_i(\Delta\varepsilon_n) - \lambda S_i\left(\frac{\partial g}{\partial\sigma_n}\right) \tag{16.21}$$

where $S_i(\Delta\varepsilon_n)$ is linear. The strength criterion is a linear function of principal stresses, so Eq.(16.19) is expressed as

$$f(\sigma_n) + f^*(\Delta\sigma_n) = 0 \tag{16.22}$$

where f^* represents the function f minus its constant term. For a stress point σ_n on the yield surface, there is $f(\sigma_n) = 0$. After considering Eq. (16.21) for the stress increment in Eq. (16.22), there is

$$f^*\left[S_n(\Delta\varepsilon_n)\right] - \lambda f^*\left[S_n\left(\frac{\partial g}{\partial\sigma_n}\right)\right] = 0 \tag{16.23}$$

The new total stress increment σ_i^N and elastic guesses σ_i^I can be expressed

as follows:

$$\sigma_i^N = \sigma_i + \Delta\sigma_i \tag{16.24}$$

$$\sigma_i^I = \sigma_i + S_i(\Delta\varepsilon_n) \tag{16.25}$$

Using the same method as above, Eq. (16.25) can be written as

$$f(\sigma_n^I) = f^*[S_n(\Delta\varepsilon_n)] \tag{16.26}$$

It can be derived from Eqs. (16.23) and (16.26) that

$$\lambda = \frac{f(\sigma_n^I)}{f^*\left[S_n\left(\dfrac{\partial g}{\partial \sigma_n}\right)\right]} \tag{16.27}$$

From Eqs. (16.21), (16.24), (16.25) and (16.27), we can obtain

$$\sigma_i^N = \sigma_i^I - \lambda S_i(\frac{\partial g}{\partial \sigma_n}) \tag{16.28}$$

Unlike metal materials, geomaterials comply with non-associated flow rules. But, so far, the non-associated flow rules have not been clearly proposed. Taking the definition of unified strength theory and the general principles of Flac-3D into consideration, a special non-associated flow rule is discussed in this case.

First, if the associated flow rule is applied, just as for the arguments used in traditional plastic mechanics, the rule can be expressed as follows:
(i) When $\tau_{12} + \beta\sigma_{12} \geq \tau_{23} + \beta_{23}$ (Take tensile stress as positive)

$$\frac{\partial g}{\partial \sigma_1} = -1 \tag{16.29}$$

$$\frac{\partial g}{\partial \sigma_2} = \frac{\alpha b}{1+b} \tag{16.30}$$

$$\frac{\partial g}{\partial \sigma_3} = \frac{\alpha}{1+b} \tag{16.31}$$

(ii) When $\tau_{12} + \beta\sigma_{12} \leq \tau_{23} + \beta_{23}$ (Take tensile stress as positive)

$$\frac{\partial g}{\partial \sigma_1} = -\frac{1}{1+b} \tag{16.32}$$

$$\frac{\partial g}{\partial \sigma_2} = -\frac{b}{1+b} \tag{16.33}$$

$$\frac{\partial g}{\partial \sigma_3} = \alpha \tag{16.34}$$

Then we can incorporate the flow rule into the modeling of Flac-3D. We find that the rock dilation is too large zones in the failure model. So a non-associated flow rule should be used here.

The flow rules used in Flac-3D derive from the associated flow rules by modifying some parameters, e.g., the forms of the Mohr-Coulomb strength theory and Drucker-Prager criterion. And, traditionally, the dilation angle is used for the evaluation of the plastic expansion of rock. So the equations are modified corresponding to the non-associated law as follows:

(i) When $\tau_{12} + \beta \sigma_{12} \geq \tau_{23} + \beta_{23}$ (Take tensile stress as positive)

$$\frac{\partial g}{\partial \sigma_1} = -1 \tag{16.35}$$

$$\frac{\partial g}{\partial \sigma_2} = \frac{\alpha' b}{1+b} \tag{16.36}$$

$$\frac{\partial g}{\partial \sigma_3} = \frac{\alpha'}{1+b} \tag{16.37}$$

(ii) When $\tau_{12} + \beta \sigma_{12} \leq \tau_{23} + \beta_{23}$ (Take tensile stress as positive)

$$\frac{\partial g}{\partial \sigma_1} = -\frac{1}{1+b} \tag{16.38}$$

$$\frac{\partial g}{\partial \sigma_2} = -\frac{b}{1+b} \tag{16.39}$$

$$\frac{\partial g}{\partial \sigma_3} = \alpha' \tag{16.40}$$

where $\alpha' = \dfrac{1-\sin(\psi)}{1+\sin(\psi)}$, and ψ is the dilation angle of the rock.

Taking the compressive stress as positive, and changing the coefficient of the first principal stress to a constant, we obtain the following:

(i) When $\tau_{12} - \beta \sigma_{12} \geq \tau_{23} - \beta_{23}$ (Take compressive stress as positive)

$$\frac{\partial g}{\partial \sigma_1} = 1 \qquad (16.41)$$

$$\frac{\partial g}{\partial \sigma_2} = b \qquad (16.42)$$

$$\frac{\partial g}{\partial \sigma_3} = -N_\psi (1+b) \qquad (16.43)$$

(ii) When $\tau_{12} - \beta\sigma_{12} \leq \tau_{23} - \beta_{23}$ (Take compressive stress as positive)

$$\frac{\partial g}{\partial \sigma_1} = 1 \qquad (16.44)$$

$$\frac{\partial g}{\partial \sigma_2} = -N_\psi \frac{b}{1+b} \qquad (16.45)$$

$$\frac{\partial g}{\partial \sigma_3} = -N_\psi \frac{1}{1+b} \qquad (16.46)$$

when $b=0$, the Mohr-Coulomb strength theory can be deduced from the unified strength theory and the expressions from Eq. (16.41) to Eq. (16.46) have the same forms of the Mohr-Coulomb flow rule used in Flac-3D. According to the equations from Eq. (16.41) to Eq. (16.46), we have

$$\frac{\partial g}{\partial \sigma_1} = 1 \qquad (16.47)$$

$$\frac{\partial g}{\partial \sigma_2} = 0 \qquad (16.48)$$

$$\frac{\partial g}{\partial \sigma_3} = -N_\psi \qquad (16.49)$$

The advantages of the flow rule used here are as follows:

(a) In common with the Mohr-Coulomb theory, a dilation angle is incorporated into functions to account for rock dilation, which is caused by the creation and propagation of cracks during rock deformation. The value of the dilation angle can be zero when the dilation needs not to be considered.

(b) Taking the effect of the intermediate principal stress into account, relationships have been perfectly established between the unified strength theory and the Flac-3D numerical modeling. (e.g. if some parameters are used in the unified strength theory for the deduction of the Mohr-Coulomb strength criterion, by choosing the same parameters in the unified strength model defined in Flac-3D, we will get the same equations for the flow rule as Mohr-Coulomb's criterion used in Flac-3D.)

When strain-hardening or strain-softening does not take place, the relationships between stresses and the criterion can be expressed as

$$F\left(\sigma_i\right) = 0, \ \ \mathrm{d}F = \frac{\partial F}{\partial \sigma_i} \mathrm{d}\sigma_i < 0 \qquad \text{(Unloading conditions)};$$

$$F\left(\sigma_i\right) = 0, \ \ \mathrm{d}F = \frac{\partial F}{\partial \sigma_i} \mathrm{d}\sigma_i = 0 \qquad \text{(Loading conditions)};$$

$$F\left(\sigma_i\right) < 0 \qquad\qquad\qquad \text{(Elastic state)}.$$

16.6 Development of Unified Strength Theory Model in Flac-3D

The methodology of writing new constitutive models in Flac-3D is called UDM (User-defined Model). The model must be developed in the C++ language and complied as a DLL file In order to create a new constitutive model, the following header files are necessary:

(a) AXES.H — specifies a particular axes system;

(b) CONMODEL.H — utility structure used to communicate with constitutive model;

(c) CONTABLE.H — defines the TABLE interface for general constitutive models;

(d) STENSOR.H— symmetric tensor storage.

Users only need to program the personal header file and classes.

(a) USERMODEL. H— user-defined head file;

(b) USERMODEL. CPP— listing of member functions.

After creating a workspace in VC++, we can create a user-defined DLL module, which contains the six files mentioned above. Before the UDM model is developed in Flac-3D, USERMODEL.DLL must be registered and loaded.

In this case, the model's name is "Double-Shear"(Twin-Shear), and the essentially parameters are bulk modulus (bulk), shear modulus (shear), dilation angle (dilation), the parameter b (bxi), the parameter α (afa) and uniaxial tensile strength (tension). In addition, the contours of the elastic modulus and Poisson's ratio can be plotted out as zones. Hence, the user-defined model can be associated and implemented in the same ways as other basic constitutive models provided in Flac-3D.

16.7 Test of User-Defined Unified Strength Theory Constitutive Model in Flac-3D

As shown in Fig. 16.1, the model is 50 mm long, 50 mm wide and 100 mm

high. First, fixing z-velocities of the top and bottom surfaces and applying 100 MPa confining pressure, we obtain a balance of the elastic model. The property parameters are listed in Table 16.1. Thereafter, the Mohr-Coulomb model is associated with the zones and the velocity is applied on the top surface in thenegative direction of the z-axis instead to the foregoing constraint of the surface. A history command is adopted to monitor the variations in the displacement and stresses. The stress-strain curves for different parameters are shown in Fig. 16.2 for the rock compression process.
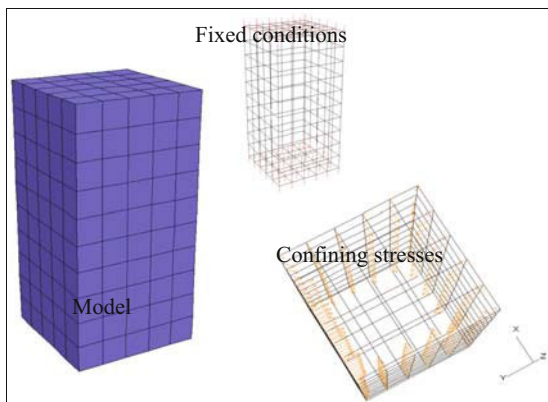
Fig. 16.1   Model zones and boundary conditions.

Table 16.1   Mohr-Coulomb strength parameters in the first simulation test

Input parameters	Values
$\sigma_2(\sigma_x)$	100 (Mpa)
$\sigma_3(\sigma_y)$	100 (MPa)
c	1 (MPa)
φ	10 (°)
Bulk	200 (MPa)
Shear	200 (MPa)

Table 16.2   Mohr-Coulomb strength parameters in the second simulation test

Input parameters	Values
$\sigma_2(\sigma_x)$	110 (Mpa)
$\sigma_3(\sigma_y)$	100 (MPa)
C	1 (MPa)
φ	10 (°)
Bulk	200 (MPa)
Shear	200 (MPa)
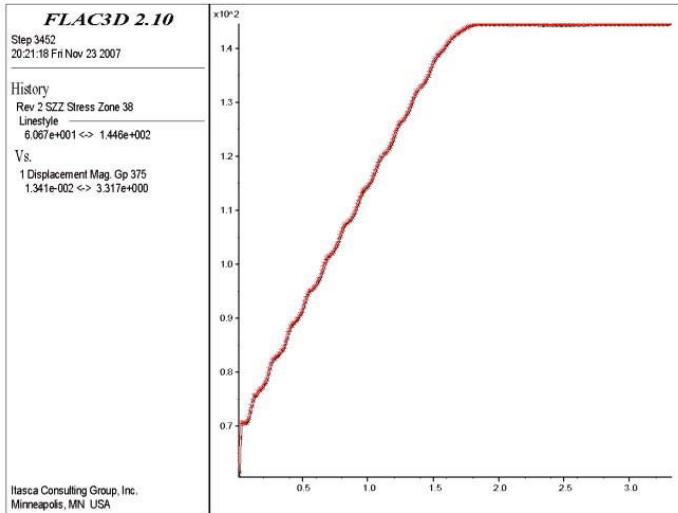
Fig. 16.2   Stress-strain curves of the two Mohr-Coulomb models with different parameters

Under the same stresses and boundary conditions, the unified strength model is used for comparison. The input parameters are shown in Table 16.3. A series of b values with $b=0$, $b=0.5$, $b=0.8$, and $b=1$ are inputted into the model in sequence and the final results can be found, as shown in Fig. 16.3.
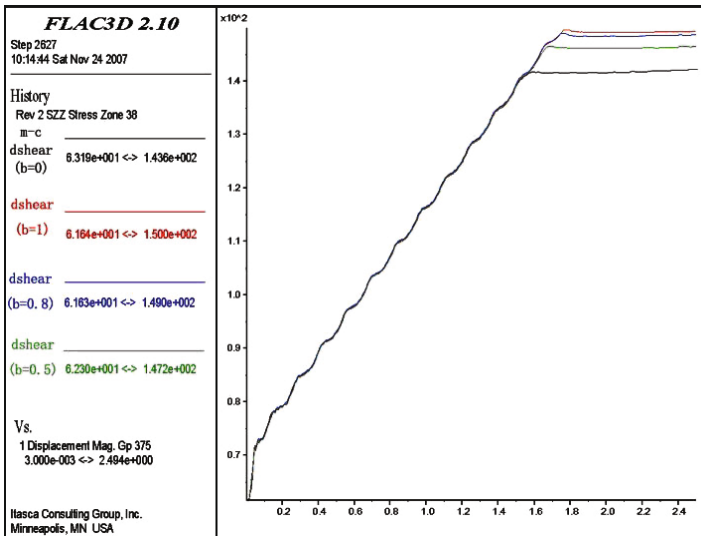
Fig. 16.3   Stress-strain curves of unified strength model with different values of b

Table 16.3   Parameters of the model associated with the unified strength theory

Input parameters	Values
$\sigma_2(\sigma_x)$	110 (MPa)
$\sigma_3(\sigma_y)$	100 (MPa)
Tensile stress	1.68 (MPa)
α	0.71 (°)
Bulk	200 (MPa)
Shear	200 (MPa)

It can be seen that the result is the same with the curve of the Mohr-Coulomb model, and the strength is about 144 MPa when $b=0$. Obviously, the intermediate principal stress makes the strength increase to 150 MPa when $b=1$. In addition, the strength is 149 MPa when $b=0.8$, and the strength is 147 MPa when $b=0.5$. Both the theoretical and test values are listed in Table 16.4.

The comparisons between numerical modeling results based on the unified strength model and theoretically analytical results based on the unified strength theory are presented in Table 16.4. It can be found from Table 16.4 that the user-defined model, i.e., unified strength model for analysis in Flac-3D, reflects very well the characteristics of the unified strength theory.

Table 16.4   Numerical simulation and theoretically analytical results based on UST

	Principal stresses	$\sigma_2(\sigma_x)$ (MPa)	$\sigma_3(\sigma_y)$ (MPa)	$\sigma_1(\sigma_z)$ (MPa)
$b=0$	Theoretically analytical result	110	100	143.6
	Numerical modeling result	110	100	143.2
$b=1$	Theoretically analytical result	110	100	150.0
	Numerical modeling result	110	100	150.3
$b=0.8$	Theoretically analytical result	110	100	149.0
	Numerical modeling result	110	100	149.4
$b=0.5$	Theoretical analytical result	110	100	147.2
	Numerical modeling result	110	100	147.9

16.8   Stability Analysis of Underground Powerhouse

16.8.1 Generation of Numerical Model and Selection of Parameters

The size of the numerical model is 240 m × 100 m × 260 m. The main power house is 22.3 m wide and 51.3 m high. The main transformer cave is 17.9 m wide and

32.2 m high. The outer boundaries have been modeled at a distance of around six tunnel widths from the tunnel in both directions to minimize the boundary effect on the analytical results. There are 44760 zones and 28017 grids in the model, which is shown in Fig. 16.4.

The in-situ stresses are applied on the boundary surfaces. The properties for the intact rock based on the experimental data are applied to the rock mass using the Hoek-Brown criterion. The properties of some rocks and the stresses are listed in Table 16.5.

Table 16.5   Property of some models

Rock type	Unit weight $(kN/m^{3)}$	Bulk modulus (GPa)	Shear modulus (GPa)	b	α	Dilation angle (°)	Rock classes CSIR	Tensile strength (MPa)
Tuff-agglomerate	27.6	21.74	17.69	0.15	0.23	0	Good rock	1.5
Andesite-tuff	27.0	22.31	17.44	0.13	0.21	0	Good rock	0.9
Interbeds of andesite-tuff and tuff-agglomerate	27.3	21.68	17.64	0.21	0.31	0	Good rock	1.36
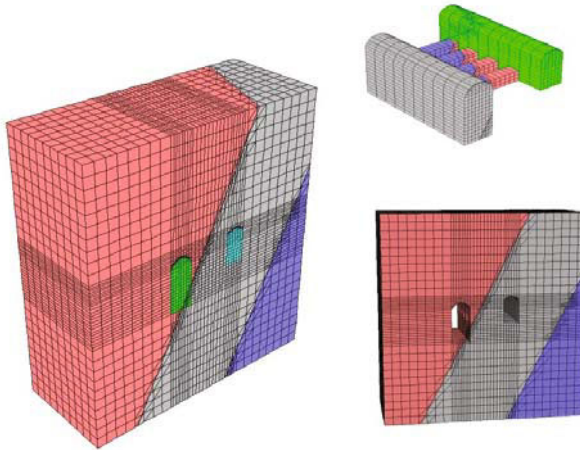
Fig. 16.4   Modeling for numerical analysis

16.8.2   Simulations for Different Excavation Schemes

The excavation of a cavern is always carried out step by step. In order to allow a reasonable step height and excavation procedures, simulations with different construction schemes are carried out. The specifications of hydraulic projects show that the step height should be about 8 m, so heights of 9 m and 12 m are

chosen in numerical modeling for the examples. There are two excavation sequences for each example with different step heights. Figures. 16.5 and 16.6 illustrate the schemes.
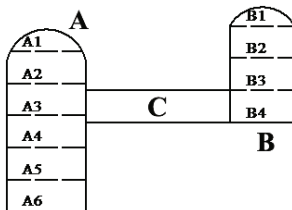
Fig. 16.6   Scheme with the step height is 12 m
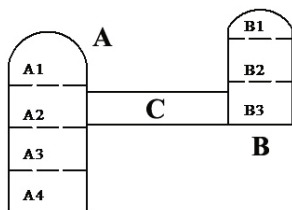
Fig. 16.5   Scheme with the step height is 9 m

The excavations cause plastic failure in certain regions. In the unified strength model, the sign shear-n shows that the zone is now in a state of shear failure, and the sign shear-p shows that the zone was previously in a state of shear failure and is elastic now. Selected results are shown in Figs. 16.7~16.11. Some researchers prioritise against displacement and a failure region by using the analytic hierarchy process method. Considering that the failure around the power house is mainly affected by the scale of the excavation and the excavation sequence makes a minor contribution, we establish the criteria for analyzing the stability of the power house based on the principles of the New Austrian Tunneling Method.

Table 16.6   Scheme of excavation procedure with 9 m height step

First sequence with step height of 9 m				Second sequence with step height of 9 m			
Excavation sequence number	Main power house	Main transformer	Omnibus bar cave	Excavation sequence number	Main power house	Main transformer	Omnibus bar cave
1	A1	B1		1	A1		
2	A2	B2		2	A2		
3	A3	B3		3	A3	B1	
4	A4	B4	C	4	A4	B2	C
5	A5			5	A5	B3	
6	A6			6	A6	B4	

Table 16.7 Scheme of excavation procedure with 12 m height step

First sequence with step height of 12 m				Second sequence with step height of 12 m			
Excavation sequence number	Main power house	Main transformer	Omnibus bar cave	Excavation sequence number	Main power house	Main transformer	Omnibus bar cave
1	A1	B1		1	A1		
2	A2	B2		2	A2	B1	
3	A3	B3	C	3	A3	B2	C
4	A4			4	A4	B3	
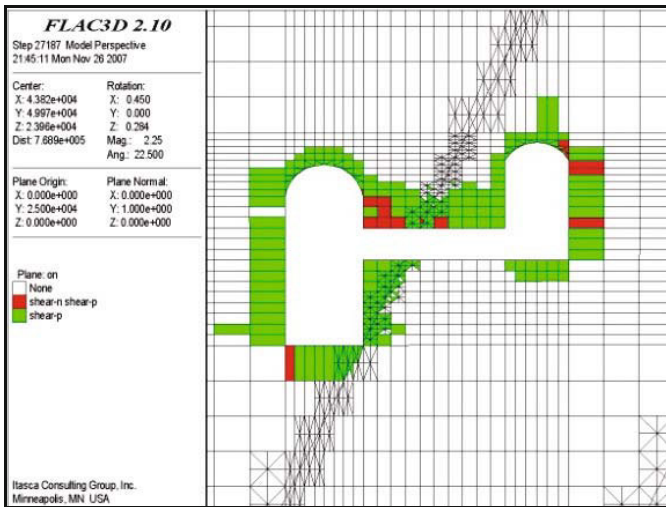
Fig. 16.7 Distributions of failure zones at last step in the first excavation sequence of the scheme

Distributions of failure zones in the first excavation sequence of the scheme are shown in Fig. 16.7 and Fig. 16.8. The step height is 9 m. Figure 16.7 shows the distributions of failure zones at the last step in the first excavation sequence of the scheme. Other failure zones at different steps are shown in Fig. 16.8. Distributions of failure zones in the second excavation sequence of the scheme are shown in Fig. 16.9. The step height is also 9 m.
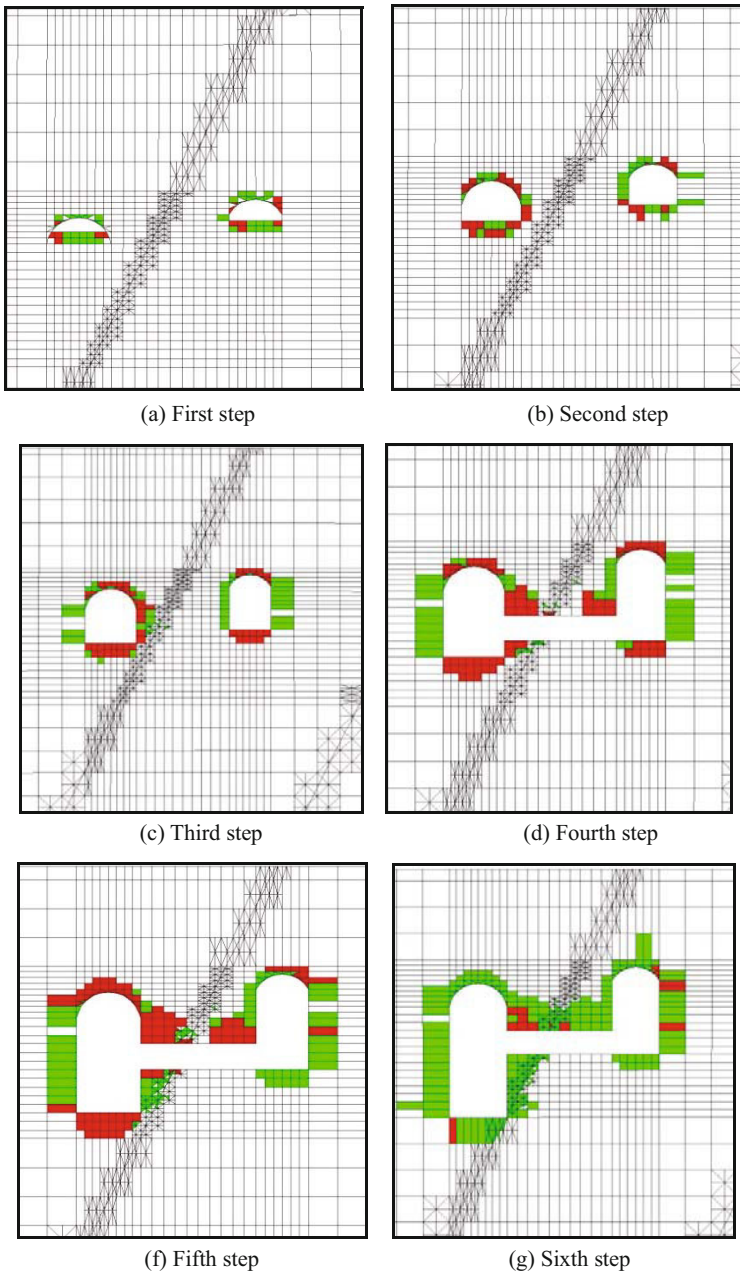
(a) First step

(b) Second step

(c) Third step

(d) Fourth step

(f) Fifth step

(g) Sixth step

Fig. 16.8   Distributions of failure zones in the first excavation sequence of the scheme

(a) First step

(b) Second step

(c) Third step

(d) Fourth step

(e) Fifth step

(f) Sixth step
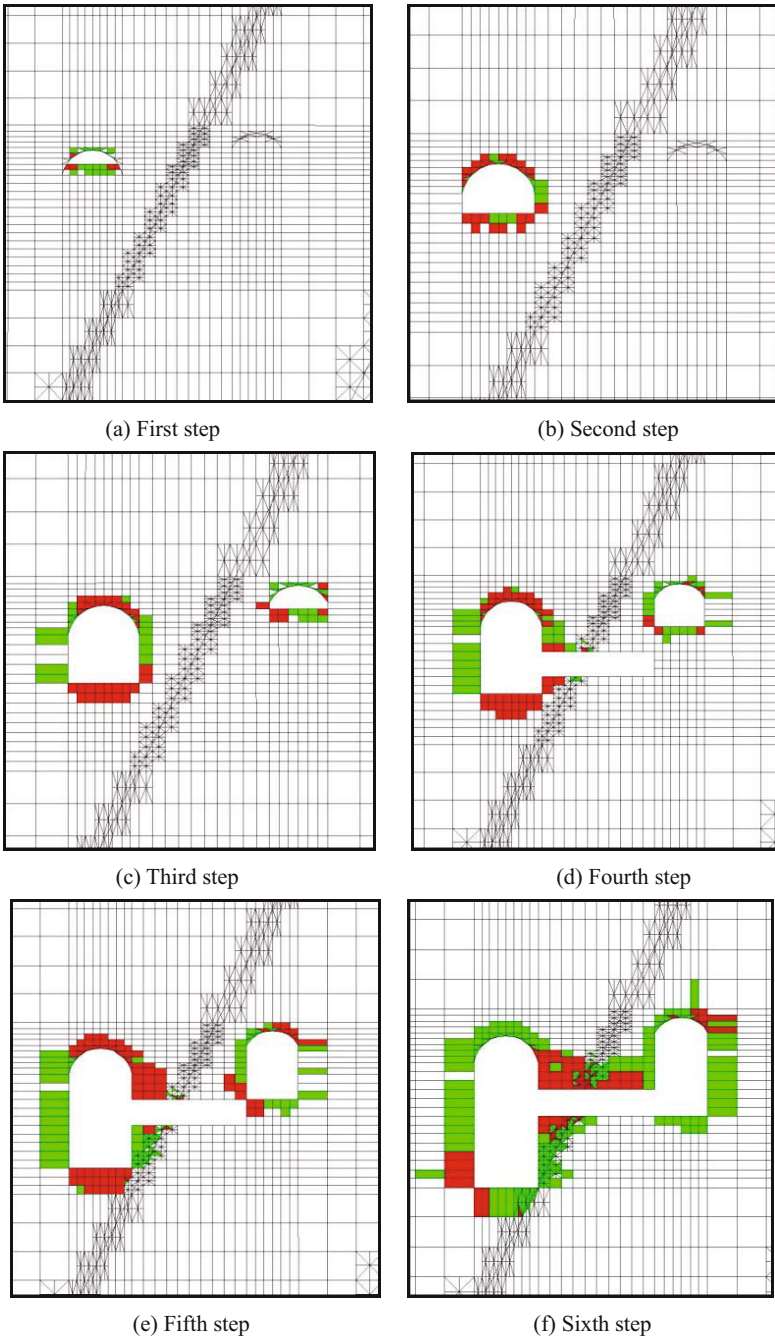
Fig. 16.9 Distributions of failure zones in the second excavation sequence of the scheme with the step height is 9 m

Distributions of failure zones in the first excavation sequence of the scheme are shown in Fig.16. 10. The step height is 12 m. Distributions of failure zones in the second excavation sequence of the scheme are shown in Fig. 16.11. The step height is also 12 m

(a) First step   (b) Second step

(c) Third step   (d) Fourth step
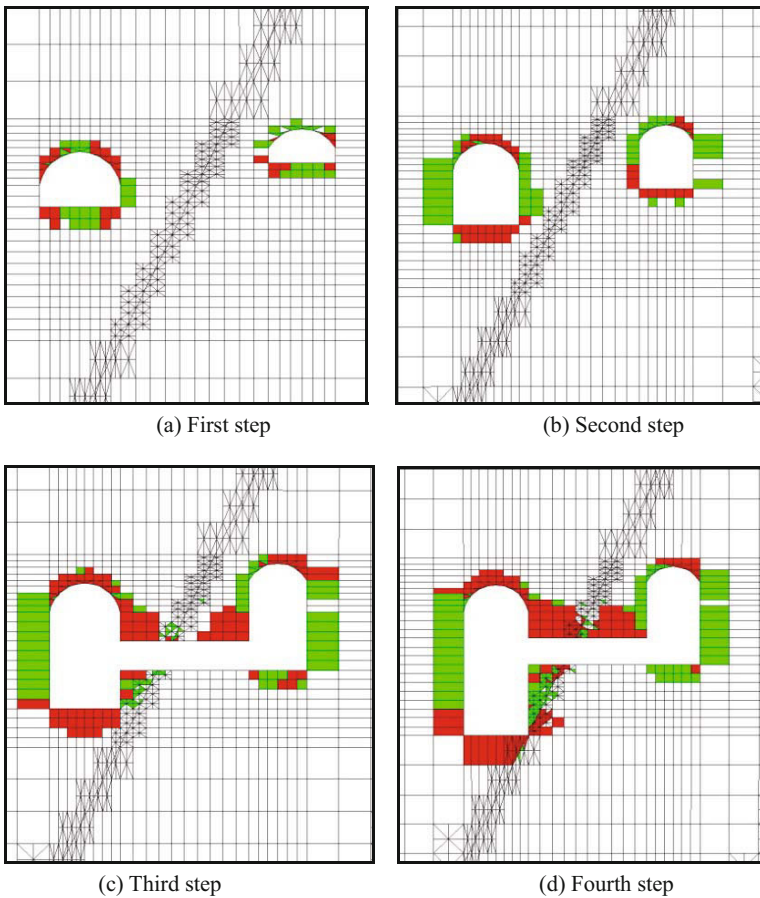
Fig. 16.10   Distributions of failure zones in the first excavation sequence of the scheme with the step height 12 m.

The New Austrian Tunneling Method (NATM) is very important for the design of tunnels. The method complies with the principles of measuring frequently, supporting in time, and closing the steel arch early. To choose a reasonable excavation procedure, which will have the minimum impact on the rock mass and where the reinforcement of the tunnel can be supported relatively earlier, a comparison of four excavation procedures is carried out. Each of the four schemes reveals the following features:

(a) First step   (b) Second step

(c) Third step   (d) Fourth step
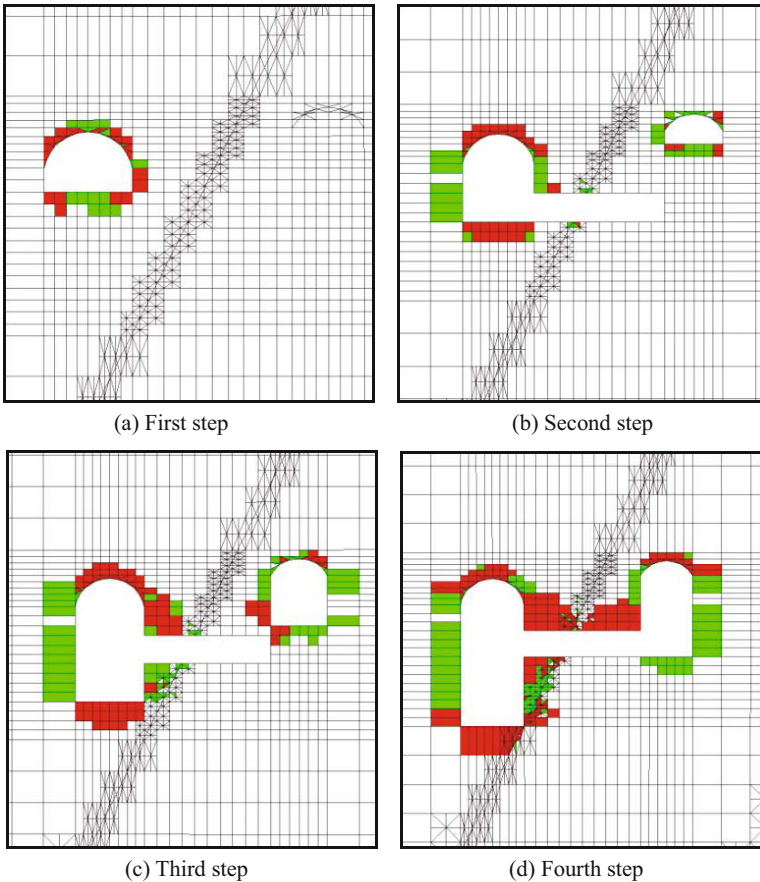
Fig. 16.11 Distributions of failure zones in the second excavation sequence of the scheme with the step height 12 m

(a) The failure region on the top of the tunnel is small, but the larger the excavation scale, the larger is the extent of the failure region.

(b) Plastic regions can be very close to each other because of the excavation of the main power house tunnel and the main transformer cave (i.e., cavern A and cavern B in Figs. 16.5 and 16.6)

(c) Omnibus bar caves (i.e., cave C in Figs. 16.5 and 16.6) excavated in the rock masses within the plastic zones are very unstable.

(d) Excavation of omnibus bar caves causes a secondary disturbance to the failure regions of the walls between the main power house tunnel and the main transformer cave.

To minimize the impact of the excavation of omnibus bar caves (i.e., cave C in Figs. 16.5 and 16.6) on the failed rock mass, to finish the excavation and the support of omnibus bar caves earlier, and to decrease the extent of the plastic region caused by the excavation of the first step, the first excavation

sequence with a 9 m height step is selected as the excavation scheme, which is subsequently used for the following supporting analysis.

16.9 Excavation and Support Modeling

The first excavation sequence with a 9 m height step is chosen for the following supporting analysis. First, supports for the initial design are given.

    Supports for the main power tunnel and the main transformer caverns:

Length of the fully grouted rebar bolt installed in top rock	5 m
Length of the fully grouted rebar bolt installed in wall	4.5 m
Rebar diameter	32 mm
Rebar bolting pattern	1.5 m×1.5 m
Length of the cable installed in wal	20 m
Cable bolting pattern	4.5 m×6 m
Tensile strength of cable	2×10^5 kg

    Supports of omnibus bar caves:

Length of the fully grouted rebar bolt	4 m
Rebar bolt diameter	28 mm
Rebar bolting pattern	3 m×3 m
Shotcrete type Chinese C20	
Liner thickness	15 cm

    The supports are illustrated in Fig. 16.12.
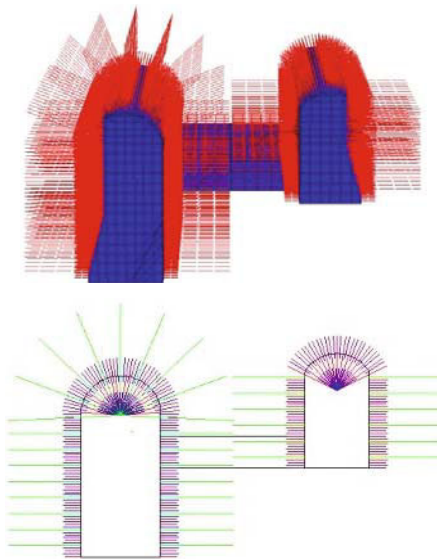
Fig. 16.12   Supports of the caverns

After a balance is reached, selected results are shown in Figs. 16.11~6.14. Distribution of the failure regions on a vertical plane is shown in Fig. 16.13. The contour of vertical displacements along the *z*-axis is shown in Fig. 16.14 and the contour of the horizontal displacement is plotted in Fig. 16.15.
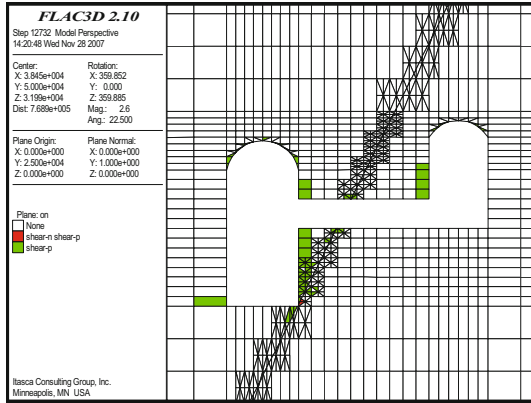
Fig. 16.13   Plastic region distribution with the support in initial design
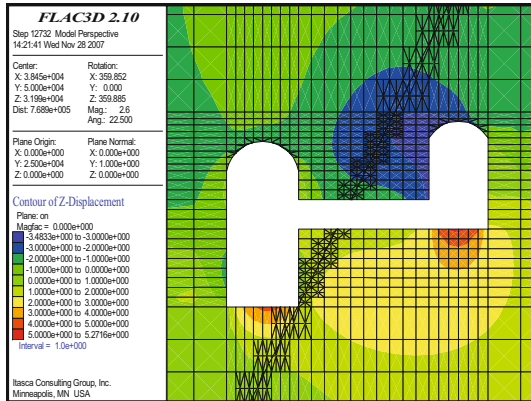
Fig. 16.14   Contour of virtical displacement with the support in initial design.

It is obvious that the tunnel is stable, the plastic zones can only be found in the wall and the extent is small. The maximum subsidence of the tunnel roof is 4 mm and the maximum vertical displacement of the main transformer cavern is located on the side and close to the main power-house. The maximum convergence in a horizontal direction is about 28 mm.

Considering that the support stiffness is high in this case, we adjusted the parameters of the support as follows:

(a) Took off the cables anchored at the top of the main power house in the initial design.

(b) Transferred the pattern of rebar bolting to 2 m×2 m.

The modeling results are shown in Figs. 16.16~16.18.
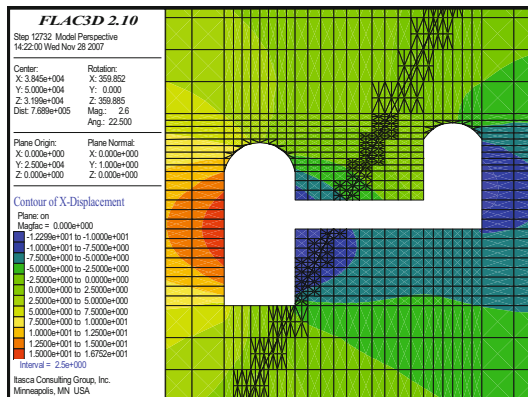
Fig. 16.15   Contour of horizontal displacement in the second design

When the stiffness of the support is degraded, the plastic region is beyond the range covered by the rebar bolts. The maximum subsidence of the tunnel roof is 7.8 mm and the maximum convergence is 55 mm. It can be seen that the support stiffness of the side walls of the main power-house tunnel in the second design is not enough, so a rebar bolt pattern of 1.5 m×1.5 m should be selected for the support of the main power-house tunnel side walls.

During the construction, the measurements based on the principles of reasonable engineering should be applied and the pattern should be tailored, on site, to the idiosyncrasy of the project. From the analysis above, the values of parameter b are both 0.33.
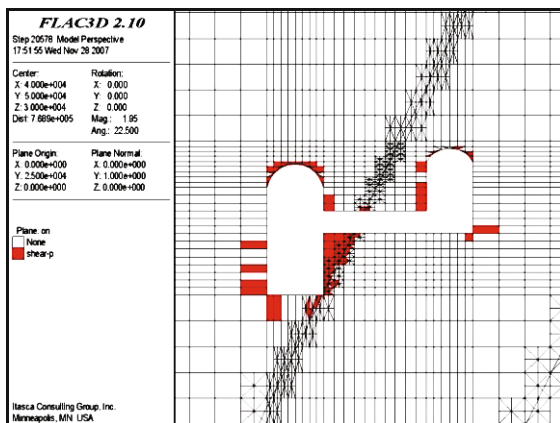
Fig. 16.16   Plastic region distribution with the support
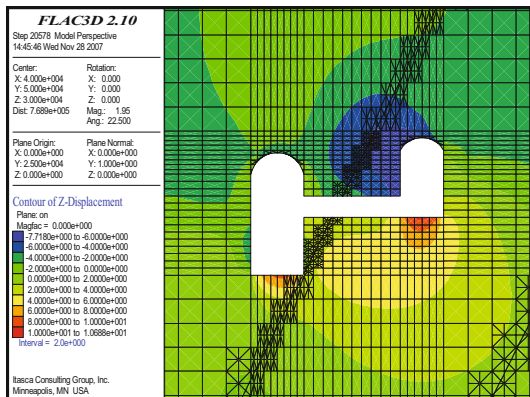
Fig. 16.17   Contour of virtical displacement with the support in second design
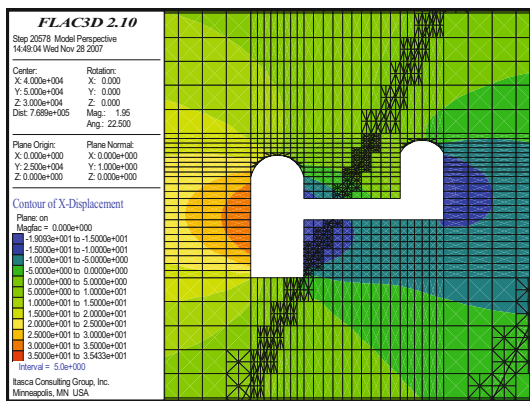
Fig. 16.18   Contour of horizontal displacement in the support second design.

16.10   Comparison of the Stabilities in these Models with Different *b* Values

The selection of different values of parameter *b* in the unified strength theory can provide a series of failure criteria, such as the single-shear (Mohr-Coulomb) yield criterion (when *b*=0) and twin-shear yield criterion (when *b*=1). Because of the variety of strength envelopes of unified strength theory on the π plane, different strength values can be obtained in the same stress state. An engineer should make a reasonable design to find which one is appropriate for the engineering objective, and which strength criterion of rock masses is the most contributing factor affecting our designs. None of the failure criteria can universally be utilized in overall rock masses, so we can compare the results obtained from different constitutive models with the same geometry, the same properties but with different

values of parameter b. The support in the second design is installed, and the results are illustrated in Figs. 16.19, 16.20 and 16.21, which show the variety of plastic region, vertical displacement and horizontal displacement of the models with different values of parameter b in the second support design
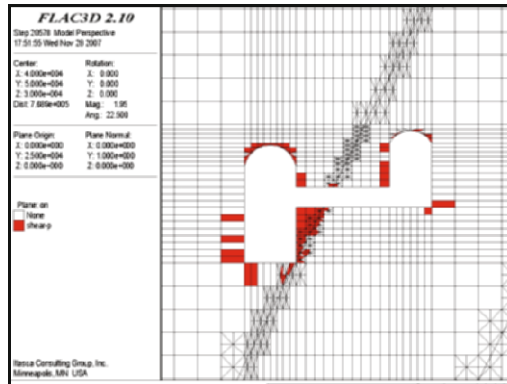
(a) UST with $b=0.3$
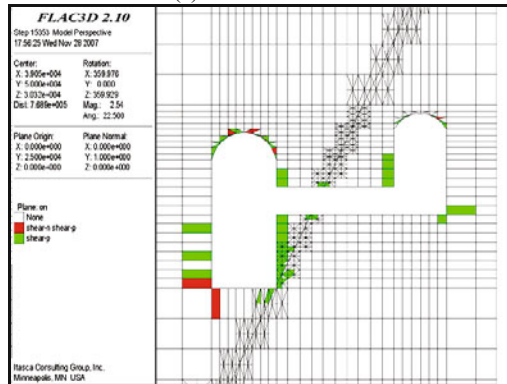
(b) UST with $b=0.5$
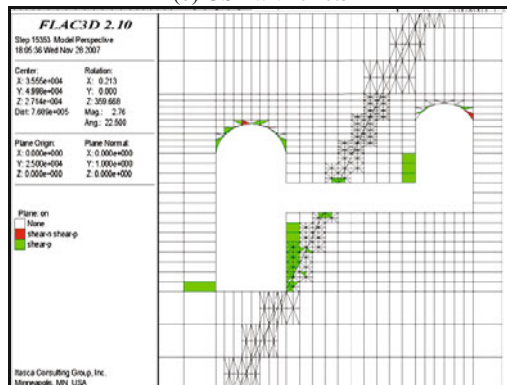
(c) UST with $b=0.8$

Fig. 16.19   Variety of plastic region of the models with different values of parameter b
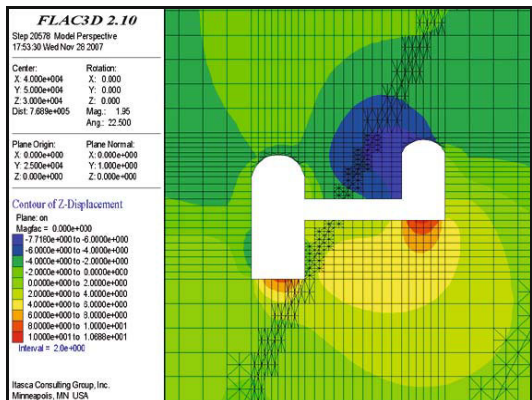
(a) UST with *b*=0.3
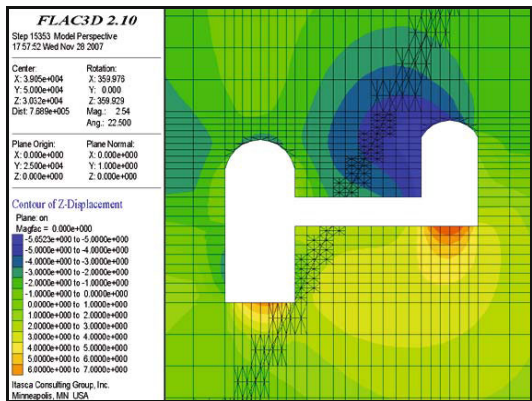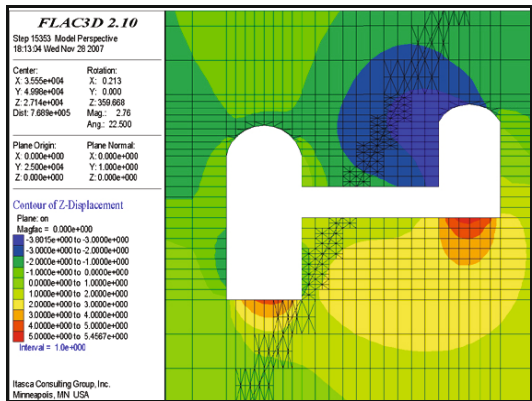
(b) UST with *b*=0.5

(c) UST with *b*=0.8

Fig. 16.20 Variety of vertical displacement of models with different parameter *b*
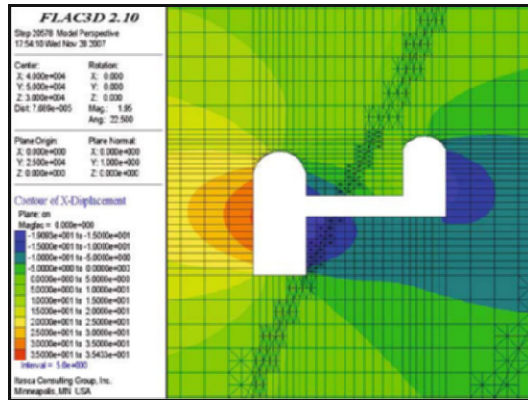
(a) UST with $b=0.3$
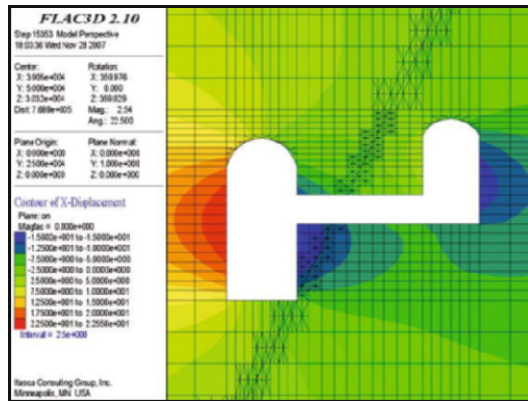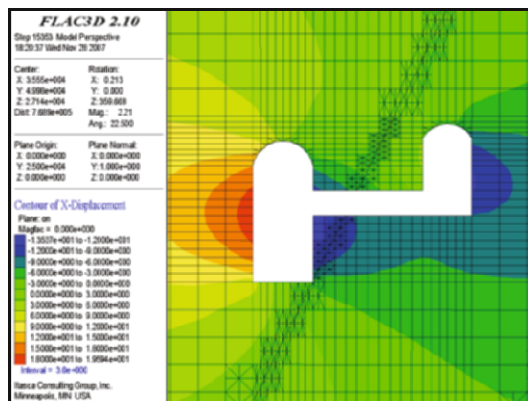
(b) UST with $b=0.5$

(c) UST with $b=0.8$

Fig. 16.21   Variety of horizontal displacement of models with different parameter b

It can be seen that the effect of the intermediate principal stress is incorporated in numerical modeling by the parameter *b* in unified strength theory, which affects the distribution of failure zones and the contour of displacements. The spread of the plastic region of the main transformer cavern and the main power-house becomes smaller when the value of parameter *b* increases from 0.3 to 0.5. The maximum roof subsidence is 5.6 mm when *b*=0.8. The parameters of support and the mechanical properties of the rock mass are the same but the range of the plastic region and the displacements of grids are all similar to those with the same support as in the initial design. In the construction of a hydraulic project, high values of stiffness and strength are usually accepted, so the stabilization results from numerical modeling with different strength criteria may be similar. But enormous economic benefits might be obtained in the construction of projects if a large plastic region is allowed.

16.11   Conclusions

Compared to the popular strength criteria used for geomaterials, the unified strength theory is selected for the stability analysis of the power station. Considering the absence of the unified strength model in Flac-3D constitutive models, a unified strength model with a non-associated flow rule is developed using the C++ language. True triaxial simulation tests are implemented, and the stress-strain curves based on the Mohr-Coulomb model and the unified strength model are obtained, respectively. According to the comparison with the simulation results, the unified strength model can reasonably represent the effect of the intermediate principal stress.

Through the numerical stability analysis of Huanren pumped storage power station using the unified strength theory, the following conclusions are made:

(a) Because of the large scale of excavation, the rock mass between the main power-house tunnel and the main transformer tunnel will fail seriously if a support system is not installed. In this case, the maximum horizontal principal stress normal to the tunnel axis is harmful to the stability of the caverns. So the principles of the New Austria Tunneling Method should be followed and the excavation of the rock mass in the tunnel roof should be carried out in small steps in order to reduce the range of failure. According to the analysis of results from the numerical modeling of unsupported tunnels, a first excavation sequence is proposed.

(b) It can be obtained from the calculated results using the unified strength model inserted in Flac-3D that the support stiffness in the initial design is high. Hence, some substitutions of the support parameters are used for further analysis. The results from the second support design show that the range of the plastic region in the tunnel side walls becomes larger, the maximum subsidence of the tunnel roof goes from from 4 mm to 7.8 mm, and the maximum convergence goes from 28 mm to 55 mm.

(c) The different values of parameter *b* make failure conditions of the caverns vary within a certain range. In this case, the stable state obtained from *b*=0.3 in the initial design is similar to that obtained from *b*=0.8 in the second design. It is shown that estimation and determination of the intermediate principal stress is important for the stability analysis and can have an important effect on the financial benefit.

References

Li XC and Xu DJ (1990) Experimental verification of the twin shear strength theory–true triaxial test research of strength of the granite in a large power station on Yellow River. Research Report (Rock and Soil 1990-52) of Institute of Rock and Soil Mechanics. Chinese Academy of Sciences (in Chinese).

Li Y (2008) In-situ Stress Measurement and Stability Analysis Based on the Unified Strength Theory in Large Scale Underground Caverns Zone. Doctoral Dissertation, Beijing Scientific and Technical University.

Mogi K (1967a) Effect of the intermediate principal stress on rock failure. J. Geophysics Res., 72: 5117-5131.

Mogi K (1967b) Effect of the triaxial stress system on fracture and flow of rock. Phys. Earth Planet Inter., 5: 318-324.

Mogi K (1979)   Flow and fracture of rocks under general triaxial compression. Proc. of 4th Int. Congress on Rock Mechanics (Montreux), Balkema, Rotterdam, Vol: 123-130.

Xu DJ and Geng NG (1984) Rock rupture and earthquake caused by change in the intermediate principal stress. Acta Seismologica Sinica, 6(2): 159-166 (in Chinese).

Xu DJ and Geng NG (1985) The variation law of rock strength with increase in intermediate principal stress. Acta Mechanics Solida Sinica, 7: 72-80 (in Chinese, English abstract).

Yu MH (1961a) General behavior of isotropic yield function. Research Report of Xi'an Jiaotong University. Xi'an, China (in Chinese).

Yu MH (1961b) Plastic potential and flow rules associated singular yield criterion. Research Report of Xi'an Jiaotong University. Xi'an, China (in Chinese).

Yu MH, He LN and Song LY (1985) Twin shear stress theory and its generalization. Scientia Sinica (Sciences in China), English edn. Series A, 28(11): 1174-1183.

Yu MH (1998) Twin Shear Theory and its Applications. Science Press: Beijing (in Chinese).

Yu MH (2004) Unified Strength Theory and its Applications. Springer: Berlin.

17

Stability of Slope

17.1 Introduction

There are more and more side slope problems and slope engineering problems every day along with the increase in human activity. These will be the most common geotechnical engineering problems needing to be addressed in the natural geological environment. The side slope in civil engineering, water conservation engineering as well as traffic engineering is extremely common. Many excellent monographs are devoted to this field (Baker and Gather, 1978; Bishop, 1955; Brand, 1989; Chen, 2003; Chen et al., 2005; Cividin, 2001; Dong et al., 2004; Duncan, 1996; Fredinnd, 1984; Hudson and Harrison, 1997; Janbu, 1973; Leshchinsky, 1990, 1992; Morgenstem, 1992; Morgenstem and Price, 1965; Pan, 1980; Zhang and Zhou, 1997; Zhou and Yang, 2005).

The high slope of the ship-lock of the Three Gorges Project is an example of one of the key technologies used in this great project. Figure 17.1 is a bird's-eye view of the ship-lock of the Three Gorges Project (Encyclopedia of Water Resources in China, Second Edition, 2006). The numerical simulation of deformation for the high slope is shown in Fig. 17.2.

The unified strength theory has been used in slip line field and characteristics analysis (Yu et al., 2006). The slip line fields of two examples are illustrated in Figs. 17.3 and 17.4. A series of results of the bearing capacity for a trapezoid structure can be obtained by using the unified slip field theory, as shown in Fig. 17.5.

Fig. 17.1   Superb view over ship-lock of the Three Gorges Project
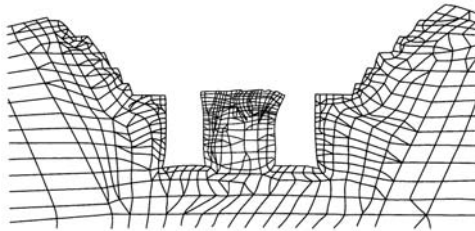
Fig. 17.2   Numerical simulation of deformation for the high slope
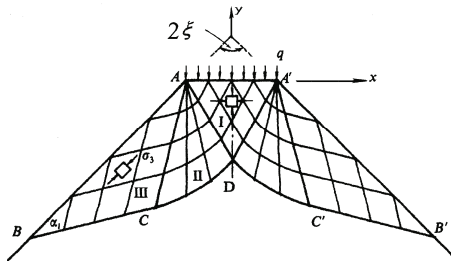
Fig. 17.3   Slip field of a trapezoid structure
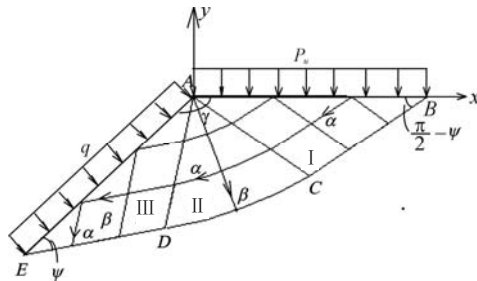
Fig. 17.4   Slip field of obtuse wedge
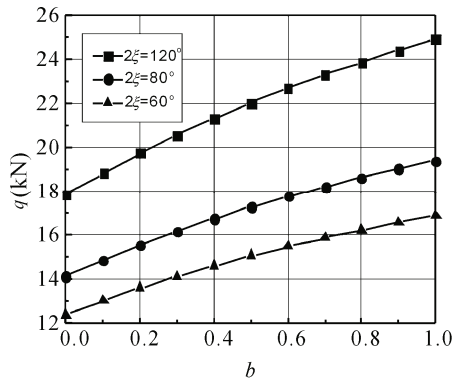
Fig. 17.5   Bearing capacity of a trapezoid structure

The UST (unified strength theory) and the slip line field theory are also implemented into ANSYS by Li and Chen (2010). According to the stress fields derived by finite element calculations, the slip line fields with UST material parameters in elastic and plastic zones were simulated. The critical slip surface on slopes was searched for through the slip line fields and the safety factor was derived so as to solve problems of slope stability. The results can be employed to analyze differences in safety factors and positions of the critical slip surfaces for various unified yield criteria, as shown in Fig. 17.6 (Li K and Chen ER, 2010). It is seen that the slip surface is dependent on the unified strength theory parameter b. The critical safety factor is also dependent on the unified strength theory parameter b.
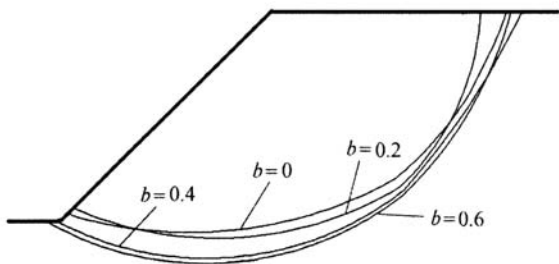
Fig. 17.6   Critical slip surfaces for various unified strength theory parameters b

Stability of a slope has been studied widely. It still remains open to debate, however, including the choice of yield criterion. The effect of yield criteria is rarely studied in this regard in the context of the safety factor, stability and excavation of vertical faces etc. The single-shear theory (Mohr-Coulomb strength theory) does not consider the effect of intermediate principal stress. A more comprehensive strength theory is also very significant.

The effect of yield criteria on the analysis of a slope, the excavation analysis of the Three Gorges ship lock (carried out by the Yangtze River Academy of

Sciences), the excavation simulation of a vertical surface face, and the numerical simulation of the slope of a highway in Guangxi Province, China (Bai, 2007) are described in this chapter. Using the unified strength theory in the computer analysis can also be a good application. A series of results are obtained by using the unified strength theory, which encompasses the Mohr-Coulomb criterion as a special case. Using the unified strength theory (Yu, 1992; 2004) it is possible for us to adopt different results of the numerical analysis to handle the effects of different materials and different structures.

17.2   Effect of Yield Criterion on the Analysis of a Slope

Stability of a slope is analysed by Dr. Ma ZY with respect to the unified strength theory, as shown in Fig. 17.7.
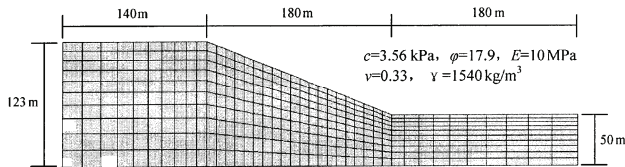
Fig. 17.7   A slope problem in Shaanxi province, China

The reason for using the unified strength theory is explained by the fact that the single-shear theory of Mohr-Coulomb or the three-shear theory of the Drucker-Prager criterion do not completely match with experimental data. It has been shown that the yield criteria of geomaterials depend not only on the maximum shear stress, but also on the intermediate principal shear stress (also on the intermediate principal stress σ_2) and the third invariant of the deviatoric stress tensor J_3. The reason that the Mohr-Coulomb theory and the Drucker-Prager criterion are not in good agreement with the experimental data is that the effect of J_3 and the effect of σ_2 are neglected.

The unified strength theory with $b=0$, $b=0.25$, $b=0.5$, $b=0.75$ and $b=1$ are used. The plastic displacements of the slope with different yield criteria under the same condition are shown in Fig. 17.8. The plastic strain based on the unified strength theory with $b=0$, $b=0.25$, $b=0.5$, $b=0.75$ and $b=1$ are given in Fig. 17.9. The difference is obvious.

The configurations of displacement vectors of a slope using different yield criteria are shown in Fig. 17.10. The configurations of deformations of finite elements of a slope are shown in Fig. 17.11. Five results using the unified strength theory with $b=0$, $b=0.25$, $b=0.5$, $b=0.75$ and $b=1$ are presented. Another three results using the Mohr-Coulomb criterion and the Drucker-Prager criterion are also presented, which are obtained by using the original material model in FLAC-2D. The differences are obvious.
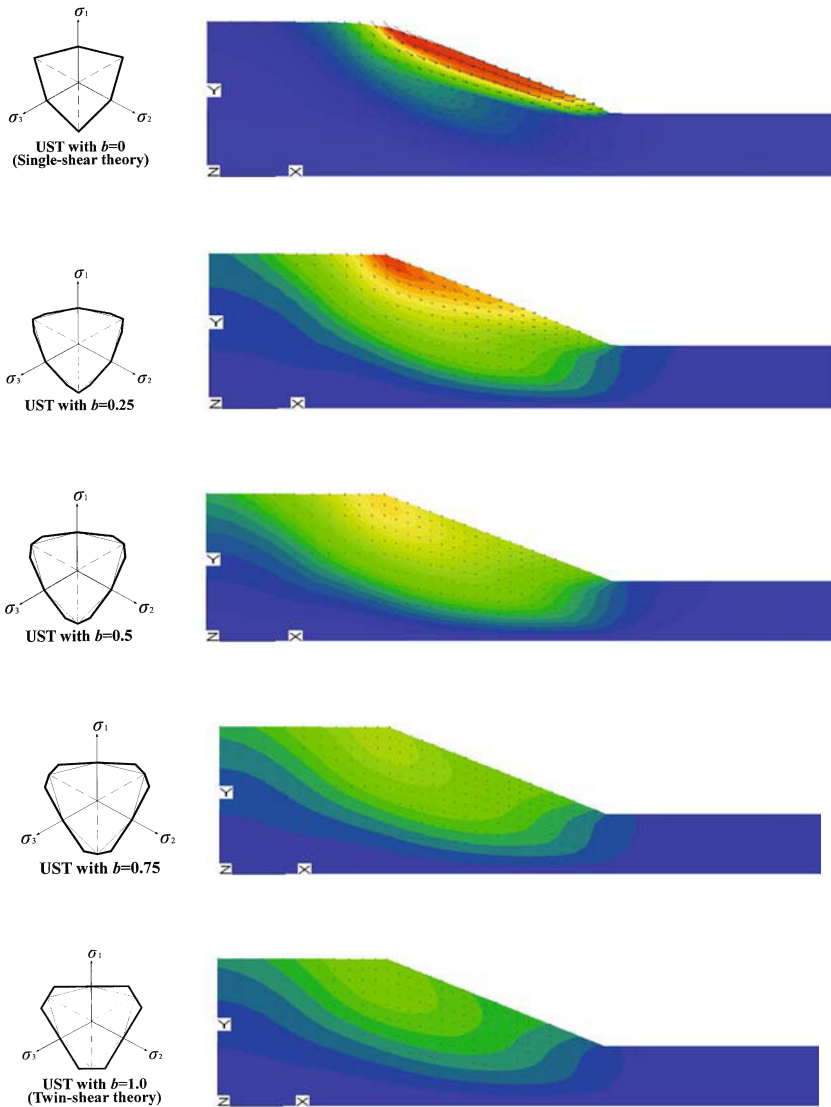
Fig. 17.8   Displacements of the slope with different yield criteria
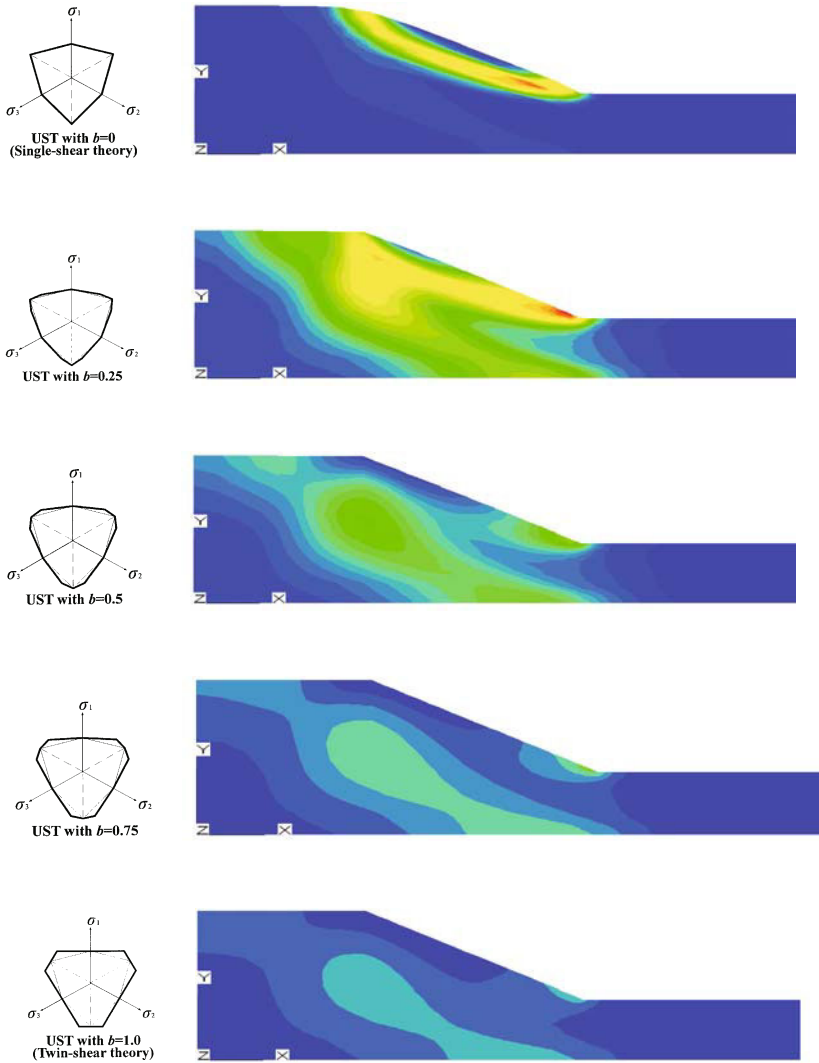
Fig. 17.9   Configuration of plastic strain of the slope with different yield criteria
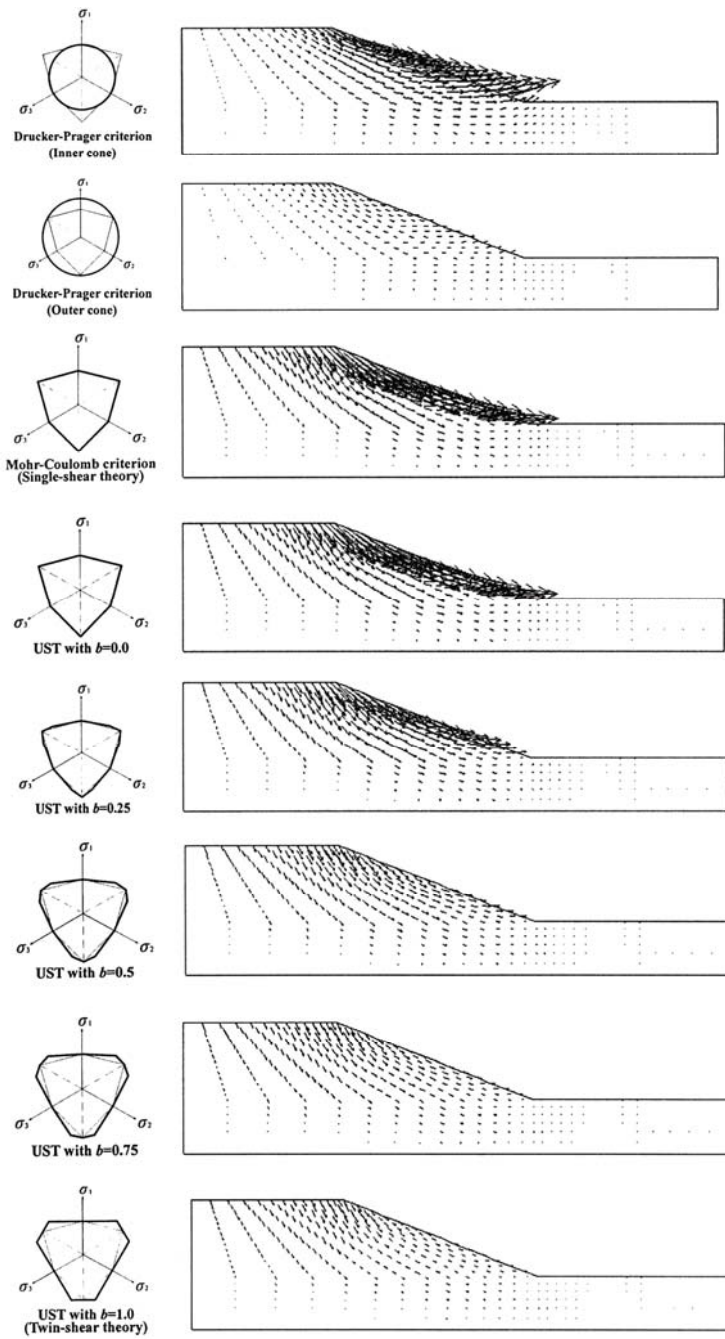
Fig. 17.10   Configuration of displacement vectors of slope using different yield criteria
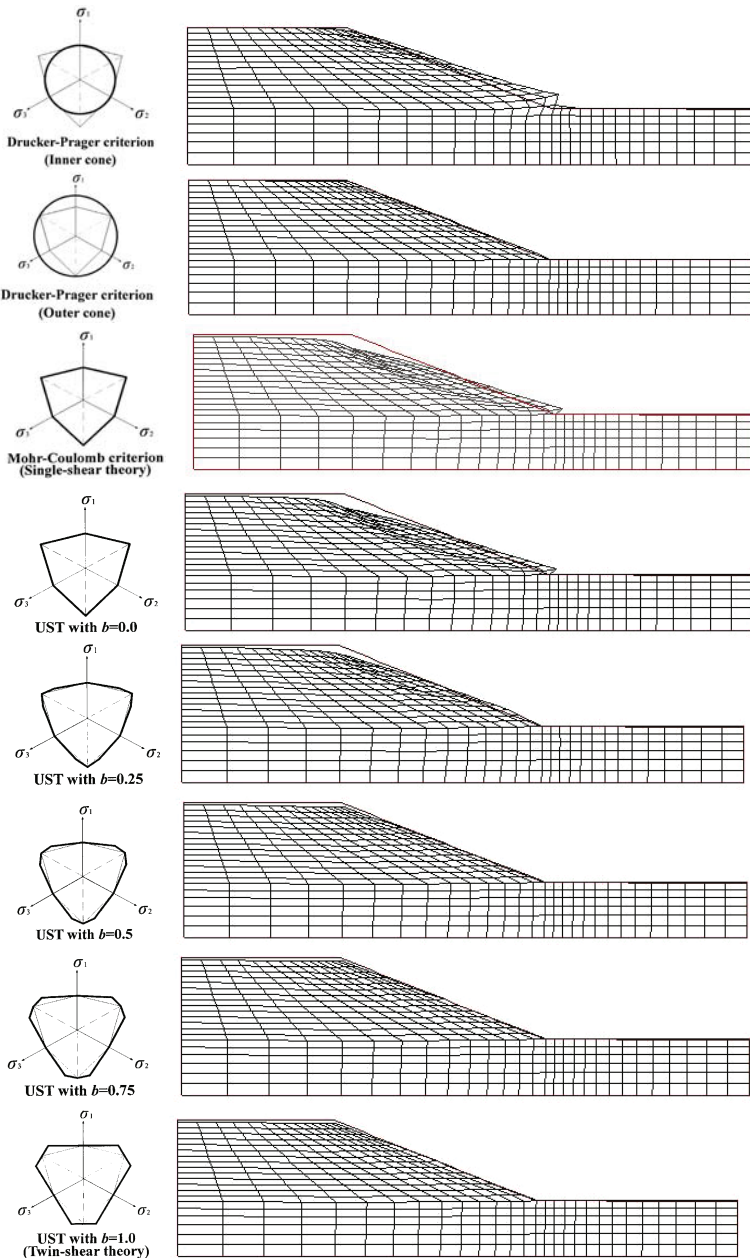
Fig. 17.11   Configuration of deformation of finite elements mesh of slope

We can see the following:

1) A series of new results are obtained using the unified strength theory with $b=0$, $b=0.25$, $b=0.5$, $b=0.75$ and $b=1$.

2) The result obtained by using the unified strength theory with $b=0$ implemented in FLAC-2D is the same as the result that is obtained from the oriented material model of the Mohr-Coulomb criterion (Single-shear theory) in FLAC-2D.

3) The outer cone of the Drucker-Prager criterion gives the minimum deformation and displacement; the inner cone of the Drucker-Prager criterion gives the maximum deformation and displacement; however, these two results are not in agreement with the real condition.

17.3 Stability of Three Gorges High Slope

The Three Gorges Project is the biggest water conservation and energy project in the world. Its five levels of continual sluices are open to navigation. After excavation,   the construction will reach as high as 170 meters on the steep side slope. It is an important waterway for the future. Extremely high stability is required (Sheng et al., 1997; Zhang and Zhou, 1997; Dong et al., 1999; Kou et al., 2001). To guarantee the stability of the Three Gorges   high side slope sluice is one of the project's important research topics. Therefore the Yangtze River Academy of Science, the Wuhan Rock and Soil Institute of Chinese Academia, Qinghua University, HeHai University, Hong Kong University, Wuhan University etc. carried out stability research of the side slope (Research Report of the Yangtze River Academy of Science, 1997-260). The excavation of the Three Gorges sluice is shown in Fig. 17.12.

Fig. 17.12   Excavation of the Three Gorges sluice
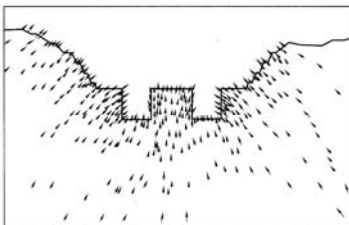
Fig. 17.13   Displacement vector field
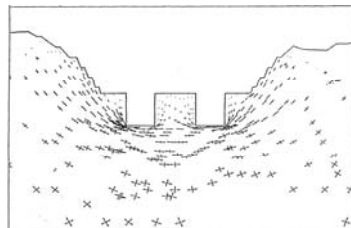
Fig. 17.14   Principal stress vector fields

The stress analysis of the ship sluice was carried out by the Yangtze River Academy of Science. The displacement vector field and principal stress fields are shown in Figs. 17.13 and 17.14 (Sheng et al., 1997; Dong et al., 1999).

The stability of the high slope of the ship lock of the Three Gorges Project has been studied (Sheng et al., 1997; Dong et al., 1999; Zhou and Yang, 2005). The plastic zone and limit equilibrium analysis for the stability of the high slope of the ship lock were presented (Sheng et al., 1997). Figure 17.15 is the plastic zone of the high slope of the ship lock using the single-shear theory (Mohr-Coulomb Theory). Figure 17.16 is the plastic zone of the high slope of the ship lock using the twin-shear theory (Yu, 1985). Figure 17.17 is the plastic zone of the high slope of the ship lock using the Drucker-Prager criterion.
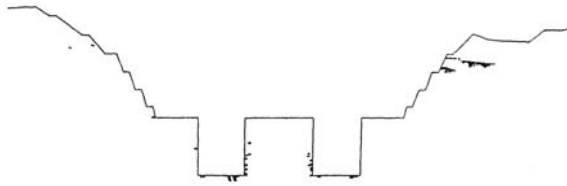
Fig. 17.15   Plastic zone for single-shear theory (Sheng et al., 1997)
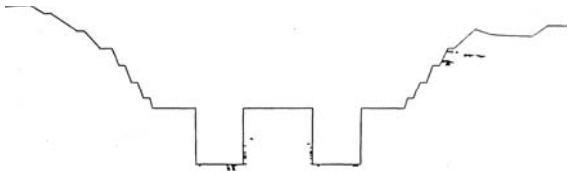
Fig. 17.16   Plastic zone for the twin-shear theory (Sheng et al., 1997)

Fig. 17.17   Drucker-Prager yield criterion (Sheng et al., 1997)

The results indicated that the deformation shape and stress field obtained from the three yield criteria show no significant difference. However, the differences in the plastic zones are larger (Sheng et al., 1997). It is seen that the spread of plastic zones using the single-shear yield criteria and the twin-shear yield criterion is similar. However, the size of the plastic zones varied widely. The difference can be illustrated from the yield surface on the deviatoric plane, as shown in Fig. 17.18.
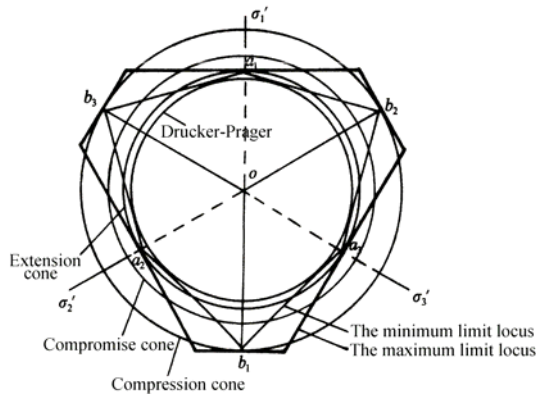
Fig. 17.18 Limit loci of various failure criteria on the deviatoric plane

As pointed out by Zienkiewicz and Pande (1977), the choice of the best limit surface is still in the hands of the analyst who has modeled the strength behavior in the best possible manner. They also indicated that the Drucker-Prager criterion and the limit loci of extension circular cones give a very poor approximation of, the real failure conditions (Humpheson and Naylor, 1975; Zienkiewicz and Pande. 1977). The choice of yield criteria has a marked effect on the prediction of the load-bearing capacities of structures. It is obvious that the Drucker-Prager criterion or other circular criterion cannot match the two experimental points a and b, as shown in Fig. 17.18.

The comparison of the single-shear theory (Mohr-Coulomb criterion) and the twin-shear theory is shown in Fig. 17.19. In fact, various yield criteria must be situated between the bounds if the convexity is considered. The lower bound is the single-shear strength theory (the Mohr-Coulomb strength theory 1900) and the upper bound is the twin-shear strength theory (Yu et al., 1985). Other failure criteria are situated between these two bounds. The limit loci of the unified strength theory cover all the regions of the convex limit loci, as shown in Fig. 17.19.
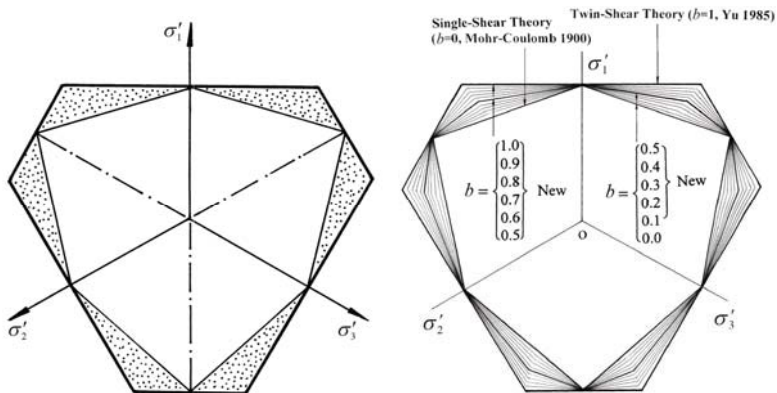
Fig. 17.19 Bounds and region of limit loci

17.4   Stability of a Vertical Cut

In the natural state, the loess soil is so resistant to erosion and so stable as to maintain indefinitely almost vertical faces in cuts, as shown in Fig. 17.20 (Hogentogler, 1937). Figure 17.21 shows an artificial vertical cut at the Green Dragon Temple near Xi'an Jiaotong University in Xi'an, China (Yoshimine, 2001). The stability of loess soil becomes troublesome when the height of the vertical cut increases. The critical height of the vertical cut was studied in the literature by using the Mohr-Coulomb theory. The computational result using the Drucker-Prager criterion with size-adjustment using the Mohr-Coulomb criterion was given by Zimmermann and Commend (2001). New bounds for the height limit of a vertical slope are given by Pastor et al. (2000). As pointed out by Pastor et al., when addressing the classic problem of the height limit of a Tresca or Mises criterion vertical slope subjected to the action of gravity, the exact solution to this problem remains unknown.

Fig. 17.20   Vertical faces of loess soil in cut

Fig. 17.21   Vertical faces of loess in Xi'an

We use a vertical cut where the material parameters are $\gamma=1.6\times10^4\,\text{N/m}^3$, $C=18$ kPa, $\varphi=30°$. The stress field of the vertical cut is shown in Fig. 17.22. The critical cut heights using the three basic criteria of the unified strength theory with $b=0$, $b=1/2$ and $b=1$ are calculated and shown in Fig. 17.23. The calculated critical heights are: $H_p=6.4$ m ($b=0$), $H_p=7.9$ m ($b=1/2$) and $H_p=9.2$ m ($b=1$). The last one is close to the height of the vertical cut of the loess as shown in Fig. 17.21.
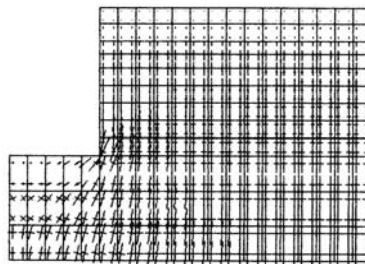
Fig. 17.22   Stress field of a vertical cut slope

(a) UST with $b=0$, $H_p=6.4$ m

(b) UST with $b=1/2$, $H_p=7.9$ m

(c) UST with $b=1$, $H_p=9.2$ m
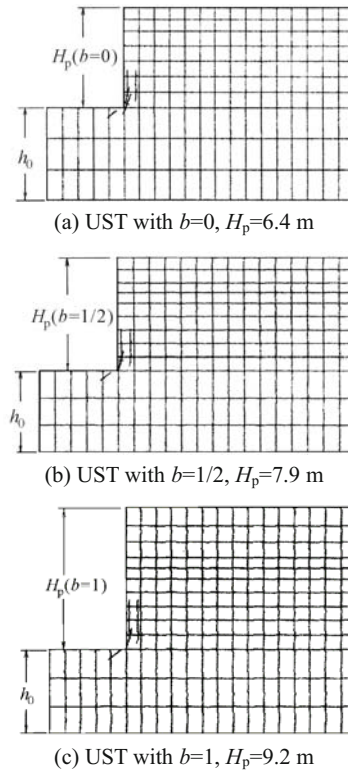
Fig. 17.23   Three critical heights obtained using the three basic criteria

17.5 Stability for a Slope of a Highway

The stability of the slope for the Baise-Luo highway in Guangxi province, China, was studied by Bai in 2005, in which the unified strength theory was used. The slope is considered as a plane strain problem. A special section of the slope and its mesh for numerical analysis is shown in Fig. 17.24. The parameters of the soil and the rock on the slope for various values of b in UST are listed in Table 17.1 (Bai, 2005; Fan W et al., 2007).
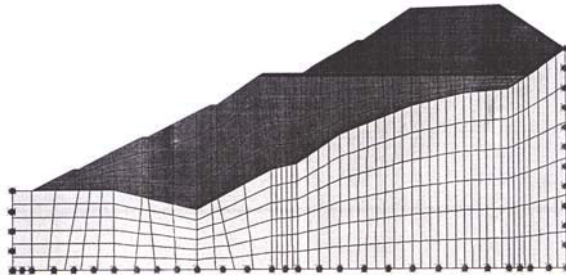
Fig. 17.24   Mesh of slope at Baise-Luo highway

Table 17.1   Parameters for various values of b in UST

Materials	Unified slip field	Unified strength theory parameter b				
		$b=0$	$b=1/4$	$b=1/2$	$b=3/4$	$b=10$
The clay loam mixes with the gravel (above water level)	C_{uni} (kPa)	19.37	20.84	21.94	22.8	23.49
	φ_{uni} (°)	30.57	33.05	34.97	36.49	37.73
The clay loam mixes with the gravel (under water level)	C_{uni} (kPa)	14.67	15.87	16.8	17.53	18.13
	φ_{uni} (°)	24.1	26.14	27.76	29.05	30.10
Rock base	C_{uni} (kPa)	30	32.07	33.64	34.88	35.88
	φ_{uni} (°)	35	36.84	38.16	39.17	39.97

The contours of the security rate for different yield criteria are shown in Figs. 17.25 to 17.29. It can be seen from Figs. 17.25 to 17.29 that the contours of the safety rate at the same stress level are different at different values of b.
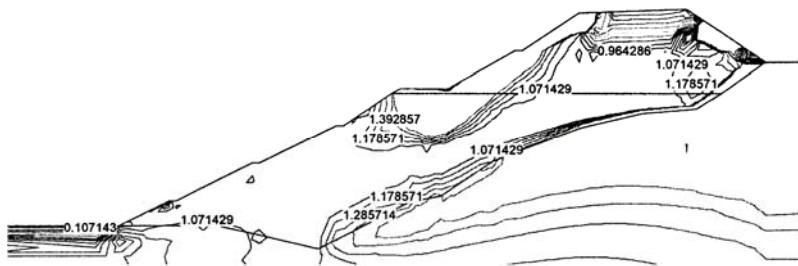
Fig. 17.25   Contours of security rate (UST with $b=0$)

Fig. 17.26   Contours of security rate (UST with *b*=0.25)

Fig. 17.27   Contours of security rate (UST with *b*=0.5)

Fig. 17.28   Contours of security rate (UST with *b*=0.75)

Fig. 17.29   Contours of security rate (UST with *b*=1.0)

The charts of the shear strain of the slope based on UST with different values of *b* are shown in Fig. 17.30 (Bai, 2005; Fan et al., 2007).
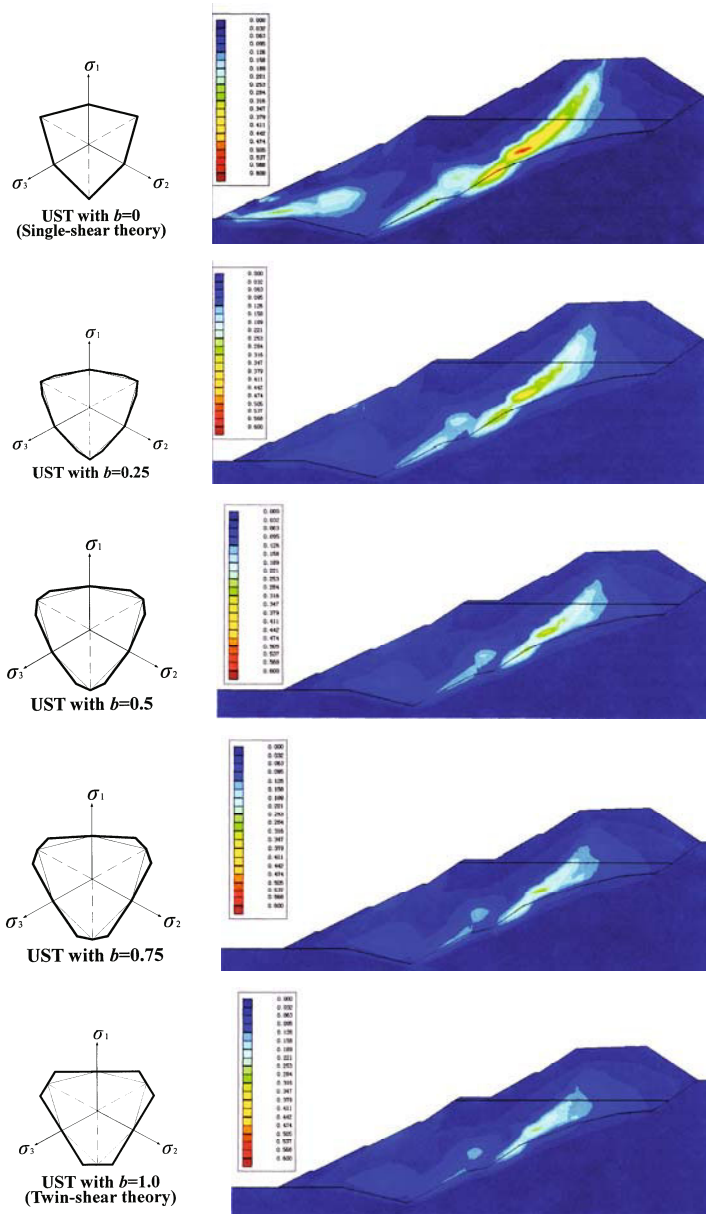
Fig. 17.30   Charts of shear strain based on UST with different values of *b*

Overall, along with the increase in the value of the UST parameter *b*, in the region of the side slope, safety coefficient changes are obviously small, the shear strain changes are obviously small and the strength of the side slope increases gradually. Therefore, the effect of the intermediate principal stress is obvious in

side slope stability analysis. The potential of the strength of materials can be played with   using the unified strength theory in which the intermediate principal stress is taken into account.

References

Bai XY (2005) The use of the unified strength theory in the stability analysis of slopes. Master Thesis, Chang'An University, Xi'an, China (in Chinese).

Baker R and Gather M (1978) Theoretical analysis of the stability of slopes. Geotechnique, 28(4): 395-413.

Bishop A W(1955) The use of the slip circle in the stability analysis of slopes. Geotechnique, 5(1): 7-17.

Brand EW (1989) Occurrence and significance of landslides in Southeast Asia. In: Landslides: extant and economic significance, Brabb & Hm'rod (eds), Balkema.

Chen WF (1975) Limit Analysis and Soil Plasticity. Elsevier.

Chen ZY (2003) Soil Slope Stability and Analysis: Theory, Methods and Programs (in Chinese). China Hydraulic and Hydropower Press: Beijing, China.

Chen ZY and Morgenstera NR(1983) Extensions to the generalized method of slices for stability analysis. Canadian Geotechnical Journal, 20(1): 104-119.

Chen ZY, Wang XG, Yang J et al. (2005) Rock Slope Stability Analysis: Theory, Methods and Programs (in Chinese). China Hydraulic and Hydropower Press: Beijing.

Cividin A (2001) Application of numerical methods to slope stability analysis. In: VaIliappan S and Khalili N editors, Computational Mechanics: New Frontiers for New Millennium. Elsevier Science Ltd: Amsterdam. pp 323-332.

Dong XS, Tian Y, Wu AQ (2004) Rock Mechanics in Hydraulic Engineering. Collection of Yangtze River Hydro-Conservancy Committee, Large and middle scale water conservation water and electricity project technology, Chinese Water Conservation and Water Electricity Press: Bejing pp 228-233 (in Chinese).

Janbu N (1973) Slope stability computations. Embankment Dam Engineering. John Wiley and Sons: New York.

Duncan JM (1996). State of the art: Limit equilibrium and finite element analysis of slopes. J. of Geotechnical Engineering, 122(7): 577-596.

Encyclopedia of Water Resources in China (2006) Second Edition. China Hydraulic and Hydropower Press: Beijing (in Chinese).

Fan W, Deng LS, Bai XY and Yu MH (2007) Application of unified strength theories to the stability of slope analysis. Coal Geology & Exploration, 35(1): 63-66.

Fredinnd DC (1984) State of the Art: Analytical methods for slope stability analysis. Proceedings of the 46th International Symposium on Landslides, Toronto, pp 229-250.

Hogentogler CA (1937) Engineering Properties of Soil. McGraw-Hill : New York.

Hudson JA and Harrison JP (1997) Engineering Rock Mechanics: An Introduction to the Principles. Elsevier Science Ltd.

Humpheson C and Naylor DJ (1975) The importance of the form of the failure criterion. C/R/243/75, University of Wales, Swansea, UK.

Janbu N (1973) Slope stability computations．Embankment Dam Engineering, 47-86.

Kou XD, Zhou WY, and Yang RQ (2001) Stability analysis on the high slopes of Three-Gorges ship-lock using FA\LAC-3D, Chinese J. Rock Mech. Eng., 20(1): 6-0.

Li K and Chen GR (2010) Finite element analysis of slope stability based on slip line field theory.J. of Hohai University (Natural Sciences),38(2): 191-195.

Morgenstem NR and Price V (1965) The analysis of the stability of general slip surface. Geotechnique, 15 (1): 79-93.

Morgenstem NR (1992) Keynote paper：The role of analysis in the evaluation of slope stability, Proceedings of Sixth Int. Symposium on Landslides, 3: 1615-1629.

Pan JZ (1980) Stability and Landslide Analysis. Hydraulic Press: Beijing (in Chinese).

Pastor J, Thai T-H and Francescato P (2000) New bounds for the height limit of a vertical slope. Int. J. for Numerical and Analytical Methods in Geomechanics, 24(2): 165-182.

Sheng Q, Xu NF and Ren F (1997) Application of the concept of plastic zone and limit equilibrium method for the stability analysis of the high slope of ship lock of Yangtze River. Three Gorges Project. Science Research Report of Yangtze River Academy of Sciences, 97-260 (in Chinese).

Yoshimine M (2001) Mechanical Properties of Loess Soil and Failure Criteria of Materials. Post-Doctor Research Report, Xi'an Jiaotong Universituy, Xi'an, China (in English).

Yu MH, He LN and Song LY (1985) Twin shear stress theory and its generalization. Scientia Sinica Series A, 28(11): 1174-83 (English edn.).

Yu MH (1992) New System of Strength Theory. Xi'an Jiaotong University Press: Xi'an (in Chinese).

Yu MH (2004) Unified Strength Theory and its Applications. Springer: Berlin.

Yu MH et al. (2006) Generalized Plasticity. Springer: Berlin.

Zienkiewicz OC and Pande GN (1977) Some useful forms of isotropic yield surfaces for soil and rock mechanics. Finite Elements in Geomechanics. Gudehus G ed. Wiley: London, pp 179-190.

Zimmermann T and Commend S (2001) Stabilized finite element applications in geomechanics. In: Valliappan S and Khalili N eds., Computational Mechanics: New Frontiers for the New Millennium. Elsevier: Amsterdam, pp 533-538.

Zhang YT and Zhou WY (1997) Deformation and Stability of Rock High Slope. China Hydraulic and Hydropower Press: Beijing (in Chinese).

Zhou WY and Yang Q (2005) Numerical Computational Methods for Rock Mechanics. China Electric Power Press: Beijing (in Chinese).

18

Unified Strength Theory and FLAC

18.1 Introduction

The unified strength theory and associated flow rule have been implemented into several finite element programs. Series numerical results can be obtained. Moreover, the equations of the unified strength theory are similar to those of the Mohr-Coulomb criterion. In fact, the Mohr-Coulomb criterion is a special case of the unified strength theory and thus it will have important significance in numerical simulation.

The equation for unified strength theory can be expressed by the strength parameters c and φ. They are transferred into the format of Lagrangian finite difference. The strain-hardening/softening model is added to the unified elasto-plastic model and the applicability of unified strength theory is enlarged. The constitutive model of unified elasto-plastic and strain-hardening /softening is implemented into the software of FLAC/FLAC^{3D} using a dynamic-link library file developed by VC++. Moreover, the unified elasto-plastic constitutive model can also be used in UDEC/3DEC. Based on the unified elasto-plastic model and unified strain-hardening/softening model, the conventional and true triaxial tests can be simulated by FLAC^{3D} respectively, and the measured data can be compared to the result of simulation. The analysis of the result suggests that unified strength theory not only describes the state of conventional triaxial stress, but also describes the mechanical behavior of materials under complex stress conditions. A fitted result is achieved between the simulation and the test data as regards different confining pressure and a different stress ratio; it shows that the influence of the intermediate principal stress σ_2 on soil strength is interesting.

Regarding the material non-linear problem for geomaterials, the smooth yield surface (for example the Huber-von Mises criterion and the Drucker-Prager criterion) was used in the majority of finite element software, but these two commonly used criteria do not conform to the experimental result and the reality to the geomaterials, as pointed out by. Zienkiewicz and others. Therefore, using another material model is also an important consideration. At present, the Mohr-Coulomb strength theory is the most widespread material strength theory used. However, the true tri-axial experiment proved that the intermediate principal stress σ_2 has to be accounted for in rock and soil mechanics and engineering.

Based on the twin-shear octahedron mechanical model, considering the effect of intermediate principal stress, Yu's unified strength theory was proposed in 1991. It has a simple mathematical expression and indicates the intensive property of the material. The application of the unified strength theory in the numerical computation enables the computation to reflect the mechanical behavior of the material under complex stress conditions. Moreover, it can further confirm the unified strength theory through numerical computation and a comparison of the measured data. Thus this has practical significance.

In choosing a non-smooth yield surface we have to process the singularity at the corner for a non-smooth yield surface, as described in Chapter 6. The FLAC^{2D} is a two-dimensional finite-difference code and an explicit Lagrangian computation scheme is used in this code. FLAC^{3D} is an extended three-dimensional edition for the two-dimensional code. The computation step using the time increment of the difference method does not need to solve the overall stiffness matrix. The calculation of the explicit expression in FLAC/FLAC^{3D} is calculated by   advancing to the next step through the increase in time. There is no need to carry on the iterative calculations for the non-linear material problem.

Zhang et al., (2008) use the Lagrange finite difference scheme for elasto-plasticity of the unified strength theory in the form of principal stress, and implement it in FLAC-3D. Ma ZY uses the Lagrange finite difference scheme for elasto-plasticity of unified strength theory in terms of the expression of invariants of the stress tensor and geomaterial parameters c and φ, and implements it in FLAC/FLAC^{3D}. He uses the C++ language compilation dynamic link storehouse document to write the unified elasto-plasticity model in FLAC/FLAC^{3D}. The C++ language has many advantages in engineering calculation. Zhang et al. indicated that "The unified strength theory is a new theory system which can almost describe the strength characteristics of most geomaterials and has been applied widely. And FLAC3D is an excellent geotechnical program. If the former can be integrated in the latter, many complex problems in engineering will be well settled. So according to this problem, the numerical scheme of the elasto-plastic unified constitutive model in FLAC3D was studied. And the numerical format of the elasto-plastic constitutive model based on the unified strength theory was derived."

"The format based on the unified strength theory in terms of the form of principal stress was derived. The implementation of the unified strength theory in FLAC-3D, unifying the unified strength theory and the finite difference method

numerical code will have a positive significance theoretically and in project application."

The idea behind the unified strength theory is the twin shear model of the orthogonal octahedron proposed by Yu. It incorporates the intermediate principal shear stress into the yield function. Thus it has vital significance in the numerical computation of computational plasticity. Here, we first introduce the unified elasto-plasticity model with parameters c and φ in the Lagrange finite difference scheme, then increase the strain hardening/softening model in the unified elasto-plasticity model. Thirdly, we compile the dynamic link storehouse document in VC++ and implement the unified elasto-plasticity and the strain-hardening /softening model in FLAC/FLAC^{3D}.

18.2   Unified Strength Theory Constitutive Model

The principal stress form of the unified strength theory can be expressed in terms of the principal stresses and material parameters c and φ (Yu, 1992; 2004), as follows.

$$f = \frac{1-\sin\varphi}{(1+\sin\varphi)(1+b)}(b\sigma_2 + \sigma_3) - \sigma_1 + \frac{2c \cdot \cos\varphi}{1+\sin\varphi}$$

$$\text{when} \quad \sigma_2 \leq \frac{1+\sin\varphi}{2}\sigma_1 + \frac{1-\sin\varphi}{2}\sigma_3 \tag{18.1a}$$

$$f' = \frac{1-\sin\varphi}{1+\sin\varphi} \cdot \sigma_3 - \frac{1}{1+b}(\sigma_1 + b\sigma_2) + \frac{2c \cdot \cos\varphi}{1+\sin\varphi}$$

$$\text{when} \quad \sigma_2 \geq \frac{1+\sin\varphi}{2}\sigma_1 + \frac{1-\sin\varphi}{2}\sigma_3 \tag{18.1b}$$

where σ_1, σ_2 and σ_3 are the three principal stresses, $\sigma_1 \geq \sigma_2 \geq \sigma_3$. Also, the tensile stress is positive and compressive stress is negative, $f \geq 0$ or $f' \geq 0$ materials occurs yield. b is a parameter reflecting the effects of the intermediate shearing stress and the corresponding normal stress.

The yield loci on the π-plane of the yield surface of Yu's unified strength theory are shown in Fig. 18.1. This becomes the single-shear theory or Mohr-Coulomb criterion when the parameter b degenerates to $b=0$. It may be seen that the yield surface of the unified strength theory exists corners at A, B and C in Figs. 18.1 and 18.2. The plastic flow vector $\dfrac{\partial f}{\partial \sigma_{ij}}$ at the corner is not uniquely defined for piecewise linear yield criterion, the direction of plastic straining is indeterminate. The processing method for corner singularity is to introduce a mean vector for point B, namely at the stress state $\sigma_2 = (1+\sin\varphi)\sigma_1/2 + (1-\sin\varphi)\sigma_3/2.$

The flow vectors at points A and C take the flow vectors of points A and C when $b=1$, which was described in Yu (1998; 2004), as shown in Fig. 18.2.
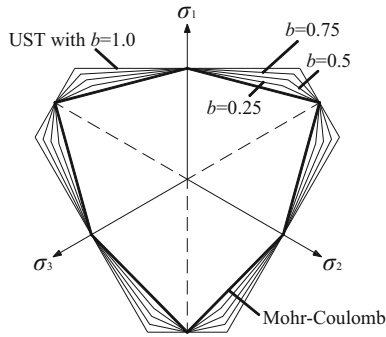
Fig. 18.1   Yield loci of the unified strength theory on π-plane
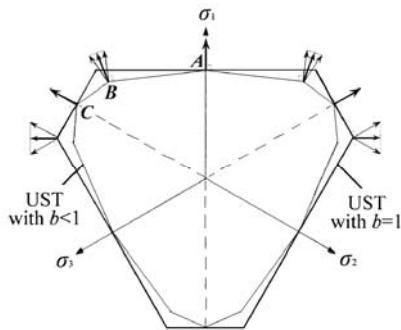
Fig. 18.2   Process of singular points

18.3   Governing Equation

18.3.1 Balance Equation

The continuous medium balance equation may be written as

$$\sigma_{ij,j} + \rho(b_i - \frac{\mathrm{d}v_i}{\mathrm{d}t}) = 0 \qquad (18.2)$$

where b_i is the volume force per unit mass for the element, ρ is the material density, $\frac{\mathrm{d}v_i}{\mathrm{d}t}$ is the acceleration. According to the virtual work principle, the power of

internal forces is

$$I = \int_V \delta\dot{\varepsilon}_i \sigma_{ij} \mathrm{d}V \tag{18.3}$$

The power rate of the external force is

$$E = \sum_{l=1}^{4} \delta v_i^{(l)} f_i^{(l)} + \int_V \delta v_i \rho (b_i - \frac{\mathrm{d}v_i}{\mathrm{d}t}) \mathrm{d}V \tag{18.4}$$

where f_i^l is the external force acting on the tetrahedron unit node; $\delta\dot{\varepsilon}_i$ and δv_i are the rate of strain and speed caused by virtual displacement. Equation (18.3) can be rewritter as

$$I = -\frac{1}{6} \sum_{l=1}^{4} (\delta v_i^{(l)} \sigma_{ij} n_j^{(l)} + \delta v_j^l \sigma_{ij} n_i^{(l)}) S^{(l)} \tag{18.5}$$

According to the symmetry of the stress tensor we have

$$I = -\frac{1}{3} \sum_{l=1}^{4} \delta v_i^{(l)} \sigma_{ij} n_j^{(l)} S^{(l)} \tag{18.6}$$

The difference format for the speed field of the tetrahedron element is

$$\delta v_i = \frac{1}{4} \sum_{l=1}^{4} \delta v_n^{(l)} \tag{18.7}$$

Equation (18.4) may be rewritten as

$$E = \sum_{l=1}^{4} \delta v_i^{(l)} [f_i^{(l)} + \frac{\rho b_i V}{4} - \frac{\rho V}{4} \int_V \frac{\mathrm{d}v_i}{\mathrm{d}t} \mathrm{d}V] \tag{18.8}$$

Equation (18.8) can also be expressed as

$$E = \sum_{l=1}^{4} \delta v_i^{(l)} [f_i^{(l)} + \frac{\rho b_i V}{4} - \frac{\rho V}{4} (\frac{\mathrm{d}v_i}{\mathrm{d}t})^l] \tag{18.9}$$

When the virtual work of the internal force equals the virtual work of the external force, the actual solution can be obtained. Equation (18.6) equals Eq. (18.9), resulting in

$$-f_i^{(l)} = \frac{1}{3} \sigma_{ij} n_j^{(l)} S^{(l)} + \frac{\rho b_i V}{4} - \frac{\rho V}{4} (\frac{\mathrm{d}v_i}{\mathrm{d}t})^l \tag{18.10}$$

Equation (18.10) is the balance equation in the difference form. The term $\rho V/4$ in Eq. (18.10) is replaced by node quality m^l for explicit computational stability.

$$-f_i^{(l)} = \frac{1}{3}\sigma_{ij}n_j^{(l)}S^{(l)} + \frac{\rho b_i V}{4} - m^l(\frac{dv_i}{dt})^l \qquad (18.11)$$

The unbalanced force of all nodes in the entire object is

$$F = \frac{1}{3}\sigma_{ij}n_jS + \frac{\rho b_i V}{4} - P_i \qquad (18.12)$$

where P_i is the resultant force of the external force and the inertia force at nodes. The object reaches a state of equilibrium when the balance force F is lower than a certain value.

18.3.2 Explicit Numerical Procedure

In explicit computation, the increase in step time is determined by the computation period and supposition of the node quality. Bathe and Wilson proposed a computing system for period of time of explicit computation in 1976,

$$T = 2\pi\sqrt{\frac{m}{k}} \qquad (18.13)$$

The increase in step time can be determined as

$$\Delta t = \frac{T}{\pi} = 2\sqrt{\frac{m}{k}} \qquad (18.14)$$

The mass of the node is calculated as

$$m^l = \frac{3K+4G}{27V}\max([n_i^{(l)}S^{(l)}]^2), \quad i = 1,3 \qquad (18.15)$$

The stable solution for numerical calculation can be obtained through the computation of the node quality.

18.3.3 Constitutive Equation

According to elasto-plasticity and generalized Hooke law, the total strain is

$$\Delta \varepsilon_i = \Delta \varepsilon_i^e + \Delta \varepsilon_i^p \tag{18.16}$$

where $\Delta \varepsilon_i^e$ is the elastic component and $\Delta \varepsilon_i^p$ is the plastic component. The generalized elastic Hooke law can be written as

$$\begin{cases} \Delta \sigma_1 = \alpha_1 \Delta \varepsilon_1^e + \alpha_2 (\Delta \varepsilon_2^e + \Delta \varepsilon_3^e) \\ \Delta \sigma_2 = \alpha_1 \Delta \varepsilon_2^e + \alpha_2 (\Delta \varepsilon_1^e + \Delta \varepsilon_3^e) \\ \Delta \sigma_3 = \alpha_1 \Delta \varepsilon_3^e + \alpha_2 (\Delta \varepsilon_1^e + \Delta \varepsilon_2^e) \end{cases} \tag{18.17}$$

where $\alpha_1 = K + 4G/3$, $\alpha_2 = K - 2G/3$, K and G are elastic bulk and shear modules.

Equation (18.17) is expressed in terms of the tensor form:

$$\Delta \sigma_i = S_i (\Delta \varepsilon_1^e, \Delta \varepsilon_2^e, \Delta \varepsilon_3^e) = S_i (\Delta \varepsilon_n^e), \quad i=1, 2, 3 \tag{18.18}$$

The plastic strain can be expressed as

$$\Delta \varepsilon_i^p = \lambda \frac{\partial g}{\partial \sigma_i} \tag{18.19}$$

where g is the plastic potential function.

According to Eqs. (18.16) and (18.17), stress increase $\Delta \sigma_i$ is

$$\Delta \sigma_i = S_i (\Delta \varepsilon_n - \Delta \varepsilon_n^p) \tag{18.20}$$

Substituting Eq. (18.19) into Eq. (18.20), we have

$$\Delta \sigma_i = S_i (\Delta \varepsilon_n - \lambda \frac{\partial g}{\partial \sigma_n}) = S_i (\Delta \varepsilon_n) - \lambda \cdot S_i (\frac{\partial g}{\partial \sigma_n}) \tag{18.21}$$

where $\lambda \cdot S_i (\frac{\partial g}{\partial \sigma_n})$ is stress at the plastic stage. $f(\sigma_n + \Delta \sigma_n)$ can be expressed as

$$f(\sigma_n + \Delta \sigma_n) = f(\sigma_n) + f(\Delta \sigma_n) - f(0) \tag{18.22}$$

in which $f(\Delta \sigma_n) - f(0)$ can be expressed by $f^*(\Delta \sigma_n)$, and $f(\sigma_n)=0$. Substituting Eq. (18.21) into Eq. (18.22), we have

$$f(\sigma_n + \Delta \sigma_n) = f^*(S_n (\Delta \varepsilon_n)) - \lambda \cdot f^*(S_n (\frac{\partial g}{\partial \sigma_n})) = 0 \tag{18.23}$$

The two expressions of stress tensors σ_i^N and σ_i^I are definite as

$$\sigma_i^N = \sigma_i + \Delta\sigma_i = \sigma_i + S_i(\Delta\varepsilon_n) - S_i(\Delta\varepsilon_n^p) \qquad (18.24)$$

$$\sigma_i^I = \sigma_i + S_i(\Delta\varepsilon_n) \qquad (18.25)$$

where $\Delta\varepsilon_n$ is total strain at the elastic stage, σ_i^I is the elastic stress tensor. σ_i^N is the stress tensor at the plastic stage, therefore

$$f(\sigma_n^I) = f(\sigma_n + S_n(\Delta\varepsilon_n)) = f^*(S_n(\Delta\varepsilon_n)) \qquad (18.26)$$

Substituting Eq. (18.26) into Eq. (18.23), the expression of λ can be obtained

$$\lambda = \frac{f(\sigma_n^I)}{f^*(S_n(\dfrac{\partial g}{\partial \sigma_n}))} \qquad (18.27)$$

Combining Eqs. (18.19), (18.24) and (18.25), the expression of σ_i^N is given as follows:

$$\sigma_i^N = \sigma_i^I - \lambda \cdot S_i(\frac{\partial g}{\partial \sigma_n}) \qquad (18.28)$$

Equation (18.28) is the finite-difference elasto-plastic constitutive equation of the material. The material non-linear relation is realized through the two stress tensors σ_i^N and σ_i^I, as shown in Fig. 18.3.

Fig. 18.3   Material nonlinearity processing of FLAC

18.4   Unified Elasto-Plastic Constitutive Model

18.4.1 Unified Elasto-Plastic Constitutive Model

The expression of the UST (Eq. (18.1)) can be transformed to another expression as follows:

$$f = \frac{b\sigma_2 + \sigma_3}{(1+b)N_\varphi} - \sigma_1 + \frac{2c}{\sqrt{N_\varphi}}, \quad \text{when} \quad \sigma_2 \leq \frac{1+\sin\varphi}{2}\sigma_1 + \frac{1-\sin\varphi}{2}\sigma_3 \quad (18.29a)$$

$$f' = \frac{\sigma_3}{N_\varphi} - \frac{\sigma_1 + b\sigma_2}{1+b} + \frac{2c}{\sqrt{N_\varphi}}, \quad \text{when} \quad \sigma_2 \geq \frac{1+\sin\varphi}{2}\sigma_1 + \frac{1-\sin\varphi}{2}\sigma_3 \quad (18.29b)$$

where $N_\varphi = (1+\sin\varphi)/(1-\sin\varphi)$. The non-associated flow rule is used. The friction angle φ in the yield function is used instead of the dilatancy angle ψ. The plastic potential function can be expressed as

$$g = \frac{b\sigma_2 + \sigma_3}{(1+b)N_\psi} - \sigma_1 \quad \text{when} \quad \sigma_2 \leq \frac{1+\sin\varphi}{2}\sigma_1 + \frac{1-\sin\varphi}{2}\sigma_3 \quad (18.30a)$$

$$g' = \frac{\sigma_3}{N_\psi} - \frac{\sigma_1 + b\sigma_2}{1+b} \quad \text{when} \quad \sigma_2 \geq \frac{1+\sin\varphi}{2}\sigma_1 + \frac{1-\sin\varphi}{2}\sigma_3 \quad (18.30b)$$

where $N_\psi = (1+\sin\psi)/(1-\sin\psi)$, $\lambda \cdot S_i(\dfrac{\partial g}{\partial \sigma_n})$ can be determined as

$$\begin{cases} S_1(\lambda\dfrac{\partial g}{\partial \sigma_1}, \lambda\dfrac{\partial g}{\partial \sigma_2}, \lambda\dfrac{\partial g}{\partial \sigma_3}) = \lambda(\dfrac{\alpha_2}{N_\psi} - \alpha_1) \\[4mm] S_2(\lambda\dfrac{\partial g}{\partial \sigma_1}, \lambda\dfrac{\partial g}{\partial \sigma_2}, \lambda\dfrac{\partial g}{\partial \sigma_3}) = \lambda\left\{\dfrac{b\cdot\alpha_1}{(1+b)N_\psi} + \alpha_2[\dfrac{1}{(1+b)N_\psi} - 1]\right\} \\[4mm] S_3(\lambda\dfrac{\partial g}{\partial \sigma_1}, \lambda\dfrac{\partial g}{\partial \sigma_2}, \lambda\dfrac{\partial g}{\partial \sigma_3}) = \lambda\left\{\dfrac{\alpha_1}{(1+b)N_\psi} + \alpha_2[\dfrac{b}{(1+b)N_\psi} - 1]\right\} \end{cases}$$

$$\text{when} \quad \sigma_2 \leq \frac{1+\sin\varphi}{2}\sigma_1 + \frac{1-\sin\varphi}{2}\sigma_3 \qquad (18.31a)$$

$$\begin{cases} S_1(\lambda\dfrac{\partial g'}{\partial \sigma_1},\lambda\dfrac{\partial g'}{\partial \sigma_2},\lambda\dfrac{\partial g'}{\partial \sigma_3})=\lambda[\alpha_2(\dfrac{1}{N_\psi}-\dfrac{b}{1+b})-\dfrac{\alpha_1}{1+b}] \\[3mm] S_2(\lambda\dfrac{\partial g'}{\partial \sigma_1},\lambda\dfrac{\partial g'}{\partial \sigma_2},\lambda\dfrac{\partial g'}{\partial \sigma_3})=\lambda[\alpha_2(\dfrac{1}{N_\psi}-\dfrac{1}{1+b})-\dfrac{\alpha_1\cdot b}{1+b}] \\[3mm] S_3(\lambda\dfrac{\partial g'}{\partial \sigma_1},\lambda\dfrac{\partial g'}{\partial \sigma_2},\lambda\dfrac{\partial g'}{\partial \sigma_3})=\lambda(\alpha_1\dfrac{1}{N_\psi}-\alpha_2) \end{cases}$$

$$\text{when}\quad \sigma_2 \ge \frac{1+\sin\varphi}{2}\sigma_1+\frac{1-\sin\varphi}{2}\sigma_3 \tag{18.31b}$$

So we have

$$\begin{cases} \sigma_1^N=\sigma_1^I-\lambda(\alpha_2\dfrac{1}{N_\psi}-\alpha_1) \\[3mm] \sigma_2^N=\sigma_2^I-\lambda\{\alpha_1\dfrac{b}{(1+b)N_\psi}+\alpha_2[\dfrac{1}{(1+b)N_\psi}-1]\} \\[3mm] \sigma_3^N=\sigma_3^I-\lambda\{\alpha_1\dfrac{1}{(1+b)N_\psi}+\alpha_2[\dfrac{b}{(1+b)N_\psi}-1]\} \end{cases}$$

$$\text{when}\quad \sigma_2 < \frac{1+\sin\varphi}{2}\sigma_1+\frac{1-\sin\varphi}{2}\sigma_3 \tag{18.32a}$$

$$\begin{cases} \sigma_1^N=\sigma_1^I-\lambda[\alpha_2(\dfrac{1}{N_\psi}-\dfrac{b}{1+b})-\dfrac{\alpha_1}{1+b}] \\[3mm] \sigma_2^N=\sigma_2^I-\lambda[\alpha_2(\dfrac{1}{N_\psi}-\dfrac{1}{1+b})-\dfrac{\alpha_1\cdot b}{1+b}] \\[3mm] \sigma_3^N=\sigma_{31}^I-\lambda(\alpha_1\dfrac{1}{N_\psi}-\alpha_2) \end{cases}$$

$$\text{when}\quad \sigma_2 \ge \frac{1+\sin\varphi}{2}\sigma_1+\frac{1-\sin\varphi}{2}\sigma_3 \tag{18.32b}$$

where the expressions for λ are

$$\lambda=\frac{f(\sigma_1^I,\sigma_2^I,\sigma_3^I)}{f(S_1(\dfrac{\partial g}{\partial \sigma_1},\dfrac{\partial g}{\partial \sigma_2},\dfrac{\partial g}{\partial \sigma_3}),S_2(\dfrac{\partial g}{\partial \sigma_1},\dfrac{\partial g}{\partial \sigma_2},\dfrac{\partial g}{\partial \sigma_3}),S_3(\dfrac{\partial g}{\partial \sigma_1},\dfrac{\partial g}{\partial \sigma_2},\dfrac{\partial g}{\partial \sigma_3}))-f(0)}$$

$$\text{when} \quad \sigma_2 \leq \frac{1+\sin\varphi}{2}\sigma_1 + \frac{1-\sin\varphi}{2}\sigma_3 \tag{18.33a}$$

$$\lambda = \frac{f'(\sigma_1^I, \sigma_2^I, \sigma_3^I)}{f'(f(S_1(\frac{\partial g}{\partial \sigma_1}, \frac{\partial g}{\partial \sigma_2}, \frac{\partial g}{\partial \sigma_3}), S_2(\frac{\partial g}{\partial \sigma_1}, \frac{\partial g}{\partial \sigma_2}, \frac{\partial g}{\partial \sigma_3}), S_3(\frac{\partial g}{\partial \sigma_1}, \frac{\partial g}{\partial \sigma_2}, \frac{\partial g}{\partial \sigma_3})) - f'(0)}$$

$$\text{when} \quad \sigma_2 \geq \frac{1+\sin\varphi}{2}\sigma_1 + \frac{1-\sin\varphi}{2}\sigma_3 \tag{18.33b}$$

For the strain hardening material, the development of the subsequent yield surface is determined by the variance in the plastic work or plastic strain. The hardening condition for isotropic hardening materials may be written as

$$f(\sigma_n) + C(q) = 0 \tag{18.34}$$

where $f(\sigma_n)$ is yield function, q is the hardening parameter and the accumulative plastic strain q is

$$q = \int (d\varepsilon^p)_i = \frac{\sqrt{2}}{3} \int \sqrt{(d\varepsilon_1^p - d\varepsilon_2^p)^2 + (d\varepsilon_2^p - d\varepsilon_3^p)^2 + (d\varepsilon_3^p - d\varepsilon_1^p)^2} \tag{18.35}$$

where $(d\varepsilon^p)_I$ is the equivalent plastic strain.

The hardening condition for linear isotropic hardening materials is

$$f(\sigma_n) + H \cdot q = 0 \tag{18.36}$$

where H is plastic modulus.

The three plastic principal strains for unified elasto-plastic model are

$$\begin{cases} \Delta\varepsilon_1^p = \lambda^s \dfrac{\partial f}{\partial \sigma_1} = -\lambda^s \\[3mm] \Delta\varepsilon_2^p = \lambda^s \dfrac{\partial f}{\partial \sigma_2} = \lambda^s \dfrac{b}{(1+b)N_\varphi} = \dfrac{\lambda^s b(1-\sin\varphi)}{(1+b)(1+\sin\varphi)} \\[3mm] \Delta\varepsilon_3^p = \lambda^s \dfrac{\partial f}{\partial \sigma_3} = \dfrac{\lambda^s}{(1+b)N_\varphi} = \dfrac{\lambda^s (1-\sin\varphi)}{(1+b)(1+\sin\varphi)} \end{cases}$$

$$\text{when} \quad \sigma_2 \leq \frac{1+\sin\varphi}{2}\sigma_1 + \frac{1-\sin\varphi}{2}\sigma_3 \tag{18.37a}$$

$$\begin{cases} \Delta\varepsilon_1^p = \lambda^s \, \dfrac{\partial f'}{\partial \sigma_1} = -\dfrac{\lambda^s}{1+b} \\[2mm] \Delta\varepsilon_2^p = \lambda^s \, \dfrac{\partial f'}{\partial \sigma_2} = -\dfrac{\lambda^s b}{1+b} \\[2mm] \Delta\varepsilon_3^p = \lambda^s \, \dfrac{\partial f'}{\partial \sigma_3} = \dfrac{\lambda^s}{N_\varphi} = \dfrac{\lambda^s (1-\sin\varphi)}{1+\sin\varphi} \end{cases}$$

$$\text{when} \quad \sigma_2 \geq \frac{1+\sin\varphi}{2}\sigma_1 + \frac{1-\sin\varphi}{2}\sigma_3 \tag{18.37b}$$

18.4.2 The Key to Implementation of the Constitutive Model

In FLAC^{3D}, this constitutive model uses C++ language compilation, the output document format for the dynamic connection storehouse document. FLAC/FLAC^{3D} writes down the dynamic connection storehouse document, the procedure to carry out the computation. Dr. Ma ZY uses the Microsoft Visual C++ 6.0 to program the platform to carry out the translation. The unified strength theory is implemented in FLAC^{3D}.

The FLAC/FLAC^{3D} constitutive development platform is the VC++ workspace format file (udm.dsw file), including the header file (.H), source file (.cpp) and the library file (.lib) in three parts. The header file defines the constitutive model of the class, member functions and objects; the source files cites and describe the file class and its member functions and objects as defined in the header file; library files can be guided to create FLAC^{3D} supported by the dynamic link library files (contains all function information). The constitutive model class is defined in the constitutive model of the class functions, the yield criteria and flow rule are implemented in the source file. User-Model calling the Run () function is defined as plastic indicator function.

18.5   Calculation and Analysis

18.5.1 Slope Stability Analysis

The unified elastic-perfectly plastic model (UST model) has been implemented in FLAC, and a two-dimensional (plane-strain) soil slope is studied and analyzed with unified strength theory. The meshes and boundary condition is

shown in Fig. 18.4. Zienkiewicz (1975), Potts (1999) and Griffiths (1999) use the strength reduction method (SRF) to analysis the problem of slope stability with associated and non-associated flow rule. The mechanical parameters of the soil are as follows: cohesive force c=16.0 kPa, internal friction angle φ=20.0°, elasticity coefficient E=5.0 MPa, Poisson ratio V=0.3, density γ=1600 kg/m^3. The mesh and dimension of the model for analysis is shown in Fig. 18.4 and the initial gravity field is established before the elastoplastic analysis.
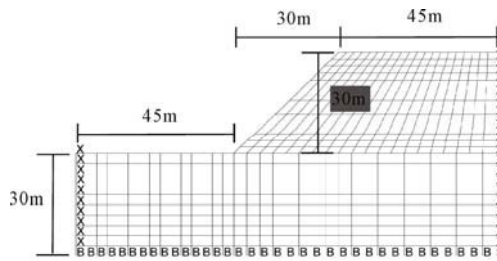
Fig. 18.4   Finite-difference meshes with the boundary condition and dimension for analysis

18.5.1.1   Associated Flow Rule

The friction angle φ in the yield function is equal to the dilatancy angle ψ when the associated flow rule is used and correspondence between the fields of stress and velocity is yielded. Figure 18.5 shows the deformed mesh plots with different strength criterion and associated flow rule. Figure 18.6 shows the factor of safety of the soil slope with different strength criteria. The failure surface occurs when the criterion of the tension cone of Drucker-Prager, Mohr-Coulomb, UST b=0.0 and UST b=0.25 are used respectively. The displacement of the slope decreases as the value of parameter b increases. The factor of safety using SRF with different criteria indicated that the results from UST use the criterion of the Drucker-Prager (compression cone) and Mohr-Coulomb, and the result using the tension cone of Drucker-Prager is slightly lower than UST b=0.25.

Exaggerated Grid Distortion
Magnification =   1.000E+00
Max Disp =   9.217E-01

Exaggerated Grid Distortion
Magnification =   1.000E+00
Max Disp =   9.065E+00

(a) Drucker-Prager compression cone   (b) Drucker-Prager tension cone

Exaggerated Grid Distortion
Magnification =   1.000E+00
Max Disp =   1.058E+01

Exaggerated Grid Distortion
Magnification =   1.000E+00
Max Disp =   1.058E+01

(c) Mohr-Coulomb   (d) UST b =0.0,

Exaggerated Grid Distortion
Magnification =   1.000E+00
Max Disp =   7.341E+00

Exaggerated Grid Distortion
Magnification =   1.000E+00
Max Disp =   3.794E+00

(e) UST b =0.25   (f) UST b =0.5

Exaggerated Grid Distortion
Magnification =   1.000E+00
Max Disp =   1.332E+00

Exaggerated Grid Distortion
Magnification =   1.000E+00
Max Disp =   8.390E-01

(g) UST b =0.75   (h) UST b =1.0

Fig. 18.5   The deformed mesh plots with different strength criteria and associated flow rule
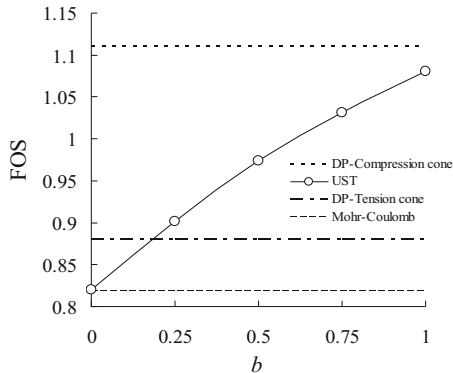
Fig. 18.6   The factor of safety of soil slope with different strength criteria

18.5.1.2   Non-associated Flow Rule

The plastic volume strain is much higher than the actual situation when the associative flow rule is used, and the non-associative flow rule could be used to reduce the plastic volume strain. For non-associative flow rule $\psi \neq \varphi$, disaccord between the fields of stress and velocity could be yielded, and the failure mechanisms with the non-associative flow rule are different from those with the associative flow rule. Figure 18.7 shows the deformed mesh with different criteria and the non-associated flow rule.

(a) Drucker-Prager compression cone

(b) Drucker-Prager tension cone

(c) Mohr-Coulomb

(d) UST b =0.0

(e) UST b=0.25

(f) UST b =0.5

(g) UST b =0.75

(h) UST b =1.0
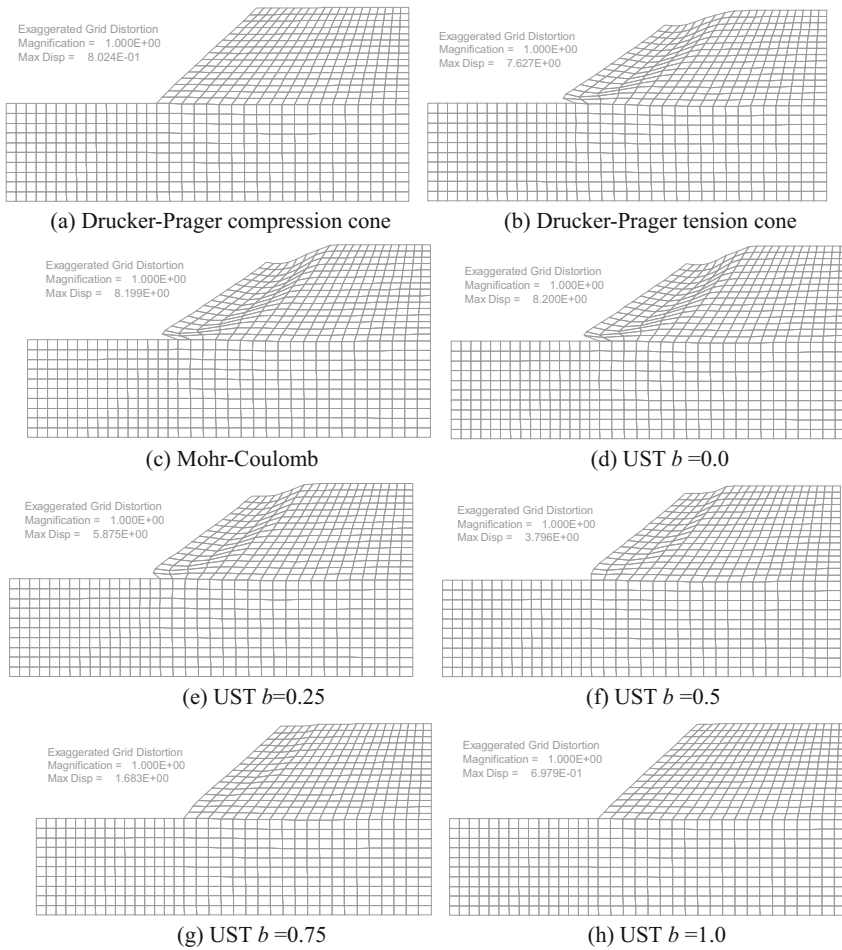
Fig. 18.7   The deformed mesh plots with different strength criteria and non-associated flow rule

18.5.2 *Thick-Walled Cylinder under Internal Pressure*

A plane-strain problem of a thick-walled cylinder under internal pressure is analyzed as shown in Fig. 18.4. The parameters for analysis follow: E=240.0 MPa, v=0.2, cohesion=1.0 kPa, friction φ=20°, dilation ψ=20°. The mesh and dimension of the model for analysis is shown in Fig. 18.7. Figure 18.9 shows the plastic zone under an internal pressure equal to 1.1645 kPa. Figure 18.10 shows the distribution of the circumferential stress in thick-walled cylinders. Figure 18.11 shows the relationship betwen the elastic and plastic limit pressure and the ratio of the outer and inner radius.
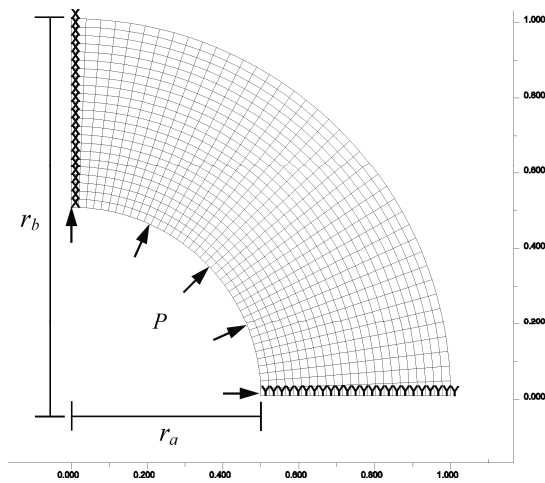
Fig. 18.8   Finite-difference meshes with the boundary condition and dimension for analysis

(a) UST b=0.0   (b) UST b=0.5   (c) UST b=1.0
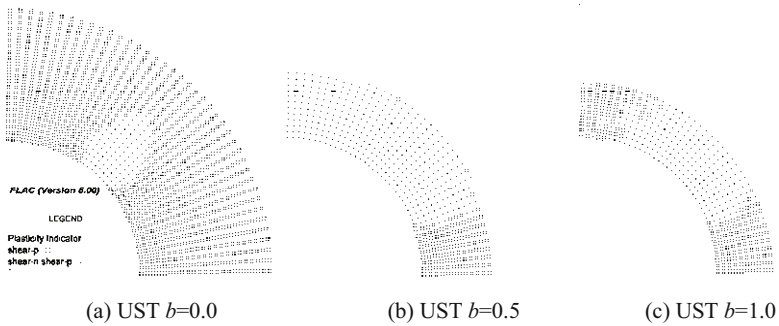
Fig. 18.9   Plastic zone under the internal pressure P=1.1645 kPa
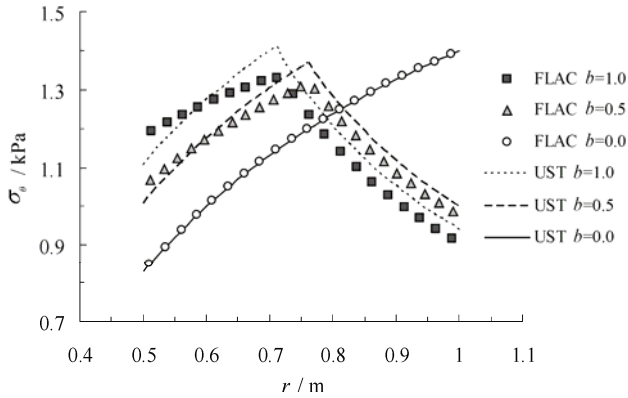
Fig. 18.10   Distribution of circumferential stress in thick-walled cylinders with UST
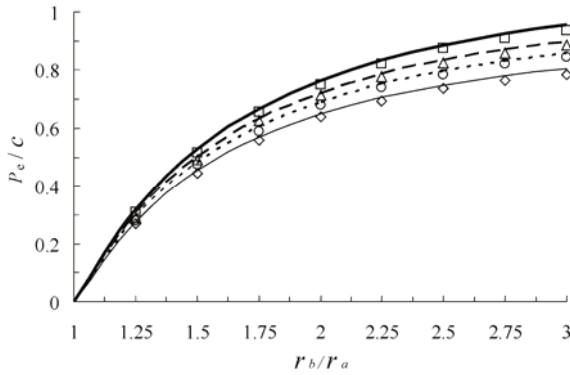
(a) Relationship between elastic limit pressure and ratio of outer and inner radius
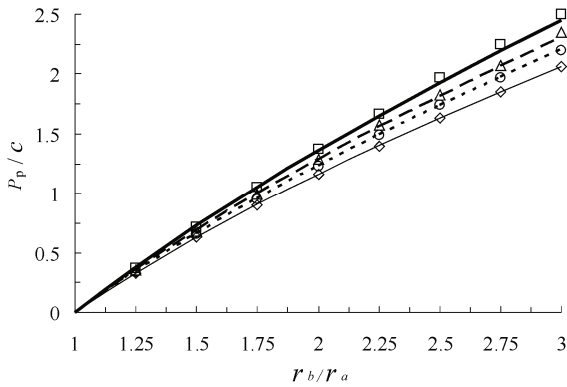
(b) Relationship between plastic limit pressure and ratio of outer and inner radius

Fig. 18.11   Relationship between limit pressure and ratio of outer and inner radius

18.5.3 Bearing Capacity of Strip Footings

Prandtl (1920) suggested the bearing capacity equation for a weightless and semi-infinite space under a vertical strip load using a characteristic method. The formula is expressed as

$$q_u = c \cdot N_c + q \cdot N_q \tag{18.38}$$

where q is the equivalent surcharge of the footing embedment, N_c and N_q are bearing capacity coefficients of cohesion and surcharge. The expression for N_c, N_q can be written as

$$N_c = \cot\varphi \cdot \left[\frac{1+\sin\varphi}{1-\sin\varphi}\exp(\pi \cdot \tan\varphi) - 1\right] \tag{18.39}$$

$$N_q = \frac{1+\sin\varphi}{1-\sin\varphi}\exp(\pi \cdot \tan\varphi) \tag{18.40}$$

Vesić (1973) proposed the following equation:

$$q_u = c \cdot N_c + q \cdot N_q + \frac{\gamma \cdot w}{2}N_\gamma \tag{18.41}$$

where γ is the unit weight, w is the footing width, N_c and N_q are the same as the formula of Prandtl, N_γ is the bearing capacity coefficient of soil self-weight and the expression for N_γ is expressed as

$$N_\gamma = 2(N_q + 1)\tan\varphi \tag{18.42}$$

Terzaghi (1943) also proposed the formulas of bearing capacity coefficients N_c, N_q and N_γ based on rigid and rough strip footing.

In the current study, the foundation soil is considered to be a linearly elastic-perfectly plastic and homogeneous material. Since the problem is symmetric, only half of the problem domain is considered and the footing width w is held constant at 0.5 m. Griffiths (1982), Frydman (1997), Yin (2001), Erickson (2002), Mabrouki (2010) and Loukidis (2009) use the finite element or finite difference method to evaluate the bearing capacity for strip or circular footings. The mesh and dimension of the model for analysis is shown in Fig. 18.12 and the other details of numerical analysis are shown in Table 18.1. The analysis was performed by applying a vertical velocity (rigid) or uniformed pressure (flexible) to simulate the load from the base of the footing. Set the horizontal displacement or force at the surface nodes below the footing to zero to simulate the rough or smooth interface between footing and soil respectively.
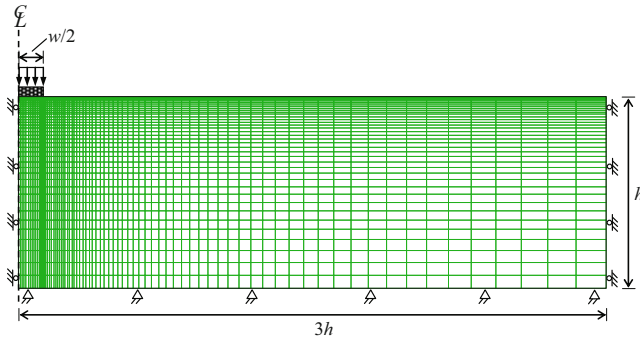
Fig. 18.12   Finite-difference meshes with the boundary condition and dimension for analysis

Table 18.1   Parameters and boundary condition for numerical analysis

Factors	h (m)	Velocity (m/step)	Elastic modulus (MPa)	Poisson's ratio	c (kPa)	q (kPa)	γ (kN/m^3)
N_c	5	1e-7	240	0.2	10	0	0
N_q	6	5e-8	240	0.2	0	15	0
N_γ	2	1e-8	240	0.2	0	0	18

The values of N_c from the *FLAC* and the characteristic method using the Unified Strength Theory for smooth footing are shown in Fig. 18.13. The values of N_c from the two methods are more closed when the friction angle is less than 30°, but the results of *FLAC* analyses become much larger than the characteristic method when the friction angle is larger than 30°. The results of bearing capacity evaluation are shown in Fig. 18.14 to Fig. 18.16.
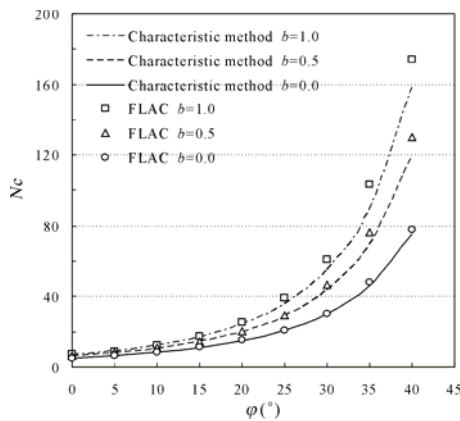
Fig. 18.13   Comparison of the values of N_c from the *FLAC* and characteristic method based on Unified Strength Theory for smooth footing
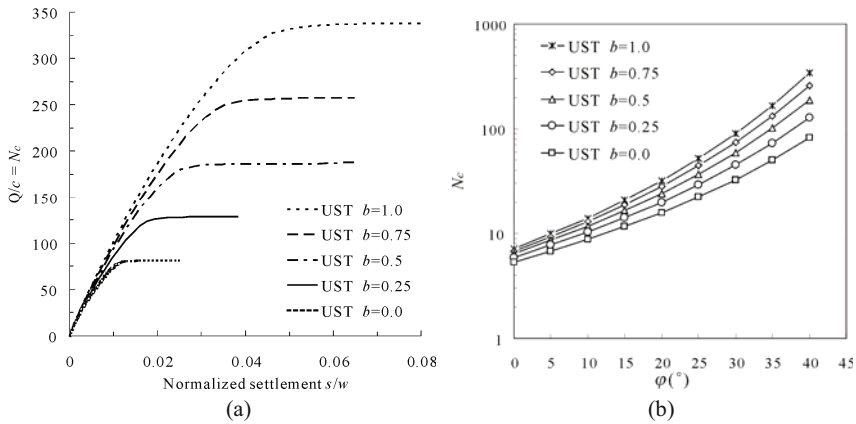
Fig. 18.14 (a) N_c versus vertical displacement for rough footing and $\varphi=\psi=40°$ with UST parameter b=0.0, 0.25, 0.5, 0.75 and 1.0. (b) Varation of N_c with friction angle for rigid and rough footing and $\psi=\varphi$ with UST
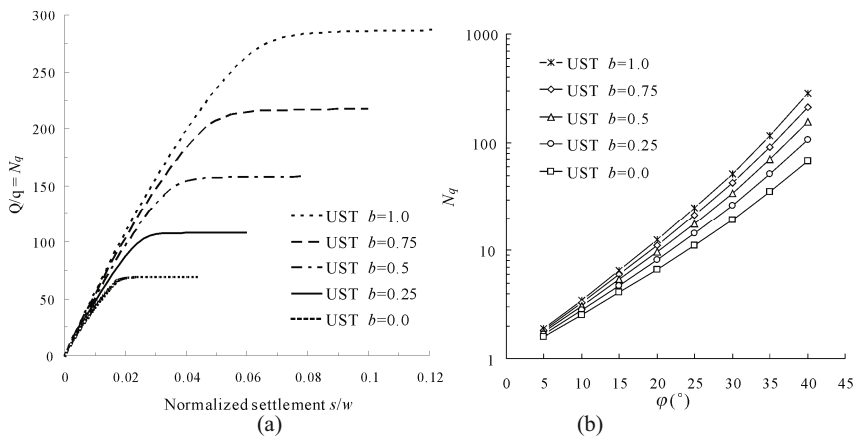
Fig. 18.15 (a) N_q versus vertical displacement for rough footing and $\varphi=\psi=40°$ with UST parameter b=0.0, 0.25, 0.5, 0.75 and 1.0. (b) Varation of N_q with friction angle for rigid and rough footing and $\psi=\varphi$ with UST.

Contours of the maximum shear strain for rigid and rough footing and $\psi=\varphi=40°$ in N_c calculation are shown in Fig. 18.17. Plastic zones (vertical displacement equals 4×10^{-4} m) for rigid and rough footing and $\psi=\varphi=40°$ in N_c calculation with UST_b=0.0, b=0.5 and b=1.0 are shown in Fig. 18.18. Contours of maximum shear strain for rigid and rough footing and $\psi=\varphi=40°$ in N_γ calculation with UST b=0.0, b=0.5 and b=1.0 are shown in Fig. 18.19. The effect of parameter b is evident.

Fig. 18.16 (a) N_γ versus vertical displacement for rough footing and $\varphi=\psi=40°$ with UST parameter b=0.0, 0.25, 0.5, 0.75 and 1.0. (b) Varation of N_γ with friction angle for rigid and rough footing and $\psi=\varphi$ with UST

(a) UST b=0.0

(b) UST b=0.5

(c) UST b=1.0
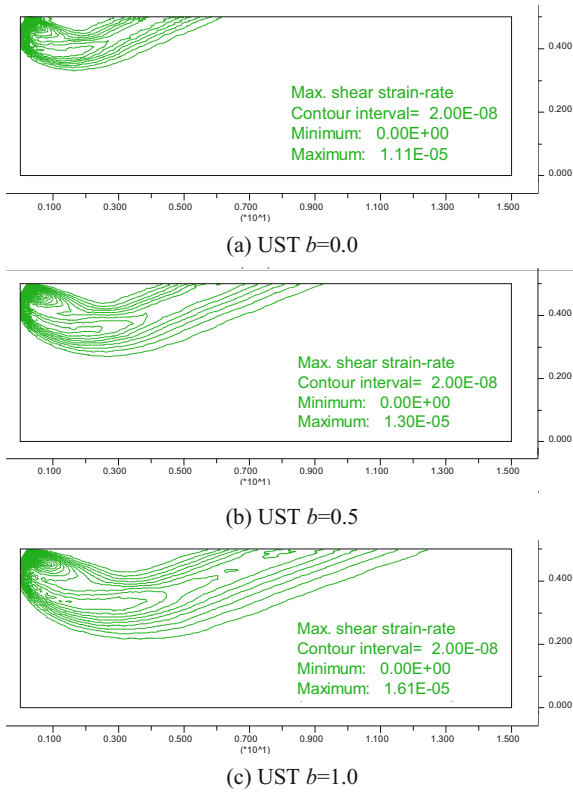
Fig. 18.17 Contours of maximum shear strain for rigid and rough footing and $\psi=\varphi=40°$ in N_c calculation
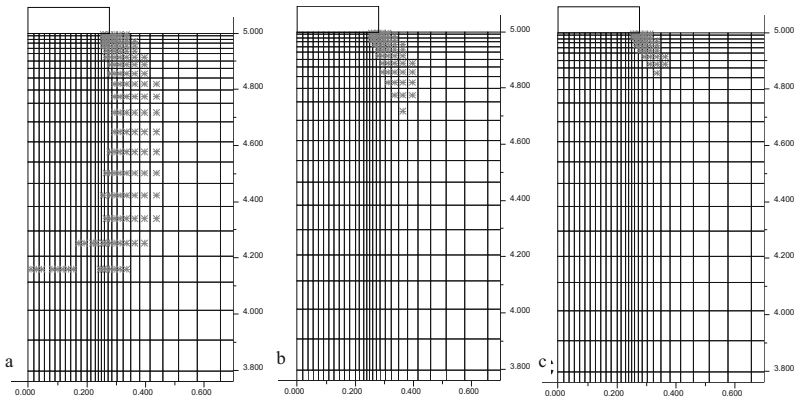
Fig. 18.18   Plastic zones (vertical displacement equals to $4{\times}10^{-4}$ m) for rigid and rough footing and $\psi{=}\varphi{=}40°$ in N_c calculation: (a) UST $b{=}0.0$; (b) $b{=}0.5$; (c) $b{=}1.0$

(a) UST $b{=}0.0$

(b) UST $b{=}0.5$

(c) UST $b{=}1.0$
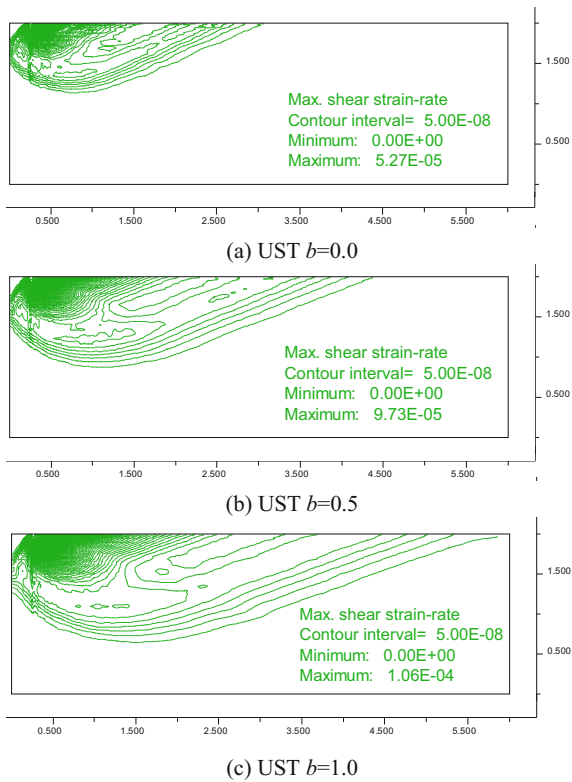
Fig. 18.19   Contours of maximum shear strain for rigid and rough footing and $\psi{=}\varphi{=}40°$ in N calculation

18.6   Three Dimensional Simulation of a Large Landslide

The loess plateau is widely distributed in northwestern China and high slopes are usually formed along the boundary of the plateau. The large height difference, steep slope and complex geological origin are common features of these high slopes. The urban city area has approached the loess plateau during the acceleration of the urbanization process in northwestern China. The arid climate of the loess area often causes a significant rise in the groundwater level due to large scale irrigation and seasonal rains. In recent years, the stability of the loess plateau boundary has been influenced significantly by climatic and anthropogenic factors. Moreover, the danger of landslides on the loess plateau caused by the variation in groundwater level has become more serious.

Figures 18.20 and 18.21 show a large landslide in Jingyang County, Shanxi Province, China. Estimation of the size and material mass of the landslide is shown in Fig. 18.21. The numerical simulation of this landslide was carried out by Ma ZY and Liao HJ using the unified strength theory in 2009. Based on the unified strength theory (Yu, 1991; 1994; 1998; 2004), elasto-plasticity theory and the non-associated flow rule are used to analyse this slope satiability problem. The elastic modulus of soil is 5.0 MPa, Poisson's ratio 0.33, the cohesion and internal friction angle of the soil is 3.56 kPa and 17.9° respectively.

(a)

(b)
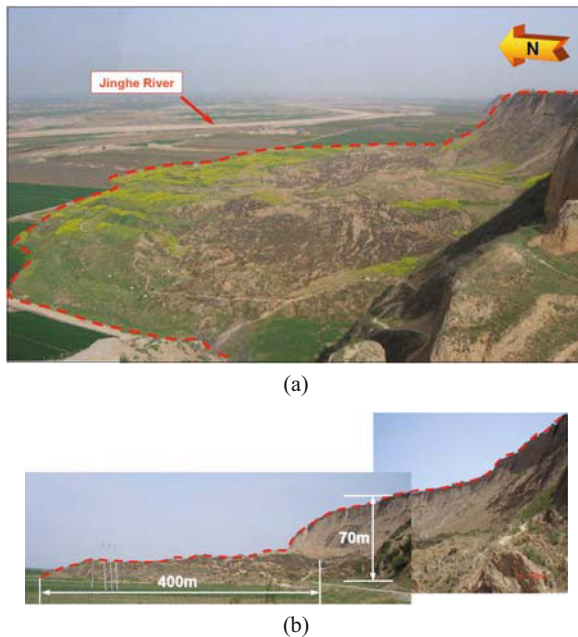
Fig. 18.20   Field photo of landslide (2003). (a) Photo from the top; (b) Photo from the bottom
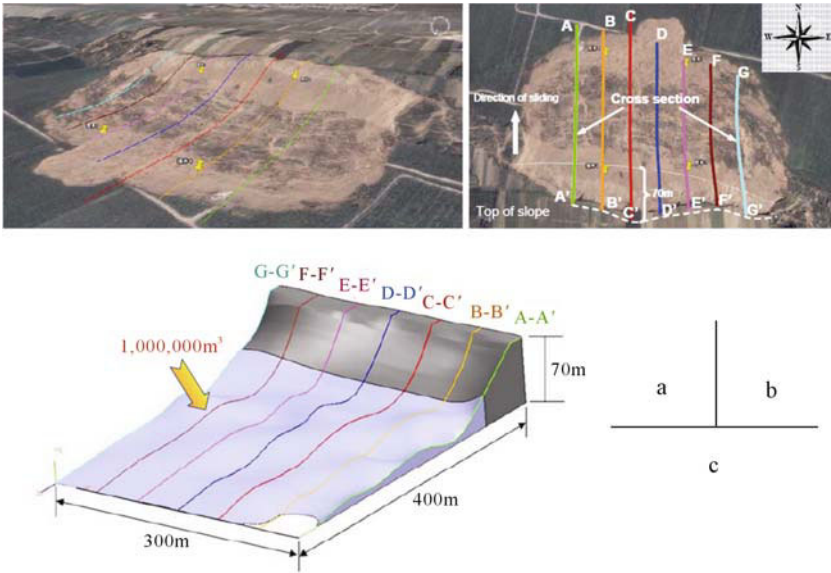
Fig. 18.21   (a) General view of landslide; (b) Cross sections of the body of landslide; (c) Estimation of the size and material mass of landslide

The boundary condition and mesh for numerical analysis is shown in Fig. 18.22. Figure 18.23 shows a horizontal displacement and maximum shear strain contours from FLAC at a depth of groundwater level h=80 m with unified strength theory (b=0.15). Figures 18.24 and 18.25 show the contours of the horizontal displacement and maximum shear strain from FLAC^{3D} analysis at a depth of groundwater level h=80m with unified strength theory (b=0.25). The slope failure occurs if the values of parameter b are lower than 0.15 and 0.25 in FLAC and FLAC^{3D} analyses respectively.
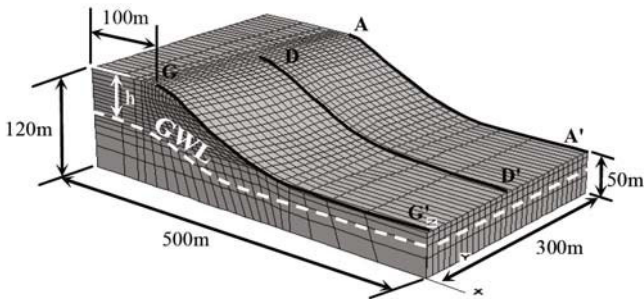
Fig. 18.22   Mesh model of slope before landslide event
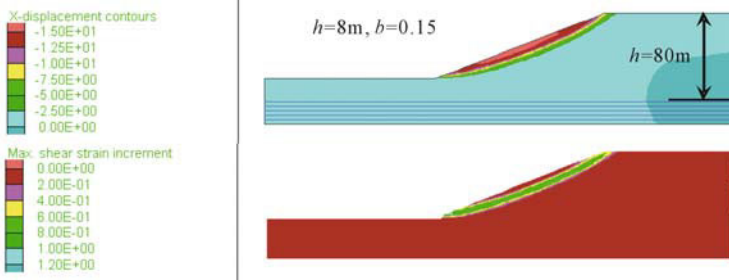
Fig. 18.23   Horizontal displacement and maximum shear strain contours from FLAC with *b*=0.15
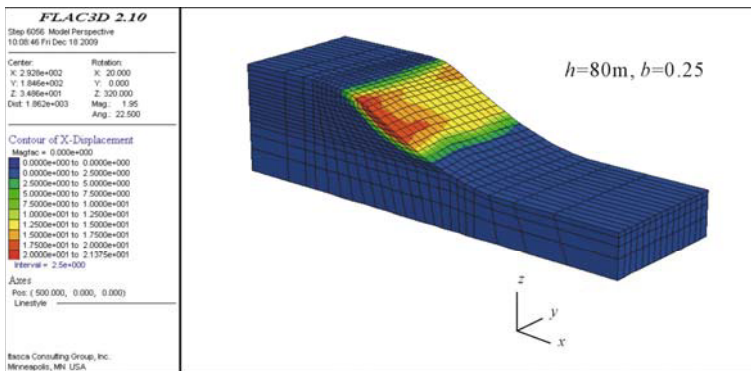
Fig. 18.24   Horizontal displacement contour from FLAC^{3D} with *b*=0.25
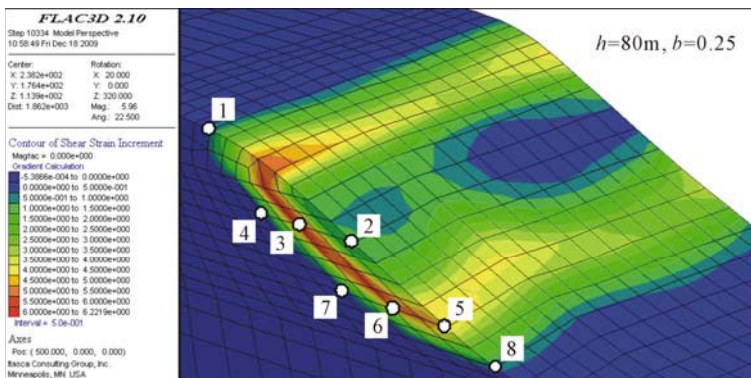
Fig. 18.25   Maximum shear strain contour from FLAC^{3D} with *b*=0.25

According to the loess landslide survey at the South-Jingyang plateau in Shanxi Province, a test specimen using the material has analyzed the scale of the landslide and the characteristics of the terrain. In order to analyze the mechanism which caused this landslide to occur, by returning the contours to their original state a three dimensional high loess slope computer model has been created.

Finally, utilizing the three dimensional Lagrange finite difference method, an analysis of the effect of intermediate principal stress on the stability of the high loess slope has been carried out, and a further study of the stability of the slope depending on different depths of the groundwater.

According to two examples with a water level of $h=80$ m and, in 1992, with a depth of $h=37$ m, the slope safety was calculated by using the strength reduction method in three-dimensions. The principle of strength reduction calculation is that the internal friction angle and cohesion are at the same time multiplied by a coefficient so that when the slope reaches a critical state of failure, this factor shall be the slope safety factor.

Because the high loess slope was stable before 1976, the stability analysis taking the influence of the intermediate principal stress into account can reflect the actual situation more accurately. The factor of safety for the high loess slope is calculated using the strength reduction method. The strength parameter of the soil mass is decreased gradually until the slope becomes unstable. The relationship between the factor of safety for the slope and the magnitude of b at two different groundwater levels in 1976 and 1992 is shown in Fig. 18.26. The same results as in the above analysis can be observed from Fig. 18.26, a decrease in the magnitude of b led to a decrease in the factor of safety for the slope and the factor of safety also decreases with a rise in the groundwater level. When the factor of safety equals 1, the magnitude of b at the groundwater level in 1976 and 1992 equals 0.3 and 0.5, respectively. Figure 18.27 shows the pore-water pressure and displacement vector of the slope at $h=37$ m and $b=0.5$. The high loess slope becomes unstable when $h=37$ m and $b=0.5$.

In order to analyze the stability of the high loess slope during the process of a rise in the groundwater level caused by rain and irrigation, an analysis was performed with a different depth ($h=35\sim50$ m) of groundwater under the loess plateau, and the groundwater level under the loess plateau is shown in Fig. 18.28. Because the velocity of the rise in the groundwater level is very low, the seepage
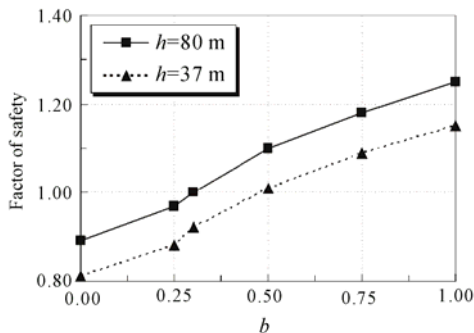
Fig. 18.26   Relations between the factor of safety and b at two groundwater levels
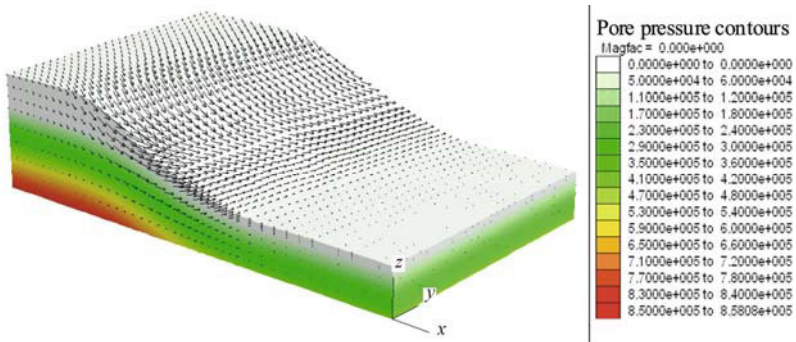
Fig. 18.27 Pore-water pressure contour and displacement vector of slope at h=37 m and b=0.5

of groundwater is neglected and the soil under the groundwater level is saturated. Figure 18.29 shows the relationship between x-direction displacement at historical point No. 1 and timesteps at different depths in the groundwater level when b=0.5. The results suggest that the x-direction displacement at historical point No. 1 increases significantly as the groundwater rises gradually, and the slope became unstable at a groundwater level of h=35 m.
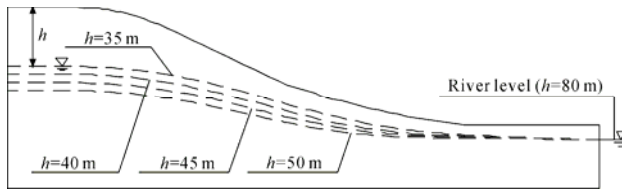
Fig. 18.28 Sketch of different depth of groundwater level
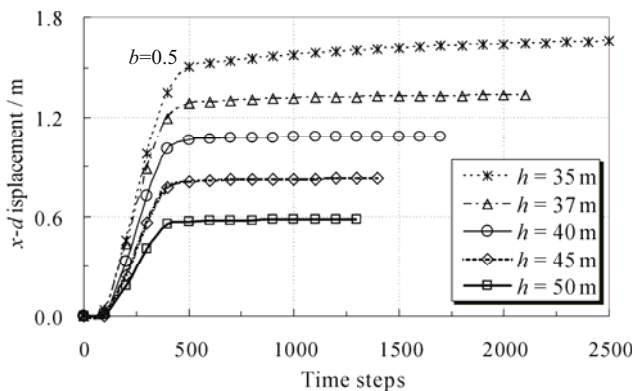
Fig. 18.29 Relationship between x-direction displacement at historical point No. 1 and timesteps

The loess plateau landslide at South Jingyang, Shaanxi Province, China, is a

useful reference for studying the mechanism of a large landslip. The result indicated that the intermediate principal stress, when considered in slope stability analysis, conforms to the actual situation. The unified strength theory provides a wide choice for slope engineering.

18.7 Conclusions

The unified strength theory is implemented into the FLAC/FLAC^{3D} code using a dynamic-link library file developed by VC++. A series of numerical analyses are carried out by FLAC with UST and the results are compared with the solution of the analytical method. The elastoplastic model of UST can be coupled with groundwater flow, dynamic and thermal analysis in FLAC/FLAC^{3D}.

(1) Unified strength theory is applied to the numerical calculation of geotechnical engineering; it has an important significance in the study of the mechanical behavior of geomaterials and structures.

(2) A series of numerical solutions can be obtained from unified strength theory using numerical methods such as FLAC/ FLAC^{3D}. Those solutions may be suitable for various materials and may be more relevant to engineering applications.

(3) The vertex singularity of unified strength theory can be processed easily in constitutive model development of FLAC/ FLAC^{3D}. The linearized criteria such as Tresca, Mohr-Coulomb and the Unified strength theory can be used in FLAC/ FLAC^{3D} directly. The Mohr-Coulomb theory is equivalent to the unified strength theory with b=0. The Tresca criterion is equivalent to the unified strength theory with α=1 and b=0. The Huber von Mises criterion is equivalent to the unified strength theory with α=1 and b=1/2.

(4) The unified strength theory considers the effect of the intermediate principal stress σ_2 and has simple mathematical formulae; it can not only make better use of the strength of materials than single shear strength theory, but   is also widely in agreement with experimental results using various materials. The unified strength theory with b=1/2 is a new criterion for SD materials. It may be used as a new reasonable failure criterion for geomaterials instead of the Drucker-Prager criterion.

(5) The results of three dimensional simulation of the Jingyang landslide show that the slope gradually stabilized when it reached a certain deformation. When considering seepage, seepage on the slope occurred during the continued deformation, when the height of the water level caused a certain degree of damage after the sudden instability. There is more danger due to the action of the seepage. Due to dry weather in loess areas, much farmland irrigation and seasonal rain causes the water level to rise significantly within a short time. Inorder to improve the stability of the high loess slope there should less reclamation of farmland and less irrigation on the edge of the loess plateau, to reduce the adverse effects of groundwater seepage on slope stability.

References

Bathe K J, Wilson E L (1976) Numerical methods in finite element analysis. Englewood Cliffs: Prentice-Hall.

Erickson H L, Drescher A (2002). Bearing capacity of circular footings. Journal of Geotechnical and Geo-environmental Engineering ASCE, 128(1): 38-43.

Fast Lagrangian Analysis of Continua in 3Dimensions' version 2.0, USA: Itasca Consulting Group, Inc., Minneapolis, 1997.

FLAC–Fast Lagrangian Analysis of Continua, version 5.0. ITASCA Consulting Group, Inc., Minneapolis, 2005.

Frydman S, Burd H J (1997) Numerical studies of bearing-capacity factor Nγ. Journal of Geotechnical and Geoenvironmental Engineering ASCE, 123(1): 20-29.

Griffiths D V (1982) Computation of bearing capacity factors using finite elements. Géotechnique, 32(3): 195-202.

Griffiths D V, Lane P A (1999) Slope stability analysis by finite elements. Géotechnique, 49(3): 387-403.

Ma ZY, Liao H J and Xie Yongli (2010) True triaxial simulation based on unified elastoplastic finite difference method. J. of Geotechnical Engineering, 32(9): 1168-1173 (in Chinese).

Mabrouki A, Benmeddour D, Frank R, Mellas M (2010) Numerical study of the bearing capacity for two interfering strip footings on sands. Computers and Geotechnics, (37): 431-439.

Liao HJ, Ma ZY, Ning CM, Liu L and Sassa K (2010) Stability analysis of high loess slope under complex stress state. In: Recent developments of geotechnical engineering, Proceedings of the fourth Japan-China geotechnical symposium, Okinawa Japan, April 12-14.

Loukidis D, Salgado R (2009) Bearing capacity of strip and circular footings in sand using finite elements: Computers and Geotechnics, (36): 871-879.

Potts D M, Lidijia Zdravkovic (1999) Finite element analysis in geotechnical engineering: theory. Thomas Telford Ltd: London.

Potts D M, Lidijia Zdravkovic (1999) Finite element analysis in geotechnical engineering: applications. Thomas Telford Ltd: London.

Prandtl, L (1920) Uber die Häete plastistischer Körper. Nachr. Ges.Wissensch, Gottingen, math.-hys. Klasse, pp 74-85.

Terzaghi K (1943) Theoretical soil mechanics. Wiley: New York.

Vesić AS (1973) Analysis of ultimate loads of shallow foundations. J Soil Mech Found Div ASCE. 99(1): 45-73.

Yin JH, Wang YJ, Selvadurai APS (2001) Influence of nonassociativity on the bearing capacity of a strip footing. Journal of Geotechnical and Geoenvironmental Engineering ASCE. 127(11): 985-989.

Yu MH, He LN and Song LY (1985) Twin shear stress theory and its generalization. Scientia Sinica Series A, 28(11): 1174-1183 (English edn.)

Yu MH (1992) New System of Strength Theory. Xi'an Jiaotong University Press: Xi'an (in Chinese).

Yu MH (1994) Unified strength theory for geomaterials and its applications. Chinese Journal of Geotechnical Engineering, 16(2): 1-9.

Yu MH(1998) Twin-Shear Theory and its Applications. Science Press: Beijing.

Yu MH (2004) Unified Strength Theory and its Applications. Springer: Berlin, Beijing.

Yu MH et al. (2006) Generalized plasticity. Berlin: Springer: Beijing.

Zhang CQ, Zhou H and Feng XT (2008) Numerical format of elastoplastic constitutive model based on the unified strength theory in FLAC^{3D}[J]. Rock and Soil Mechanics, 29(3): 596-601

Zienkiewicz O C, Humpheson C, Lewis R W (1975) Associative and non-associative visco- plasticity and plasticity in soil mechanics. Géotechnique, 25(4): 671-689.

Zienkiewicz O C, Taylor R L (2009) The finite element method for solid and structural mechanics. Elsevier: Singapore.

19

Mesomechanics and Multiscale Modelling for Yield Surface

19.1 Introduction

Mechanical modelling is an abstraction, a formation of an idea or ideas that may involve the physics of solids with specific geometric configurations. Mathematical models may involve relationship between continuous functions of space and time for describing the homogeneity and/or isotropy of a material or the formation of conservation laws (Meyer, 1985; Tayler, 1986; Besseling and Liessen, 1994). The results based on these models for describing a phenomenon should agree with existing measurements within a specified accuracy and can be used with confidence to predict future observations and events.

Useful models provide valuable analogies for new situations. The challenge lies in finding a model that is simple and yields useful information, but it sufficiently diversified to give all the information required with sufficient accuracy (Meyer, 1985; Tayler, 1986; Besseling and Liessen, 1994).

Models can be built with varying degree of details at the different scale levels. A super-macro model for universe is similar a high-power telescope. A macro-model for material and structure is similar to naked eye; it takes global picture of the object at large fine details. A meso-model is similar to a low-power microscope. A micro-model is equivalent to a high-power microscope where the view of vision is narrow down to a local region giving the fine details (Meyer, 1985; Tayler, 1986). The multi-scale analysis of materials and structures on various scales are presented (Ortiz, 2008; Sadowski, 2005; Ottosen and Ristinmaa, 2005; Ma et al., 2004; 2008; Li et al., 2010; Schrefler, 2009; Zohdi and Wridggers, 2001; Ladevdz and Fish, 2003). It can be illustrated by a picture as shown in Fig. 19.1 (Li et al., 2007).

Multiscale modeling applied to meso and macro scale continuum calculations is a broad field with a long history. It encompasses hardening relations based on

dislocation density, porosity related ductile failure models, crystal plasticity, composite media and numerous other general topics dating back more than half a century. There are also a myriad of more recent activities that can be grouped under this subject heading (Becker, 2007; McDowell, 2010).

Emphasis will be placed on the research of yield criterion of element or unit cell under complex stress state in this chapter.
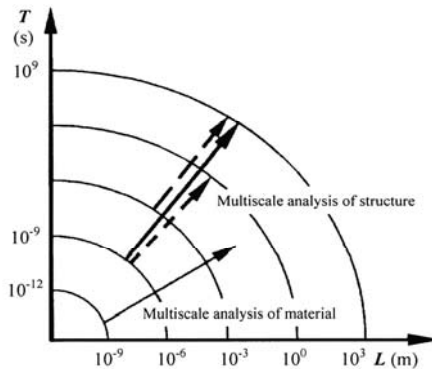
Fig. 19.1   The multiscale analysis of material and structure (Li et al., 2007)

Plastic yield criterion of metallic glass based on atomistic basis was studied by Schuh and Lund (2003). Atomic-scale study of plastic-yield criterion in nanocrystalline CU is given by Dongare et al. (2010).

The theory of the plastic distortion of a polycrystalline aggregate under combined stresses were studied by Bishop and Hill (1951), Kröner (1961) as well as Lin and Ito (1965; 1966) and others. The yield loci of polycrystalline aggregates under the combined stress (σ~τ) were studied by Lin and Ito (1965; 1966). The calculate models of Lin and Ito for polycrystalline aggregates are shown in Fig. 19.2. Three yield loci (dotted line) corresponding to the three plastic strain increment $\Delta\varepsilon=0$, $\Delta\varepsilon=0.01\times10^{-6}$ and $\Delta\varepsilon=2\times10^{-6}$ were given, as shown in the three dotted lines in Fig. 19.3 (Lin and Ito, 1965; 1966).
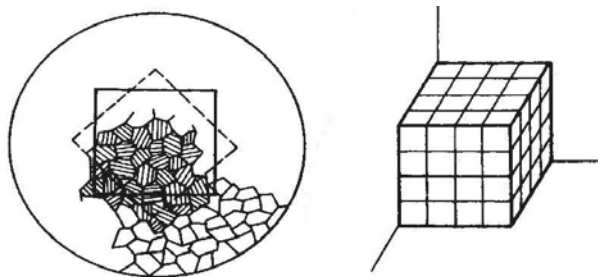
Fig. 19.2   Simulate model of polycrystalline aggregates (Lin and Ito, 1965; 1966)
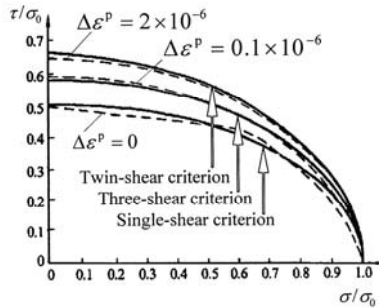
Fig. 19.3   Three yield loci of polycrystalline aggregates

The three solid lines in Fig. 19.3, top to bottom respectiuely correspond to the twin shear yield criterion (Yu, 1961) or the maximum deviatoric stress criterion (Haythornthwaite, 1961), three-shear yield criterion (Huber-von Mises criterion) and the single-shear yield criterion (Tresca criterion), in which the two yield loci of the Huber-von Mises criterion and the Tresca criterion were given by Lin and Ito (1965; 1966), and the third yield locus of the twin-shear yield criterion was added by Yu and Zeng in 1993 in the Collection of Papers Dedicated to Professor Tung-Hua Lin in Celebration of His 80th Birthday (Yu and Zeng, 1993).

The multi-scale analysis of materials and structures crosses wide fields of research (Becker, 2007; Ghosh et al., 1995; 1996; Ghosh et al., 2001; Tomasz Sadowski, 2005; Ottosen and Ristinmaa, 2005; Kröner, 1977; Fish and Yu, 2001; Jasiuk and Strarzewski, 1994; 1998; Li et al., 2010; Liu et al., 2004, McDowell et al., 1985 to 2010; Picu, 2003; Raabe, 1998; Schrefler, 2009; Faria et al., 2010). A serial symposium and proceedings on meso-mechanics are organized and edited by Sih GC, such as the proceedings of an Int. Conf. of Role of Mechanics for Development of Science and Technology, held at Xi'an Jiaotong University, Xi'an, China, June 13-16, 2000 (Sih, 2000). A plenary lecture on material model in mesomechanics and macromechanics was presented by Yu at this Conference (Yu, 2000).

Many models have been proposed in applied mechanics. In what follows, the discussion will be confined to the strength models of materials under the complex stress state within the framework of continuum mesomechanics and macromechanics. The multi-scale analysis with emphasis on the yield surface of element (unit cell) under complex stress will be described in this chapter. The interaction yield surface of structures under combined loading is also discussed briefly. The multi-scale analysis of strength of material under various scale complex stress is illustrated as shown in Fig. 19.4.
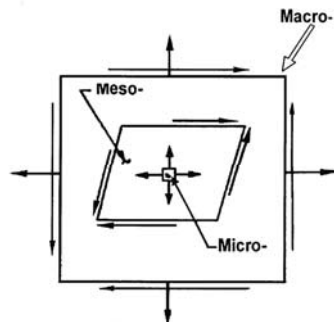
Fig. 19.4   The multi-scale analysis of strength of material under various scales of complex stress

19.2   Interaction Yield Surface of Structures

The cross-section of an element of structure, in the general case, is loaded by a combination of a normal force, bending moments at different directions, shear force, a torsion moment etc. All these quantities can be referred as the generalized force, denoted by the symbol $Q^*=Q(N_z, Q_x, Q_y, M_x, M_y, T_z)$. $N_z, Q_x, Q_y, M_x, M_y, T_z$, which are the plastic limit force of tension/compression, shear force, bending moment and torque moment, respectively. Interaction yield surface for generalized force for different structures are discussed by Hodge (1959), Save and Massonet (1972), Zyczkowski (1981), Sawczuk (1989), Stronge and Yu (1993). Detail description of interaction yield surfaces can be seen in Zyczkowski (1981).

Figure 19.5 shows the elastic-plastic state for a simply supported circular plate. The generalized yield surface, or interaction yield surface for circular plate obeying the unified yield criterion is shown in Fig. 19.6 (Liu and Jiang, 2008). Similar results can be found in structural plasticity (Yu et al., 2009) and plastic analysis of structures (Hodge, 1959; Zyczkowski, 1981, Stronge and Yu, 1993).
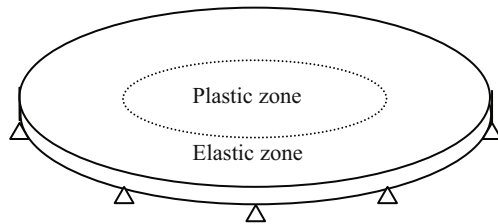
Fig. 19.5   Elastic-plastic state for a simply supported circular plate
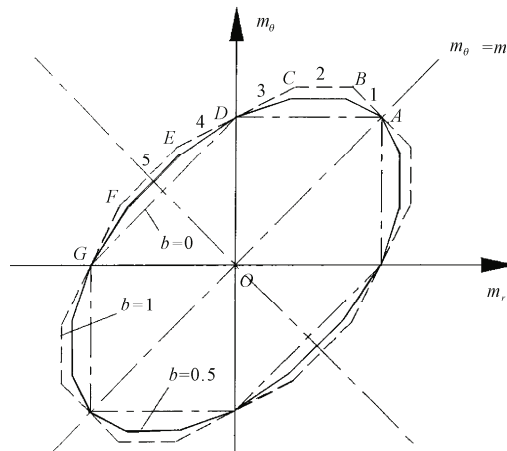
Fig. 19.6   The generalized yield surface for a circular plate obeying the unified yield criterion (Liu and Jiang, 2008)

19.3 Models in Mesomechanics and Macromechanics

A host of material models have been proposed in meso-mechanics. They include those for dislocation (Bomert et al., 1994), shear stress slip model, polycrystalline aggregate model (Lin and Ito, 1965; Dvorak and Bahei-E1-Din, 1997; Gologanu et al., 1993), equivalent inclusion (Hashin, 1962; 1983; Hashin and Shtrikman, 1964), Dugdale crack and Dugdale damage (Christeensen and Lo, 1979; Gologanu et al., 1997), continuum damage (Gurson, 1977), damage of domain of microcrack growth (Dvorak, 1999) , and the differential self-consistent model etc. Continuum micro-mechanics of elastoplastic polycrystals was presented by Hill (1965).

19.3.1 RVE and HEM Model

Representative volume element (RVE) model (Hashin, 1962; 1983; Sun and Vaidya, 1996) and homogeneous equivalent medium (HEM) model are defined such that there prevails a sufficient number of volumes or subvolumes, subjected to macroscopically uniform stress, strain, or temperature change. The bulk properties are not dependent on its size (de Buhan and de Pelice, 1997). RVE model and HEM model have been used widely in mesomechanics.

19.3.2 Equivalent Inclusion Model

The elastic field for an ellipsoidal inclusion has been determined in Hashin (1962). The important result is that the strain field in the inclusion is uniform.

19.3.3 CSA and CCA Models

A direct and simple way to represent the matrix connectedness of a composite material was proposed. The composite spheres assemblage (CSA) model applies to an isotropic particulate while the composite cylinders assemblage (CCA) model introduced later has been used for fiber-reinforced transversely isotropic materials. The latter pertains to unbounded set of contiguous similar composite spheres of all sizes, including those that tends to zero such that the voids between the sphere could be filled.

19.3.4 Gurson Homogenized Model

The Gurson homogenized model (Gurson, 1977) for porous ductile metals is based on an approximate limit-analysis for hollow spheres made of rigid ideal-plastic material using the von Mises yield criterion. Some Gurson models consider the influence of void shape. The effect of strong gradients of macroscopic fields were proposed.

19.3.5 Periodic Distribution Model

Figure 19.12 shows some isotropic distributed patterns of periodic distribution model (PDM) (Christeensen and Lo, 1979).

19.3.6 PHA Model and 3-Fold Axissymmetrical Model

The periodic hexagonal array (PHA) model deals with a microstructure that consists of hexagonal and dodecahedral cylindrical fibers (Gologanu et al., 1993). A 3-fold axis of rotational symmetry model has been proposed (Dvorak and Bahei-E1-Din, 1997).

19.3.7 A Unit Cell of Masonry

A continuum model for assessing the ultimate failure of masonry as a homogenized material can be found in the literature. The unit cell is a rhombic model. Several other models have been used in the analyses of reinforced concrete and reinforced plastic.

19.3.8 Topological Disorder Models

Disorder models dispersion patterns of fibres were proposed (Pyrz and Bochenek, 1998).

19.3.9 Random Field Models of Heterogeneous Materials

The random field models of heterogeneous materials were presented by Ostoja-Strarzewski (1993; 1994; 1998).

   The idea of a unit cell and other models were used. Several models of composite and heterogeneous materials were presented (Hashin, 1962; l Gurson, 1977; Christeensen and Lo, 1979; Ostoja-Strarzewski, 1993; 1994; 1998; Dvorak and Bahei-E1-Din, 1997; Pyrz and Bochenek, 1998; Dvorak, 1999), which are shown in Fig. 19.7.
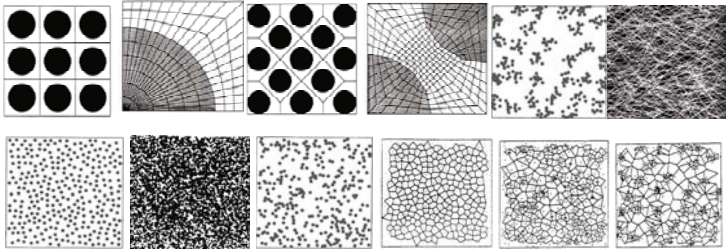
Fig. 19.7   Several models of composite and heterogeneous materials

19.4 Failure Surface for Cellular Materials under Multiaxial Loads and Damage Surfaces of a Spheroidized Graphite Cast Iron

In many applications, foams, including rigid polymer foam, lightweight cellular concrete, metallic foams and ceramic foam are subjected to multiaxial stresses. Systematic investigations regarding the multiaxial failure of foams were done at MIT (Massachu-setts Institute of Technology), Cambridge University and Harvard University. Failure surfaces for cellular materials under multiaxial loads are presented by by Gibson and Ashby (1987; 1997), Gibson et al. (1989), Triantafillou and Zhang (1989), Triantafillou and Gibson (1990). Theocaris (1991), Ashby et al. (2000), Deshpande and Fleck (2000), Gibson (2000), Gioux et al. (2000), Sridhar and Fleck (2000). A yield surface is developed using an analysis of an idealised foam. It may be referred to as the GAZT (Gibson et al., 1989) yield surface. The failure criterion for tensile rupture of foams is written as follows:

$$F(I_1, J_2) = \pm\sqrt{J_2} - 0.2aI_1 = \sigma_{cr} \qquad (19.1)$$

   This equation is similar to the Drucker–Prager criterion for soils. The limit surfaces in stress space consist of two intersecting surfaces of conical shape associated with the tensile and compressive limit (Triantafillou and Gibson, 1990).

The yield surfaces of aluminum alloy foams for a range of axisymmetric compressive stress states have been investigated by Deshpande and Fleck (2000). The yield surfaces of compacted composite powders under triaxial testing were measured and studied by Sridhar and Fleck (2000). A design guide for metal foams was given by Ashby et al. (2000). A review for mechanical behavior of metallic foams was given by Gibson (2000).

Aluminum foams are currently being considered for use in lightweight structural sandwich panels and in energy-absorption devices. In both applications, they may be subjected to multiaxial loads. Designers require a criterion to evaluate the combination of multiaxial loads that cause failure. The Drucker-Prager criterion and a yield surface for compaction of powders are used. Both phenomenological yield surfaces give a description of the multiaxial failure of the aluminum foams tested by Gioux et al. (2000).

Multi-axial yield behaviour of polymer foams is found to be described adequately by the inner envelope of a quadratic function of mean stress and octahetral-shear stress and a maximun compressive principal stress criterion (Deshpande and Fleck, 2000).

The global extremal yield surfaces of a unit cell are constructed with the numerical experiments by Schrefler (2009).

The Huber-von Mises type functions are always used in damage mechanics (Kachanov, 1986; Lou, 1991; Lemaitre, 1992; Yu and Feng, 1997; Voyiadjis et al., 1998). A theoretical and experimental study of damage surfaces for spheroidized graphite cast iron was presented by Hayakawa and Murakami (1998) and Murakami et al. (1998). Damage evolution and fundamental aspects of damage surface of a spheroidized graphite cast iron were observed. The existence and the development of the damage surface, together with the condition of loading, unloading and neutral loading, are elucidated. The initial, subsequent and final damage surfaces were obtained by Hayakawa and Murakami (1998), as shown in Fig. 19.8.
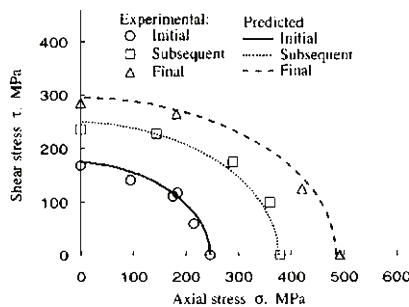
Fig. 19.8   Damage surfaces under combined stress space (Hayakawa and Murakami, 1998)

The damage surfaces can be described by a first quadrant of an ellipse in the space of axial tensile and shear stress. The ellipse of the initial damage surface has the aspect ratio of $\sigma/\tau=1.46$, the ellipse of the subsequent damage surface is $\sigma/\tau=1.62$, which are in contrast to the ellipse ($\sigma/\tau=1.733$) of the initial yield surface of von Mises type yield criterion. A theoretical damage surface under

combined stress was proposed by Murakami et al. (1998), it is closed to the experimental results as shown in Fig. 19.8.

It is interesting that the ellipse of the initial damage surface has the aspect ratio of $\sigma/\tau=1.46$, which is closed well to the twin-shear yield criterion with the ratio of $\sigma/\tau=1.5$. A twin-shear damage surface, a generalized twin-shear damage surface or the unified typed damage surface may be available. The generalized twin-shear strength criterion (Yu, 1985) and the unified strength theory (Yu, 1991) can be matched to the pressure sensitively materials.

19.5 Mesomechanics Analysis of Composite Using UST

The strength prediction for composite materials is very important in engineering. The homogenization method by using a unit cell is an effective method to evaluate the elastic stiffness property for the composite materials by many researchers. Micromechanical analysis of composite by the method of unit cell was summarized and reviewed by Aboudi (1989), Pindera and Aboudi (1989), Ju and Tseng (1996), Zhu et al. (1998). The analysis leads to the prediction of the overall behavior of various types of composites from the known material properties of fiber and matrix. The capability of the theory in providing the response of elastic, thermoelastic, viscoelastic, and viscoplastic composites, as well as their initial yield surfaces, strength envelopes, and fatigue failure curves, is demonstrated by Aboudi (1989).

The evaluations of strength of composites under the biaxial stresses by using the unified yield criteria were given by Li YM and Ishii (1998a; 1998b). A series of biaxial loads were applied to the laminate sample of boron fiber unidirectional reinforced aluminum in material principal directions, and through a meso-unit-cell to get the corresponding macroscopic elasto-plastic behavior. The unified yield criterion was used as an elasto-plastic flow potential function to evaluate strength of composite. This approach ensures the uniformity of the stress field and has no any so called slip generally in the grips during the experiment. It means that one can get a preliminary understanding of the macroscopic nonlinear elasto-plastic properties easily by numerical analysis. The corresponding FEM analysis system were developed by Quint Co. in Japan (1993; 1994).

For the flow potential function at the mesoscopic level, the unified yield criterion was used (Li and Ishii, 1998). The coefficient b in the unified yield criterion could be determined by pure shear test. Since the pure shear test is usually difficult to be carried out, the b can be taken in a range of $0 \le b \le 1$ for various materials. Equation (10.2) should be turned to be the Tresca yield criterion when $\alpha =1$ and $b=0$, or the Twin Shear Stress (TSS) criterion (Yu, 1961) when $\alpha =1$ and $b=1$, or it is closes to the Huber von Mises yield criterion with linearity when $\alpha =1$ and $b=0.5$. It is easy to find that the coefficient b is obviously a parameter reflecting the strength property on π -plane when stress state is close to the pure shear stress state. In fact, include all possible existing criteria which

satisfy the convex postulate on π -plane by $0 \le b \le 1$. So, one can select a different value of b for using different yield function by installing the unified yield criterion only into FE-code.

The unified yield criterion was used in meso-unit-cell for getting macroscopic elasto-plastic responses. This model can be considered as an experimental sample of the unidirectional reinforced laminate, and the biaxial uniform loading is applied to the two directions X_1 and X_2 as shown in Fig. 19.9.
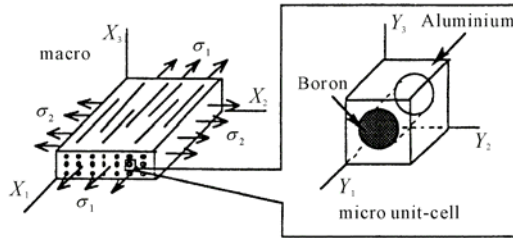
Fig. 19.9   The sample model: macro and meso

The meso-scopic properties for fiber and matrix are:

Boron: $E_f = 413.7$ GPa, $v_f = 0.21$, $\sigma_f^0 = 3200$ MPa;

Aluminum: $E_m = 68.9$ GPa, $v_f = 0.33$, $\sigma_m^0 = 262$ MPa.

Here, it is assumed that the boron fiber and aluminum matrix are of ideal elasto-plastic properties.

Figure 19.10(a) is the stress-strain properties for the tension loading in fiber direction only, and it is found that there is almost no difference among the macroscopic stress-strain curves with three yield criteria. For the tension loading in transverse direction only, however, the nonlinear stress-strain curves appear very different as shown in Fig. 19.10(b).

(a) Fiber direction loading only   (b) Transverse loading only
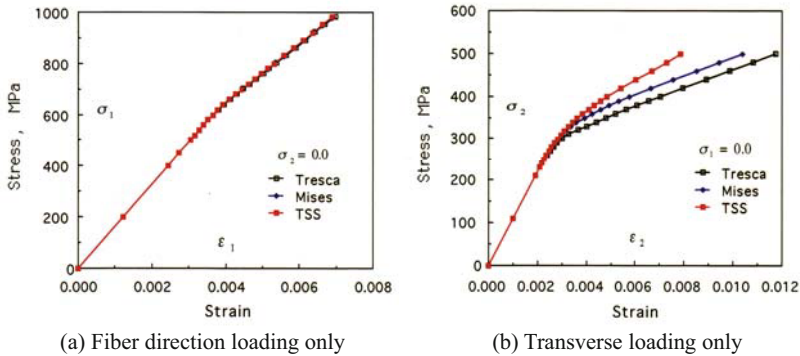
Fig. 19.10   Stress-strain curves for composite (Li and Ishii)

Obviously, the difference of nonlinear stress-strain properties is depended on the load condition by using various yield criteria at meso-scopic level. The plastic zones with different yield criteria are shown in Fig. 19.11. Figure 19.11 shows that the twin-shear yield criterion (Yu, 1961) gives a smaller plastic zone, and the single-shear yield criterion (Tresca, 1864) gives a bigger plastic zone in the unit-cell under same load.

(a) Tresca material   (b) von Mises material   (c)Twin-shear material
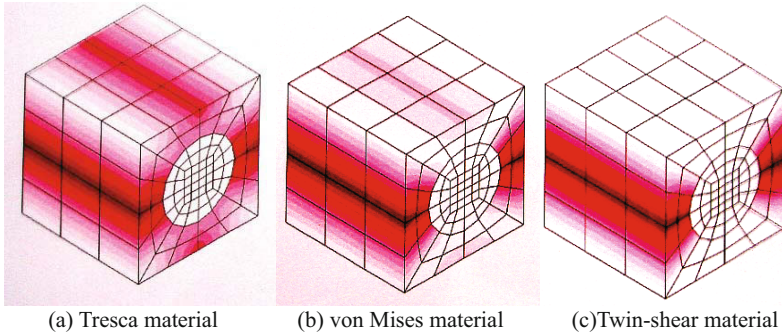
Fig. 19.11   Plastic zones in meso-unit-cell under same load (Li and Ishii)

The conclusion obtained by Li and Ishii is that the installation of the unified yield criterion makes it easy to use various yield criteria to evaluate the strength property of composite.

The unified yield criterion and the approach Li and Ishii used may be extended for more complex meso-construction composite materials, such waved fiber, honeycomb, of which the strength relation evaluation between macro and micro is not very clear until now.

The unified strength theory give us with a effect and powerful theoretical basic to study the effect of failure criterion on the evaluation of elasto-plastic behaviour of composite and other materials at macro and meso levels. Multiscale modelling of damage and fracture processes in composite materials was summarized by Sadowski (2005).

19.6   Multiscale Analysis of Yield Criterion of Metallic Glass Based on Atomistic Basis (Schuh and Lund, 2003)

Plastic yield criterion of metallic glass based on atomistic basis was studied by Schuh and Lund in 2003. The simulation model on atomistic basis is shown in Fig. 19.12 (Schuh and Lund 2003; Lund and Schuh, 2005).
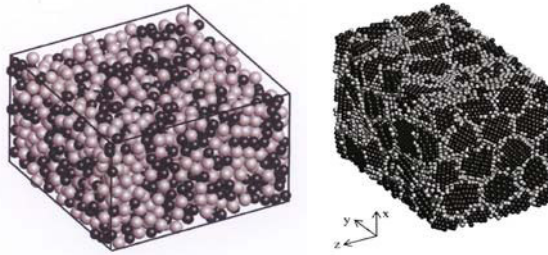
Fig. 19.12   Simulation model on atomistic basis (Schuh and Lund, 2003)

The two simulation results of metallic glass under plane stress on atomic basis given by Schuh and Lund are shown in Fig. 19.13 and Fig. 19.14. It indicted that metallic glass is tension-compression asymmetry; the Huber von Mises criterion and the Tresca criterion cannot be adapted for metallic glass. The comparison of the simulation results of yield locus with the Mohr-Coulomb yield locus (solid line) is shown in Fig. 19.14.
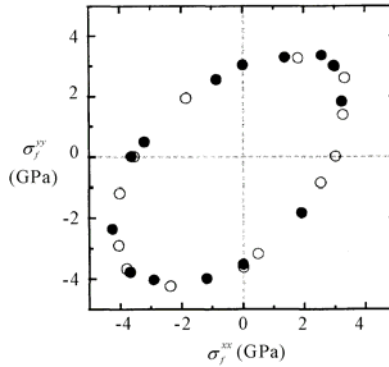
Fig. 19.13   Simulation results (Schuh and Lund, 2003)
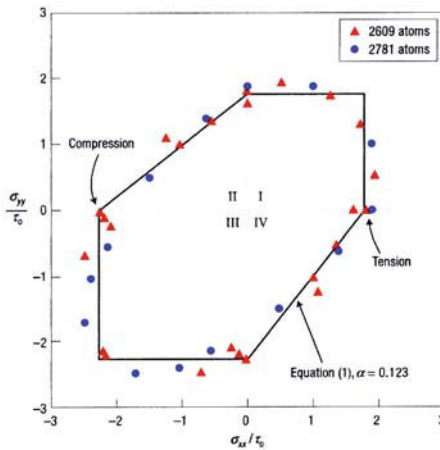
Fig. 19.14   Simulation results (Schuh and Lund, 2003)

19.7 Multiscale Analysis of Yield Criterion of Molybdenum and Tungsten Based on Atomistic Basis (Groger et al., 2008)

Multiscale modeling of plastic deformation of molybdenum and tungsten is studied by Groger et al. (2008). Yield surface for single crystals based on atomistic studies is obtained by Groger et al. as shown in Fig. 19.15.
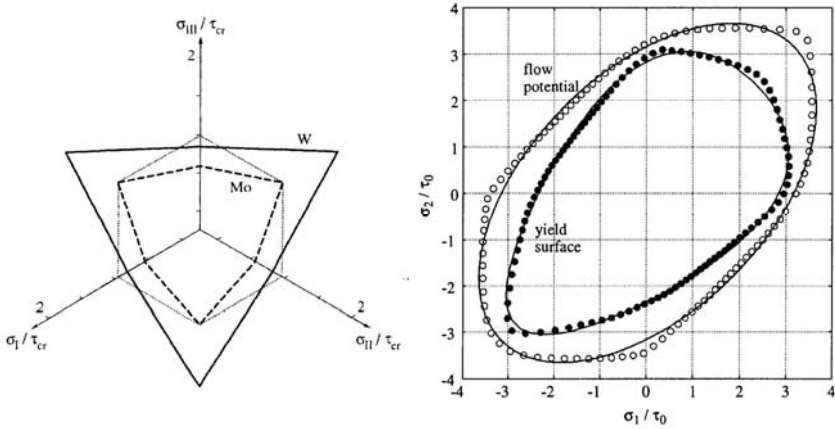
Fig. 19.15 Yield and flow surfaces predicted from a Taylor model for bcc Mo (Groger et al., 2008)

Simple isotropic functions that accurately describe computed yield and flow surfaces for random bcc poly-crystals obtained from calculations, such as those shown in Fig. 19.15, are given by Groger (2008). They constructed the analytical yield criteria as

$$F = \sqrt{3}[(J_2)^{3/2} + bJ_3]^{1/3} ; \quad G = \sqrt{3J_2} \tag{19.2}$$

where $J_2 = s_{kl} s_{kl} / 2$ and $J_3 = s_{ij} s_{jk} s_{ki} / 3$ are the second and third invariants of the deviatoric stress tensor.

19.8 Phase Transformation Yield Criterion of Shape-Memory Alloys

Mechanical behavior and yield surface of shape memory alloy (SMA) under multiaxial stress has been studied widely. It has been found that the "yield" (transformation start stress in stress induced phase transformation) surface does neither really match the Huber-von Mises yield criterion nor the Tresca yield

criterion. The possibility of using such a "yield" surface to predict the behavior of a SMA under other stress conditions. "Yield" surfaces of shape memory alloys and their applications were studied by Huang (1999), Lim and McDowell (1999), Gall et al. (1998), Novák and Šittner (2004) The "yield" surfaces of four polycrystalline SMAs (NiTi, NiAl, CuZnGa, and CuAlNi) are investigated by Lexcellent et al. (2002; 2004; 2007; 2010). Phenomenological simulation of yield surfaces of NiTi polycrystal for different temperatures was presented by Lexcellent et al. (2002). A generalized macroscopic J_2-J_3 criterion to describe the transformation onset is proposed and identified (Bouvet et al., 2002). Determination and transport of phase transformation yield surfaces for shape memory alloys are also given by Gibeau, Laydi and Lexcellent (2010). Yield surface of Cu-Al-Be polycrystalline was presented by Lexcellent et al. (2004).

Experimental yield surface of phase transformation initiation for bicompression and tension (compression)–internal pressure tests for CuAlBe polycrystalline was obtained by Lexcellent et al. (2002; 2007; 2010). A general formula to describe these "yield" surfaces is found by Lexcellent et al. The parameters in this formula can be calculated by using the "yield" stresses of tension and compression of a particular SMA. The analytical results agree well with reported experimental data of NiTi.

The simulation and experimental yield surfaces of phase transformation for shape memory ally (Lexcellent, 2010), as shown in Fig. 19.16.
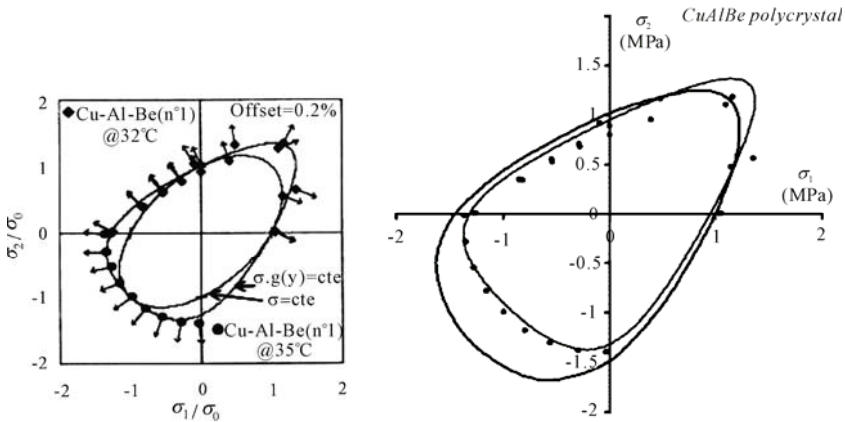
Fig. 19.16 Simulation and experimental yield surface of phase transformation for CuAlBe shape memory alloy (Lexcellent, 2010)

A new yield surface is presented by Kolupaev and Altenbach (2010), which is illustrated by red line in Fig. 19.17. It is interesting that the Kolupaev-Altenbach yield surface is similar to the simulation and experimental yield surfaces of shape memory alloy, as shown in Fig. 19.16 (Lexcellent, 2010).
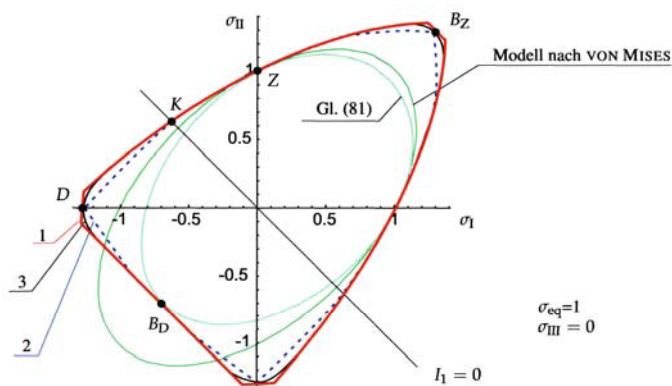
Fig. 19.17 New yield surface (Kolupaev-Altenbach, 2010)

The transformation yield surface of shape-memory alloys was also studied by Bhattacharya and Schlömerkemper (2004).

19.9 Atomic-Scale Study of Yield Criterion in Nanocrystalline CU

Atomic-scale study of plastic-yield criterion in nanocrystalline CU is given by Dongare et al. (2010). Initial configuration of nanocrystalline Cu with an average grain size of 6nm. System consists of approximately 1.2 million atoms arranged in 122 grains, as shown in Fig. 19.18. Molecular dynamics (MD) simulations for yield surface are presented. Plot of the calculated yield stress and flow (peak) stress in tension and compression at strain rates $1 \times 10^9 \, s^{-1}$ to $8 \times 10^9 \, s^{-1}$, respectively is given in Fig. 19.19. It is seen that yield stress and limit stress values are greater in compression and the difference increases with increasing strain rates. So, the single parameter yield criterion cannot be adopted for nanocrystalline CU.
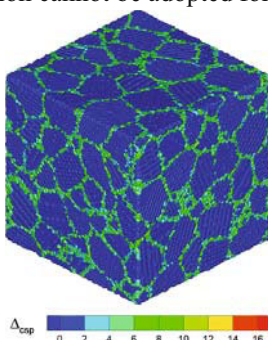
Fig. 19.18 Initial configuration of nanocrystalline Cu with an average grain size of 6 nm
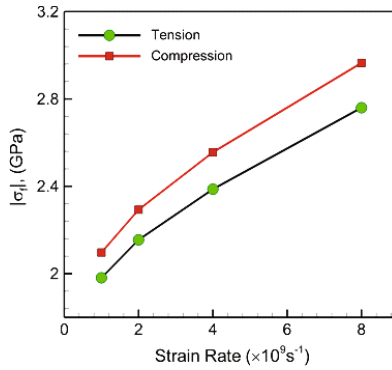
Fig. 9.19 Plot of the calculated yield stress and limit (peak) stress in tension and compression

In the work of Dongare et al. (2010), the biaxial yield surface is calculated by plotting the yield/limit stresses during loading of the nanocrystalline metal by equal/unequal amounts in the X and Y directions and keeping the stress in the Z direction constant ($\sigma_x=\sigma_1$, $\sigma_y=\sigma_2$, and $\sigma_3=\sigma_z=0$). The calculated yield stresses and limit stresses under combined biaxial loading conditions (X-Y) give a locus of points that can be described with a traditional ellipse. However, the center of the ellipse deviated from the center of coordinate (solid lines) a small value, as shown in Fig. 19.20. Dashed lines indicate the shifted center of the ellipse.

(a) Yield stress (0.2% offset stress)   (b) Limit stress (peak value of stress)
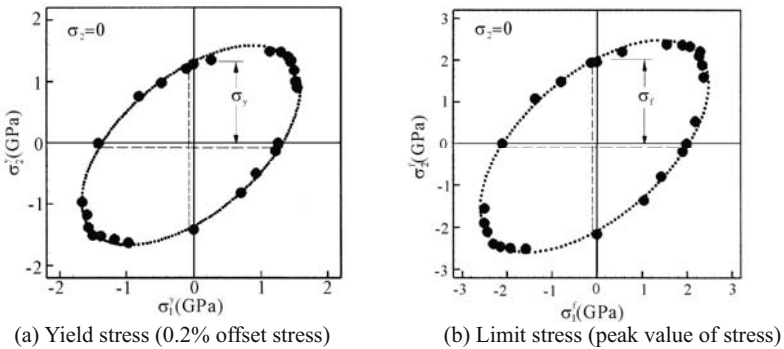
Fig. 19.20 Yield loci for biaxial loading in the X and Y directions and zero stress in the Z direction

The deviation of shifted center of the ellipse is due to the SD (Strength Difference) effect of material, or the tension-compression asymmetry in yield stress and limit stress. It is need to find other theory and method to match these results. A two-parameters yield criterion (or limit criterion), which the SD effect is taken into account, is necessary. The strength ratio of material in tension and in compression $\alpha=\sigma_t/\sigma_c$ is introduced that allows for the incorporation of the tension compression asymmetry. The strength ratio of material in tension and in

compression is $\alpha = \sigma_t / \sigma_c = 0.88$ to $\alpha = \sigma_t / \sigma_c = 0.9$ in this case. The traditional von Mises yield criterion and Tresca yield criterion cannot be fitted to the results.

It is interesting that the results are situated between two convex bounds, as shown in Fig. 19.21. The SD effect is taken into account in these two convex bounds. The inner bound (dotted line) is the Mohr-Coulomb theory.

(a) Yield stress (0.2% offset stress)   (b) Limit stress (peak value of stress)
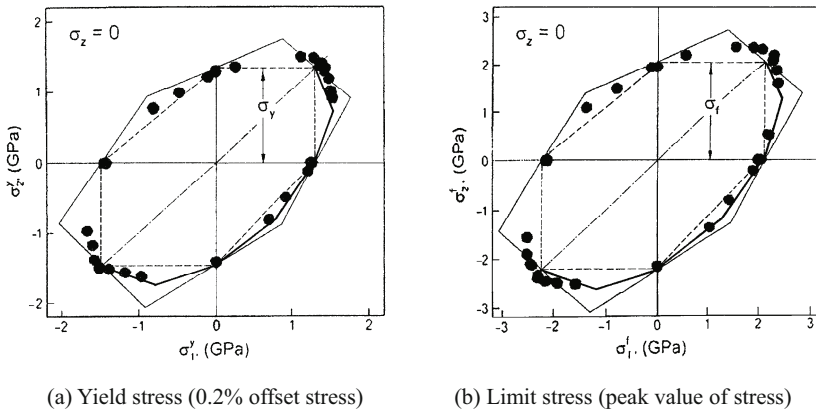
Fig. 19.21   The results situated between two convex bounds

19.10 A General Yield Criteria for Unit Cell in Multiscale Plasticity

Consider a unit cell on the mesoscale with the length of all edges equal to l_ε, as shown in Fig. 19.22. Within this unit cell, the cell is sufficiently small, higher order displacement gradients can be ignored and the strain field varies linearly as the Hooke law. It is assumed that the essential structure of conventional plasticity is preserved on the micro-scale. The Huber-von Mises criterion was always used as the micro-scale effective stress and strain analysis.

In general, the yield behavious of unit cell in meso-scale and micro-scale is always strength asymmetric in tension and in compression. So, a two parameter yield criterion is need.
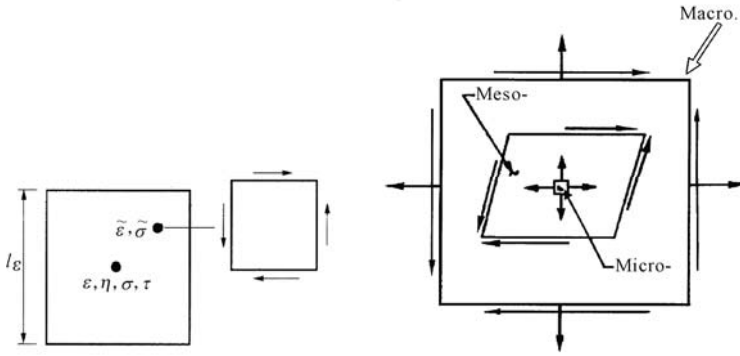
Fig. 19.22   Macro-meso-micro analysis of element (or unit cell) under complex stress

The material models are widely used in mesomechanics and macromechanics. It is hopeful that a simple model could be found to give useful information. It should also be sufficiently general and yield accurate results. Moreover, the formulation should contain the least number of state variables.

It is assumed that:

1) The strength of unit cell at different direction is identical, but the strength is different in tension and in compression. The cell is a SD material. The SD material is also referred as strength asymmetrical in tension and in compression.

2) The strength of unit cell is different at different scales. Denoted the strength as $\Sigma^t{}_v$ tensile strength of unit cell, $\Sigma^c{}_v$ compressive strength of unit cell.

3) The principal stresses acted on the each sides is denoted as Σ_1, Σ_2 and Σ_3.

So, the single parameter criteria, such as the Tresca criterion, the Huber-von Mises criterion and the twin-shear single parameter criterion (Yu, 1961) or the maximum deviatoric stress criterion (Schmidt, 1932; Ishlinsky, 1940; Hill, 1950; Haythornthwaite, 1961, see: Chapter 3) cannot be adopted.

According to the UST, a simple general yield criterion for unit cell may be proposed as follows:

$$F = \Sigma_1 - \frac{\alpha}{1+b}(b\Sigma_2 + \Sigma_3) = \Sigma_t, \text{ when } \Sigma_2 \le \frac{\Sigma_1 + \alpha\Sigma_3}{1+\alpha}, \tag{19.3a}$$

$$F' = \frac{1}{1+b}(\Sigma_1 + b\Sigma_2) - \alpha\Sigma_3 = \Sigma_t, \text{ when } \Sigma_2 \ge \frac{\Sigma_1 + \alpha\Sigma_3}{1+\alpha} \tag{19.3b}$$

where $\alpha = \Sigma^t/\Sigma^c$ is strength ratio of unit cell in tension and in compression. b is a parameter for the choice of yield criterion.

The yield loci of this criterion in plane stress state are illustrated in Fig. 19.23 for two different ratio of $\alpha = \Sigma^t/\Sigma^c$.

(a) α=0.3   (b) α=0.7
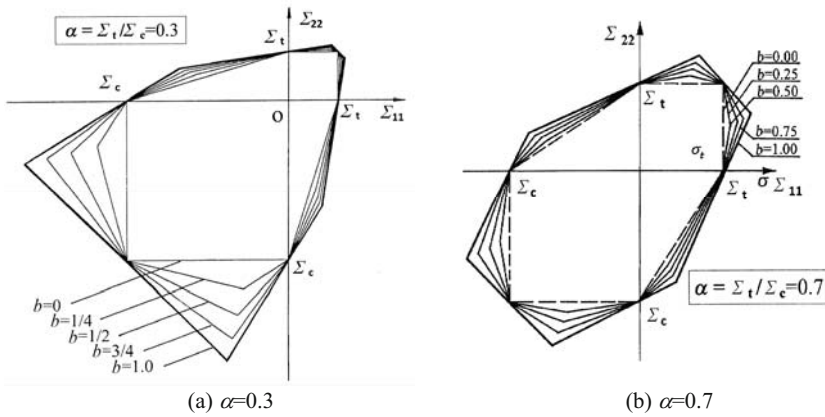
Fig. 19.23 Strength difference in tension and in compression

This general yield criterion for unit cell can be also extended to the non-convex yield loci when the parameter $b<0$ or $b>1$. The convex yield loci and non-convex yield loci of the unified yield loci of unit cell for α=0.5 material are shown in Fig. 19.24. Many problems regarding the non-convex yield surface remain open. A Plenary Lecture on "Nonconvex Plasticity and Microstructure" was presented by Ortiz at 22nd International Congress of Theoretical and Applied Mechanics, Adelaide, Australia, August 27, 2008.
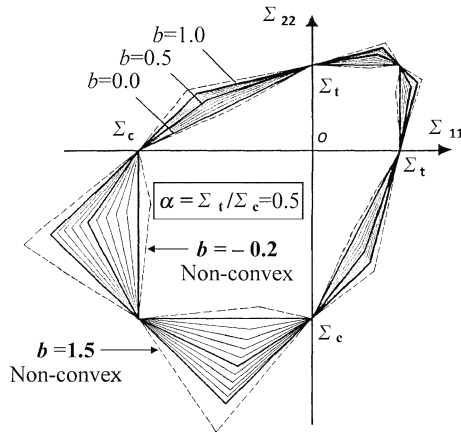
Fig. 19.24 Convex yield loci and non-convex yield loci

This general yield criterion for unit cell is a very simple criterion. However, it is better to match many new results. The calculative results of metallic grass at atomic base have been obtained by Schuh et al. (2003; 2005), as shown in Figs. 19.13 and 19.14. They are shown again with the comparison to yield criterion in Fig. 19.25 and Fig. 19.26. The yield surfaces of simulation results for metallic glass are convex and strength asymmetric in tension and in compression,

which are situated between the two bounds as shown in Fig. 19.25. The comparisons of the UST $b=0$ (inner bound), $b=0.5$ (median) and $b=1$ (upper bound) with simulation result of Schuh et al. are given.

Obviously, the results show the strength asymmetric in metallic grass (Schuh and Lund, 2003). The Tresca criterion and Huber-von Mises criterion cannot be adopted. The Mohr-Coulomb criterion may be used for match the results. It is noted that the general yield criterion for unit cell with $b=0.5$ is also adapted for this result, as shown in Figs. 19.25 and 19.26.

Atomic-scale study of plastic-yield criterion in nanocrystalline CU is given by Dongare, et al. (2010), as stated in section 19.9. The results indicate that:

1) The strength of nanocrystalline CU is tension-compression asymmetry. It has been indicated in Fig. 19.20. The strength ratio of material in tension and in compression is $\alpha=\sigma_t/\sigma_c=0.88$ to $\alpha=\sigma_t/\sigma_c=0.9$. So a two-parameter yield criterion is needed.
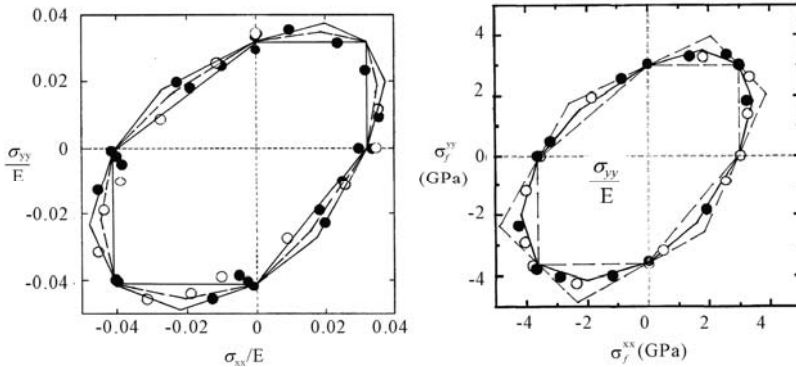
Fig. 19.25   Comparison of the UST $b=0$, $b=0.5$ and $b=1$ with simulation result of Schuh et al.
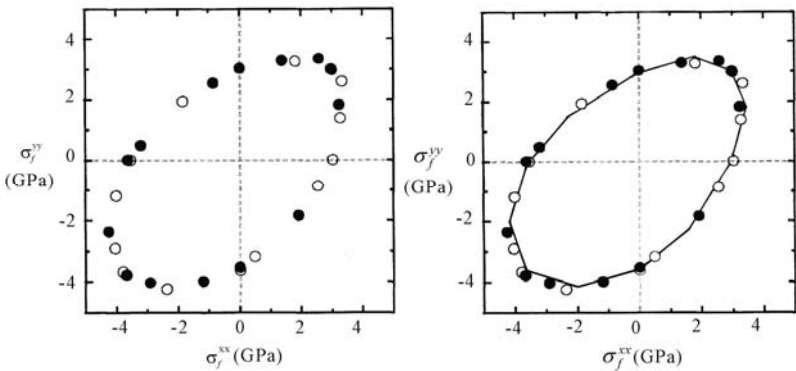
(a) Simulation results for metallic glass   (b) Match of simulation results with $b=1/2$

Fig. 19.26   Comparison of the UST $b=0.5$ with simulation result of Schuh et al.
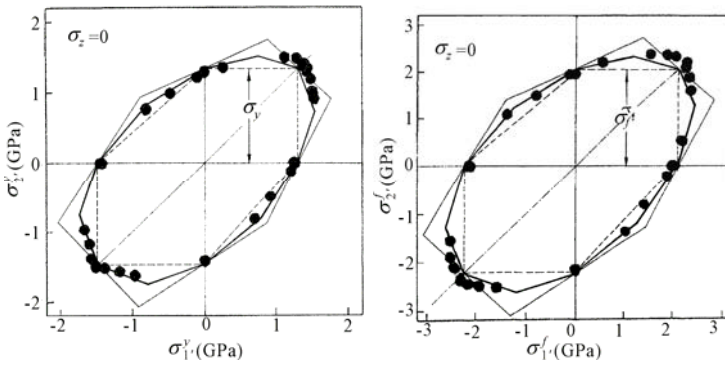
Fig. 19.27 The comparison of the calculated yield loci and the general yield criterion for unit cell with parameter $b=1/2$

2) The yield loci (yield locus and limit locus) obtained from MD simulations are situated between two convex bounds, as shown in Fig. 19.21.

3) The calculated biaxial yield loci for the yield stress and limit stress can be fit to the general yield criterion for unit cell, described in equations 19.3a and 19.3b. A series of yield loci is shown in Figs. 19.23 and 19.24.

4) Significant work is needed to evaluate the parameter b to plasticity under multiaxial loading conditions and, in turn, the yield criterion to predict the macroscopic behavior of these metals at different loading conditions.

5) The comparison of the calculated biaxial yield surface for the yield and limit stresses and the general yield criterion for unit cell with parameter $b=1/2$ are shown in Fig. 19.27.

The shape of yield loci of the unified strength theory will be changed if the strength ratio of material in tension and in compression $\alpha=\sigma_t/\sigma_c$ is decreased. Fig. 19.28 shows the yield loci of the unified strength theory with five typed cases ($b=0$, $b=1/4$, $b=1/2$, $b=3/4$, $b=1$) and three typed cases ($b=0$, $b=1/2$, $b=1$) when the strength ratio of material in tension and in compression $\alpha=\sigma_t/\sigma_c=1/2$.
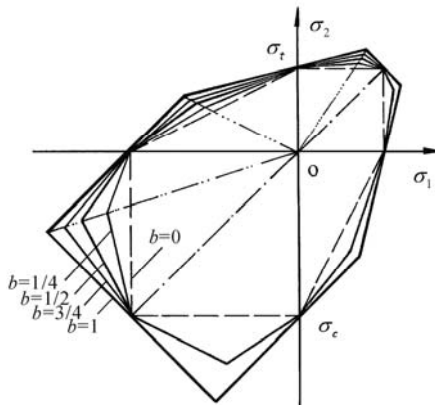
(a) UST with five and three typed cases
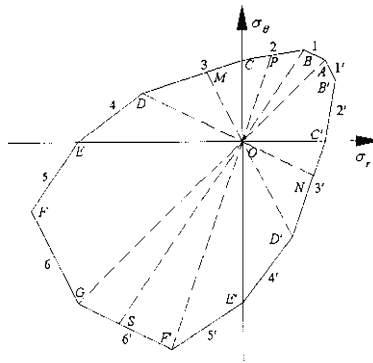
(b) UST with $b=1/2$

Fig. 19.28   Yield loci of the UST in plane stress state(for $\alpha=\sigma_t/\sigma_c=1/2$ material)

19.11   Virtual Material Testing Based on Crystal Plasticity Finite Element Simulations

The CPFE (Crystal Plasticity Finite Element) method is studied systematically by Raabe et al. (Raabe, 1998; Kraska et al., 2009; Roters et al., 2010). The effects of microstructure and texture and their evolution during deformation are taken into account. The example in this section presents an application of the CPFE method for the concept of virtual material testing using a representative volume element (RVE) approach (Kraska et al., 2009). By using such numerical test protocols it becomes possible to determine the actual shape of the yield locus, and to use this information to calibrate empirical constitutive models used. Along with standard uniaxial tensile tests, other strain paths are numerically monitored, such as biaxial

tensile, compressive or shear tests. The use of the CPFE method for virtual testing of yield locus is demonstrated by Roters et al. for a low-carbon steel grade.

19.12   Meso-Mechanical Analysis of Failure Criterion for Concrete

The computational modelling of failure criteria for concrete materials was studied by Buyukozturk et al. (1970), and Liu et al. (1972). The unit cell of concrete combined by circular aggregate and mortar was used. Needleman (1994) gave a summary relating the computational modelling of materials failure.

The model of concrete composited by circular aggregate and mortar is shown in Fig. 19.29. The failure criterion for concrete was obtained by Liu et al. (1972) as shown in Fig. 19.30, in which the dotted lines is the analysis result, and the solid point is the experimental result.
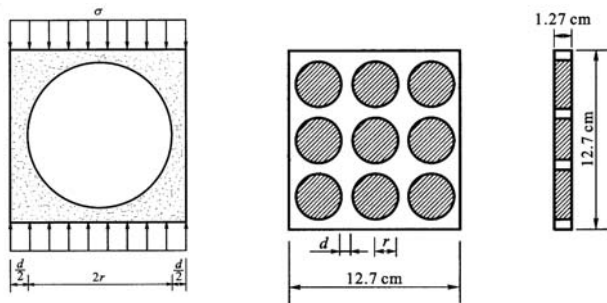
Fig. 19.29   Analysis model of concrete composited by circular aggregate and mortar
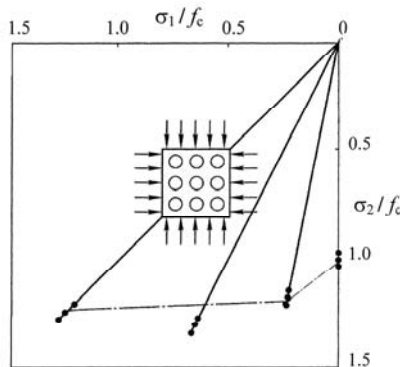
Fig. 19.30   Simulated limit locus for concrete under biaxial compression (Liu et al., 1972)

The computational simulation of failure criterion for concrete was done by Yu and Zeng (1993) and Zeng and Wei (1998). The concrete was regarded as a

composite material composed of big aggregates (1), small aggregates (2), water bubble (3), air bubble (4), and mortar (5) as shown in Figs. 19.31 (a)~19.31(c). The Unified Elasto-Plastic Program and the twin-shear strength theory were used under plane stress condition and plane strain condition.

Various stress combinations were calculated. Different model and different stress state σ_1, σ_2, $\sigma_3=0$ ($\varepsilon_3 \neq 0$) gave different limit value. Twenty-two stress combinations were calculated as shown in Fig. 10.32. The failure locus of concrete with big aggregate is smallest, and anisotropic. The failure loci obtained according to three meso-models are shown by the solid curve, the dotted curve and the broken curve, respectively. The horizontal compressive strength of model with big aggregate is larger than that of vertical. The failure locus of concrete becomes larger and isotropic when the size of aggregates decreased.

(a) Large aggregates   (b) Moderate aggregates   (c) Small aggregates
1: Large aggregates;   2: Small aggregates;   3: Water bubble;   4: Air bubble;   5: Mortar;
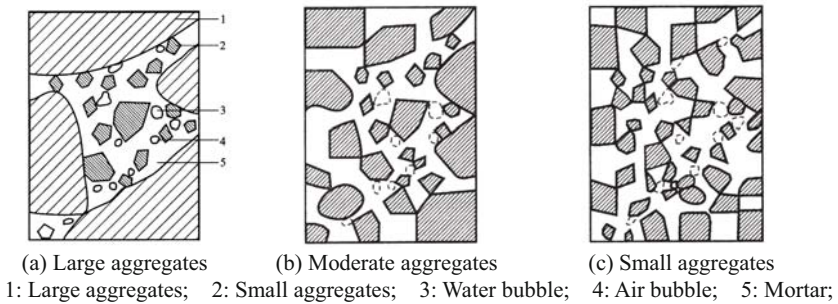
Fig. 19.31   Three meso-concrete models with different aggregate gradation
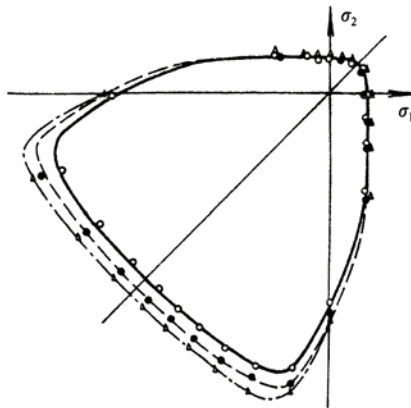
Fig. 19.32   Failure loci of three meso-concrete models under plastic stress conditions

Figure 19.33 shows the computational failure loci of the meso-model under the plane strain condition σ_1, σ_2, $\varepsilon_3 = 0$ ($\sigma_3 \neq 0$) by using of the Mohr-Coulomb strength theory and the twin-shear strength theory. The outer failure locus (line 2) is obtained using the twin-shear strength theory, and the inner failure locus (line 1) is obtained using the Mohr-Coulomb strength theory. The solid points are the

experimental results. The biaxial compressive strength of concrete at the compressive stress zone under the plane strain condition is larger than that of the plane stress condition, which agrees with the experimental results.

1: Single-shear theory   2: Twin-shear theory
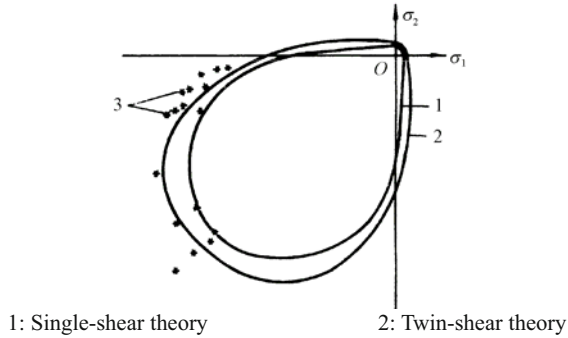
Fig. 19.33   Failure loci of meso-concrete models under plastic strain condition

Recently, a meso-mechanical analysis of concrete specimens under biaxial loading was presented by Caballero et al. (2007). Finite element mesh for concrete and rigid platens and numerical results under plane stress are shown in Fig. 19.34. Seventeen simulation results (above the diagonal $\sigma_1=\sigma_2$) under different loading paths with different proportions of σ_1 and σ_2 are obtained as shown in Fig. 19.34. The failure locus is obtained by connecting these 17 points and using the symmetric condition about the diagonal $\sigma_1=\sigma_2$.
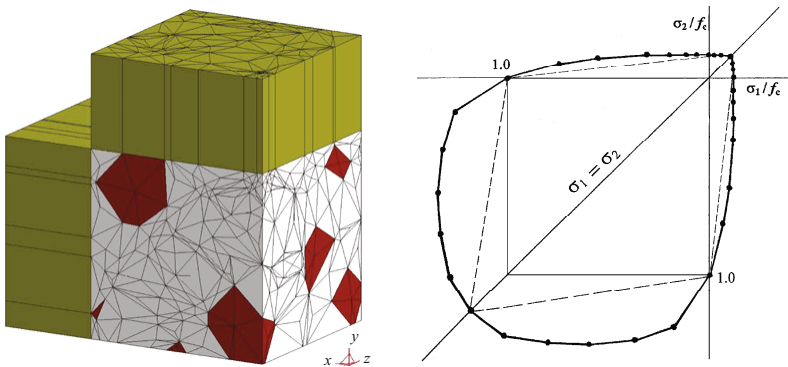
Fig. 19.34   FE mesh for concrete and rigid platens and numerical failure locus for concrete under plane stress (Caballero et al., 2007)

The results show that the tensile strength and compressive strength of concrete is different ($f_c \neq f_t$). It means that the single-parameter criteria are not suitable. The results also show that the strength of concrete under equal bi-axial compression is not equal to uniaxial compressive strength ($f_{cc} \neq f_c$), therefore, the three-parameter criterion is better. The two-parameter criterion of single-shear theory

(Mohr-Coulomb strength theory) and the three-parameter criterion of single-shear theory (dashed line) are plotted in Fig. 19.34. The simulated results do not match them.

The simulation results can also be fitted by using the experience curve. But the curve equation is not easy for using.

This simulation result may be matched by a three-parameter criterion reduced from the three-parameter unified strength theory. Comparison of the micromechanical analysis of concrete under plane stress with the three-parameter unified strength theory is shown in Fig. 19.35. In the figure, the dashed line is the three-parameter single-shear theory (or the three-parameter unified strength theory with $b=0$); the solid line is the three-parameter unified strength theory with $b=1$; dot dashed line is the three-parameter unified strength theory with $b=1/2$. They showed an intersection relationship between the simulated results and the three-parameter unified strength theory with $b=1/2$.
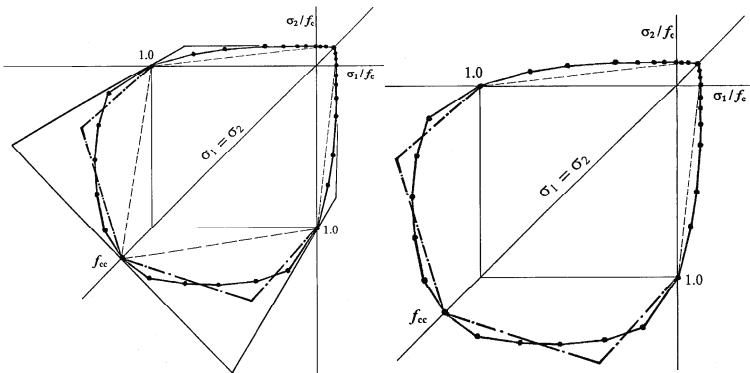
Fig. 19.35   The comparison of the micromechanical analysis of concrete under plane stress with the three-parameter unified strength theory

19.13   Brief Summary

Mesomechanics and multiscale modelling for yield surface are studied in this chapter. The prediction of strength of materials and structures for different scale yield surface is influenced strongly by the choosing of the material model. It is very important that how to choose the reasonable strength theory (yield criteria, failure criterion, or material model in FEM code) in the research and design. The change in shape and size of the yield surface of various failure criteria is great. A general, but simple and thereby suited for many potential users may be developed.

The interaction yield surface of structures, yield loci of polycrystalline aggregates under the combined stress ($\sigma\sim\tau$) (Lin and Ito), models in meso and macro mechanics, failure surface for cellular materials under multiaxial loads, multiscale analysis of composite using UST (Li and Ishii), multiscale analysis of

yield criterion of metallic glass based on atomistic basis (Schuh and Lund), atomic-scale study of plastic-yield criterion in nanocrystalline CU (Dongare et al., 2010), multiscale analysis of yield criterion of molybdenum and tungsten based on atomistic basis (Groger), phase transformation yield criterion of shape-memory alloys (Lexcellent et al., 2002; 2004; 2007; Gibeau, 2010; Bhattacharya and Schlömerkemper, 2004), extremal yield surfaces of a unit cell (Schrefler, 2009), damage surface under combined stress (Murakami, Hayakawa and Liu Y)), virtual material testing based on crystal plasticity finite element simulations (Roters et al,. 2010) and meso-mechanical analysis of failure criterion for concrete (Liu et al., 1972; Yu and Zeng, 1993; Caballero, 2007) are described in this chapter.

A general yield criterion for unit cell in multiscale plasticity is proposed in Section 19.10, and several comparisons between yield surfaces of material in multiscale plasticity are given in Sections 19.10 and 19.12.

References

Aboudi UJ (1989) Micromechanical analysis of composites by the method of cells. Appl. Mech. Rev., 42(7): 193-221.

Ashby MF, Evans AG, Fleck NA, Gibson LJ, Hutchinson JW and Wadley HNG (2000) Metal Foams: A Design Guide. Butterworth Heinemann: Oxford.

Becker R（2002）Developments and trends in continuum plasticity. Journal of Computer-Aided Materials Design, 9(2): 145-163.

Besseling JE and der Liessen E (1994) Mathematical Modeling of Inelastic Deformation. Chapman & Hall: London.

Bhattacharya K and Schlömerkemper A (2004) Transformation yield surface of shape memory alloys. J. Phys. IV France, 115: 155-2.

Bishop JFW and Hill R (1951) A theory of the plastic distortion of a polycrystalline aggregate under combined stresses. Philos Mag, 42：414-27.

Bishop JFW and Hill R (1951) A theoretical derivation of the plastic properties of a polycrystalline face centered metal. Philos Mag, 42: 1298-307.

Bomert M, Herve E, Stolz C, Zaoui A (1994) Self-consistent approaches and strain heterogeneities in two-phase elastoplastic materials. Appl. Mech. Review, 47(1): Part 2, 66-76.

Bouvet C, Calloch S and Lexcellent C (2002) Mechanical behavior of a Cu-Al-Be shape memory alloy under multiaxial proportional and nonproportional loadings. J. Eng. Mater. Technol, 124(2): 112-124.

Bouvet C, Calloch S and Lexcellent C (2004) A phenomenological model for pseudoelasticity of shape memory alloys under multiaxial proportional and non-proportional loadings．Eur J. of Mech A Solids, 23: 37-61.

Buyukozturk O, Nilson AH and State FO (1970) Stress-strain response and fracture of a concrete model in biaxial loading. Journal ACI, 68(8): 590-595.

de Buhan P and de Pelice G (1997) A homogenization approach to the ultimate strength of brick masonry. 3~Mechanics and Physics of Solids, 45 (7): 1085-1104.

Caballero A, Carol I and Lopez CM (2007) A 3D meso-mechanical analysis of concrete specimens under biaxial loading. Fatigue and Fracture of Engineering Materials and Structures,30(9): 877-886.

Chen SH and Wang ZQ (2009) Micro-scale plasticity mechanics. University of Science and Technology of China Press: Hefei, China.

Christeensen RM and Lo KH (1979) Solutions for effective shear properties in three phase sphere and cylinder models, Journal of the Mechanics and Physics of Solids, 27: 315-330.

Deshpande VS and Fleck NA (2000) Isotropic constitutive models for metallic foams. J. Mech. Phys. Solids, 48: 1253-283.

Dongare AM, Rajendran AM, Lamattina B, Brenner DW, Zikry MA (2010) Atomic-scale study of plastic-yield criterion in nanocrystalline CU at high strain rates. Metallurgical and Materials Transactions A, 41A(2): 523-31.

Dvorak GJ, Bahei-E1-Din (1997) An inelastic composite materials: Transformation analysis and experiments. In: Continuum Micromechanics, P. Suquet (ed.), Springer: Wien.

Dvorak GJ (1999) Composite materials: inelastic behavior, damage, fatigue and fracture. In: Research Trends in Solid Mechanics, G.J. Dvorak (ed.). Pergamon: New York.

Faria SH, Hutter K, Kirchner N and Wang Y (2010) Continuum Description of Granular Materials. Springer: Berlin.

Fish J and Yu Q (2001) Multiscale damage modeling for composite materials: theory and computational framework. Int. J. for Numerical Methods in Engineering, 52: l61-192.

Gall K, Sehitoglu H, Maier HI and Jacobus K (1998) Stress-induced Martensitic Phase Transformations in Polycrystalline CuZnAl Shape Memory Alloys under Different Stress States, Met Mat Trans A., 29A: 765-73.

Ghosh S. and Moorthy S (1995) Elastic–plastic analysis of arbitrary heterogeneous materials with the Voronoi cell finite element method. Comp. Meth. Appl. Mech. Eng., 121: 373-09.

Ghosh S., Lee K. and Moorthy S (1995) Multiple scale analysis of heterogeneous elastic structures using homogenization theory and Voronoi cell finite element method. Int. J. Solids Struct., 321: 27-2.

Ghosh S, Lee K and Moorthy S (1996) Two scale analysis of heterogeneous elastic–plastic materials with asymptotic homogenization and Voronoi cell finite element model. Comp. Meth. Appl. Mech. Engrg., 132: 63-16.

Ghosh S, Lee K and Raghavan P (2001) A multilevel computational model for multi-scale damage analysis in composite and porous materials. Inter. J. of Solids and Structures,38: 2335-385.

Gibeau E, Laydi MR and Lexcellent C (2010) Determination and transport of phase transformation yield surfaces for shape memory alloys. Journal of Applied Mathematics and Mechanics / Zeitschrift für Angewandte Mathematik

und Mechanik (ZAMM), 90(7): 595-695.

Gibson LJ, Ashby MF, Zhang J and Triantafillou TC (1989) Failure surface for cellular mateerials under multiaxial loads-(1) modelling. Int. J. Mech. Sci., 31: 635-63.

Gibson LJ and Ashby MF (1987, 1997) Cellular Solids: Structure and Propertties.Press Syndicate of the University of Cambridge: London.

Gibson LJ (2000) Mechanical behavior of metallic foams. Annu. Rev. Mater. Sci., 30: 191-27.

Gioux G, McCormark TM and Gibson LJ (2000) Failure of aluminum foams under multiaxial loads. Int. J. Mech. Sci. 42: 1097-117.

Gologanu M et al. (1993) Approximate models for ductile metals containing non-spherical voids-case of asisymmetric prolate ellipsoidal cavities, J. of the Mechanics and Physics of Solids,41: 1723-1754.

Gologanu M, Leblond JB, Perrin G, Devaux J (1997) Recent extensions of Gurson's Model for porous ductile metals. In: Continuum Micromechanics, P. Suquet (ed.) Springer: Wien, pp 61-130,.

Groger R, Racherla V, Bassani JL and Vitek V (2008) Multiscale modeling of plastic deformation of b molybdenum and tungsten：Ⅱ. Yield Criterion for single crystals based on atomistic studies of glide of 1/2(11) Screw dislocations. Acta Materialia, 56: 5412-5425

Gurson AL (1977) Continuum theory of ductile rupture by void nucleation and growth, I. Yield criteria and flow rules for porous ductile media. J. Eng. Mater. Tech.,99: 2-15.

Hashin Z (1962) The elastic moduli of heterogeneous materials, J. Applied Mech.,29: 143-150.

Hashin Z and Shtrikman S (1964) A variational approach to the theory of the elastic behavlour of multiphase materials，Mech. Phys. Sci., 11(2): 127-41.

Hashin Z (1983) Analysis of composite materials—A survey. J. Appl. Mech., 50: 481-05.

Hayakawa K and Murakami S (1998) Space damage conjugate force and damage potential of elastic-plastic damage materials. In: Damage Mechanics in Engineering Materials. Edited by Voyiadjis GZ, Ju J-WW and Chaboche J-L, Elsevier.

Haythornthwaite RM (1961) Range of yield condition in ideal plasticity. J. Engrg. Mech., 87: 117-33.

Hill R (1965) Continuum micro-mechanics of elastoplastic polycrystals. J. Mech. Phys. Solids, 13: 89-101.

Hodge PG (1959) Plastic Analysis of Structures. McGraw-Hill: New York.

Huang W (1999) "Yield" surfaces of shape memory alloys and their applications. Acta Materialia, 47(9): 2769-2776.

Jasiuk I and Ostoja-Strazewski M eds (1994) Micromechanics of Random Media Ⅰ. Applied Mechanics Reviews, 47(1): Part 2:Special Supplement.

Jasiuk I and Ostoja-Strazewski M eds (1998) Micromechanics of Random Media Ⅱ. Int. J. Solids and Structures, 35(19): 2383-2569.

Ju J and Tseng K (1996) Effective elastoplastic behavior of two-phase ductile matrix composites: a micromechanical framework. Int. J. Solids Struct., 3329: 4267-291.

Kachanov LM (1986) Introduction to Continum Damage Mechanics. Martinus Nijhoff Publishers: Netherlands.

Kolupaev VA and Altenbach H (2010) Einige Überlegungen zur Unified Strength Theory von Mao-Hong Yu (Considerations on the Unified Strength Theory due to Mao-Hong Yu), Forschung im Ingenieurwesen (Forsch Ingenieurwes) Springer-Link 29 May 2010 (in German, English Abstract).

Kraska M, Doig M, Tikhomirov D, Raabe D and Roters F (2009) Virtual material testing for stamping simulations based on polycrystal plasticity. Comput Mater Sci, 46: 383-92.

Kröner E (1961) On the plastic deformation of polycrystals. Acta Metall, 9: 155-61.

Kröner E (1977) Bounds for effective elastic moduli of disordered materials，Mech. Phys Sci, 25(2): l37-55.

Ladevdz EC and Fish J (2003) Preface to special issue on multiscale computational mechanics for materials and structure. Computer Methods in Applied Mechanics and Engineering,192: 28-0.

Lemaitre J (1992) A Course on Damage Mechanics. Springer-Verlag.

Lexcellent C, Vivet A, Bouvet C, Calloch S and Blanc P (2002) Experimental and numerical determinations of the initial surface of phase transformation under biaxial loading in some polycrystalline shape-memory alloys. J Mech Phys Solids, 50: 2717-735.

Lexcellent C and Blanc P (2004) Phase transformation yield surface determination for some shape memory alloys. Acta Mater 52: 2317-324.

Lexcellent C and Schl6merkemper A (2007) Comparison of several models for the determination of the phase transformation yield surface in shape memory alloys with experimental data. Acta Materialia, 55: 2995-3006.

Li YM and Ishii K (1998a) The evaluation of the elasto-plastic behavior of composite materials under biaxial stress with homogenization method. In: Proc. of the Conference on Computational Engineering and Science, 3: 1023-026.

Li YM and Ishii K (1998b) The evaluation of strength for the composite materials. In: Strength Theory: Applications, Developments and Prospects for the 21st Century. Yu MH and Fan SC eds. Science Press: New York, Beijing, 337-42.

Li YY, Zheng JL, Cui JZ and Long SY (2010) Iterative multi-scale finite element predicting method for the elasticity mechanical parameters of the concrete with multi-graded rocks. Chinese Journal of Computational Mechanics, 27(1): 115-119 (in Chinese).

Li ZX, Sun ZH, Guo L et al. (2007) Multi-objective concurrent approaching of simulating for civil infrastructure. J. of Southeast University (Natural Science Edn.), 37(02):251-260 (in Chinese).

Lim TJ and McDowell DL (1999) Mechanical behavior of Ni-Ti shape memory alloys under axial-torsional proportional and nonproportional loading. J Eng Mat and Techn, 121: 9-8.

Lin TH and Ito YM (1965) Theoretical plastic distortion of a polycrystalline aggregate under combined and revered stress. J. Mech. Phys. Solids.,13:103-15.

Lin TH and Ito YM (1966) Theoretical plastic stress-strain relationship of a polycrystal and comparisions with Mises and Tresca plasticity theories. Int. J. Engng. Sci., 4: 543-61.

Liu D and Jiang CZ (2008) Plastic limit analysis of circular plates based on twin-shear unified strength theory. Engineering Mechanics, 25(8): 77-84 (in Chinese).

Liu TCY, Nilson AH and Slate FO (1972) Biaxial stress-strain relation for concrete, Proc. ASCE, Journal of Structural Division, 98(5): 1025-1034.

Liu TCY, Nilson AH and Slate FO (1972) Stress-strain response and fracture of concrete in uniaxial and biaxial compression. Journal ACI, 69(5): 191-195.

Liu WK, Qian D and Horstemeyer ME (2004) Preface to special issue on multiple scale methods for nanoscale mechanics and materials. Computer Methods in Applied Mechanics and Engineering, 193: l7-20.

Lou ZW (1991) Foundation of Damage Mechanics. Xi'an Jiaotong University Press: Xi'an (in Chinese).

Lu XZ, Lin XC, Ye LP (2008) Multiscale finite element modeling and its application in structural analysis. Journal of Huazhong University of Science and Technology (Urban Science Edition), 25(4): 76-80 (in Chinese).

Lund AC and Schuh CA (2005) Strength asymmetry in nanocrystalline metals under multiaxial loading. Acta Material, 53: 3173-3205.

Ma HF, Chen HQ, Li BK (2004) Progress in concrete meso-mechanics research and comment on. Chinese Journal of Water Resources and Hydropower Research, 2004(2).

Ma HF, Chen HQ, Wu JP, Li BK (2008) Study on numerical algorithm of 3D meso-mechanics model of dam concrete. Chinese J. of Computational Mechanics, 25(2): 244-247.

McDowell DL(1985) An experimental study of the structure of constitutive equations for nonproportional cyclic plasticity, ASME Journal of Engineering Materials and Technology, 107: 307-315.

McDowell DL, Stock SR, Stahl D and Antolovich SD (1988) Biaxial path dependence of deformation substructure of type 304 stainless steel, Metallurgical Transactions, 19: A 1277-1293.

McDowell DL, Marin E, and Bertoncelli C (1993) A combined kinematic-isotropic hardening theory for porous inelasticity of ductile metals, Int. J. of Damage Mechanics, 2: 137-161.

McDowell DL(1999) Non-associative aspects of multiscale evolutionary phenomena. In: Picu, R.C., Krempl, E. (Eds.), Proceedings 4th International Conference on Constitutive Laws for Engineering Materials, pp 54-57.

McDowell DL(2001) Materials design: a useful research focus for inelastic behavior of structural metals. In: Sih GC, Panin VE (Eds.), Special Issue of the Theoretical and Applied Fracture Mechanics, Prospects of Mesomechanics in the 21st Century: Current Thinking on Multiscale Mechanics Problems, vol. 37, pp 245-259.

McDowell DL(2007) Simulation-assisted materials design for the concurrent design of materials and products, JOM., 59 (9): 21-25.

McDowell DL and Olson GB (2008) Concurrent design of hierarchical materials and structures, Scientific Modeling and Simulation (CMNS), 15(1): 207.

McDowell DL, Choi H-J, Panchal J, Austin R, Allen JK and Mistree F (2007) Plasticity-related microstructure–property relations for materials design, Key Engineering Materials, 340-341: 21-30.

McDowell DL (2010) A perspective on trends in multiscale plasticity. Khan International Medal Lecture , Int. J. of Plasticity.

Meyer WJ (1985) Concepts of Mathematical Modeling. McGraw-Hill, Singapore.

Murakami S, Hayakawa K and Liu Y (1998) Damage evolution and damage surface of elastic-plastic-damage materials under multiaxial loading. Int. Journal of Damage Mechanics, 7(2):103-128.

Novák V and Šittner P (2004) Micromechanics modelling of NiTi polycrystalline aggregates transforming under tension and compression stress. Mat Sci Eng A, 378: 490-498.

Ortiz M (2008) Multiscale modeling of materials: Linking microstructure and macroscopic behavior. Invited Lecture, Seminarios Interuniversitarios de Mecanica y Materiales, Barcelona, Zaragoza, Seville, Spain.

Ortiz M (2008) Nonconvex Plasticity and Microstructure. Rodney Hill Prize Plenary Lecture, 22nd International Congress of Theoretical and Applied Mechanics, Adelaide, Australia.

Ostoja-Strarzewski M (1993) Micromechanics as a basis of random elastic continuum approximations. Probablistic Engineering Mechanics, 8(2): 107-114.

Ostoja-Strarzewski M (1994) Micromechanics as a basis of continuum random fields. Applied Mechanics Reviews (Special Issue: Micromechanics of Random Media), 47(1) Part 2: S221-230.

Ostoja-Strarzewski M (1994) Random field models of heterogeneous matrials. Int. J. Solids and Structures, 35(19): 2429-2455..

Ottosen NS and Ristinmaa M (2005) The Mechanics of Constitutive Modeling. Elsevier.

Picu RC (2003) Foreword to special issue on linking discrete and continuum models. Int. Multiscale Computational Engng, 1(1): vii-viii.

Pindera M-J and Aboudi J (1989) Micromechanical investigation of the convexity of yield surfaces of metal matrix composites. In: Advances in Plasticity A.S. Khan and M. Tokuda (eds.), pp 129-132.

Raabe D (1998) Computational Materials Science: The Simulation of Materials Microstructures and Properties. Wiley-VCH Verlag: London.

Roters F. Eisenlohr P, Hantcherli L, Tjahjanto DD, Bieler TR and Raabe D (2010) Overview of constitutive laws, kinematics, homogenization and multiscale methods in crystal plasticity finite-element modeling: Theory, experiments, applications. Acta Materialia, 58(4): 1152-1211.

Sadowski T(2005) Multiscale Modelling of Damage and Fracture Processes in Composite Materials. Springer: Berlin.

Save MA and Massonnet CE (1972) Plastic Analysis and Design of Plates, Shells

and Disks. North-Holland: Amsterdam.

Sawczuk A (1989) Mechanics and Plasticity of Structures. Ellis Horwood: Chichester.

Schrefler BA (2009) Multiscale Modelling. In: Zienkiewicz OC and Taylor RL (2009) The Finite Element Method for Solid and Structural Mechanics. Sixth edn.Elsevier, Amsterdam and Elsevier (Singapore) Pte Ltd, pp 547-589.

Schuh CA and Lund AC (2003) Atomic basis for the plastic yield criterion of metallic glass. Nature Materials, 2: 499-452.

Sih GC ed (2000) Role of Mechanics for Development of Science and Technology. Proceedings of an Int. Conf. of Role of Mechanics for Development of Science and Technology, held at Xi'an Jiaotong University, China, June Tsinghua University press: Xi'an.

Sridhar I and Fleck NA (2000) Yield behaviour of cold compacted composite powders. Acta Materials, 48(13): 3341-3352.

Stronge WJ and Yu TX (1993) Dynamic Models for Structural Plasticity. Springer: Berlin.

Sun CT and Vaidya RS (1996) Prediction of composite properties from a representative volume element. Composites Science and Technology, 56(2): 171-179.

Tayler AB (1986) Mathematical Models in Applied Mechanics. Clarendon Press: Oxford.

Tailard K, Blanc P, Calloch and Lexcellent (2006) Phase transformation yiels surface of anisotropic shape memory allys. Materials Science and Engineering, A 438-440: 436-440.

Theocaris PS (1991) The elliptic paraboloid failure criterion for cellular solids and brittle foams. Acta Mechanica, 89: 93-121.

Triantafillou TC, Zhang J et al (1989) Failure surface for cellular Mateerials under multiaxial loads-(2) Comparison of models with experment. Int. J. Mech. Sci., 31(9): 665-678

Triantafillou TC and Gibson LJ (1990) Multiaxial failure criteria for brittle foams. Int. J. Mech. Sci., 32(6): 479-496.

Voyiadjis GZ, Ju JW and Chaboche JL eds (1998) Damage Mechanics in Engineering Materials, Elsevier.

Wu BJ, Li ZX and Tang KK (2007) Multi-scale modeling and damage analyses of large civil structure: multi-scale mechanics from material to structure. Advances in Mechanics, 37(3): 321-336.

Yu MH (1961a) General behaviour of isotropic yield function. Res. Report of Xi'an Jiaotong University. Xi'an, China (in Chinese).

Yu MH (1961b) Plastic potential and flow rules associated singular yield criterion. Res. Report of Xi'an Jiaotong University. Xi'an, China (in Chinese).

Yu MH (1983) Twin shear stress yield criterion. Int. J. of Mech. Science, 25(1): 71-74.

Yu MH et al. (1985) Twin shear theory and its generalization. Science in China, Series A,English edition,28 (11): 1174-1183.

Yu MH and He LN (1991) A new model and theory on yield and failure of

materials under the complex stress state, Mechanical Behaviour of Materials-6, (ICM-6), Jono M and Inoue T (eds.), Pergamon Press: Oxford, 3: 841-846.

Yu MH and Zeng WB (1993a) Twin-shear plasticity and mesomechanics. In: Collection of Papers Dedicated to Professor Tung-Hua Lin in Celebration of His 80th Birthday (Wang ZQ, Xu BY and Huang ZP eds. Peking University Press: Beijing (in Chinese).

Yu MH and Zeng WB (1993b) Mesomechanical simulation of failure criterion for a composite material. Macro-Meso-micro Mechanical Properties of Materials. Tokuda M and Xu BY eds. Mie Academic Press: Mie, Japan, pp 571-576.

Yu MH (2000) Material Model in Mesomechanics and Macromechanics. Plenary lecture. In: Mesomechanics 2000, Tsinghua University Press, pp 239-246.

Yu SW and Feng XQ (1997) Damage Mechanics. Tsinghua University Prtess: Beijing.

Zeng WB and Wei XY (1998) Computer simulation of failure criteria for concrete. Strength Theory: Applications, Developments and Prospects for the 21st Century. Yu MH and Fan SC eds. Science Press: New York, Beijing, pp 639-642.

Zhu H, Sankar BV and Marrey RV (1998) Evaluation of failure criteria for fiber composites using finite element micromechanics Journal of Composite Materials, 32(8): 766-782.

Zienkiewicz OC and Taylor RL (2009) The Finite Element Method for Solid and Structural Mechanics. Sixth edn.Elsevier: Amsterdam and Elsevier (Singapore) Pte Ltd.

Zohdi TI and Wridggers P (2001) Computational micro-macro material testing. Archives of Computational Methods in Engineering, 8(2): 131-228.

Zyczkowski M (1981) Combined Loadings in the Theory of Plasticity. Polish Scientific Publishers: PWN and Nijhoff.

20

Miscellaneous Issues:
Ancient Structures, Propellant of Solid Rocket, Parts of Rocket and Generator

20.1 Introduction

The stability of `an ancient city wall and the foundation of an ancient pagoda, the strength of the parts of a rocket and generator, a plastic analysis of a thick-walled cylinder and 2D and 3D finite element simulations of a solid rocket motor grain are studied in this chapter. The unified strength theory is used in all these problems. Finally, several comments, reviews and research on the unified strength theory are presented from published papers and books.

More than 5000 city walls existed in China before the 1950s. Most of them were destroyed between the 1950s and 1970s. Fortunately, several ancient structures built during the Tang Dynasty 1350 years ago and the Ming Dynasty 620 years ago in Xi'an are well preserved. The Ming City Wall in Xi'an is now the only large city wall preserved in China, as shown in Fig. 20.1 and Fig. 20.2 (Yu et al., 2009).

Several ancient Pagoda in the Xi'an area are shown in Fig. 20.3. They are the Big Goose Pagoda, Small Goose Pagoda and the Famen Temple Pagoda. The Big Goose Pagoda was constructed during the Tang Dynasty in A.D. 653 and was repaired in A.D. 930. The pagoda is 64.1 meters high from the spire to the ground.

Fig. 20.1   South-east corner of Xi'an City Wall (Yu, 2009)

Fig. 20.2   South-west corner of Xi'an City Wall (Yu, 2009）

(a)Big Goose Pagoda   (b) Small Goose Pagoda   (c) Famen Temple Pagoda

Fig. 20.3   Ancient Pagoda at Xi'an area built in Tang Dynasty (AD 652-930)

The circumference of the city wall of the Ming Dynasty is 14 km, but the length of the bomb shelters (caves) inside or under the city wall reach 41 km. One-third of the caves were built in the 1940s to protect against Japanese bombing and two-thirds were built in the 1970s at the call of Mao Zedong to "Dig the cave deeply". Some city walls were destroyed, as shown in Fig. 20.4.

Fig. 20.4   Destroyed city wall due to the dug caves

Half the Famen Temple Pagoda collapsed on Aug. 24th, 1981 (Fig. 20.5). The Big Goose Pagoda is leaning somewhat to the west, as shown in Fig. 20.6. All the pagodas have an underground mausoleum chamber. There is a need for research into the bearing capacity of the city wall and pagoda foundations (Yu et al., 2008; 2009).

Fig. 20.5 Half collapsed Pagoda   **Fig. 20.6** The lining of the Big Goose Pagoda

In order to investigate the bearing capacity of the foundations of an ancient pagoda, we firstly researched the strength behaviour of the loess in Xi'an. The tensile strength and compressive strength of materials of ancient architectures are always unequal. They are referred to as SD materials (strength difference in tension and in compression). Therefore, the Tresca failure criterion, the Huber-von Mises failure criterion and the twin-shear yield criterion for metallic materials are not adapted. The test also illustrates that the intermediate principal stress σ_2 has a strong influence on the strength of the loess and should be taken into account in numerical analysis for geomechanics and geotechnical engineering.

A series of failure criteria for SD materials of the unified strength theory have been described in Chapter 4. The unified strength theory is represented as follows:

$$F = \sigma_1 - \frac{\alpha}{1+b}(b\sigma_2 + \sigma_3) = \sigma_t \quad \text{when} \quad \sigma_2 \leq \frac{\sigma_1 + \alpha\sigma_3}{1+\alpha} \tag{20.1a}$$

$$F' = \frac{1}{1+b}(\sigma_1 + b\sigma_2) - \alpha\sigma_3 = \sigma_t \quad \text{when} \quad \sigma_2 \geq \frac{\sigma_1 + \alpha\sigma_3}{1+\alpha} \tag{20.1b}$$

$$F'' = \sigma_1 = \sigma_t \quad \text{when} \quad \sigma_1 > \sigma_2 > \sigma_3 > 0 \tag{20.1c}$$

When choosing different values of parameter b, the unified strength theory can represent or approach various existing yield criteria. The Mohr-Coulomb's single-shear strength theory is obtained when $b=0$; it is the generalized twin-shear strength theory when $b=1$; when $b=1/2$ it is a new yield criterion between the former two theories. Their limit loci on the deviatoric plane in the stress space is shown in Fig. 20.7.
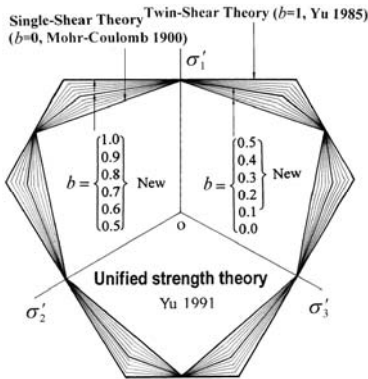
Fig. 20.7   The limit loci of
the unified strength theory
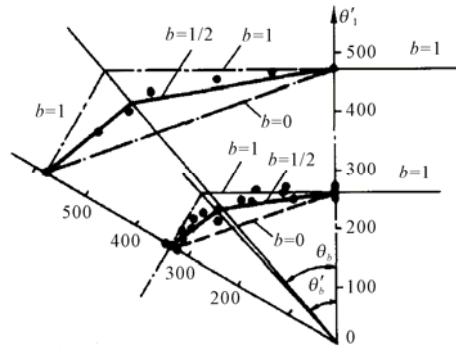
Fig. 20.8   The comparison between the
unified strength theory and the experiment result

Many test results indicate that the yield strength of loess is situated between two bounds (the twin-shear strength theory and the single-shear theory). The test results for loess in Xi'an carried out by Xing et al. (1992) are shown in Fig. 20.8. The dotted line in the figure is the Mohr-Coulomb strength theory; on the other hand, the solid line is a particular case of the unified strength theory, namely unified strength theory with $b=1/2$, shown as the dodecagon when $b=1/2$ in Fig. 20.7.

20.2   Stability of Ancient City Wall in Xi'an

The ancient city of the Ming Dynasty in Xi'an is the most completely preserved among all the ancient city relics in China. It is a famous historic city relic of worldwide reputation. The city wall has collapsed several times in history. To solve the problem, a research group started a study on the stability of the city wall in the 1980s, cooperating with the Xi'an City Ring Construction Committee. Yu MH, Zeng WB, Ma GW, Yang SY, He LN and Wang Y programmed a finite-element computational program UEPP (unified elastic-plastic program) based on the unified strength theory and associated flow rule (see: Chapters 4–6). Some research on the bearing capacity of the ancient city wall was carried out using UEPP (Yu et al., 2008; 2009). The mesh of the city wall is shown in Fig. 20.9.

Figure 20.10 shows the spread of the plastic region in the load process on the Xi'an ancient city wall. Figure 20.11 shows the displacement of the ancient city wall. It can be seen that the original failure started from the cave.
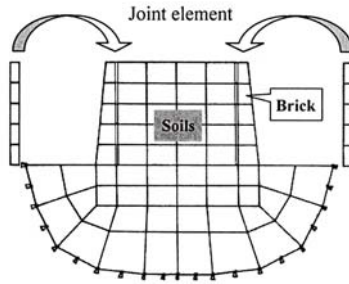
Fig. 20.9   Mesh of city wall for FEM
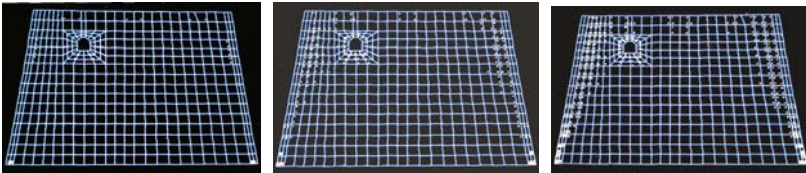
Fig. 20.10   Spread of plastic region of ancient city wall in the load process
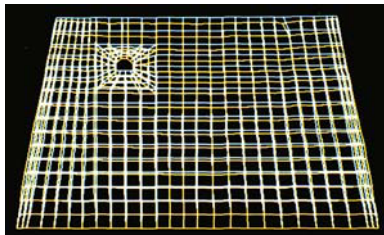
Fig. 20.11   Displacement of the ancient city wall

Figure 20.12 shows the plastic zones surrounding the cave that was dug inside and under the ancient Xi'an city wall. The result of the calculation indicates that these caves made a great contribution to the collapse of the city wall. They are the main reason for the collapse, especially the caves in the upper part of the wall. The city wall has higher strength, but the strength will decrease seriously when the wall is soaked and becomes saturated (Yu, 1993; 2009). Therefore, settlement caused by the soaking of the loess of the city wall is another reason why it collapsed. These conclusions have become an important basis for the preservation and repair of the ancient Xi'an city wall.

The deformations of the city wall under five different load cases are shown in Fig. 20.13. Case(e) is the dangerous one.

The effect of the yield criterion on the plastic zone is also obvious, as shown in Fig. 20.14. The single-shear theory gives the maximum plastic zone, and the twin-shear theory gives the minimum plastic zone under the same load. It can be illustrated from Fig. 20.14(f).
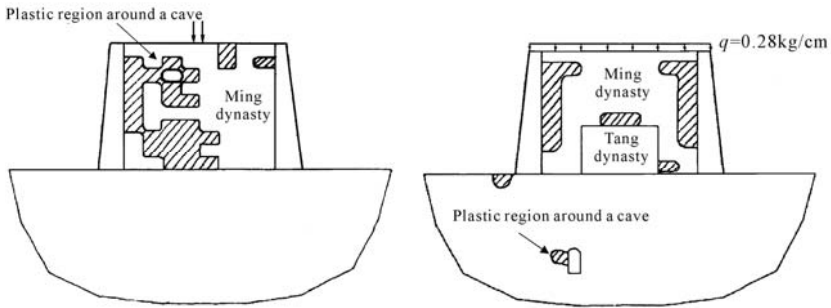
Fig. 20.12   The plastic failure of city wall around a cave in the wall

(a)   (b)

(c)   (d)   (e)
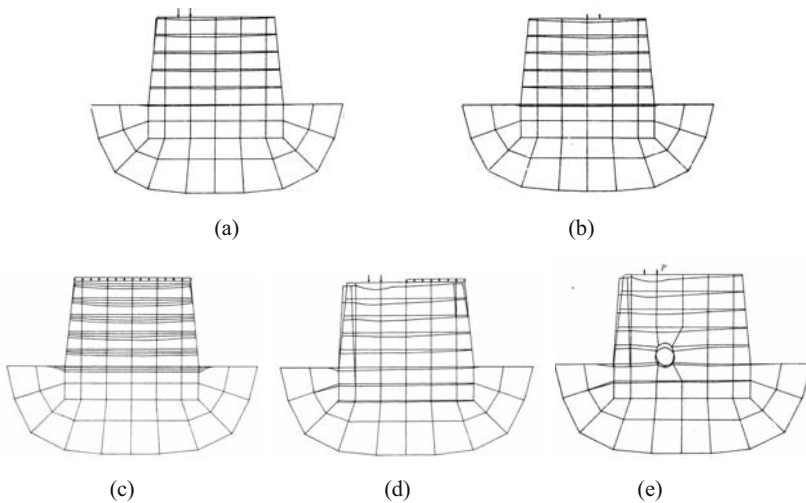
Fig. 20.13   The deformations of city wall under the five load cases

In a normal situation, the ancient Xi'an city wall gains enough strength to resist breaking down, when the safety factor is more than 3. It provides a theoretical basis for the safety of the annual Xi'an City Wall International Marathon. Nowadays, the Xi'an City Wall International Marathon has become one of the representative activities of Xi'an. There are about ten thousand people from around 50 countries all over the world who come to Xi'an to participate in the race. Moreover, the number of people who climb up on the city wall to celebrate the Lantern Festival is more than 100,000. More descriptions can be seen in (Yu et al., 2009; 2011).

(a) UST with *b*=0 (Single-shear theory)

(b) UST with *b*=1/4 (New criterion)

(c) UST with *b*=1/2 (New criterion)

(d) UST with *b*=3/4 (New criterion)

(e) UST with *b*=1.0 (Twin-shear theory)

(f) Five typical criteria
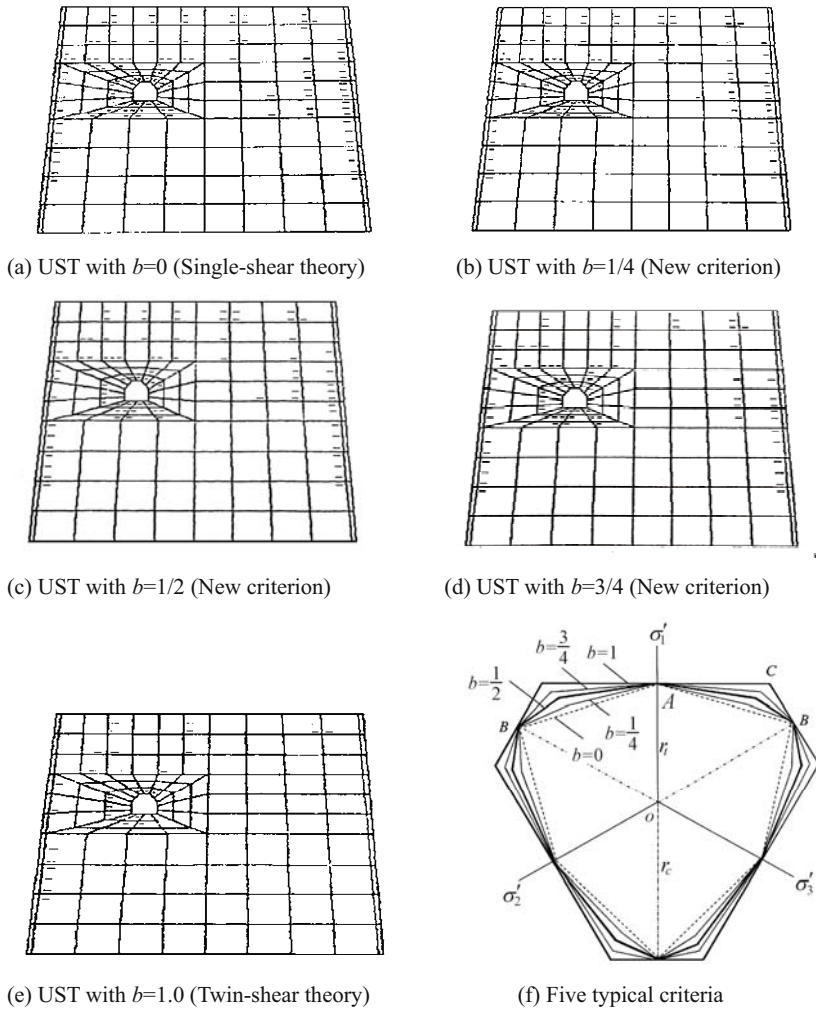
Fig. 20.14   Effect of yield criteria on the spread of plastic zone of city wall

20.3   Stability of the Foundation of Ancient Pagoda

20.3.1 Structure of Foundation of Ancient Pagoda

The Big Goose pagoda is now a brick-soil structure 7 storeys high and 64.1 m from top to bottom, as shown in Fig. 20.3(a). It is built on a base which is 45.9 m from east to west, 48.9 m from south to north and 4.2 m high. The main body of

the pagoda is 51.63 m high and is a square-pyramid shape. The length of each side of the base square is 25 m. The body of the tower binds the loess on the inside to the outside brick. This is similar to modern high-rise tube structures. The Pagoda had very good earthquake resistance.

The Big Goose Pagoda has national key protection among cultural relics and is a world-renowned Buddhist site. Any destructive testing is prohibited. The shape of the foundation is unknown. Therefore, based on several documents and the historical records of other ancient pagodas in Xi'an, which were built at a similar period to that of the Big Goose Pagoda, Yu Mao-hong proposed and divided the foundation structure of the Big Goose Pagoda into four main forms: rectangular foundation structure, stepped foundation structure, inverted stepped foundation structure, inverted stepped foundation structure with underground chamber, as shown in Fig. 20.15. The structure is simplified to a spatial axial symmetric structure. The bearing capacity of the foundation of the Big Goose Pagoda has been studied (Gu, 1993; Gao, 1995; Yu and Meng, 1994; Yu et al., 2008; 2009; 2011).

(a) Rectangular foundation   (b) Stepped foundation

(c) Inverted stepped foundation   (d) Inverted stepped foundation with chamber
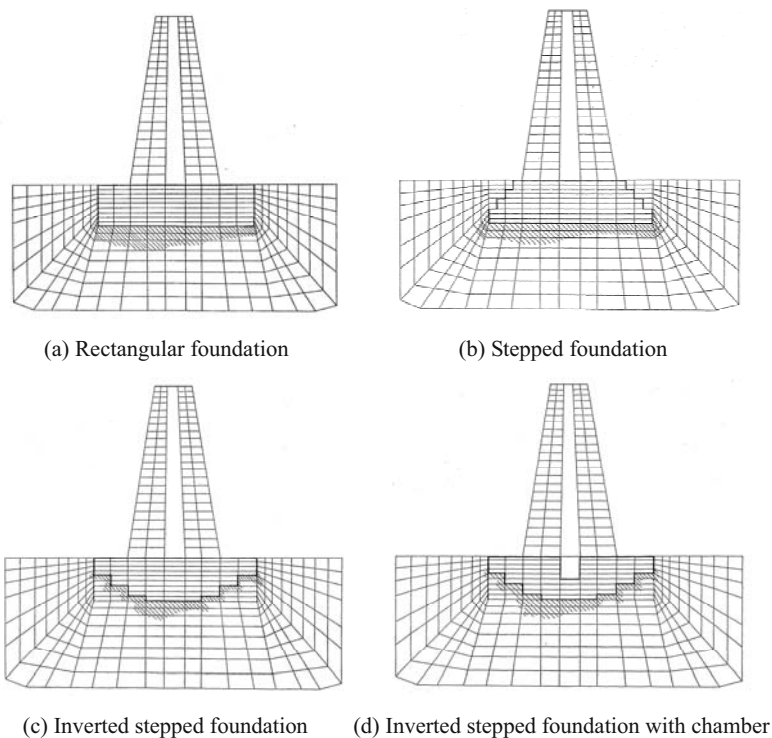
Fig. 8.15   The possible structure of the foundation of the Big Goose Pagoda

20.3.2   The Effect of Yield Criterion on Plastic Zone of Soil Foundation of Pagoda

The mesh of the finite element analysis for a high ancient pagoda in Xi'an is shown in Fig. 20.16(a). This is a simulation of the Big Goose Pagoda built during the Tang Dynasty. The plastic zones using different yield criteria for the rectangular foundation of the pagoda under the same load are obtained as shown in Figs. 20.16(b), 20.16 (c) and 20.16 (d). It is seen that the spreads of the plastic zone of the soil foundation of the ancient pagoda are strongly influenced by the choice of the yield criterion.

(a) FE Mesh   (b) Plastic zone with Drucker-Prager

(c) UST with $b=0$ (Single-shear theory)   (d) UST with $b=1$ (Twin-shear theory)
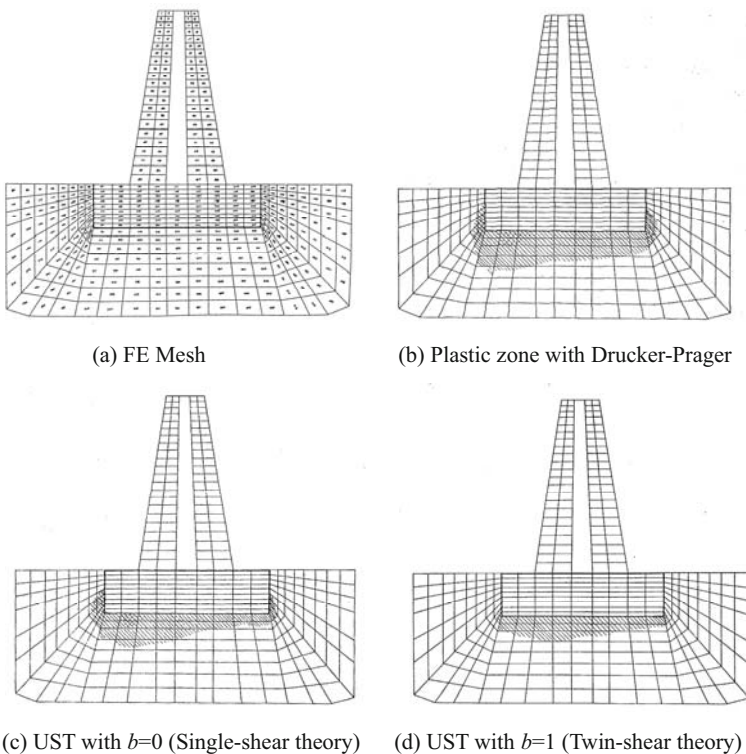
Fig. 20.16   Plastic zones for rectangular foundation

If the structural shape of the foundation of the Pagoda has changed, the effect of yield criteria on the plastic analysis is also noticed. Plastic zones obeying the single-shear theory and twin-shear theory for the stepped foundation, reverse-stepped foundation and reverse-stepped foundation with underground chamber, are shown in Figs. 20.17, 20.18 and 20.19, respectively.
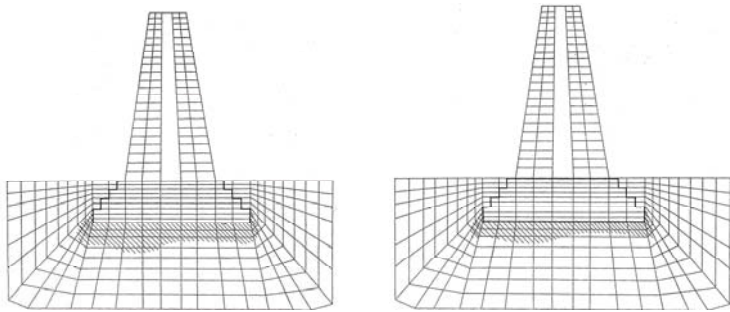
(a) UST with $b=0$ (Single-shear theory)   (b) UST with $b=1$ (Twin-shear theory)

Fig. 20.17   Plastic zones for stepped foundation
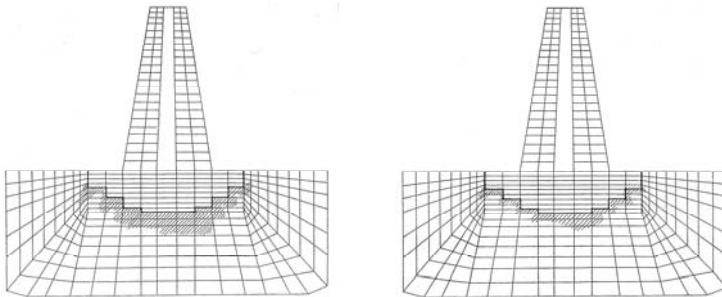
(a) UST with $b=0$ (Single-shear theory)   (b) UST with $b=1$ (Twin-shear theory)

Fig. 20.18   Plastic zones for reverse-stepped foundation
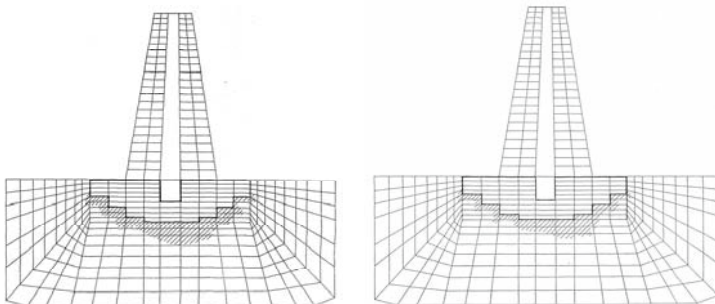
(a) UST $b=0$ (Single-shear theory)   (b) UST $b=1$(Twin-shear theory)

Fig. 20.19   Plastic zones for reverse-stepped foundation with a chamber

The results of the research indicate the following:

(1) The size of the plastic area decreases as parameter b increases. Under the same load and the same foundation structure, the area of the plastic zone is largest when $b=0$; the area of the plastic zone is smallest when $b=1$. It can be concluded that considering the effect of intermediate principal stress, the limiting load of the

structure will increase. Therefore, it is important to choose a proper value of the UST parameter b in order to make efficient use of material.

(2) With respect to different foundation shapes, while using the same yield criterion, the results show that the size of the plastic area of the stepped foundation structure is larger than that of the inverted stepped foundation.

(3) It can be said that where there is a pagoda, there could be an underground chamber. A Buddhist temple also has an underground chamber. Ancient pagodas of the Tang Dynasty are mostly in Shaanxi Province. The protection of ancient pagodas should include the protection of the underground chamber. The influence of the underground chamber on the size of the plastic region is not remarkable.

According to the results of analysis, the frequency of four foundation structures (rectangular, stepped, inverted stepped with and without underground chamber) differs little one from the other. Their first-order frequency is 1.25 Hz, close to the test result (1.3~1.4 Hz). Furthermore, from research on the two different foundation structures of the Small Goose Pagoda, a similar conclusion is also obtained. The results show that the strength of the foundation of the Small Goose Pagoda has big potential. According to the result of a triaxial test on the loess of ancient architectures (Yu et al., 2008; 2009), loess has relatively high strength. However, when it is soaked and becomes saturated, the strength decreases sharply. The main reason for the collapse of the pagoda of the FaMen Temple is that there was much rain that year and the foundation was soaked, causing a decrease in the strength of the loess.

The plastic zones for four foundations using the single-shear theory and twin-shear theory are shown in Fig. 20.20 and Fig. 20.21.

(a) Rectangular   (b) Stepped   (c) Reverse-stepped   (d) With chamber
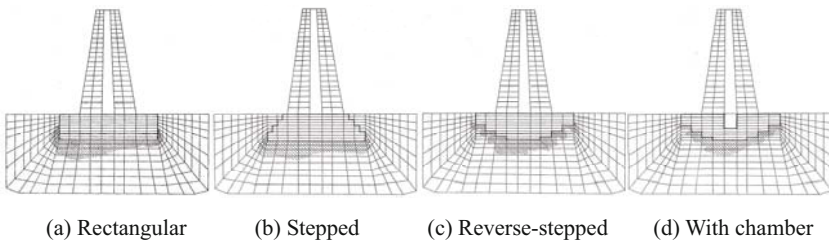
Fig. 20.20   The plastic zones for four foundations using UST with $b=0$ (Single-shear theory)

(a) Rectangular   (b) Stepped   (c) Reverse-stepped   (d) With chamber
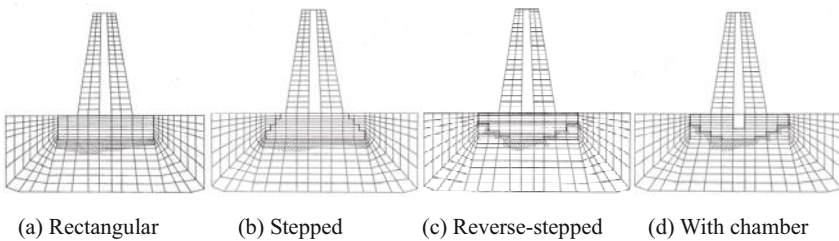
Fig. 20.21   The plastic zones for four foundations using UST with $b=1$ (Twin-shear theory)

20.4 Plastic Analysis of Thick-Walled Cylinder

Plastic analysis of a thick-walled cylinder for non-SD materials was carried out by
Li JC and Fan LF in 2009, in which the unified yield criterion with $b=0$, $b=1/4$,
$b=1/2$, $b=3/4$, and $b=1$ were used. These five typical
criteria cover the entire convex region of failure
criteria. Five results for the plastic analysis of
structures were obtained. The scheme of a
thick-walled cylinder is shown in Fig. 20.22.

The relation between the circumferential stress
σ_θ and the normalized radius r/r_a is shown in
Fig. 20.23. The relation between the radial stress σ_r
and the normalized radius r/r_a is shown in Fig. 20.24.
Figure 20.25 shows the relation between the elastic
limit pressure p_e and the normalized radius r/r_a.
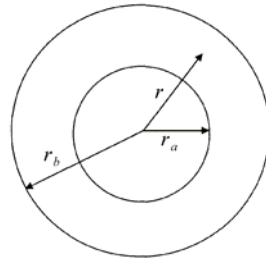
Fig. 20.22   Scheme for a
thick-walled cylinder
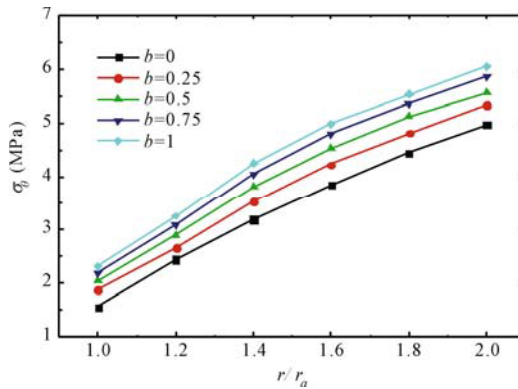
Fig. 20.23   Relation between the circumferential stress σ_θ and radial stress σ_r with r/r_a
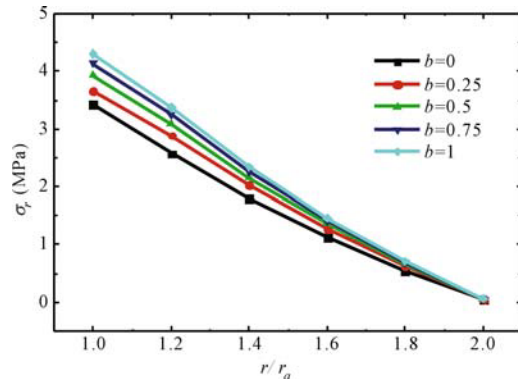
Fig. 20.24   The relation between the radial stress σ_r with r/r_a
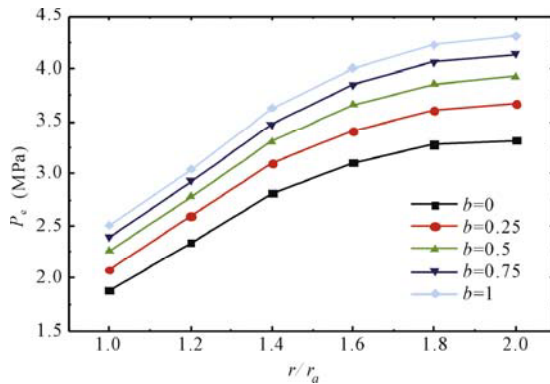
Fig. 20.25 The relation between p_e and r/r_a

The five elastic limit pressures of the thick-walled cylinder for non-SD materials (r/r_a =1) with five parameters $b=0$, $b=1/4$, $b=1/2$, $b=3/4$ and $b=1$ are obtained and shown in Fig. 20.26. The numerical results agree well with the analytical results. The analytical solution for non-SD materials and SD materials can be seen in sections 10.5 to 10.7 in (Yu et al., 2004).
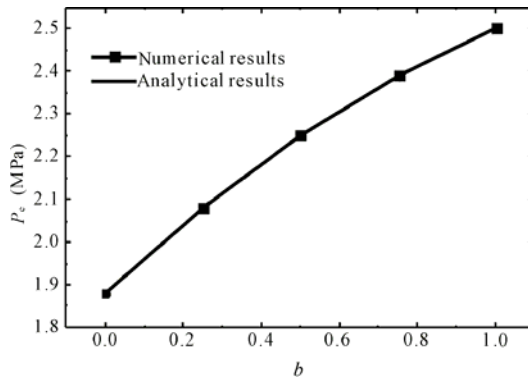
Fig. 20.26 Elastic limit pressure p_e versus the UST parameter b

Figure 20.27 shows the plastic regions of the thick cylinder using the unified strength theory with five parameters $b=0$, $b=1/4$, $b=1/2$, $b=3/4$ and $b=1$ under the same load.

(a) UST with b=0.0   (b) UST with b=0.25

(c) UST with b=0.5   (d) UST with b=0.75   (e) UST with b=1.0
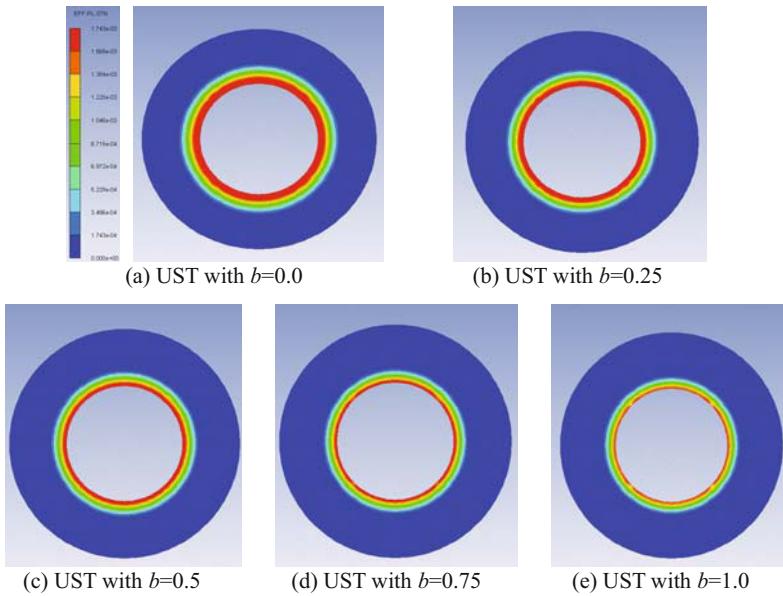
Fig. 20.27   Plastic region distribution at the same load

20.5   Plastic Analysis of the Structural Part of a Rocket

The rocket is always used to launch communication satellites and meteorological
satellites (Hu et al., 2010) as shown in Fig. 20.28. The structure of a part of a
rocket is shown in Fig. 20.29.

Fig. 20.28   Launch of communication satellite and meteorological satellite
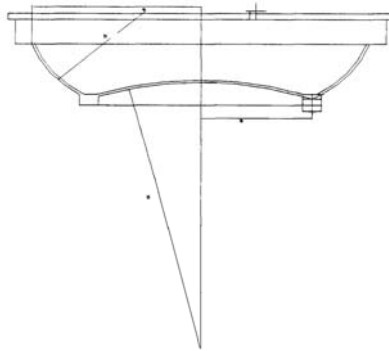
Fig. 20.29   The structure of a part of a rocket

A stress analysis of this part is shown in Fig. 20.30. Several results are illustrated in Fig. 20.31. The important result is the limit pressure shown in Fig. 20.32.
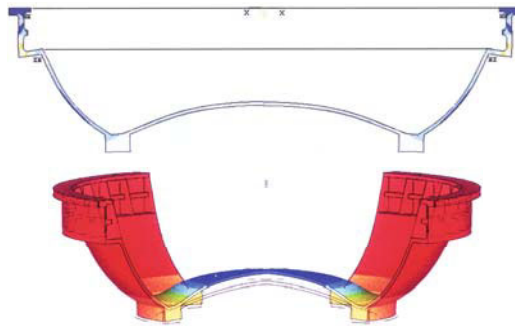
Fig. 20.30   Plastic analysis of a part of a rocket

(a)

(b)

(c)

(d)
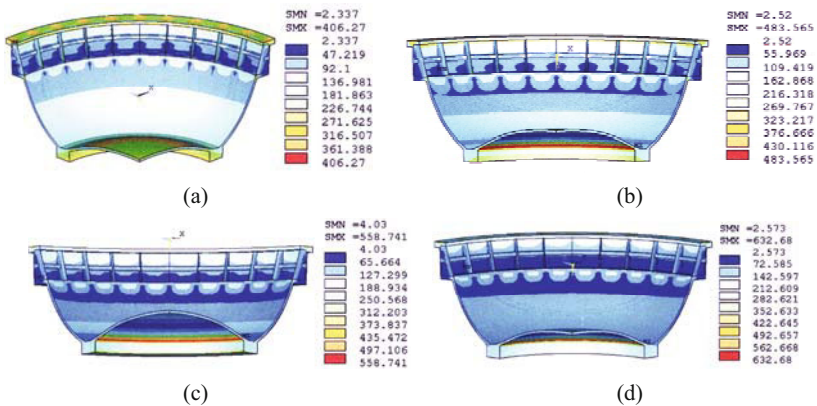
Fig. 20.31   Several results of numerical analysis

The Tresca yield criterion (i.e. unified yield criterion with $b=0$) is always used for the design of this part of a rocket. If the unified yield criterion with $b=1$ is used, the thickness of the bottom of this part can be decreased by about 5mm. The weight of the rocket can be decreased.
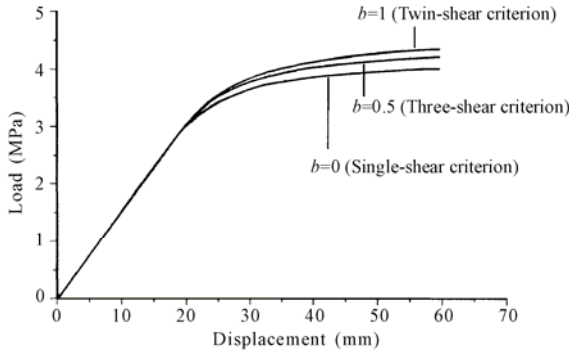
Fig. 20.32   Limit pressure of a part of a rocket

20.6   Numerical Analysis of Rocket Motor Grain

The mechanical behavior of the propellant and the strength and reliability of the solid rocket motor grain were studied by Qiang (1998), Qiang et al. (2008), Li et al. (2008), Zhang (2010). The unified strength theory and elasto-visco-plastic FE Program (UEPP) were used for rocket motor grain by Qiang et al. (2008). The failure criteria for rocket motor grain are complex, because the tensile strength is not equal to the compressive strength for grain. The Tresca criterion and the Huber-von Mises criterion cannot be adapted for the numerical simulation. The test results show the tensile yield strength of a grain is $\sigma_t=0.95$ MPa, the compressive yield strength of a grain is $\sigma_c=4.07$ MPa, the strength ratio of grain in tension and in compression is $\alpha=0.234$. The three yield criteria of the unified strength theory with parameters $b=1$, $b=1/2$ and $b=0$ are used. They can be introduced from the unified strength theory Eq. (20.1) as follows.

(1) $b=1$

$$F = \sigma_1 - \frac{\alpha}{2}(\sigma_2 + \sigma_3) = \sigma_t, \quad \text{when} \ \sigma_2 \leq \frac{\sigma_1 + \alpha\sigma_3}{1+\alpha} \tag{17.2a}$$

$$F' = \frac{1}{2}(\sigma_1 + \sigma_2) - \alpha\sigma_3 = \sigma_t, \quad \text{when} \ \sigma_2 \geq \frac{\sigma_1 + \alpha\sigma_3}{1+\alpha} \tag{17.2b}$$

(2) $b=1/2$

$$F = \sigma_1 - \frac{\alpha}{3}(\sigma_2 + 2\sigma_3) = \sigma_t, \quad \sigma_2 \leq \frac{\sigma_1 + \alpha\sigma_3}{1+\alpha} \tag{17.3a}$$

$$F' = \frac{1}{3}(2\sigma_1 + \sigma_2) - \alpha\sigma_3 = \sigma_t, \quad \sigma_2 \geq \frac{\sigma_1 + \alpha\sigma_3}{1+\alpha} \tag{17.3b}$$

(3) $b=0$

$$F = F' = \sigma_1 - \alpha\sigma_3 = \sigma_t \tag{17.4}$$

The structure of a solid rocket motor is shown in Fig. 20.33. The grain in the rocket motor can be considered as an axial symmetric problem. Figure 20.34 shows the numerical simulation mesh for structure A.
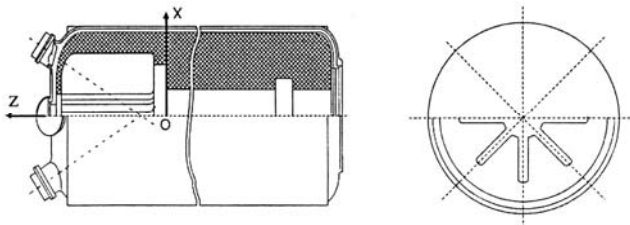
Fig. 20.33   The structure of a solid rocket motor
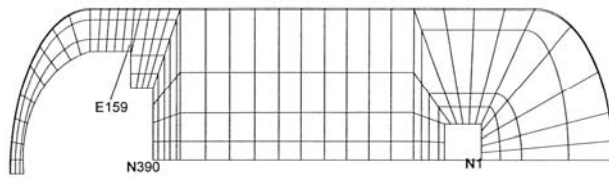
Fig. 20.34   Axial symmetric mesh of a solid rocket motor grain (Structure A)

The numerical simulation shows the plastic yield starts from element E159 of structure A (Fig. 20.34), as shown in Fig. 20.35.

(a) UST with $b=0$ (b) UST with $b=0.5$ (c) UST with $b=1$ (Twin-shear theory)
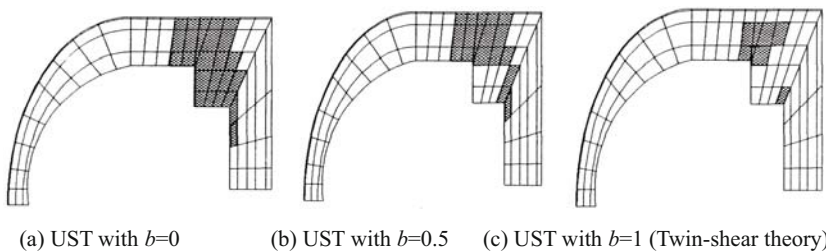
Fig. 20.35   Plastic zones of motor grain (Structure A) for three criteria

The stress-time steps of element E159 obeying the three yield criteria are shown in Fig. 20.36. The displacement-time steps of element E390 obeying the

three yield criteria are shown in Fig. 20.37. The results are dependent on the yield criterion.
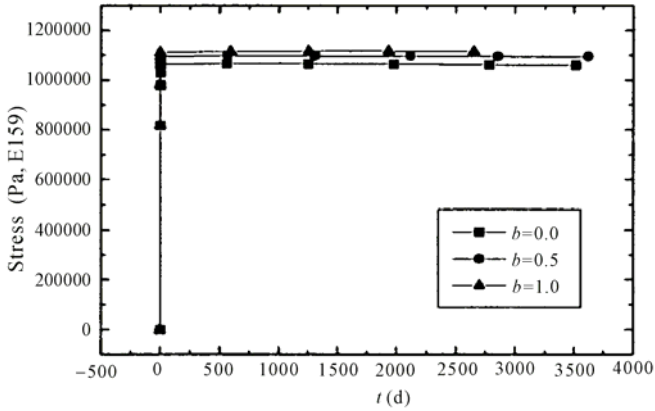
Fig. 20.36   Stress-time steps of element E159 (Structure A)
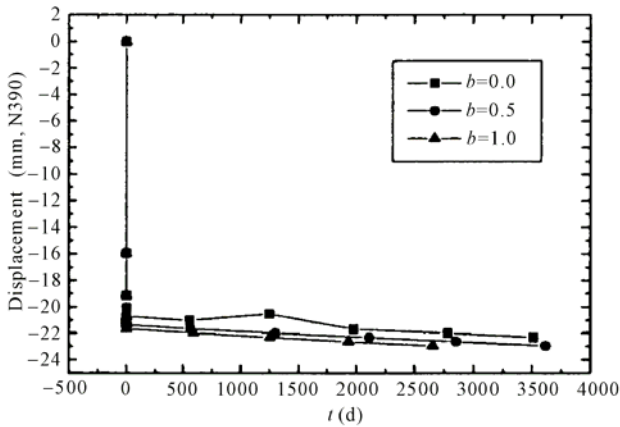
Fig. 20.37   The displacement-time steps of element E390

The numerical simulation mesh for structure B is shown in Fig. 20.38. The plastic yield starts from the element E184 (Fig. 20.38) of structure B, as shown in Fig. 20.38. The spread of the plastic zone of the three yield criteria under the same conditions are similar. However, the size of the plastic zone is dependent on the choice of yield criterion.
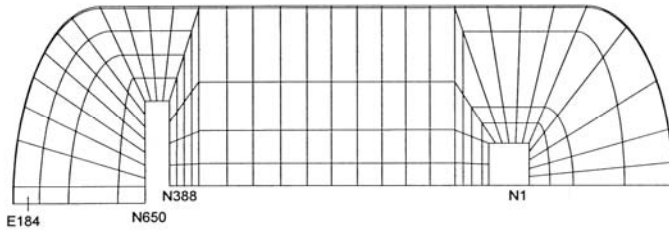
Fig. 20.38   Axial symmetric mesh of a solid rocket motor grain (Structure B)

(a) UST with b=0   (b) UST with b=0.5   (c) UST with b=1 (Twin-shear theory)
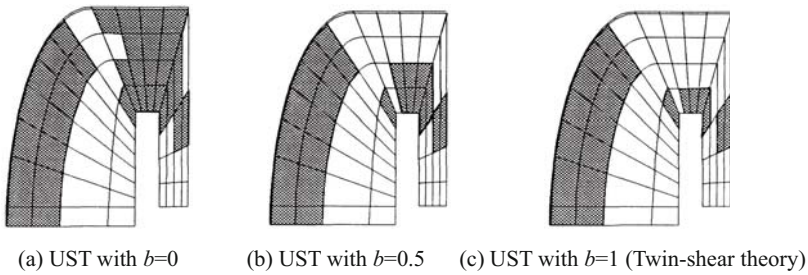
Fig. 20.39   Plastic zones of motor grain (Structure B) for three criteria

20.7   3D Numerical Simulation for a Solid Rocket Motor

The 3D numerical simulation for a solid rocket motor was conducted by Qiang (1998). The structural mesh of a solid rocket motor is shown in Figs. 20.40(a) and 20.40(b). Owing to the symmetry and the periodicity of the structure (Fig. 20.33), a one-eighth mesh is constructed, as shown in Fig. 20.40. The finite element mesh is divided into 1248 elements, 5709 nodes. The shell part has a total of 186 elements and the number of nodes is 633; the grain part has a total of 1062 elements and the number of nodes is 5709. This can be very close to the actual boundary conditions of a solid motor, so the results maintain a high accuracy. The 3D finite element mesh of a missile solid rocket motor including metal shell and inner grain are shown in Fig. 20.40.

Distribution of the radial stress σ_r, circumferential stress σ_θ and vertical stress σ_z in grain are shown in Figs. 20. 41, 20.42 and 20.43, respectively. Figure 20.44 is the effective stress analysis based on the unified strength theory with parameter b=0.5.

The numerical simulations of a solid missile motor under the condition of vertical storage are shown in Figs. 20.45, 20.46, and 20.47. Effective stress analysis based on the unified strength theory with b=0.5 is illustrated in Fig. 20.48.

(a) Shell of rocket motor   (b) Grain
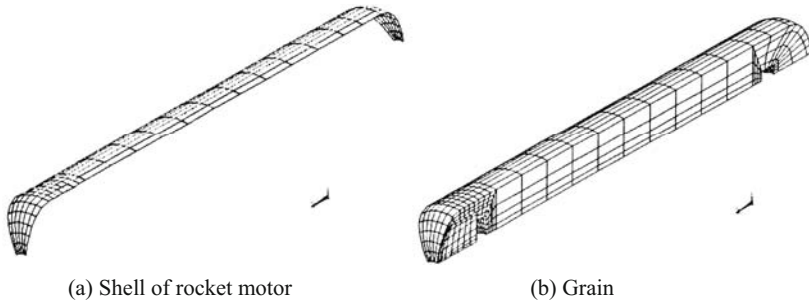
Fig. 20.40   The mesh of a solid rocket motor
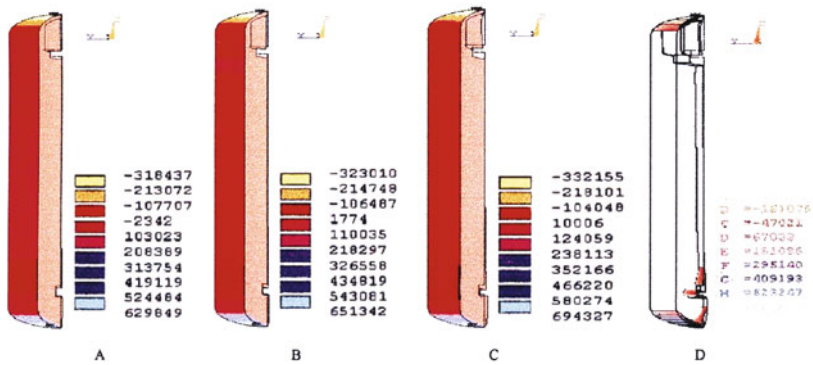
Fig. 20.41   Distribution of radial stress σ_r
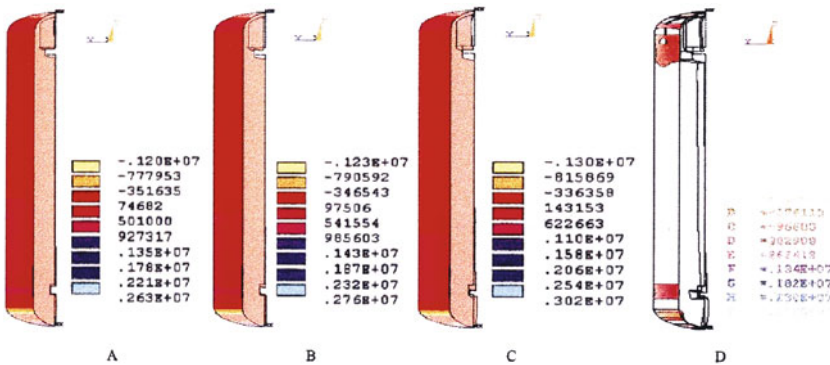
Fig. 20.42   Distribution of circumferential stress σ_θ
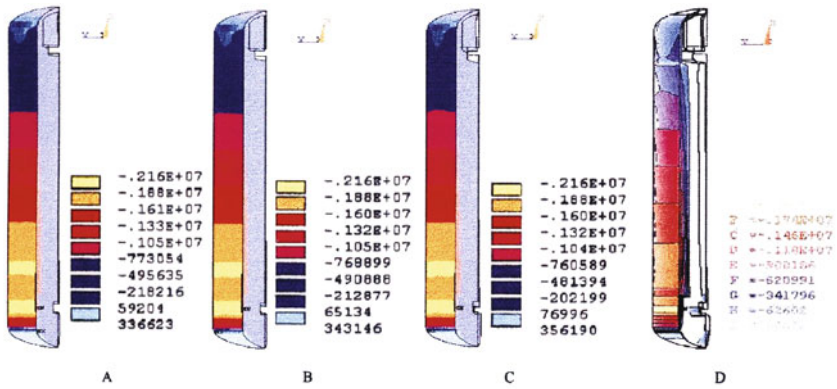
Fig. 20.43   Distribution of vertical stress σ_z
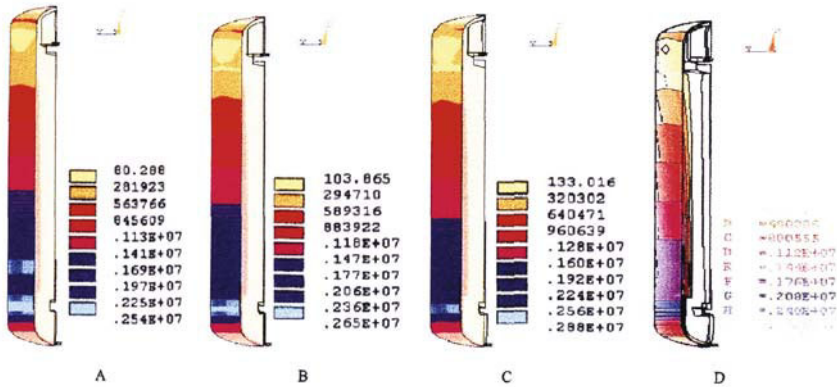
Fig. 20.44   Effective stress based on the unified strength theory with b=0.5.
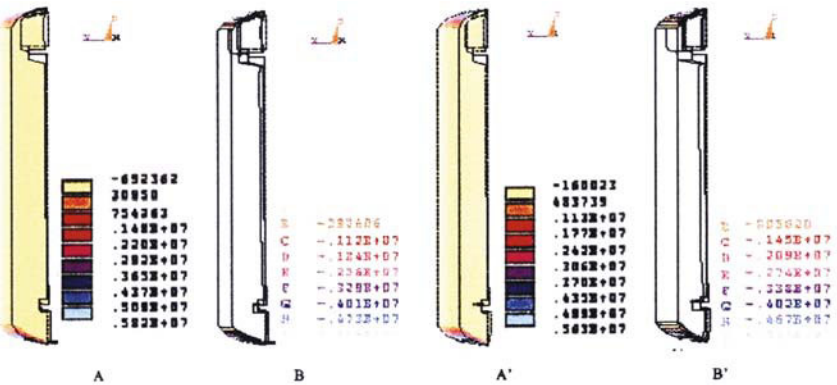
Fig. 18.45   Distribution of horizontal stress σ_x
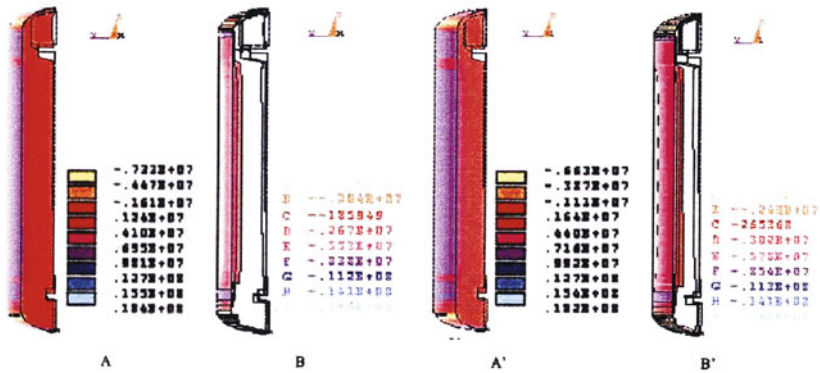
Fig. 18.46   Distribution of circumferential stress σ_θ
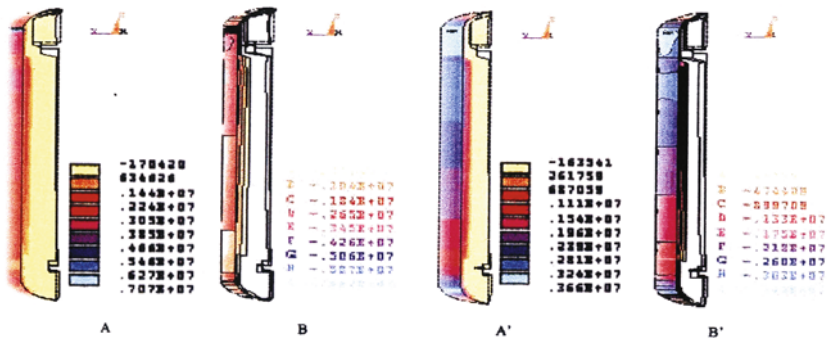
Fig. 18.47   Distribution of vertical stress σ_z
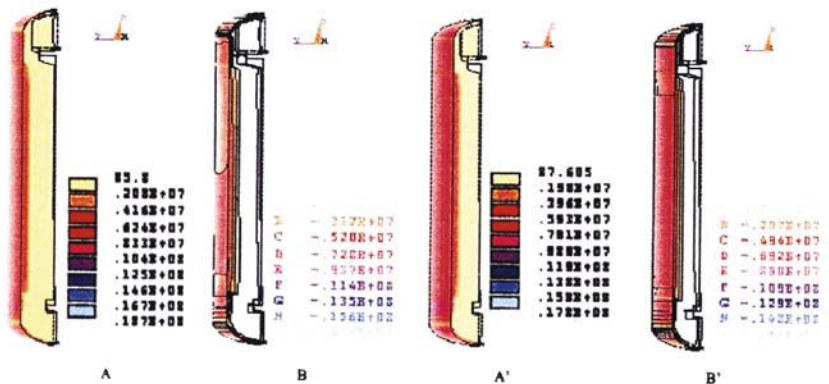
Fig. 20.48   Effective stress based on the unified strength theory with $b=0.5$

The numerical simulations of a solid missile motor under curing and reduction in temperature, as well as the storage conditions, were conducted. The simulation results are basically consistent with the process of curing and the reduction in temperature. They also agree with the condition of the vertical storage of the missile.

20.8   Structural Part of the Generator of Nuclear Power Station

The pressure ring is a structural part of a turbo-generator stator, which is used to press the silicon steel pieces of the stator, as shown in Fig. 20.49. It can be simplified to a spatial axisymmetric problem. The finite element mesh is also shown in Fig. 20.49 (Yu et al., 1992).
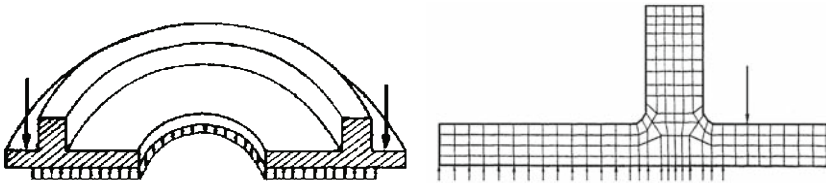
Fig. 20.49   Pressure ring of turbo-generator stator and its simulation mesh

The finite element analysis of the pressure ring for a 600 MW generator stator of a nuclear power station is shown in Fig. 20.50(a). Figure 20.50(b) shows the stress field in the pressure ring.
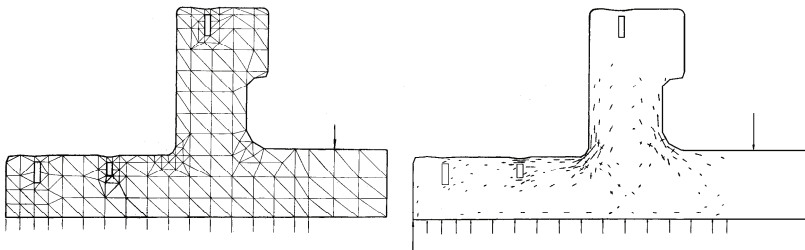
Fig. 20.50   FE mesh and stress field of a large pressure ring of turbo-generator stator

Elasto-plastic analysis was carried out for the pressure ring of a 300 MW turbo-generator. Four yield criteria of the unified yield criterion with $b=0$, $b=1/2$, $b=1$ and the Huber-von Mises yield criterion are used. The different plastic zones of the pressing ring using a different yield criterion at the same load are given in Figs. 20.35(a)~20.35(d).

(a) Unified yield criterion with $b=0$ (b) Huber-von Mises criterion

(c) Unified yield criterion with $b=1/2$ (d) Unified yield criterion with $b=1$
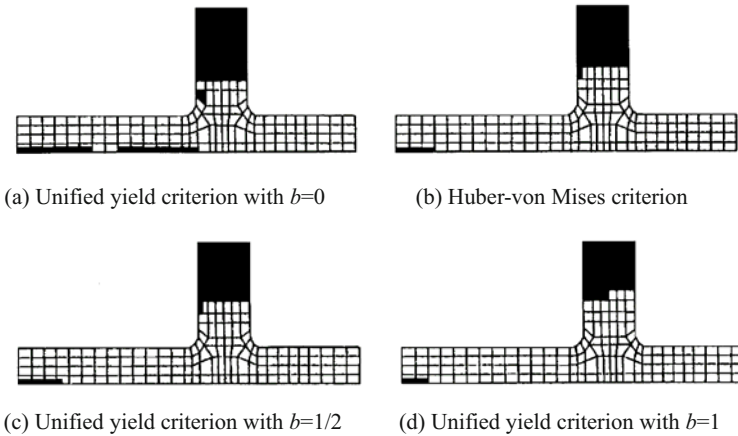
Fig. 20.51   Plastic zones of the pressing ring

The unified yield criterion and associated elasto-plastic constitutive model have been implemented into a special finite element program and used for the analysis of the pressure ring of different generators. The effect of the intermediate principal stress is taken into account. It can be adapted for all the materials which have the same yield stress in tension and in compression. It can be easily used for elasto-plastic analysis of the structures. The comparison between different zones of the pressing ring using a different parameter b of the unified yield criterion indicates that the plastic zone using twin shear model ($b=1$) is smaller than that using the unified yield criterion ($0<b<1$). The plastic zones using the unified yield criterion with $b=1/2$ and the Huber-von Mises criterion are similar. These results agree with the prediction of the theoretical analysis. The unified yield criterion with $\alpha=1$ and $b=1/2$ may be referred to as the linear approximation of the Huber-von Mises criterion.

20.9 The Effect of Yield Criterion on the Spread of the Shear Strain of Structure

The UST (unified strength theory) has been used in many fields. Figures 20.52 and 20.53 show a new example presented by Ma and Liao (2010). Generalized shear strain contours of a slope using UST with different parameters of b are shown in Fig. 20.52. The generalized shear strain contours of a slope using the Drucker-Prager criterion are also presented for comparison (Liao et al., 2010; Ma and Liao, 2010). The effect of the yield criterion on the spread of the shear strain of a structure is obvious.

(a) UST with *b*=0

(b) UST with *b*=0.25

(c) UST with *b*=0.5

(d) UST with *b*=0.75

| 7.8050e-005 to 5.0000e-003 |
| 1.0000e-002 to 1.5000e-002 |
| 2.0000e-002 to 2.5000e-002 |
| 3.0000e-002 to 3.5000e-002 |
| 4.0000e-002 to 4.5000e-002 |
| 5.0000e-002 to 5.5000e-002 |
| 6.0000e-002 to 6.5000e-002 |
| 7.0000e-002 to 7.5000e-002 |
| 7.5000e-002 to 7.5000e-002 |

(e) UST with *b*=1.0
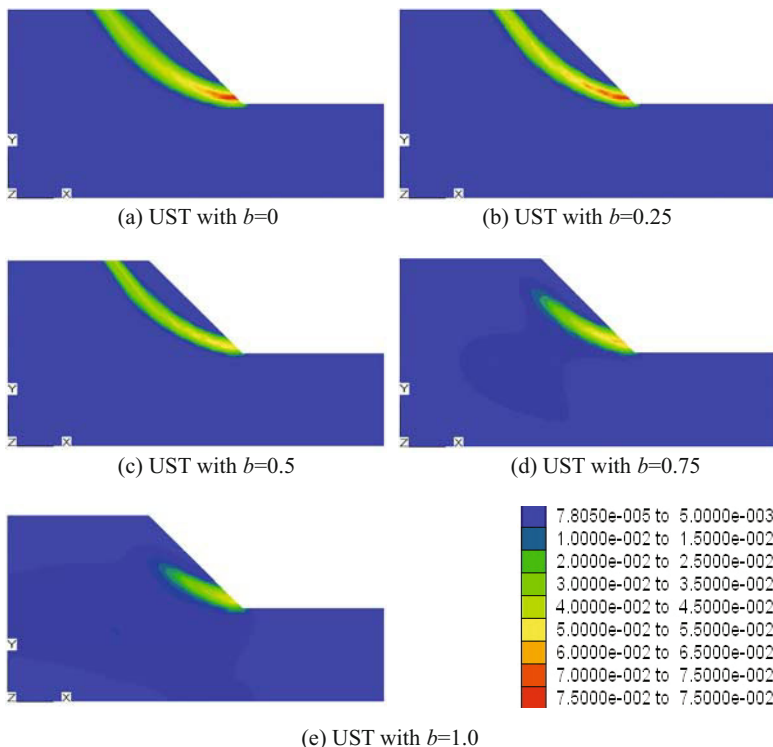
Fig. 20.52   Generalized shear strain contours of slope using UST with different parameter of *b*

(a) Outer cone yield surface of D-P criterion

(b) Inner cone yield surface of D-P criterion
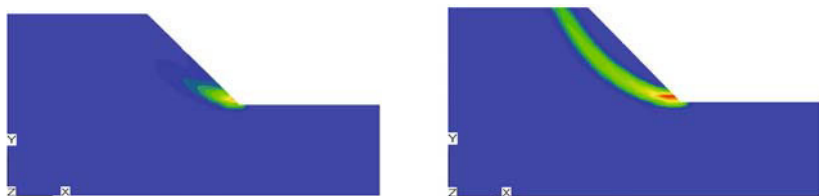
Fig. 20.53   Generalized shear strain contours of slope using the Drucker-Prager criterion

20.10 About the Unified Strength Theory: Reviews and Comments

The UST (Unified Strength Theory) has achieved widespread application and been the subject of much research. Several comments, reviews and research on UST, which are presented in published papers and books, are introduced as follows.

In 2006, "Zentralblatt MATH" (Mathematics Digest) published comments of the applied mathematician and scholar of mechanics, Academician Petre P.

Teodorescu of the European Mathematics Society, relating to "Unified Strength Theory and its Applications" the monograph (Yu, 2004) , as follows.

"Strength theories focus on the limit states of stress and strain in order to compare them with admissible stresses and strains. Uniaxial experiments and results are no longer sufficient and two- or three-axial studies are needed. Because different materials have different mechanical behavior under complex stress-strain states, yield criteria and failure criteria play an important part. The goal of these theories is to ensure the safety of civil and mechanical structures. But,in general, such a theory can be applied to a small number of materials and states of stress and strain in their deterministic aspects, and does not cover the area of all problems which may arise, so that unified theories have been looked for.

Here, starting from the idea of twin-shear and twin-shear yield criterion, the author sets up a twin-shear strength theory and then a unified strength theory, the limit loci of which cover all regions of the convex limit loci and can be extended to the region of non-convex limit loci. The present book is not only a presentation of the theory, experiments, applications and history, but also a monograph on the own research of the author as evidenced by its contents.

The book is intended for a large community of readers and represents an important contribution to the field. The present book is not only a presentation of the theory, experiments, applications and history, but is also a monograph on the author's own research".

In 2008, Altenbach and Kolupaev published a paper entitled "Remarks on Model of Mao-Hong Yu" (Altenbach and Kolupaev, 2008). They indicate that "The development of unified strength theory (UST) is an event in phenomenological material science. UST provides a new family of material models. It contains a number of new models and highlights an interrelation between known models. The UST-model can be fitted to different materials and therefore is suitable for the analysis of experimental results. The material parameters can be computed showing results of only three experiments (e.g. tension, compression and torsion)". The variety of the unified strength theory is shown in Fig. 20.54 (Altenbach and Kolupaev, 2008). The comparison of experimental results with polymers using the unified strength theory is shown in Fig. 20.55 (Altenbach and Kolupaev, 2010).
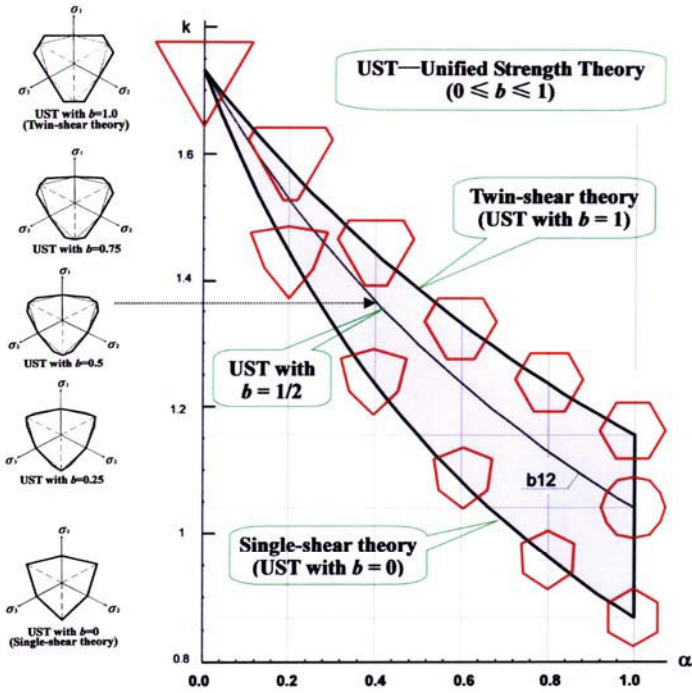
Fig. 20.54 UST covers all the region
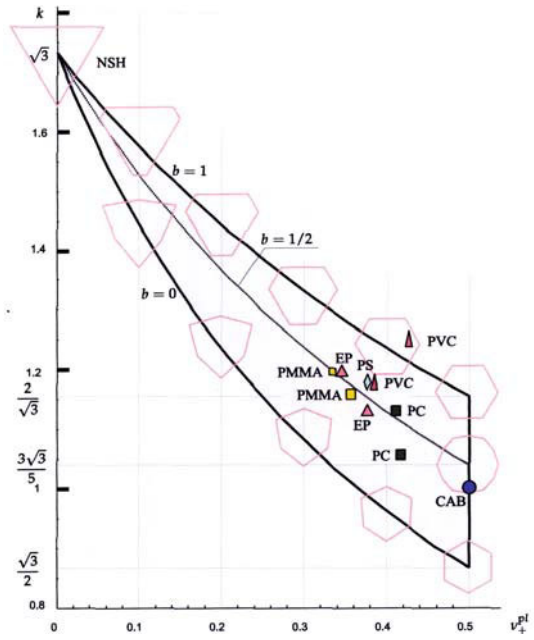
Fig. 20.55 Test results of plastics situated in the region of UST (Altenbach and Kolupaev)

A paper was presented by the State Key Laboratory of Geomechanics and Geotechnical Engineering, Institute of Rock and Soil Mechanics, Chinese Academy of Sciences, Wuhan, China in 2008. One of the authors is Professor Feng XT, the president of the International Society for Rock Mechanics and Engineering (Zhang et al., 2008). The abstract stated that:

"The unified strength theory is a new theory system which can almost describe the strength characteristics of most geomaterials and has been applied widely. And FLAC^{3D} is an excellent geotechnical program. If the former can be integrated into the latter, many complex problems in engineering will be well settled. So according to this problem, the numerical scheme of an elasto-plastic unified constitutive model in FLAC^{3D} was studied. And the numerical format of the elasto-plastic constitutive model based on the unified strength theory was derived. The corresponding UDM interface codes were programmed. Finally, a circular tunnel case is analyzed using this program. The corresponding simulated results are presented and compared with the analytical solution. The comparison expresses good agreement with the analytical solution and verifies the validity of the numerical scheme and the codes. The merits of the unified strength theory and the FLAC^{3D} program will be utilized well in geo-engineering after their combination."

The conclusion of the paper is "The unified strength theory for geomaterials was proposed by Professor Yu Mao-hong in 1991. It established a theory as suitable for each kind of material; it has a unified mathematical expression; it contains each kind of main strength theory and some new strength theories not before expressed. Moreover, the unified strength theory considers well the effect of the intermediate principal stress on the rock strength, and can match the results of true triaxial tests for geomaterials. It has achieved widespread application in geotechnical engineering."

"The unified strength theory has a solid rationale and can express the strength characteristics for each kind of geomaterial. There has been also widespread application of the new strength theory. FLAC^{3D} has formidable computational analysis functions and it is also aimed specifically at geotechnical project development by the widespread application of numerical analysis software. If can unify the theory and code which,, without doubt, can greatly promote the solution of correlation problems in geotechnical projects."

In 2006, the twin shear unified strength theory was included in "*China's Water Conservancy Encyclopedia*" (2006) and the "*Handbook of Engineering Mechanics, Rock Mechanics, Engineering Structures and Materials*" (Zhao, 2006). It states that: "Twin-shear stress strength theory was first proposed by Chinese scholar Mao-Hong Yu in 1961. In the subsequent 20 years, Mao-Hong Yu turned his attention to the progressive development of the theory to create a unified system of generalized twin-shear strength theory and, in 1991, it became officially known as the unified strength theory. The unified strength theory can explain not only the plastic yield, but also explain the tensile failure, shear failure, compressive failure and a variety of biaxial and tri-axial failures, suitable for metal, concrete, geotechnical and other materials. The theory is of important academic interest and has powerful application potential."

The introduction to the monograph "Unified Strength Theory and its Applications" is written by the Multidisciplinary Center for Earthquake Engineering Research (MCEER), USA. MCEER is a national center of excellence dedicated to the discovery and development of new knowledge, tools and technologies that equip communities to become more disaster resilient in the face of earthquakes and other extreme events.

"This text introduces a new theory dealing with the yield and failure of materials under multi-axial stresses. It provides a system of yield and failure criteria adopted for most materials, from metallic materials to rocks, concrete, soils and polymers. It describes the unified strength theory and shows how a series of results can be obtained with its use. An experimental verification, engineering applications, a detailed historical review and more than 1000 references are provided. It is intended primarily for researchers, practitioners and students."

In 2008, the Chairman of the Chinese Society of Rock Mechanics and Engineering, and Chairman of the Science and Technology Commission of the PLA General Staff Headquarters, Academician Qian Qihu, presented an invited lecture at the Sun Jun Fellow's Lecture of Tongji University in Shanghai, a Lectur "rock, rock strength and dynamic failure criterion" was reported. He pointed out that "The further development of single-shear theory is the twin-shear theory, the further development of twin-shear strength theory is the unified strength theory. Single- shear theory, twin-shear theory and the other failure criteria between the single-shear and twin-shear theories are special cases of the unified strength theory or linear approximation. It can be said that the unified strength theory is making an outstanding contribution to the developmental history of strength theory."

Recently, "Considerations on the Unified Strength Theory due to Mao-Hong Yu" were presented by Kolupaev and Altenbach (2010) in Germany. The English abstract states:

"As a basis for systematization of different models, the unified strength theory (UST) was proposed by Yu．It can be used in order to describe incompressible inelastic material behavior as well as compressible materials with different behavior in tension and in compression. In this paper Yu's theory is analyzed, compared to the existing models and approximated by simpler ones".

"For UST and other models the Poisson's ratio and the hydrostatic stress are computed. Using the Poisson's ratio for tension as well as for simple stress relations, different models are compared to each other. Constraints on the parameters of the model based on the latter values can be provided. In order to reduce the number of models, an alternative systematization based on the geometrical properties of the equivalent stresses is suggested. In this systematization Yu's model plays a quite important role."

"The beauty of the twin-shear-unified strength theory is its feasibility in defining the convex shape of the surfaces". It is the conclusion of a paper presented by a professor of Nanyang Technological University, Singapore (Fan and Qiang, 2001).

More reviews, introductions, descriptions, applications and comments on the

unified strength theory can be found in the published papers and books, in which the unified strength theory (UST) was used. The unified strength theory is a family of yield criteria and failure criteria. The yield surfaces of UST cover all regions from the lower bound to upper bound. It is possible for us to adopt different values of the unified strength theory parameter b to meet the requirements of different materials and structures. The unified strength theory can be used in all those fields in which the Tresca yield criterion, the Huber von Mises criterion or the Mohr-Coulomb theory was used. However, a higher limit load of structures can be obtained using the unified strength theory. It is advantageous in material and energy saving and also advantageous in environmental protection.

The Unified Strength Theory, as n important original innovation in applied mechanics and engineering design, has been written in more than 260 scientific monographes, handbook of engineering mechanics and textbooks. In 2011, the unified strength theory is awarded the one of the highest science award in China: National Natural Science Award.

20.11   Signification and Determination of the UST Parameter b

The unified strength theory, its implementation in FE codes and its applications have been studies in above chapters. The parameter b is an important idea. What are the physical meaning of UST parameter b and how to determine the value of UST parameter b for various materials? It is interesting and important.

20.11.1   Signification of the UST Parameter b

The unified strength theory parameter b has clear physical meaning. It offers a variety of attractions.

1) b is a parameter that reflects the influence of the intermediate principal shear stress.

In the expression of the mathematical modeling of the unified strength theory, the parameter b was displayed originally in 1991 (Yu, 1991; 1992; 2004). It is rewritten as

$$F = \tau_{13} + b\tau_{12} + \beta(\sigma_{13} + b\sigma_{12}) = C, \quad \text{when} \quad \tau_{12} + \beta\sigma_{12} \geq \tau_{23} + \beta\sigma_{23} \quad (20.5a)$$

$$F' = \tau_{13} + b\tau_{23} + \beta(\sigma_{13} + b\sigma_{23}) = C, \quad \text{when} \quad \tau_{12} + \beta\sigma_{12} \leq \tau_{23} + \beta\sigma_{23} \quad (20.5b)$$

It can be seen, b is a parameter that reflects the influence of the intermediate principal shear stress τ_{12} (or τ_{23}) and respective normal stresses σ_{12} (or σ_{23}) acting on the sections that the intermediate principal shear stress τ_{12} (or τ_{23}) acted.

2) *b* is a parameter that reflects the influence of the intermediate principal stress.

The unified strength theory is expressed in terms of the three principal stresses as

$$F = \sigma_1 - \frac{\alpha}{1+b}(b\sigma_2 + \sigma_3) = \sigma_t, \text{ when } \sigma_2 \le \frac{\sigma_1 + \alpha\sigma_3}{1+\alpha}, \quad (20.6a)$$

$$F' = \frac{1}{1+b}(\sigma_1 + b\sigma_2) - \alpha\sigma_3 = \sigma_t, \text{ when } \sigma_2 \ge \frac{\sigma_1 + \alpha\sigma_3}{1+\alpha}, \quad (20.6b)$$

It is seen, *b* is a parameter that reflects the influence of the intermediate principal stress σ_2

3) *b* is a choice parameter of the yield criterion.

The mathematical modeling and the mathematical expression of UST with *b*=0 is deduced to

$$F = F' = \tau_{13} + \beta\sigma_{13} = C, \quad F = F' = \sigma_1 - \alpha\sigma_3 = \sigma_t \quad (20.8)$$

It is the familiar Mohr-Coulomb strength theory. Obviously, only single shear stress τ_{13} and respective normal stress σ_{13} are taken into account in mathematical modeling (Eq. (20.7)), and the intermediate principal stress σ_2 is not displayed in the mathematical expression (Eq. (20.8)). So, it may be referred as the single-shear theory.

The mathematical expression of UST Eq.20.6 is deduced to the twin-shear theory when the parameter *b* equals *b*=1, as

$$F = \sigma_1 - \frac{\alpha}{2}(\sigma_2 + \sigma_3) = \sigma_t, \quad \text{when } \sigma_2 \le \frac{\sigma_1 + \alpha\sigma_3}{1+\alpha} \quad (20.9a)$$

$$F' = \frac{1}{2}(\sigma_1 + \sigma_2) - \alpha\sigma_3 = \sigma_t, \quad \text{when } \sigma_2 \ge \frac{\sigma_1 + \alpha\sigma_3}{1+\alpha} \quad (20.9b)$$

A series of new yield criteria can be obtained when 0<*b*<1.

4) *b* is a control parameter of the shape and size of yield surface.

The yield surfaces of the unified strength theory on deviatoric plane are represented in Fig. 20.56. It is seen, *b* is a control parameter of the shape and size of yield criteria, which reflects the influence of the shape and size for yield surface, as shown in Fig. 20.56. The yield loci are hexagonal when *b*=0 and *b*=1, and the yield loci are a dodecagonal locus when 0<*b*<1.
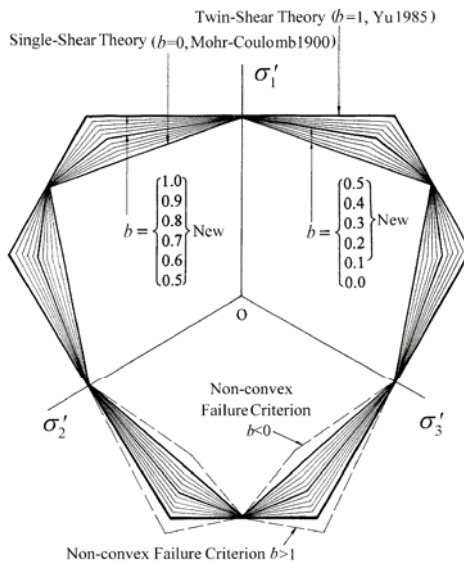
Fig. 20.56 Convex and non-convex yield loci of UST

5) b is a critical parameter of the convexity of yield criterion.

The yield loci of UST are convex when yield criterion parameter b ($0 \leq b \leq 1$), and the yield loci of UST are non-convex when yield criterion parameter $b<0$ or $b>1$, as shown in Fig. 20.56. The non-convex yield criterion is rare studied up to now.

6) b is a parameter that reflects the shear strength of materials.

It will be discussed as follows.

20.11.2   Determination of the UST Parameter b

The UST parameter b can be determined by different methods.

1) Complex stress test

The values of parameter b can be determined by comparison with experimental verification for various materials. The comparisons between the unified strength theory and several experiment results are shown in Fig. 20.8. It is very expensive, however, because of the expense of the experimental facilities in which the materials can be acted under complex stress.

2) Pure shear test

The stress state of pure shear is $\sigma_1=\tau$, $\sigma_1=0$, $\sigma_3=-\tau$, the yield state at pure shear is $\sigma_1=\tau_0$, $\sigma_2=0$, $\sigma_3=-\tau_0$. This state coincidence the condition $\sigma_2 \leq \dfrac{\sigma_1 + \alpha\sigma_3}{1+\alpha}$, the Eq. (20.6a) is used.

$$\sigma_1 - \frac{\alpha}{1+b}(b\sigma_2 + \sigma_3) - \sigma_t = \tau_0 - \frac{\alpha}{1+b}(-\tau_0) - \sigma_t = 0 \qquad (20\text{-}10)$$

where $\alpha = \sigma_t/\sigma_c$ is ratio of material strength in tension and in compression. The relationship among shear strength τ_0, the uniaxial tensile strength σ_t, uniaxial compressive strength σ_c and unified strength theory parameter b can be determined as follows:

$$b = \frac{(1+\alpha)\tau_0 - \sigma_t}{\sigma_t - \tau_0} = \frac{\alpha\tau_0}{\sigma_t - \tau_0} - 1, \quad \alpha = \frac{\sigma_t}{\sigma_c} \qquad (20.11)$$

Eq. 20-11 can be simplified to Eq. 20-12 for non-SD materials, as follows

$$b = \frac{2\tau_0 - \sigma_t}{\sigma_t - \tau_0} = \frac{\tau_0}{\sigma_t - \tau_0} - 1 \qquad (20.12)$$

3) Plane strain test
Unified strength theory can be also expressed by the stress invariant, stress angle and material parameters cohesion and friction angle, as (see Chapter 4)

$$F = \frac{2I_1}{3}\sin\varphi + \frac{2\sqrt{J_2}}{1+b}\left[\sin\left(\theta + \frac{\pi}{3}\right) - b\sin\left(\theta - \frac{\pi}{3}\right)\right] + \frac{2\sqrt{J_2}}{(1+b)\sqrt{3}} \times$$
$$\left[\sin\varphi\cos\left(\theta + \frac{\pi}{3}\right) + b\sin\varphi\cos\left(\theta - \frac{\pi}{3}\right)\right] = 2C_0\cos\varphi, \quad 0° \le \theta \le \theta_b \quad (20.13a)$$

$$F' = \frac{2I_1}{3}\sin\varphi + \frac{2\sqrt{J_2}}{1+b}\left[\sin\left(\theta + \frac{\pi}{3}\right) - b\sin\theta\right]$$
$$+ \frac{2\sqrt{J_2}}{(1+b)\sqrt{3}}\left[\sin\varphi\cos(\theta + \frac{\pi}{3}) + b\sin\varphi\cos\theta\right] = 2C_0\cos\varphi, \quad \theta_b \le \theta \le 60° \quad (20.13b)$$

where C_0 is material cohesion parameters and φ is friction angle of material, which are always obtained by a conventional tri-axial test, i.e. triaxial confined pressure experiment.

The relationship of friction angle φ_0 under trial-axial test and unified friction angle φ_{unified} in terms of the unified strength theory (Fig. 20.57) has been established by Yu in 1997, and represented in (Yu et al., 2006). It is expressed as follows

$$\sin\varphi_{uni} = \frac{2(b+1)\sin\varphi_0}{2 + b(1 + \sin\varphi_0)} \qquad (20.14)$$
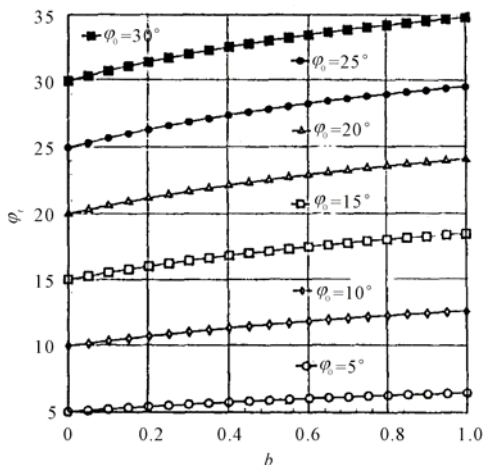
Fig. 20.57   Relation between UST parameter b with friction angle

The unified strength theory parameter b can be determined as

$$b = \frac{2(\sin\varphi_{uni} - \sin\varphi_0)}{2\sin\varphi_0 - \sin\varphi_{uni}\sin\varphi_0 - \sin\varphi_{uni}} \tag{20.15}$$

20.12   Brief Summary

Several ancient structures and parts of rocket and generator are studied. A lot of results can be obtained by using of the unified strength theory and associated flow rule. It can be adapted for more materials and structures. It is evident that

1) The unified strength theory with $b=0$ (single-shear theory) gives the lower limit load and the unified strength theory with $b=1$ (twin-shear theory) gives the upper limit load.

2) The unified strength theory with $b=0$ gives the larger plastic zone, and the unified strength theory with $b=1$ gives the smaller plastic zone under the same load.

3) It means that more materials in structure are contributed for the bearing capacity of structure when the unified strength theory parameter $b>0$, and the highest limit load can be obtained when the UST parameter $b=1$ is used.

4) The limit bearing capacity of structure can be obtained when the material parameter $b>0$. It is also means that the weight of structure may be decreased. It is advantageous especially for airplane and rocket structures, also for traffic structures.

5) The unified strength theory provides us a theoretical base and more practical applications. The unified strength theory (UST) can be used in all those

fields that the Tresca-Mohr-Coulomb theory (lower bound), the Huber-von Mises-Drucker-Prager criterion or the twin-shear strength theory (upper bound) was used. More new results will also be obtained.

6) The development of strength theories can be summarized briefly as shown in Fig. 20.58.

Fig. 20.58 The development of strength theories

7) The application of the unified strength theory can be illustrated by an example as show in Fig. 20.59.
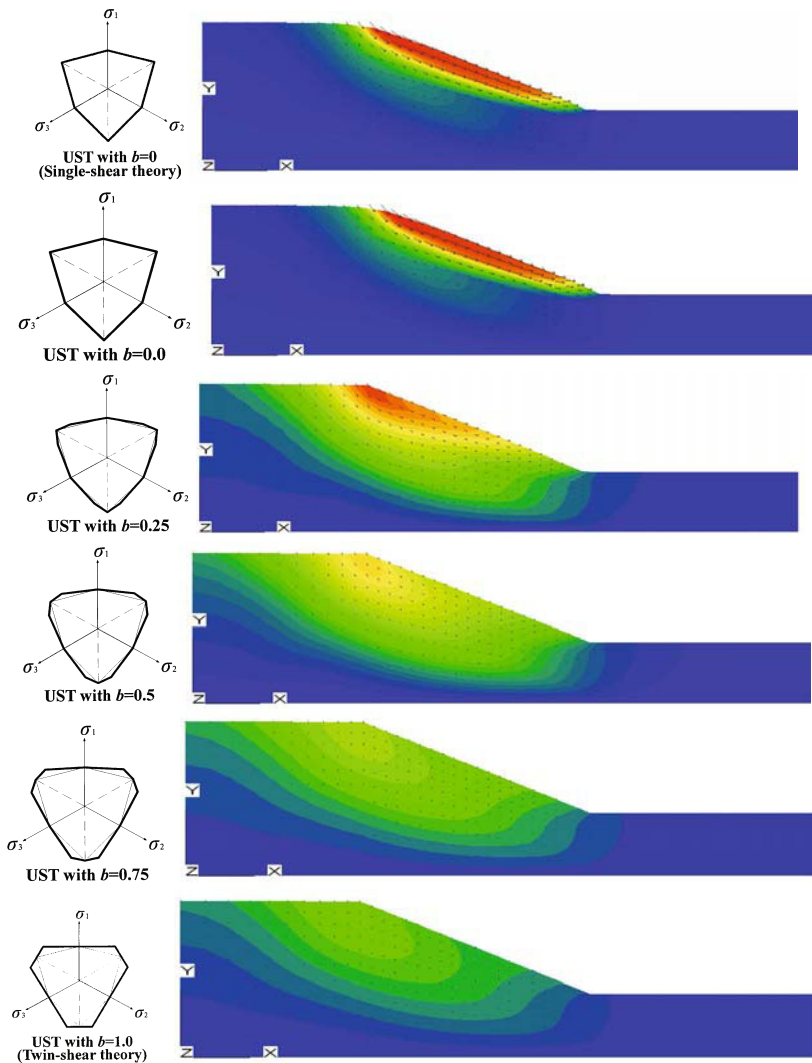
Fig. 20.59   Shear strain spread with several yield criteria for a slope

Unified strength theory is important and interesting not only in theory form a series of yield criterion, which covering all convex regions from the inner boundary to outer oundary. It is also important and interesting in structural analysis and engineering applications, a series of new results can be obtained for engineering application. It provides us more information and choice. This is a series of results for the plastic analysis of a slope.

References

Altenbach H and Kolupaev VA (2008) Remarks on Model of Mao-Hong Yu.. In: The Eighth International Conference on Fundamentals of Fracture (ICFF VIII), Zhang TY, Wang B and Feng XQ eds. pp 270-271.

Chinese National Historical Relic Bureau (1992) Summary of Appraisal Meeting of Rescue and Restoration Project of Arrow Tower of North City Gate of Xi'an. in: Yu MH, Fang DP. Research of Ancient City Wall of Xi'an: Architecture Structure and Seismic Performance. Xi'an: Jiaotong University Press: Xi'an, pp 84-85 (in Chinese).

Encyclopedia of China Water Conservancy (2nd edition 2006). China Water Conservancy and Hydropower Press: Beijing, Vol. II, pp 940.

Fan SC and Qiang HF (2001) Normal high-velocity impaction concrete slabs-a simulation using the meshless SPH procedures. In: Computational Mechanics–New Frontiers for New Millennium, Valliappan S. and Khalili N. eds. Elsevier Science Ltd, pp 1457-1462.

Gu J (1993) Elastic-plastic Analysis of the Foundation of the Big Goose Pagoda: Master's Dissertation, Xi'an Jiaotong University (in Chinese).

Gao DF (1995) Investigation of Earthquake and Wind Resistance and the Limiting Bearing Capacity of the Foundation of the Small Goose Pagoda. Master's Dissertation. Xi'an: Xi'an Jiaotong University (in Chinese).

Hu WF, Shen L, Yang JM and He WL (2010) Analysis and Improved design of structural dynamics for an advanced upper stage. Missiles and Space Vehicles, (3):1-7 (in Chinese).

Kolupaev VA and Altenbach H (2009) Application of the Unified Strength Theory of Mao-Hong Yu to Plastics. In: Tagung Deformations und Bruchverhalten von Kunststoffen. Book of Abstracts ed. by W. Grellmann, Merseburg, pp 320-339 (in German).

Kolupaev, VA and Altenbach H (2009) Anwendung der Unified Strength Theory (UST) von Mao-Hong Yu auf unverstärkte Kunststoffe. In: 12. Tagung Problemseminar "Deformation und Bruchverhalten von Kunststoffen" -Merseburg, S. 1-8.

Kolupaev VA. Bolchoun A and Altenbach H (2009) Unified representation and evaluation of the strength hypotheses. In: Proceedings of 12th International Conference on Fracture. Ottawa : NRCanCANMET, pp 1-10.

Kolupaev VA and Altenbach H (2010) Einige Überlegungen zur Unified Strength Theory von Mao-Hong Yu (Considerations on the Unified Strength Theory due to Mao-Hong Yu), Forschung im Ingenieurwesen (Forsch Ingenieurwes) Springer: Berlin (in German, English Abstract).

Li JT, Lei YJ. Tang GJ, Mong SY and Yu DC (2008) Crack analysis for solid rocket motor grain. Missiles and Space Vehicles, (5):471-474 (in Chinese).

Liao HJ, Ma ZY, Ning CM, Liu L and Sassa K (2010) Stability analysis of high loess slope under complex stress state. In: Recent developments of geotechnical engineering, Proceedings of the fourth Japan-China geotechnical symposium, Okinawa Japan, April 12-14.

Ma ZY and Liao HJ (2010) Study on the constitutive model of twin shear unified elasto-plastic and strain hardening/softening based on FLAC3D. J. of Geotechnical Engineering(in Chinese).

Qiang HF (1998) Numerical Analysis and Experimental Researches on the Structural Integrity of Solid Rocket Motor Grain. Doctoral Dissertation, Xi'an Jiaotong University, Xi'an (in Chinese).

Qiang HF, Cao DZ and Zhang Y (2008) A new criterion based on the unified strength theory and its application in the study on the crack of solid rocket motor grain. Solid Rocket Technology, 31(4): 340-343 (in Chinese).

Qian QH and Qi CZ (2008) Dynamic strength and dynamic fracture criteria of rock and rock mass. J. of Tongji University (Natural Science Edition), 36(12):1599-1605(in Chinese, English abstract).

Teodorescu PP (2006) Review of "Unified strength theory and its Applications. Springer, Berlin, 2004" Zentralblatt MATH 2006, Cited in Zbl. Reviews, 1059.74002 (02115115).

Wang Y (1996) Structural Analysis of City Tower of East Gate of Xi'an. Master's Dissertation, Xi'an Jiaotong University (in Chinese).

Xing RC, Liu ZD and Zheng YR (1992) A failure criterion of loess. J. Hydraulic Engineering (1), 12-19 (in Chinese, English abstract).

You JF, Chen RX and Li SL (2008) Experimental stress calculate method for the shell of solid rocket motor. Missiles and Space Vehicles, (4): 386-388 (in Chinese).

Yu MH (1992) New System of Strength Theory. Xi'an Jiaotong University Press: Xi'an. (in Chinese).

Yu MH and Meng XM (1992) Twin shear stress yield model and its application in soil engineering. Chin. J. Geotech. Eng., 14(3): 71-75 (in Chinese).

Yu MH, He LN, Liu CY (1992) Generalized twin shear stress yield criterion and its generalization. Chinese Science Bulletin (Eng. Edn) 37(24): 2085-2089.

Yu MH, Lu N, Yang SY, Gao DF (1994) Research on Column Foundation Structure and Bearing Capacity. In: The Collection of the 7th National Soil Engineering & Foundation Engineering Conference. China Architecture & Building Press: Beijing. pp 309-312.

Yu MH (1994) Unified strength theory for geomaterials. Chin. J. Geotech. Eng., (2): 1-10 (in Chinese).

Yu MH, Zeng WB, Lu N (1994) New theory of engineering structural analysis and its application. Engineering Mechanics, 11(1): 9-20 (in Chinese).

Yu MH et al. (1997) Unified plane strain slip line theory. China Civil Engineering Journal, 30(2): 14-26 (in Chinese, English Abstract).

Yu MH (1998) Twin Shear Theory and Its Application. The Science Press: Beijing. (in Chinese).

Yu MH and Liu FY (2001) Researches on the stability of ancient city wall in Xi'an. In: Studies in Ancient Structures (Proceedings of the 2nd International Congress). Yildiz Technical University Publication: pp 365-370.

Yu MH (2003) Studies on the History, Art and Scientific Characteristics of Ancient Structures. Invited Lecture at the Chinese Conference on Structural Engineering.

Engineering Mechanics, 20 (Additional): 435-438(in Chinese).

Yu MH (2004) Unified Strength Theory and its Applications. Springer: Berlin.

Yu MH, Oda Yoshiya, Fang DP (2008) Advances in Structural Mechanics of Ancient Architectures. Frontiers of Architecture and Civil Engineering in China- Selected Publications from Chinese Universities, Higher Education Press and Springer-Verlag, 2(1): 1-25.

Yu MH, Wang Y, Yu T and Dietermam D (2009) Ancient City Wall, Bell Tower and Drum Tower: Second Edition (Color edition), 2011. History, Art and Science. Xi'an Jiaotong University Press: Xi'an (in Chinese).

Zhang CQ, Zhou H and Feng XT (2008) Numerical format of elastoplastic constitutive model based on the unified strength theory in FLAC^{3D}[J]. Rock and Soil Mechanics, 29(3): 596-601 (in Chinese).

Zhang Y (2010) Experimental and Theoretical Research on Failure Criterion of HTPB composite Solid Propellant. Doctoral thesis of Xi'an High Technology Institute, Xi'an, China (in Chinese).

Zhao Guang-Heng, Chief ed. (2006) Handbook of Engineering Mechanics, Rock Mechanics, Engineering Structures and Materials. China's Water Conservancy Resources and Hydropower Press: Beijing, pp 20-21 (in Chinese).

Index